SHAPE DESIGN BY OPTIMAL FLOW CONTROL AND REDUCED BASIS TECHNIQUES: APPLICATIONS TO BYPASS CONFIGURATIONS IN HAEMODYNAMICS

THÈSE N^{O} 3400 (2005)

PRÉSENTÉE À LA FACULTÉ SCIENCES DE BASE

Institut d'analyse et de calcul scientifique

SECTION DE MATHÉMATIQUES

ÉCOLE POLYTECHNIQUE FÉDÉRALE DE LAUSANNE

POUR L'OBTENTION DU GRADE DE DOCTEUR ÈS SCIENCES

PAR

Gianluigi ROZZA

Laurea in Ingegneria Aerospaziale, Politecnico di Milano, Italie
et de nationalité italienne

acceptée sur proposition du jury:

Prof. A. Quarteroni, directeur de thèse
Prof. V. Agoshkov, rapporteur
Prof. A. Patera, rapporteur
Prof. J. Rappaz, rapporteur

Lausanne, EPFL
2005

Ai miei Nonni,
Rosa e Luigi, Giuseppina ed Ernesto

Abstract

The purpose of this thesis is to develop numerical methods for optimization, control and shape design in computational fluid dynamics, more precisely in haemodynamics.
The application studied is related with the shape optimization of an aorto-coronaric bypass. The optimization process has to keep into account aspects which are very different and sometimes conflicting, for this reason the process has been organized in more levels dealing with a geometrical scale. Moreover we have chosen to use simplified low fidelity models during the application of the complex optimization tools and to verify in feed-back with higher fidelity models the configurations previously obtained. In our case we deal with fluid models based on Stokes and Navier-Stokes equations, for lower and higher fidelity approach respectively, also in the unsteady formulation.
At an outer level of the optimization process, efficient numerical methods based on parametrized partial differential equations have been developed to get real-time and accurate information concerning the preliminary configurations, and to get a sensitivity analysis on geometrical quantities of interest and on functionals, related with fluid mechanics quantities. This approach is carried out by reduced basis methods which let us rebuild approximate solutions for parametrized equations by other solutions already computed and stored, allowing huge computational savings.
At an inner level we have developed local shape optimization methods by optimal flow control theory based on adjoint approach. Two different approaches have been developed: the former is based on the local displacement of each node on the boundary, the latter is based on small perturbation theory into a reference domain. This approach is more complex but let us avoid mesh reconstruction at each iteration and study the problem into a deeper context from a theoretical point of view and do a generalization dealing with unsteady flows.

Version abrégée

Le but de cette thèse est le développement de méthodes numériques pour l'optimisation, le contrôle et le project de forme dans le cadre de la dynamique des fluides, notamment en hémodynamique.
On étudie en particulier une application de ces méthodes à l'optimisation d'un bypass aorto-coronaire.
Le processus d'optimisation est basé sur des aspects différents et des exigences parfois contradictoires; pour cette raison il a été structuré sur plusieurs niveaux correspondants à différentes echelles géométriques. En outre, on a choisi d'utiliser des modèles simplifiés pour l'application des complexes outils d'optimisation et de vérifier les états optimaux à posteriori par des modèles plus précis. Dans notre cas, il s'agit de modèles portant respectivement sur les équations de Stokes et Navier-Stokes, éventuellement non stationnaires.
Dans un niveau extérieur (par rapport au processus d'optimisation) on a développé des méthodes numériques efficaces basées sur des équations parametrisées qui donnent des informations précises "en temps réel" sur une configuration indicative à considerer à travers l'analyse de sensitivité pour les quantites d'intérêt et les fonctionneles typiques de la dynamique des fluides. Cette approche utilise les méthodes dites "à bases réduites", qui permettent de reconstruire des solutions approchées d'équations parametrisées en fonction d'autres solutions déjà calculées et disponibles, ce qui réduit énormément les réssources de calcul nécessaires.
Dans un niveau interne on a développé des méthodes d'optimisation de forme locale par la théorie du contrôle optimal des fluxes en utilisant la formulation basée sur l'état adjoint. On a étudié deux approches: une première portant sur le déplacement des noeuds du bord, et une deuxième qui utilise une technique de pérturbations sur un domaine de référence. Cette dernière approche, même si plus complexe, a l'avantage d'éviter la réconstruction du maillage et permet d'étudier le problème d'une façon plus profonde, ainsi que de le généraliser.

Estratto

L'obiettivo di questo lavoro di tesi è quello di sviluppare metodi numerici di ottimizzazione, controllo e progetto di forma in fluidodinamica computazionale, precisamente in emodinamica. L'applicazione studiata è relativa all'ottimizzazione della forma di un bypass aorto-coronarico. Il processo di ottimizzazione deve tenere conto di aspetti molto diversi ed esigenze spesso contrastanti, per questo motivo è stato organizzato su più livelli di scala geometrica. Inoltre, si è scelto di usare modelli semplificati a bassa fedeltà durante l'applicazione dei complessi strumenti di ottimizzazione e di verificare successivamente in feed-back le configurazioni ottenute con modelli a più alta fedeltà. Nel nostro caso si tratta rispettivamente di modelli basati sulle equazioni di Stokes e di Navier-Stokes, anche non stazionarie.

Ad un livello più esterno del processo di ottimizzazione si sono sviluppati metodi numerici efficienti basati su equazioni parametrizzate che permettono di ottenere informazioni accurate in tempo reale circa la configurazione di massima da considerare, mediante un'analisi di sensitività su grandezze geometriche di interesse e funzionali legati a grandezze fluidodinamiche. Tale approccio è costituito da metodi a basi ridotte che permettono di ricostruire delle soluzioni approssimate per equazioni parametrizzate in funzione di altre soluzioni già calcolate e memorizzate, garantendo notevoli risparmi computazionali.

A un livello più interno si sono sviluppati metodi di ottimizzazione di forma locale mediante la teoria del controllo ottimale dei flussi nella formulazione basata sul problema aggiunto. Sono stati sperimentati due approcci: uno si basa direttamente sullo spostamento dei nodi del contorno, mentre l'altro su piccole perturbazioni in un dominio di riferimento.

Il secondo approccio, più complesso, permette però di evitare la ricostruzione della griglia e di studiare il problema in maniera più approfondita da un punto di vista teorico, e di farne una generalizzazione.

Acknowledgements

First of all, I would like to thank Prof. Alfio Quarteroni for being more than a thesis supervisor during these years at EPFL with his human qualities and kindness. He gave me unique opportunities to study and learn new branches of applied mathematics and numerical analysis since my master degree thesis, leading enthusiastically my research activity and always providing new ideas, suggestions and insights.

I am very grateful to Prof. Anthony T. Patera, who has given me the opportunity to visit his research team at Massachusetts Institute of Technology and opened the doors of the reduced basis world. I am particularly grateful for his availability, kindness, patience during the several video conferences between EPFL and MIT and in revising my work.

Special thanks to Prof. Valery Agoshkov of Russian Academy of Sciences for his strong contributions and guidelines on optimal control and adjoint approach during his visiting periods at EPFL.

I thank all the members of the jury, especially Prof. Jacques Rappaz, director of IACS, Institute of Analysis and Scientific Computing, and Prof. Charles Stuart for presiding the jury.

Several people contributed to the achievement of this work. Special recognition goes to all my colleagues of the Chair of Modelling and Scientific Computing (CMCS) of EPFL, past and present members, for sharing with me a part of their precious time, for their friendship and their availability and for creating a lively and nice place and a great team. Special thanks to our information technology team and my office mates.
Thanks to M.me J. Mosetti and M.me C. Craman, our secretaries, for their work and their kindness, and to all other people with whom I interacted during my period at EPFL, especially all the members and colleagues of IACS.

I mention also other three professional environments in which I have been involved: members of MOX –Modelling and Scientific Computing Center– at Politecnico di Milano, especially Prof. L. Formaggia, Prof. F. Saleri, Prof. A. Veneziani and Dr. S. Perotto, with whom I shared many parts of my professional life and I had always suggestions and encouragement; the Haemodel project group to be not only a network but also a big family after several

meetings and conferences; and all the A.T. Patera's group at Fluids Laboratory at MIT, especially Dr. Karen Veroy and Dr. Martin Grepl for creating a very exciting place to work and collaborate.

This work has also benefited from the collaboration with Luca Dedè and Annalisa Quaini who carried out their master thesis under my supervision.

Acknowledgements to Bernoulli Center of EPFL for the special semester organized on the mathematical modelling of the cardiovascular system in 2003.
I acknowledge the European Community's Human Potential Programme (contract HPRN-CT-2002-00270), the European Union Research Training Network –Haemodel Project– and the OFES –Swiss Federal Office for Education and Schools– which supported my activity during these three years at EPFL.

Personally, I would like to remember all people with whom I interacted during my PhD –the list would be too long and incomplete– for understanding, support, interest and affection, especially all my friends.

Last but not least, a very special thanks to my parents, for their support, their love and patience. This work is dedicated to my grandparents to remember everything they made for our family.

Lausanne, November 2005

"In motu igitur sanguinis explicando easdem offendimus insuperabiles difficultates, quae nos impediunt omnia plane opera Creatoris accuratius prescrutari; ubi perpetuo multo magis summan sapientiam cum omnipotentia coniunctam admirari ac venerari debemus, cum ne sumum quidem ingenium humanum vel levissimae vibrillae veram structuram percipere atque explicare valeat."
Leonhard Euler (1707-1783).

"Mathematics seems to endow one with something like a new sense."
Charles Darwin (1809-1882).

"È nelle difficoltà che si prova la fedeltà e la costanza
–Omnia possum in Eo qui me confortat (St.Paul, Philipp. 4,13)–."
Francesca Cabrini (1850-1917).

Contents

List of Tables

List of Figures

Chapter 1

Introduction and Motivation

The theory of optimal control based on variational systems of equations is applied in order to optimize the shape of the incoming branch of the bypass (the toe) into the coronary. At this level two different options are addressed for shape design: one implements local boundary variations in the computational domain, the other, based on the theory of small perturbations, makes use of a linearized design in a reference domain. As a pre-processing stage, reduced basis methodologies based on parametrized partial differential equations are developed to provide (a) a sensitivity analysis for geometrical quantities of interest in bypass complete configurations and (b) rapid and reliable prediction of integral functional outputs. The aim of this work is (i) to provide design indications for arterial surgery in the perspective of future development for prosthetic bypasses, (ii) to develop multi-level numerical methods for optimization and shape design by optimal control, and (iii) to provide input-output relationships led by models with lower complexity (i.e simplified flow models) and competitive computational costs to be validated with higher fidelity models in feed-back.
In this introduction multi-level geometrical approaches in the study of aorto-coronaric bypass anastomoses configurations and their optimization are briefly discussed.

1.1 Bypass clinical aspects: surgery, materials, state of the art

The surgical realization of a bypass to overcome a critically stenosed artery is a very common practice in everyday cardiovascular clinic (see Figure 1.1 [126]).
When a coronary artery is affected by a stenosis, the heart muscle cannot be properly oxygenated through blood. Aorto-coronaric anastomosis restores the oxygen amount through a bypass surgery downstream an occlusion (see Figure 1.2).
At present, different kind and shape for aorto-coronaric bypass anastomoses are available and consequently different surgery procedures are used to set up a bypass.

A bypass can be made up either by organic material (e.g. the saphena vein taken from patient's legs or the mammary artery) or by prosthetic material. The current saphenous bypass solution requires the extraction of saphena vein with possible complications. In this respect,

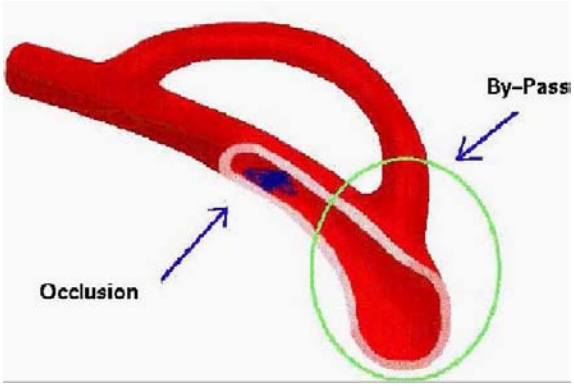

Figure 1.1: Simplified bypass model.

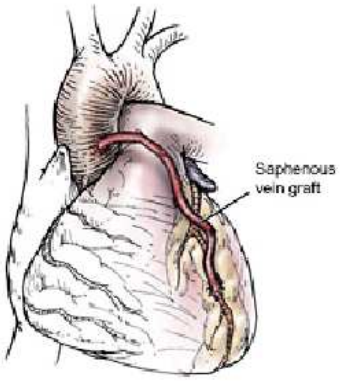

Figure 1.2: Heart, coronary arteries and bypass.

prosthetic bypasses are less invasive. They may feature very different shape for bypass anastomoses, such as, e.g., cuffed arteriovenous access grafts (Figure 1.3 and 1.4). Different cuffed models are used and analyzed such as Taylor patch [28] and Miller cuff bypass [30], but also standard end-to-side anastomoses at different graft angle [29] or other shaped carbon-fiber prostheses. For a discussion and a comparative approach based on fluid mechanics considerations see Cole *et al.* [27], [26].

In the cardiovascular system altered flow conditions such as separation, flow reversal, low and oscillatory shear stress areas and abnormal pulse pattern are all recognized as potentially important factors in the development of arterial diseases (White *et al.* [165], Loth *et al.* [87]). A detailed understanding of local haemodynamics phenomena and the effect of vascular wall modification on flow patterns can have useful clinical applications especially in surgical procedures or prostheses tailoring (see Steinman *et al.* [147], Moore *et al.* [99]). Concerning bypass setting, lots of different aspects and post-surgical complications have to be taken into consideration, among them we mention intimal thickening hyperplasia (near suture lines), which is a narrowing of coronaries, restenosis, surgical injury, long term graft failure. Every year 8% of all patients risk bypass occlusion, after ten years 80% bypasses must be replaced (data from HeartCenterOnLine©). Repeating procedures typically carry a higher risk of

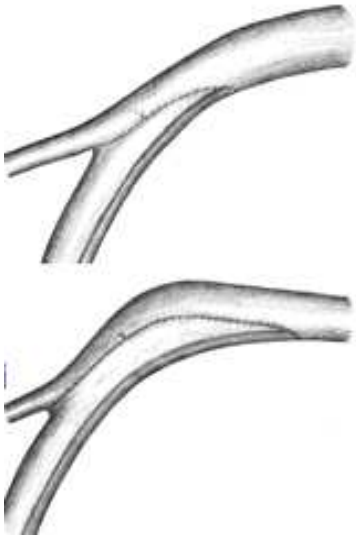

Figure 1.3: Different anastomoses configurations: end-to-side (top) and cuffed on the bed (bottom).

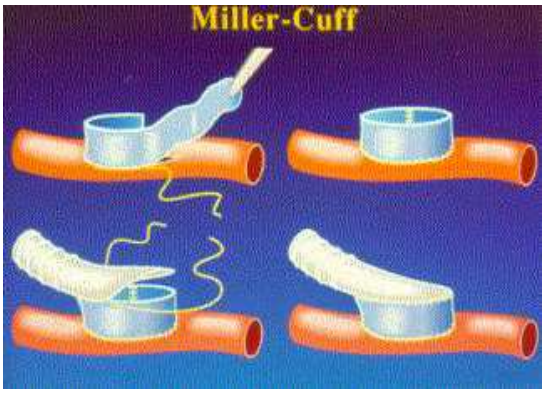

Figure 1.4: Miller cuffed bypass model.

complications.
Because of all these different aspects the design and analysis of artificial arterial bypass is a very complex problem. Carbon fiber, bioartificial and collagen cuffed grafts instead of natural saphenous vein can be used in bypass shape design without needing "in loco" reconstruction. In this framework, optimal flow control and shape optimization provide a new interesting approach to the problem, aimed at improving arterial bypass graft on the basis of a better understanding of fluid dynamics aspects involved in the bypass studying. A parametric analysis on inflow conditions, branch angle and upstream geometry for bypass graft, considering also secondary flows due to the particular configuration studied, has been provided recently by Sherwin and Doorly [141].

1.2 Framework: mathematical modelling in haemodynamics

Improvement in the understanding of the genesis of coronary diseases is very important as it allows to reduce surgical and post-surgical failures. It may also suggest new means in bypass surgical procedures with less invasive methods and to devise new shape in bypass configuration (see Perktold *et al.* [112], O'Brien and McGloughin [107]).
Generally speaking, mathematical modelling and numerical simulation can allow better understanding of phenomena involved in vascular diseases (see Abdoulaev *et al.* [1], Quarteroni, Tuveri and Veneziani [125], Quarteroni and Formaggia [126], Fung [39] and more recently Gerbeau and Chapelle [42]).
In this work we aim at providing design indications for bypasses surgical procedures by applying numerical optimization methods at two different geometrical levels: the former is based on the local shape of the incoming branch, the latter is devoted to a complete bridge configuration.
At each geometrical level we have developed different approaches based on either low fidelity steady Stokes flows and on high fidelity unsteady Navier-Stokes. The idea is to use complex optimization tools with low fidelity fluid model, then to verify results in feedback on the complete (high fidelity) fluid model.
At a fine geometrical level the background provided by mathematical modelling and numerical simulation has led us to apply the optimal control theory of systems governed by partial differential equations (PDEs) with the aim of optimizing the (local) shape of a simplified bypass model.
At a coarser geometrical level efficient schemes for reduced basis methodology (see Patera *et al.* [118]) applied to parametrized partial differential equations (P^2DEs) are being used to provide useful and quick indications (outputs) for bypass complete configuration in a repetitive design environment as shape design requires. With the reduced basis approach also a sensitivity analysis of the initial configuration and a study of important geometrical quantities in bypass can be obtained. (see [135] for an introduction and [111] for details). Figure 1.5 clarifies our geometrical double-level of interest for bypass design.

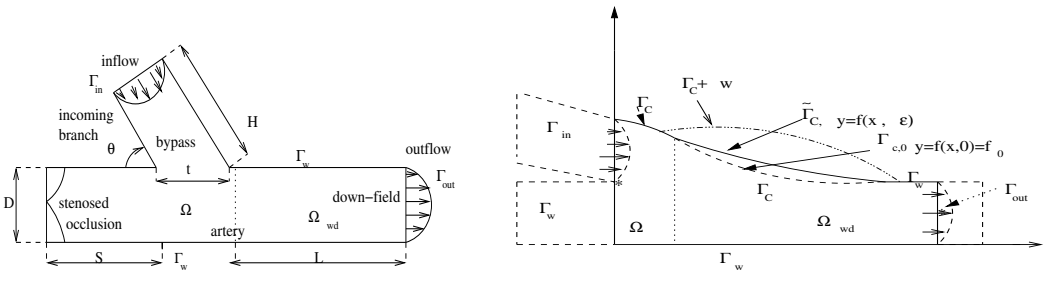

Figure 1.5: Bypass schemes: coarse geometrical configuration (left), parametrized by H, L, S, t, D, θ and local configuration (right), where $\Gamma_{C,0}$ represents the initial configuration, $\tilde{\Gamma}_C$ the one optimized by small perturbation techniques and $\Gamma_C + w$ the one optimized by local boundary variations.

The ultimate goal is to build an input-output relationship hold by different models characterized by an increasing degree of complexity (dealing with different fluid models and optimization methods) and focused on different geometrical levels. The outputs of interest are design quantities and fluid mechanics indexes, while the inputs are typically geometrical quantities. The multilevel approach is introduced in Figure 1.6.

1.2.1 On control approaches

At a local geometrical level optimal control of one (or several) aspect of the problem entails the minimization of a *cost functional* which describes physical quantities involved in the specific problem. Optimization process is carried out by a *control function* which, depending upon the context, may represent initial or boundary conditions, shape of the domain (by boundary variations), force terms, sources, etc. In computational fluid dynamics two different kind of optimal control problems can be faced.

The former is called *Data Control*, in which case the control is on different variables of the problem such as initial and boundary conditions, force terms, sources and coefficients. Control function can act either on the boundary or part of it, or on the whole computational domain or part of it. When control is put on the flux we have a *flow control* problem (Becker [14], Berggren [17], Hinze and Kunish [57], Ravindran and Hou [58], [59], Gunzburger [49], Slawig [142]).

The other field is called *Domain Control*, since the solution of the system of PDEs is controlled by boundary variations of the domain itself. This field is related with *shape optimization and optimal shape design*, see e.g. the work by Jameson *et al.* [66], [67], [68], Pironneau [115], Mohammadi and Pironneau [97], Kawohl *et al.* [70], Di Césaré [33], in the context of aerodynamics for external flows (wings and airfoils design) and internal flows (nozzles, channels).

The problem we are considering is related both with *optimal shape design* (see also J.Haslinger and R.A.E. Makinen [52]) and *flow control* (see Gunzburger [50]) in haemodynamics, involved in the observation of the evolving system and in cost functionals, such as vorticity or wall shear stress. Optimization process is carried out by a *control function* used as parameter in modelling the shape of the domain.

At this level two control approaches have been used: in the former the control function is used to define directly the boundary shape (local boundary variation method) in the true domain (see [123]); in the latter, the control function is used to define the mapping transformation from the reference domain to the true one. In this case the design problem becomes an optimal control problem on coefficients and the analysis can be based on small perturbation theory in fluid mechanics (see [4]). Theoretical investigation based on perturbation theory analysis and linearized shape design provides results on existence and uniqueness of solution and on the well-posedness of the problem, and permits us to better understand the problem from a theoretical point of view. In this second approach also an unsteady fluid model has been used during control process. In both cases the adjoint approach, proposed for example by J.L. Lions [82], Marchuk [95] and Agoshkov *et al.* [96], to get cost functionals gradient in problem

with distributed or boundary control and observation, has been developed. In the functional optimization process a descent gradient-type method (with fixed optimized step size) is used (see Ciarlet [25]). Numerical approximation is based on the Galerkin-Finite Element Method [127]. Algorithms were developed for control and optimization as well as for the coupling between state and adjoint problems.
At the end of these first investigation stages based on optimal design a cuffed bypass is found with a shape which resembles the Taylor arterial patch [26]. A feedback validation procedure has then been implemented by solving the unsteady Navier-Stokes equations in the original configuration as well as in the final configuration obtained after applying the shape optimization processes. The original elements dealing with this part of the work are the use of small perturbation techniques in fluid mechanics combined with optimal flow control, the use of reference domain formulation to avoid mesh reconstruction at each iteration, the setting of a shape optimization problem as an optimal control problem on coefficients, representing coordinates transformations. This approach has been used both for steady and unsteady flows.

1.2.2 Reduced basis methods for pre-process and real time optimization

Especially in the field of optimization or design, where the evaluation of many different possible configurations is required – corresponding to different choices of the design parameters – even for modest-complexity problems, the computational cost is unacceptably high. To more efficiently utilize the existing computational resources, reliable methods that reduce the complexity of the problem while at the same time preserve all relevant information, are becoming very important.

Input-Output relationship

Central to every design, optimization, or control problem is the evaluation of an "input-output" relationship. The set of input parameters μ, which we will collectively denote as "inputs," identify a particular configuration of the system or of one of its components. These inputs may represent design or decision variables, such as geometry or physical properties – for example, control variables in optimization studies; or characterization variables, such as physical properties, in inverse problems. The output parameters $s(\mu)$, which we will collectively denote as "outputs", are performance indexes for the particular input μ – for example stresses, velocity, flow rates. These outputs are typically expressed as functionals of field variables associated with a set of parametrized partial differential equations which describe the physical behavior of the system or its components. Then we are interested in calculating the outputs $s(\mu) = \mathcal{F}(\mu)$, for many different inputs/configurations μ chosen from a parameter space $\mathcal{D} \subset \mathbb{R}^P$, where P is the number of input parameters. Here, $\mathcal{F}$ encompasses the mathematical description of the physical problem at different levels of complexity.
For the evaluation of $\mathcal{F}$ the underlying equations have to be solved. Usually, an analytical solution is not easy to obtain, rather a discretization procedure like the finite-element method, is used; then $\mathcal{F}$ is replaced by $\mathcal{F}_h$, a discrete form amenable to numerical solution. The

basic premise, is that as the discretization "length" $h \to 0$, then $\mathcal{F}_h \to \mathcal{F}$, and consequently $s_h(\mu) \to s(\mu)$, $\forall \mu \in \mathcal{D}$ *but* as $h \to 0$ the cost of evaluating $\mathcal{F}_h$ becomes prohibitive. Especially in the context of design, control, or parameter identification where "real-time" response or many "input-output" evaluations are required, a balance between computational cost and accuracy/certainty is essential.

Computational method

Identifying the problem in the high dimensionality of the discrete problems, model-order reduction techniques have been developed. The critical observation is that instead of using projection spaces with general approximation properties — like in finite element method— we choose problem-specific approximation spaces and use these for the discretization of the original problem. Using such spaces, we can construct a model that represents with sufficient accuracy the physical problem of interest using a significantly smaller number of degrees of freedom. Depending on the choice of the global approximation spaces many possible reductions are available.
The computational methods developed in this work permit *rapid* and *reliable* evaluation of this input-output relationship induced by partial differential equations *in the limit of many queries* — that is, in the design, optimization, control, and characterization contexts. In designing new methods, certain qualities must be considered:

- *Efficiency* is crucial for the problems in consideration. To achieve efficiency, we shall use the reduced-basis method; a weighted-residual Galerkin-type method, where the solution is projected onto low-dimensional spaces with certain problem-specific approximation properties.

- *Relevance.* Usually in a design or optimization procedure we are not interested in the field solution, but rather in certain design measures such as the drag coefficient in the case of flow past a bluff body, or the average temperature on a surface in the case of heat conduction. The methods developed as part of this work give accurate approximations to these outputs of interest, defined as functional outputs of the field solution.

- *Reliability.* To quantify the error introduced by the reduced-basis method, an error analysis must be invoked on outputs of interest.

In our field of interest, reduced basis approximation provides not only high computational savings, a rapid (real-time) and accurate methodological pre-process to detect the essential feature of the optimization process itself, but also the study of a geometrical sensitivity analysis of a complete bypass configuration. By selecting a limited number of relevant geometrical parameters (bypass diameter t, artery diameter D, stenosis length S, graft angle θ, bypass bridge height H, see Figure 1.5) and a moderate number (N) of sample parameters

$$\boldsymbol{\mu}_k = \{t_k, D_k, S_k, \theta_k, H_k\},\ k = 1, \ldots, N,$$

we solve the parametrized equations that govern the physical problem in a reference domain Ω, properly mapped by coordinate transformations [135]. Then we build properly reduced

basis functional approximation spaces for velocity and pressure to guarantee approximation and algebraic stability. For a new sample $\boldsymbol{\mu}_k$ we look for a new solution which is given by a weighted combination of previously computed and stored solutions. Weights are given by the solution of a state problem on the subspace of the reduced basis by a Galerkin projection (see [111]). In this thesis reduced basis methods have been applied especially to Stokes and Navier Stokes problem. A more pedagogical introduction to elliptic operators is presented in the **Appendix A** in order to set up the ground for an unfamiliar reader for a better understanding when addressing the Stokes and Navier-Stokes problem, while advection-diffusion operators are considered in the conclusive part dealing with perspectives and developments. The most original contribution are concerned with the pressure treatment in Stokes and Navier-Stokes problem, the introduction of geometrical parametrization of domain by affine and non-affine maps, the study of different options to guarantee approximation stability of reduced basis approximation and, finally, basis orthonormalization to achieve algebraic stability for reduced basis. This methodological development highlights the great potential of reduced basis methods in optimal flow control and shape optimization, not only for pre-process optimization. Reduced basis can be seen as methods to solve in real-time complex problem with great computational savings without loosing accuracy and fast convergence.

1.2.3 Thesis outline

The thesis is organized as follows. **Part I** deals with optimal flow control and local shape optimization.
In **Chapter 2** we deal with local shape optimization by optimal control (briefly recalled) using local boundary variations and Stokes equations. Design quantities of interest are introduced and motivated. A simplified bypass model is considered. Preliminary feedback procedures are described. In this chapter we introduce also methodological algorithms to solve our problem.
In **Chapter 3** we deal with small perturbation techniques in fluid mechanics. The linearized shape design problem is described using an optimal control approach in a reference domain using Stokes equations. Theoretical results on well-posedness of the problem, existence and uniquiness of solution are discussed.
In **Chapter 4** we extend our work considering unsteady Stokes equations and introducing a generalization of our approach. Numerical results are presented in each chapter.

Part II is devoted to reduced basis techniques for optimization problems. In **Chapter 5** we introduce the reduced basis problem for Stokes equations where we focus our attention on geometrical parametrization using Cartesian geometries, and proof of stability. Preliminary results on sensitivity analysis of bypass configuration are described. Different outputs are considered and the dual residual weighted approach is introduced to improve the accuracy of the output calculation.
In **Chapter 6** we deal with a more complex problem introducing non-affine coordinate transformations and curved geometries.
In **Chapter 7** reduced basis methods are discussed for steady Navier-Stokes equations. Other

feedback results are introduced considering bypass configurations. This chapter concludes the study of the bypass optimization and provides a comparison between low fidelity models, based on Stokes equations, and high fidelity models based on Navier-Stokes equations.
In **Chapter 8** several further aspects are considered, such as the possibility to use reduced basis for an optimal control problem (the example deals with advection-diffusion operators), combined also with shape sensitivity. Finally a reduced basis methodology for an unsteady version of the problem is suggested. This chapter provides some perspectives towards the solution of solving parametrized optimal control problems and some conclusions.

Appendix A provides an introduction on reduced basis techniques to explain the methodology and all its aspects dealing with elliptic operators. In this appendix is shown also how to build a parametrized geometrical configuration.

To summarize, the first part of this thesis is focused on shape optimization techniques for local configurations: local boundary variations, small perturbation techniques led by optimal flow control. The second part of the dissertation deals with the optimization of global configurations and is led by the development of reduced basis techniques in parametrized domain with an approach based on a "step-by-step" increasing complexity. The "glue" between the two parts is represented from one side by the kind of application that is considered and, from the other side, by the methodological aspects that are developed. To help the reader following the logical flow of the work, in Figure 1.7 we present the general organization of the thesis with theoretical, methodological and conceptual links highlighted. More interpretation paths can be outlined. For example, in Figure 1.8 we provide the same scheme focusing on the application point of view.

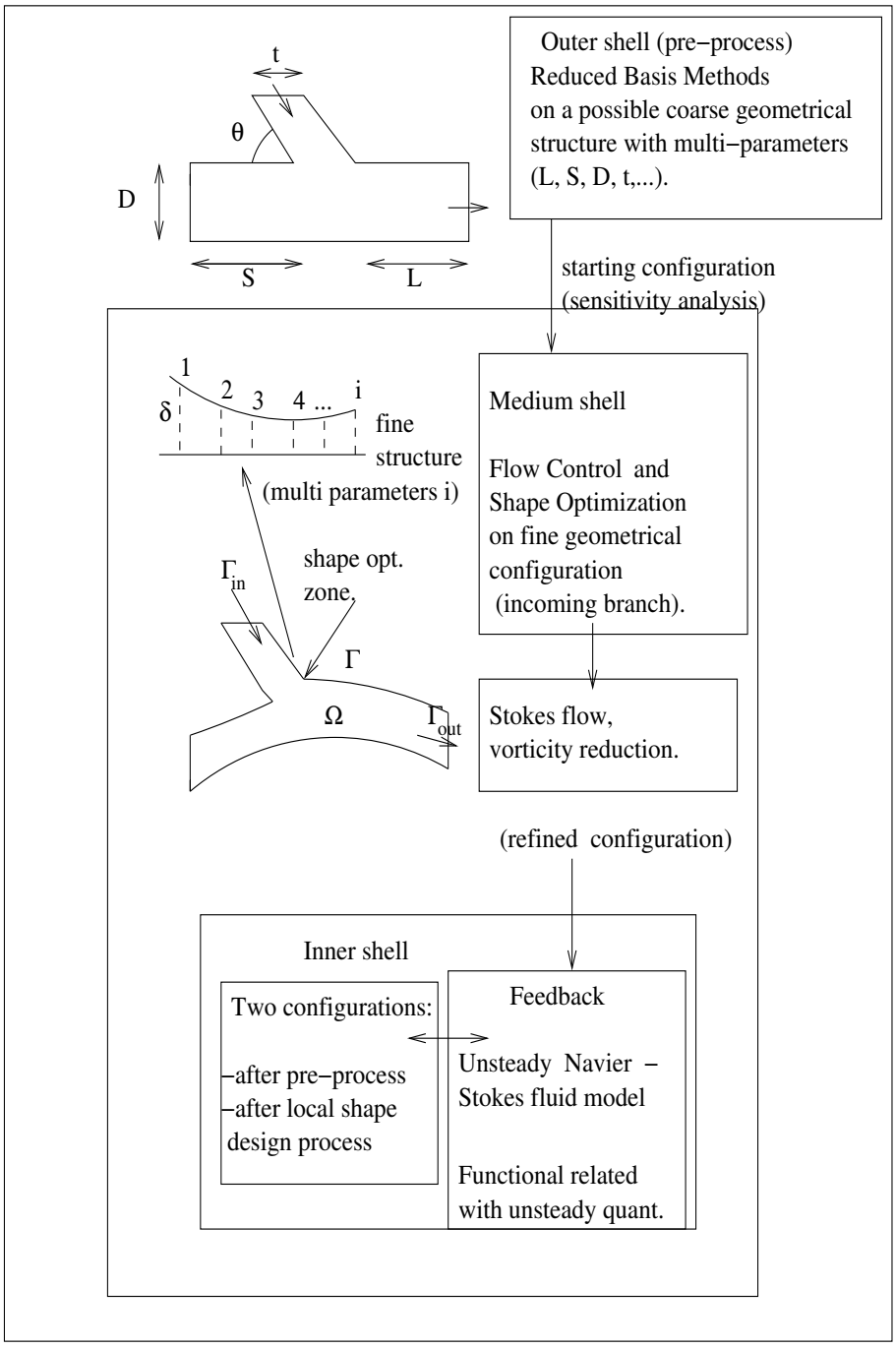

Figure 1.6: A double level of interest: local shape optimization and complete configuration.

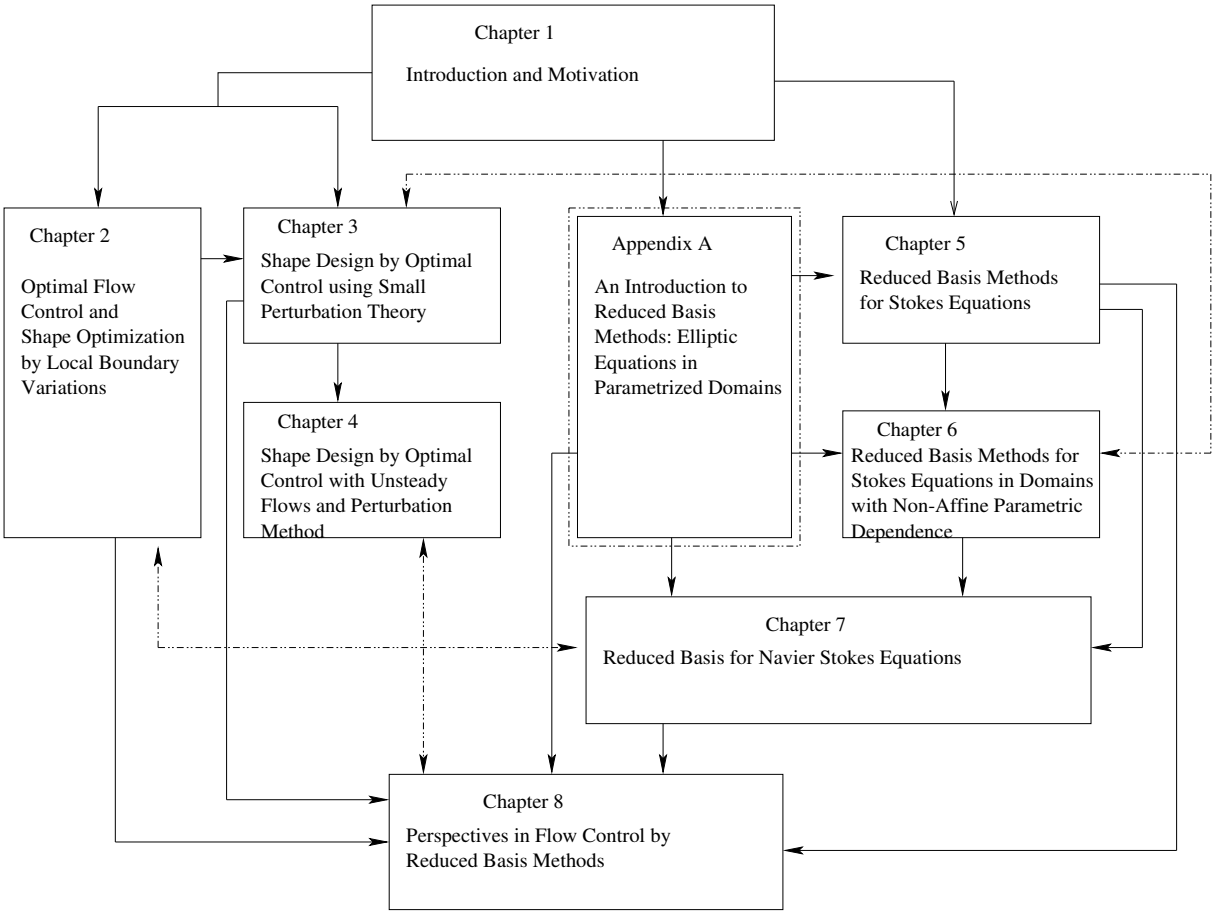

Figure 1.7: Thesis organization: theoretical and conceptual links.

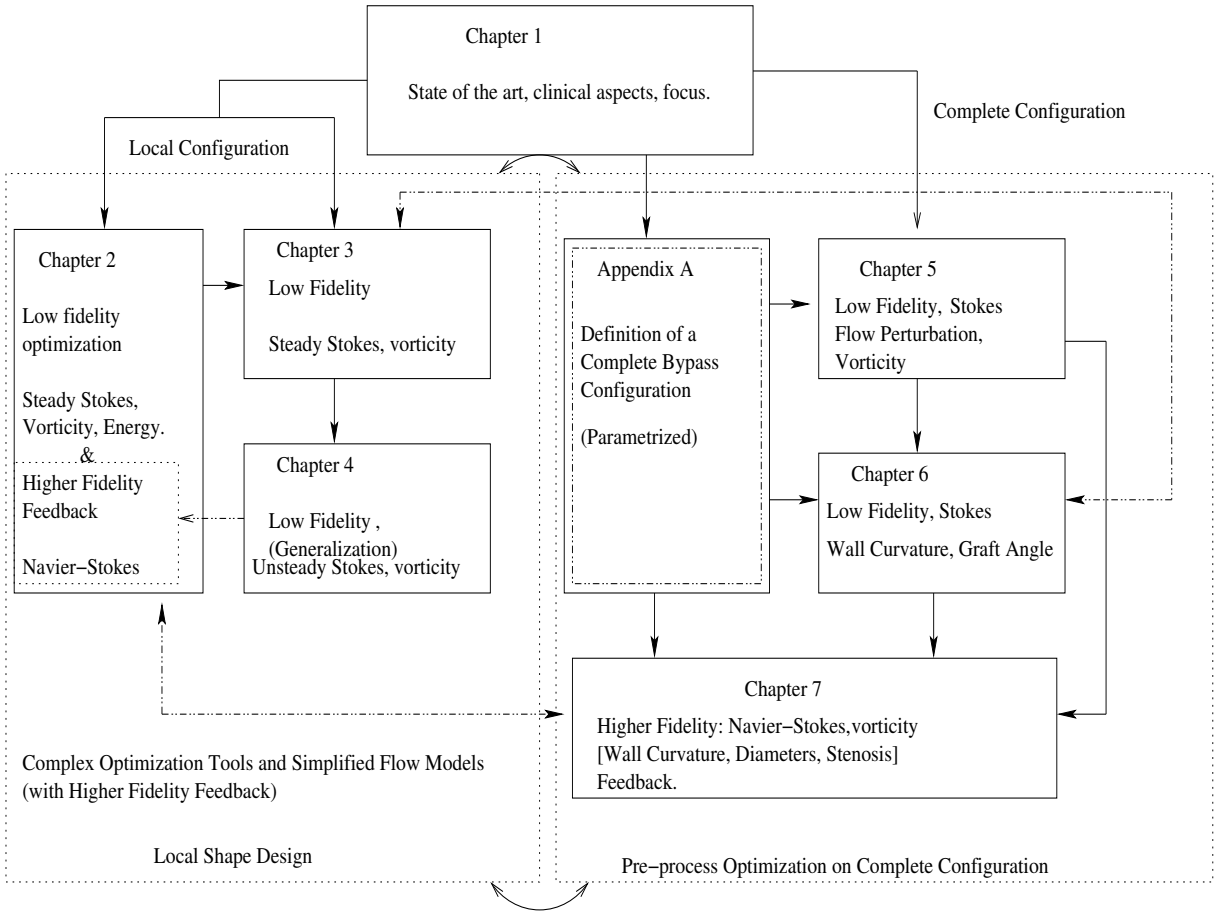

Figure 1.8: Thesis organization: application to bypass optimization.

Part I

Optimal Flow Control and Shape Optimization

Chapter 2

Optimal Control and Shape Optimization by Local Boundary Variations

In this chapter we present the first approach in the study of Aorto-Coronaric bypass anastomoses. The theory of optimal control based on adjoint formulation is introduced and applied in order to optimize the shape of the zone of the incoming branch of the bypass (the toe) into the coronary using a local boundary variations method led by the gradient of a cost functional. The aim is to provide design indications in the perspective of future development for prosthetic bypasses. With a reduced model based on Stokes equations and a vorticity functional in the down-field zone of bypass, a Taylor like patch is found. A feedback procedure by Navier-Stokes fluid model based on the analysis of wall shear stress and its related indexes is proposed.
The chapter is organized as follows: firstly we make some remarks on optimal control theory, then we turn our attention to design quantities of interest for the specific bypass configuration problem and we set up a geometrical framework to analyze our problem. Then we describe a first shape optimization algorithm and provide several numerical results. For a general introduction on the bypass anastomoses problem we suggest to see Perktold et al. [80].

2.1 A control approach: looking for cost functional optimization

In this section we briefly review the optimal control theory. This will provide the ground for the set up of our shape optimization algorithms. For a general presentation of the optimal control theory the interested reader can refer to Lions [82], [83] and Aziz *et al.* [9]. For functional analysis elements see Yosida [167], Brezzi and Gilardi [20].
In the optimal control problems the following mathematical ingredients will set the stage:

- A *control function* u which belongs to a functional space $\mathcal{U}_{adm} \subset \mathcal{U}$, called *admissible control space*.

- A *state system* $y(u)$ associated to the control u, y belongs to the *Hilbert* space $\mathcal{V}$ and is the solution of a PDE problem defined on the domain Ω:

$$Ay(u) = f + Bu, \tag{2.1.1}$$

  where f is a given function (source term), while A is an operator defined on $\mathcal{V}$ with values in $\mathcal{V}'$ and B is a linear operator defined on $\mathcal{U}$ and valued in $\mathcal{V}'$, respectively. The latter equation is called *state equation* and represents the physical system to control and optimize. Note that $u \to y(u)$ is an affine map.

- An *observation function* $z(u)$ belonging to a suitable space $\mathcal{Z}$ which is related to $y(u)$ through an operator $\mathcal{C}$, $z(u) = \mathcal{C}y(u)$. Our observation will coincide with the restriction of $z(u)$ upon a convenient subset of the computational domain Ω, so in our case $\mathcal{C}$ is indeed a restriction operator.

- A *cost functional* $J(u)$ (to be minimized) which is a non-negative quantity depending on the observation $z(u)$.

The general formulation of an *optimal control problem* reads:

- *Find a function* $u \in \mathcal{U}_{adm}$ so that:

$$J(u) = \inf\{J(v), \quad \forall v \in \mathcal{U}_{adm}\}. \tag{2.1.2}$$

Note that the formulation (2.1.1) covers the case where the control variable is either a boundary condition or a source term. Optimal shape design can be regarded as a special case of control theory where the control is the boundary itself. More precisely, $u \to \Omega(u) \to y(u)$, where $u \to \Omega(u)$ is the parametrization of the domain by a control parameter u and the problem is to minimize a functional $J(u, y(u))$, which depends on u through $y(u)$, but also directly (for instance J is an integral of a quantity depending on $y(u)$ extended to a region depending on u). See Mohammadi and Pironneau [97]. In our problem the control will be a subset of the domain boundary $\Gamma(u)$.
In the following section we will construct some cost functionals of our interest.

2.2 Design control quantities

As already seen in the previous section, cost functionals are related with the observation of physical quantities in the system.
Our interest is for the use of optimal control strategies in the context of improving and optimizing the shape of aorto-coronaric bypasses (see Figure 1.1). In the literature several physical quantities (often called "indexes") have been proposed in order to asses and measure, at some extent, arteries occlusion risk (or re-occlusion after bypass surgery). These indexes have been introduced in order to enlight some specific mechanism that could be correlated to the narrowing of coronaries (phenomena called intimal thickening). A first index stems from

the observation that a crucial role is played by blood flow oscillations during the diastolic phase of every single heart beat. Another index attemps at measuring the rapid variations of the shear stress (2.2.2) on the vascular wall. In any case these and other indexes (that we are going to review briefly) could be considered as a starting point on the way to synthesize the enormous amount of information given by numerical simulation for the bypass design and they can be used to build cost functionals of interest for our problem.
The *Oscillatory Shear Index* (OSI) was introduced in 1983 by Zarins and Giddens [168] to identify the occlusion risk zones. It is defined as follows:

$$OSI = \frac{1}{2}\left(1 - \frac{\int_0^T \tau_w dt}{\int_0^T |\tau_w| dt}\right), \tag{2.2.1}$$

where $[0, T)$ is the time interval of a single heart beat ($T \simeq 1$ sec) and τ_w is the *wall shear stress*, indicated with WSS and defined for a Newtonian fluid as:

$$\tau_w = \mu \frac{\partial \mathbf{u}}{\partial \hat{\mathbf{n}}} \cdot \hat{\mathbf{t}}, \tag{2.2.2}$$

where $\mathbf{u}$ is the blood velocity field, μ is the blood viscosity, $\hat{\mathbf{n}}$ and $\hat{\mathbf{t}}$ are, respectively, normal and tangential unit vector on the arterial wall. OSI measures the temporal oscillations of the shear stress *pointwise*, without taking into account the shear stress trend in the immediate neighborhood of a specific (critical) point.
Another indicator of occlusion risk zones is the *Mean Wall Shear Stress Gradient (MWSSG)* (see Veneziani [156] and Wells *et al.* [164]) defined as:

$$MWSSG = \frac{1}{T}\int_0^T |WSSG| dt, \tag{2.2.3}$$

where the *Wall Shear Stress Gradient* (WSSG) is defined as:

$$WSSG = \frac{\partial \tau_w}{\partial \hat{\mathbf{t}}} = \nabla \tau_w \cdot \hat{\mathbf{t}}. \tag{2.2.4}$$

According to MWSSG, the zones featuring occlusion risk or abnormal flow pattern are those where strong variations in the shear stress along the wall occur. This index is dual to OSI, since it weighs spatial variations.
An alternative to OSI is the *Oscillatory Flow Index* (OFI), see Taylor *et al.* [149]:

$$OFI = \frac{1}{2}\left(1 - \frac{\int_0^T Q dt}{\int_0^T |Q| dt}\right), \tag{2.2.5}$$

where Q is the *flow rate* across an artery section Γ_f,

$$Q = \int_{\Gamma_f} \rho \mathbf{u} \cdot \hat{\mathbf{n}} d\Gamma, \tag{2.2.6}$$

being ρ the blood density. It quantifies temporal oscillations in flow rate.
A problem arising when using one of the previous functionals for optimization purposes is

that they don't have a quadratic form. We can use these quantities for feed-back processes, but we need functionals which can provide a good average in time and in space of shear stress trend. With this aim, we propose other integral quantities that can be defined along the artery wall Γ_w (or a critical part of it). Set for all $t > 0$:

$$\Sigma(t) = \int_{\Gamma_w} \Big(\frac{\partial \tau_w(t)}{\partial t}\Big)^2 d\Gamma, \tag{2.2.7}$$

and

$$\mathcal{Q}(t) = \int_{\Gamma_w} \Big(\frac{\partial Q(t)}{\partial t}\Big)^2 d\Gamma. \tag{2.2.8}$$

Then we define:

$$J_\tau = mean_{[0,T]}\Sigma(t) = \frac{1}{T}\int_0^T \Sigma(t)dt = \frac{1}{T}\int_0^T \int_{\Gamma_w} \Big(\frac{\partial}{\partial t}\tau_w(t)\Big)^2 d\Gamma dt, \tag{2.2.9}$$

which is the $L^2 - norm$ of the wall shear stress rate ($L^2 - WSSR$). Similarly, we define the analogous $L^2 - norm$ of the flow rate Q ($L^2 - FR$):

$$J_Q = mean_{[0,T]}\mathcal{Q}(t) = \frac{1}{T}\int_0^T \mathcal{Q}(t)dt = \frac{1}{T}\int_0^T \int_{\Gamma_f} \Big(\frac{\partial}{\partial t}Q\Big)^2 d\Gamma dt. \tag{2.2.10}$$

These new indexes J_τ and J_Q could be seen as a lumped and complete information from the previous cost functionals because they take into account both of spacial and temporal oscillation of fluid mechanics quantities.
In the perspective of using low fidelity methods for control process (to reduce computational time and costs) and then higher fidelity methods in feedback we are going also to measure other fluid mechanics quantities such as vorticity and energy dissipation (due to viscous terms) in distributed zone of flow field (and not pointwise quantities), above all when using steady fluid models. These indexes (vorticity, viscous energy dissipation) contain many information on flow properties and their links with geometry variation.

2.3 Mathematical modelling of the problem.

Blood is a very complex fluid which interacts with the compliant arterial vessels. Some simplificatory assumptions are in order in view of applying a control procedure. Concerning the fluid model we consider blood as a *Newtonian fluid*, modelled by Navier-Stokes equations (or even by the simplified Stokes model). This model is an acceptable approximation when studying blood flow in large or medium-size arteries. In coronary arteries blood is also characterized by a low velocity profile. The *Reynolds* number (the ratio between inertial and viscous forces) is rather low, so the flow can be regarded as *laminar*.

2.3.1 The geometrical model

To model the incoming branch of a bypass, different bypass anastomoses models have been taken into consideration. We have simplified our model by considering a longitudinal section

in the mean plane reducing it to a two-dimensional problem. As initial configuration we have used a fiberglass model developed at the Surgical Vascular Division of *Aahrus University Hospital* (Denmark). See Figure 2.1. To define anastomoses geometry for numerical simulation,

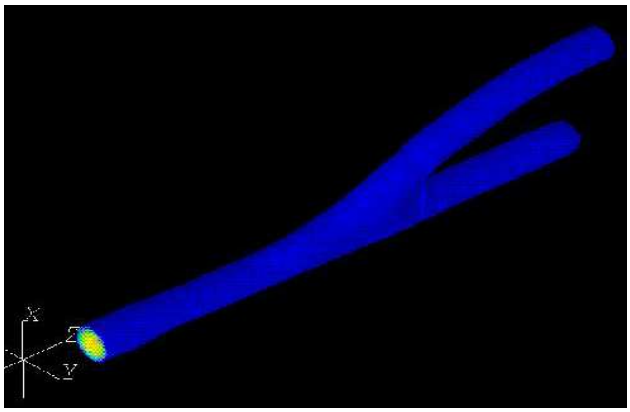

Figure 2.1: 3-D Anastomoses fiberglass model (Aahrus University Hospital, Denmark)

different aspects have to be accounted for:

- Fluid dynamics phenomena in the bypass are strictly related with the shape assumed, such as the presence of blood re-circulating zones, flow separation and vorticity. Blood pulsatility due to heart beat influences our analysis and this aspect will be considered in the next chapters. The most critical zone in the bypass design is the toe and must be carefully modelled. The toe, in fact, models the incoming branch of the bypass and influences the way in which the blood approaches in the host artery from the bypass bridge device. See Figure 2.2.
- Another important aspect to keep into consideration is the graft angle between the incoming branch and the occluded artery. This aspect will be discussed in details in the second part of this thesis.
- The diameter of the occluded branch (the lower branch) is $D = 3.5$ mm and the one taken in this first investigation for the bypass is $0.96 \cdot D$, as suggested in Quarteroni and Formaggia [126] and used in surgery procedures. This quantity will be studied more deeply in the second part of the thesis.

A curvature in the vascular wall is introduced to model coronary arteries in order to take into consideration the presence of the heart muscle. Figure 2.2 shows the mean plane before applying the shape optimization process. These simple considerations already underline the importance of the study of a complete parametrized bypass configuration taking into account graft angle, curvature and other quantities to define the complete device scheme.

2.3.2 The state problem: Navier-Stokes and Stokes equations

In our optimal control process we use as state equations the steady Stokes equations which are however well suited for modelling Newtonian flows at low Reynolds number. In reality, because

of flow pulsatility we should consider the unsteady Navier-Stokes equations. Unfortunately, such as a complete fluid model would be too complex and expensive to control because of evolution terms, non linearity in the adjoint problem and the fact that the shape of our computational domain depends on time. Nonetheless, after performing shape optimization on our reduced model governed by steady Stokes equations, we will turn our attention to the complete Navier-Stokes model for feed-back procedures considering design cost functionals such as the ones presented in Section 2.2. We focus therefore on the steady Stokes problem. The Stokes equations in a two-dimensional computational domain Ω with velocity vector $\mathbf{u} = (u, v)^T$ and pressure p (which is divided by the constant blood density ρ) read:

$$\begin{cases} -\nu\Delta\mathbf{u} + \nabla p = \mathbf{f} \quad in\ \Omega \subset \mathbb{R}^2, \\ \nabla \cdot \mathbf{u} = 0 \quad in\ \Omega, \\ \mathbf{u} = \mathbf{0}\ on\ \Gamma_w, \\ \mathbf{u} \cdot \hat{\mathbf{t}} = 0,\ \mathbf{u} \cdot \hat{\mathbf{n}} = g_{in}\ on\ \Gamma_{in}, \\ \nu \frac{\partial \mathbf{u}}{\partial \hat{\mathbf{n}}} - p\hat{\mathbf{n}} = \mathbf{0}\ on\ \Gamma_{out}, \end{cases} \tag{2.3.1}$$

where $\mathbf{f}$ is a force field (for example gravity $\mathbf{f} = (0, 9.8)^T ms^{-2}$), $\hat{\mathbf{n}}$ and $\hat{\mathbf{t}}$ are, respectively, normal and tangential unit vector on the domain boundary $\partial\Omega$. The latter is partitioned in three components: Γ_{in} is the inflow boundary, Γ_{out} the outflow boundary and Γ_w the boundary corresponding to the arterial wall; Figure 2.2 represents schematically the computational geometry and the symbols used.

Concerning boundary conditions, no-slip conditions are imposed on all vascular walls of Γ_w,

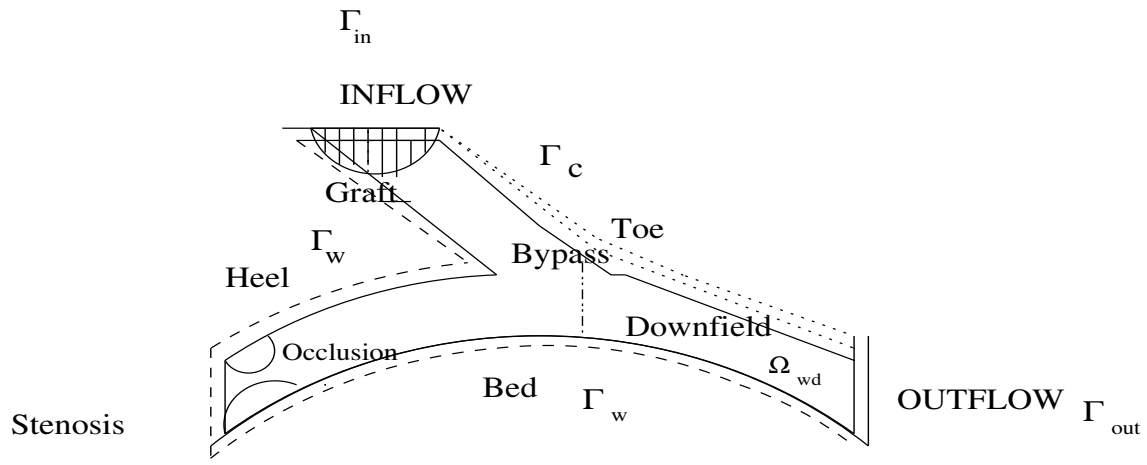

Figure 2.2: Anastomosis schematic model and symbolic notation used for domain and boundaries, with down-field observation zone Ω_{wd}.

over the stenosed artery portion (if we consider a complete occlusion, otherwise we have to consider this section in the same way of the inflow section but with a reduction of flow rate) and on the incoming branch of bypass. At inflow section Γ_{in}, a Hagen-Poiseuille's velocity profile g_{in} is imposed, while on outflow section Γ_{out} of the artery a free-stress, Neumann-type, boundary condition has been imposed. Velocity values at the inflow are chosen in such a

way that the Reynolds number $Re = \frac{\bar{u}D}{\nu}$ has order 10^3. Blood kinematic viscosity $\nu = \frac{\mu}{\rho}$ is $4 \cdot 10^{-6}\ m^2\ s^{-1}$, blood density $\rho = 1\ g\ cm^{-3}$ and dynamic viscosity $\mu = 4 \cdot 10^{-2}\ g\ cm^{-1}s^{-1}$; $\bar{u}$ is a mean inflow velocity (in absolute value) related with g_{in}, while D is the arterial diameter (3.5 mm). Arterial thickness is about 0.5 mm [126].

The role of control

In our problem the control w represents the shape Γ_w itself or a part Γ_c of it (typically the incoming branch). Precisely, we write (see Figure 2.2):

$$\Gamma_w = \Gamma_{w(rigid)} \cup \Gamma_{c(toe)}, \tag{2.3.2}$$

where

$$\Gamma_{w(rigid)} = \Gamma_{w(bed)} \cup \Gamma_{w(heel)} \cup \Gamma_{w(graft)} \cup \Gamma_{w(stenosis)}, \tag{2.3.3}$$

then we can build our geometrical model for Γ_c (double-dotted in Figure 2.2) made up of M branches $\Gamma_c^j(w)$ represented by:

$$\Gamma_c = \bigcup_{j=0}^{M} \Gamma_c^j(w),\ \Gamma_c^j(w) = \overline{\Gamma_c^j} + w^j, \tag{2.3.4}$$

where w^j is the control variable (control shape function) which changes by δw_k^j at each iteration of the optimization process. At the $k-th$ iteration we have:

$$w_k^j = \sum_{m=0}^{k-1} (\delta w_m^j), \tag{2.3.5}$$

its expression will be derived in Section 2.5. Further, we take the curves (of order up to N)

$$\overline{\Gamma_c^j}(s) = \sum_{i=0}^{N} \alpha_i^j f_i^j(s), \tag{2.3.6}$$

which represent the initial shape, s is the horizontal abscissa that parametrizes the curve Γ_c, $f_i^j(s) = \sum_{k=0}^{i} a_k s^k$ are given shape polynomial functions of i^{th} order and α_i^j are suitable weights (clearly each branch describing the initial shape must be properly set to guarantee a boundary with sufficient regularity).

Weak formulation for the state problem

We introduce a weak formulation for the state problem (2.3.1), see [127]: find $\mathbf{u} \in V = (H^1(\Omega))^2$, $p \in Q = L^2(\Omega)$ s.t.

$$\begin{cases} a(\mathbf{u}, \mathbf{v}) + b(p, \mathbf{v}) = F(\mathbf{v})\ \forall \mathbf{v} \in \mathbb{X}, \\ b(q, \mathbf{u}) = 0\ \forall q \in L^2(\Omega), \\ \mathbf{u} = \mathbf{u}_{in}\ on\ \Gamma_{in}, \end{cases} \tag{2.3.7}$$

where

$$a(\mathbf{u},\mathbf{v}) = \int_\Omega \nu \nabla \mathbf{u} \cdot \nabla \mathbf{v} d\Omega,$$

$$b(p,\mathbf{v}) = -\int_\Omega p \nabla \cdot \mathbf{v} d\Omega,\ F(\mathbf{v}) = \int_\Omega \mathbf{f} \cdot \mathbf{v} d\Omega,$$

$$\mathbb{X} := \{\mathbf{v} : \mathbf{v} \in (H^1(\Omega))^2, \mathbf{v} = \mathbf{0}\ on\ \Gamma_{in} \cup \Gamma_w\},$$

and $\mathbf{u}_{in}$ is $g_{in}\hat{\mathbf{n}}$ *on* Γ_{in} and $\mathbf{0}$ *on* Γ_w. Note that the second equation in system (2.3.7) may be also written in the equivalent form: $-b(q,\mathbf{u}) = 0$; after numerical discretization, the latter formulation will lead to an algebraic system which is no longer symmetric but always positive definite ([127]). This alternative will be adopted to build the adjoint problem.

Galerkin approximation

The Galerkin approximation for the Stokes equations (2.3.7) is the following: find $\mathbf{u}_h \in V_h$, $p_h \in Q_h$ such that

$$\begin{cases} a(\mathbf{u}_h,\mathbf{v}_h) + b(p_h,\mathbf{v}_h) = (\mathbf{f},\mathbf{v}_h) - a(\mathbf{R}_h,\mathbf{v}_h) & \forall \mathbf{v}_h \in V_h, \\ -b(q_h,\mathbf{u}_h) = b(q_h,\mathbf{R}_h) & \forall q_h \in Q_h, \end{cases} \tag{2.3.8}$$

here $\mathbf{R}_h \in V_h$ and $\mathbf{R}_h|_{\Gamma_{in}} = \mathbf{u}_{in_h}$. The spaces $V_h \subset V$ and $Q_h \subset Q$ are two families of subspaces of finite dimension depending on the discretization parameter h. For the proof concerning the existence and uniqueness of solution of problem (2.3.8) and approximation stability aspects we suggest to see [127]. We denote

$$\{\boldsymbol{\varphi}_j \in V_h\}, \quad \{\phi_k \in Q_h\},$$

the basis functions for the spaces V_h and Q_h, respectively. We can develop $\mathbf{u}_h$ and p_h on their basis getting

$$\mathbf{u}_h(\mathbf{x}) = \textstyle\sum_{j=1}^{\mathcal{N}} U_j \boldsymbol{\varphi}_j(\mathbf{x}), \quad p_h(\mathbf{x}) = \sum_{k=1}^{\mathcal{M}} p_k \phi_k(\mathbf{x}), \tag{2.3.9}$$

where $\mathcal{N} = \dim(V_h)$, $\mathcal{M} = \dim(Q_h)$. We get the following linear system for the state problem:

$$\begin{cases} \mathrm{A}\mathbf{U} + \mathrm{B}^T\mathbf{P} = \mathbf{F}, \\ \mathrm{B}\mathbf{U} = \mathbf{0}, \end{cases} \tag{2.3.10}$$

where $\mathrm{A} \in \mathbb{R}^{\mathcal{N}\times\mathcal{N}}$ and $\mathrm{B} \in \mathbb{R}^{\mathcal{M}\times\mathcal{N}}$ are matrices related to bilinear forms $a(\cdot,\cdot)$ and $b(\cdot,\cdot)$, with elements given by

$$\mathrm{A} = (a_{ij}) = (a(\boldsymbol{\varphi}_j,\boldsymbol{\varphi}_i)),$$

$$\mathrm{B} = (b_{km}) = (b(\phi_k,\boldsymbol{\varphi}_m)),$$

while $\mathbf{U}$ and $\mathbf{P}$ are vectors of unknowns,

$$\mathbf{U} = (U_j), \quad \mathbf{P} = (p_j).$$

Remark on stabilization

We have based our approximation on Galerkin-Finite element method and we use, for example, piecewise linear elements for velocity (φ) and pressure ϕ. This choice of elements with the same polynomial degree has to be accompanied by a stabilization procedure. We use the SUPG stabilization (see, e.g., Quarteroni and Valli [127]). We introduce a relaxation on the incompressibility constraint: find $\mathbf{u}_h \in V_h$, $p_h \in Q_h$ such that:

$$\begin{cases} a(\mathbf{u}_h, \mathbf{v}_h) + b(\mathbf{v}_h, p_h) = (\mathbf{f}, \mathbf{v}_h) & \forall \mathbf{v}_h \in V_h, \\ b(\mathbf{u}_h, q_h) = \Phi_h(q_h) & \forall q_h \in Q_h, \end{cases} \tag{2.3.11}$$

where Φ_h has a linear dependence on the test function q_h, but can also depend on $\mathbf{u}_h, p_h, \mathbf{f}$ and h. An example of Φ_h in the case of linear finite elements $\mathbb{P}^1 - \mathbb{P}^1$ is:

$$\Phi_h(q_h) = \sum_{K \in \mathcal{T}_h} h_K^2 \int_K \nabla p_h \cdot \nabla q_h,$$

where $\mathcal{T}_h$ is the finite element triangulation whose elements are indicated with K.

2.3.3 The observation on the system

After having described the control strategy on the boundary and introduced the state problem (and its approximation) we have to choose a cost functional. We consider a distributed observation in the down-field zone of the incoming branch of the bypass indicated as Ω_{wd} (see Figure 2.2). For this preliminary study our observation will be the vorticity $\omega = \nabla \times \mathbf{u} = \frac{\partial v}{\partial x} - \frac{\partial u}{\partial y}$; $\mathbf{u}$ is the solution of the Stokes equations (2.3.1) and we control the system by minimizing the following functional:

$$J(w) = \frac{1}{2} \int_{\Omega_{wd}} | \nabla \times \mathbf{u} |^2 \, d\Omega + \alpha \|w\|^2, \quad (0 < \alpha \ll 1). \tag{2.3.12}$$

where the last term provides the minimum shape deformation and guarantees existence of the solution. The symbol $\|.\|$ denotes the norm of $L^2(\Omega_{wd})$. By this observation we can draw information on the vorticity distribution. The curl of the vorticity will provide a source term of the adjoint problem, whose solution represents the sensitivity of the cost functional to the observation (related with state solution) and will be used during our optimization procedure to get the gradient of the cost functional allowing computational savings. For further aspects on vorticity reduction problems see Berggren [17].

We underline that we consider not only what happens on the vascular wall (i.e. on part of the domain boundary) but also in the fluid domain. For this reason this investigation is also a flow control problem and not only a shape optimization problem, because an optimal shape design problem is usually based only on the boundary observation. In this approach we have also taken into consideration another important aspect, concerning wall stiffness and elasticity. In fact we can rewrite the cost functional of interest into a different form, replacing the term $\alpha\|w\|^2$ of (2.3.12) with the following one including the minimization of the wall

deformation (which will depend on mechanical properties of the wall), in the zone where the bypass merges with the artery:

$$J(w) = \frac{1}{2}\int_{\Omega_{wd}} |\nabla \times \mathbf{u}|^2 \, d\Omega + \frac{E_0}{\xi}\sum_j \Big(\int_{\Gamma_c^j(w)} d\Gamma - \widetilde{l}_j\Big)^2. \tag{2.3.13}$$

Here $\widetilde{l}_j$ is the original length of the vascular wall $\overline{\Gamma}_c^j(w)$, ξ is a suitable weight, while E_0 is Young's elasticity modulus ($3\cdot 10^6$ *dyne* cm^{-2}). We are thus considering a *multi-objective optimization* of a prosthetic device. The last term in (2.3.13) describes the elastic wall behavior and provides a measure for elastic energy and wall deformation. The two quantities on the right end side of (2.3.13) have to be weighed by the choice of ξ.
The choice of a vorticity based functional to extract information can be better understood looking at Figures 2.3 and 2.4 where vortices structures in the downfield zone of a bypass are shown.

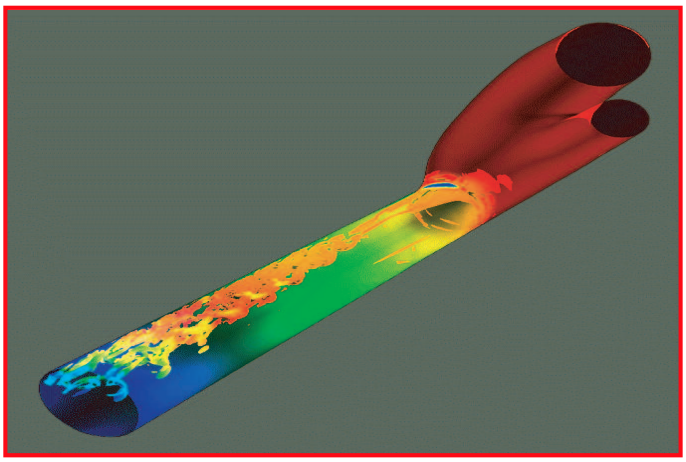

Figure 2.3: Vorticity in the down-field zone of a bypass (from a numerical simulation carried out by Fischer, Lee, Loth; University of Illinois and Argonne National Laboratories by permission).

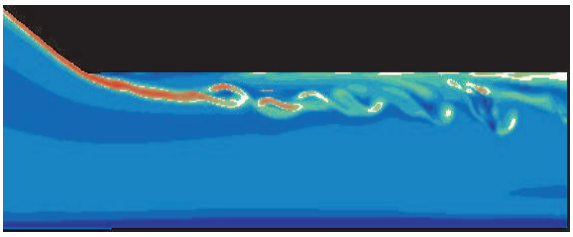

Figure 2.4: Vorticity in the downfield zone of a bypass: 2D details at the incoming branch (from a numerical simulation carried out by Fischer, Lee, Loth; University of Illinois and Argonne National Laboratories by permission).

2.3.4 The adjoint problem

As already mentioned, during the optimization process we must solve another PDE problem, the so-called adjoint problem. Considering the cost-functional (2.3.12), the state problem (2.3.7) and replacing test functions $\mathbf{v}$ and q with $\mathbf{p}$ and σ, respectively, the associate Lagrangian reads:

$$\mathcal{L}(\mathbf{u}, p; \mathbf{p}, \sigma; w) = J(w) - a(\mathbf{u}, \mathbf{p}) - b(p, \mathbf{p}) + (\mathbf{f}, \mathbf{p}) + b(\sigma, \mathbf{u}), \tag{2.3.14}$$

whose derivative with respect to $(\mathbf{u}, p)$ imposed equal to zero gives us the adjoint problem (see Gunzburger [50]):

$$\mathcal{L}_{\mathbf{u},p}(\mathbf{u}, p; \mathbf{p}, \sigma; w)[\boldsymbol{\delta}\mathbf{u}, \delta p] = -\int_\Omega \nu \nabla \boldsymbol{\delta}\mathbf{u} \cdot \nabla \mathbf{p} d\Omega + \int_\Omega \delta p \nabla \cdot \mathbf{p} d\Omega - \int_\Omega \sigma \nabla \cdot \boldsymbol{\delta}\mathbf{u} d\Omega +$$
$$+ \int_{\Omega_{wd}} (\nabla \times \mathbf{u}) \cdot (\nabla \times \boldsymbol{\delta}\mathbf{u}) d\Omega = 0, \ \forall [\boldsymbol{\delta}\mathbf{u}, \delta p],$$

which,using the notation already introduced for the state problem, can be written in the weak form as: find $\mathbf{p} \in \mathbb{X}$, $\sigma \in L^2(\Omega)$ s.t.

$$\begin{cases} a(\mathbf{p}, \mathbf{q}) - b(\sigma, \mathbf{q}) = H(\mathbf{q}) \ \forall \mathbf{q} \in \mathbb{X}, \\ b(\hat{\sigma}, \mathbf{p}) = 0 \ \forall \hat{\sigma} \in L^2(\Omega), \end{cases} \tag{2.3.15}$$

where $\mathbf{p}$ and σ denote the adjoint velocity and pressure, respectively. We have replaced the test functions $\boldsymbol{\delta}\mathbf{u}$ and δp with $\mathbf{q}$ and $\hat{\sigma}$ respectively, while the observation term is

$$H(\mathbf{q}) = \int_{\Omega_{wd}} (\nabla \times \mathbf{u}) \cdot (\nabla \times \mathbf{q}) d\Omega =$$

$$= \int_{\Omega_{wd}} \mathbf{q} \cdot (\nabla \times \nabla \times \mathbf{u}) d\Omega + \int_{\Gamma_{wd}} \hat{\mathbf{n}} \cdot (\mathbf{q} \times \nabla \times \mathbf{u}) d\Gamma,$$

using in the last step *Green's identities*. This term is related with an internal source defined in the down-field zone and its boundary, see for details Berggren [17] where a similar problem is studied. A no-slip condition is imposed on the vascular wall $\Gamma_w(w)$ and also on Γ_{in}, while a "free-stress" condition $\nu \frac{\partial \mathbf{p}}{\partial \hat{\mathbf{n}}} + \sigma \hat{\mathbf{n}} = \mathbf{0}$ is imposed on Γ_{out}.
The discretization of this problem is carried out using the Galerkin-Finite Element method as introduced for the state problem (2.3.8): find $\mathbf{p}_h \in V_h$, $\sigma_h \in Q_h$ such that

$$\begin{cases} a(\mathbf{p}_h, \mathbf{q}_h) - b(\sigma_h, \mathbf{q}_h) = H(\mathbf{q}_h) & \forall \mathbf{q}_h \in V_h, \\ b(\hat{\sigma}_h, \mathbf{p}_h) = 0 & \forall \hat{\sigma}_h \in Q_h, \end{cases} \tag{2.3.16}$$

An important role is played by the adjoint solution to get the quantity $J'(w)$, which is used to provide indications on the shape modification of Γ_w^j. In fact, $J'(w) = G(\mathbf{p}, \mathbf{u}, w)$: a detailed analysis will follow in Section 2.5 after introducing some notions on optimization algorithm (Section 2.4).

We anticipate here, just to clarify, that at $k-th$ iteration of the optimization algorithm described in Section 2.4.3 we will have

$$\delta w_k^j = -\xi_j(s)\lambda_k^j J_k'(w_k^j), \tag{2.3.17}$$

where λ_k^j is a relaxation parameter for descent gradient-based method, called step-size (see Quarteroni, Sacco and Saleri [129]), while $\xi_j(s)$ is a weight for the shape variation, used to satisfy congruence geometrical conditions such as shape continuity and guarantee that the internal arterial diameter cannot go below a certain threshold.
The cost functional depends on k ($J_k(w_k)$) to underline that at each iteration the integral is computed in a zone of the domain $(\Omega_{wd})_k$ whose shape is changing at each iteration. During the shape optimization process we have two degrees of freedom available (x, y) in the mean plane of the bypass. We only consider a normal displacement with respect to the original boundaries (as done also by Gunzburger [50] and Mohammadi and Pironneau [97]). For this reason the weight parameter $\xi_j(s)$ is a function of linear abscissa only.

2.4 Optimization and control algorithm

Before the description of the algorithm for the solution of the discretized control problem (state and adjoint equations) introduced in Sections 2.3.2-2.3.4 we recall some elements dealing with cost functional optimization and geometrical topology to manage with shape variations.

2.4.1 Gradient method

Let $\mathcal{U}$ be a Hilbert space, $(.,.)$ its associated scalar product, and $w \in \mathcal{U} \to J(w) \in \mathbb{R}$ then $J'(w)$ is a linear operator from $\mathcal{U}$ to $\mathbb{R}$ such that

$$J(w+\delta w) = J(w) + J'(w)\delta w + o(\|\delta w\|_{\mathcal{U}})$$

At the basis of gradient methods is the Taylor expansion

$$J(w+\rho z) = J(w) + \rho(Grad_w J(w), z) + o(\rho\|z\|_{\mathcal{U}})\ \forall w, z \in \mathcal{U},\ \forall \rho \in \mathbb{R}, \tag{2.4.1}$$

where $Grad_w J(w)$ is the element of $\mathcal{U}$ defined by

$$(Grad_w J(w), z) = J_w'(w)z\ \forall z \in \mathcal{U},$$

given by *Riesz' Theorem*. By taking $z = -Grad_w J(w)$ in (2.4.1), with $0 < \rho \ll 1$ we find:

$$J(w+\rho z) - J(w) = -\rho\|Grad_w J(w)\|_{\mathcal{U}}^2 + o(\rho\|Grad_w J(w)\|_{\mathcal{U}}).$$

Hence if ρ is small enough the first term on the right-hand side will dominate the remainder and the sum will be negative:

$$\rho\|Grad_w J(w)\|_{\mathcal{U}}^2 > o(\rho\|Grad_w J(w)\|_{\mathcal{U}}) \Rightarrow J(w+\rho z) < J(w).$$

Thus the sequence defined by:

$$w_{n+1} = w_n - \rho Grad_w J(w_n), \quad n = 0, 1, 2, \ldots \tag{2.4.2}$$

makes the sequence of real numbers $J(w_n)$ monotonically decreasing. We have the following result:

Theorem 2.4.1 *(from Pironneau [70]). If J is continuously differentiable, bounded from below, and $+\infty$ at infinity, then all accumulation points w^* of w_n, generated by (2.4.2) satisfies*

$$Grad_w J(w^*) = 0$$

This is the so-called *optimality condition* of the first order of the problem. If J is convex then w^* is a minimum; if J is strictly convex the minimum is unique. By taking the best ρ in the descent direction $z_n = -Grad_w J(w_n)$,

$$\rho_n = argmin_\rho\{J(w_n + \rho z_n)\},$$

that is

$$J(w_n + \rho_n z_n) = min_\rho\{J(w_n + \rho z_n)\},$$

we obtain the so-called *method of steepest descent with optimal step size.* Indeed, thanks to the analysis in [116], it is enough to find ρ_n with the following property (Armijo rule) to guarantee convergence: find ρ such that for $0 < \alpha < \beta < 1$:

$$-\rho\beta\|z\|^2 < J(w_n + \rho z) - J(w_n) < -\rho\alpha\|z\|^2$$

to have $w_{n+1} = w_n + \rho z$. An approximate Armijo rule takes only one line of slope $\alpha\|z\|^2$ and first finds the largest ρ of the form $\rho = \rho_0 2^{\pm k}$ which gives a decrement for J below the line for ρ and above the line for 2ρ: choose $\rho_0 > 0, \alpha \in (0, 1)$ and find $\rho = \rho_0 2^{\pm k}$ where k is the smallest signed integer (k can be negative) such that

$$J(w_n + \rho z) - J(w_n) < -\rho\alpha\|z\|^2$$

and

$$-2\rho\alpha\|z\|^2 \leq J(w_n + 2\rho z) - J(w_n).$$

A good choice is $\rho_0 = 1$, $\alpha = \frac{1}{2}$.

2.4.2 Shape variation and control

In functional spaces, as in finite dimension, optimization methods require the gradient of the cost functional J and for this we need to define an underlying Hilbert structure for the parameter space, in our case the shapes (see Zolésio [144]). Two strategies can be pursued:

- All the admissible shapes are obtained by a mapping transformation from a reference domain $\tilde{\Omega} : \Omega = T(\tilde{\Omega})$. Then the parameter is $T : \mathbb{R}^d \to \mathbb{R}^d$. This approach will be used and illustrated in detail in the next two chapters.

- It is possible to guarantee the Hilbert structure (the existence of a scalar product) only for small variations of the shape $\partial\Omega$. Dealing with local shape variations δw defined about a reference boundary Γ we consider:

$$\Gamma'(w) = \{x + \delta w(x)\hat{\mathbf{n}}(x) : x \in \Gamma\},$$

where $\hat{\mathbf{n}}$ is the outer normal to Γ at x and Ω is the domain which is on the left side of the oriented boundary $\Gamma'(w)$. The Hilbert structure is placed on w, for instance $w \in H^m(\Gamma)$. Considering a small perturbation Σ' of $\Sigma \subset \Gamma$ given by $\delta w = -\lambda J'(w)$, using a gradient method, we have:

$$\Sigma' = \{x - \lambda J'(w)\hat{\mathbf{n}} : x \in \Sigma\}$$

where w is a function of $x \in \Sigma$, Σ is endowed with sufficient regularity, and λ is a positive number destined to tend to zero. We denote the "new" domain $\Omega' = \Omega(\Sigma')$. For any $f \in H^1(C)$, where C is a subset of $\Omega \cup \Omega'$ we have

$$\int_{\Omega'} f - \int_{\Omega} f = \int_{\Sigma} \delta w f + o(\lambda). \tag{2.4.3}$$

This strategy has been used in this chapter and illustrated in the following sections.

2.4.3 The iterative process

The generic step of an algorithm for the solution of the control problem described in Section 2.3 can be devised as follows. Note that the pedix h referring to discretized solution is omitted for simplicity of notation and the index k refers to iteration index.

- Solve the state problem (2.3.8) with velocity components u_k and v_k in the domain Ω_k with the moving boundary $\Gamma^j_{c_k}(w_{k-1})$ obtained from the previous iteration of the control cycle.
- Compute the vorticity $\nabla \times \mathbf{u}_k$ in the domain $(\Omega_{wd})_k$.
- Evaluate the cost functional (2.3.12) or (2.3.13).
- Solve the adjoint problems (2.3.16) for $\mathbf{p}_k$ and σ_k with source term H depending on $(\nabla \times \mathbf{u}_k)$.
- Use the stopping test on the quantity $J'_k(w_k)$ related with $\mathbf{u}_k$ and the adjoint state $(\mathbf{p_k}, \sigma_k)$:

$$\|J'_k(w_k)\|_{\mathcal{U}} \leq \ tol, \tag{2.4.4}$$

for a suitable tolerance tol.

- Estimate the shape variation δw^j_k ($\delta w^j_0 = 0$) on the boundary $\Gamma^j_{c_k}(w^j_k)$ by a descent gradient-type method (see Kawohl *et al.* [70]). Then using (2.4.2):

$$\delta w^j_k|_{\Gamma^j_{c_k}} = -\lambda^j_k J'_k(w^j_k) = -\tilde{\lambda}^j_k G_k(\mathbf{p_k}, \mathbf{u}_k, w_k) \tag{2.4.5}$$

with $0 < \lambda^j_k \ll 1$, which causes a vertical shape displacement δw^j_k in (2.3.4).

- Update the boundary shape:

$$\Gamma^j_{c_{k+1}}(w_k) \simeq \overline{\Gamma^j_c} + w^j_k + \delta w^j_k = \overline{\Gamma^j_c} + \sum_{m=0}^{k} (\delta w^j_m). \tag{2.4.6}$$

- Modify the boundary and re-construct or adapt the computational grid (see Section (2.4.4)).

Figure 2.5 shows a general scheme for a flow control and shape optimization problem (discretization aspects are understood in the scheme focused on optimization algorithm). For more on optimal shape design techniques by boundary variations and shape parameters see e.g. Di Césaré [33].

2.4.4 Mesh strategy

During the shape optimization process, introduced above, the mesh is subject to be modified by boundary variations. There are two different strategies for mesh treatment at every step:

- Mesh reconstruction. This process is computationally expensive, even if new elements can be added.
- Mesh stretching and elements adaptivity after boundary variations operated by small deformation. This approach is faster and cheaper than the previous one. Mesh is usually stretched only in the computational domain surrounding the boundary Γ_c subject to shape changes. This technique is better because, when applicable, it guarantees the continuity of the solution (for both state and adjoint problem) during the optimization process (at different iterations).

Our approach used both strategies: the mesh was completely re-built only after a certain number of iterations, when the elements lost some of their properties set to guarantee regularity, while at each step mesh was stretched by locally boundary variations and adapted. In this process regularity conditions were put on grid quality such as on the control of minimum angles or maximum side-lengths. See Hecht *et al.* [55] and [53]. To preserve regular meshes during shape deformation we may reduce the step-size of the gradient method (to limit shape deformation) or introduce some regularization procedures.

Smoother

To avoid boundary oscillations (and irregular shapes) and due to the fact that the gradient method produces shape variations δw_k which have necessarily less regularity than the original parametrization we can apply the following smoothing operator over the shape, defined in Ω_k, as proposed and demonstrated by Mohammadi and Pironneau [97]:

$$\begin{cases} (I - \epsilon\Delta)\delta w = \delta\tilde{w}, \\ \delta w = 0 \ on \ \Gamma_{in} \ \cup \ \Gamma_{out}, \\ \frac{\partial \delta w}{\partial \vec{\mathbf{n}}} = 0 \ on \ \Gamma_c, \\ \delta w = \delta\tilde{w} \ on \ \Gamma_w \backslash \Gamma_c \end{cases} \tag{2.4.7}$$

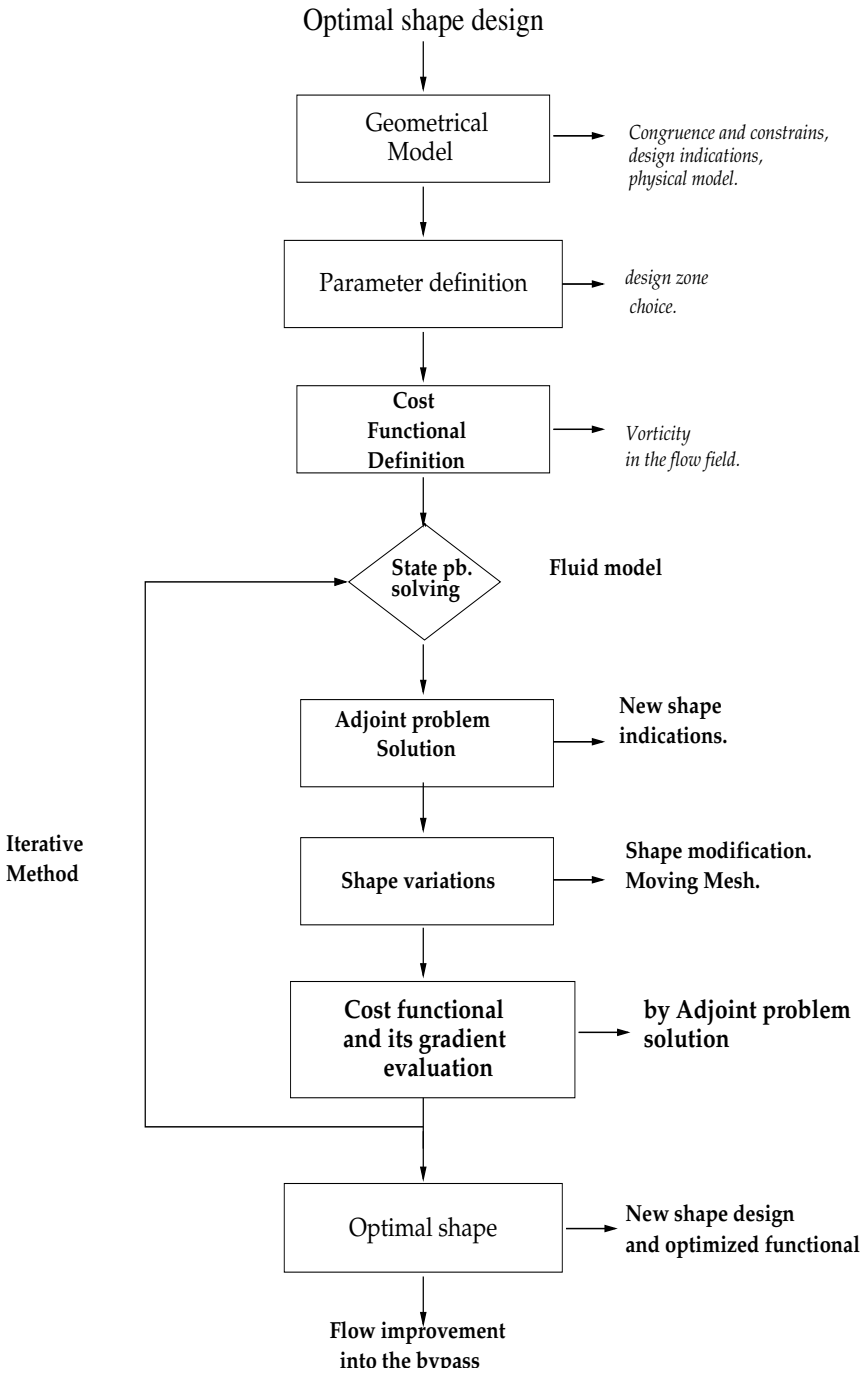

Figure 2.5: Optimal shape design by flow control: scheme of the algorithm.

where $\delta\tilde{w}$ is the shape variation to be regularized and δw the smoothed one, while ϵ is a viscosity parameter to be set to avoid mesh degeneration. For this reason a control over geometrical quantities such as minimum angle or maximum side-length has been used. We use this smoothing procedure at each iteration between steps (2.4.5) and (2.4.6); the value of the "viscosity" parameter at convergence is set to zero, so that we have an identity operator

in (2.4.7). To better understand the necessity of regularization we can say that if we desire $\delta w \in C^1(\Gamma)$, where Γ is a portion of the boundary of $\Omega \subset \mathbb{R}^2$, the gradient method does not necessarily produce $C^1(\Gamma)$ variation of δw but only $L^2(\Gamma)$ and therefore we need to project them thanks to (2.4.7).

2.5 An equivalent interpretation of the problem

The cost functional (2.3.12) represents the square of the vorticity in the down-field (host vessel) zone of the bypass. In the adjoint problem (2.3.15) we have considered the source field

$$H(\mathbf{q}) = \int_{\Omega_{wd}} \mathbf{q} \cdot (\nabla \times \nabla \times \mathbf{u}) d\Omega + \int_{\Gamma_{wd}} \hat{\mathbf{n}} \cdot (\mathbf{q} \times \nabla \times \mathbf{u}) d\Gamma.$$

Let us consider the particular case where $\Omega_{wd} \equiv \Omega$ and the state problem has Dirichlet conditions on the whole boundary or, alternatively, as it happens in our case, a free-stress Neumann boundary condition on the outflow, where $\hat{\mathbf{n}} = (1, 0)^T$ and Dirichlet conditions on inflow and arterial walls. Then the boundary term of $H(q)$ is zero. Note that the boundary term of $H(\mathbf{q})$ can be written also as $\int_{\Gamma_{wd}} (\nabla \mathbf{u} \cdot \hat{\mathbf{n}}) \mathbf{q} d\Gamma$.
The following identity holds:

$$\nabla \times \omega = \nabla \times \nabla \times \mathbf{u} = \nabla(\nabla \cdot \mathbf{u}) - \Delta \mathbf{u}$$

and since we are considering incompressible flows ($\nabla \cdot \mathbf{u} = 0$) it would have been equivalent, from a physical point of view, using the source term $-\Delta \mathbf{u}$ for the adjoint problem (2.3.15) instead of $\nabla \times \nabla \times \mathbf{u}$. The corresponding new cost functional (multiplied by the viscosity ν) becomes:

$$J(\mathbf{u}) = \frac{1}{2} \nu \int_{\Omega} |\nabla \mathbf{u}|^2 d\Omega,$$

and represents the minimization of the energy of the system dissipated by viscous stresses (related with viscous drag). From now we will therefore consider this new functional.
To analyze this new problem (see also [97]), let us consider a domain Ω' representing a small perturbation of Ω. Its boundary $\Gamma' = \partial\Omega'$ can be represented as follows,

$$\Gamma' = \{x + \delta w(x) \hat{\mathbf{n}}(x) \ \forall \ x \in \Gamma = \partial\Omega\},$$

where δw is regular (for example $\delta w \in C^2$) and small. We define also:

$$\boldsymbol{\delta} \mathbf{u} = \mathbf{u}(\Omega') - \mathbf{u}(\Omega) \equiv \mathbf{u}' - \mathbf{u}$$

where $\mathbf{u}$ has been extended from Ω to Ω' such that $\mathbf{u} = 0$ in $\Omega' \backslash \Omega$. This extension is possible because we have zero Dirichlet boundary condition on the wall subject to shape variations. We will see that $\boldsymbol{\delta} \mathbf{u}$ (and hence $\mathbf{u}'$) can be obtained solving an additional problem. We introduce

$$\delta J \equiv J(\Omega', \mathbf{u}') - J(\Omega, \mathbf{u}) = \frac{1}{2} \nu \Big(\int_{\Omega'} |\nabla \mathbf{u}'|^2 d\Omega - \int_{\Omega} |\nabla \mathbf{u}|^2 d\Omega \Big),$$

we have stressed the domain on which the cost functional is defined. We rewrite δJ as

$$\delta J = \frac{1}{2}\nu\delta\Big(\int_\Omega |\nabla \mathbf{u}|^2 d\Omega\Big) = \frac{1}{2}\nu\int_{\delta\Omega} |\nabla \mathbf{u}|^2 d\Omega + \nu\int_\Omega \nabla\boldsymbol{\delta}\mathbf{u}\cdot\nabla\mathbf{u} d\Omega + o(\delta\Omega, \boldsymbol{\delta}\mathbf{u}), \tag{2.5.1}$$

where $\delta\Omega = \Omega' - \Omega$. We suppose that $\nabla\mathbf{u}$ is smooth, and we rewrite the first term of (2.5.1), related with $\delta\Omega$ as an "extension" of the value of $|\nabla\mathbf{u}|$ on Γ:

$$\frac{1}{2}\nu\int_{\delta\Omega} |\nabla \mathbf{u}|^2 d\Omega = \frac{1}{2}\nu\int_\Gamma \delta w|\nabla\mathbf{u}|^2 d\Gamma + o(\|\delta w\|_{C^2}) = \frac{1}{2}\nu\int_\Gamma \delta w|\frac{\partial\mathbf{u}}{\partial\hat{\mathbf{n}}}|^2 d\Gamma + o(\|\delta w\|_{C^2}), \tag{2.5.2}$$

having exploited the fact that the tangential derivative $\frac{\partial\mathbf{u}}{\partial\hat{\mathbf{t}}} = 0$ since $\mathbf{u} = \mathbf{0}$ on Γ. To rewrite the second term of (2.5.1) it is possible to show that $\boldsymbol{\delta}\mathbf{u}$ is a solution to the following problem (now referring to the domain considered in Section 2.3) representing small flow perturbation in Ω. Then rewriting problem (2.3.1) we have: find $\delta\mathbf{u}$ and δp in Ω such that

$$\begin{cases} -\nu\Delta\boldsymbol{\delta}\mathbf{u} + \nabla\delta p = \mathbf{0} \;\; in\ \Omega\subset\mathbb{R}^2, \\ \nabla\cdot\boldsymbol{\delta}\mathbf{u} = 0 \quad in\ \Omega, \\ \boldsymbol{\delta}\mathbf{u} = \mathbf{0}\ on\ \Gamma_w\backslash\Gamma_c, \\ \boldsymbol{\delta}\mathbf{u} = \mathbf{0}\ on\ \Gamma_{in}, \\ \nu\frac{\partial\boldsymbol{\delta}\mathbf{u}}{\partial\hat{\mathbf{n}}} - \delta p\hat{\mathbf{n}} = \mathbf{0}\ on\ \Gamma_{out}, \\ \boldsymbol{\delta}\mathbf{u} = -\delta w\frac{\partial\mathbf{u}}{\partial\hat{\mathbf{n}}}\ on\ \Gamma_c, \end{cases} \tag{2.5.3}$$

Here we assume $\Gamma_c \subset \Gamma$ as a portion of the boundary subject to shape optimization (perturbation is only on Γ_c which becomes Γ_c'). The only non-obvious relation is the boundary condition on Γ_c (we recall that $\mathbf{u}$ is already known). By a Taylor expansion we rewrite $\mathbf{u}'|_{\Gamma_c'} = \mathbf{u}'(x + \delta w\hat{\mathbf{n}})$ as

$$\mathbf{u}'(x+\delta w\hat{\mathbf{n}}) = \mathbf{u}'(x) + \delta w\frac{\partial\mathbf{u}'}{\partial\hat{\mathbf{n}}}|_{\Gamma_c} + o(|\delta w|) = \mathbf{0},$$

which is set to zero to satisfy non-slip conditions between fluid and wall on the new boundary Γ_c'. Being $\mathbf{u}'(x) = \mathbf{u}'|_{\Gamma_c}$ We get:

$$\mathbf{u}'|_{\Gamma_c} = -\delta w\frac{\partial\mathbf{u}'}{\partial\hat{\mathbf{n}}}|_{\Gamma_c},$$

but $\boldsymbol{\delta}\mathbf{u}|_{\Gamma_c} = \mathbf{u}'|_{\Gamma_c} - \mathbf{u}|_{\Gamma_c}$ and $\mathbf{u}|_{\Gamma_c} = \mathbf{0}$ so:

$$\delta\mathbf{u}|_{\Gamma_c} = -\delta w\frac{\partial\mathbf{u}}{\partial\hat{\mathbf{n}}}|_{\Gamma_c}.$$

Now we consider (2.3.15) in the weak form and with the new right-hand-side $-\nu\Delta\mathbf{u}$ (instead of $\nabla\times\nabla\times\mathbf{u}$), we multiply by $(\boldsymbol{\delta}\mathbf{u}, \delta p)$ and integrate by parts, obtaining:

$$\begin{cases} \nu\int_\Omega \nabla\mathbf{p}\cdot\nabla\boldsymbol{\delta}\mathbf{u} d\Omega - \nu\int_{\Gamma_c}\frac{\partial\mathbf{p}}{\partial\hat{\mathbf{n}}}\cdot\boldsymbol{\delta}\mathbf{u} d\Gamma + \int_\Omega \sigma\nabla\cdot\boldsymbol{\delta}\mathbf{u} d\Omega = \nu\int_\Omega\nabla\mathbf{u}\cdot\nabla\boldsymbol{\delta}\mathbf{u} d\Omega - \nu\int_{\Gamma_c}\frac{\partial\mathbf{u}}{\partial\hat{\mathbf{n}}}\cdot\boldsymbol{\delta}\mathbf{u} d\Gamma, \\ \int_\Omega \delta p\nabla\cdot\mathbf{p} d\Omega = 0. \end{cases} \tag{2.5.4}$$

Using equation (2.5.3) multiplied by $(\mathbf{p}, \sigma)$ we have:

$$\begin{cases} \nu\int_\Omega\nabla\mathbf{p}\cdot\nabla\boldsymbol{\delta}\mathbf{u} d\Omega - \int_\Omega \delta p\nabla\cdot\mathbf{p} d\Omega = 0, \\ \int_\Omega \sigma\nabla\cdot\boldsymbol{\delta}\mathbf{u} d\Omega = 0, \end{cases} \tag{2.5.5}$$

and so, comparing (2.5.4) and (2.5.5) the only term surviving is

$$-\nu \int_{\Gamma_c} \frac{\partial \mathbf{p}}{\partial \hat{\mathbf{n}}} \cdot \boldsymbol{\delta}\mathbf{u} d\Gamma = \nu \int_{\Omega} \nabla \mathbf{u} \cdot \nabla \boldsymbol{\delta}\mathbf{u} d\Omega - \nu \int_{\Gamma_c} \frac{\partial \mathbf{u}}{\partial \hat{\mathbf{n}}} \cdot \boldsymbol{\delta}\mathbf{u} d\Gamma,$$

where $\boldsymbol{\delta}\mathbf{u}|_{\Gamma_c} = -\delta w \frac{\partial \mathbf{u}}{\partial \hat{\mathbf{n}}}|_{\Gamma_c}$, so

$$-\nu \int_{\Gamma_c} (\frac{\partial \mathbf{p}}{\partial \hat{\mathbf{n}}} - \frac{\partial \mathbf{u}}{\partial \hat{\mathbf{n}}}) \cdot \boldsymbol{\delta}\mathbf{u} d\Gamma = \nu \int_{\Omega} \nabla \mathbf{u} \cdot \nabla \boldsymbol{\delta}\mathbf{u} d\Omega. \tag{2.5.6}$$

Finally from (2.5.2) and (2.5.6) we can rewrite (2.5.1) as:

$$\delta J = \frac{1}{2}\nu \int_{\Gamma_c} \delta w |\frac{\partial \mathbf{u}}{\partial \hat{\mathbf{n}}}|^2 d\Gamma + \nu \int_{\Gamma_c} \delta w (\frac{\partial \mathbf{p}}{\partial \hat{\mathbf{n}}} - \frac{\partial \mathbf{u}}{\partial \hat{\mathbf{n}}}) \cdot \frac{\partial \mathbf{u}}{\partial \hat{\mathbf{n}}} d\Gamma,$$

or

$$\delta J = \nu \int_{\Gamma_c} \delta w (\frac{\partial \mathbf{p}}{\partial \hat{\mathbf{n}}} - \frac{1}{2}\frac{\partial \mathbf{u}}{\partial \hat{\mathbf{n}}}) \cdot \frac{\partial \mathbf{u}}{\partial \hat{\mathbf{n}}} d\Gamma.$$

In our algorithm we are interested in $J'(w)$ and recalling that

$$\delta J = \int_{\Gamma_c} J'(w) \delta w d\Gamma$$

we can say that the new $\delta w|_{\Gamma_c} = -\rho J'(w) = -\rho\nu((\frac{\partial \mathbf{p}}{\partial \hat{\mathbf{n}}} - \frac{1}{2}\frac{\partial \mathbf{u}}{\partial \hat{\mathbf{n}}}) \cdot \frac{\partial \mathbf{u}}{\partial \hat{\mathbf{n}}}) = -\rho G(\mathbf{p}, \mathbf{u}, w)$. In this analysis we can better understand the role of the adjoint variables to get the gradient of cost functional and the new shape.

2.6 Some numerical results

In this section we present some results carried out by local boundary variations algorithm to optimize a preliminary bypass configuration, to obtain vorticity reduction and a feedback procedure to prevent wall shear stress oscillations with the functional (2.2.9). Numerical tests and simulations have been carried out using *Bamg* [55], a Bi-dimensional Anisotropic Mesh Generator and *FreeFem* [54], a finite element Library developed at INRIA, the French National Institute for Research in Computer Science and Control, with the development of algorithms based on control theory and shape optimization. Several remarks carried out from intensive preliminary numerical investigations are in order:

- The wall curvature in the host artery (to model arteries near the heart muscle) increases vorticity.
- The graft angle of the incoming branch of the bypass influences vorticity, by reducing the angle also vorticity is reduced in the down-field observation zone (keeping fixed the configuration provided by other quantities such as arterial and bypass diameter).
- Bypass configuration causes an increase of vorticity in the downfield area of about 35% than the previous idealized 2D configuration without bypass bridge and coronary occlusion.

- After obtaining the new optimal shape for the incoming branch in 25 iterations, vorticity reduction, in our specific modelling context led by optimal control, is about of 45% in comparison with the starting idealized 2D configuration.

Figures 2.6-2.10 provide an account of numerical results and show the optimal shape of the bypass obtained using steady Stokes equations in an optimal control problem with cost functionals (2.3.12) and (2.3.13). As we can see the shape that is found resembles the Taylor patch configuration [26], a little cuffed shape. The effect of the Taylor patch is to reduce gradually the average velocity of the blood as it approaches the distal anastomosis, since the cross-sectional area of the bypass is steadily becoming larger. This prevents the sudden deceleration experienced in the conventional model with the fluid returning to the host vessel. There is a gradual reduction in the momentum of the blood while approaching the junction, in fact, the blood is guided more smoothly through the vessel thanks to the gradually changing geometry. Flow disturbances are abated, undesirable flow separation at the toe of the bypass diminished.

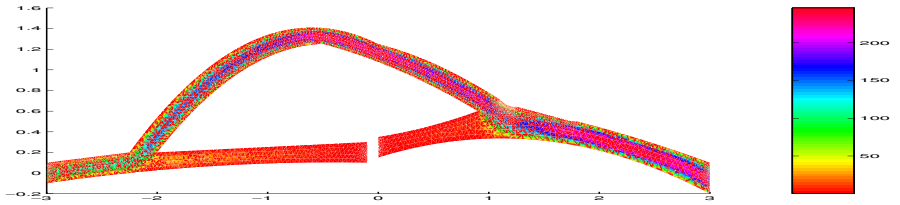

Figure 2.6: Complete bypass configuration (bridge) before optimal shape design process: iso-velocity $[ms^{-1} \cdot 10^{-2}]$.

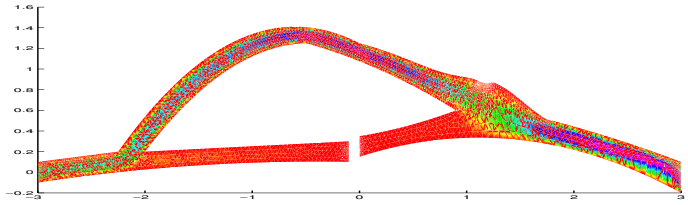

Figure 2.7: Complete bypass configuration at the end of shape optimization: iso-velocity, same colorbar of the previous picture.

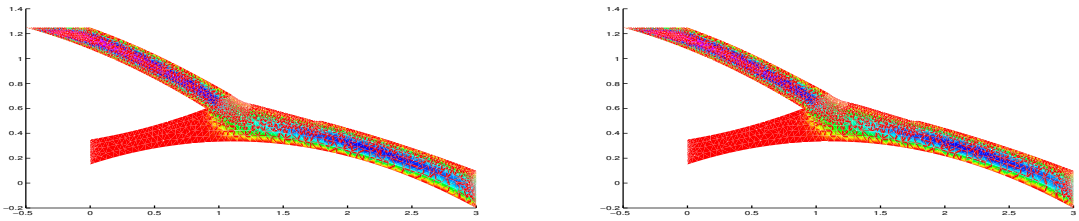

Figure 2.8: Bypass configuration near the incoming branch before shape optimization (left) and with 11% vorticity reduction (right).

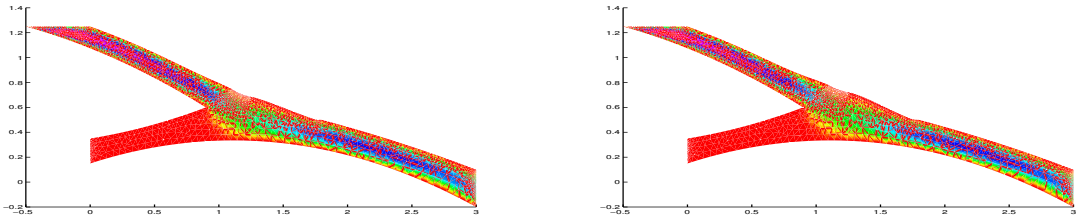

Figure 2.9: Bypass configuration near the incoming branch with 22% (left) and with 32% vorticity reduction (right). The colorbar is the same of pictures in the previous page.

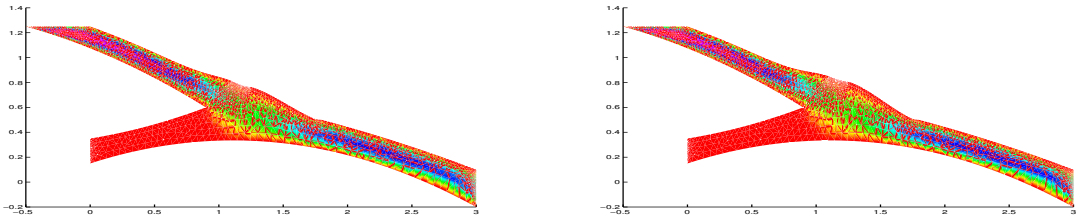

Figure 2.10: Bypass configuration near the incoming branch with 38% (left) and with 45% vorticity reduction (right).

2.7 Feedback procedures and results interpretation

A feedback procedure has been implemented by solving the unsteady Navier-Stokes equations in the original configuration as well as in the final configuration obtained after applying the optimal shape design process on a reduced model, based on steady Stokes equations. The full Navier-Stokes problem reads, for all $0 < t < T$:

$$\begin{cases} \frac{\partial \mathbf{u}}{\partial t} - \nu \Delta \mathbf{u} + (\mathbf{u} \cdot \nabla)\mathbf{u} + \nabla p = \mathbf{f} \quad in\ \Omega, \\ \nabla \cdot \mathbf{u} = 0 \quad in\ \Omega, \\ \mathbf{u} = \mathbf{0}\ on\ \Gamma_w \\ \mathbf{u} \cdot \hat{\mathbf{t}} = 0,\ \mathbf{u} \cdot \hat{\mathbf{n}} = g_{in}(t)\ on\ \Gamma_{in} \\ \nu \frac{\partial \mathbf{u}}{\partial \hat{\mathbf{n}}} - p\hat{\mathbf{n}} = \mathbf{0}\ on\ \Gamma_{out}, \end{cases} \tag{2.7.1}$$

We used Hagen-Poiseuille inflow pulsatory condition (*Womersley* profile with period $T = 1s$). Time discretization is based on backward Euler method with a time step $\Delta t = 0.01s$. Figures 2.11-2.12 show unsteady flows at different time steps.
During the feedback procedure we used the functional (2.2.9) to provide useful information about unsteady fluid dynamics phenomena such as wall shear stress oscillations during pulsatory systolic and diastolic phases. This quadratic functional is complete because it keeps into consideration WSS variations in time and the functional is not pointwise but defined on Γ_c, the vascular wall we are modelling by optimal shape design. In the specific modelling context that we have considered, shape optimization process guarantees a reduction of 45% of vorticity using steady Stokes flow model and a reduction of 25% in wall shear stress oscillations in time (on the vascular wall Γ_c we are modelling). In general, the flow at the distal junction exhibits considerable spatial and temporal variations. With the adaptation operated by shape optimization technique we find, as already seen, a graft which resembles the Taylor patch configuration in which the anastomotic flow is less disturbed, a less adverse shear stress distribution prevails and furthermore flow separation is reduced [26]. Intimal thickening hyperplasia, which causes restenosis, should be alleviated at the toe in the new bypass configuration proposed.

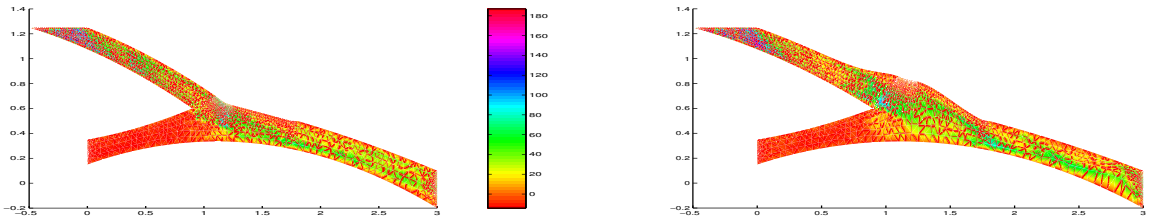

Figure 2.11: Fluid dynamics unsteady phenomena into the incoming branch of bypass at $t = 0.3s$, velocity $[ms^{-1} \cdot 10^{-2}]$.

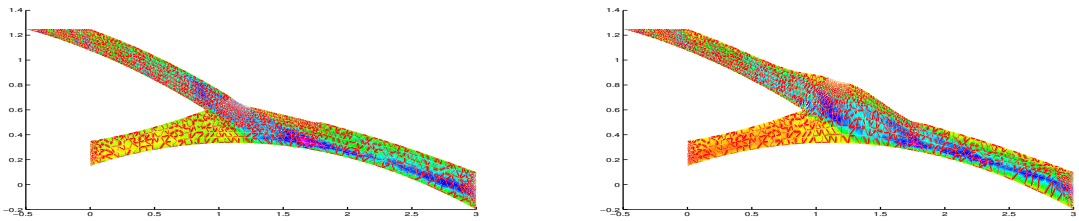

Figure 2.12: Fluid dynamics unsteady phenomena into the incoming branch of bypass at $t = 0.5s$.

In Figure 2.13 an integral quantity of interest is plotted, it is the wall shear stress variation in time $\Sigma(t)$ (2.2.7) on Γ_c, its calculation has been done to get information about functional J_τ (2.2.9) which provides integral information in time $(0, T)$ for $\Sigma(t)$. As we can see the oscillatory behavior of $\Sigma(t)$ on Γ_c is strongly reduced after applying shape optimization.

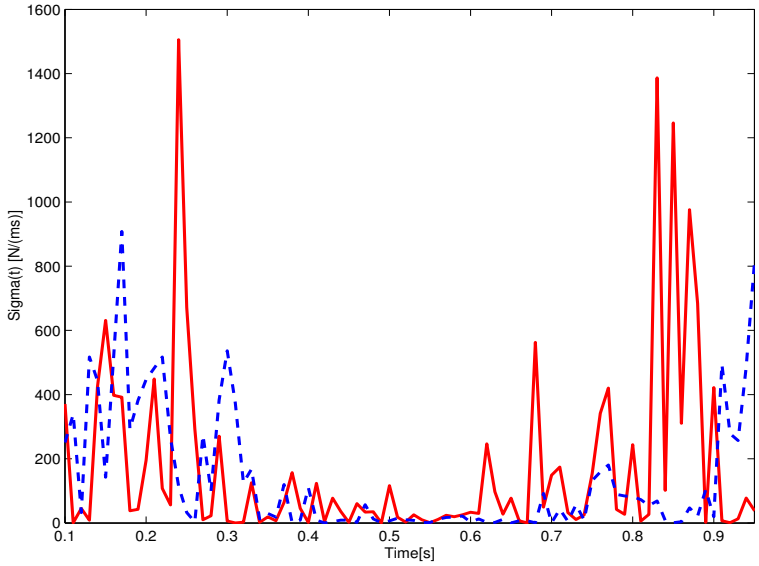

Figure 2.13: Variations in time of the Wall Shear Stress $\Sigma(t)$ $[Nm^{-1}s^{-1}]$ (2.2.7) along Γ_c (pulsatory inflow condition) in the two different bypass configurations, at the beginning (continuous line) and at the end (dashed line) of optimal shape design process.

It is also possible to develop algorithm to apply optimal control and shape optimization to fully unsteady incompressible Navier-Stokes equations (see Laporte [75] and Le Tallec [76]) and eventually to consider the coupled fluid-structure problem (Moubachir and Zolésio [100]). In our case at this step the interest is to develop efficient algorithms based on reduced fluid models to provide preliminary design indications concerning surgical prosthesis realizations to be verified in feedback and supported by other efficient optimization methods such as reduced basis applied to parametrized domains.
We have also seen that our control approach based on a vorticity functional is related (and equivalent from a physical point of view) with the one based on the minimization of viscous dissipation. For this reason we can conclude that the use of the unsteady functional J_τ related with shear stresses (and so the gradient of velocity, considering a Newtonian fluid) in feedback is strictly related with the functional used in the shape optimization process.
As conclusion of this chapter we introduce a theoretical explanation of results, achieved after the optimization approach, and related with fluid mechanics phenomena in the bypass, especially in the host artery.
Applying the $2D$ version of *Stokes Theorem* (*Green Theorem*, see for example Adams [3]) we can say that the cost functional calculated in down-field zone of the bypass is given by:

$$J(\mathbf{u}) = \int_{\Omega_{wd}} (\frac{\partial v}{\partial x} - \frac{\partial u}{\partial y}) d\Omega = \int_{\Gamma_{wd}} (udx + vdy) d\Gamma, \tag{2.7.2}$$

in our case the boundary conditions on Γ_{wd} in the down-field zone provides a contribution only at the inflow (the intersection between the bypass and the host artery) and at the outflow (of bypass configuration considered). See scheme in Figure 2.14.

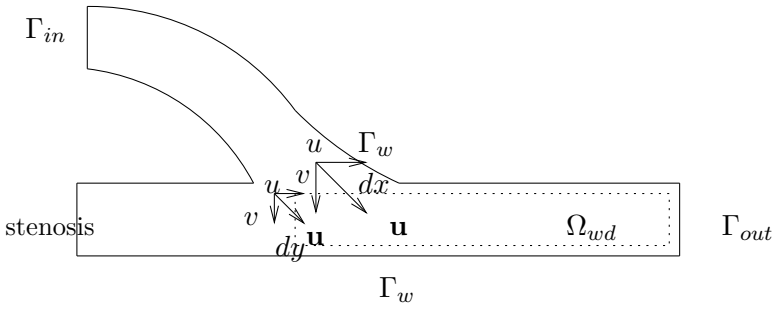

Figure 2.14: Bypass Scheme and Green's Theorem interpretation.

The intersection zone between the bypass and the artery is becoming larger and the mean velocity of the blood is diminished so the term udx is becoming smaller and if the fluid is less disturbed also the term vdy (representing a distorsion of the main stream) is small in the down-field zone. The relationship (2.7.2) tells us that while studying (stationary) vorticity we can get information on velocity field and viscous dissipation as well. In this framework we can unify results already available in literature and trying to better understand our own optimization results.

Chapter 3

Shape Design by Optimal Control using Small Perturbation Theory

In this chapter we present another shape design approach using small perturbation theory. The theory of optimal control based on adjoint formulation is applied to a state problem representing the flow perturbation induced by shape variation (first order problem) in order to optimize the incoming branch of the bypass (the toe) into the coronary. We use a method based on the reference domain formulation described by a map whose coefficients have to be optimized so that we show how to solve a shape design problem without dealing with shape functions and boundary variations (that would invoke mesh adaptation, re-meshing and smoothing). Rather, we will have to solve an optimal control problem on the coefficients of the transformation map.

3.1 An alternative approach to local boundary variations

This second proposed approach for local shape design is based on a map from the real domain Ω to a (rectangular) reference one $\tilde{\Omega}$ using a variable transformation:

$$\tilde{x} = x, \ \tilde{y} = \frac{1}{f(x,\varepsilon)} y, \tag{3.1.1}$$

where $f(x,\varepsilon)$ represents, for example, in our case, the upper shape of the bypass and can be developed as

$$f(x,\varepsilon) = f_0(x) + \varepsilon f_1(x) + \varepsilon^2 f_2(x) + ..., \tag{3.1.2}$$

being $f_0(x)$ the given (non-optimized) shape and ε is a small parameter. Assuming that the state problem has a solution $\mathbf{u}, p$ that is infinitely differentiable with respect to ε:

$$\mathbf{u} = \mathbf{u}_0 + \varepsilon \mathbf{u}_1 + \varepsilon^2 \mathbf{u}_2 + ...,$$

$$p = p_0 + \varepsilon p_1 + \varepsilon^2 p_2 + ...,$$

and using small perturbation techniques (see Van Dyke [154]), we can derive the equations for $\mathbf{u}_k, p_k$ starting from the state problem and then mapping Ω to the reference domain $\tilde{\Omega}$. Here

$(\mathbf{u}_0, p_0)$ represents the solution of the state problem in the domain Ω_0 with upper boundary $f_0(x)$, while $(\mathbf{u}_1, p_1)$ represents the flow perturbation due to the first order shape variation $f_1(x)$, $(\mathbf{u}_k, p_k)$ are velocity and pressure perturbation induced by $f_k(x)$. At this point we can use optimal control techniques to solve the problem for $\mathbf{u}_1, p_1$ (the first corrections), the function $f_1(x)$ which represents a perturbation in the shape $f_0(x)$ (weighted by ε) is another unknown for the problem and is used as control variable. In this context Masmoudi *et al.* [47] have investigated a complementary approach based on high order derivatives and Taylor expansion of cost functional with respect to shape parameters.
The structure of this chapter is the following: in Section 3.2 we recall the problem based on the same fluid model of the previous chapter (a generalization to unsteady flows will be introduced in the next chapter) and we develop small perturbation techniques in Section 3.3, then we deal with shape optimization problem in Section 3.4 and with the optimal control framework in Section 3.5. Then we study theoretical aspects of the problem such as existence and uniqueness of solutions in Section 3.6, we propose an algorithm in Section 3.7 and we describe numerical results in Section 3.8. A comparison between local boundary variations method and small perturbation is provided in Section 3.9.

3.2 Problem statement

Let Ω be a bounded domain of $\mathbb{R}^2$, $\Gamma \equiv \partial\Omega$ is the boundary of Ω, $\overline{\Omega} = \Omega \cup \partial\Omega$, $\mathbf{x} = (x, y)^T$ is a point of $\overline{\Omega}$. In the sequel aggregation of vector quantities $\mathbf{u}$ with scalar quantities p are indicated with $\underline{Q}$ ($\underline{Q} = (\mathbf{u}, p)$), $\underline{\Phi}$ or $\underline{\hat{\Phi}}$.
We consider again an idealized, two-dimensional bypass bridge configuration as in Figure 3.1 and the domain of Figure 3.2, where the dotted line represents the geometry of the complete anastomosis; Γ_{w_2} is the section of the original artery, Γ_{in} is the new anastomosis inflow after bypass surgery, Γ_{out} is the anastomosis outflow. We consider a boundary value problem for

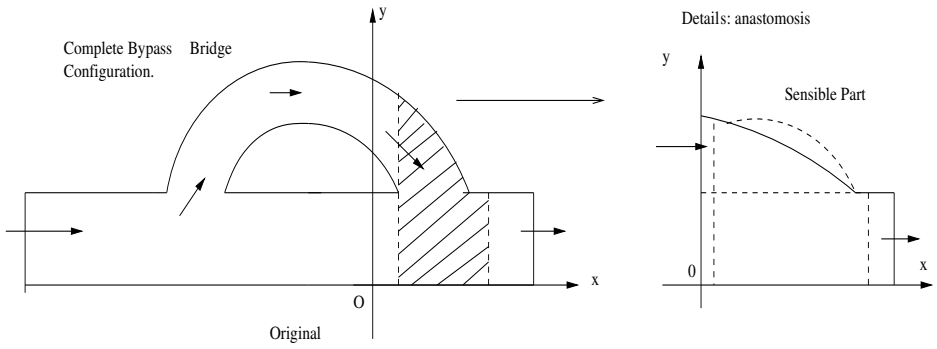

Figure 3.1: Idealized, 2-D bypass bridge configuration (left) and detail of the sensible part for the optimization process (right), where the dotted curve represents a possible shape variation.

the Stokes equations, see for example Zeytounian [169], used as in the previous chapter to

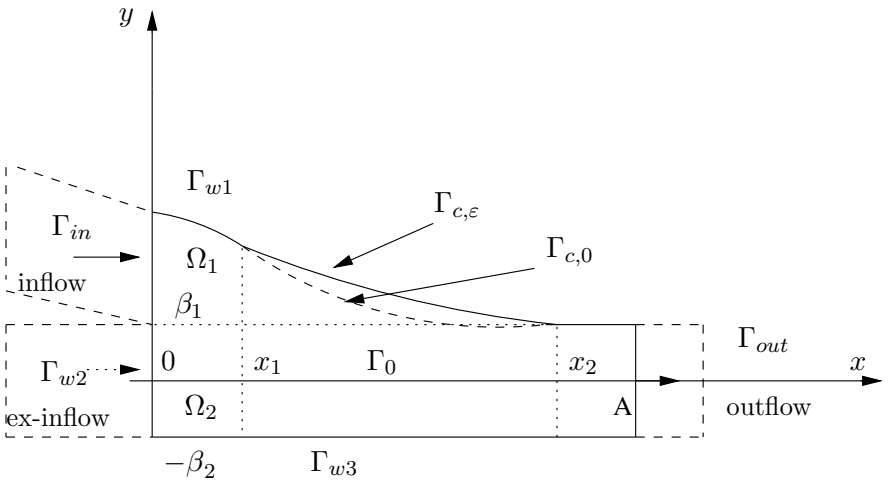

Figure 3.2: $\overline{\Omega} = \overline{\Omega}_1 \cup \overline{\Omega}_2, \Gamma_w = \Gamma_{w_1} \cup \Gamma_{w_2} \cup \Gamma_{w_3}, \Gamma_0 = \partial\Omega_1 \cap \partial\Omega_2$.

model low Reynolds blood flow in the optimization process. The problem reads: find $\mathbf{u}, p$ s.t.

$$\begin{cases} -\nu\Delta\mathbf{u} + \nabla p = \mathbf{f} \quad in\ \Omega, \\ \nabla \cdot \mathbf{u} = 0 \quad in\ \Omega, \\ \mathbf{u} = \mathbf{u}_{in}\ on\ \Gamma_{in},\ \mathbf{u} = \mathbf{0}\ on\ \Gamma_{w_1} \cup \Gamma_{w_3}, \\ -p\hat{\mathbf{n}} + \nu\frac{\partial \mathbf{u}}{\partial \hat{\mathbf{n}}} = \mathbf{g}_{out}\ on\ \Gamma_{out} \cup \Gamma_{w_2}, \end{cases} \tag{3.2.1}$$

where $\hat{\mathbf{n}} = (n_1, n_2)^T$ is the outward unit normal vector on Γ, $\mathbf{f} = \mathbf{f}(x, y)$, $\mathbf{u}_{in} = \mathbf{u}_{in}(x, y)$, $\mathbf{g}_{out} = \mathbf{g}_{out}(x, y)$ are given vector functions, $\nu = const > 0$ and $\mathbf{u}_f = \{\mathbf{u}_{in}\ on\ \Gamma_{in}; \mathbf{0}\ on\ \Gamma_{w_1} \cup \Gamma_{w_3}\}$. In the following we may need to impose some additional restriction on p (for example $\int_\Omega p d\Omega = 0$ if $\Gamma_{in} = \Gamma$).

The weak statement of (3.2.1) reads: find $\mathbf{u} \in (H^1(\Omega))^2$, $p \in L^2(\Omega)$ s.t.

$$\begin{cases} a(\mathbf{u}, \mathbf{v}) = b(p, \mathbf{v}) + G(\mathbf{v})\ \forall \mathbf{v} \in \mathbb{X}, \\ b(q, \mathbf{u}) = 0\ \forall q \in L^2(\Omega), \\ \mathbf{u} = \mathbf{u}_f\ on\ \Gamma_{in} \cup \Gamma_{w_1} \cup \Gamma_{w_3}, \end{cases} \tag{3.2.2}$$

where with $\mathbf{v}$ and q we indicate test functions and:

$$a(\mathbf{u}, \mathbf{v}) = \int_\Omega \nu \nabla\mathbf{u} \cdot \nabla\mathbf{v} d\Omega$$

$$b(p, \mathbf{v}) = \int_\Omega p\nabla \cdot \mathbf{v} d\Omega,\ G(\mathbf{v}) = \int_\Omega \mathbf{f} \cdot \mathbf{v} d\Omega + \int_{\Gamma_{out} \cup \Gamma_{w_2}} \mathbf{g}_{out} \cdot \mathbf{v} d\Gamma,$$

$$\mathbb{X} := \{\mathbf{v} : \mathbf{v} \in (H^1(\Omega))^2, \mathbf{v} = 0\ on\ \Gamma_{in} \cup \Gamma_{w_1} \cup \Gamma_{w_3}\}.$$

For further mathematical aspects of the problem see, for example, Lions [85]. The subset $\Gamma_{c,\varepsilon}$ of Γ_{w_1} is parametrized by a function $f(x, \varepsilon)$ of $x \in [x_1, x_2]$ and of a small parameter $\varepsilon \in [-\varepsilon_0, \varepsilon_0]$, $\varepsilon_0 = const$. More precisely we assume that $f(x, \varepsilon)$ can be developed as follows:

$$f(x, \varepsilon) = f_0(x) + \varepsilon f_1(x) + \varepsilon^2 f_2(x) + \ldots, \tag{3.2.3}$$

where $f_k \in \mathbb{W}^{1,\infty}(x_1, x_2)$, for $k = 0$, (we recall that $\mathbb{W}^{1,\infty}(x_1, x_2)$ is the space of functions $f_k \in L^\infty(x_1, x_2)$ such that the distributional derivative of first order of f_k belongs to $L^\infty(x_1, x_2)$) while for $k \geq 1$ $f_k \in \mathbb{W}_0^{1,\infty}(x_1, x_2)$ with $f_k(x_1) = f_k(x_2) = 0, k \geq 1$. Here the function $f_0(x) > 0$ describes the original subset $\Gamma_{c,0}$ (corresponding to $\Gamma_{c,\varepsilon}$ for $\varepsilon = 0$) of the boundary $\Gamma_{w0} \equiv \partial\Omega_0$ of a given non-optimized domain Ω_0, see Figure 3.3 (in perturbation theory this is often called "unperturbed domain"), while $f_k(x), k \geq 1$, could be unknown when dealing with control problem (see Section 3.4).

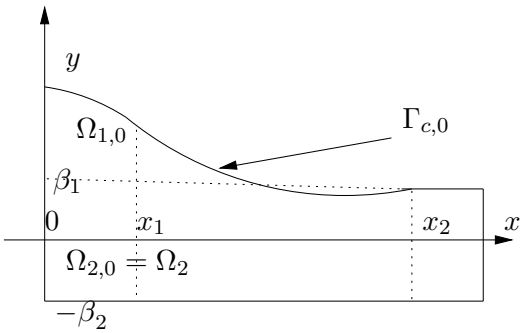

Figure 3.3: The original "unperturbed domain" Ω_0.

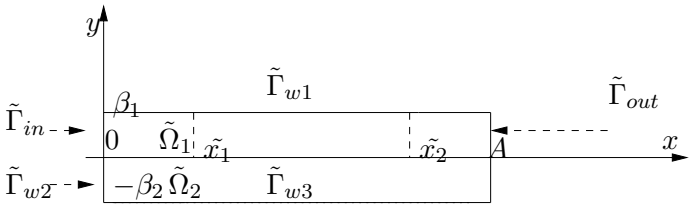

Figure 3.4: The "simple" domain $\tilde{\Omega}$.

Although $a(.,.), b(.,.)$ and $G(.)$ depend on the parametrization f of the part $\Gamma_{c,\varepsilon}$, this dependence has been understood for simplicity of notations.

3.3 The problem for the perturbation functions

Let us introduce the reference (simple-shaped) domains $\tilde{\Omega}_1 = \{0 < \tilde{x} < A, 0 < \tilde{y} < \beta_1 \equiv \beta\}$, $\tilde{\Omega}_2 = \{0 < \tilde{x} < A, -\beta_2 < \tilde{y} < 0\}$, and $\overline{\tilde{\Omega}} = \overline{\tilde{\Omega}}_1 \cup \overline{\tilde{\Omega}}_2$ (see Figure 3.4). Then we assume that $f(x, \varepsilon) > 0$ and consider the following variable transformation:

$$\mathrm{T}_f : \overline{\Omega}_1 \cup \overline{\Omega}_2 \to \overline{\tilde{\Omega}},\ \tilde{\mathbf{x}} = \mathrm{T}_f(\mathbf{x}),$$

such that T_f is the identity in Ω_2, while $\mathrm{T}_f(x, y) = (x, \frac{\beta}{f(x,\varepsilon)} y)$ in Ω_1.
We set $\tilde{\mathbf{x}} = (\tilde{x}, \tilde{y})^T$ and define

$$\tilde{\mathbf{u}}(\tilde{\mathbf{x}}) := \mathbf{u} \circ \mathrm{T}_f^{-1}(\tilde{\mathbf{x}}) = \mathbf{u}(\tilde{x}, \tilde{y} f(\tilde{x}, \varepsilon)/\beta).$$

where $\tilde{\mathbf{u}} = (\tilde{u}, \tilde{v})^T$. Then,

$$dxdy = \frac{f(\tilde{x}, \varepsilon)}{\beta} d\tilde{x} d\tilde{y}$$

and the following relations hold:

$$\begin{cases} \frac{\partial \phi}{\partial y}(\tilde{\mathbf{x}}) = \frac{\beta}{f(\tilde{x},\varepsilon)} \frac{\partial \tilde{\phi}(\tilde{\mathbf{x}})}{\partial \tilde{y}}, \\ \frac{\partial \phi}{\partial x}(\tilde{\mathbf{x}}) = \frac{\partial \tilde{\phi}(\tilde{\mathbf{x}})}{\partial \tilde{x}} - \tilde{y} \frac{f_x(\tilde{x},\varepsilon)}{f(\tilde{x},\varepsilon)} \frac{\partial \tilde{\phi}(\tilde{\mathbf{x}})}{\partial \tilde{y}} \quad \big(with\ f_x := \frac{df}{dx}\big), \end{cases} \tag{3.3.1}$$

$$\begin{cases} \tilde{\mathcal{D}}(f)\tilde{\mathbf{u}}(\tilde{\mathbf{x}}) := ((\nabla \cdot \mathbf{u}) \circ \mathrm{T}_f^{-1})(\tilde{\mathbf{x}}) = \frac{\partial \tilde{u}}{\partial \tilde{x}} - \tilde{y} \frac{f_x(\tilde{x},\epsilon)}{f(\tilde{x},\varepsilon)} \frac{\partial \tilde{u}}{\partial \tilde{y}} + \frac{\beta}{f(\tilde{x},\varepsilon)} \frac{\partial \tilde{v}}{\partial \tilde{y}}, \\ \tilde{\mathcal{R}}(f)\tilde{\mathbf{u}}(\tilde{\mathbf{x}}) := ((\nabla \times \mathbf{u}) \circ \mathrm{T}_f^{-1})(\tilde{\mathbf{x}}) = \frac{\partial \tilde{v}}{\partial \tilde{x}} - \tilde{y} \frac{f_x(\tilde{x},\epsilon)}{f(\tilde{x},\varepsilon)} \frac{\partial \tilde{v}}{\partial \tilde{y}} - \frac{\beta}{f(\tilde{x},\varepsilon)} \frac{\partial \tilde{u}}{\partial \tilde{y}}. \end{cases} \tag{3.3.2}$$

Then in $\tilde{\Omega}$ we have:

$$\tilde{\mathcal{D}}(f)\tilde{\mathbf{u}} = m_2 \tilde{\nabla} \cdot \tilde{\mathbf{u}} + m_1 \tilde{\mathcal{D}}(f)\tilde{\mathbf{u}},\ \tilde{\mathcal{R}}(f)\tilde{\mathbf{u}} = m_2 \tilde{\nabla} \times \tilde{\mathbf{u}} + m_1 \tilde{\mathcal{R}}(f)\tilde{\mathbf{u}},$$

where $\tilde{\nabla}\phi := \big(\frac{\partial \phi}{\partial \tilde{x}}, \frac{\partial \phi}{\partial \tilde{y}}\big)$, while m_s is the characteristic function of Ω_s $(s = 1, 2)$. Now the functional spaces $\mathbb{X}$ and L^2 are defined on the domain $\tilde{\Omega}$. To simplify our notation from now on we will set (unless otherwise specified):

$$\mathbf{x} = \tilde{\mathbf{x}},\ \mathbf{u}(x, y) = \tilde{\mathbf{u}}(\tilde{x}, \tilde{y}),\ u = \tilde{u},\ v = \tilde{v}, \ldots, \mathcal{D} = \tilde{\mathcal{D}}, \mathcal{R} = \tilde{\mathcal{R}},\ \Omega \equiv \tilde{\Omega},\ \Gamma_{w_k} \equiv \tilde{\Gamma}_{w_k},$$

$$\Omega_1 \equiv \tilde{\Omega}_1, \Omega_2 \equiv \tilde{\Omega}_2$$

Then problem (3.2.2) in the new variables and in the new domains reads as follows:

$$\begin{cases} a(f; \mathbf{u}, \mathbf{v}) = b(f; p, \mathbf{v}) + G(f; \mathbf{v})\ \forall \mathbf{v} \in \mathbb{X}, \\ b(f; q, \mathbf{u}) = 0\ \forall q \in L^2(\Omega), \\ \mathbf{u} = \mathbf{u}_f\ on\ \Gamma_{in} \cup \Gamma_{w_1} \cup \Gamma_{w_3}. \end{cases} \tag{3.3.3}$$

We have emphasized the dependence of $a(f; ., .), b(f; ., .)$, and $G(f; .)$ on the shape function f. Precisely, we have:

$$a(f; \mathbf{u}, \mathbf{v}) = a_1(f; \mathbf{u}, \mathbf{v}) + a_2(\mathbf{u}, \mathbf{v}),$$

$$a_1(f; \mathbf{u}, \mathbf{v}) = \int_{\Omega_1} \frac{f\nu}{\beta} \Big(\big(\frac{\partial \mathbf{u}}{\partial x} - \frac{y f_x}{f} \frac{\partial \mathbf{u}}{\partial y} \big) \cdot \big(\frac{\partial \mathbf{v}}{\partial x} - \frac{y f_x}{f} \frac{\partial \mathbf{v}}{\partial y} \big) + \frac{\beta^2}{f^2} \frac{\partial \mathbf{u}}{\partial y} \cdot \frac{\partial \mathbf{v}}{\partial y} \Big) d\Omega,$$

$$a_2(\mathbf{u}, \mathbf{v}) = \int_{\Omega_2} \nu \big(\frac{\partial \mathbf{u}}{\partial x} \cdot \frac{\partial \mathbf{v}}{\partial x} + \frac{\partial \mathbf{u}}{\partial y} \cdot \frac{\partial \mathbf{v}}{\partial y} \big) d\Omega,$$

$$b(f; p, \mathbf{v}) = b_1(f; p, \mathbf{v}) + b_2(p, \mathbf{v}),$$

$$b_1(f; p, \mathbf{v}) = \int_{\Omega_1} \frac{f}{\beta} p \mathcal{D}(f)\mathbf{v} d\Omega,\quad b_2(p, \mathbf{v}) = \int_{\Omega_2} p \nabla \cdot \mathbf{v} d\Omega,$$

$$G(f; \mathbf{v}) = G_1(f; \mathbf{v}) + G_2(\mathbf{v}),$$

$$G_1(f; \mathbf{v}) = \int_{\Omega_1} \frac{f}{\beta} \mathbf{f} \cdot \mathbf{v} d\Omega + \int_{(\Gamma_{out} \cup \Gamma_{w2}) \cap \partial\Omega_1} \mathbf{g}_{out} \cdot \mathbf{v} d\Gamma,$$

$$G_2(\mathbf{v}) = \int_{\Omega_2} \mathbf{f} \cdot \mathbf{v} d\Omega + \int_{(\Gamma_{out} \cup \Gamma_{w2}) \cap \partial\Omega_2} \mathbf{g}_{out} \cdot \mathbf{v} d\Gamma.$$

Assume that the problem (3.3.3) has a solution $\mathbf{u}, p$ that is infinitely differentiable with respect to ε:

$$\begin{cases} \mathbf{u} = \mathbf{u}_0 + \varepsilon \mathbf{u}_1 + \varepsilon^2 \mathbf{u}_2 + \dots \\ p = p_0 + \varepsilon p_1 + \varepsilon^2 p_2 + \dots \end{cases} \tag{3.3.4}$$

where $p_k \in L^2(\Omega), \mathbf{u}_k \in \mathbb{X},\ k \geq 0$. Using (3.2.3), (3.3.4) and small perturbation techniques we can derive the equations for $\mathbf{u}_k, p_k,\ k \geq 0$. In particular, for $k = 0$ $\mathbf{u}_0$ and p_0 satisfy the following zero-order problem, for which velocity and pressure are obtained without considering a shape variation:

$$\begin{cases} a(f_0; \mathbf{u}_0, \mathbf{v}) = b(f_0; p_0, \mathbf{v}) + G(f_0; \mathbf{v})\ \forall \mathbf{v} \in \mathbb{X}, \\ b(f_0; q, \mathbf{u}_0) = 0\ \forall q \in L^2(\Omega), \\ \mathbf{u}_0 = \mathbf{u}_f\ on\ \Gamma_{in} \cup \Gamma_{w_1} \cup \Gamma_{w_3}. \end{cases} \tag{3.3.5}$$

Note that the test functions $\mathbf{v},\ q$ in (3.3.3) can be assumed to be independent of ε in the sequel.
Correspondingly we define:

$$\mathcal{R}_{obs,0} := \mathcal{R}(f_0)\mathbf{u}_0 \tag{3.3.6}$$

representing the vorticity mapped into the simple (reference) domain. For $k = 1$ the functions $\mathbf{u}_1$ and p_1, representing small perturbations in the velocity and pressure fields, respectively, are the solution of the equations:

$$\begin{cases} a(f_0; \mathbf{u}_1, \mathbf{v}) = b(f_0; p_1, \mathbf{v}) + \frac{\partial}{\partial \varepsilon} b(f; p_0, \mathbf{v})|_{\varepsilon=0} + \\ + \frac{\partial}{\partial \varepsilon} G(f; \mathbf{v})|_{\varepsilon=0} - \frac{\partial}{\partial \varepsilon} a(f; \mathbf{u}_0, \mathbf{v})|_{\varepsilon=0}\ \forall \mathbf{v} \in \mathbb{X}, \\ b(f_0; q, \mathbf{u}_1) + \frac{\partial}{\partial \varepsilon} b(f; q, \mathbf{u}_0)|_{\varepsilon=0} = 0\ \forall q \in L^2(\Omega), \\ \mathbf{u}_1 = \mathbf{0}\ on\ \Gamma_{in} \cup \Gamma_{w_1} \cup \Gamma_{w_3}, \end{cases} \tag{3.3.7}$$

where we have some new terms depending on the new configuration (f_1) but evaluated with respect to the zero-order solution $\mathbf{u}_0$ and p_0:

$$\frac{\partial}{\partial \varepsilon} b(f; p_0, \mathbf{v})|_{\varepsilon=0} = b_f(f_1, p_0, \mathbf{v}) = \int_{\Omega_1} \frac{f_1}{\beta} p_0 \mathcal{D}(f_0)\mathbf{v} d\Omega + \int_{\Omega_1} \frac{f_0}{\beta} p_0 \mathcal{D}_f(f_1, \mathbf{v}) d\Omega,$$

with

$$\mathcal{D}_f(f_1, \mathbf{v}) = \frac{\partial}{\partial \varepsilon} \mathcal{D}(f)\mathbf{v}|_{\varepsilon=0} = -\big[y\big(\frac{f_{1,x} f_0 - f_{0,x} f_1}{f_0^2}\big)\frac{\partial \hat{u}}{\partial y} + \frac{\beta f_1}{f_0^2}\frac{\partial \hat{v}}{\partial y}\big]$$

$$\mathcal{D}_f(f_1, \mathbf{u}_0) = \frac{\partial}{\partial \varepsilon} \mathcal{D}(f)\mathbf{u}_0|_{\varepsilon=0} (:= \mathcal{D}_f f_1\ in\ the\ sequel),$$

$$\frac{\partial}{\partial \varepsilon} G(f; \mathbf{v})|_{\varepsilon=0} = G_1(f_1; \mathbf{v}) = \int_{\Omega_1} \frac{f_1}{\beta} \mathbf{f} \cdot \mathbf{v} d\Omega,$$

$$\frac{\partial}{\partial \varepsilon} a(f; \underline{v}_0, \mathbf{v})|_{\varepsilon=0} = a_f(f_1; \mathbf{u}_0, \mathbf{v}) = \int_{\Omega_1} \frac{f_1 \nu}{\beta} \big(\big(\frac{\partial \mathbf{u}_0}{\partial x} - \frac{y f_{0,x}}{f_0}\frac{\partial \mathbf{u}_0}{\partial y}\big) \cdot \big(\frac{\partial \mathbf{v}}{\partial x} - \frac{y f_{0,x}}{f_0}\frac{\partial \mathbf{v}}{\partial y}\big) + \frac{\beta^2}{f_0^2}\frac{\partial \mathbf{u}_0}{\partial y} \cdot \frac{\partial \mathbf{v}}{\partial y}\big) d\Omega +$$

$$- \int_{\Omega_1} \frac{f_0 \nu}{\beta} y \frac{(f_{1,x} f_0 - f_{0,x} f_1)}{f_0^2} \big(\frac{\partial \mathbf{u}_0}{\partial y} \cdot \big(\frac{\partial \mathbf{v}}{\partial x} - \frac{y f_{0,x}}{f_0}\frac{\partial \mathbf{v}}{\partial y}\big) + \big(\frac{\partial \mathbf{u}_0}{\partial x} - \frac{y f_{0,x}}{f_0}\frac{\partial \mathbf{u}_0}{\partial y}\big) \cdot \frac{\partial \mathbf{v}}{\partial y}\big) d\Omega$$

$$-\int_{\Omega_1}\frac{f_0\nu}{\beta}\Big(\frac{2\beta^2 f_1}{f_0^3}\Big)\frac{\partial \mathbf{u}_0}{\partial y}\cdot\frac{\partial \mathbf{v}}{\partial y}d\Omega.$$

Therefore the problem for $\mathbf{u}_1,\ p_1$ reads as follows: find $\mathbf{u}_1\in\mathbb{X},\ p_1\in L^2(\Omega)$ s.t.:

$$\begin{cases} a(f_0;\mathbf{u}_1,\mathbf{v})-b(f_0;p_1,\mathbf{v})=b_f(f_1;p_0,\mathbf{v})+G_1(f_1;\mathbf{v})-a_f(f_1;\mathbf{u}_0,\mathbf{v})\ \forall\mathbf{v}\in\mathbb{X},\\ b(f_0;q,\mathbf{u}_1)+b_f(f_1;q,\mathbf{u}_0)=0\ \forall q\in L^2(\Omega), \end{cases} \tag{3.3.8}$$

This is a generalized Stokes problem (see Galdi [40]) representing the perturbations in the system due to the induced shape variation. By a similar technique we can derive the equations for $\mathbf{u}_k,\ p_k$ with $k\geq 2$. However we will not further carry on this development in this work. At the end of the chapter in Section 3.10 we are going to discuss how to deal with higher orders and non-linear problems. The general guidelines to build the problem at different order is based on the idea of replacing in the state equations the development of velocity, pressure and shape and then solving the problem at various orders of ε, see also Hinch [56] and Kevorkian [71]. In particular, our shape optimization and control problem will be considered as a first-order problem and it will deal with flow perturbation.

3.4 The shape optimization problem

Suppose now that in (3.3.7) the function $f_1(x)$ is unknown and so are $\mathbf{u}_1,\ p_1$. To complete problem (3.3.7) we will have to formulate some "additional equations", or, alternatively, we should require that f_1 be determined by minimizing a suitable cost functional.
Problem (3.2.2) can be supplemented by the "additional equation":

$$\mathcal{C}(f,\mathbf{u},p)=0 \tag{3.4.1}$$

where $\mathcal{C}$ is an operator (linear or nonlinear) defined on $H_0^1(x_1,x_2)\times\mathbb{X}\times L^2(\Omega)$. (We consider now $f\ \in H_0^1$ for convenience). We assume $\mathcal{C}$ have a regular dependence on $f,\mathbf{u},p$. Using the representations (3.2.3) and (3.3.4) we derive from (3.4.1) the following equation:

$$\mathcal{C}(f,\mathbf{u},p)=\mathcal{C}_0(f_0,\mathbf{u}_0,p_0)+\varepsilon\mathcal{C}_1(f_1,\mathbf{u}_1,p_1)+\mathcal{O}(\varepsilon^2)=0,\quad\forall\varepsilon\in[-\varepsilon_0,\varepsilon_0] \tag{3.4.2}$$

where

$$\mathcal{C}_1(f_1,\mathbf{u}_1,p_1):=\frac{\partial\mathcal{C}}{\partial\varepsilon}(f,\mathbf{u},p)|_{\varepsilon=0}. \tag{3.4.3}$$

If we assume, for example, that the data of our problems are such that $\mathcal{C}_0(f_0,\mathbf{u}_0,p_0)=0$, then we can use

$$\mathcal{C}_1(f_1,\mathbf{u}_1,p_1)=0 \tag{3.4.4}$$

as additional equation to complete (3.3.7). An alternative approach would consist in replacing the *exact controllability* equation (3.4.4) by the following minimization problem:

$$\inf_{f_1}\int_\Omega\frac{f_0}{\beta}|\mathcal{C}_1(f_1,\mathbf{u}_1,p_1)|^2d\Omega, \tag{3.4.5}$$

where we assume that $\mathcal{C}_1$ has image in $L^2(\Omega)$. Note that (3.4.5) is a weak statement of (3.4.4).

In the next sections we apply the approach described above for the completion of (3.3.7); moreover we will use the following special choice of (3.4.1):

$$\mathcal{C}(f,\mathbf{u}) := (\nabla\times\mathbf{u})\circ \mathrm{T}_f^{-1} - \mathcal{R}_{obs,\varepsilon}\ in\ \Omega_{wd}\subseteq\Omega, \tag{3.4.6}$$

where Ω_{wd} is a suitable subset of Ω in which we want our additional equation (or our "control") to take place. In our application Ω_{wd} is the down-field zone of the domain, where the the bypass is hosted into the artery.
Moreover

$$\mathcal{R}_{obs,\varepsilon} = \mathcal{R}_{obs,0} + \varepsilon\mathcal{R}_{obs,1} + \varepsilon^2\mathcal{R}_{obs,2} + \dots\ ,\ with\ \mathcal{R}_{obs,0} := ((\nabla\times\mathbf{u}_0)\circ \mathrm{T}_{f_0}^{-1}). \tag{3.4.7}$$

Then we have: $\mathcal{C}_0(f_0,\mathbf{u}_0) = 0$ (to consider the additional equation only for the first-order problem), while the equation (3.4.4) reads:

$$\mathcal{C}_1(f_1,\mathbf{u}_1) = \mathcal{R}(f_0)\mathbf{u}_1 + m_1\mathcal{R}_f f_1 - \mathcal{R}_{obs,1} = 0\ in\ \Omega_{wd}, \tag{3.4.8}$$

where

$$\mathcal{R}(f_0)\mathbf{u}_1 = (\nabla\times\mathbf{u}_1)\circ \mathrm{T}_{f_0}^{-1}(x,y) = \frac{\partial v_1}{\partial x} - \frac{y f_{0,x}}{f_0}\frac{\partial v_1}{\partial y} - \frac{\beta}{f_0}\frac{\partial u_1}{\partial y},$$

$$\mathcal{R}_f f_1 := \mathcal{R}_f(f_1,\mathbf{u}_0) = -y\frac{(f_{1,x}f_0 - f_{0,x}f_1)}{f_0^2}\frac{\partial v_0}{\partial y} + \frac{\beta f_1}{f_0^2}\frac{\partial u_0}{\partial y},$$

which represents two contributes to vorticity due to flow perturbation ($\mathbf{u}_1$) and shape perturbation f_1, respectively. Finally, $\mathcal{R}_{obs,1}$ is a given function (for example $\mathcal{R}_{obs,1} = -\mathcal{R}_{obs,0}$ to reduce vorticity by a shape optimization process on f_1 and flow perturbation $\mathbf{u}_1$ and p_1). Therefore we have the problem on the domain reported in Figure 3.4: find $\mathbf{u}_1\in\mathbb{X}$, $p_1\in L^2(\Omega)$, $f_1\in H_0^1(x_1,x_2)$ s.t.

$$\begin{cases} a(f_0;\mathbf{u}_1,\mathbf{v}) = b(f_0;p_1,\mathbf{v}) + b_f(f_1;p_0,\mathbf{v}) + G_1(f_1;\mathbf{v}) - a_f(f_1;\mathbf{u}_0,\mathbf{v})\ \forall\mathbf{v}\in\mathbb{X}, \\ b(f_0;q,\mathbf{u}_1) + b_f(f_1;q,\mathbf{u}_0) = 0\ \forall q\in L^2(\Omega), \\ \mathcal{R}(f_0)\mathbf{u}_1 + m_1\mathcal{R}_f f_1 - \mathcal{R}_{obs,1} = 0\ in\ \Omega_{wd}. \end{cases} \tag{3.4.9}$$

Problem (3.4.9) is an "exact controllability problem". These kind of problems have solutions in some particular cases only. For this reason we replace (3.4.9) by the following optimal control problem: find $\mathbf{u}_1\in\mathbb{X}$, $p_1\in L^2(\Omega)$, $f_1\in H_0^1(x_1,x_2)$ s.t.

$$\begin{cases} a(f_0;\mathbf{u}_1,\mathbf{v}) - b(f_0;p_1,\mathbf{v}) = b_f(f_1;p_0,\mathbf{v}) + G_1(f_1;\mathbf{v}) - a_f(f_1;\mathbf{u}_0,\mathbf{v})\ \forall\mathbf{v}\in\mathbb{X}, \\ b(f_0;q,\mathbf{u}_1) + b_f(f_1;q,\mathbf{u}_0) = 0\ \forall q\in L^2(\Omega), \\ \inf_{f_1} = \frac{\alpha}{2}||f_1||^2_{H_0^1(x_1,x_2)} + \gamma_1 J_1(f_1,\underline{v_1}), \end{cases} \tag{3.4.10}$$

where

$$J_1(f_1,\mathbf{u}_1) = \frac{1}{2}\int_\Omega m_{wd}\frac{f_0}{\beta}(\mathcal{R}(f_0)\mathbf{u}_1 + m_1\mathcal{R}_f f_1 - \mathcal{R}_{obs,1})^2 d\Omega, \tag{3.4.11}$$

$\alpha = const \geq 0$ is a small regularization parameter, $\gamma_1 > 0$ is a weight coefficient, m_{wd} is the characteristic function of Ω_{wd}. Problem (3.4.10) is called "first-order problem" since it provides the solution of the first order terms in the developments (3.2.3) and (3.3.4).

Note that the third equation from (3.4.9) is considered in (3.4.10) in the least square sense; then when $\alpha = 0$ (3.4.10) represents the weak statement of problem (3.4.9). Otherwise the solution $v_1 = v_1(\alpha),\ p_1 = p_1(\alpha),\ f_1 = f_1(\alpha)$ of (3.4.10) will represent an approximate (regularized) solution of (3.4.9).
We will also consider a generalized optimal control problem, still given by (3.4.10); however now instead of J_1 we use

$$J(f_1, \mathbf{u}_1, p_1) = \gamma_1 J_1(f_1, \mathbf{u}_1) + \gamma_2 J_2(f_1, \mathbf{u}_1, p_1).$$

Here $\gamma_2 = const \geq 0$ is a weight coefficient, while $J_2(f_1, \mathbf{u}_1, p_1)$ is an additional functional that we assume to be quadratic. A few examples of $J_2(f_1, \mathbf{u}_1, p_1)$ follow.

Example 3.4.1

$$J_2(f_1, \mathbf{u}_1, p_1) := J_2(\mathbf{u}_1, p_1) = \frac{1}{2}(||p_1 - p_{out,1}||^2_{L^2(\Gamma_{out})} + \int_{\Gamma_{out}} |\mathbf{u}_1 - \mathbf{u}_{out,1}|^2 d\Gamma) \qquad (3.4.12)$$

where $p_{out}, \mathbf{u}_{out}$ are given.

Example 3.4.2 *Now let Ω_{obs} be a "small" subdomain of Ω with boundary Γ_{obs} and $\Gamma_{w_3} \subset \Gamma_{obs}$:*

$$\Omega_{obs} = (0, A) \times (-\beta_2, -\beta_2 + \delta),\ with\ 0 < \delta \ll \beta_1.$$

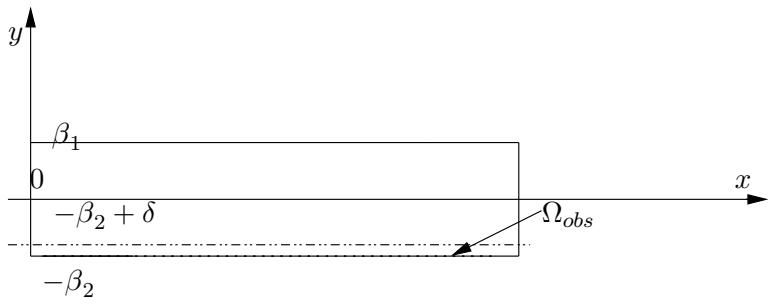

Figure 3.5: Subdomain Ω_{obs}.

If $\Omega = \Omega_1$ (i.e. $\beta_2 = 0$), we can take

$$J_2(f_1, \mathbf{u}_1, p_1) := J_2(\mathbf{u}_1) = \frac{1}{2} \int_{\Omega_{obs}} |\mathbf{u}_1 - \mathbf{u}_{obs,1}|^2 \frac{f_0}{\beta} d\Omega, \qquad (3.4.13)$$

where $\mathbf{u}_{obs}$ is a prescribed vector-function.

Example 3.4.3 *Take $\Omega_1 = \Omega$, and use: $\int_\Omega p_1 d\Omega = 0$,*

$$J_2(f_1, \mathbf{u}_1, p_1) := J_2(\mathbf{u}_1) = \frac{1}{2} \int_{\Gamma_{w_3}} |\frac{\partial \mathbf{u}_1}{\partial \hat{\mathbf{n}}} - \mathbf{g}_{1,obs}|^2 d\Gamma, \qquad (3.4.14)$$

for a given $\mathbf{g}_{1,obs}$.

Example 3.4.4 *Finally we may consider:*

$$\Omega_1 = \Omega,$$
$$J_2(f_1, \mathbf{u}_1, p_1) := J_2(\mathbf{u}_1) = \frac{1}{2}\int_{\Omega_{obs}} \frac{f_0}{\beta}|\frac{\beta}{f_0}\frac{\partial \mathbf{u}_1}{\partial y} - \mathbf{g}_{2,obs}|^2 d\Omega, \tag{3.4.15}$$

with a given $\mathbf{g}_{2,obs}$.

Remark 3.4.1 *The term J_2 can be considered as an "overdetermination" of the problem, as in principle it allows the control of further quantities of physical interest. Using such a J_2 makes easier to prove uniqueness but more troublesome to analyze existence for the optimal control problem.*

3.5 The variational equations of the optimal control problem

While considering (3.4.10) we have taken into cosideration the simple domain $\tilde{\Omega}$ of Figure 3.4. Another possibility consists of using the new variable transformation

$$\mathbf{x} = T_{f_0}^{-1}(\tilde{\mathbf{x}}),\ \tilde{\mathbf{x}} \in \tilde{\Omega},\ \mathbf{x} \in \Omega_0, \tag{3.5.1}$$

which is the identity in $\tilde{\Omega}_2$, while $T_{f_0}^{-1}(\tilde{x}, \tilde{y}) = (\tilde{x}, \frac{f_0(\tilde{x})}{\beta}\tilde{y})$ in $\tilde{\Omega}_1$. After applying (3.5.1) we will work in the "unperturbed" domain Ω_0 (see Figure 3.6) where the expressions for the bilinear forms in (3.4.10) become simpler. Indeed, with the help of transformation (3.5.1), problem

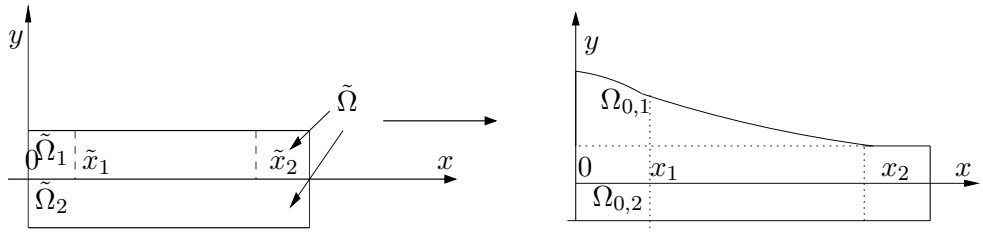

Figure 3.6: Transformation of the simple domain into the unperturbed domain Ω_0 .

(3.4.10) reads upon its reformulation in Ω_0: find $\mathbf{u} := \mathbf{u}_1$, $p := p_1$,$f := f_1$[1] s.t.

$$\begin{cases} a_0(\mathbf{u}, \mathbf{v}) - b_0(p, \mathbf{v}) = b_f(f; p_0, \mathbf{v}) + G_1(f; \mathbf{v}) - a_f(f; \mathbf{u}_0, \mathbf{v})\ \forall \mathbf{v} \in \mathbb{X} \\ b_0(q, \mathbf{u}) + b_f(f; q, \mathbf{u}_0) = 0\ \forall q \in L^2(\Omega), \\ \inf_f = \frac{\alpha}{2}||f||^2_{H_0^1(x_1,x_2)} + J(f, \mathbf{u}, p), \end{cases} \tag{3.5.2}$$

[1]From now on we denote $\mathbf{u}_1 = \mathbf{u},\ p_1 = p,\ f_1 = f$ however we should keep in mind that now $\mathbf{u}, p, f$ represent the "first corrections" of $\mathbf{u}_0,\ p_0,\ f_0$ on the unperturbed domain.

where

$$a_0(\mathbf{u},\mathbf{v}) = \int_{\Omega_0} \nu\big(\frac{\partial \mathbf{u}}{\partial x}\cdot\frac{\partial \mathbf{v}}{\partial x} + \frac{\partial \mathbf{u}}{\partial y}\cdot\frac{\partial \mathbf{v}}{\partial y}\big)d\Omega.$$

$$b_0(p,\mathbf{v}) = \int_{\Omega_0} p\nabla\cdot\mathbf{v}d\Omega,$$

$$b_f(f,p_0,\mathbf{v}) = \int_{\Omega_{0,1}} p_0\mathcal{D}_f(f,\mathbf{v})d\Omega + \int_{\Omega_{0,1}} \frac{f}{f_0}p_0\nabla\cdot\mathbf{v}d\Omega,$$

$$\mathcal{D}_f(f,\mathbf{v}) = -\big[y\big(\frac{f_x f_0 - f_{0,x}f}{f_0^2}\big)\frac{\partial \hat{u}}{\partial y} + \frac{f}{f_0}\frac{\partial \hat{v}}{\partial y}\big],$$

$$\mathcal{D}_f(f,v_0) := \mathcal{D}_f f,$$

$$G_1(f;\mathbf{v}) = \int_{\Omega_{0,1}} \frac{f}{f_0}\mathbf{f}\cdot\mathbf{v}d\Omega,$$

$$a_f(f;\mathbf{u}_0,\mathbf{v}) = \int_{\Omega_{0,1}} \frac{f\nu}{f_0}\nabla\mathbf{u}_0\cdot\nabla\mathbf{v}d\Omega - \int_{\Omega_{0,1}} \nu y\frac{(f_x f_0 - f_{0,x}f)}{f_0^2}\big(\frac{\partial \mathbf{u}_0}{\partial y}\cdot\frac{\partial \mathbf{v}}{\partial x} + \frac{\partial \mathbf{u}_0}{\partial x}\cdot\frac{\partial \mathbf{v}}{\partial y}\big)d\Omega +$$

$$- \int_{\Omega_{0,1}} \frac{2f\nu}{f_0}\frac{\partial \mathbf{u}_0}{\partial y}\cdot\frac{\partial \mathbf{v}}{\partial y}d\Omega.$$

$$J(f,\mathbf{u},p) = \gamma_1 J_1(f,\mathbf{u}) + \gamma_2 J_2(f,\mathbf{u},p),$$

$$J_1(f,\mathbf{u}) = \frac{1}{2}\int_{\Omega_0} m_{wd}|\nabla\times\mathbf{u} + m_1\mathcal{R}_f f - \mathcal{R}_{obs,1}|^2 d\Omega,$$

$$\mathcal{R}_f f := \mathcal{R}_f(f,\mathbf{u}_0) = -y\frac{(f_x f_0 - f_{0,x}f)}{f_0^2}\frac{\partial v_0}{\partial y} + \frac{f}{f_0}\frac{\partial u_0}{\partial y}.$$

$$\nabla\times\mathbf{u} = \frac{\partial v}{\partial x} - \frac{\partial u}{\partial y},\ \nabla\cdot\mathbf{u} = \frac{\partial u}{\partial x} + \frac{\partial v}{\partial y}$$

and $J_2(f,\mathbf{u},p)$ are given by corresponding expressions. At this step we have developed our problem in two levels (zero and first order) and rewritten the first order problem in a simpler way on the domain Ω_0. In order to derive the operator form of problem (3.5.2) and formulate the problem in an optimal control setting we introduce the following functional spaces:

$$\mathbb{X} \subseteq (L^2(\Omega))^2 \subseteq \mathbb{X}^*, \mathbb{H}^p \subseteq L^2(\Omega) \subseteq \mathbb{H}^{p*},$$

$$\mathbb{H}_f \ \subseteq L^2(x_1,x_2) \subseteq \mathbb{H}_f^*,$$

$$\mathbb{W} := \mathbb{X}\times\mathbb{H}^p \subseteq \mathbb{H}_0 := (L^2(\Omega))^2 \times L^2(\Omega) \subseteq \mathbb{W}^*,$$

where $\mathbb{X}^*$, $\mathbb{H}^{p*}$, $\mathbb{H}_f^*$ and $\mathbb{W}^*$ are the dual spaces of $\mathbb{X}$, $\mathbb{H}^p$, $\mathbb{H}_f$ and $\mathbb{W}$, respectively. Let us reformulate (3.5.2) in the following form: find $\underline{\Phi} := (\mathbf{u},p) \in \mathbb{W} = (\mathbb{X}\times\mathbb{H}^p)$, $f \in \mathbb{H}^f$, s.t.

$$\begin{cases} \mathcal{L}(\underline{\Phi},\hat{\underline{\Phi}}) = B(f,\hat{\underline{\Phi}})\ \forall\hat{\underline{\Phi}} = (\mathbf{v},q) \in \mathbb{W}, \\ \inf_{f\in\mathbb{H}_f} = \frac{\alpha}{2}||f||^2_{H^1} + J(f,\underline{\Phi}), \end{cases} \tag{3.5.3}$$

where

$$\mathcal{L}(\underline{\Phi},\hat{\underline{\Phi}}) := a_0(\mathbf{u},\mathbf{v}) - b_0(p,\mathbf{v}) + b_0(q,\mathbf{v}),$$

$$B(f,\hat{\underline{\Phi}}) := b_f(f,p_0,\mathbf{v}) + G_1(f,\mathbf{v}) - a_f(f,\mathbf{u}_0,\mathbf{v}) - b_f(f,q,\mathbf{u}_0).$$

Should $\underline{\Phi}$ be a solution of (3.5.3), then

$$\alpha(f,\hat{f})_{\mathbb{H}_f} + \langle J'_\Phi(f,\underline{\Phi}),\underline{\Phi}_{\hat{f}}\rangle + \langle J'_f(f,\underline{\Phi}),\hat{f}\rangle = 0, \tag{3.5.4}$$

for any $\hat{f} \in \mathbb{H}_f$ ($\hat{f}$ is the independent variation), where $\underline{\Phi}_{\hat{f}} \in \mathbb{W}$ satisfies the following equation:

$$\mathcal{L}(\underline{\Phi}_{\hat{f}},\hat{\underline{\Phi}}) = B(\hat{f},\hat{\underline{\Phi}}) \ \forall \hat{\underline{\Phi}} \in \mathbb{W}. \tag{3.5.5}$$

In (3.5.4), $J'_\Phi = \frac{\partial J}{\partial \Phi}$ and $J'_f = \frac{\partial J}{\partial f}$ are partial derivatives of J, while $\langle Q,\underline{\Phi}\rangle$ is the duality between $\mathbb{W}$ and $\mathbb{W}^*$ and $\langle g,f\rangle$ the duality between $\mathbb{H}_f$ and $\mathbb{H}_f^*$. Then we can rewrite (3.5.3) as a system of "optimality conditions":

$$\begin{cases} \mathcal{L}(\underline{\Phi},\hat{\underline{\Phi}}) = B(f,\hat{\underline{\Phi}}) \ \forall \hat{\underline{\Phi}} \in \mathbb{W}, \\ \alpha(f,\hat{f})_{\mathbb{H}^f} + \langle J'_\Phi(f,\underline{\Phi}),\underline{\Phi}_{\hat{f}}\rangle + \langle J'_f(f,\underline{\Phi}),\hat{f}\rangle = 0 \ \forall \hat{f} \in \mathbb{H}_f. \end{cases} \tag{3.5.6}$$

The element $\underline{\Phi}_{\hat{f}}$ can be eliminated from (3.5.6) by introducing the adjoint problem: find $\underline{Q} := (\mathbf{q},\sigma)^T \in \mathbb{W}$ s.t.

$$\mathcal{L}^*(\underline{Q},\hat{\underline{W}}) := \mathcal{L}(\hat{\underline{W}},\underline{Q}) = \langle J'_\Phi(f,\underline{\Phi}),\hat{\underline{W}}\rangle \ \forall \hat{\underline{W}} \in \mathbb{W}. \tag{3.5.7}$$

Since $\underline{\Phi}_{\hat{f}} \in \mathbb{W}$ we can choose $\hat{\underline{W}} = \underline{\Phi}_{\hat{f}}$ in (3.5.7), yielding

$$\langle J'_\Phi(f,\underline{\Phi}),\underline{\Phi}_{\hat{f}})\rangle = \mathcal{L}(\underline{\Phi}_{\hat{f}},\underline{Q}) = B(\hat{f},\underline{Q}) \tag{3.5.8}$$

and the system of variational equations (3.5.6) reads now as follows:

$$\begin{cases} \mathcal{L}(\underline{\Phi},\hat{\underline{\Phi}}) = B(f,\hat{\underline{\Phi}}) \ \forall \hat{\underline{\Phi}} \in \mathbb{W}, \\ \mathcal{L}^*(\underline{Q},\hat{\underline{W}}) = \langle J'_\Phi(f,\underline{\Phi}),\hat{\underline{W}}\rangle \ \forall \hat{\underline{W}} \in \mathbb{W}, \\ \alpha(f,\hat{f})_{\mathbb{H}_f} + B(\hat{f},\underline{Q}) + \langle J'_f(f,\underline{\Phi}),\hat{f}\rangle = 0 \ \forall \hat{f} \in \mathbb{H}_f. \end{cases} \tag{3.5.9}$$

The first equation is the state equation, the second is the adjoint one and the third equation is the optimality condition. Let us define the following operators (see Lions and Magenes [84], Lions [82] and Agoshkov [6]):

$$L : \mathbb{W} \to \mathbb{W}^*, \ (L\underline{\Phi},\hat{\underline{\Phi}})_{\mathbb{H}_0} := \mathcal{L}(\underline{\Phi},\hat{\underline{\Phi}}), \ \forall \underline{\Phi}, \ \hat{\underline{\Phi}} \in \mathbb{W},$$

$$L^* : \mathbb{W} \to \mathbb{W}^*, \ (\hat{\underline{W}},L^*\underline{Q})_{\mathbb{H}_0} = (L\hat{\underline{W}},\underline{Q})_{\mathbb{H}_0}, \forall \underline{Q},\hat{\underline{W}} \in \mathbb{W},$$

$$B : \mathbb{H}_f \to \mathbb{W}^*, \ (Bf,\underline{\Phi})_{\mathbb{H}_0} = B(f,\underline{\Phi}) \ \forall f,\underline{\Phi},$$

$$\Lambda_w : \ \mathbb{W}^* \to \mathbb{W}^*, \ (\Lambda_w J_\Phi(f,\underline{\Phi}),\hat{\underline{W}})_{\mathbb{H}_0} := \langle J'_\Phi(f,\underline{\Phi}),\hat{\underline{W}}\rangle,$$

$$\Lambda_f : \ \mathbb{H}_f^* \to \mathbb{H}_f^*, \ (\Lambda_f J_f(f,\underline{\Phi}),\hat{f})_{L^2(x_1,x_2)} := \langle J'_f(f,\underline{\Phi}),\hat{f}\rangle.$$

Now the system (3.5.9) can be written in operator form as follows:

$$\begin{cases} L\underline{\Phi} = Bf \ \ (in \ \mathbb{W}^*), \\ L^*\underline{Q} = \Lambda_w J_\Phi(f,\underline{\Phi}) \ \ (in \ \mathbb{W}^*), \\ \alpha\Lambda_c f + B^*\underline{Q} + \Lambda_f J_f(f,\underline{\Phi}) = 0 \ \ (in \ (\mathbb{H}_f)^*), \end{cases} \tag{3.5.10}$$

where Λ_c is the extension to $\mathbb{H}_f$ of the following operator $\Lambda_{c,0}$ (defined on $H^2 \cap \mathbb{H}_f$):

$$\Lambda_{c,0} f := -f_{xx} + f,$$

Remark 3.5.1 *The system (3.5.10) with a cost functional $J(\underline{\Phi}) = \|C\underline{\Phi} - \underline{\Psi}\|^2_{\mathbb{H}_{ob}}$, where $C : \mathbb{W} \to \mathbb{H}_{ob}$ is a given operator and $\underline{\Psi} \in \mathbb{H}_{ob}$ a given observation function, is analyzed in Agoshkov [6]. In this case $J'_f = 0$ and $\Lambda_w J'_\Phi(f, \underline{\Phi}) = C^*(C\underline{\Phi} - \underline{\Psi})$ and we find a "classical" optimal control problem in the sense of J.L. Lions' formulation.*

3.6 Existence and uniqueness results

We analyze the particular cases where the cost functional J is chosen as outlined by Example 3.4.1 to obtain some uniqueness and existence results. See also Isakov [61].

Let J be the functional J_2 of Example 3.4.1. Then

$$J(f, \underline{\Phi}) = J(f, \mathbf{u}, p) = \frac{\gamma_1}{2} \int_{\Omega_0} m_{wd} |\nabla \times \mathbf{u} + m_1 \mathcal{R}_f f - \mathcal{R}_{obs,1}|^2 d\Omega + \tag{3.6.1}$$

$$+ \frac{\gamma_2}{2} \int_{\Gamma_{out}} \Big(|p - p_{out}|^2 + |\mathbf{u} - \mathbf{u}_{out}|^2 \Big) d\Gamma$$

To study the problem in this case we assume that $\Omega_{wd} = \Omega_0$ and we define:

$$\mathbb{X} := \{\mathbf{u} : \mathbf{u} \in (H^2(\Omega))^2, \mathbf{u} = \mathbf{0} \text{ on } \Gamma_{in} \cup \Gamma_{w_1} \cup \Gamma_{w_3}\},$$

$$\mathbb{H}^p := H^1(\Omega_0), \ \mathbb{H}_f \ := H^2(x_1, x_2) \cap H^1_0(x_1, x_2).$$

Here we consider H^2 as velocity space in order to be allowed to use the uniqueness continuation theorem (see Weck [162], Fabre and Lebeau [35]). The derivatives $J'_\Phi(f, \underline{\Phi})$ and $J'_f(f, \underline{\Phi})$ become

$$\langle J'_\Phi(f, \underline{\Phi}), \hat{\underline{\Phi}} \rangle = \gamma_1 \int_{\Omega_0} m_{wd} (\nabla \times \mathbf{u} + m_1 \mathcal{R}_f f - \mathcal{R}_{obs,1}) \cdot (\nabla \times \mathbf{v}) d\Omega +$$

$$+ \gamma_2 \int_{\Gamma_{out}} (p - p_{out}) q d\Gamma + \gamma_2 \int_{\Gamma_{out}} (\mathbf{u} - \mathbf{u}_{out}) \cdot \mathbf{v} d\Gamma,$$

$$\langle J'_f(f, \underline{\Phi}), \hat{f} \rangle = \gamma_1 \int_{\Omega_0} m_{wd} (\nabla \times \mathbf{u} + m_1 \mathcal{R}_f f - \mathcal{R}_{obs,1}) \mathcal{R}_f \hat{f} d\Omega,$$

$$\forall \ \hat{\underline{\Phi}} = (\mathbf{v}, q)) \text{ and } \forall \ \hat{f}.$$

The system of variational equations (3.5.6) reads: find $\mathbf{u}_f \in \mathbb{X}, \ p_f \in \mathbb{H}^p$

$$\begin{cases} a_0(\mathbf{u}_f, \mathbf{v}) = b_0(p_f, \mathbf{v}) + F(f, \mathbf{v}) \ \forall \mathbf{v} \in \mathbb{X}, \\ b_0(q, \mathbf{u}_f) + b_f(f; q, \mathbf{u}_0) = 0 \ \forall q \in \mathbb{H}^p(\Omega), \\ \alpha(f, \hat{f})_{\mathbb{H}_f} + \gamma_1 \int_{\Omega_0} m_{wd} (\nabla \times \mathbf{u}_f + m_1 \mathcal{R}_f f - \mathcal{R}_{obs,1}) \cdot (\nabla \times \mathbf{u}_{\hat{f}} + m_1 \mathcal{R}_f \hat{f}) d\Omega + \\ + \gamma_2 \int_{\Gamma_{out}} ((p_f - p_{out}) p_{\hat{f}} + (\mathbf{u}_f - \mathbf{u}_{out}) \cdot \mathbf{u}_{\hat{f}}) d\Gamma = 0 \ \forall \ \hat{f} \in \mathbb{H}_f, \end{cases} \tag{3.6.2}$$

where

$$F(f,\mathbf{v}) := b_f(f,p_0,\mathbf{v}) + G_1(f,\mathbf{v}) - a_f(f,\mathbf{u}_0,\mathbf{v}),$$

and for every $\hat{f}$, $\mathbf{u}_{\hat{f}} = \mathbf{u}_f(\hat{f})$, $p_{\hat{f}} = p_f(\hat{f})$ denote the solution of the system given by the first and second equations in (3.6.2) corresponding to a right end side $f = \hat{f}$. The system (3.5.9) is: find $\mathbf{u}_f \in \mathbb{X}$, $p_f \in \mathbb{H}^p$

$$\left\{\begin{array}{l} a_0(\mathbf{u}_f,\mathbf{v}) = b_0(p_f,\mathbf{v}) + F(f,\mathbf{v})\ \forall \mathbf{v} \in \mathbb{X}, \\ b_0(q,\mathbf{u}_f) + b_f(f;q,\mathbf{u}_0) = 0\ \forall q \in \mathbb{H}^p(\Omega), \\ a_0(\hat{\mathbf{q}},\mathbf{q}) = -b_0(\sigma,\hat{\mathbf{q}}) + \gamma_1 \int_{\Omega_0} m_{wd}(\nabla\times\mathbf{u}_f + m_1\mathcal{R}_f f - \mathcal{R}_{obs,1})\cdot(\nabla\times\hat{\mathbf{q}})d\Omega + \\ +\gamma_2 \int_{\Gamma_{out}} (\mathbf{u}_f - \mathbf{u}_{out})\cdot\hat{\mathbf{q}} d\Gamma\ \forall \hat{\mathbf{q}} \in \mathbb{X}, \\ -b_0(\hat{\sigma},\mathbf{q}) = \gamma_2 \int_{\Gamma_{out}} (p_f - p_{out})\hat{\sigma} d\Gamma\ \forall \hat{\sigma} \in \mathbb{H}^p, \\ \alpha(f,\hat{f})_{\mathbb{H}_f} + F(\hat{f},\mathbf{q}) - b_f(\hat{f};\sigma,\mathbf{u}_0) + \\ +\gamma_1 \int_{\Omega_0} m_{wd}(\nabla\times\mathbf{u}_f + m_1\mathcal{R}_f f - \mathcal{R}_{obs,1}) m_1\mathcal{R}_f\hat{f} d\Omega = 0\ \forall \hat{f} \in \mathbb{H}_f. \end{array}\right. \tag{3.6.3}$$

In the sequel we assume that the generalized Stokes problem (3.3.7) has a unique solution for any given $\mathbf{u}_0$, p_0 (the solution in the unperturbed domain Ω_0) and for each $f \in \mathbb{H}_f$. (See Galdi [40], Fabre and Lebeau [36], Girault and Raviart [43]).
Consider now the problem (3.6.3) for $\alpha > 0$.

Proposition 3.6.1 *For any $\alpha > 0$ problem (3.6.3) has a unique solution for any given $\underline{\mathcal{R}}_{obs,1}$.*

Proof. Following Agoshkov [6], we formally invert L and L^* in the first and second equations of (3.5.10) then we substitute $\underline{\Phi}$, $\underline{Q}$ into the third equation and we obtain the following weak problem: for $f \in \mathbb{H}_f$:

$$\alpha(f,\hat{f})_{\mathbb{H}_f} + (Af, A\hat{f})_{L^2(x_1,x_2)} = (G, A\hat{f})_{L^2(x_1,x_2)}\ \forall \hat{f} \in \mathbb{H}_f, \tag{3.6.4}$$

where A is a linear operator, which depends on previous operators from variational equations, while G will depend on the data. More precisely from (3.6.2) we obtain:

$$(f,\hat{f})_{\mathbb{H}_f} = (\Lambda_f f, \hat{f})_{L^2(x_1,x_2)},$$

$$(Af, A\hat{f})_{L^2(x_1,x_2)} = \gamma_1 \int_\Omega m_{wd}(\nabla\times\mathbf{u} + m_1\mathcal{R}_f f)\cdot(\nabla\times\mathbf{u}_{\hat{f}} + m_1\mathcal{R}_f\hat{f}) d\Omega +$$

$$+\gamma_2 \int_{\Gamma_{out}} (pp_{\hat{f}} + \mathbf{u}\cdot\mathbf{u}_{\hat{f}}) d\Gamma,$$

$$(G, A\hat{f})_{L^2(x_1,x_2)} = \gamma_1 \int_\Omega m_{wd}\mathcal{R}_{obs,1}\cdot(\nabla\times\mathbf{u}_{\hat{f}} + m_1\mathcal{R}_f\hat{f}) d\Omega + \gamma_2 \int_{\Gamma_{out}} (p_{out}p_{\hat{f}} + \mathbf{u}_{out}\cdot\mathbf{u}_{\hat{f}}) d\Gamma,$$

where $\underline{\Phi} = (\mathbf{u},p) = L^{-1}Bf$, $\underline{\Phi}_{\hat{f}} = (\mathbf{u}_{\hat{f}}, p_{\hat{f}}) = L^{-1}B\hat{f}, \forall \hat{f} \in \mathbb{H}_f$.
We see that problem (3.6.4) has a unique solution which satisfies $\|f\|^2_{\mathbb{H}_f} \le \|G\|^2/(2\alpha) < \infty$. Correspondingly, we can construct $\mathbf{u}$, p, $\mathbf{q}$, σ, which together with f provides the unique

solution of (3.6.3). □

Consider now the problem (3.6.3) with $\alpha = 0$.

Proposition 3.6.2 *Assume that: i) The solution of the generalized Stokes problem satisfies* $\left(\frac{\partial v_0}{\partial y}\right)^2 + \left(\frac{\partial u_0}{\partial y}\right)^2 > 0$ *at* $y = 0,\ x \in (x_1, x_2)$ *ii) problem (3.6.3) has a solution. Then the solution of (3.6.3) is unique in the class* $(H^2(\Omega))^2 \times H^1(\Omega) \times \mathbb{W}^{1,\infty}(x_1, x_2)$.

Proof. Let $(\mathbf{u}_1, \ldots, f_1)$ and $(\mathbf{u}_2, \ldots, f_2)$ be two solutions of (3.6.3). Then for $\mathbf{u} = \mathbf{u}_1 - \mathbf{u}_2, \ldots, f = f_1 - f_2$ from (3.6.2) we obtain:

$$\begin{cases} a_0(\mathbf{u}, \mathbf{v}) = b_0(p, \mathbf{v}) + F(f, \mathbf{v})\ \forall \mathbf{v} \in \mathbb{X}, \\ b_0(q, \mathbf{u}) + b_f(f; q, \mathbf{u}_0) = 0\ \forall q \in \mathbb{H}^p(\Omega), \\ \nabla \times \mathbf{u} + m_1 \mathcal{R}_f f = 0\ in\ \Omega, \\ p = 0,\ \mathbf{u} = 0\ on\ \Gamma_{out}. \end{cases} \tag{3.6.5}$$

Consider the second and third equation from (3.6.5) in $\Omega_{2,0}$

$$\nabla \cdot \mathbf{u} = 0,\ \nabla \times \mathbf{u} = 0\ in\ \Omega_{2,0}.$$

Then $\Delta \mathbf{u} = \mathbf{0}$ in $\Omega_{2,0}$. Considering $\mathbf{v}$ with $supp(\mathbf{v}) \subseteq \Omega_{2,0}$ from the first equation of (3.6.5) we find $\nabla p = \mathbf{0}$, then $p = const$ in $\Omega_{2,0}$ and $-p\hat{\mathbf{n}} + \nu \frac{\partial \mathbf{u}}{\partial \hat{\mathbf{n}}} = \mathbf{0}$ *on* Γ_{out}. Since $p = 0$ *on* Γ_{out} then $p = 0$ *in* $\Omega_{2,0}$ and $\nu \frac{\partial \mathbf{u}}{\partial \hat{\mathbf{n}}} = \mathbf{0}$ *on* Γ_{out} too. Consequently, $\mathbf{u}$ satisfies:

$$\Delta \mathbf{u} = \mathbf{0}\ in\ \Omega_{2,0},\ \mathbf{u} = \nu \frac{\partial \mathbf{u}}{\partial \hat{\mathbf{n}}} = \mathbf{0}\ on\ \Gamma_{out}.$$

This problem has only the trivial solution $\mathbf{u} = \mathbf{0}$ *in* $\Omega_{2,0}$. Since $\mathbf{u} \in (H^2(\Omega))^2$ then

$$\mathbf{u} = \frac{\partial \mathbf{u}}{\partial \hat{\mathbf{n}}} = \mathbf{0}\ on\ \Gamma_0 := \{(x, y) : y = 0, x_1 < x < x_2\}.$$

Consider now the second and third equations from (3.6.5) in $\Omega_{1,0}$:

$$\begin{cases} \nabla \cdot \mathbf{u} - \left[y\left(\frac{f_x f_0 - f_{0,x} f}{f_0^2}\right)\frac{\partial u_0}{\partial y} + \frac{f}{f_0}\frac{\partial v_0}{\partial y}\right] = 0\ in\ \Omega_{1,0}, \\ \nabla \times \mathbf{u} - \left[y\left(\frac{f_x f_0 - f_{0,x} f}{f_0^2}\right)\frac{\partial v_0}{\partial y} - \frac{f}{f_0}\frac{\partial u_0}{\partial y}\right] = 0\ in\ \Omega_{1,0}. \end{cases} \tag{3.6.6}$$

On Γ_0 we have:

$$\nabla \cdot \mathbf{u} - \frac{f}{f_0}\frac{\partial v_0}{\partial y} = 0,\ \nabla \times \mathbf{u} + \frac{f}{f_0}\frac{\partial u_0}{\partial y} = 0,$$

$$|f(x)| = f_0 \frac{\left[(\nabla \cdot \mathbf{u})^2 + (\nabla \times \mathbf{u})^2\right]^{1/2}}{\left[\left(\frac{\partial v_0}{\partial y}\right)^2 + \left(\frac{\partial u_0}{\partial y}\right)^2\right]^{1/2}}\ on\ \Gamma_0,$$

(the dependence of the right end side on x and y is understood). Since $\mathbf{u} = \frac{\partial \mathbf{u}}{\partial \mathbf{n}} = \frac{\partial \mathbf{u}}{\partial y} = 0 \; on \; \Gamma_0$, then

$$\nabla \cdot \mathbf{u}|_{y=0} = \frac{\partial u}{\partial x} + \frac{\partial v}{\partial y}|_{y=0} = 0, \; \nabla \times \mathbf{u}|_{y=0} = \frac{\partial v}{\partial y} - \frac{\partial u}{\partial x}|_{y=0} = 0, \; x \in (x_1, x_2).$$

i.e. $f(x) = 0$. Therefore, $\mathbf{u} = 0, \; p = 0$ too. $\square$

Let us note once more, that if $\gamma_2 > 0$ we account for the cost functional J_2, then we overdeterminate the initial problem with (3.4.4) for $\alpha = 0$. Therefore in this case usually we have uniqueness results, but not existence results. However in some physical problems the above overdeterminations (and the presence of term $\alpha \|f\|^2_{\mathbb{H}_f}$) have a physical sense, therefore in these cases we can consider the optimal control problems like (3.4.5). This problem becomes independent of the initial problem (where we have only J_1). Here, we have also existence results and can name these optimal control problems as the "optimal shape design problems". Nevertheless, it is interesting to investigate well posedness of the above variational problems when $\alpha = \gamma_2 = 0$.

3.7 Iterative processes

In this section we propose some iterative processes which are well suited for solving the variational equations obtained in the previous sections and we will use them for our numerical tests.
Consider the problem (3.5.10); if for $k = 0, 1, \ldots$ $f^{(k)}$ is known, then $f^{(k+1)}$ can be determinated by solving the following equations ([6]):

$$\begin{cases} L\Phi^{(k)} = Bf^{(k)}, \\ L^* \underline{Q}^{(k)} = \Lambda_w J_\Phi(f^{(k)}, \underline{\Phi}^{(k)}), \\ \Lambda_c w^{(k)} = B^* \underline{Q}^{(k)} + \Lambda_f J_f(f^{(k)}, \underline{\Phi}^{(k)}), \\ f^{(k+1)} = f^{(k)} - \tau_k(\alpha f^{(k)} + w^{(k)}), \end{cases} \tag{3.7.1}$$

where $\{\tau_k\}$ is a family of parameters whose determination follows from the theory of extremal problems (see Vasiliev [155]), the general theory of iterative processes (Marchuk [94], Quarteroni and Valli [127], Quarteroni, Sacco and Saleri [129]), and the ill-posed problems theory (see Tikhonov and Arsenin [151], Vainikko and Veretennikov [153]). The step (3.7.1) would read as follows for the variational form (3.5.9) of problem (3.5.10):

$$\begin{cases} \mathcal{L}(\underline{\Phi}^{(k)}, \hat{\underline{\Phi}}) = B(f^{(k)}, \hat{\underline{\Phi}}) \; \forall \hat{\underline{\Phi}} \in \mathbb{W}, \\ \mathcal{L}(\hat{\underline{W}}, \underline{Q}^{(k)}) = \langle J'_\Phi(f^{(k)}, \underline{\Phi}^{(k)}), \hat{\underline{W}} \rangle \; \forall \hat{\underline{W}} \in \mathbb{W}, \\ (w^{(k)}, \hat{f})_{\mathbb{H}_f} = B(\hat{f}, \underline{Q}^{(k)}) + \langle J'_f(f^{(k)}, \underline{\Phi}^{(k)}), \hat{f} \rangle \; \forall \hat{f} \in \mathbb{H}_f, \\ f^{(k+1)} = f^{(k)} - \tau_k(\alpha f^{(k)} + w^{(k)}). \end{cases} \tag{3.7.2}$$

Consider now problem (3.6.2) (with $\Omega_{wd} \subseteq \Omega$). The iterative process (3.7.2) for this problem

reads as follows:

$$\begin{cases} a_0(\mathbf{u}^{(k)},\mathbf{v}) = b_0(p^{(k)},\mathbf{v}) + F(f^{(k)},\mathbf{v})\ \forall \mathbf{v}\in\mathbb{X}, \\ b_0(q,\mathbf{u}^{(k)}) + b_f(f^{(k)};q,\mathbf{u}_0) = 0\ \forall q\in\mathbb{H}^p(\Omega), \\ a_0(\hat{\mathbf{q}},\mathbf{q}^{(k)}) = -b_0(\sigma^{(k)},\hat{\mathbf{q}}) + \gamma_1\int_{\Omega_0} m_{wd}(\nabla\times\mathbf{u}^{(k)} + m_1\mathcal{R}_f f^{(k)} - \mathcal{R}_{obs,1})\cdot \\ \cdot(\nabla\times\hat{\mathbf{q}})d\Omega + \gamma_2\int_{\Gamma_{out}}(\mathbf{u}^{(k)} - \mathbf{u}_{out})\cdot\hat{\mathbf{q}}d\Gamma\ \forall\hat{\mathbf{q}}\in\mathbb{X}, \\ -b_0(\hat{\sigma},\mathbf{q}^{(k)}) = \gamma_2\int_{\Gamma_{out}}(p^{(k)} - p_{out})\hat{\sigma}d\Gamma\ \forall\hat{\sigma}\in\mathbb{H}^p, \\ (w^{(k)},\hat{f})_{\mathbb{H}_f} = F(\hat{f},\mathbf{q}^{(k)}) - b_f(\hat{f};\sigma^{(k)},\mathbf{u}_0) + \\ +\gamma_1\int_{\Omega_0} m_{wd}(\nabla\times\mathbf{u}^{(k)} + m_1\mathcal{R}_f f^{(k)} - \mathcal{R}_{obs,1})m_1\mathcal{R}_f\hat{f}d\Omega\ \forall\hat{f}\in\mathbb{H}_f, \\ f^{(k+1)} = f^{(k)} - \tau_k(\alpha f^{(k)} + w^{(k)}),\quad k=0,1,\dots. \end{cases} \tag{3.7.3}$$

Consider now the *finite dimensional case* in which the functions $f,\{f^{(k)}\},\hat{f}$ all are sought for in a finite-dimensional subspace $\mathbb{H}_{f,N}\subset\mathbb{H}_f$ of dimension $N<\infty$, whose basis $\varphi_i\in\mathbb{W}^{1,\infty}(x_1,x_2), i=1,2,\dots,N$. Then the following theorem holds.

Theorem 3.7.1 . *Assume that* $\Omega_{wd}=\Omega$, $\left(\frac{\partial v_0}{\partial y}\right)^2+\left(\frac{\partial u_0}{\partial y}\right)^2>0$ *at* $y=0, x\in(x_1,x_2)$. *Then:*

1. *The problem (3.6.2) is correctly solvable (solution exists and is unique) for* $\alpha\geq 0$ *and all* $N<\infty$*;*

2. *The iterative process (3.7.3) is convergent for any* $\alpha>0,\ N<\infty$ *and provided the parameters* $\tau_k>0,\ k=0,1,2,\dots.$ *are small enough;*

3. *If* α *is sufficiently small while* k *is sufficiently large, then* $\{\mathbf{u}^{(k)},p^{(k)},f^{(k)}\}$ *can be taken as an approximate solution of problem (3.6.2).*

Proof:

1. The existence of the solution for $\alpha>0$ has been proved early. Let us consider the case $\alpha=0$. Since $f=\Sigma_{i=1}^N a_i\varphi_i\in\mathbb{H}_{f,N}$ then in the form (3.6.4) with $\alpha=0$ we conclude that this equation is correctly solvable (because the problem (3.6.2) can have only unique solution in $\mathbb{X}\times\mathbb{H}^p\times\mathbb{H}_f$, see Proposition 3.6.2). We assume the generalized Stokes problem to be correctly solvable for any given $f\in\mathbb{H}_f$. Hence the problem (3.6.2) is correctly solvable too.

2. If $\alpha>0$ then the bilinear form on the left hand side of (3.6.4) is coercive and continuous with respect to the norm $\|f\|_{A,\alpha}=\sqrt{\alpha\|f\|^2_{\mathbb{H}_f}+\|Af\|^2_{L^2(x_1,x_2)}}$. Then according to the general theory of iterative algorithm the process given by

$$(f^{(k+1)},\hat{f})_{\mathbb{H}_f} = (f^{(k)},\hat{f})_{\mathbb{H}_f} - \tau(\alpha(f^{(k)},\hat{f})_{\mathbb{H}_f} + (Af^{(k)},A\hat{f})_{L^2(x_1,x_2)}) -$$

$$-(G,A\hat{f})_{L^2(x_1,x_2)},\ k=0,1,\dots$$

is convergent for small $\tau>0$. Hence the process (3.7.3) is convergent also and

$$\|\mathbf{u}^{(k)}-\mathbf{u}\|_{\mathbb{X}} + \|p^{(k)}-p\|_{\mathbb{H}^p} + \|f-f^{(k)}\|_{\mathbb{H}_f}\to 0,\ k\to\infty. \tag{3.7.4}$$

If $\Lambda_C^{-1}A^*A \in [C_1, C_2], C_1, C_2 = const$, and $\tau_k = 2/(2\alpha + C_1 + C_2)$ then (3.7.4) becomes (see Agoshkov [6]):

$$\|\mathbf{u}^{(k)} - \mathbf{u}\|_{\mathbb{X}} + \|p^{(k)} - p\|_{\mathbb{H}^p} + \|f - f^{(k)}\|_{\mathbb{H}_f} \leq C\Big(\frac{C_2 - C_1}{2\alpha + C_1 + C_2}\Big)^k \to 0,\ k \to \infty. \quad (3.7.5)$$

3. Let $\mathbf{u}_0,\ p_0,\ f_0$ be a solution of (3.6.2) when $\alpha = 0$. According to the theory of ill-posed problems (Tikhonov and Arsenin [151], Vainikko and Veretennikov [153]) we have: $\|f_0 - f_\alpha\|_{\mathbb{H}^p} \to 0$ as $\alpha \to 0^+$, where $(f_\alpha, \mathbf{u}_\alpha, p_\alpha)$ is the solution of (3.6.2) for $\alpha > 0$. Hence

$$\|\mathbf{u}_0 - \mathbf{u}_\alpha\|_{\mathbb{X}} + \|p_0 - p_\alpha\|_{\mathbb{H}^p} \to 0,\ as\ \alpha \to 0^+.$$

Then owing to (3.7.4) we conclude that the statements of the theorem holds true also.
The simple schemes in Figure 3.7 can be considered as examples of the above problems when $f \in \mathbb{H}_{f,N}$ for small N (the dimension of $\mathbb{H}_{f,N}$).

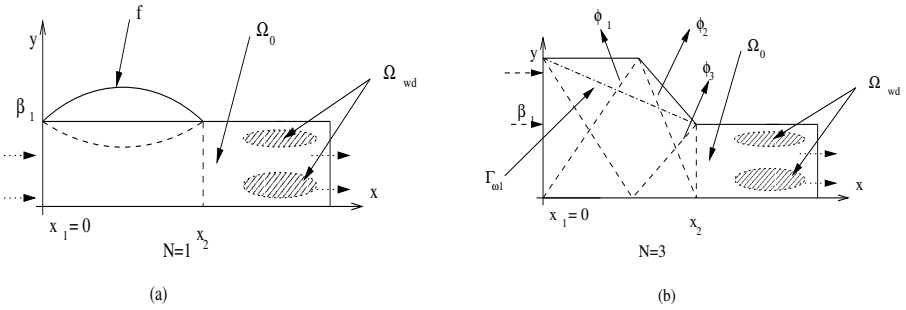

Figure 3.7: Domain Ω with N shape functions: (a) $N = 1$, $f = \beta_1 + a\varphi_0(x)$, $\varphi_0 = x(x_2 - x)$; (b) $N = 3$, $f = \beta_1 + \Sigma_{i=1}^3 a_i\phi_i$.

3.8 Test problem and numerical results

We consider some test problems on simplified arterial bypass configurations. Numerical simulations have been carried out using also in this case the *Bamg* –Bi-dimensional Anisotropic Mesh Generator– and the finite element library *FreeFem*, used to develop algorithms based on control theory and adjoint formulation for generalized Stokes problem. For application of finite element method to incompressible flow see also Gresho and Sani [46]. In this section we present numerical results using as cost functional the L^2 norm of the vorticity in the down-field zone of the new incoming branch of the bypass.
Wall curvature was considered only in the zone of the incoming branch of the bypass ($-2 \leq x \leq 0$) where we set $f_0 = 1 - sin(\frac{x\pi}{4})$; in other parts we used piecewise constant function. The graft angle of the bypass incoming branch (which influences vorticity) is equal to zero (between the artery and the new incoming branch there isn't a relative angle). This aspect will be studied better in the next chapters dealing with a complete bypass configurations and

parametrization.
The original configuration is very similar to the one studied by Lee, Loth and Fisher (see Lee *et al.* [77] and Figure 3.8). Velocity values $\mathbf{u}_{in}$ at the inflow are chosen in such a way that the Reynolds number $Re = \frac{\bar{u}D}{\nu}$ has order 10^3. We recall that blood kinematic viscosity $\nu = \frac{\mu}{\rho}$ is equal to $4 \cdot 10^{-6}\ m^2\ s^{-1}$, blood density $\rho = 1\ g\ cm^{-3}$ and dynamic viscosity $\mu = 4 \cdot 10^{-2}\ g\ cm^{-1}s^{-1}$; $\bar{u}$ is a mean inflow velocity (absolute value) related with $\mathbf{u}_{in}$, while D is the arterial diameter (3.5 mm) [126].

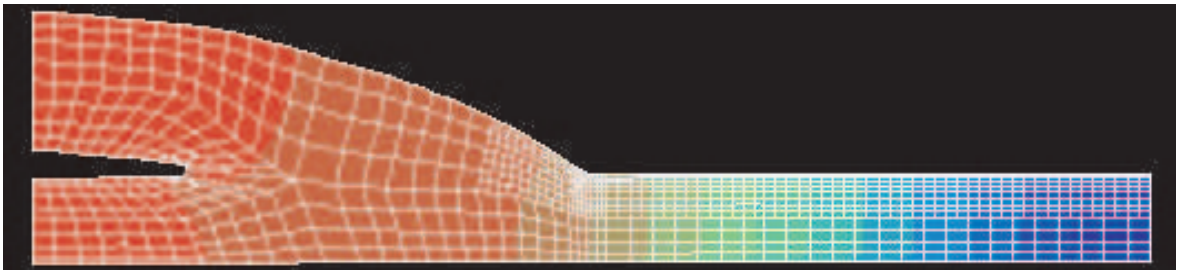

Figure 3.8: Example of configuration proposed and studied by Lee, Loth and Fisher [77].

Figures 3.9-3.11 provide a preliminary account of numerical results and show how the shape of the bypass using generalized steady Stokes equations in an optimal control problem is smoothed out at the corner, which represents a singularity. Figure 3.9 refers to the original configuration; whereas Figure 3.10 to the configuration obtained after 25 iterations of the optimization algorithm (the vorticity has been reduced by about the 30%). Figure 3.11 shows the most sensible zone of the bypass with respect to the cost functional to be minimized. In the picture, first order shape variation (correction) $f_1 y/\beta$ has been plotted in the reference domain. This quantity is related with the adjoint solution, representing the shape sensitivity with respect to the gradient of the cost functional: the "hot" zone is the one at the corner.

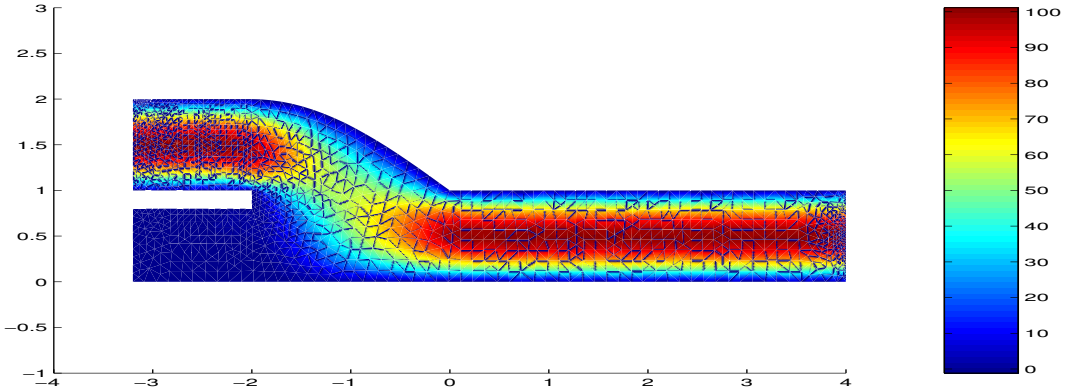

Figure 3.9: Idealized 2-D bypass configuration before optimal shape design process: isovelocity $[ms^{-1} \cdot 10^{-2}]$.

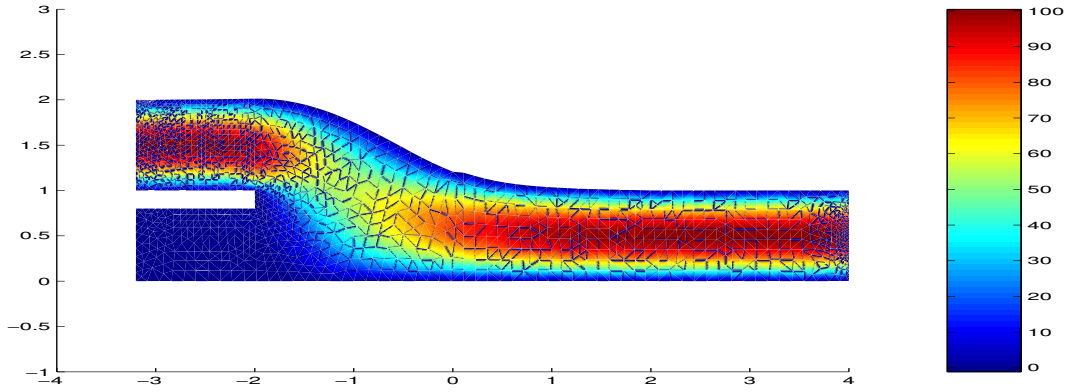

Figure 3.10: Bypass configuration at the end of shape optimization using first corrections: iso-velocity $[ms^{-1} \cdot 10^{-2}]$.

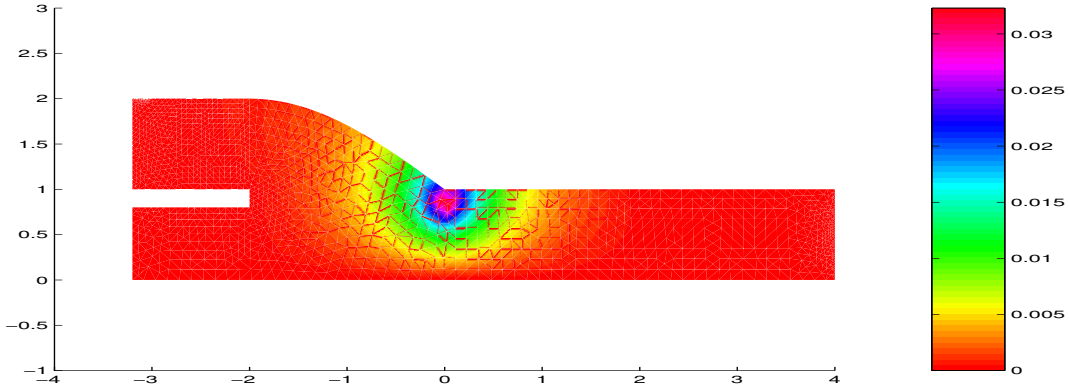

Figure 3.11: First correction $\frac{f_1}{\beta} y$, quantity which is related with the adjoint solution $(\mathbf{q}, \sigma)$ and represents the shape variation in bypass configuration (reported in the reference domain) $[m \cdot 10^{-2}]$.

The results that are obtained by applying shape optimization to first order problem provide a regularization of the shape between the incoming branch of the bypass and the host artery. These results provide a validation of our methodological approach: the shape found is the one presented as "optimized" (minimizing wall shear stress) by Lei, Archie et Kleinstreuer in [78] as an alternative one with respect to the Taylor patch, reducing wall shear stress. We recall that the vorticity cost functional is related with the viscous dissipation dealing with incompressible flows and that the distributed vorticity is related with the velocity field too in the boundary of the region we considered. See Section 2.7.

3.9 A comparison between the two methods

At the end of this first investigation stage, preliminary reported in [4] for the small perturbation theory, we present below some numerical results obtained by applying both the optimal control by local boundary variation (Figure 3.12) and the small perturbations techniques (Figure 3.13), starting from the same configuration. Results by local boundary variations give a shape more similar to Taylor patch (see for a comparison [78]). We have to consider that in this case we are not dealing with a first order perturbation problem. The idea we propose is to iterate our algorithm and restart the optimization process with a new initial shape $\tilde{f}_0$ which is the optimized one $\tilde{f}_0 = f_0 + \varepsilon f_1$ from the previous iterative process. Figure 3.14 shows the shape sensitivity with respect with the cost functional for the problem studied by local boundary variations, while Figure 3.15 shows the reduction of the cost functional (3.4.11) during the optimization processes and a comparison between the two methods. The vorticity reduction during the linearized shape design process (by small perturbation) is shown in Figure 3.15 for the first iterative process. It is possible to iterate the process to get the same configuration provided by local boundary variations approach (Figure 3.12) and a more consistent vorticity reduction as in the local boundary variations case.
The method proposed in this chapter has allowed us (i) to study a shape optimization problem as a control problem on a set of coefficients representing shape functions, (ii) to set the problem in the theoretical framework of a generalized Stokes problem and (iii) to avoid all the topological aspects related with shape optimization with nodal variations in the computational mesh.

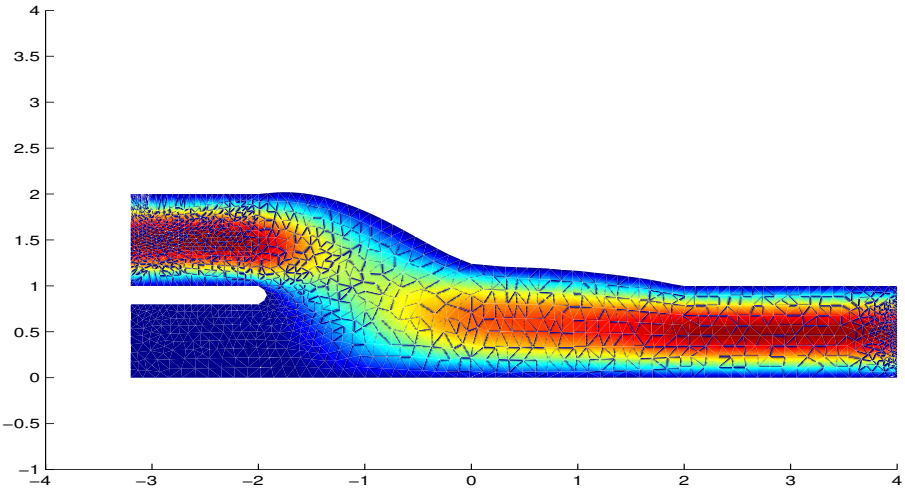

Figure 3.12: Bypass configuration (velocity $[ms^{-1} \cdot 10^{-2}]$, same colorbar of Fig. 3.10) near the incoming branch after shape optimization by boundary variations (30 iterations, 40% vorticity reduction).

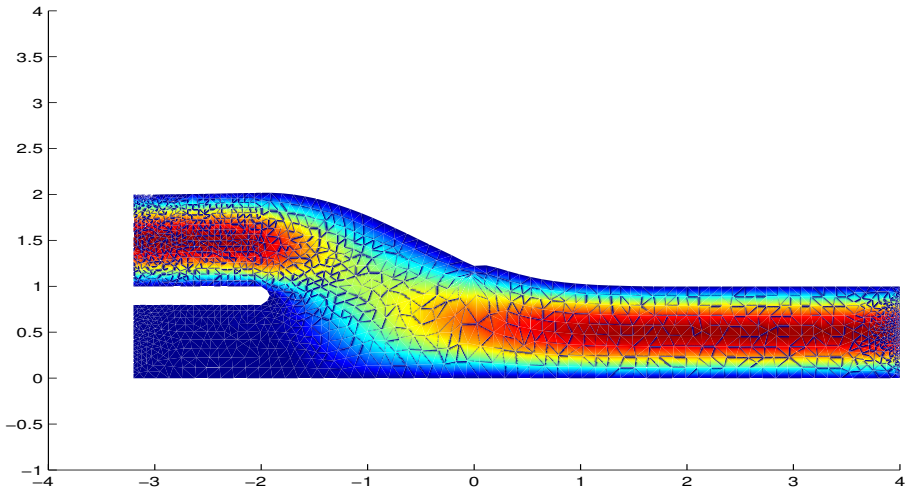

Figure 3.13: Bypass configuration (velocity $[ms^{-1} \cdot 10^{-2}]$, same colorbar of Fig. 3.10, 25 iterations and 30% vorticity reduction) after design by small perturbations.

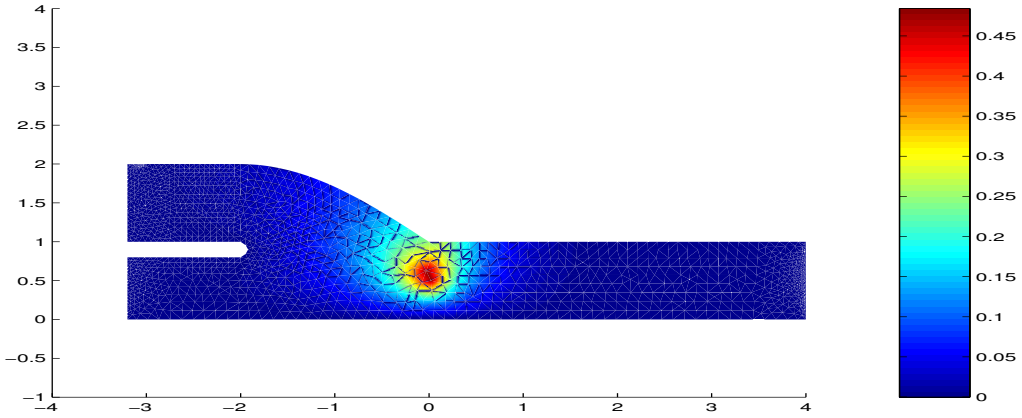

Figure 3.14: Bypass configuration and its shape sensitivity in reference domain with respect to the cost functional (quantity related with adjoint solution) to underline the most sensible zone related with observation $[m \cdot 10^{-2}]$.

3.10 Further developments

In this chapter we have focused on the problem of determining the first corrections for the shape design of simplified two-dimensional bypass configurations.
We recall here that we are in the perspective of using low order models for optimal control and shape optimization algorithms, but this methodology may be applied to fully unsteady incompressible Stokes (as we will do in the next chapter) and Navier-Stokes equations and consider the coupled fluid-structure problem. The setting of the problem in a three-dimensional geometry will provide more realistic design indications concerning surgical prosthesis realizations. The development of tools for geometry reconstruction from medical data (medical imaging and other non-invasive means) and their integration with numerical simulation could provide

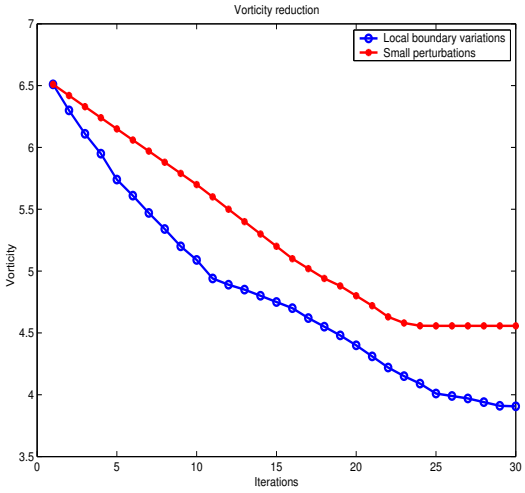

Figure 3.15: Distributed vorticity $[m^2 s^{-1}]$ reduction achieved during the two optimization processes: shape design by local boundary variations and small perturbations.

improvements in disease diagnosis procedures and more realistic models. Also the integration of numerical models with experimental ones could allow to get a more complete study framework, see for example Bertolotti *et al.* [18].

An important application of the numerical method developed in this chapter is the possibility to realize the iterative process for solving initial non-linear problems. For that it is sufficient to consider $f = f_0 + \varepsilon f_1$, where f_0 is the initial configuration and f_1 the computed first correction, as the new f_0, then to calculate a new first correction and so on.

A further useful development may be devoted to build domain decomposition methods (see Quarteroni and Valli [128]) based on optimal control approaches. What we are going to develop in the next chapters of this thesis, after a generalization of the approach we have proposed here, are efficient schemes for reduced-basis methodology approximations (see Patera, Maday, Prud'homme, Rovas, Veroy and Turinici in [118] and/or [119]) to study complete parametrized bypass configuration. This methodology will be more efficient for the use in a repetitive design environment as optimal shape design methodology requires.

Chapter 4

Shape Design by Optimal Control with Unsteady Flows and Perturbation Method

In this chapter we present an approach for the study of the Aorto-Coronaric bypass anastomoses using unsteady Stokes equations. Our aim is still to develop optimization methods based on simplified fluid models. This approach can be seen as a methodological generalization of the results of the previous chapter; as a matter of fact, the shape optimization process takes into account unsteady flow phenomena over a period T to build an optimized shape which is not time dependent. The small perturbation method, coupled with optimal control, is extended to unsteady flows, moreover existence and uniqueness results are generalized to the unsteady case.

4.1 Introduction

In this chapter we still apply optimal control for the shape optimization of Aorto-Coronaric bypass anastomoses. We consider unsteady (rather than steady) Stokes equations with the aim of providing a better understanding of the blood flow dynamics. We analyze the "first correction" method which is derived by applying a perturbation method to the initial unsteady problem in a space-time domain $\Omega \times (0,T)$ with $\Omega \subset \mathbb{R}^2$. The boundary $\partial\Omega$ of Ω is parametrized by a suitable function f. In this chapter we extend the approach and the results already introduced in the previous chapter (and preliminary reported in [4]) to the case where the *non-stationary* Stokes equations are used. An outline of this chapter is as follows. In Section 4.2 we formulate our problem, in Section 4.3 we deal with the problem of perturbed functions in the generalized unsteady Stokes equations framework. In Section 4.4 we introduce the shape optimization problem and its equations in the optimal control framework dealing with unsteady cost functionals (Section 4.5). In Section 4.6 uniqueness and existence results are extended, then in Section 4.7 an iterative optimization algorithm is proposed. Section 4.8 deals with a test problem and numerical results, finally some conclusions are drawn in

Section 4.9.

4.2 The non-stationary problem

Let Ω be a bounded domain of $\mathbb{R}^2$ with boundary Γ, $\mathbf{x} = (x, y)^T$ is a point of $\overline{\Omega}$, $t \in [0, T], T < \infty$, is the time variable. As before we consider the idealized, two-dimensional bypass bridge configuration of Figure 4.1 and the domain on Figure 4.2, where the dotted line represents the geometry of the complete anastomosis; Γ_{w_2} is the section of the original artery, Γ_{in} is the new anastomosis inflow after bypass surgery, Γ_{out} is the anastomosis outflow.

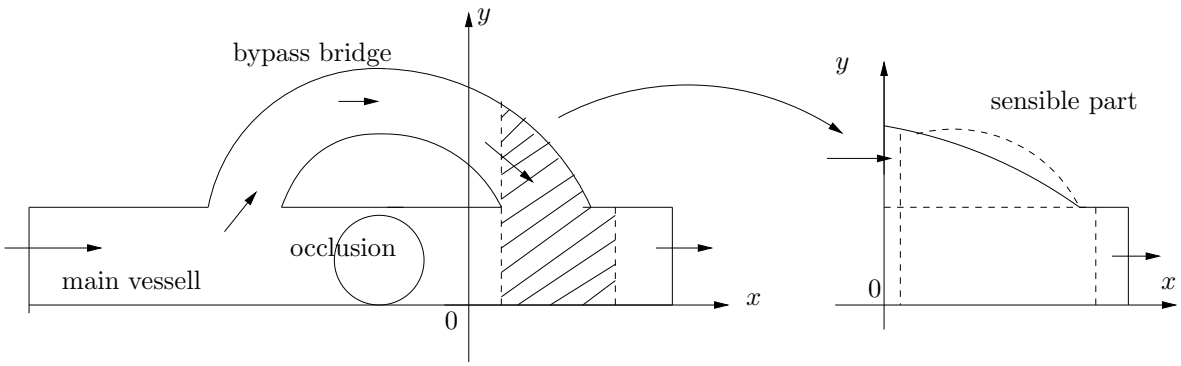

Figure 4.1: Idealized, 2-D bypass bridge configuration (left) and detail of the sensible part for the optimization process (right). The dotted curve represents the portion of the boundary that is subjected to change.

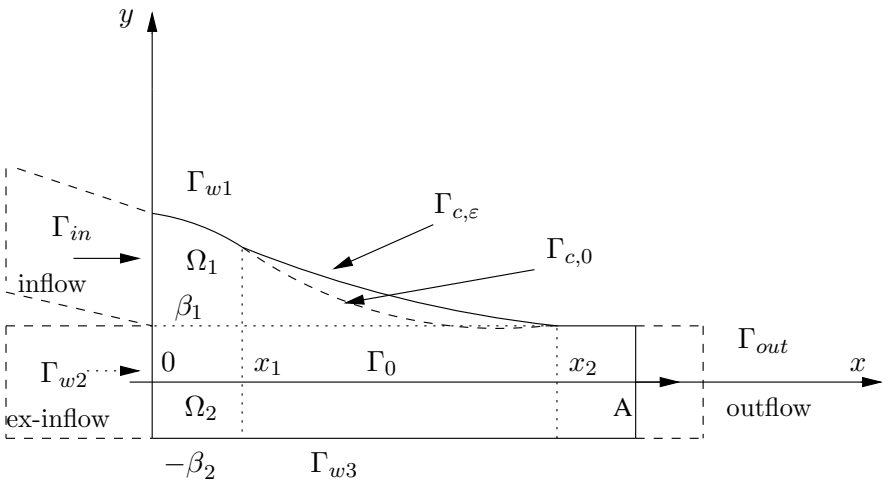

Figure 4.2: Main notations: $\overline{\Omega} = \overline{\Omega}_1 \cup \overline{\Omega}_2, \Gamma_w = \Gamma_{w_1} \cup \Gamma_{w_2} \cup \Gamma_{w_3}, \Gamma_0 = \partial\Omega_1 \cap \partial\Omega_2$

We consider the following boundary-value problem for the unsteady Stokes equations, used

to model blood flow at low Reynolds number: find $\mathbf{u}, p$ s.t.

$$\begin{cases} \mathbf{u}_t - \nu\Delta\mathbf{u} + \nabla p = \mathbf{f} \;\; in\ \Omega \times (0,T), \\ \nabla \cdot \mathbf{u} = 0 \quad in\ \Omega \times (0,T), \\ \mathbf{u} = \mathbf{u}_{in}\ on\ \Gamma_{in},\ \mathbf{u} = \mathbf{0}\ on\ \Gamma_{w_1} \cup \Gamma_{w_3}\ \forall t \in (0,T), \\ -p\hat{\mathbf{n}} + \nu\frac{\partial \mathbf{u}}{\partial \hat{\mathbf{n}}} = \mathbf{g}_{out}\ on\ \Gamma_{out} \cup \Gamma_{w_2}\ \forall t \in (0,T,) \\ \mathbf{u} = \mathbf{u}^*\ at\ t = 0\ in\ \Omega, \end{cases} \tag{4.2.1}$$

where $\mathbf{u}_t := \frac{\partial \mathbf{u}}{\partial t}$, $\mathbf{u}^*$ is a given vector function such that $\nabla \cdot \mathbf{u}^* = 0$ in Ω, $\hat{\mathbf{n}} = (n_1, n_2)^T$ is the outward unit normal vector on Γ, $\mathbf{f} = \mathbf{f}(x,y,t)$, $\mathbf{u}_{in} = \mathbf{u}_{in}(x,y,t)$, $\mathbf{g}_{out} = \mathbf{g}_{out}(x,y,t)$ are given vector functions, $\nu = const > 0$ and $\mathbf{u}_f = \{\mathbf{u}_{in}\ on\ \Gamma_{in}; \mathbf{0}\ on\ \Gamma_{w_1} \cup \Gamma_{w_3}\}$. As seen previously, the subset $\Gamma_{c,\varepsilon}$ of Γ_{w_1} is parametrized by a function $f(x,\varepsilon)$ of $x \in [x_1, x_2]$ and $\varepsilon \in [-\varepsilon_0, \varepsilon_0]$, $\varepsilon_0 = const$ is a small parameter. More precisely we assume that $f(x,\varepsilon)$ is time independent and can be developed as follows:

$$f(x,\varepsilon) = f_0(x) + \varepsilon f_1(x) + \varepsilon^2 f_2(x) + \dots, \tag{4.2.2}$$

where $f_k \in \mathbb{W}^{1,\infty}(x_1, x_2)$, for $k = 0$, and $f_k \in \mathbb{W}_0^{1,\infty}(x_1, x_2)$, for $k \geq 1$, so that $f_k(x_1) = f_k(x_2) = 0, k \geq 1$. Here the function $f_0(x) > 0$ describes the original subset $\Gamma_{c,0}$ of the boundary of the "unperturbed domain", $\Gamma_{w0} \equiv \partial\Omega_0$ (see Figure 4.3), while $f_k(x), k \geq 1$, could be unknown when considering a control problem (see Section 4.4).

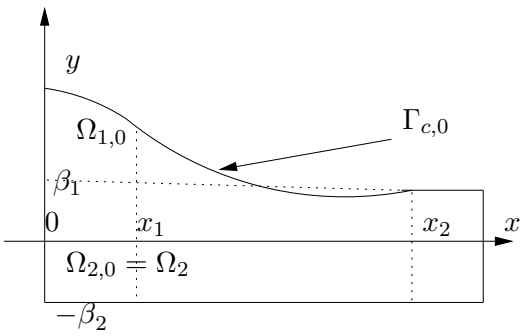

Figure 4.3: The original "unperturbed domain" Ω_0.

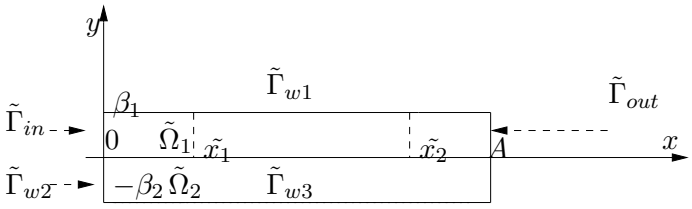

Figure 4.4: The "simple" domain $\tilde{\Omega}$.

We introduce the following real Hilbert spaces:

$$\mathbb{X} := \{\mathbf{v} : \mathbf{v} \in (H^1(\Omega))^2, \mathbf{v} = \mathbf{0} \; on \; \Gamma_{in} \cup \Gamma_{w_1} \cup \Gamma_{w_3}\},$$

$$H := L^2(\Omega \times (0,T)) \equiv H^*, \; Y := L^2(0,T;\mathbb{X}),$$

$$W := \{\mathbf{u} : \mathbf{u} \in Y, \mathbf{u}_t \in L^2(0,T;Y^*), \mathbf{u}(x,y,T) = \mathbf{0}\}.$$

The weak statement of Eq.(4.2.1) reads: find $\mathbf{u} \in L^2(0,T;(H^1(\Omega))^2)$, $p \in H$ s.t.

$$\begin{cases} a(\mathbf{u},\mathbf{v}) - b(p,\mathbf{v}) = G(\mathbf{v}) \; \forall \mathbf{v} \in W, \\ b(q,\mathbf{u}) = 0 \; \forall q \in H, \\ \mathbf{u} = \mathbf{u}_f \; on \; \Gamma_{in} \cup \Gamma_{w_1} \cup \Gamma_{w_3} \; \forall \; t \; \in \; (0,T), \end{cases} \tag{4.2.3}$$

we recall that with $\mathbf{v}$ and q we indicate test functions and:

$$a(\mathbf{u},\mathbf{v}) = \int_0^T \int_\Omega \nu \nabla \mathbf{u} \cdot \nabla \mathbf{v} d\Omega dt - \int_0^T \int_\Omega \mathbf{u} \cdot \mathbf{v}_t d\Omega dt,$$

$$b(p,\mathbf{v}) = \int_0^T \int_\Omega p \nabla \cdot \mathbf{v} d\Omega dt,$$

$$G(\mathbf{v}) = \int_0^T \int_\Omega \mathbf{f} \cdot \mathbf{v} d\Omega dt + \int_0^T \int_{\Gamma_{out} \cup \Gamma_{w_2}} \mathbf{g}_{out} \cdot \mathbf{v} d\Gamma dt + \int_\Omega \mathbf{u}^* \cdot \mathbf{v}(x,y,0) d\Omega.$$

The forms $a(.,.), b(.,.)$ and $G(.)$ depend on the parametrization f of $\Gamma_{c,\varepsilon}$, however this dependence will be understood for simplicity of notations.

4.3 The unsteady problem for the perturbed functions

Let us introduce the reference (simple-shaped) domains $\tilde{\Omega}_1 = \{0 < \tilde{x} < A, 0 < \tilde{y} < \beta_1 \equiv \beta\}$, $\tilde{\Omega}_2 = \{0 < \tilde{x} < A, -\beta_2 < \tilde{y} < 0\}$, and $\overline{\tilde{\Omega}} = \overline{\tilde{\Omega}}_1 \cup \overline{\tilde{\Omega}}_2$ (see Figure 4.4). Then we assume that $f(x,\varepsilon) > 0$ and consider the following variable transformation:

$$\mathrm{T}_f : \overline{\Omega}_1 \cup \overline{\Omega}_2 \to \overline{\tilde{\Omega}}, \; \tilde{\mathbf{x}} = \mathrm{T}_f(\mathbf{x});$$

T_f is the identity in Ω_2, while $\mathrm{T}_f(x,y) = (x, \frac{\beta}{f(x,\varepsilon)} y)$ in Ω_1. We set $\tilde{\mathbf{x}} = (\tilde{x}, \tilde{y})$ and define

$$\tilde{\mathbf{u}}(\tilde{\mathbf{x}},t) := \mathbf{u} \circ \mathrm{T}_f^{-1}(\tilde{\mathbf{x}},t) = \mathbf{u}(\tilde{x}, \tilde{y} f(\tilde{x},\varepsilon)/\beta, t).$$

where $\tilde{\mathbf{v}} = (\tilde{u}, \tilde{v})$. Then,

$$dxdy = \frac{f(\tilde{x},\varepsilon)}{\beta} d\tilde{x} d\tilde{y}$$

and for every $\tilde{\phi} : \tilde{\Omega} \times (0,T) \to \mathbb{R}$ and $\phi = \tilde{\phi} \circ T_f$ the following relations hold (with $f_x := df/dx$):

$$\frac{\partial \phi}{\partial y}(\tilde{\mathbf{x}},t) = \frac{\beta}{f(\tilde{x},\varepsilon)} \frac{\partial \tilde{\phi}(\tilde{\mathbf{x}},t)}{\partial \tilde{y}}, \; \frac{\partial \phi}{\partial x}(\tilde{\mathbf{x}},t) = \frac{\partial \tilde{\phi}(\tilde{\mathbf{x}},t)}{\partial \tilde{x}} - \tilde{y} \frac{f_x(\tilde{x},\varepsilon)}{f(\tilde{x},\varepsilon)} \frac{\partial \tilde{\phi}(\tilde{\mathbf{x}},t)}{\partial \tilde{y}}, \tag{4.3.1}$$

$$\begin{cases} \tilde{\mathcal{D}}(f)\tilde{\mathbf{u}}(\tilde{\mathbf{x}},t) := ((\nabla\cdot\mathbf{u})\circ \mathrm{T}_f^{-1})(\tilde{\mathbf{x}},t) = \frac{\partial\tilde{u}}{\partial\tilde{x}} - \tilde{y}\frac{f_x(\tilde{x},\epsilon)}{f(\tilde{x},\varepsilon)}\frac{\partial\tilde{u}}{\partial\tilde{y}} + \frac{\beta}{f(\tilde{x},\varepsilon)}\frac{\partial\tilde{v}}{\partial\tilde{y}}, \\ \tilde{\mathcal{R}}(f)\tilde{\mathbf{u}}(\tilde{\mathbf{x}},t) := ((\nabla\times\mathbf{u})\circ \mathrm{T}_f^{-1})(\tilde{\mathbf{x}},t) = \frac{\partial\tilde{v}}{\partial\tilde{x}} - \tilde{y}\frac{f_x(\tilde{x},\epsilon)}{f(\tilde{x},\varepsilon)}\frac{\partial\tilde{v}}{\partial\tilde{y}} - \frac{\beta}{f(\tilde{x},\varepsilon)}\frac{\partial\tilde{u}}{\partial\tilde{y}}. \end{cases} \tag{4.3.2}$$

Then in $\tilde{\Omega}$ we have:

$$\tilde{\mathcal{D}}(f)\tilde{\mathbf{u}} = m_2\tilde{\nabla}\cdot\tilde{\mathbf{u}} + m_1\tilde{\mathcal{D}}(f)\tilde{\mathbf{u}},\ \tilde{\mathcal{R}}(f)\tilde{\mathbf{u}} = m_2\tilde{\nabla}\times\tilde{\mathbf{u}} + m_1\tilde{\mathcal{R}}(f)\tilde{\mathbf{u}},$$

where $\tilde{\nabla}\phi := \left(\frac{\partial\phi}{\partial\tilde{x}}, \frac{\partial\phi}{\partial\tilde{y}}\right)$, while m_s is the characteristic function of $\tilde{\Omega}_s$ $(s = 1, 2)$. To simplify the notations from now on we will set (unless otherwise specified):

$$\mathbf{x} = \tilde{\mathbf{x}},\ \mathbf{u}(x,y,t) = \tilde{\mathbf{u}}(\tilde{x},\tilde{y},t),\ u = \tilde{u},\ v = \tilde{v}, \ldots,$$

$$\mathcal{D} = \tilde{\mathcal{D}}, \mathcal{R} = \tilde{\mathcal{R}},\ \Omega \equiv \tilde{\Omega},\ \Gamma_{w_k} \equiv \tilde{\Gamma}_{w_k}.$$

Then problem (4.2.3) in the new reference frame $\tilde{\Omega}$, now renamed Ω, reads as follows:

$$\begin{cases} a(f;\mathbf{u},\mathbf{v}) - b(f;p,\mathbf{v}) = G(f;\mathbf{v})\ \forall\mathbf{v}\in W, \\ b(f;q,\mathbf{u}) = 0\ \forall q\in H, \\ \mathbf{u} = \mathbf{u}_f\ on\ \Gamma_{in}\cup\Gamma_{w_1}\cup\Gamma_{w_3}\forall t\in(0,T). \end{cases} \tag{4.3.3}$$

We have emphasized the dependence of $a(f;.,.), b(f;.,.)$, and $G(f;.)$ on f. Precisely, upon writing Ω_1 instead of $\tilde{\Omega}_1$ and Ω_2 instead of $\tilde{\Omega}_2$ for simplicity of notation we have (unless otherwise specified, integration is carried out with respect to $d\Omega dt$):

$$a(f;\mathbf{u},\mathbf{v}) = a_1(f;\mathbf{u},\mathbf{v}) + a_2(\mathbf{u},\mathbf{v}),$$

$$a_1(f;\mathbf{u},\mathbf{v}) = \int_0^T\int_{\Omega_1}\frac{f\nu}{\beta}\Big(\Big(\frac{\partial\mathbf{u}}{\partial x} - \frac{yf_x}{f}\frac{\partial\mathbf{u}}{\partial y}\Big)\cdot\Big(\frac{\partial\mathbf{v}}{\partial x} - \frac{yf_x}{f}\frac{\partial\mathbf{v}}{\partial y}\Big) + \frac{\beta^2}{f^2}\frac{\partial\mathbf{u}}{\partial y}\cdot\frac{\partial\mathbf{v}}{\partial y}\Big) -$$

$$-\int_0^T\int_{\Omega_1}\frac{f}{\beta}\mathbf{u}\cdot\mathbf{v}_t,$$

$$a_2(\mathbf{u},\mathbf{v}) = \int_0^T\int_{\Omega_2}\nu\Big(\frac{\partial\mathbf{u}}{\partial x}\cdot\frac{\partial\mathbf{v}}{\partial x} + \frac{\partial\mathbf{u}}{\partial y}\cdot\frac{\partial\mathbf{v}}{\partial y}\Big) - \int_0^T\int_{\Omega_2}\mathbf{u}\cdot\mathbf{v}_t,$$

$$b(f;p,\mathbf{v}) = b_1(f;p,\mathbf{v}) + b_2(p,\mathbf{v}),$$

$$b_1(f;p,\mathbf{v}) = \int_0^T\int_{\Omega_1}\frac{f}{\beta}p\mathcal{D}(f)\mathbf{v},\quad b_2(p,\mathbf{v}) = \int_0^T\int_{\Omega_2}p\nabla\cdot\mathbf{v},$$

$$G(f;\mathbf{v}) = G_1(f;\mathbf{v}) + G_2(\mathbf{v}),$$

$$G_1(f;\mathbf{v}) = \int_0^T\int_{\Omega_1}\frac{f}{\beta}\mathbf{f}\cdot\mathbf{v} + \int_0^T\int_{(\Gamma_{out}\cup\Gamma_{w2})\cap\partial\Omega_1}\mathbf{g}_{out}\cdot\mathbf{v}d\Gamma dt +$$

$$+\int_{\Omega_1}\frac{f}{\beta}\mathbf{u}^*(x,y)\cdot\mathbf{v}(x,y,0)d\Omega,$$

$$G_2(\mathbf{v}) = \int_0^T\int_{\Omega_2}\mathbf{f}\cdot\mathbf{v} + \int_0^T\int_{(\Gamma_{out}\cup\Gamma_{w2})\cap\partial\Omega_2}\mathbf{g}_{out}\cdot\mathbf{v}d\Gamma dt +$$

$$+\int_{\Omega_2}\mathbf{u}^*(x,y)\cdot\mathbf{v}(x,y,0)d\Omega.$$

Assume that problem (4.3.3) has a solution $\mathbf{u}, p$ that is infinitely differentiable with respect to ε:

$$\begin{cases} \mathbf{u} = \mathbf{u}_0 + \varepsilon \mathbf{u}_1 + \varepsilon^2 \mathbf{u}_2 + \dots \\ p = p_0 + \varepsilon p_1 + \varepsilon^2 p_2 + \dots \end{cases} \tag{4.3.4}$$

where $p_k \in H, \mathbf{u}_k \in Y,\ k \geq 1$, the test functions $\mathbf{v},\ q$ appearing in (4.3.3) and in the sequel can be assumed as independent of ε.
Using (4.2.2)-(4.3.4) and the small perturbation technique we can deduce the equations satisfied by $\mathbf{u}_k, p_k,\ k \geq 0$. In particular, for $k = 0$, $\mathbf{u}_0$ and p_0 satisfy

$$\begin{cases} a(f_0; \mathbf{u}_0, \mathbf{v}) - b(f_0; p_0, \mathbf{v}) = G(f_0; \mathbf{v}) \ \ \forall \mathbf{v} \in W, \\ b(f_0; q, \mathbf{u}_0) = 0 \ \ \forall q \in H, \\ \mathbf{u}_0 = \mathbf{u}_f \ on\ \Gamma_{in} \cup \Gamma_{w_1} \cup \Gamma_{w_3} \ \forall t \in (0, T). \end{cases} \tag{4.3.5}$$

Correspondingly we define:

$$\mathcal{R}_{obs,0} := \mathcal{R}(f_0)\mathbf{u}_0. \tag{4.3.6}$$

We introduce some further functional spaces $\mathbb{H}^p$ and $\mathbb{H}_f$ for p and $\{f_k\}$, respectively, which satisfy:

$$\mathbb{H}^p \subseteq H \subseteq \mathbb{H}^{p*},\ \mathbb{H}_f \subseteq L^2(x_1, x_2) \subseteq \mathbb{H}_f^*,$$

$$\mathbb{W} := W \times \mathbb{H}^p \subseteq \mathbb{H}_0 := L^2(\Omega \times (0,T))^2 \times L^2(\Omega \times (0,T)) \subseteq \mathbb{W}^*.$$

Then we set:

$$\mathbb{Y} := Y \times \mathbb{H}^p \subseteq \mathbb{H}_0 \subseteq \mathbb{Y}^*,$$

Then for $k = 1$ the functions $\mathbf{u}_1, p_1$, considered as the components of the vector-function $\underline{\Phi_1} := (\mathbf{u}_1, p_1) \in \mathbb{Y}$, $f_1 \in \mathbb{H}_f$, satisfy the equation:

$$\mathcal{L}(\underline{\Phi_1}, \hat{\underline{\Phi}}) = B(f_1, \hat{\underline{\Phi}}) \quad \forall \hat{\underline{\Phi}} := (\mathbf{v}, q) \in \mathbb{W}, \tag{4.3.7}$$

where

$$\mathcal{L}(\underline{\Phi_1}, \hat{\underline{\Phi}}) := a_0(f_0; \mathbf{u}_1, \mathbf{v}) - b_0(f_0; p_1, \mathbf{v}) + b_0(f_0; q, \mathbf{u}_1),$$

$$B(f_1, \hat{\underline{\Phi}}) := b_f(f_1; p_0, \mathbf{v}) + G_1(f_1; \mathbf{v}) - a_f(f_1; \mathbf{u}_0, \mathbf{v}) - b_f(f_1; q, \mathbf{u}_0),$$

$$b_f(f_1; p_0, \mathbf{v}) := \frac{\partial}{\partial \varepsilon} b(f; p_0, \mathbf{v})|_{\varepsilon=0} = \int_0^T \int_{\Omega_1} \frac{f_1}{\beta} p_0 \mathcal{D}(f_0)\mathbf{v} +$$

$$+ \int_0^T \int_{\Omega_1} \frac{f_0}{\beta} p_0 \mathcal{D}_f(f_1, \mathbf{v}),$$

$$\mathcal{D}_f(f_1, \mathbf{v}) := \frac{\partial}{\partial \varepsilon} \mathcal{D}(f)\mathbf{v}|_{\varepsilon=0} = -\big[y\big(\frac{f_{1,x} f_0 - f_{0,x} f_1}{f_0^2}\big)\frac{\partial \hat{u}}{\partial y} + \frac{\beta f_1}{f_0^2}\frac{\partial \hat{v}}{\partial y}\big],$$

$$\mathcal{D}_f(f_1, \mathbf{u}_0) := \frac{\partial}{\partial \varepsilon} \mathcal{D}(f)\mathbf{u}_0|_{\varepsilon=0} (:= \mathcal{D}_f f_1 \ in\ the\ sequel),$$

$$G_1(f_1; \mathbf{v}) := \frac{\partial}{\partial \varepsilon} G(f; \mathbf{v})|_{\varepsilon=0} = \int_0^T \int_{\Omega_1} \frac{f_1}{\beta} \mathbf{f} \cdot \mathbf{v} + \int_{\Omega_1} \frac{f_1}{\beta} \mathbf{u}_0(x, y) \cdot \mathbf{v}(x, y, 0) d\Omega,$$

$$a_f(f_1;\mathbf{u}_0,\mathbf{v}) := \frac{\partial}{\partial\varepsilon}a(f;\underline{v}_0,\mathbf{v})|_{\varepsilon=0} =$$

$$= \int_0^T\int_{\Omega_1}\frac{f_1\nu}{\beta}\Big(\big(\frac{\partial\mathbf{u}_0}{\partial x}-\frac{yf_{0,x}}{f_0}\frac{\partial\mathbf{u}_0}{\partial y}\big)\cdot\big(\frac{\partial\mathbf{v}}{\partial x}-\frac{yf_{0,x}}{f_0}\frac{\partial\mathbf{v}}{\partial y}\big)+\frac{\beta^2}{f_0^2}\frac{\partial\mathbf{u}_0}{\partial y}\cdot\frac{\partial\mathbf{v}}{\partial y}\Big)-$$

$$-\int_0^T\int_{\Omega_1}\frac{f_0\nu}{\beta}y\frac{(f_{1,x}f_0-f_{0,x}f_1)}{f_0^2}\big(\frac{\partial\mathbf{u}_0}{\partial y}\cdot\big(\frac{\partial\mathbf{v}}{\partial x}-\frac{yf_{0,x}}{f_0}\frac{\partial\mathbf{v}}{\partial y}\big)+\big(\frac{\partial\mathbf{u}_0}{\partial x}-\frac{yf_{0,x}}{f_0}\frac{\partial\mathbf{u}_0}{\partial y}\big)\cdot\frac{\partial\mathbf{v}}{\partial y}\big)$$

$$-\int_0^T\int_{\Omega_1}\frac{f_0\nu}{\beta}\big(\frac{2\beta^2f_1}{f_0^3}\big)\frac{\partial\mathbf{u}_0}{\partial y}\cdot\frac{\partial\mathbf{v}}{\partial y}-\int_0^T\int_{\Omega_1}\frac{f_1}{\beta}\mathbf{u}_0\cdot\mathbf{v}_t.$$

Problem (4.3.7) is a weak statement for the non-stationary Stokes problem. In the sequel we assume that this problem has a unique solution for any given $\mathbf{u}_0,\ p_0$ (the solution in the unperturbed domain Ω_0), and for each $f_1\in\mathbb{H}_f$.

4.4 The shape optimization problem: unsteady cost functionals

In this section our mathematical derivation will be formal, in the sense that we allow ourselves the regularity that is necessary for our manipulation. Suppose now that the (time independent) function f_1 in problem (4.3.7) is unknown and so are $\mathbf{u}_1,\ p_1$. To complete problem (4.3.7) we will have to either provide some additional equations or require that f_1 be determined by minimizing a suitable (time dependent) cost functional.
In general terms, problem (4.3.7) will be supplemented by the additional equation:

$$\mathcal{C}(f,\mathbf{u},p)=0 \tag{4.4.1}$$

where $\mathcal{C}$ is an operator (linear or nonlinear) defined on $H_0^1(x_1,x_2)\times Y\times\mathbb{H}^p$. (We consider now $f\in H_0^1(\Omega)$ for convenience). We assume $\mathcal{C}$ to depend smoothly on its variables $f,\mathbf{u},p$. Using the representations (4.2.2) and (4.3.4) we derive from (4.4.1) the following equation:

$$\mathcal{C}(f,\mathbf{u},p)=\mathcal{C}_0(f_0,\mathbf{u}_0,p_0)+\varepsilon\mathcal{C}_1(f_1,\mathbf{u}_1,p_1)+\mathcal{O}(\varepsilon^2)=0,\quad\forall\varepsilon\in[-\varepsilon_0,\varepsilon_0] \tag{4.4.2}$$

where

$$\mathcal{C}_1(f_1,\mathbf{u}_1,p_1) := \frac{\partial\mathcal{C}}{\partial\varepsilon}(f,\mathbf{u},p)|_{\varepsilon=0}. \tag{4.4.3}$$

If we assume that the data of our problems are such that $\mathcal{C}_0(f_0,\mathbf{u}_0,p_0)=0$, then we can replace (4.4.2) by the approximate equation

$$\mathcal{C}_1(f_1,\mathbf{u}_1,p_1)=0 \tag{4.4.4}$$

and use it to complete (4.3.7), yielding an *exact controllability problem.* An alternative approach would consist in replacing (4.4.4) by the following equivalent *minimization problem*:

$$\inf_{f_1}\int_0^T\int_\Omega\frac{f_0}{\beta}|\mathcal{C}_1(f_1,\mathbf{u}_1,p_1)|^2d\Omega dt, \tag{4.4.5}$$

where we assume that $\mathcal{C}_1$ has image in $\mathbb{H}^p$. In the next sections we apply the approaches (4.4.4)-(4.4.5) described above for the completion of (4.3.7) and we will move from the following special choice of (4.4.1):

$$\mathcal{C}(f,\mathbf{u}) := ((\nabla\times\mathbf{u})\circ \mathrm{T}_f^{-1})(x,y,t) - \mathcal{R}_{obs,\varepsilon}(x,y,t) \ in\ \Omega_{wd}\subseteq\Omega\ \forall t\geq 0, \tag{4.4.6}$$

where we recall that Ω_{wd} is a suitable subset of Ω in which we want our additional equation (or our "control") to take place. Moreover

$$\mathcal{R}_{obs,\varepsilon} = \mathcal{R}_{obs,0} + \varepsilon\mathcal{R}_{obs,1} + \varepsilon^2\mathcal{R}_{obs,2} + \dots\ ,\ \mathcal{R}_{obs,0} := ((\nabla\times\mathbf{u}_0)\circ \mathrm{T}_{f_0}^{-1}). \tag{4.4.7}$$

Then we have: $\mathcal{C}_0(f_0,\mathbf{u}_0)=0$, while the equation (4.4.4) corresponding to the special choice (4.4.6) reads:

$$\mathcal{C}_1(f_1,\mathbf{u}_1) = \mathcal{R}(f_0)\mathbf{u}_1 + m_1\mathcal{R}_f f_1 - \mathcal{R}_{obs,1} = 0 \ in\ \Omega_{wd},\ \forall t, \tag{4.4.8}$$

where

$$\mathcal{R}(f_0)\mathbf{u}_1 = (\nabla\times\mathbf{u}_1)\circ \mathrm{T}_{f_0}^{-1}(x,y) = \frac{\partial v_1}{\partial x} - \frac{y f_{0,x}}{f_0}\frac{\partial v_1}{\partial y} - \frac{\beta}{f_0}\frac{\partial u_1}{\partial y},$$

$$\mathcal{R}_f f_1 := \mathcal{R}_f(f_1,\mathbf{u}_0) = -y\frac{(f_{1,x}f_0 - f_{0,x}f_1)}{f_0^2}\frac{\partial v_0}{\partial y} + \frac{\beta f_1}{f_0^2}\frac{\partial u_0}{\partial y}.$$

In conclusion we consider the following problem: find $\underline{\Phi_1} = (\mathbf{u}_1, p_1)\in\mathbb{Y}$, $f_1\in H_0^1(x_1,x_2)$ s.t.

$$\begin{cases} \mathcal{L}(\underline{\Phi_1},\underline{\hat{\Phi}}) = B(f_1,\underline{\hat{\Phi}})\ \forall\underline{\hat{\Phi}} = (\mathbf{v},q)\in\mathbb{W}, \\ \mathcal{R}(f_0)\mathbf{u}_1 + m_1\mathcal{R}_f f_1 - \mathcal{R}_{obs,1} = 0 \ in\ \Omega_{wd}\ \forall t\geq 0, \end{cases} \tag{4.4.9}$$

where $\mathcal{R}_{obs,1}$ is a given function (for example in our case it could be $\mathcal{R}_{obs,1} = -\mathcal{R}_{obs,0}$). Problem (4.4.9) is an "exact controllability problem". These problems have solutions in some particular cases only. For this reason we replace (4.4.9) by the following generalized optimal control problem: find $\underline{\Phi_1} = (\mathbf{u}_1, p_1)\in\mathbb{Y}$, $f_1\in H_0^1(x_1,x_2)$ s.t.

$$\begin{cases} \mathcal{L}(\underline{\Phi_1},\underline{\hat{\Phi}}) = B(f_1,\underline{\hat{\Phi}})\ \forall\underline{\hat{\Phi}} = (\mathbf{v},q)\in\mathbb{W}, \\ \inf_{f_1} = \frac{\alpha}{2}||f_1||^2_{H_0^1(x_1,x_2)} + J(f_1,\mathbf{u}_1,p_1), \end{cases} \tag{4.4.10}$$

where

$$J(f_1,\mathbf{u}_1,p_1) = \gamma_1 J_1(f_1,\mathbf{u}_1) + \gamma_2 J_2(f_1,\mathbf{u}_1,p_1) + \gamma_3 J_3(f_1,\mathbf{u}_1,p_1),$$

$$J_1(f_1,\mathbf{u}_1) = \frac{1}{2}\int_0^T\int_\Omega m_{wd}\frac{f_0}{\beta}(\mathcal{R}(f_0)\mathbf{u}_1 + m_1\mathcal{R}_f f_1 - \mathcal{R}_{obs,1})^2,$$

$\alpha = const \geq 0$ is a small regularization parameter, $\gamma_1,\gamma_2,\gamma_3$ are non-negative constant weights, m_{wd} is the characteristic function of Ω_{wd}. The functional $J_1(f_1,\mathbf{u}_1)$ allows the control of the vorticity over a period T which is, as already seen, a relevant clinical index related also with velocity and viscous dissipation (more specifically to shear stresses), while $J_2(f_1,\mathbf{u}_1,p_1)$ and $J_3(f_1,\mathbf{u}_1,p_1)$ are additional functionals that are assumed to be quadratic. Note that the second equation in (4.4.9) is considered in (4.4.10) in the least square sense; then (4.4.10) for $\alpha = 0, \gamma_2 = \gamma_3 = 0$ provides the weak statement of problem (4.4.9). For

$\alpha > 0$ the solution $v_1 = v_1(\alpha),\ p_1 = p_1(\alpha),\ f_1 = f_1(\alpha)$ of (4.4.10) represents an approximate (regularized) solution of (4.4.9).
An example of $J_2(f_1, \mathbf{u}_1, p_1)$ follows:

$$J_2(f_1, \mathbf{u}_1, p_1) = J_2(\mathbf{u}_1, p_1) := \tag{4.4.11}$$
$$= \frac{1}{2}\Big(||p_1 - p_{out,1}||^2_{L^2(\Gamma_{out}\times(0,T))} + ||\mathbf{u}_1 - \mathbf{u}_{out,1}||^2_{L^2(\Gamma_{out}\times(0,T))^2}\Big)$$

The functional J_3 is introduced in order to enhance the smoothness in time of $\mathbf{u}_1, p_1$. There we will take:

$$J_3(f_1, \mathbf{u}_1, p_1) = J_3(\tau; p_1) := \frac{1}{2}\|\mathcal{J}(p_1 - p_{out,1})\|^2_{L^2(\Gamma_{out}\times(0,T))},$$

where

$$\mathcal{J}(p) := \frac{p(x,y,t) - p(x,y,t-\tau)}{\tau},$$

where $\tau \geq 0$ is a parameter, while it is assumed that the functions $p_1, p_{out,1}$ be extended by parity to the negative values of t (i.e. $p(x,y,t) := p(x,y,-t)$ as $t < 0, (x,y) \in \Omega$, etc). If $p_1, p_{out,1} \in H^1(0,T;L^2(\Omega))$ and $\tau \to 0$ then $J_3 \to \frac{1}{2}\|p_{1,t} - (p_{out,1})_t\|^2_{L^2(\Gamma_{out}\times(0,T))}$. Otherwise said, J_3 in fact imposes a regularity restriction on p_1. If $\tau \to \infty$, then $J_3 \to 0$ and no additional restriction holds on p_1. If $0 < \tau < \infty$ then the introduction of J_3 can be regarded as a tool that yields a regularization condition for p_1 on $\Gamma_{out} \times (0,T)$. (Of course there are other ways to introduce similar regularity restrictions).

4.5 The optimal control formulation for unsteady flows

When considering (4.4.10) we have considered the simple domain of Figure 4.4, that we have previously denoted with Ω. An alternative possibility (that we are going to follow) consists of using the new variable transformation

$$\mathbf{x} = T_{f_0}^{-1}(\tilde{\mathbf{x}}),\ \tilde{\mathbf{x}} \in \Omega,\ \mathbf{x} \in \Omega_0, \tag{4.5.1}$$

which is the identity in Ω_2, while $T_{f_0}^{-1}(\tilde{x}, \tilde{y}) = (\tilde{x}, \frac{f_0(\tilde{x})}{\beta}\tilde{y})$ in Ω_1, then working in the "unperturbed" domain Ω_0 (see Figure 4.5), as done in the previous chapter, the expressions for the bilinear forms in (4.4.10) become simpler.
Indeed in $\Omega_0 \times (0,T)$ problem (4.4.10) can be reformulated as follows: find $\underline{\Phi} = (\mathbf{u}, p) := \underline{\Phi_1} = (\mathbf{u}_1, p_1) \in \mathbb{Y}$, $f := f_1 \in \mathbb{H}_f$[2], such that

$$\begin{cases} \mathcal{L}(\underline{\Phi}, \hat{\underline{\Phi}}) = B(f, \hat{\underline{\Phi}})\ \forall \hat{\underline{\Phi}} := (\mathbf{v}, q) \in \mathbb{W}, \\ \inf_{f\in\mathbb{H}_f} = \frac{\alpha}{2}||f||^2_{H_0^1(x_1,x_2)} + J(f, \underline{\Phi}), \end{cases} \tag{4.5.2}$$

where

$$\mathcal{L}(\underline{\Phi}, \hat{\underline{\Phi}}) = a_0(\mathbf{u}, \mathbf{v}) - b_0(p, \mathbf{v}) + b_0(q, \underline{v}),$$

[2]From now on we denote $\mathbf{u}_1 = \mathbf{u},\ p_1 = p,\ f_1 = f$ however we should keep in mind that now $\mathbf{u}, p, f$ represent the "first corrections" of $\mathbf{u}_0,\ p_0,\ f_0$ on the unperturbed domain.

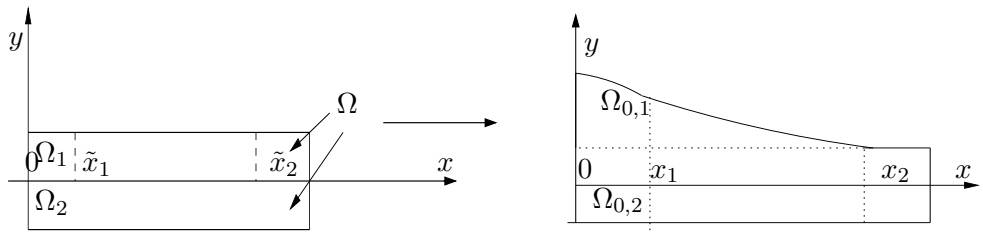

Figure 4.5: Transformation of the simple domain into the unperturbed domain Ω_0.

$$B(f,\hat{\underline{\Phi}}) := b_f(f,p_0,\mathbf{v}) + G_1(f,\mathbf{v}) - a_f(f,\mathbf{u}_0,\mathbf{v}) - b_f(f,q,\mathbf{u}_0),$$

$$a_0(\mathbf{u},\mathbf{v}) = \int_0^T \int_{\Omega_0} \nu\big(\frac{\partial \mathbf{u}}{\partial x}\cdot\frac{\partial \mathbf{v}}{\partial x} + \frac{\partial \mathbf{u}}{\partial y}\cdot\frac{\partial \mathbf{v}}{\partial y}\big) - \int_0^T \int_{\Omega_0} \mathbf{u}\cdot\mathbf{v}_t,$$

$$b_0(p,\mathbf{v}) = \int_0^T \int_{\Omega_0} p\nabla\cdot\mathbf{v},$$

$$b_f(f,p_0,\mathbf{v}) = \int_0^T \int_{\Omega_{0,1}} p_0\mathcal{D}_f(f,\mathbf{v}) + \int_0^T \int_{\Omega_{0,1}} \frac{f}{f_0} p_0\nabla\cdot\mathbf{v},$$

$$\mathcal{D}_f(f,\mathbf{v}) = -\big[y\big(\frac{f_x f_0 - f_{0,x} f}{f_0^2}\big)\frac{\partial \hat{u}}{\partial y} + \frac{f}{f_0}\frac{\partial \hat{v}}{\partial y}\big],$$

$$\mathcal{D}_f(f,v_0) := \mathcal{D}_f f,$$

$$G_1(f;\mathbf{v}) = \int_0^T \int_{\Omega_{0,1}} \frac{f}{f_0}\mathbf{f}\cdot\mathbf{v} + \int_{\Omega_{0,1}} \frac{f}{f_0}\mathbf{u}_0\cdot\mathbf{v}(x,y,0)d\Omega,$$

$$a_f(f;\mathbf{u}_0,\mathbf{v}) = \int_0^T \int_{\Omega_{0,1}} \frac{f\nu}{f_0}\nabla\mathbf{u}_0\cdot\nabla\mathbf{v} - \int_0^T \int_{\Omega_{0,1}} \nu y\frac{(f_x f_0 - f_{0,x} f)}{f_0^2}\big(\frac{\partial \mathbf{u}_0}{\partial y}\cdot\frac{\partial \mathbf{v}}{\partial x} + \frac{\partial \mathbf{u}_0}{\partial x}\cdot\frac{\partial \mathbf{v}}{\partial y}\big) +$$

$$- \int_0^T \int_{\Omega_{0,1}} \frac{2f\nu}{f_0}\frac{\partial \mathbf{u}_0}{\partial y}\cdot\frac{\partial \mathbf{v}}{\partial y},$$

$$J(f,\mathbf{u},p) = \gamma_1 J_1(f,\mathbf{u}) + \gamma_2 J_2(f,\mathbf{u},p) + \gamma_3 J_3(\tau;p),$$

$$J_1(f,\mathbf{u}) = \frac{1}{2}\int_0^T \int_{\Omega_0} m_{wd}|\nabla\times\mathbf{u} + m_1\mathcal{R}_f f - \mathcal{R}_{obs,1}|^2, \tag{4.5.3}$$

$$\mathcal{R}_f f := \mathcal{R}_f(f,\mathbf{u}_0) = -y\frac{(f_x f_0 - f_{0,x} f)}{f_0^2}\frac{\partial v_0}{\partial y} + \frac{f}{f_0}\frac{\partial u_0}{\partial y},$$

$J_2(f,\mathbf{u},p)$ and $J_3(\tau,p)$ are defined similarly. Let us derive the operator form of problem (4.5.2). Should $\underline{\Phi}$ be a solution of (4.5.2), then

$$\alpha(f,\hat{f})_{\mathbb{H}_f} + \langle J'_\Phi(f,\underline{\Phi}),\underline{\Phi}_{\hat{f}}\rangle + \langle J'_f(f,\underline{\Phi}),\hat{f}\rangle = 0, \tag{4.5.4}$$

for any $\hat{f}\in\mathbb{H}_f$ ($\hat{f}$ is the independent variation), where $\underline{\Phi}_{\hat{f}}\in\mathbb{W}$ satisfies the following equation:

$$\mathcal{L}(\underline{\Phi}_{\hat{f}},\hat{\underline{\Phi}}) = B(\hat{f},\hat{\underline{\Phi}})\ \forall\hat{\underline{\Phi}}\in\mathbb{W}. \tag{4.5.5}$$

In (4.5.4), $J'_\Phi = \frac{\partial J}{\partial \underline{\Phi}}$ and $J'_f = \frac{\partial J}{\partial f}$ are partial derivatives of J, while $\langle Q, \underline{\Phi}\rangle$ stands for ${}_{\mathbb{W}}\langle Q, \underline{\Phi}\rangle_{\mathbb{W}^*}$ the duality between $\mathbb{W}$ and $\mathbb{W}^*$ and $\langle g, f\rangle$ for the duality ${}_{\mathbb{H}_f}\langle g, f\rangle_{\mathbb{H}^*_f}$ between $\mathbb{H}_f$ and $\mathbb{H}^*_f$. Then we can write for (4.5.2) the system of "optimality conditions":

$$\begin{cases} \mathcal{L}(\underline{\Phi}, \hat{\underline{\Phi}}) = B(f, \hat{\underline{\Phi}}) \ \forall \hat{\underline{\Phi}} \in \mathbb{W}, \\ \alpha(f, \hat{f})_{\mathbb{H}_f} + \langle J'_\Phi(f, \underline{\Phi}), \underline{\Phi}_{\hat{f}}\rangle + \langle J'_f(f, \underline{\Phi}), \hat{f}\rangle = 0 \ \forall \hat{f} \in \mathbb{H}_f. \end{cases} \tag{4.5.6}$$

The element $\underline{\Phi}_{\hat{f}}$ can be eliminated from (3.5.6) by introducing the adjoint problem: find $\underline{Q} := (\mathbf{q}, \sigma) \in \mathbb{W}$ s.t.

$$\mathcal{L}^*(\underline{Q}, \hat{\underline{W}}) := \mathcal{L}(\hat{\underline{W}}, \underline{Q}) = \langle J'_\Phi(f, \underline{\Phi}), \hat{\underline{W}}\rangle \ \forall \hat{\underline{W}} \in \mathbb{Y}. \tag{4.5.7}$$

Since $\underline{\Phi}_{\hat{f}} \in \mathbb{Y}$ we can choose $\hat{\underline{W}} = \underline{\Phi}_{\hat{f}}$ in (4.5.7), yielding

$$\langle J'_\Phi(f, \underline{\Phi}), \underline{\Phi}_{\hat{f}})\rangle = \mathcal{L}(\underline{\Phi}_{\hat{f}}, \underline{Q}) = B(\hat{f}, \underline{Q}) \tag{4.5.8}$$

and the system of variational equations (4.5.6) reads now as follows:

$$\begin{cases} \mathcal{L}(\underline{\Phi}, \hat{\underline{\Phi}}) = B(f, \hat{\underline{\Phi}}) \ \forall \hat{\underline{\Phi}} \in \mathbb{W}, \\ \mathcal{L}^*(\underline{Q}, \hat{\underline{W}}) = \langle J'_\Phi(f, \underline{\Phi}), \hat{\underline{W}}\rangle \ \forall \hat{\underline{W}} \in \mathbb{Y}, \\ \alpha(f, \hat{f})_{\mathbb{H}_f} + B(\hat{f}, \underline{Q}) + \langle J'_f(f, \underline{\Phi}), \hat{f}\rangle = 0 \ \forall \hat{f} \in \mathbb{H}_f. \end{cases} \tag{4.5.9}$$

The first equation is the state equation. By means of the following operators (see Lions and Magenes [84], Lions [82] and Agoshkov [6]):

$$L : \mathbb{Y} \to \mathbb{W}^*, \ (L\underline{\Phi}, \hat{\underline{\Phi}})_{\mathbb{H}_0} := \mathcal{L}(\underline{\Phi}, \hat{\underline{\Phi}}),$$

$$L^* : \mathbb{W} \to \mathbb{Y}^*, \ (\hat{\underline{W}}, L^*\underline{Q})_{\mathbb{H}_0} = (L\hat{\underline{W}}, \underline{Q})_{\mathbb{H}_0},$$

$$B : \mathbb{H}_f \to \mathbb{W}^*, \ (Bf, \underline{\Phi})_{\mathbb{H}_0} = B(f, \underline{\Phi})$$

$$\Lambda_w : \mathbb{Y}^* \to \mathbb{Y}^*, \ (\Lambda_w J_\Phi(f, \underline{\Phi}), \hat{\underline{W}})_{\mathbb{H}_0} := \langle J'_\Phi(f, \underline{\Phi}), \hat{\underline{W}}\rangle,$$

$$\Lambda_f : \mathbb{H}^*_f \to \mathbb{H}^*_f, \ (\Lambda_f J_f(f, \underline{\Phi}), \hat{f})_{L^2(x_1, x_2)} := \langle J'_f(f, \underline{\Phi}), \hat{f}\rangle,$$

the system (4.5.9) can be written in operator form as follows:

$$\begin{cases} L\underline{\Phi} = Bf \ \ (in \ \mathbb{W}^*), \\ L^*\underline{Q} = \Lambda_w J_\Phi(f, \underline{\Phi}) \ \ (in \ \mathbb{Y}^*), \\ \alpha\Lambda_c f + B^*\underline{Q} + \Lambda_f J_f(f, \underline{\Phi}) = 0 \ \ (in \ (\mathbb{H}_f)^*), \end{cases} \tag{4.5.10}$$

there Λ_c is the extension to $\mathbb{H}_f$ of the operator:

$$\Lambda_{c,0} f := -f_{xx} + f$$

whose domain is $D(\Lambda_{c,0}) = H^2(\Omega) \cap \mathbb{H}_f$.

4.6 Existence and uniqueness results for unsteady case

We analyze the particular cases where the cost functional J is chosen as outlined in Section 4.4, and we extend uniqueness and existence results proven to the unsteady case. Let J be a weighted sum of the functionals J_1, J_2, J_3 of Section 4.4. Then

$$J(f,\underline{\Phi}) = J(f,\mathbf{u},p) = \frac{\gamma_1}{2}\int_0^T\int_{\Omega_0} m_{wd}|\nabla\times\mathbf{u} + m_1\mathcal{R}_f f - \mathcal{R}_{obs,1}|^2 d\Omega dt + \tag{4.6.1}$$

$$+\frac{\gamma_2}{2}\int_0^T\int_{\Gamma_{out}}\Big(|p-p_{out}|^2 + |\mathbf{u}-\mathbf{u}_{out}|^2\Big)d\Gamma dt + \frac{\gamma_3}{2}\int_0^T\int_{\Gamma_{out}}|\mathcal{J}(p-p_{out})|^2 d\Gamma dt$$

We assume that $\Omega_{wd} = \Omega_0$ and we define the spaces:

$$\mathbb{X} := \{\mathbf{u} : \mathbf{u}\in (H^2(\Omega))^2, \mathbf{u} = 0 \ on\ \Gamma_{in}\cup\Gamma_{w_1}\cup\Gamma_{w_3}\},$$

$$\mathbb{H}^p := L^2(0,T;H^1(\Omega_0)),\ \mathbb{H}_f := H^2(x_1,x_2)\cap H_0^1(x_1,x_2).$$

Also here we pretend that the velocity be in H^2 in order to use the uniqueness continuation theorem. The derivatives $J'_\Phi(f,\underline{\Phi})$ and $J'_f(f,\underline{\Phi})$ become

$$\langle J'_\Phi(f,\underline{\Phi}),\hat{\underline{\Phi}}\rangle = \gamma_1\int_0^T\int_{\Omega_0} m_{wd}(\nabla\times\mathbf{u} + m_1\mathcal{R}_f f - \mathcal{R}_{obs,1})\cdot(\nabla\times\mathbf{v})d\Omega dt +$$

$$+\gamma_2\int_0^T\int_{\Gamma_{out}}(p-p_{out})q d\Gamma dt + \gamma_2\int_0^T\int_{\Gamma_{out}}(\mathbf{u}-\mathbf{u}_{out})\cdot\mathbf{v} d\Gamma dt +$$

$$+\gamma_3\int_0^T\int_{\Gamma_{out}}\mathcal{J}(p-p_{out})\cdot\mathcal{J}(q)d\Gamma dt,$$

$$\langle J'_f(f,\underline{\Phi}),\hat{f}\rangle = \gamma_1\int_0^T\int_{\Omega_0} m_{wd}(\nabla\times\mathbf{u} + m_1\mathcal{R}_f f - \mathcal{R}_{obs,1})\mathcal{R}_f\hat{f} d\Omega dt,$$

$$\forall\ \hat{\underline{\Phi}} = (\mathbf{v},q)\ and\ \forall\ \hat{f}.$$

The system of variational equations (4.5.6) becomes: find $\underline{\Phi_f} = (\mathbf{u}_f, p_f)\in Y\times\mathbb{H}^p$ s.t.

$$\begin{cases} \mathcal{L}(\underline{\Phi_f},\hat{\underline{\Phi}}) = B(f,\hat{\underline{\Phi}})\ \forall\hat{\underline{\Phi}}\in W\times\mathbb{H}^p, \\ \alpha(f,\hat{f})_{\mathbb{H}_f} + \gamma_1\int_0^T\int_{\Omega_0} m_{wd}(\nabla\times\mathbf{u}_f + m_1\mathcal{R}_f f - \mathcal{R}_{obs,1})\cdot(\nabla\times\mathbf{u}_{\hat{f}} + \\ +m_1\mathcal{R}_f\hat{f})d\Omega dt + \gamma_2\int_0^T\int_{\Gamma_{out}}((p_f-p_{out})p_{\hat{f}} + (\mathbf{u}_f-\mathbf{u}_{out})\cdot\mathbf{u}_{\hat{f}})d\Gamma dt \\ +\gamma_3\int_0^T\int_{\Gamma_{out}}\mathcal{J}(p_f-p_{out})\mathcal{J}(p_{\hat{f}})d\Gamma dt = 0\ \forall\hat{f}\in\mathbb{H}_f, \end{cases} \tag{4.6.2}$$

where for every $\hat{f}$, $\mathbf{u}_{\hat{f}} = \mathbf{u}_f(\hat{f})$, $p_{\hat{f}} = p_f(\hat{f})$ denote the solution of the system given by the first equation in (4.6.2) corresponding to a right end side $f = \hat{f}$. The system (4.5.9) becomes: find $\underline{\Phi_f} = (\mathbf{u}_f, p_f)\in Y\times\mathbb{H}^p, \underline{Q} = (\mathbf{q},\sigma)\in W\times\mathbb{H}^p$ s.t.

$$\begin{cases} \mathcal{L}(\underline{\Phi_f},\hat{\underline{\Phi}}) = B(f,\hat{\underline{\Phi}})\ \forall\hat{\underline{\Phi}}\in W\times\mathbb{H}^p, \\ \mathcal{L}^*(\underline{Q},\hat{\underline{W}}) = \langle J'_\Phi(f,\underline{\Phi}),\hat{\underline{W}}\rangle\ \forall\hat{\underline{W}}\in Y\times\mathbb{H}^p, \\ \alpha(f,\hat{f})_{\mathbb{H}_f} + B(\hat{f},\underline{Q}) + \\ +\gamma_1\int_0^T\int_{\Omega_0} m_{wd}(\nabla\times\mathbf{u}_f + m_1\mathcal{R}_f f - \mathcal{R}_{obs,1})m_1\mathcal{R}_f\hat{f}d\Omega dt = 0\ \forall\hat{f}\in\mathbb{H}_f, \end{cases} \tag{4.6.3}$$

where

$$\langle J'_\Phi(f,\underline{\Phi}),\underline{\hat{W}}\rangle = \gamma_1\int_0^T\int_{\Omega_0} m_{wd}(\nabla\times\mathbf{u}_f + m_1\mathcal{R}_f f - \mathcal{R}_{obs,1})\cdot(\nabla\times\hat{\mathbf{q}})d\Omega dt+$$

$$+\gamma_2\int_0^T\int_{\Gamma_{out}}(\mathbf{u}_f-\mathbf{u}_{out})\cdot\hat{\mathbf{q}}d\Gamma dt + \gamma_2\int_0^T\int_{\Gamma_{out}}(p_f-p_{out})\hat{\sigma}d\Gamma dt+$$

$$+\gamma_3\int_0^T\int_{\Gamma_{out}}\mathcal{J}(p_f-p_{out})\cdot\mathcal{J}(\hat{\sigma})d\Gamma dt.$$

Consider now the problem (4.6.3) for $\alpha>0$.

Proposition 4.6.1 *For any $\alpha>0$ problem (4.6.3) has a unique solution for any given $\underline{\mathcal{R}}_{obs,1}$.*

Proof. Following [6] and what already seen in the previous chapter for steady flow, we formally invert L and L^* in the first and second equations of (4.5.10), then we substitute $\underline{\Phi}$, $\underline{Q}$ into the third equation and we obtain the following weak problem, $f\in\mathbb{H}_f$ satisfies:

$$\alpha(f,\hat{f})_{\mathbb{H}_f} + (Af,A\hat{f})_{L^2(x_1,x_2)} = (G,A\hat{f})_{L^2(x_1,x_2)}\ \forall\hat{f}\in\mathbb{H}_f. \tag{4.6.4}$$

A is a linear operator, while G depends on the data. Precisely, from (4.6.2) we obtain:

$$(f,\hat{f})_{\mathbb{H}_f} = (\Lambda_f f,\hat{f})_{L^2(x_1,x_2)},$$

$$(Af,A\hat{f})_{L^2(x_1,x_2)} = \gamma_1\int_0^T\int_\Omega m_{wd}(\nabla\times\mathbf{u}+m_1\mathcal{R}_f f)\cdot(\nabla\times\mathbf{u}_{\hat{f}}+m_1\mathcal{R}_f\hat{f})d\Omega dt+$$

$$+\gamma_2\int_0^T\int_{\Gamma_{out}}(pp_{\hat{f}}+\mathbf{u}\cdot\mathbf{u}_{\hat{f}})d\Gamma dt + \gamma_3\int_0^T\int_{\Gamma_{out}}\mathcal{J}(p)\cdot\mathcal{J}(p_{\hat{f}})d\Gamma dt,$$

$$(G,A\hat{f})_{L^2(x_1,x_2)} = \gamma_1\int_0^T\int_\Omega m_{wd}\mathcal{R}_{obs,1}\cdot(\nabla\times\mathbf{u}_{\hat{f}}+m_1\mathcal{R}_f\hat{f})d\Omega dt+$$

$$+\gamma_2\int_0^T\int_{\Gamma_{out}}(p_{out}p_{\hat{f}}+\mathbf{u}_{out}\cdot\mathbf{u}_{\hat{f}})d\Gamma dt + \gamma_3\int_0^T\int_{\Gamma_{out}}\mathcal{J}(p_{out})\cdot\mathcal{J}(p_{\hat{f}})d\Gamma dt,$$

where $\underline{\Phi}=(\mathbf{u},p)=L^{-1}Bf$, $\underline{\Phi}_{\hat{f}}=(\mathbf{u}_{\hat{f}},p_{\hat{f}})=L^{-1}B\hat{f},\ \forall\hat{f}\in\mathbb{H}_f$.
We see that if $\alpha>0$ then problem (4.6.4) has a unique solution which satisfies $\|f\|^2_{\mathbb{H}_f}\le\|G\|^2/(2\alpha)<\infty$. Correspondingly, we can construct $\mathbf{u}$, p, $\mathbf{q}$, σ, which together with f provide the unique solution of (4.6.3). □
Consider now problem (4.6.3) with $\alpha=0$.

Proposition 4.6.2 *Assume that:*
i) The solution of the generalized non-stationary Stokes problem (4.3.7) satisfies:

$$\Big(\frac{\partial v_0}{\partial y}\Big)^2+\Big(\frac{\partial u_0}{\partial y}\Big)^2>0\ at\ y=0,\ x\in(x_1,x_2);$$

ii) problem (4.6.3) has a solution in the class $(L^2(0,T;H^2(\Omega)^2)\times L^2(0,T;H^1(\Omega))\times W^{1,\infty}(x_1,x_2)$. *Then this solution is unique.*

PROOF. Let $(\mathbf{u}_1,p_1,f_1)$ and $(\mathbf{u}_2,p_2,f_2)$ be two solutions of (4.6.3). Then for $\mathbf{u}=\mathbf{u}_1-\mathbf{u}_2, p=p_1-p_2, f=f_1-f_2$ from (4.6.2) we obtain:

$$\begin{cases} a_0(\mathbf{u},\mathbf{v})-b_0(p,\mathbf{v})=F(f,\mathbf{v})\ \forall\mathbf{v}\in W,\\ b_0(q,\mathbf{u})+b_f(f;q,\mathbf{u}_0)=0\ \forall q\in\mathbb{H}^p,\\ \nabla\times\mathbf{u}+m_1\mathcal{R}_f f=0\ in\ \Omega\times(0,T),\\ p=0,\ \mathbf{u}=\mathbf{0}\ on\ \Gamma_{out}\times(0,T). \end{cases} \tag{4.6.5}$$

Consider the classical form of the second and the third equation from (4.6.5) in $\Omega_{2,0}\times(0,T)$

$$\nabla\cdot\mathbf{u}=0,\ \nabla\times\mathbf{u}=0\ in\ \Omega_{2,0}\times(0,T).$$

Then $\Delta\mathbf{u}=\mathbf{0}$ in $\Omega_{2,0}\ \forall t\in(0,T)$. Considering $\mathbf{v}$ with $supp(\mathbf{v})\subseteq\Omega_{2,0}$ from the first equation of (4.6.5) we find $\nabla p=\mathbf{0}$, then $p=const$ in $\Omega_{2,0}$ and $-p\hat{\mathbf{n}}+\nu\frac{\partial\mathbf{u}}{\partial\hat{\mathbf{n}}}=\mathbf{0}$ *on* $\Gamma_{out}\ \forall t$. Since $p=0$ *on* Γ_{out} then $p=0$ *in* $\Omega_{2,0}$ and $\nu\frac{\partial\mathbf{u}}{\partial\hat{\mathbf{n}}}=\mathbf{0}$ *on* Γ_{out} too. Consequently, for all $t\in(0,T)$, $\mathbf{u}$ satisfies:

$$\Delta\mathbf{u}=\mathbf{0}\ in\ \Omega_{2,0},\ \mathbf{u}=\nu\frac{\partial\mathbf{u}}{\partial\hat{\mathbf{n}}}=\mathbf{0}\ on\ \Gamma_{out}.$$

Owing to the uniqueness continuation theorem this Cauchy problem has only the trivial solution $\mathbf{u}=\mathbf{0}$ *in* $\Omega_{2,0}$. Since $\mathbf{u}\in L^2(0,T;H^2(\Omega)^2)$ then

$$\mathbf{u}=\frac{\partial\mathbf{u}}{\partial\hat{\mathbf{n}}}=\mathbf{0}\ on\ \Gamma_0:=\{(x,y):y=0,x_1<x<x_2\},\ \forall t\in(0,T).$$

Consider now the second and third equations from (4.6.5) in $\Omega_{1,0}$ in their classical form, $\forall\, t\in(0,T)$:

$$\begin{cases} \nabla\cdot\mathbf{u}-\left[y\left(\frac{f_xf_0-f_{0,x}f}{f_0^2}\right)\frac{\partial u_0}{\partial y}+\frac{f}{f_0}\frac{\partial v_0}{\partial y}\right]=0\ in\ \Omega_{1,0},\\ \nabla\times\mathbf{u}-\left[y\left(\frac{f_xf_0-f_{0,x}f}{f_0^2}\right)\frac{\partial v_0}{\partial y}-\frac{f}{f_0}\frac{\partial u_0}{\partial y}\right]=0\ in\ \Omega_{1,0}. \end{cases} \tag{4.6.6}$$

On Γ_0 we have:

$$\nabla\cdot\mathbf{u}-\frac{f}{f_0}\frac{\partial v_0}{\partial y}=0,\ \nabla\times\mathbf{u}+\frac{f}{f_0}\frac{\partial u_0}{\partial y}=0,$$

$$|f(x)|=f_0\frac{\left[(\nabla\cdot\mathbf{u})^2+(\nabla\times\mathbf{u})^2\right]^{1/2}}{\left[\left(\frac{\partial v_0}{\partial y}\right)^2+\left(\frac{\partial u_0}{\partial y}\right)^2\right]^{1/2}}\ on\ \Gamma_0,$$

(the dependence of the right end side on x and y is understood). Since $\mathbf{u}=\frac{\partial\mathbf{u}}{\partial\hat{\mathbf{n}}}=\frac{\partial\mathbf{u}}{\partial y}=0$ *on* Γ_0, then

$$\nabla\cdot\mathbf{u}|_{y=0}=\frac{\partial u}{\partial x}+\frac{\partial v}{\partial y}|_{y=0}=0,\ \nabla\times\mathbf{u}|_{y=0}=\frac{\partial v}{\partial y}-\frac{\partial u}{\partial x}|_{y=0}=0,\ x\in(x_1,x_2).$$

i.e. $f(x)=0$. Therefore, $\mathbf{u}=0,\ p=0$ too, $\forall t\in(0,T)$. □

4.7 The iterative process in the non-stationary case

In this section we propose some iterative processes for solving the space-time variational equations obtained in the previous sections. These algorithms are an extension of those introduced in the previous chapter. Consider the problem (4.5.10); if for $k = 0, 1, \dots$ $f^{(k)}$ is known, then $f^{(k+1)}$ can be determinated by solving the following equations [6]:

$$\begin{cases} L\Phi^{(k)} = Bf^{(k)}, \\ L^*\underline{Q}^{(k)} = \Lambda_w J_\Phi(f^{(k)}, \underline{\Phi}^{(k)}), \\ \Lambda_c \underline{w}^{(k)} = B^*\underline{Q}^{(k)} + \Lambda_f J_f(f^{(k)}, \underline{\Phi}^{(k)}), \\ f^{(k+1)} = f^{(k)} - \tau_k(\alpha f^{(k)} + w^{(k)}), \end{cases} \tag{4.7.1}$$

where $\{\tau_k\}$ is a family of parameters whose determination follows from the theory of extremal problems (see Vasiliev [155]), the general theory of iterative processes (see Marchuk [94], Quarteroni and Valli [127], Quarteroni, Sacco and Saleri [129]), and the ill-posed problems theory (Tikhonov and Arsenin [151], Vainikko and Veretennikov [153]). Its variational form reads as:

$$\begin{cases} a_0(\mathbf{u}^{(k)}, \mathbf{v}) - b_0(p^{(k)}, \mathbf{v}) = F(f^{(k)}, \mathbf{v}) \ \forall \mathbf{v} \in W, \\ b_0(q, \mathbf{u}^{(k)}) = -b_f(f^{(k)}; q, \mathbf{u}_0) \ \forall q \in \mathbb{H}^p, \\ a_0(\hat{\mathbf{q}}, \mathbf{q}^{(k)}) + b_0(\sigma^{(k)}, \hat{\mathbf{q}}) = G_k(\hat{\mathbf{q}}) \ \forall \hat{\mathbf{q}} \in Y, \\ -b_0(\hat{\sigma}, \mathbf{q}^{(k)}) = g_k(\hat{\sigma}) \ \forall \hat{\sigma} \in \mathbb{H}^p, \\ (w^{(k)}, \hat{f})_{\mathbb{H}_f} = d_k(\hat{f}) \ \forall \hat{f} \in \mathbb{H}_f, \\ f^{(k+1)} = f^{(k)} - \tau_k(\alpha f^{(k)} + w^{(k)}), \quad k = 0, 1, \dots, \end{cases} \tag{4.7.2}$$

where

$$F(f^{(k)}, \mathbf{v}) = b_f(f^{(k)}, p_0, \mathbf{v}) + G_1(f^{(k)}, \mathbf{v}) - a_f(f^{(k)}, \mathbf{u}_0, \mathbf{v}),$$

$$G_k(\hat{\mathbf{q}}) = \gamma_1 \int_0^T \int_{\Omega_0} m_{wd}(\nabla \times \mathbf{u}^{(k)} + m_1 \mathcal{R}_f f^{(k)} - \mathcal{R}_{obs,1}) \cdot (\nabla \times \hat{\mathbf{q}}) d\Omega dt +$$

$$+\gamma_2 \int_0^T \int_{\Gamma_{out}} (\mathbf{u}^{(k)} - \mathbf{u}_{out}) \cdot \hat{\mathbf{q}} d\Gamma dt,$$

$$g_k(\hat{\sigma}) = \gamma_2 \int_0^T \int_{\Gamma_{out}} (p^{(k)} - p_{out}) \hat{\sigma} d\Gamma dt + \gamma_3 \int_0^T \int_{\Gamma_{out}} \mathcal{J}(p^{(k)} - p_{out}) \cdot \mathcal{J}\hat{\sigma} d\Gamma dt,$$

$$d_k(\hat{f}) = F(\hat{f}, \mathbf{q}^{(k)}) - b_f(\hat{f}; \sigma^{(k)}, \mathbf{u}_0) +$$

$$+\gamma_1 \int_0^T \int_{\Omega_0} m_{wd}(\nabla \times \mathbf{u}^{(k)} + m_1 \mathcal{R}_f f^{(k)} - \mathcal{R}_{obs,1}) m_1 \mathcal{R}_f \hat{f} d\Omega dt.$$

Consider now the *finite dimensional case* in which the function $f, \{f^{(k)}\}, \hat{f}$ all are sought for in a finite-dimensional subspace $\mathbb{H}_{f,N} \subset \mathbb{H}_f$ of dimension $N < \infty$, whose basis $\varphi_i \in \mathbb{W}^{1,\infty}(x_1, x_2), i = 1, 2, \dots, N$. Then the following theorem holds true.

Theorem 4.7.1 *Assume that:*

$$\Omega_{wd} = \Omega,$$

$$\Big(\frac{\partial v_0}{\partial y}\Big)^2 + \Big(\frac{\partial u_0}{\partial y}\Big)^2 > 0 \text{ at } y = 0,\ x \in (x_1, x_2).$$

Then:

1. *For $\alpha \geq 0$ and any $N < \infty$ the problem (4.6.2) is well posed (i.e. it admits a unique solution that depends continuously on the data);*

2. *The iterative process (4.7.2) is convergent for any $\alpha > 0,\ N < \infty$, provided the parameters $\tau_k > 0,\ k = 0, 1, 2, \ldots$ are small enough;*

3. *If α is sufficiently small while k is sufficiently large, then $\{\mathbf{u}^{(k)}, p^{(k)}, f^{(k)}\}$ can be regarded as an approximate solution of problem (4.6.2).*

Proof:

1. For $\alpha > 0$ the existence was proven earlier in Proposition 4.6.1. Let us consider the case $\alpha = 0$, since $f = \Sigma_{i=1}^{N} a_i \varphi_i \in \mathbb{H}_{f,N}$, then (4.6.4) is well posed (because problem (4.6.2) can have only unique solution in $\mathbb{X} \times \mathbb{H}^p \times \mathbb{H}_f$, see Proposition 4.6.2). We assume the unsteady Stokes problem to be well posed for given $f \in \mathbb{H}_f$. Hence the problem (4.6.2) is well posed too.

2. If $\alpha > 0$ then the bilinear form on the left hand side of (4.6.4) is coercive and continuous with respect to the norm

$$\|f\|_{A,\alpha} = \sqrt{\alpha \|f\|^2_{\mathbb{H}_f} + \|Af\|^2_{L^2(x_1,x_2)}}.$$

Then the process given by

$$(f^{(k+1)}, \hat{f})_{\mathbb{H}_f} = (f^{(k)}, \hat{f})_{\mathbb{H}_f} - \tau(\alpha(f^{(k)}, \hat{f})_{\mathbb{H}_f} + (Af^{(k)}, A\hat{f})_{L^2(x_1,x_2)}) -$$

$$-(G, A\hat{f})_{L^2(x_1,x_2)},\ k = 0, 1, \ldots$$

is convergent for small $\tau > 0$. Hence also the process (3.7.3) is convergent and

$$\|\mathbf{u}^{(k)} - \mathbf{u}\|_Y + \|p^{(k)} - p\|_{\mathbb{H}^p} + \|f - f^{(k)}\|_{\mathbb{H}_f} \to 0,\ k \to \infty. \tag{4.7.3}$$

If $\Lambda_C^{-1} A^* A \in [C_1, C_2], C_1, C_2 = const$, choosing $\tau_k = 2/(2\alpha + C_1 + C_2)$ we obtain (see Agoshkov [6]):

$$\|\mathbf{u}^{(k)} - \mathbf{u}\|_Y + \|p^{(k)} - p\|_{\mathbb{H}^p} + \|f - f^{(k)}\|_{\mathbb{H}_f} \leq C\Big(\frac{C_2 - C_1}{2\alpha + C_1 + C_2}\Big)^k \tag{4.7.4}$$

which tends to zero as $k \to \infty$.

3. Let $\mathbf{u}_0,\ p_0,\ f_0$ be a solution of (3.6.2) when $\alpha = 0$. According to the theory of ill-posed problems ([151] and [153]) we have: $\|f_0 - f_\alpha\|_{\mathbb{H}_f} \to 0$ as $\alpha \to 0^+$, where $(f_\alpha, \mathbf{u}_\alpha, p_\alpha)$ is the solution of (3.6.2) for $\alpha > 0$. Hence

$$\|\mathbf{u}_0 - \mathbf{u}_\alpha\|_Y + \|p_0 - p_\alpha\|_{\mathbb{H}^p} \to 0,\ as\ \alpha \to 0^+.$$

Owing to (4.7.3) this concludes our proof. □

4.8 Numerical results for unsteady generalized Stokes problem

To test and extend our methodology we consider some test problems on the initial configuration already used in the previous test case.
Velocity values $\mathbf{u}_{in}$ at the inflow are chosen in such a way that the Reynolds number $Re = \frac{\bar{u}D}{\nu}$ be of the order 10^3, the mean Reynolds number is 1250, the maximum is 2500. The inlet Poiseuille velocity profile has a pulsatile nature over the period $T = 1s$ (heart beat) and the law considered was: $\mathbf{u}_{in} = -0.475(y-1)(y-2)(1-t)\hat{\mathbf{n}}$, see Figure 4.8. Blood kinematic viscosity $\nu = \frac{\mu}{\rho}$ is equal to $4 \cdot 10^{-6}\ m^2\ s^{-1}$, blood density $\rho = 1\ g\ cm^{-3}$ and dynamic viscosity $\mu = 4 \cdot 10^{-2}\ g\ cm^{-1}s^{-1}$; $\bar{u}$ is the mean inflow velocity $\overline{u} = \left(\frac{\int_{\Gamma_{in}} \int_0^T |\mathbf{u}_{in} \cdot \hat{\mathbf{n}}| d\Gamma dt}{\int_{\Gamma_{in}} \int_0^T d\Gamma dt}\right)$ which yields the desired Reynolds number, while D is the arterial diameter (3.5 mm), see Quarteroni and Formaggia [126], Quarteroni, Tuveri and Veneziani [125].
Dealing with unsteady blood flow into the coronaries (from the Aorta artery) we have to face some difficulties and fix some hypotheses to model the pulsatile flow and the fluid mechanical phenomena in the endograft region (see for preliminary considerations Bertolotti *et al.* [18]). The first aspect deals with the fact that we consider a complete stenosis into the artery (the flow rate from the stenosed section is set to zero), and this yields a retrograde flow, see Kute and Vorp [74]. The second aspect deals with the way blood flow is modelled into the coronaries. Being embedded on the heart surface muscle, coronaries do not share the same behavior similar the other arteries during systolic and diastolic phases. In fact, during systolic phase, the left ventricle contracts and squeezes the coronaries. To take that into account, we have adopted the same pulsatile flow at the inlet of the bypass bridge as the one of the aortic vessel from the opening of the coronaries to the end of the period. The flow-rate function goes from a maximum quantity to zero. For more details we suggest to see Sankaranarayanan *et al.* [140]. Figures 4.6 and 4.7 show the flow-rate waveform for the Aorta and the left coronary, respectively; we can see that the flow-rate in the aorta goes from zero to a maximum and then to zero in the systolic phase and remains at zero during diastolic phase. To model blood flow into the bypass bridge we have adopted the aorta flow-rate waveform but from the time step in which the coronaries are open (and not squeezed): for this reason in the bypass we have a flow-rate waveform starting from a maximum and going to zero.

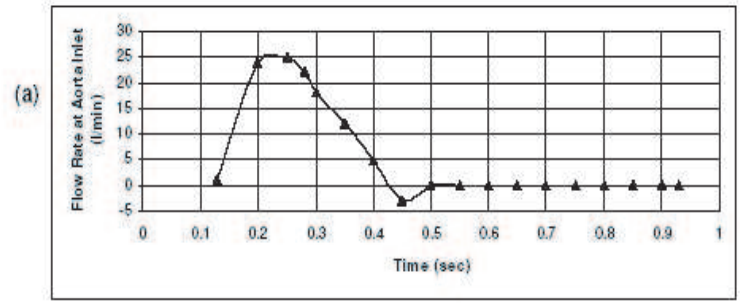

Figure 4.6: Flow-rate waveform at the inlet of the ascending Aorta from [140].

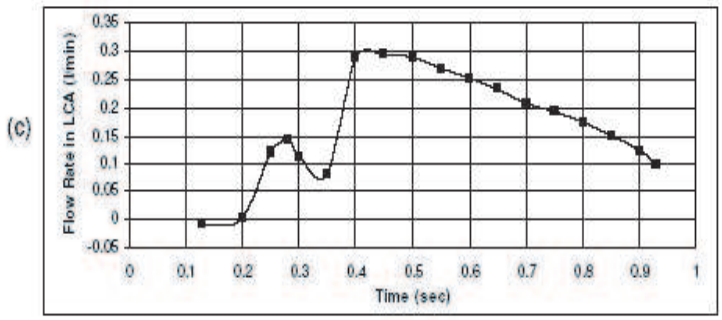

Figure 4.7: Flow-rate waveform at the left coronary from [140].

In this section we present numerical results using as cost functional $J(f, \mathbf{u}) = J_1(f, \mathbf{u})$ (introduced in Equation (4.5.3)). This is equivalent to the L^2 norm of the vorticity on $(\Omega_{wd} \times (0, T))$ (restricted in the downfield zone of the new incoming branch of the bypass, where the observation is made). We have set $\mathcal{R}_{obs,1} = -0.45 \cdot \mathcal{R}(f_0)\mathbf{u}$.
For the space approximation of the unsteady Stokes equations we use $\mathbb{P}^1 - \mathbb{P}^1$ (piecewise linear) finite elements and SUPG stabilization (see [127]). Time discretization is based on first order backward differentiation (which is unconditionally stable).
In figures 4.9-4.14 we report the numerical results obtained and show how the shape of the bypass is changed to reduce downfield vorticity. The shape is smoothed out at the upper corner and a slightly cuffed incoming branch is created. These results provide a shape which resembles the Taylor patch (see Cole *et al.* [26]). We have shown original bypass configuration (and horizontal velocity to show relevant fluid dynamics phenomena) at different time-steps ($t_1 = 0.1$ s, $t_2 = 0.4$ s, $t_3 = 0.7$ s) and then the configurations obtained at different iterations of our optimization process (i.e. at $N_1 = 5$, $N_2 = 11$ and $N_3 = 17$). These results can be regarded as an improvement of previous results that were obtained using a steady fluid flow model. The similarity between the present results and those obtained in [4] (and introduced in the previous chapter) can be ascribed to the fact that shape $f^{(k)}$ does not depend on time, moreover the shape variation at each optimization step $\delta f^{(k)}$ is given by the sum of the contributions from all time-steps in $(0, T)$ and the first contribution is the one that dominates

(when considering a pulsatile flow). In these simulations we can find the typical flow reversal caused by the stenosed zone and the other related aspects described for instance in Lei *et al.* [79]. Figure 4.15 shows pointwise vorticity ($[1/s]$) in bypass configuration before and at the end of the control process. Vorticity is diminished near the upper corner (in the original configuration we have a concentrated vorticity at the singularity) but also in the bed of the artery in the down-field zone: this indicates that the flow is less disturbed and the main flow decreases its attitude to recirculate in the stenosed zone. These phenomena are due to the fact that the bypass section is smoothed and increased and the flow is guided more smoothly through the section. Figure 4.16 shows the variation of corrections $(x, \delta f^n(x)y/\beta)$ at the first iteration and after 14 iterations of the shape design process. These plots represent a measure of shape variation (first corrections) with respect to the problem. Note that δf^n is related with state and adjoint solutions. At the beginning of the process we can see (plot on the left) that the corner is the most sensible zone of the domain, after 14 iterations of the process (plot on the right) the shape variation is reduced (max $\delta f^{(n)}$ is 10% of the one at the first step). In Figure 4.17 we report total vorticity ($[m^2/s]$) in down-field zone during the control process at different time steps. We underline that only for the curve at $t = 1$ s we have a complete result dealing with vorticity reduction over a period T, other curves represent partial results considering a fraction of T (optimization is carried out over a period T at each iteration). The most important contribution to total vorticity is given by the flow behavior in the first part of the period considered. The total vorticity reduction is quite substantial. Figure 4.17 shows the total vorticity trend in time. At the end of the process we can see that the vorticity behavior in time has the same trend, however its value is reduced.

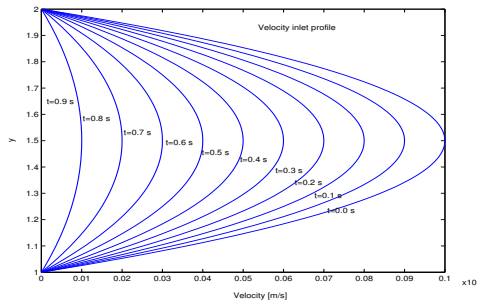

Figure 4.8: Unsteady (pulsatile) Stokes velocity profiles at the inflow $[ms^{-1}]$.

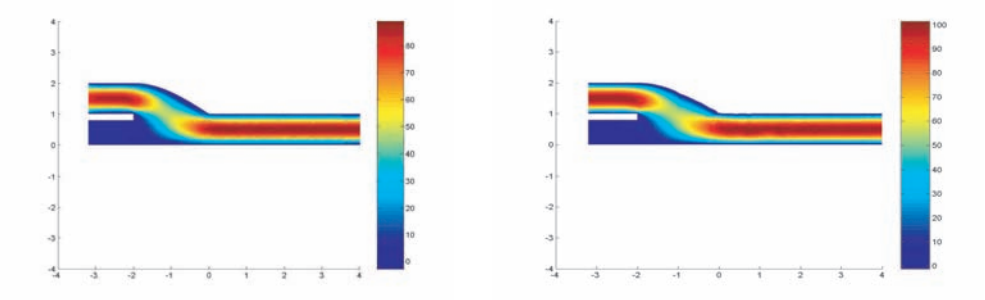

Figure 4.9: Horizontal velocity $[ms^{-1} \cdot 10^{-2}]$ at $t = 0.1s$ for initial test configuration (left) and after 5 iterations (right).

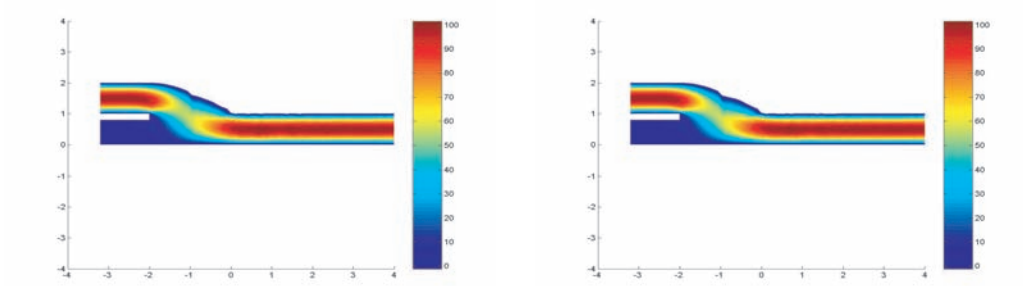

Figure 4.10: Horizontal velocity $[ms^{-1} \cdot 10^{-2}]$ after $t = 0.1s$ at 11 (left) and 17 (right) iterations.

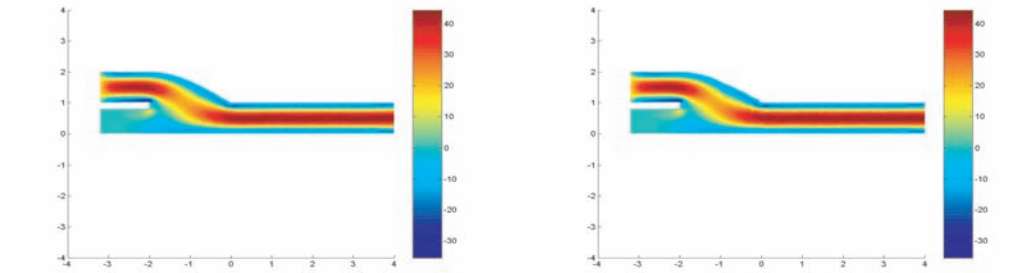

Figure 4.11: Horizontal velocity $[ms^{-1} \cdot 10^{-2}]$ at $t = 0.4s$ for initial test configuration (left) and after 5 iterations (right).

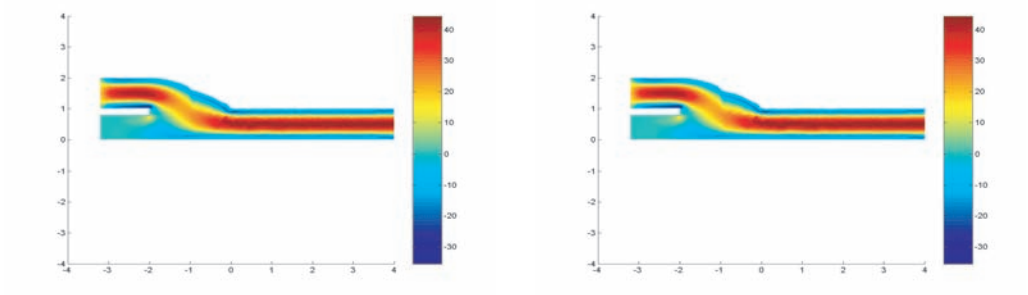

Figure 4.12: Horizontal velocity $[ms^{-1} \cdot 10^{-2}]$ after $t = 0.4s$ at 11 (left) and 17 (right) iterations.

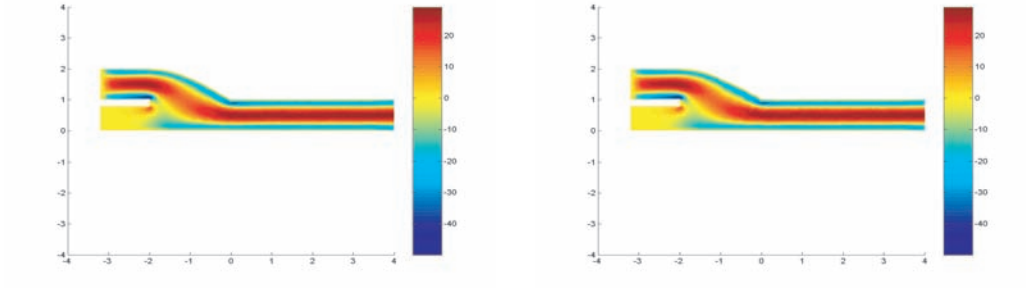

Figure 4.13: Horizontal velocity $[ms^{-1} \cdot 10^{-2}]$ at $t = 0.7s$ for initial test configuration (left) and after 5 iterations (right).

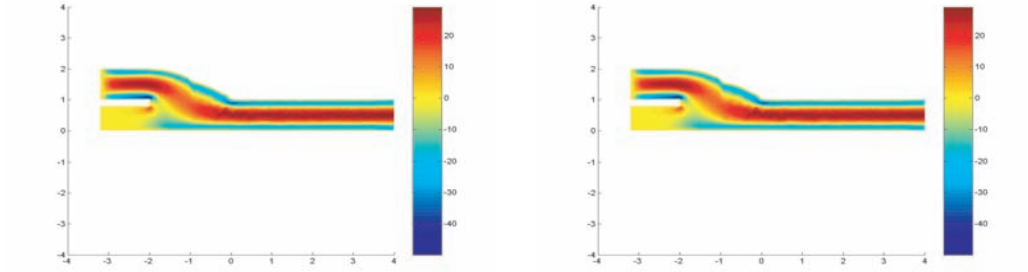

Figure 4.14: Horizontal velocity $[ms^{-1} \cdot 10^{-2}]$ after $t = 0.7s$ at 11 (left) and 17 (right) iterations.

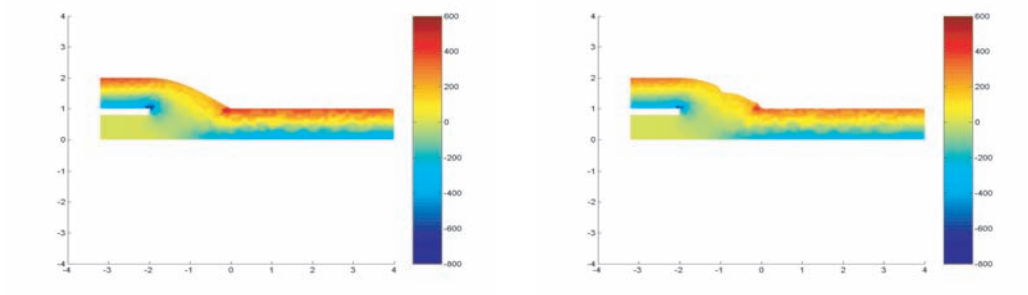

Figure 4.15: Distributed vorticity $[s^{-1} \cdot 10^{-2}]$ in original configuration (left) and at the end of the optimization process (right). Vorticity in the upper corner and in the bed of the artery is diminished.

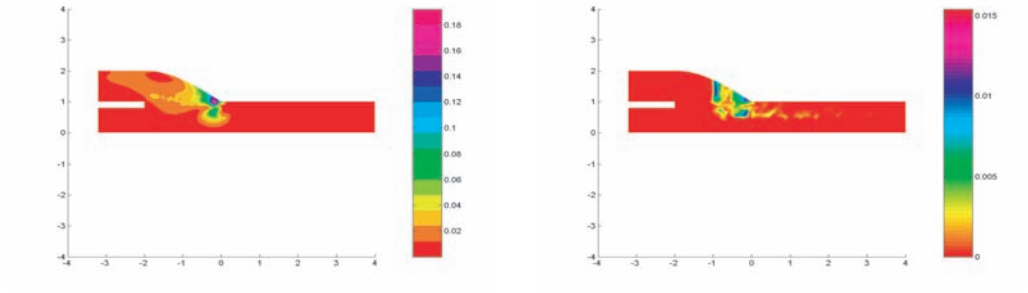

Figure 4.16: Variation of corrections $(x, \delta f^n(x) y/\beta)$ at the first iteration (left) and after 14 iterations of the process (right) $[m \cdot 10^{-2}]$.

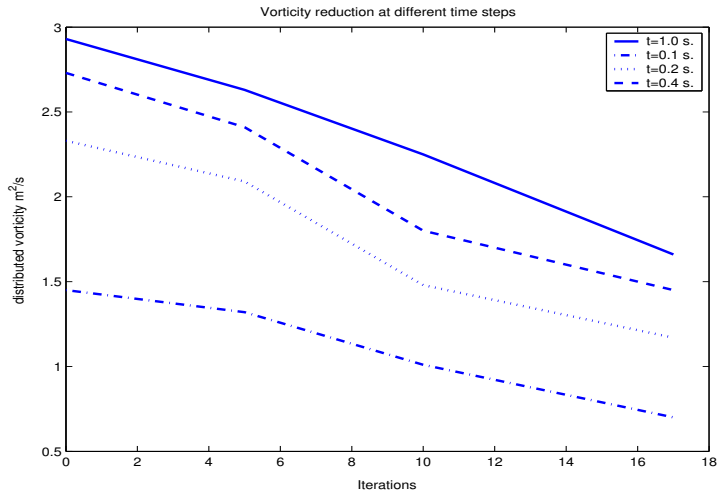

Figure 4.17: Total vorticity $[m^2 s^{-1}]$ reduction at different time steps during shape optimization.

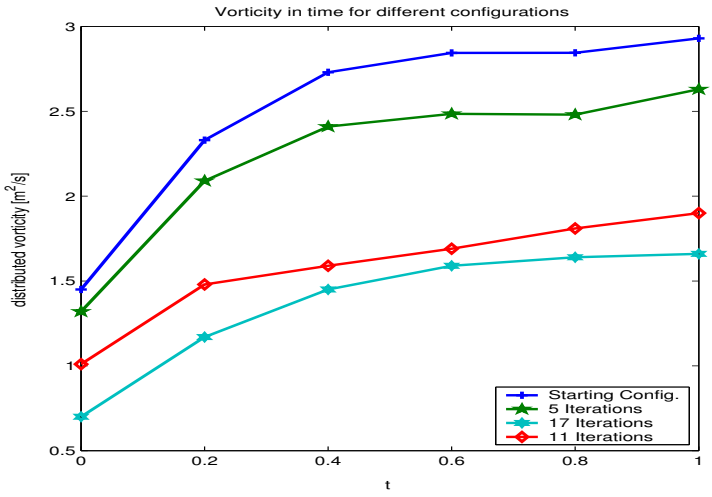

Figure 4.18: Total vorticity $[m^2 s^{-1}]$ in time during shape optimization for different configurations.

4.9 Conclusions about Part I

In the first part of this thesis we have proposed several mathematical approaches based on optimal flow control techniques for shape optimization problem. They both use simplified fluid models to be verified in feed-back and are based on local boundary variations and small perturbation theory. Using a vorticity cost functional we tried to unify different approaches about bypass configurations already available in literature in which cost functionals depend on velocity field, viscous dissipation and stresses: all these quantities can indeed be related to vorticity. In the last approach we have also modelled the unsteady flow rate in the coronary after bypass implanting procedures.

The approach proposed and discussed in this chapter and in the previous one, based on small perturbation in fluid mechanics and set into a reference domain, is more general than the one discussed in Chapter 2 and has permitted us to investigate the problem from a theoretical point of view and to generalize the approach dealing with transient flows and to use a unique computational mesh.

The results we have analyzed in this part of the work underline the importance of an accurate modelling of the incoming branch of the bypass, in particular with cuffed and/or patched shapes, which provide an enlarged section between the bypass and the host artery. Some of the results found using shape optimization and optimal flow control were already known in literature, but not validated yet by optimization techniques and not interpreted and unified using vorticity cost functional.

What ought be done to generalize and validate our results on the local shape of the incoming branch of the bypass is to study a complete bridge configuration depending on a certain number of parameters. This aspect will be considered in the second part of the thesis by reduced basis techniques where we will deal both with Stokes and Navier-Stokes equations.

Another issue is how to reduce computational costs in solving optimal control problems, like the ones proposed in Chapters $2-4$, which are very expensive: reduced basis methods can be adopted also in this respect and, in the last part, it will be shown how to use reduced basis to solve optimal control problems.

Part II

Reduced Basis Techniques for Optimization

Chapter 5

Reduced Basis Methods for Stokes Equations

In this chapter we extend reduced basis techniques[3] *to Stokes equations in domains with affine (or approximately affine) parameter dependence to have a rapid and reliable prediction of linear-functional outputs. Particular attention is given to the approximation problem: (i) to the pressure treatment of incompressible Stokes problem; (ii) to find an equivalent inf-sup condition to guarantee stability of reduced basis solutions enriching the reduced basis velocity approximation space with the solutions of a supremizer problem; (iii) to provide algebraic stability of the problem by bounding the condition number of reduced basis matrices using an orthonormalization procedure applied to functions used as basis; (iv) to improve accuracy of outputs estimation by a dual residual method based on adjoint problem approach;(v) to reduce computational costs in order to have real time solution of parametrized problem; (vi) finally, by considering more complex ("non-compliant") outputs.*
The motivation in developing reduced basis techniques is the set-up of computational methods which allow huge computational savings to solve also the problems introduced in the first part of this thesis. In this chapter we will derive a methodology focusing on bypass optimization problem, however we will also address some issues and results which are interesting independently of the problem considered in the previous chapters.

5.1 Reduced basis for viscous flows

In this chapter we are going to introduce the reduced basis formulation for a pre-process optimization on a Cartesian geometry for a simplified bypass configuration. Preliminary applications of reduced basis techniques to incompressible viscous flows problems are given in Peterson [113], in Ito and Ravindran [64] and also [62] for optimal control problems; however in these papers the pressure approximation is not considered and stability of solutions is not discussed. More recent works dealing with free divergence velocity spaces and physical parameters and focused on a posteriori error estimates are the ones by Patera, Veroy *et*

[3]For an introduction on reduced basis methods and related aspects see **Appendix A**.

al. [159], [104], and [160]. This chapter (which generalizes the results of [111]) is organized as follows: in Section 5.2 we formulate the problem for parametrized Stokes equations. In Section 5.3 we introduce the Stokes reduced basis formulation and analyze the stability of the approximation. In Section 5.4 we study a procedure to control N (the number of reduced basis functions) more tightly and to apply an adaptive procedure for the basis construction using a suitable error projection. In Section 5.5 we analyze the inf-sup condition which is necessary for the stability of reduced basis approximation. Then in the Section 5.6 we present some numerical results based on three different test cases. In Section 5.7 we deal with algebraic stability problem and we present possible solutions to achieve it by an orthonormalization procedure. In Section 5.8 we introduce some sensitivity results based on geometrical quantities of interest for the bypass configuration. In Section 5.9 we start dealing with more complex outputs related with fluid mechanics quantities and based on a dual residual approach. A recent interesting approach to parametrized domains is provided by Maday and Rønquist [88], where a reduced basis element method based on a domain decomposition approach is proposed. The idea is to decompose the computational domain into a series of subdomains that are deformations of a few reference domains into geometrically similar parts ("elements"). Associated with each reference subdomain there are precomputed solutions corresponding to the same governing partial differential equation (the case deals with steady Stokes equations), but solved for different choices of parameters deforming the subdomains and mapped onto the reference shape. In our case we do not consider a domain decomposition approach and we deform the complete parametrized domain. Our approach is an extension of the one used to introduce the parametrization of physical quantities by affine (and then non-affine) maps.

5.2 The parametrized Stokes problem

We start considering parametrized Stokes equations in the same "T" domain introduced in Appendix A with one more parameter, H, the bypass bridge height as in Figure 5.1. Referring to the following steady Stokes problem in a domain $\hat{\Omega}$

$$\begin{cases} -\nu\triangle\hat{\mathbf{u}} + \nabla\hat{p} = \hat{\mathbf{f}} \ in \ \hat{\Omega}, \\ \nabla\cdot\hat{\mathbf{u}} = 0 \ in \ \hat{\Omega}, \\ \hat{\mathbf{u}} = \mathbf{0} \ on \ \hat{\Gamma}_w; \ \hat{\mathbf{u}} = \hat{\mathbf{g}}_{in} \ on \ \hat{\Gamma}_{in}, \nu\frac{\partial\hat{\mathbf{u}}}{\partial\hat{\mathbf{n}}} - \hat{p}\hat{\mathbf{n}} = \mathbf{0} \ on \ \hat{\Gamma}_{out}, \end{cases} \tag{5.2.1}$$

its weak formulation reads: find $\hat{\mathbf{u}} \in Y = H^1_{\Gamma_D}(\Omega) \times H^1_{\Gamma_D}(\Omega)$, $\hat{p} \in Q = L^2(\Omega)$, $\Omega \subset \mathbb{R}^2$ such that:

$$\begin{cases} \nu\displaystyle\int_{\hat{\Omega}} \nabla\hat{\mathbf{u}}\cdot\nabla\hat{\mathbf{w}}d\Omega - \int_{\hat{\Omega}} \hat{p}\,\nabla\cdot\hat{\mathbf{w}}d\Omega = \int_{\hat{\Omega}} \hat{\mathbf{f}}\cdot\hat{\mathbf{w}}d\Omega + \langle\hat{F^0},\hat{\mathbf{w}}\rangle \ \forall\hat{\mathbf{w}} \in Y, \\ \displaystyle\int_{\hat{\Omega}} \hat{q}\,\nabla\cdot\hat{\mathbf{u}}d\Omega = \langle\hat{G^0},\hat{q}\rangle \ \ \forall\hat{q} \in Q, \end{cases} \tag{5.2.2}$$

$\hat{F^0}, \hat{G^0}$ are terms due to non-homogeneous Dirichlet boundary condition ($\mathbf{u} = \mathbf{g}_{in}$) on $\hat{\Gamma}_{in}$, $\hat{\Gamma}_D = \hat{\Gamma}_{in} \cup \hat{\Gamma}_w$, on $\hat{\Gamma}_{out}$ we have a free stress Neumann condition. In our case the true

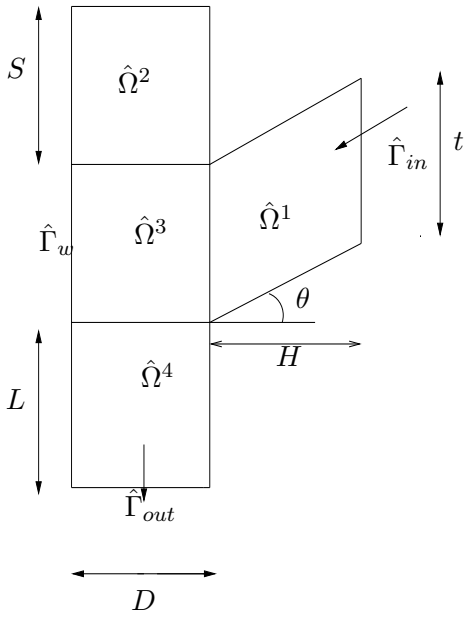

Figure 5.1: True physical domain: sub-domains and parameters.

domain is made up of $R = 4$ subdomains: $\hat{\Omega} = \bigcup_{r=1}^{R} \hat{\Omega}^r$, so that the bilinear and linear forms of the problem weak statement read for $1 \leq i, j \leq d = 2$ and $\hat{\nu}_{i,j} = \nu\delta_{i,j}$ as:

$$\langle \hat{\mathcal{A}}\hat{\mathbf{u}}, \hat{\mathbf{w}} \rangle = \sum_{r=1}^{R} \int_{\hat{\Omega}^r} \frac{\partial \hat{\mathbf{u}}}{\partial \hat{x}_i} \hat{\nu}_{ij} \frac{\partial \hat{\mathbf{w}}}{\partial \hat{x}_j} d\hat{\Omega}, \tag{5.2.3}$$

$$\langle \hat{\mathcal{B}}\hat{p}, \hat{\mathbf{w}} \rangle = -\sum_{r=1}^{R} \int_{\hat{\Omega}^r} \hat{p} \nabla \cdot \hat{\mathbf{w}} d\hat{\Omega}, \tag{5.2.4}$$

$$\langle \hat{F}, \hat{\mathbf{w}} \rangle = \langle \hat{F}_s, \hat{\mathbf{w}} \rangle + \langle \hat{F}^0, \hat{\mathbf{w}} \rangle, \tag{5.2.5}$$

and

$$\langle \hat{F}_s, \hat{\mathbf{w}} \rangle = \sum_{r=1}^{R} \int_{\hat{\Omega}^r} \hat{f}\hat{\mathbf{w}} d\hat{\Omega}, \langle \hat{F}^0, \hat{\mathbf{w}} \rangle = -\langle \hat{\mathcal{A}}\hat{\mathbf{g}}_{in}, \hat{\mathbf{w}} \rangle, \ \langle \hat{G^0}, \hat{q} \rangle = \langle \hat{\mathcal{B}}\hat{q}, \hat{\mathbf{g}}_{in} \rangle. \tag{5.2.6}$$

Then we write:

$$\begin{cases} \langle \hat{\mathcal{A}}\hat{\mathbf{u}}, \hat{\mathbf{w}} \rangle + \langle \hat{\mathcal{B}}\hat{p}, \hat{\mathbf{w}} \rangle = \langle \hat{F}, \hat{\mathbf{w}} \rangle \ \ \forall \hat{\mathbf{w}} \in Y, \\ -\langle \hat{\mathcal{B}}\hat{q}, \hat{\mathbf{u}} \rangle = \langle \hat{G^0}, \hat{q} \rangle \ \ \forall \hat{q} \in Q. \end{cases} \tag{5.2.7}$$

We want to build a system of P^2DEs (Parametrized Partial Differential Equations) depending on a set of geometrical coefficients $\boldsymbol{\mu}$, that we call parameters. Then (5.2.7) is traced back to a *reference domain* (Fig.5.2) by an *affine mapping* of the subdomains $\hat{\Omega}^r$ into Ω^r. For any $\hat{x} \in \hat{\Omega}^r$, $r = 1, \ldots, R$, its image $x \in \Omega^r$ is given by

$$x = \mathcal{G}^r(\mu; \hat{x}) = G^r(\mu)\hat{x} + g^r, \quad 1 \leq r \leq R; \tag{5.2.8}$$

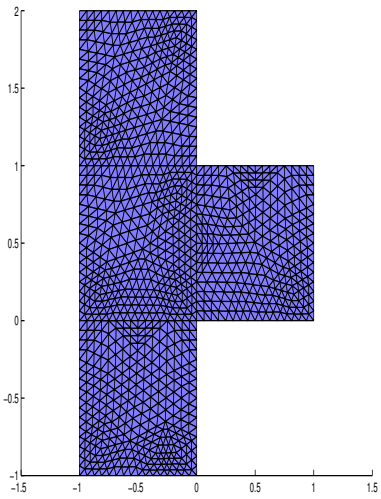

Figure 5.2: Reference domain Ω.

we thus write

$$\frac{\partial}{\partial \hat{x}_i} = \frac{\partial x_j}{\partial \hat{x}_i}\frac{\partial}{\partial x_j} = G^r_{ji}(\mu)\frac{\partial}{\partial x_j} \tag{5.2.9}$$

and we get in the reference domain Ω:

$$\langle \mathcal{A}\mathbf{u}, \mathbf{w}\rangle = \sum_{r=1}^{R}\int_{\Omega^r} \frac{\partial \mathbf{u}}{\partial x_i}\Big(G^r_{ii'}(\mu)\hat{\nu}_{i'j'}G^r_{jj'}(\mu)det(G^r(\mu))^{-1}\Big)\frac{\partial \mathbf{w}}{\partial x_j}d\Omega \ \forall \mathbf{w} \in Y, \tag{5.2.10}$$

$$\langle \mathcal{B}p, \mathbf{w}\rangle = -\sum_{r=1}^{R}\int_{\Omega^r} p\Big(G^r_{ij}(\mu)det(G^r(\mu))^{-1}\Big)\frac{\partial w_j}{\partial x_i}d\Omega \ \forall \mathbf{w} \in Y, \tag{5.2.11}$$

$$\langle F, \mathbf{w}\rangle = \langle F_s, \mathbf{w}\rangle + \langle F^0, \mathbf{w}\rangle, \tag{5.2.12}$$

where

$$\langle F_s, \mathbf{w}\rangle = \sum_{r=1}^{R}\int_{\Omega^r}\Big(\hat{f}^r det(G^r(\mu))^{-1}\Big)\mathbf{w}d\Omega; \langle F^0, \mathbf{w}\rangle = -\langle \mathcal{A}g_{in}, \mathbf{w}\rangle; \ \langle G^0, q\rangle = \langle \mathcal{B}q, g_{in}\rangle. \tag{5.2.13}$$

We introduce a vector of parameters $\boldsymbol{\mu} = \{t, D, L, S, H, \theta\} \in \mathcal{D}^\mu \subset \mathbb{R}^P$, $\mathcal{D}^\mu$ is given by: $[t_{min}, t_{max}] \times [D_{min}, D_{max}] \times [L_{min}, L_{max}] \times [S_{min}, S_{max}] \times [H_{min}, H_{max}] \times [\theta_{min}, \theta_{max}]$. The *transformation tensors* for bilinear viscous terms are defined as follows:

$$\nu^r_{ij}(\mu) = G^r_{ii'}(\mu)\hat{\nu}_{i'j'}G^r_{jj'}(\mu)det(G^r(\mu))^{-1}, 1 \le i, j \le 2, r = 1, ..., R,$$

then in our case:

$$\nu^1 = \nu\begin{bmatrix} \frac{t}{H} & -\tan\theta \\ -\tan\theta & \frac{1+\tan^2\theta}{t}H \end{bmatrix}; \ \nu^2 = \nu\begin{bmatrix} \frac{S}{D} & 0 \\ 0 & \frac{D}{S} \end{bmatrix}; \tag{5.2.14}$$

$$\nu^3 = \nu \begin{bmatrix} \frac{t}{D} & 0 \\ 0 & \frac{D}{t} \end{bmatrix};\ \nu^4 = \nu \begin{bmatrix} \frac{L}{D} & 0 \\ 0 & \frac{D}{L} \end{bmatrix}. \tag{5.2.15}$$

The tensors for *pressure and divergence forms* are:

$$\chi^r_{ij}(\mu) = G^r_{ij} det(G^r(\mu))^{-1}$$

and are given by:

$$\chi^1 = \begin{bmatrix} t & -H\tan\theta \\ 0 & H \end{bmatrix};\ \chi^2 = \begin{bmatrix} S & 0 \\ 0 & D \end{bmatrix}; \tag{5.2.16}$$

$$\chi^3 = \begin{bmatrix} t & 0 \\ 0 & D \end{bmatrix};\ \chi^4 = \begin{bmatrix} L & 0 \\ 0 & D \end{bmatrix}. \tag{5.2.17}$$

Furthermore, we may define

$$\Theta^{q(i,j,r)}(\mu) = \nu^r_{ij}(\mu),\ \langle \mathcal{A}^{q(i,j,r)}\mathbf{u}, \mathbf{w}\rangle = \int_{\Omega^r} \frac{\partial \mathbf{u}}{\partial x_i}\frac{\partial \mathbf{w}}{\partial x_j} d\Omega, \tag{5.2.18}$$

$$\Phi^{s(i,j,r)}(\mu) = \chi^r_{ij}(\mu),\ \langle \mathcal{B}^{s(i,j,r)}p, \mathbf{w}\rangle = -\int_{\Omega^r} p\frac{\partial w_i}{\partial x_j} d\Omega, \tag{5.2.19}$$

for $1 \le r \le R$, $1 \le i, j \le d = 2$ (q and s are condensed indexes of i, j, r quantities) and we apply affine decomposition:

$$\mathcal{A}(\Theta(\mu), \mathbf{u}, \mathbf{w}) = \sum_{q=1}^{Q^a} \Theta^q(\mu)\mathcal{A}(\mathbf{u}, \mathbf{w})^q\ ;$$

$$\mathcal{B}(\Phi(\mu), p, \mathbf{w}) = \sum_{s=1}^{Q^b} \Phi^s(\mu)\mathcal{B}(p, \mathbf{w})^s\ ;$$

in our case $Q^a = 20$ and $Q^b = 9$, in reality: $\max(Q^a) = d \times d \times d \times R = 32,\ \max(Q^b) = d \times d \times R = 16$;

The Stokes problem rewritten on the reference domain Ω reads: find $(\mathbf{u}(\mu), p(\mu)) \in Y \times Q$such that:

$$\begin{cases} \mathcal{A}(\mu; \mathbf{u}(\mu), \mathbf{w}) + \mathcal{B}(\mu; p(\mu), \mathbf{w}) = \langle F, \mathbf{w}\rangle\ \forall\ \mathbf{w} \in\ Y, \\ \mathcal{B}(\mu; q, \mathbf{u}(\mu)) = \langle G^0, q\rangle\ \forall\ q \in\ Q. \end{cases} \tag{5.2.20}$$

A necessary condition for the well posedness of this problem is the so-called *inf-sup* condition (LBB) [127]:

$$\exists\ \beta_0 > 0 :\ \beta(\mu) = \inf_{q\in Q}\sup_{\mathbf{w}\in Y} \frac{\mathcal{B}(\mu, q, \mathbf{w})}{\|\mathbf{w}\|_Y \|q\|_Q} \ge \beta_0, \forall\ \mu\ \in\ \mathcal{D}^\mu, \tag{5.2.21}$$

where $Y = H^1_0 \times H^1_0$. To verify it let us introduce a supremizer operator T^μ: $Q \to Y$ defined as follows:

$$(T^\mu q, \mathbf{w})_Y = \mathcal{B}(\mu; q, \mathbf{w}),\ \forall\ \mathbf{w}\ \in\ Y. \tag{5.2.22}$$

It is readily shown that:

$$T^\mu q = \arg\sup_{\mathbf{w}\in Y} \frac{\mathcal{B}(\mu; q, \mathbf{w})}{\|\mathbf{w}\|_Y}, \tag{5.2.23}$$

then

$$\beta^2(\mu) = \inf_{q\in Q} \frac{(T^\mu q, T^\mu q)_Y}{\|q\|_Q^2}, \tag{5.2.24}$$

by definition (5.2.22):

$$\|T^\mu q\|_Y^2 = \mathcal{B}(\mu; q, T^\mu q),$$

and by applying (5.2.23) and (5.2.21)

$$\inf_{q\in Q} \frac{(T^\mu q, T^\mu q)_Y}{\|q\|_Q^2} = \inf_{q\in Q} \frac{\|T^\mu q\|_Y^2}{\|q\|_Q^2} =$$

$$= \inf_{q\in Q} \Big[\sup_{\mathbf{w}\in Y} \frac{(T^\mu q, \mathbf{w})_Y}{\|\mathbf{w}\|_Y \|q\|_Q} \Big]^2 = \inf_{q\in Q} \Big[\sup_{\mathbf{w}\in Y} \frac{\mathcal{B}(\mu, q, \mathbf{w})}{\|\mathbf{w}\|_Y \|q\|_Q} \Big]^2 = \beta^2(\mu),$$

this proofs (5.2.24). In our numerical approximation the Stokes problem has been solved by Galerkin-Finite Element Method using Taylor-Hood $\mathbb{P}^2 - \mathbb{P}^1$ elements for velocity and pressure, respectively. See Girault and Raviart [43], Gresho and Sani [46], and Gunzburger [48].

5.3 The reduced basis formulation of the Stokes equations

In the reduced basis approximation we take some "$\boldsymbol{\mu}$" samples $S_N^{\boldsymbol{\mu}} = \{\boldsymbol{\mu}^1, \ldots, \boldsymbol{\mu}^N\}$, where $\boldsymbol{\mu}^n \in \mathcal{D}^{\boldsymbol{\mu}}$, $n = 1, \ldots, N$.

The *reduced basis pressure space* is $Q_N = \text{span}\,\{\xi_n,\ n = 1, \ldots, N\}$, where $\xi_n = p(\mu^n)$.

We can build the *reduced basis velocity space* as $Y_N^\mu = \text{span}\,\{\zeta_n,\ n = 1, \ldots, N; T^\mu \xi_n,\ n = 1, \ldots, N\}$, where $\zeta_n = \mathbf{u}(\mu^n)$. The reduced basis approximation problem reads:
find $(\mathbf{u}_N(\mu), p_N(\mu)) \in Y_N^\mu \times Q_N$ s.t.:

$$\begin{cases} \mathcal{A}(\mu; \mathbf{u}_N(\mu), \mathbf{w}) + \mathcal{B}(\mu; p_N(\mu), \mathbf{w}) = \langle F, \mathbf{w}\rangle \ \forall\ \mathbf{w} \in\ Y_N^\mu, \\ \mathcal{B}(\mu; q, \mathbf{u}_N(\mu) = \langle G, q\rangle \ \forall\ q \in\ Q_N. \end{cases} \tag{5.3.1}$$

Problem (5.3.1) is subject to an equivalent reduced basis inf-sup condition.

Lemma 5.3.1 *We define*

$$\beta_N(\mu) = \inf_{q\in Q_N} \sup_{\mathbf{w}\in Y_N^\mu} \frac{\mathcal{B}(\mu, q, \mathbf{w})}{\|\mathbf{w}\|_Y \|q\|_Q}.$$

Then we can prove that

$$\beta_N(\mu) \geq \beta(\mu) \geq \beta_0 > 0, \forall \mu \in \mathcal{D}^\mu.$$

Proof:

$$\beta(\mu) = \inf_{q\in Q} \sup_{\mathbf{w}\in Y} \frac{\mathcal{B}(\mu, q, \mathbf{w})}{\|\mathbf{w}\|_Y \|q\|_Q} \leq \inf_{q\in Q_N} \sup_{\mathbf{w}\in Y} \frac{\mathcal{B}(\mu, q, \mathbf{w})}{\|\mathbf{w}\|_Y \|q\|_Q} = \inf_{q\in Q_N} \frac{\mathcal{B}(\mu; q, T^\mu q)}{\|T^\mu q\|_Y \|q\|_Q} \leq$$

$$\leq \inf_{q\in Q_N} \sup_{\mathbf{w}\in Y_N^\mu} \frac{\mathcal{B}(\mu, q, \mathbf{w})}{\|\mathbf{w}\|_Y \|q\|_Q} = \beta_N(\mu). \qquad \square$$

To demonstrate the Lemma above we have applied the fact that $Q_N \subset Q$, the definition of the supremizer and the fact that the velocity space is enriched by supremizers, respectively. For further elements dealing with supremizer operator and the reduced basis framework see Rovas [134] for the general non-coercive problem and Patera *et al.* [161] especially for Helmholtz and Burgers equations.

We rewrite for computationally convenience Y_N^μ using the *affine dependence* of $\mathcal{B}(\mu, q, \mathbf{w})$ on the parameter and the *linearity* of T^μ: $T^\mu \xi = \sum_{q=1}^{Q^b} \Phi^q(\mu) T^q \xi$ for any ξ and μ, which allows us to write:

$$Y_N^\mu = \text{span}\,\{\sum_{k=1}^{\overline{Q}^b} \Phi^k(\mu)\sigma_{kn},\ n = 1, \ldots, 2N\},$$

where $\overline{Q}^b = Q^b + 1, \Phi^{\overline{Q}^b} = 1$. For $n = 1, \ldots, N$:

$$\sigma_{kn} = 0, for\ k = 1, \ldots, Q^b; \sigma_{\overline{Q}^b n} = \zeta_n = \mathbf{u}(\mu^n).$$

For $n = N+1, \ldots, 2N$:

$$(\sigma_{kn}, \mathbf{w})_Y = \mathcal{B}(\xi_{n-N}, \mathbf{w})^k, \forall \mathbf{w} \in Y, for\ k = 1, \ldots, Q^b; \tag{5.3.2}$$

$$\sigma_{\overline{Q}^b n} = 0.$$

For a new "$\boldsymbol{\mu}$" we want a solution given by a combination of previously computed stored solutions as basis functions:

$$\mathbf{u}_N(\mu) = \sum_{j=1}^{2N} \mathbf{u}_{Nj}(\mu)\Big(\sum_{k=1}^{\overline{Q}^b} \Phi^k(\mu)\sigma_{kj}\Big),$$

$$p_N(\mu) = \sum_{l=1}^{N} p_{Nl}(\mu)\xi_l,$$

whose weights $\mathbf{u}_{Nj}$ and p_N are given by the following reduced basis linear system:

$$\begin{cases} \sum_{j=1}^{2N} A_{ij}^\mu \mathbf{u}_{Nj}(\mu) + \sum_{l=1}^{N} B_{il}^\mu p_{Nl}(\mu) = F_i^\mu, & 1 \le i \le 2N, \\ \sum_{j=1}^{2N} B_{jl}^\mu \mathbf{u}_{Nj}(\mu) = G_l^\mu, & 1 \le l \le N, \end{cases} \tag{5.3.3}$$

where the sub-matrices A and B are given by:

$$A_{ij}^\mu = \sum_{k=1}^{Q^a} \sum_{k'=1}^{\overline{Q}^b} \sum_{k''=1}^{\overline{Q}^b} \Theta^k(\mu)\Phi^{k'}(\mu)\Phi^{k''}(\mu)\mathcal{A}(\sigma_{k'i}, \sigma_{k''j})^k,\ 1 \le i, j \le 2N,$$

$$B_{il}^\mu = \sum_{k=1}^{\overline{Q}^b} \sum_{k'=1}^{\overline{Q}^b} \Phi^k(\mu)\Phi^{k'}(\mu)\mathcal{B}(\sigma_{k'i}, \xi_l)^k,\ 1 \le i \le 2N,\ 1 \le l \le N,$$

and:

$$F_i^\mu = \sum_{k'=1}^{\overline{Q}^b} \Phi^{k'}(\mu)\langle F, \sigma_{k'i}\rangle,\ 1 \le i \le 2N;\ G_l^\mu = \langle G^0, \xi_l\rangle,\ 1 \le l \le N.$$

Finally problem (5.7.10) can be written in compact form as

$$\begin{pmatrix} \underline{A} & \underline{B} \\ \underline{B}^T & 0 \end{pmatrix} \begin{pmatrix} \underline{\mathbf{u}}_N \\ \underline{p}_N \end{pmatrix} = \begin{pmatrix} \underline{F} \\ \underline{G} \end{pmatrix}. \tag{5.3.4}$$

This linear system whose unknowns are the coefficients of the linear combination of previously computed off-line solutions has the same structure of a finite element Stokes problem. Using reduced basis we deals with matrix of smaller dimension (of order of N) and with full matrices (instead of sparse ones).

5.3.1 Outputs of interest

As outputs of interest we may consider, for example, the mean value of the velocity components:

$$s_1(\mu) = \sum_{r=1}^{R} \frac{\int_{\Omega^r} u_1 d\Omega}{\int_{\Omega^r} d\Omega};\ s_2(\mu) = \sum_{r=1}^{R} \frac{\int_{\Omega^r} u_2 d\Omega}{\int_{\Omega^r} d\Omega} \tag{5.3.5}$$

other outputs are derived from velocity such as vorticity:

$$s_v(\mu) = \sum_{r=1}^{R} \int_{\Omega_r} \Big(\frac{\partial u_2(\mu)}{\partial x_1} - \frac{\partial u_1(\mu)}{\partial x_2} \Big) d\Omega, \tag{5.3.6}$$

where we have set $\mathbf{u} = (u_1, u_2)^T$ and $\mathbf{x} = (x_1, x_2)^T$, or wall shear stress:

$$s_\tau(\mu) = \int_{\Gamma_w} \nu \frac{\partial \mathbf{u}(\mu)}{\partial \hat{\mathbf{n}}} \cdot \hat{\mathbf{t}} d\Gamma, \tag{5.3.7}$$

where $\hat{\mathbf{t}}$ is the tangential unit vector. In the last two examples we may introduce a dual residual correction based on an adjoint problem to improve output accuracy. See Section 5.9.

5.3.2 Reduced basis on-line complexity

We have the following computational costs to build (on-line) reduced basis matrix, given also the supremizer component in the velocity space: $O(Q^a(\overline{Q}^b)^2 4N^2)$ for sub-matrix $\underline{A}$, $O((\overline{Q}^b)^2 2N^2)$ for $\underline{B}$, $O(\overline{Q}^b 2N)$ for $\underline{F}$ and $O(9N^3)$ for the inversion of the full reduced basis matrix (5.3.4). Note that the approach presented to build reduced basis velocity space is only one of the possible solutions and the space Y_N^μ, in this case, is depending on the value of the on-line $\boldsymbol{\mu}$ parameter. Other options that avoid ill conditioning problems characterized by different computational costs are available and will be presented in Section 5.7.

5.4 Off-line optimized basis assembling: adaptive procedure

In this case an adaptive procedure based on H^1 max relative error projection for velocity E_{H^1} has been developed, optionally we can also considering and combining L^2 max relative error projection for pressure E_{L^2}. We underline that, given the higher powers of N that appear

in our cost computing estimation, it is crucial (both as regards online and offline effort) to control N more tightly. To this end, we may gainfully apply our off line assembling procedure adaptively, see also Veroy *et al.* [161] and Prud'homme [121]. We first construct, offline, an approximation that, over most of the domain, exhibits an error ϵ (E_{H^1} or E_{L^2} or both) less than ϵ_d^{prior}: we begin with a first point $\mu^1(S_{N'=1} = \{\mu^1\})$; we next (inexpensively) evaluate error $\epsilon_{N'=1}(\mu)$ over a large test sample of parameter points in $\mathcal{D}^\mu$, denoted with Σ^{prior}; we then choose for μ^2 (and hence $S_{N'=2} = \{\mu^1, \mu^2\}$) the maximizer of $\epsilon_{N'=1}(\mu)$ over Σ^{prior}. We repeat this process until the maximum of $\epsilon_{N'=N^{prior}}(\mu)$ over Σ^{prior} is less than ϵ_d^{prior}. Then, online, given a new value of the parameter, μ, and an error tolerance $\epsilon_d^{post}(\mu)$, we essentially repeat this adaptive process - but now our sample points are drawn from $S_{N^{prior}}$, and the test sample is a singleton - μ. Typically we choose $\epsilon_d^{prior} \ll \epsilon_d^{post}(\mu)$ since our test is not exhaustive; and therefore, typically, $N^{post}(\mu) \ll N^{prior}$. With the adaptive process we get higher accuracy at lower N: modest reductions in N can translate into measurable performance improvements. This procedures is very important not only to get a computationally cheaper and faster procedure but also to avoid ill-conditioning in matrix assembling procedures. Error projection procedure, described below, has permitted us to have an off-line adaptive (and optimized) assembling procedure which is very fast and inexpensive, without reduced basis matrix assembling procedures, but only the solution of a linear system.

5.4.1 L^2 pressure error projection

Given a new μ and hence a new approximated $p_h(\mu)$ pressure solution we solve the following linear system:

$$\sum_j^N \int_\Omega \xi_i \xi_j c_j = \int_\Omega \xi_i p_h(\mu), 1 \le i \le N, \tag{5.4.1}$$

where ξ_i are N pressure solutions used as basis given by: $\xi_i = \sum_{k=1}^{\mathcal{N}_P} p_{i_k} \Phi_k$, computed solving a finite element problem on $\mathcal{N}_P$ pressure nodes of the mesh; Φ_k are finite element local functions for the pressure. Expanding (5.4.1) by finite element approximation we can write:

$$\sum_{j=1}^{N} \sum_{l=1}^{\mathcal{N}_P} \sum_{k=1}^{\mathcal{N}_P} p_{i_l} (\int_\Omega \Phi_l \Phi_k) p_{j_k} c_j = \sum_{m=1}^{\mathcal{N}_P} \sum_{n=1}^{\mathcal{N}_P} p_{i_m} (\int_\Omega \Phi_m \Phi_n) p_{h_n}(\mu), 1 \le i \le N,$$

$$(\underline{p}_i^T \underline{M}^p \underline{p}_j) \underline{c} = \underline{p}_i^T \underline{M}^p \underline{p}_h(\mu),$$

$$\underline{\hat{M}}^p \underline{c} = \underline{F}^p.$$

Once we have $\underline{c}$ we write the L^2 pressure error E_{L^2} as:

$$E_{L^2}^2 = \|p_h(\mu)\|_{L^2}^2 - \sum_{i=1}^{N} \sum_{j=1}^{N} c_i (\int_\Omega \xi_i \xi_j) c_j,$$

where $(\int_\Omega \xi_i \xi_j)$ is the *pressure mass* matrix $\underline{\hat{M}}_{ij}^p = \sum_{l=1}^{\mathcal{N}_P} \sum_{k=1}^{\mathcal{N}_P} p_{i_l} (\int_\Omega \Phi_l \Phi_k) p_{j_k}$, $1 \le i, j \le N$, i.e. $\underline{p}_i^T \underline{M}^p \underline{p}_j$.

5.4.2 H^1 velocity error projection

Given a new μ and hence a new approximated velocity solution $u_h(\mu)$ we solve the following linear system

$$\sum_{j}^{2N}(\int_\Omega \zeta_i\zeta_j + \int_\Omega \nabla\zeta_i \cdot \nabla\zeta_j)c_j = \int_\Omega \zeta_i u_h(\mu) + \int_\Omega \nabla\zeta_i \cdot \nabla u_h(\mu), 1 \leq i \leq 2N, \tag{5.4.2}$$

where ζ_i are $2N$ velocity solutions used as basis, made up of finite element approximated velocities and supremizer solutions, written as: $\zeta_i = \sum_{k=1}^{\mathcal{N}} u_{i_k}\Psi_k$ on $\mathcal{N}$ velocity nodes by Ψ_k finite element velocity local functions. Expanding the system (5.4.2) by finite element approximation (on $\mathcal{N}$ nodes) we get, for $1 \leq i \leq 2N$:

$$[\sum_{j=1}^{2N}\sum_{l=1}^{\mathcal{N}}\sum_{k=1}^{\mathcal{N}} u_{i_l}(\int_\Omega \Psi_l\Psi_k)u_{j_k} + \sum_{j=1}^{2N}\sum_{l=1}^{\mathcal{N}}\sum_{k=1}^{\mathcal{N}} u_{i_l}(\int_\Omega \nabla\Psi_l \cdot \nabla\Psi_k)u_{j_k}]c_j =$$

$$= \sum_{m=1}^{\mathcal{N}}\sum_{n=1}^{\mathcal{N}} u_{i_m}(\int_\Omega \Psi_m\Psi_n)u_{h_n}(\mu) + \sum_{m=1}^{\mathcal{N}}\sum_{n=1}^{\mathcal{N}} u_{i_m}(\int_\Omega \nabla\Psi_m \cdot \nabla\Psi_n)u_{h_n}(\mu),$$

$$(\underline{u}_i^T(\underline{M} + \underline{K})\underline{u}_j)\underline{c} = \underline{u}_i^T(\underline{M} + \underline{K})\underline{u}_h(\mu),$$
$$\hat{\underline{M}}^u\underline{c} = \underline{F}^u.$$

Once we have $\underline{c}$ we write the H^1 velocity error E_{H^1} as:

$$E_{H^1}^2 = \|u_h(\mu)\|_{H^1}^2 - \sum_{i=1}^{2N}\sum_{j=1}^{2N} c_i(\int_\Omega (\zeta_i\zeta_j + \nabla\zeta_i \cdot \nabla\zeta_j)c_j,$$

where $(\int_\Omega \zeta_i\zeta_j)$ is the *velocity mass* matrix $\sum_{l=1}^{\mathcal{N}}\sum_{k=1}^{\mathcal{N}} u_{i_l}(\int_\Omega \Psi_l\Psi_k)u_{j_k}$, i.e. $\underline{u}_j^T\underline{M}\underline{u}_i$ and $(\int_\Omega \nabla\zeta_i \cdot \nabla\zeta_j) = \sum_{l=1}^{\mathcal{N}}\sum_{k=1}^{\mathcal{N}} u_{i_l}(\int_\Omega \nabla\Psi_l \cdot \nabla\Psi_k)u_{j_k}$ the *velocity stiffness* matrix, i.e. $\underline{u}_j^T\underline{K}\underline{u}_i$.

5.5 The computation of the constant β of the inf-sup condition

The calculation of the constant of the inf-sup condition for finite element (β) and reduced basis method (β_N) has been carried out as a test to guarantee approximation stability.

- In the case in which we want to calculate β we have a generalized eigenvalue problem on sparse matrices (see Gresho and Sani [46], Malkus [93], and Quarteroni and Valli [127]):

$$(\underline{G}^T\underline{K}^{-1}\underline{G})\underline{x} = \underline{S}\underline{x} = \lambda\underline{M}^p\underline{x} \tag{5.5.1}$$

  $\underline{K}$ is the finite element (velocity) stiffness matrix ($\int_\Omega \nabla\Psi_l \cdot \nabla\Psi_k$), $\underline{G}$ is the velocity-divergence finite element matrix ($\int_\Omega \Phi_l\nabla \cdot \Psi_k$), $\underline{M}^p$ is the finite element pressure mass matrix ($\int_\Omega \Phi_l\Phi_k$), λ are eigenvalues and $\underline{x}$ eigenvectors. The β constant is given by

$$\beta = \sqrt{\lambda_{min}} \tag{5.5.2}$$

- To calculate β_N we have a generalized eigenvalues problem on reduced basis (full) matrices (previously defined):

$$(\underline{B}^T \underline{A}^{-1} \underline{B}) \underline{x}_N = \underline{S}_N \underline{x}_N = \lambda_N \underline{\hat{M}}^p \underline{x}_N \tag{5.5.3}$$

$$\beta_N = \sqrt{\lambda_{N_{min}}} \tag{5.5.4}$$

- We have tested that equivalent reduced basis inf-sup parameter condition: $\beta_N(\mu) \geq \beta(\mu) \geq \beta_0 > 0, \forall \mu \in \mathcal{D}^\mu$ has been satisfied. Table 5.1 shows a test driven to calculate the constant β of the *inf-sup* condition studying a one-parameter varying configuration (the diameter D, for example) at different N.

D	β	β_N, $N=1$	β_N, $N=2$	β_N, $N=3$
0.63	2.0249	3.9096	2.7895	2.531
0.68	2.0286	3.9316	2.8708	2.6625
0.73	2.0274	3.952	2.9456	2.7992
0.78	2.0257	3.971	3.0145	2.9386
0.83	2.0237	3.9888	3.0781	3.0729
0.88	2.0216	4.0054	3.137	3.0729
0.93	2.0192	4.0208	3.1918	3.186
0.98	2.0167	4.0353	3.243	3.264
1.03	2.0139	4.0487	3.291	3.3466
1.08	2.011	4.0612	3.3361	3.3759

Table 5.1: β and β_N in one parameter dependent configuration (D for example). Other parameters are frozen.

5.6 Some preliminary numerical results

Several numerical tests were carried out to develop all the Stokes reduced basis toolbox and to study different related aspects: affine mapping transformation in reference domains, off-line optimization basis assembling procedure, approximation and algebraic stability (LBB inf-sup equivalent condition fulfillment and condition number control). Different meshes have been used (from coarse to fine). Using finer mesh CPU (Pentium IV, 2GHZ) operation time increases a lot during computing procedures such as assembling off-line adaptive calculations (i.e. reduced basis approximation spaces and matrix assembling, error estimation and, eventually, orthogonalization) and it is maintained reasonable during on-line calculation. A mesh adaptation procedure in some zones has been achieved. Taylor-Hood finite elements have been used: $\mathbb{P}^2 - \mathbb{P}^1$ elements (for velocity and pressure respectively) [127]. Different solver for finite element and reduced basis systems have been used: both iterative (such as *Bi-CGSTAB, Conjugate Gradient Method, GMRES*) and direct, see [129]. The reduced basis solutions have been compared directly with true finite element solutions by computing H^1 relative error for velocity and L^2 relative error for pressure.

5.6.1 First Test: homogeneous Dirichlet boundary conditions, forced flow, 3(1) varying parameter(s)

The first test we introduce deals with a forced Stokes flow in the "T" domain with all zero Dirichlet boundary conditions (flow closed into a cavity), varying only three parameters available (depending by one adimensional quantity: τ). Data and relationships for geometrical parameters used to solve the problem follow (see also Figure 5.1).

- (I) The bypass diameter is $t = 3 - 2\tau$, the stenosis length $S = \tau$ and the outflow length $L = \tau$.
- (II) The viscosity is $\nu = 0.04\ m^2 s^{-1}$, the force field is $\hat{\mathbf{f}} = (0, 10x)^T m s^{-2}$ in the true domain $\hat{\Omega}$.
- (III) The parameter τ is ranging in $[0.1, 1.45]$. All other parameters are frozen: the bridge height $H = 1$, the arterial diameter $D = 1$ and the graft angle $\theta = 0$.

Figures 5.3 and 5.4 show examples of flow solution: velocity and pressure for two configuration with τ_{min} and τ_{max}; Figure 5.5 shows the error reduction using the adaptive optimized procedure of Section 5.4 during basis assembling procedure, based on H^1 relative (projected) error minimization, on the left, and the parameters distribution during basis assembling procedure, on the right. Figure 5.6 shows true relative error reduction (H^1 for velocity and L^2 for pressure) considering a great number of different geometrical configurations. Tables 5.2-5.3 show error reduction (and its magnitude); Table 5.4 shows the proofs of approximation stability of reduced basis formulation computing β_N, the LBB inf-sup equivalent constant and its comparison with β from Galerkin (FEM) approximation. Table 5.5 shows true error on a possible output of interest, for example $s(\mu) = \int_\Omega \mathbf{f} \cdot \mathbf{u}(\mu) d\Omega$. Results on outputs are reported also in Figure 5.7.

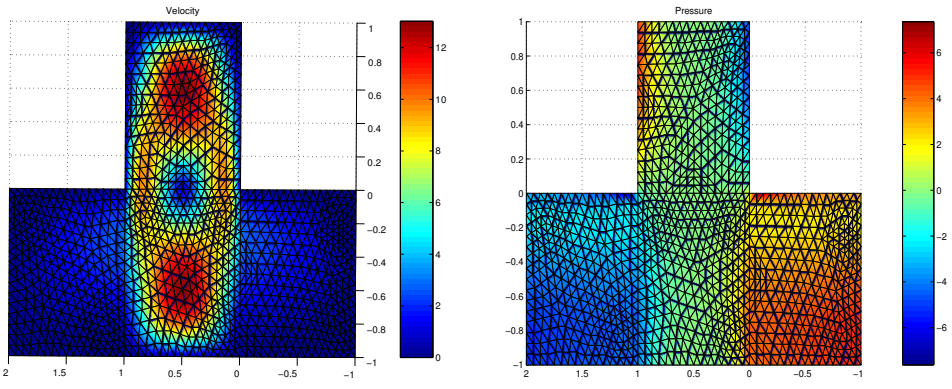

Figure 5.3: Velocity and pressure solution for $\tau = 0.1$.

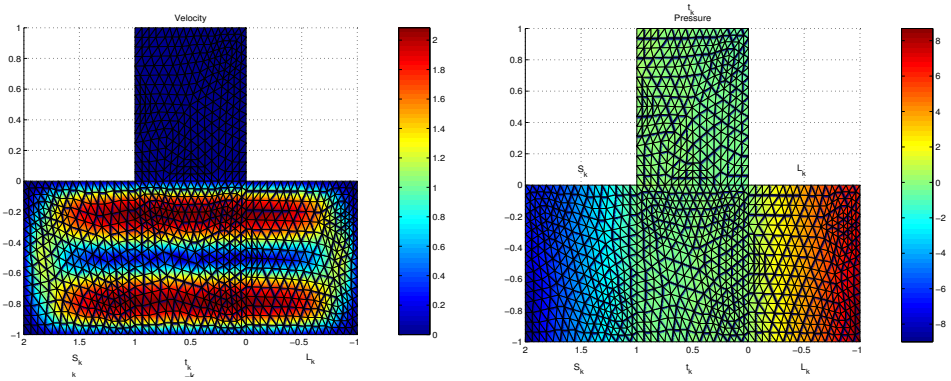

Figure 5.4: Velocity and pressure solution for $\tau = 1.45$.

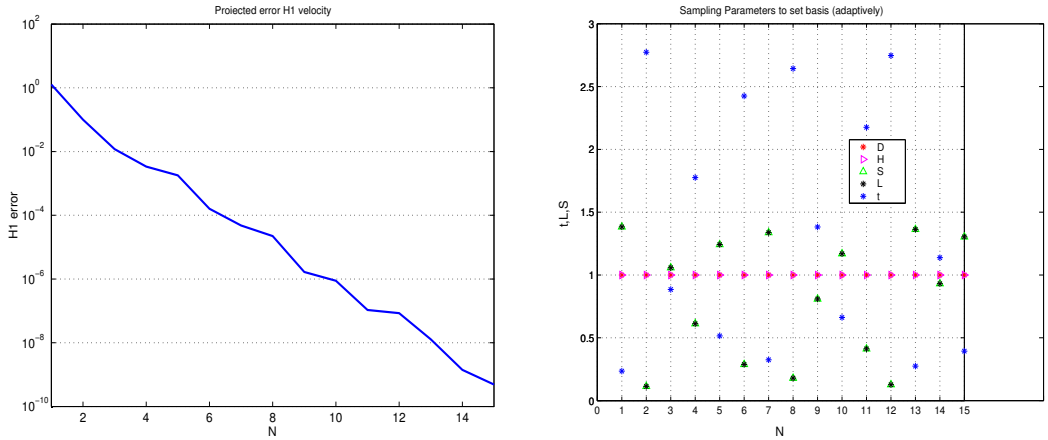

Figure 5.5: Relative max projected H^1 error (see Section 5.4.2) on velocity at each iteration during adaptive basis assembling (left) and parameters distribution during off-line reduced basis assembling procedure (right).

N	Rel. Err. H^1 Max	Rel. Err. H^1 mean	Rel. Err. L^2 Max	Rel. Err. L^2 mean
1	$9.8900e-001$	$5.9138e-001$	$2.5790e-001$	$1.0878e-001$
2	$2.1583e-001$	$7.8312e-002$	$2.0387e-002$	$1.1826e-002$
3	$2.3301e-002$	$1.0174e-002$	$5.9742e-003$	$1.4583e-003$
4	$3.7543e-003$	$8.7714e-004$	$4.4999e-004$	$5.5973e-005$
5	$3.2670e-003$	$5.0383e-004$	$3.2752e-004$	$3.3635e-005$
6	$1.4271e-004$	$3.6446e-005$	$2.8591e-005$	$1.7688e-006$
7	$8.4314e-005$	$1.8559e-005$	$2.7009e-005$	$1.5313e-006$

Table 5.2: Table of H^1 and L^2 relative errors on velocity and pressure, respectively, 50 test configurations, 3(1) parameters, $N < 7$.

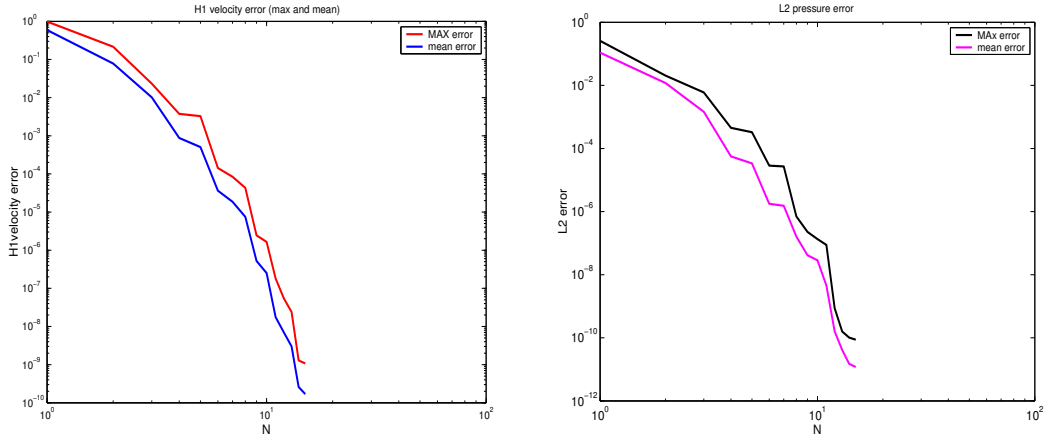

Figure 5.6: Left: relative true H^1 velocity errors, max and mean error over a large test sampling (50 configurations). Right: relative true L^2 pressure errors, max and mean error over a large test sampling (50 configurations); errors in log-log scale.

N	Rel. Err. H^1 Max	Rel. Err. H^1 mean	Rel. Err. L^2 Max	Rel. Err. L^2 mean
8	$4.3142e-005$	$7.4860e-006$	$7.0025e-007$	$1.6084e-007$
9	$2.4504e-006$	$5.2102e-007$	$2.2660e-007$	$4.1354e-008$
10	$1.6485e-006$	$2.5155e-007$	$1.3400e-007$	$2.8537e-008$
11	$1.8195e-007$	$1.7635e-008$	$8.8023e-008$	$4.5140e-009$
12	$5.3852e-008$	$6.9109e-009$	$8.6392e-010$	$1.5917e-010$
13	$2.4053e-008$	$2.9963e-009$	$1.5813e-010$	$4.1002e-011$
14	$1.2923e-009$	$2.5982e-010$	$1.0129e-010$	$1.4957e-011$
15	$1.0702e-009$	$1.6946e-010$	$8.7277e-011$	$1.1840e-011$

Table 5.3: Table of H^1 and L^2 relative errors on velocity and pressure, respectively, 50 test configurations, 3(1) parameters, $N > 7$.

N	β_N	N	β_N	N	β_N
1	$6.5012e+000$	6	$5.7051e+000$	11	$5.6263e+000$
2	$5.8811e+000$	7	$5.7048e+000$	12	$5.6245e+000$
3	$5.7978e+000$	8	$5.7047e+000$	13	$5.6087e+000$
4	$5.7876e+000$	9	$5.7056e+000$	14	$5.5935e+000$
5	$5.7344e+000$	10	$5.6309e+000$	15	$5.4651e+000$

Table 5.4: β_N equiv. LBB inf-sup constant. $\beta = 5.0164$ ($\tau = 0.76$).

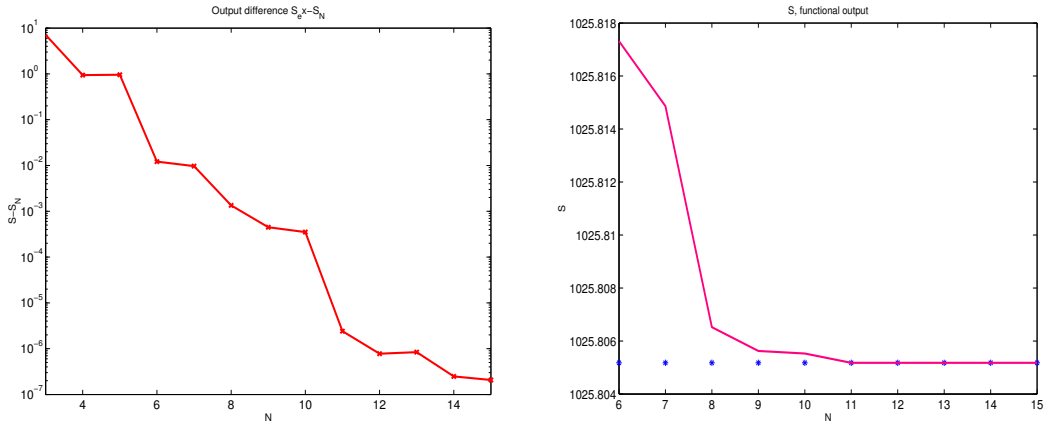

Figure 5.7: Left: Functional output difference $\Delta s = (s - s_N)$; $s = \int_\Omega \mathbf{f} \cdot \mathbf{u}$. Right: convergence of s_N to s $(*)$ versus N $(\tau = 0.356)$.

N	Δs	N	Δs	N	Δs
1	$9.4249e+002$	6	$1.2142e-002$	11	$2.4146e-006$
2	$4.0905e+000$	7	$9.6898e-003$	12	$7.7663e-007$
3	$7.0984e+000$	8	$1.3454e-003$	13	$8.4071e-007$
4	$9.3965e-001$	9	$4.4785e-004$	14	$2.4822e-007$
5	$9.5652e-001$	10	$3.5133e-004$	15	$2.0706e-007$

Table 5.5: Output error: $\Delta s = s - s_N$ for $\tau = 0.356$.

5.6.2 Second Test: mixed Dirichlet/Neuman boundary conditions, 5(2) varying parameters

The second test deals with a flow in the "T" shape bypass geometry with Neumann homogeneous boundary conditions on inflow Γ_{in} and outflow Γ_{out} and zero Dirichlet condition on the wall Γ_w. We deal with five varying parameters (bound by 3 relationships depending on two quantities τ and ρ). Data and values used follow.

- The bypass diameter is $t = 3 - 2\tau$, the stenosis length is $S = \tau$, the outflow length is $L = \tau$, the artery diameter is $D = \rho$, the bypass height is $H = 1 - \rho$.
- The viscosity is 0.04 $m^2 s^{-1}$, while the force field is $\mathbf{f} = (0, 10)^T m s^{-2}$ in true domain $\hat{\Omega}$.
- The parameters range is $\tau \in [0.1, 1.45]$ and $\rho \in [0.1, 1.9]$.

Figure 5.8 shows an example of flow solution (velocity) for a certain parameters combination; Figure 5.9 shows on the left the off-line parameters distribution during basis assembling procedures based on the reduction of the H^1 relative projected error using the adaptive procedure; on the right we have max and mean output error Δs over a large number of different configurations, considering, for example, $s(\mu) = \int_\Omega \mathbf{f} \cdot \mathbf{u}(\mu) d\Omega$. Figure 5.10 shows the true relative error reduction (H^1 for velocity and L^2 for pressure) considering a great number of different geometrical configurations. Table 5.6 shows error reduction (and its magnitude) and Table 5.7 the true error over the output of interest.

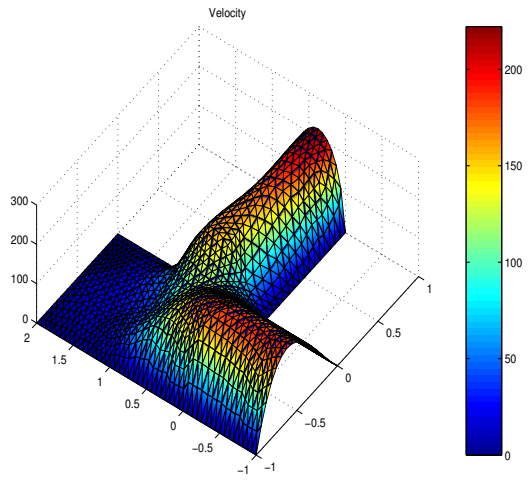

Figure 5.8: Example of flow solution (velocity $[m s^{-1} \cdot 10^{-2}]$) in the "T" shape parametrized domain.

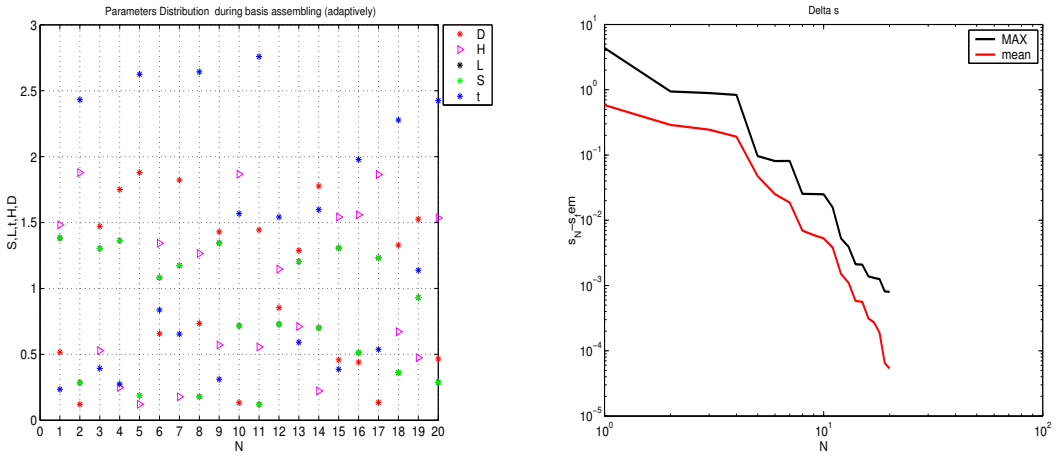

Figure 5.9: Basis assembling: parameters distribution during off-line reduced basis optimized assembling procedure (left). Functional output difference $\Delta s = (s - s_N)$; $s = \int_\Omega \mathbf{f} \cdot \mathbf{u}$: max and mean error over large test sample configurations (right).

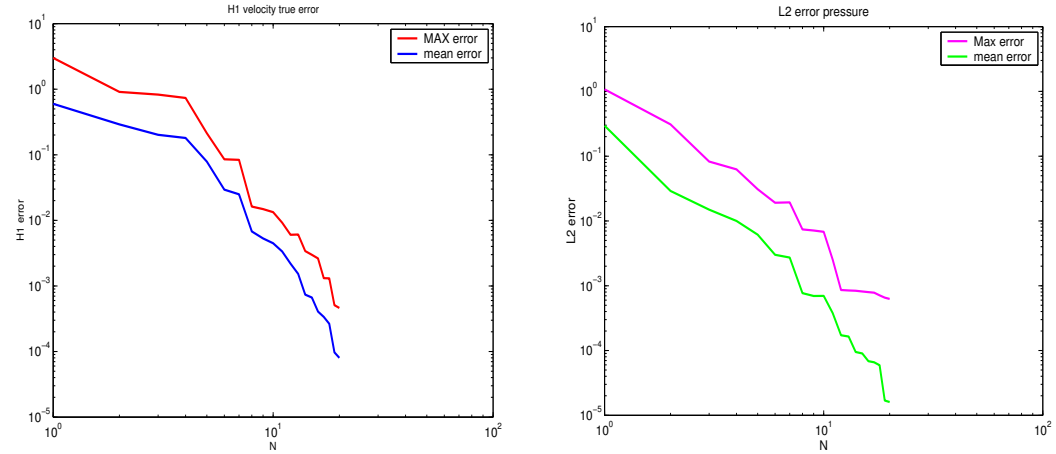

Figure 5.10: Left: relative true H^1 velocity errors: max and mean error over a large test sampling (50 configurations). Right: relative true L^2 pressure errors: max and mean error over a large test sampling (50 configurations); errors in log-log scale.

N	Rel. Err. H^1 Max	Rel. Err. H^1 mean	Rel. Err. L^2 Max	Rel. Err. L^2 mean
5	$2.93e-001$	$7.86e-002$	$3.09e-002$	$6.14e-003$
10	$1.33e-002$	$4.47e-003$	$6.79e-003$	$6.96e-004$
15	$2.98e-003$	$6.65e-004$	$8.16e-004$	$9.021e-005$
20	$4.61e-004$	$8.01e-005$	$6.24e-004$	$1.60e-005$

Table 5.6: Table of H^1 relative errors on velocity and L^2 relative errors on pressure, 50 test configurations, 5(2) parameters, $N \leq 20$.

N	Δs max	N	Δs mean
5	$9.62e-002$	5	$4.73e-002$
10	$2.49e-002$	10	$5.27e-003$
15	$2.09e-003$	15	$5.63e-004$
20	$7.68e-004$	20	$5.35e-005$

Table 5.7: $\Delta s = s - s_N$: max and mean error over output s for 50 configurations.

5.6.3 Third Test: homogeneous Dirichlet boundary conditions, forced flow, 6(3) varying parameters

The third test we carried out considered a forced Stokes flow in the "T" domain with all zero Dirichlet boundary conditions, varying all the six parameters available (depending by two quantities: τ, ρ), including the graft angle θ. Data and relationship used in this test are reported below.

- The bypass diameter is $t = 3 - 2\tau$, the stenosis length is $S = \tau$, the outflow length is $L = \tau$, the artery diameter is $D = \rho$, the bypass height is $H = 2 - \rho$ and the graft angle is θ.
- The viscosity is 0.04 $m^2 s^{-1}$, the force field is $\hat{\mathbf{f}} = (0, 10x)^T m s^{-2}$ in the true domain $\hat{\Omega}$.
- The parameters range are: $\tau \in [0.1, 1.45]$, $\rho \in [0.1, 1.9]$ and for the graft angle $\theta \in [0, \pi/3]$.

Figure 5.11 shows the projected error reduction (as shown in Section 5.4.2) using the adaptive procedure in basis assembling, based on H^1 error minimization and parameters distribution during basis assembling procedure. Figure 5.12 shows true error reduction (H^1 for velocity and L^2 for pressure) considering a great number of different geometrical configurations. The plateau in pressure error plot is due to the fact that we are optimizing reduced basis velocity approximation space with adaptive procedures, but nothing is done with pressure. Table 5.8 shows error reduction (and its magnitude) and Table 5.9 the true error on an output of interest: $s(\mu) = \int_\Omega \mathbf{f} \cdot \mathbf{u}(\mu) d\Omega$. A second option is carried out using and adaptive off-line

procedure based on total projected error (velocity and pressure). Figure 5.13 shows total (projected) error reduction using the adaptive procedure during basis assembling. Figure 5.14 shows true error reduction (H^1 for velocity and L^2 for pressure) considering different geometrical configurations. In this case the plateau in pressure error behavior disappears because we are optimizing reduced basis velocity and pressure approximation spaces with adaptive procedures minimizing off-line error.

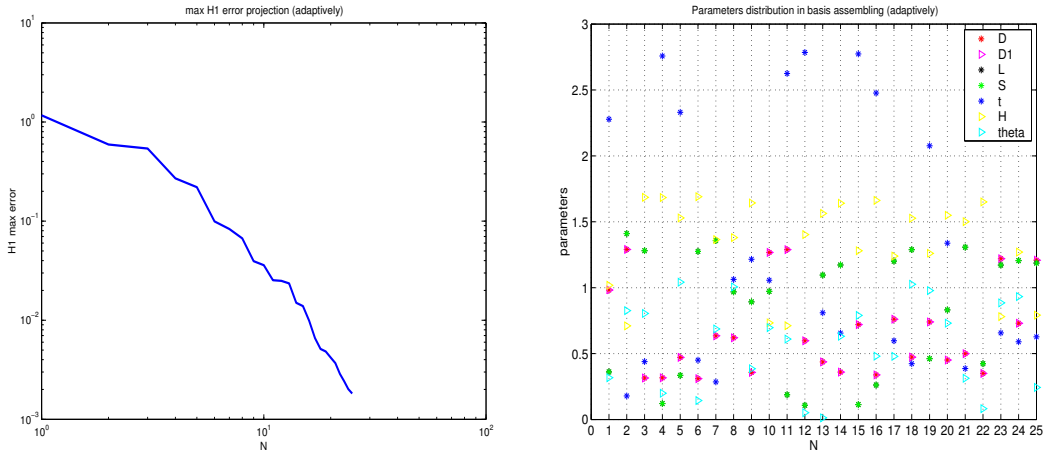

Figure 5.11: Basis assembling: total H^1 velocity (projected) error reduction during basis assembling (left) and parameters distribution during off-line reduced basis assembling (right).

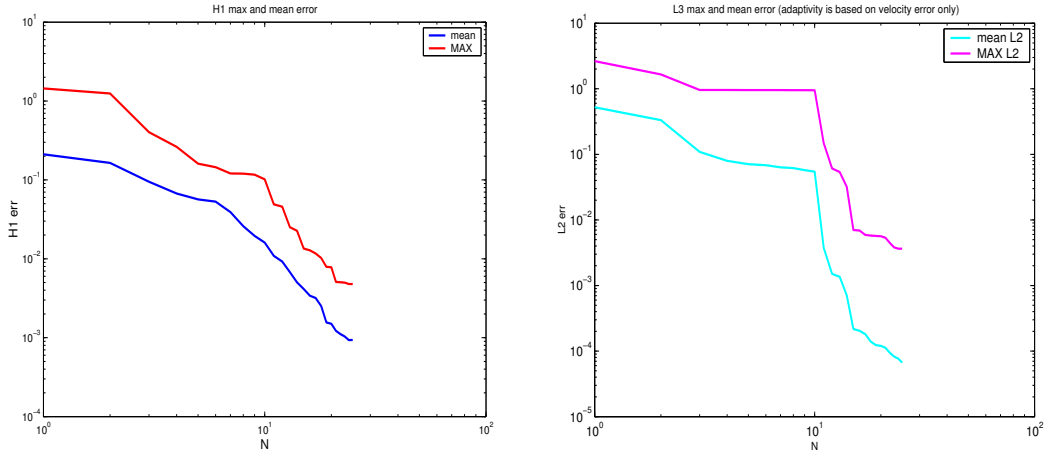

Figure 5.12: Left: relative true H^1 velocity errors: max and mean error over a large test sampling (90 configurations.). Right: relative true L^2 pressure errors: Max and mean error over a large test sampling (90 configurations); errors in log-log scale.

N	Rel. Err. H^1 Max	Rel. Err. H^1 mean	Rel. Err. L^2 Max	Rel. Err. L^2 mean
5	$1.60e-001$	$5.65e-002$	$9.55e-001$	$7.08e-002$
10	$1.01e-001$	$1.60e-002$	$9.48e-001$	$5.74e-002$
15	$1.348e-002$	$4.14e-003$	$7.02e-003$	$2.17e-004$
20	$7.82e-003$	$1.49e-003$	$5.64e-003$	$1.20e-004$
25	$4.79e-003$	$9.37e-004$	$3.63e-003$	$6.66e-005$

Table 5.8: Table of velocity relative errors H^1 and pressure L^2, 90 test configurations, 6(3) parameters, $N \leq 25$.

N	Δs Max	N	Δs mean
5	$1.34e-001$	5	$3.26e-002$
10	$1.26e-001$	10	$6.91e-003$
15	$4.064e-003$	15	$6.87e-004$
20	$2.50e-003$	20	$2.92e-004$
25	$1.38e-003$	25	$2.31e-004$

Table 5.9: Max and mean for 90 configurations Functional output difference $\Delta s = (s - s_N)$: Max and mean values for 90 configurations $s = \int_\Omega \mathbf{f} \cdot \mathbf{u}$.

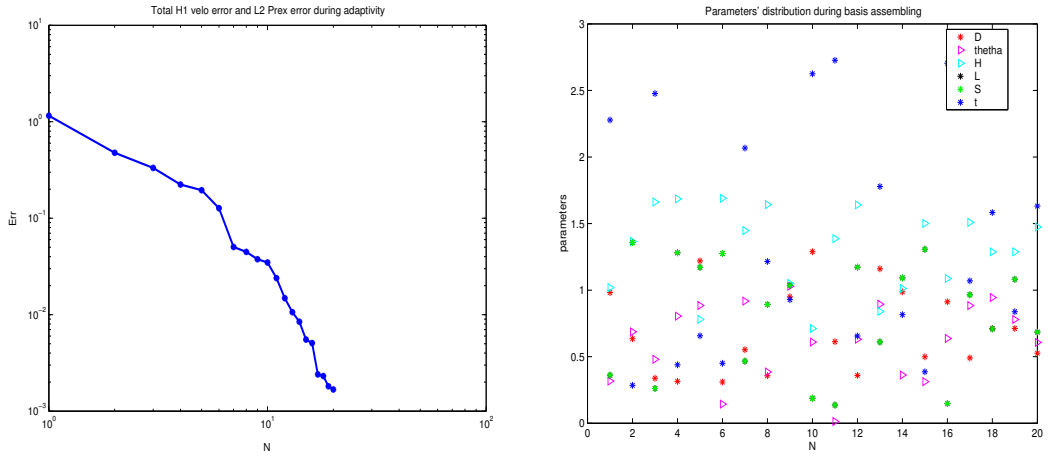

Figure 5.13: Basis assembling: total H^1 velocity and L^2 pressure (projected) errors reduction during basis assembling (left) and corresponding parameters distribution during off-line reduced basis assembling (right).

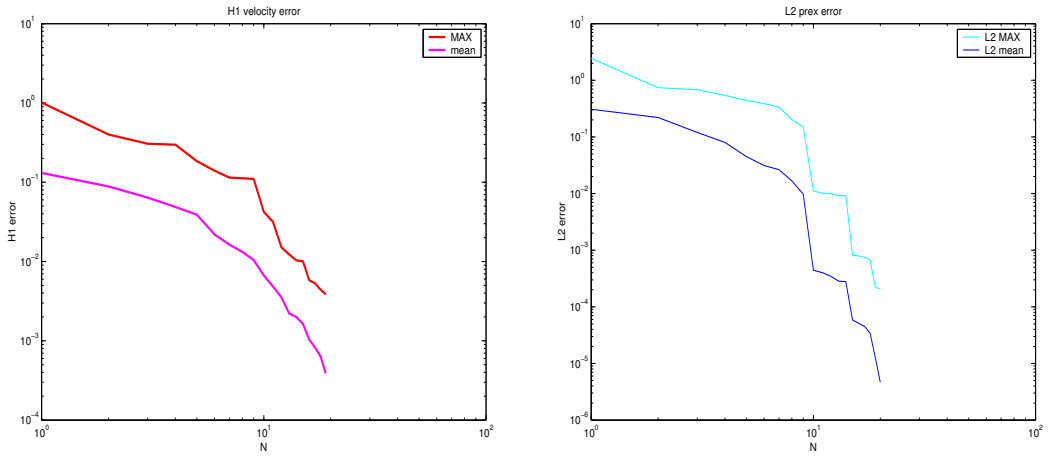

Figure 5.14: Left: relative true H^1 velocity errors: max and mean error over a large test sampling (90 configurations). Right: relative true L^2 pressure errors: Max and mean error over a large test sampling (90 configurations); errors in log-log scale.

5.6.4 On computational costs

In Table 5.10 we report some computational costs (CPU time) versus N. Finite element solution is obtained with a CPU time of 112.23, adopting a mesh with $O(10^3)$ elements, see Figure 5.2. Note the computational savings in the on-line step once we have assembled reduced basis matrix. In the same table we have inserted H^1 error indication to compare the computational costs and precision reached. The example refers to the case of a single parameter D, the arterial diameter.

N	$CPUtime$	H^1 error	%	N	$CPUtime$	H^1 error	%
1	1.597	$6.24E-1$	1.4	2	2.445	$2.16E-1$	2.2
3	3.225	$6.58E-3$	2.9	4	4.937	$5.30E-4$	4.4
5	5.908	$1.92E-4$	5.2	6	5.908	$1.006E-4$	5.2
7	6.68	$5.27E-5$	5.9	8	7.55	$3.36E-5$	6.7
9	8.442	$6.83E-7$	7.52	10	9.314	$1.11E-7$	8.3
11	10.615	$2.66E-8$	9.45	12	14.11	$1.98E-8$	12.57
13	14.38	$1.25E-8$	12.81	14	17.895	$2.91E-12$	15.9
15	20.601	$1.38E-12$	18.4	16	24.646	$4.05E-13$	21.9
17	24.625	$2.20E-13$	21.9	18	23.614	$2.74E-14$	21.1
19	24.025	$2.19E-14$	21.4	20	25.257	$1.39E-15$	22.5

Table 5.10: Computational costs (CPU time) varying N (and H^1 velocity error) and comparison with computational cost of FEM solution (%).

5.7 On algebraic and approximation stability

To control the condition number of reduced basis matrix we have adopted an orthonormalization procedure applied to velocity and pressure basis functions. After orthonormalization (to achieve algebraic stability) we have to satisfy the approximation stability condition on β_N, the equivalent reduced basis (RB) LBB *inf-sup* constant. But if we apply orthonormalization algorithm to reduced basis approximation spaces, assembled as proposed in Section 5.3, we may loose the validity of Lemma 5.3.1 to guarantee the stability of the approximation. For this reason we are going to propose other options in building the reduced basis velocity space.

5.7.1 Orthonormalization: Gram-Schmidt (GS) algorithm

We recall very briefly the main step of GS orthonormalization:

- Given: $\mathbf{z}_j, j = 1, ..., N$ a family vector of functions;
- we obtain $\mathbf{q}_j = \frac{P_j \mathbf{z}_j}{||P_j \mathbf{z}_j||}$, where P_j is an orthogonal projector onto the orthogonal complement of $< \mathbf{q}_1, \mathbf{q}_2, ..., \mathbf{q}_{j-1} >$.
- Each $\mathbf{q}_j$ is orthogonal to $\mathbf{q}_1, \mathbf{q}_2, ..., \mathbf{q}_{j-1}$ and lies in $< \mathbf{z}_1, \mathbf{z}_2, ..., \mathbf{z}_j >$.
- Each $||\mathbf{q}_j|| = 1$.
- $P_j = I - Q_{j-1} Q_{j-1}^T$; $Q_{j-1} = \{\mathbf{q}_1, ..., \mathbf{q}_{j-1}\}$;
- $P_j \mathbf{z}_j = \mathbf{z}_j - (\mathbf{q}_1^T \mathbf{z}_j)\mathbf{q}_1 - (\mathbf{q}_2^T \mathbf{z}_j)\mathbf{q}_2 - ... - (\mathbf{q}_{j-1}^T \mathbf{z}_{j-1})\mathbf{q}_{j-1}$;
- $\{\mathbf{q}_1, ..., \mathbf{q}_N\}$ is an orthogonal basis of $< \mathbf{z}_1, \mathbf{z}_2, ..., \mathbf{z}_N >$.

The norm $\|.\|$ used is the $Y = (H^1(\Omega))^2$ for velocity (and supremizers) and $L^2(\Omega)$ for pressure. The scalar product $\mathbf{q}_i^T \mathbf{z}_j$ is the one induced by the functional space and the norm we use. The orthonormalization procedure has been applied to reduced basis functions. For velocity and pressure the procedure is standard. For the supremizer we have to introduce some considerations. Referring to previous supremizer formulation of Equation 5.3.2 and to the compact notation already introduced, for $n = N+1, \ldots, 2N$ in the reference domain we have:

$$(\sigma_n, \mathbf{v})_{H^1} = \sum_{q=1}^{Q^b} \Phi^q(\mu)(\sigma_{qn}, \mathbf{v})_{H^1} = \sum_{q=1}^{Q^b} \Phi^q(\mu)\mathcal{B}(\xi_{n-N}, \mathbf{v})^q \quad \forall\, \mathbf{v} \in (H^1_{\Gamma_D}(\Omega))^2,$$

where

$$(\sigma_n, \mathbf{v})_{H^1} = \mathcal{B}(\mu, \xi_{n-N}, \mathbf{v}), \tag{5.7.1}$$

we recall that

$$(\sigma_{qn}, \mathbf{v})_{H^1} = \mathcal{B}(\xi_{n-N}, \mathbf{v})^q \tag{5.7.2}$$

and

$$\mathcal{B}(\mu, \xi, \mathbf{v}) = \sum_{q=1}^{Q^b} \Phi^q(\mu)\mathcal{B}(\xi, \mathbf{v})^q.$$

At this point we have two possibilities (referring to $n-th$ supremizer σ_n, $n = N+1, \ldots, 2N$) in applying orthonormalization:
i) an orthonormalization (GS) directly on σ_n done on-line (being σ_n dependent on μ) to obtain $\sigma_n^{\perp}$ as new element (basis function) to enrich RB velocity space:

$$\sigma_n^{\perp} = \frac{P_n^{\perp}\sigma_n}{||P_n^{\perp}\sigma_n||},$$

$$\sigma_n^{\perp} = \frac{P_n^{\perp}(\sum_{q=1}^{Q^b}\Phi_q(\mu)\sigma_{qn})}{||P_n^{\perp}(\sum_{q=1}^{Q^b}\Phi_q(\mu)\sigma_{qn})||},$$

$$P_n^{\perp} = I - Q_{n-1}Q_{n-1}^T, Q_i = \{\sigma_1^{\perp}, ..., \sigma_i^{\perp}\};$$

ii) an orthonormalization (GS) on components σ_{qn} made off-line (σ_{qn} are not depending on μ) to get $\sigma_{qn}^{\perp *}$:

$$\sigma_{qn}^{\perp *} = \frac{P_{qn}^{\perp}\sigma_{qn}}{||P_{qn}^{\perp}\sigma_{qn}||},$$

$$P_{qn}^{\perp} = I - Q_{q(n-1)}Q_{q(n-1)}^T, Q_{qi} = \{\sigma_{q1}^{\perp *}, ..., \sigma_{qi}^{\perp *}\},$$

$$\sigma_{qn}^{\perp *} = \sum_{k=1}^{n-1}\gamma_{qn}^k\sigma_{qk}^{\perp *},$$

Figure 5.15 shows the reduction of the condition number of Stokes reduced basis linear system matrix by orthonormalizing reduced basis functions (using method (i) for supremizer, including also orthonormalization for velocity and pressure basis functions). A very interesting

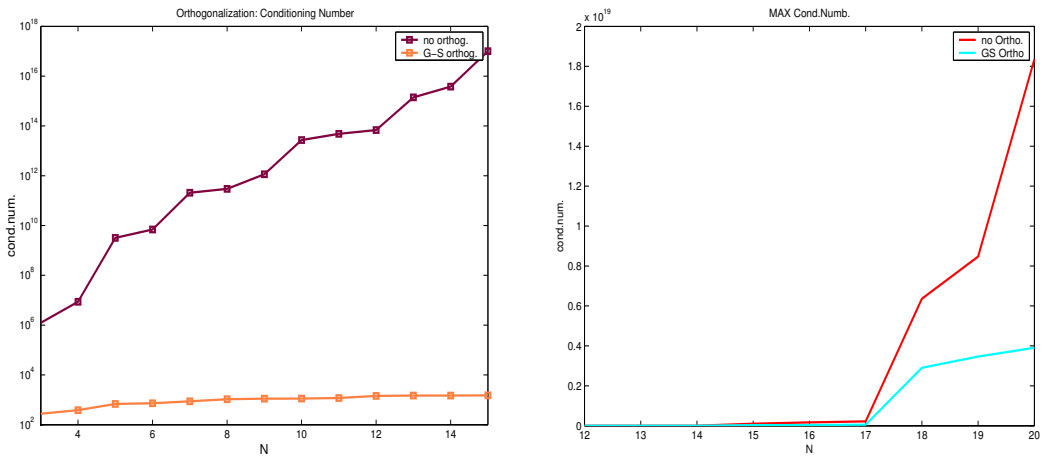

Figure 5.15: Orthonormalization: condition number of reduced basis Stokes linear system matrix with complete orthonormalized basis (left) and with a partial orthonormalization only on velocity and pressure (right), but not on supremizer.

property (visible also in Figure 5.15) is the following:

Property 5.7.1 *The condition number is limited and bounded after orthonormalization. The upper bound is given by the ratio between continuity and coercivity constant associated with the bilinear form.*

Proof
We define the coercivity and continuity constant, associated with the bilinear form $\mathcal{A}$, as:

$$\alpha(\mu) \equiv inf_{\mathbf{v}\in Y} \frac{\mathcal{A}(\mu, \mathbf{v}, \mathbf{v})}{\|\mathbf{v}\|_Y^2}, \tag{5.7.3}$$

$$\gamma(\mu) \equiv sup_{\mathbf{v}\in Y} \frac{\mathcal{A}(\mu, \mathbf{v}, \mathbf{v})}{\|\mathbf{v}\|_Y^2}. \tag{5.7.4}$$

We now assume that our basis functions $\sigma_n, n = 1, \ldots, 2N$ are orthonormal, that is,

$$(\sigma_i, \sigma_j)_Y = \delta_{i,j},\ 1 \leq i, j \leq 2N, \tag{5.7.5}$$

and we wish to bound the condition number of the reduced basis matrix A^μ given by

$$A_{ij}^\mu = \mathcal{A}(\mu, \sigma_i, \sigma_j). \tag{5.7.6}$$

We note that for any $\underline{\phi} \in \mathbb{R}^{2N}$,

$$\underline{\phi}^T \underline{A}^\mu \underline{\phi} = \sum_{i=1}^{2N}\sum_{j=1}^{2N} \phi_i\phi_j \mathcal{A}(\mu, \sigma_i, \sigma_j)$$

$$\geq \alpha(\mu) \sum_{i=1}^{2N}\sum_{j=1}^{2N} \phi_i\phi_j (\sigma_i, \sigma_j)_Y =$$

$$= \alpha(\mu) \sum_{i=1}^{2N} \phi_i^2.$$

Similarly

$$\underline{\phi}^T \underline{A}^\mu \underline{\phi} \leq \gamma(\mu) \sum_{i=1}^{2N} \phi_i^2. \tag{5.7.7}$$

It then follows that

$$\alpha(\mu) \leq \frac{\underline{\phi}^T \underline{A}^\mu \underline{\phi}}{\underline{\phi}^T \underline{\phi}} \leq \gamma(\mu)\ \forall\ \underline{\phi}\ \in\ \mathbb{R}^{2N}, \tag{5.7.8}$$

and therefore the condition number of $\underline{A}$ is bounded by $\gamma(\mu)/\beta(\mu)$. $\square$

5.7.2 Approximation stability: other supremizer options

By orthonormalizing the supremizer solutions according to the approach (i) we could lose approximation stability (guaranteed by Lemma 5.3.1) in the attempt of preserving algebraic stability by reducing the condition number. We can orthonormalize just using method (i) pressure ξ and velocity ζ basis functions and not the supremizer σ_n solutions and use the approach (ii) to orthogonalize the supremizer on its component σ_{kn} (before summation) to preserve Lemma 5.3.1.
To achieve this goal we may introduce two further different options in assembling the supremizer solutions for stabilization procedure by building in a different way the reduced basis velocity approximation space so that we may guarantee both approximation and algebraic stability.

First option

We have considered the following reduced basis spaces:

$$Y_N = \text{span}\,\{\sigma_n, n = 1, \ldots, N\overline{Q}^b\},$$

where $\overline{Q}^b = Q^b + 1$. For $n = 1, \ldots, N$:

$$\sigma_n = \zeta_n = \mathbf{u}(\mu^n).$$

For $n = N+1, \ldots, N\overline{Q}^b$, condensing index m and k in n, we have: $(\sigma_n, \mathbf{w})_Y = (\tilde{\sigma}_{mk}, \mathbf{w})_Y$, where

$$(\tilde{\sigma}_{mk}, \mathbf{w})_Y = \mathcal{B}(\xi_m, \mathbf{w})^k, \forall \mathbf{w} \in Y,\ k = 1, \ldots, Q^b,\ m = 1, \ldots, N;$$

$$\mathbf{u}_N(\mu) = \sum_{j=1}^{N\overline{Q}^b} \mathbf{u}_{Nj}(\mu)\sigma_j,$$

$$p_N(\mu) = \sum_{l=1}^{N} p_{Nl}(\mu)\xi_l;$$

the reduced basis system becomes:

$$\begin{cases} \sum_{j=1}^{N\overline{Q}_b} A_{ij}^{\mu}\mathbf{u}_{Nj}(\mu) + \sum_{l=1}^{N} B_{il}^{\mu} p_{Nl}(\mu) = F_i, & 1 \le i \le N\overline{Q}_b, \\ \sum_{j=1}^{N\overline{Q}_b} B_{jl}^{\mu}\mathbf{u}_{Nj}(\mu) = G_l, & 1 \le l \le N, \end{cases} \tag{5.7.9}$$

where:

$$A_{ij}^{\mu} = \sum_{k=1}^{Q^a} \Theta^k(\mu)\mathcal{A}(\sigma_i, \sigma_j)^k,\ 1 \le i, j \le N\overline{Q}_b,$$

$$B_{il}^{\mu} = \sum_{k=1}^{\overline{Q}^b} \Phi^k(\mu)\mathcal{B}(\sigma_i, \xi_l)^k,\ 1 \le i \le N\overline{Q}_b,\ 1 \le l \le N,$$

$$F_i = \langle F, \sigma_i\rangle,\ 1 \le i \le N\overline{Q}_b,\ G_l = \langle G^0, \xi_l\rangle,\ 1 \le l \le N.$$

In this case the basis is no longer μ (on line) dependent, the reduced basis velocity space, enriched by supremizers, has a bigger dimension ($N\overline{Q}_b > 2N$) than previously. The computational costs are as follows: $O(Q^a(\overline{Q}^b)^2N^2)$ for sub-matrix $\underline{A}$, $O((\overline{Q}^b)^2N^2)$ for $\underline{B}$, $O(\overline{Q}^bN)$ for $\underline{F}$, but the cost for inversion of the full reduced basis matrix (6.4.6) increases now to $O((\overline{Q}^b + 1)^3N^3)$. This approach has the big advantage to preserve Lemma 5.3.1, to let us apply orthonormalization (method (ii)) and to preserve the mentioned Lemma also after orthonormalization. This approach is the best if we want to be sure to preserve both algebraic and approximation stability after orthonormalization, if necessary. Figure 5.16 shows errors behavior by testing this first new supremizer option over a large test sampling (zero Dirichlet conditions and 3 geometrical parameters).

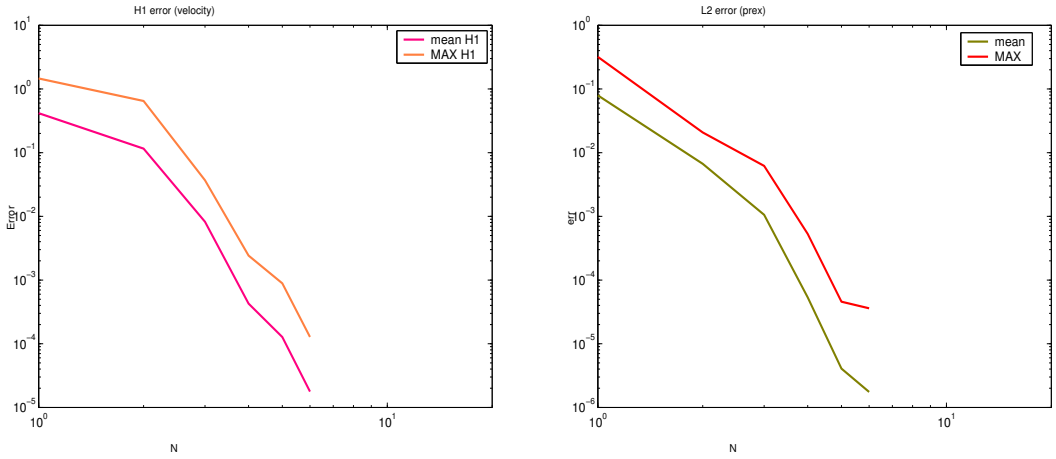

Figure 5.16: New supremizer first option, H^1 relative error (for velocity) and L^2 relative error (for pressure) using 50 configurations.

Second option

Another approach is based on the idea that supremizers are built upon summation using the same μ^j values used to store velocity $\zeta_j(\mu^j)$ and pressure solutions $\xi_j(\mu^j)$ (also in this case the basis for velocity is not dependent on the on-line value of μ and it is completely assembled off-line):

$$Y_N = \text{span}\,\{\sigma_n = \sum_{k=1}^{\overline{Q}^b} \Phi^k(\mu^n)\sigma_{kn},\ n = 1,\dots,2N\},$$

where $\overline{Q}^b = Q^b + 1, \Phi^{\overline{Q}^b} = 1$. For $n = 1,\dots,N$:

$$\sigma_{kn} = 0, for\ k = 1,\dots,Q^b; \sigma_{\overline{Q}^b n} = \zeta_n = \mathbf{u}(\mu^n).$$

For $n = N+1,\dots,2N$:

$$(\sigma_{kn}, \mathbf{w})_Y = \mathcal{B}(\xi_{n-N}, \mathbf{w})^k, \forall \mathbf{w} \in Y, for\ k = 1,\dots,Q^b;$$

$$\sigma_{\overline{Q}^b n} = 0.$$

The reduced basis solution is given by

$$\mathbf{u}_N(\mu) = \sum_{j=1}^{2N} \mathbf{u}_{Nj}(\mu)\Big(\sum_{k=1}^{\overline{Q}^b} \Phi^k(\mu^j)\sigma_{kj}\Big),$$

$$p_N(\mu) = \sum_{l=1}^{N} p_{Nl}(\mu)\xi_l,$$

by solving the system:

$$\begin{cases} \sum_{j=1}^{2N} A_{ij}^{\mu}\mathbf{u}_{Nj}(\mu) + \sum_{l=1}^{N} B_{il}^{\mu}p_{Nl}(\mu) = F_i, \quad 1 \le i \le 2N, \\ \sum_{j=1}^{2N} B_{jl}^{\mu}\mathbf{u}_{Nj}(\mu) = G_l, \quad 1 \le l \le N; \end{cases} \tag{5.7.10}$$

where:

$$A_{ij}^{\mu} = \sum_{k=1}^{Q^a} \Theta^k(\mu)\mathcal{A}(\sigma_i, \sigma_j)^k =$$

$$= \sum_{k=1}^{Q^a}\sum_{k'=1}^{\overline{Q}^b}\sum_{k''=1}^{\overline{Q}^b} \Theta^k(\mu)\Phi^{k'}(\mu^i)\Phi^{k''}(\mu^j)\mathcal{A}(\sigma_{k'i}, \sigma_{k''j})^k, \ 1 \le i, j \le 2N;$$

$$B_{il}^{\mu} = \sum_{k=1}^{\overline{Q}^b} \Phi^k(\mu)\mathcal{B}(\sigma_i, \xi_l)^k =$$

$$= \sum_{k=1}^{\overline{Q}^b}\sum_{k'=1}^{\overline{Q}^b} \Phi^k(\mu)\Phi^{k'}(\mu^i)\mathcal{B}(\sigma_{k'i}, \xi_l)^k, \ 1 \le i \le 2N, \ 1 \le l \le N;$$

$$F_i = \langle F, \sigma_i\rangle = \sum_{k'=1}^{\overline{Q}^b} \Phi^{k'}(\mu^i)\langle F, \sigma_{k'i}\rangle, \ 1 \le i \le 2N, \ G_l = \langle G^0, \xi_l\rangle, \ 1 \le i, l \le N.$$

This option is also competitive concerning computational costs dealing with $3N \times 3N$ reduced basis matrices (5.3.4) instead of $(\overline{Q}^b+1)N \times (\overline{Q}^b+1)N$ matrix (usually $(\overline{Q}^b+1) \gg 3$). We have the following computational costs to build reduced basis matrices, given also the supremizer components in the velocity space: $O(Q^a 4N^2)$ for sub-matrix $\underline{A}$, $O(\overline{Q}^b 2N^2)$ for $\underline{B}$, $O(N)$ for $\underline{F}$ and $O(9N^3)$ for the inversion of the full reduced basis matrix (5.3.4).
Using this option we cannot demonstrate that Lemma 5.3.1 is preserved (even without orthonormalization). We have tested numerically this option and we can argue that also this approximation is reasonably stable. Numerical results are shown in Figure 5.17 where we have reported errors behavior always testing a large number of configurations (Dirichlet conditions and 3 varying parameters). Convergence is very fast in this case. Figure 5.18 shows condition number reduction of reduced basis linear system and a comparison of condition number of the matrix without orthonormalization.

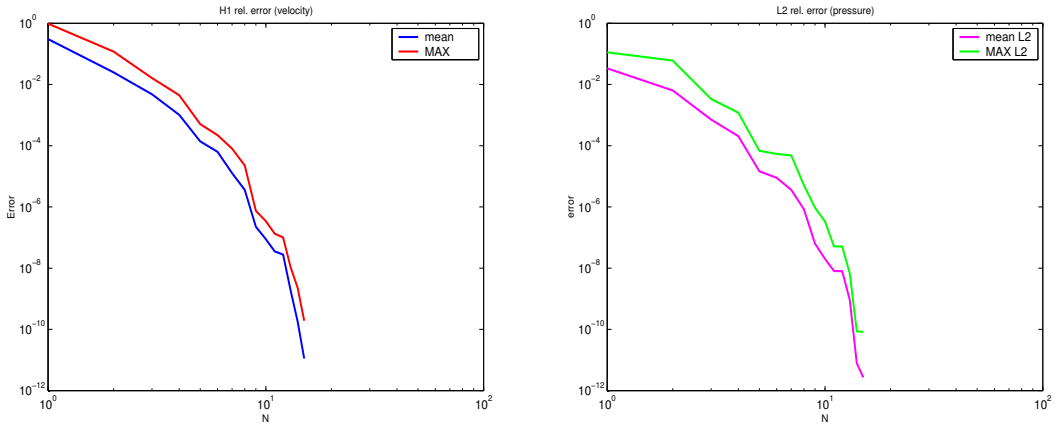

Figure 5.17: New supremizer second option, H^1 relative error (velocity) and L^2 relative error (pressure) over 50 configurations.

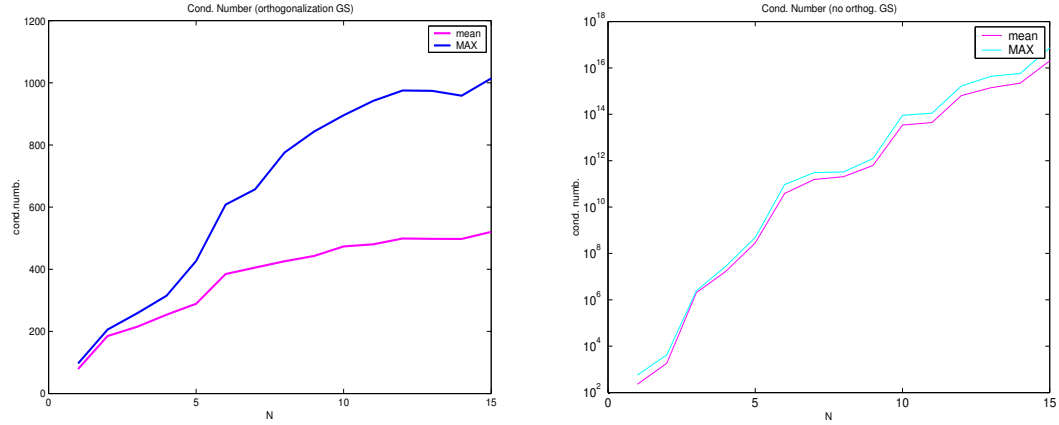

Figure 5.18: Condition number (max and mean) for the Stokes reduced basis system, with the new supremizer second option. On the left results with orthonormalization, on the right without it.

5.8 Some preliminary results on bypass configurations

As preliminary reported in [136] and [137] we start introducing some results on the complete bypass configurations using reduced basis techniques. We refer to the configuration reported in Figure 5.19. The idea has been the use of reduced basis (with also different approximation spaces) to test a huge number of different bypass configurations (i.e. a great number of parameters combinations).
As measure of blood flow perturbation we have considered for example the mean blood velocity:

$$s(\mu) = s_1(\mu) + s_2(\mu) = \sum_{r=1}^{R} \frac{\int_{\Omega_r} u_1 d\Omega}{\int_{\Omega_r} d\Omega} + \sum_{r=1}^{R} \frac{\int_{\Omega_r} u_2 d\Omega}{\int_{\Omega_r} d\Omega}. \tag{5.8.1}$$

We underline that, as seen in Chapter 2, also the velocity field is an interesting quantity to be studied in parametrized configuration, above all if we consider inflow and outflow of the downfield zone of the bypass configuration (being related with vorticity by Green's Theorem). In our case the inflow is the intersection between the new bridge and the host artery which is the zone studied in the local shape optimization approach.

We underline that, as seen in Chapter 2, also the velocity field is an interesting quantity to be studied in parametrized configuration, above all if we consider inflow and outflow of the downfield zone of the bypass configuration (being related with vorticity by Green's Theorem). In our case the inflow is the intersection between the new bridge and the host artery which is the zone studied in the local shape optimization approach.

With great computational costs savings we can provide in real time useful clinical indication dealing with a great number (i.e. hundreds) of bypass configurations and to understand the role of each geometrical parameter and their reciprocal influence. Numerical results indicate a very good convergence behavior and a tight control on the maximum N. Numerical tests on the bypass configuration (Figure 5.19) have been carried out imposing a mean Reynolds number of 10^3, a blood kinematic viscosity $\nu = 4{\cdot}10^{-6}\ m^2\ s^{-1}$ and a force field: $\mathbf{f} = (0, 9.8)^T m s^{-2}$. Solutions used as basis functions are always obtained by Galerkin-Finite Element method with Taylor-Hood elements ($\mathbb{P}^2$ and $\mathbb{P}^1$ for velocity and pressure, respectively). Figure 5.20 shows good convergence of the relative mean errors (H^1 for velocity and L^2 for pressure) testing a great number of configurations. We have carried out three different tests on parametrized families of bypass configurations by our *input-output* methodology. Figure 5.21 shows the first case of study where we have investigated the bypass graft angle perturbation (other parameters are frozen) measuring the increase of our output of interest (5.8.1): varying θ form ~ 0 to $\frac{\pi}{3}$ the increase of the mean blood flow is very high in the range $[0, \pi/6]$ and smoothed in the range $[\pi/6, \pi/3]$. Results are shown for different N to underline the fidelity of approximation with a few basis functions. Experimental results reported in [146] and other numerical simulations described in [152], [140], [141] and [60] provide the same interpretation of the role played by graft angle into an end-to-side anastomosis concerning flow separation and perturbation. Figure 5.22 shows the flow perturbations with respect to the quantity

$\frac{S}{D}$: the ratio between the stenosis length and the arterial diameter (best performances when $\frac{S}{D} \geq 1$) and the quantity $\frac{t}{D}$ (improving performances when the ratio is less than unity, i.e. bypass diameter smaller than arterial diameter). These results can be linked with the ones obtained during shape optimization where we find that it is better to get a flow which is diminishing its velocity when it is approaching the host artery (section is becoming larger, i.e. $D > t$, but also $S > D$). These results are a consequence of the continuity equation and of the fact that we are dealing with incompressible fluids.

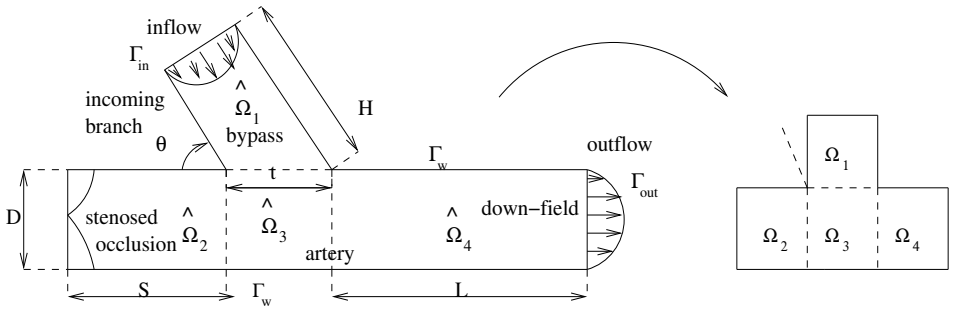

Figure 5.19: Schematic bypass configuration and reference domain.

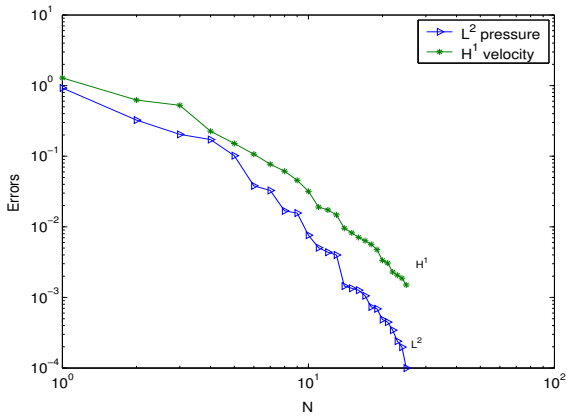

Figure 5.20: Reduced basis convergence results: mean error on velocity and pressure.

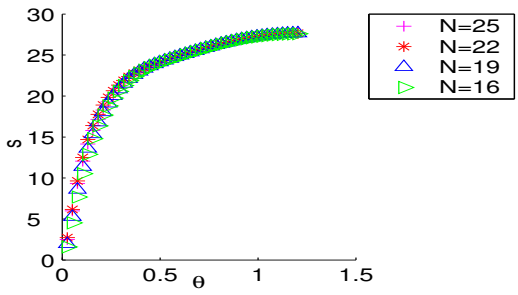

Figure 5.21: Output s $[ms^{-1} \cdot 10^{-2}]$ versus the parameter θ at different N.

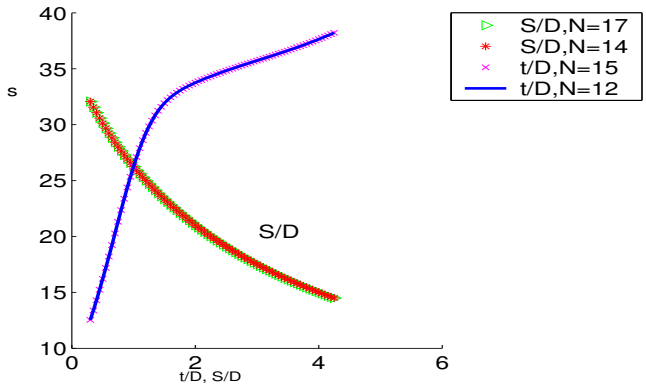

Figure 5.22: Output s $[ms^{-1} \cdot 10^{-2}]$ versus the ratios $\frac{t}{D}$ and $\frac{S}{D}$ at different N.

5.9 Non-compliant outputs: dual residual approach

Finally, as it is typical in engineering practice, we assume that we are not interested in calculating only the solution of parametrized problem (5.3.1). Rather we are interested in obtaining performance measures that characterize the particular configuration $\mu \in \mathcal{D}$ and have physical importance like, for example, flow-rate, vorticity, shear stress. Given the solution $[\mathbf{u}(\mu), p(\mu)]$ to (5.3.1), the output of interest can be written as:

$$s(\mu) = \ell^O([\mathbf{u}(\mu), p(\mu)]; \mu) = \ell_u^O(\mathbf{u}(\mu); \mu) + \ell_p^O(p(\mu); \mu); \tag{5.9.1}$$

with $\ell_u^O(\cdot; \mu) \in Y'$, $\forall \mu \in \mathcal{D}$ and $\ell_p^O(\cdot; \mu) \in Q'$, $\forall \mu \in \mathcal{D}$, which implies that $\ell^O(\cdot; \mu) \in (Y \times Q)'$, $\forall \mu \in \mathcal{D}$ is a bounded linear functional. We also require in the following a dual, or adjoint, problem associated with $\ell^O(\cdot; \mu)$: find $[\psi(\mu), \lambda(\mu)] \in Y \times Q$ such that

$$\begin{cases} \mathcal{A}(\mathbf{v}, \psi(\mu); \mu) + \mathcal{B}(\mathbf{v}, \lambda(\mu); \mu) = -\ell_u^O(\mathbf{v}; \mu) \ \forall \mathbf{v} \in Y, \\ \mathcal{B}(\psi(\mu), q; \mu) = -\ell_p^O(q; \mu) \ \forall q \in Q. \end{cases} \tag{5.9.2}$$

We note that $\mathcal{A}$ and $\mathcal{B}$ are the continuous bilinear forms introduced in (5.2.10) and (5.2.11), respectively. The adjoint problem (5.9.2) is subject to the same inf-sup condition (5.2.21) of the state problem.

Finally, we make the assumption of affine parameter dependence also for the linear form representing the output:

$$\ell^O([\mathbf{w}, q]; \mu) = \sum_{q=1}^{M_O} \pi_O^q(\mu) \ell_O^q([\mathbf{w}, q]), \tag{5.9.3}$$

$\forall \mathbf{w} \in Y$, $\forall q \in Q$, where M_O is an integer that depend on the problem (and output) in consideration. For a general overview on the adjoint problem and its reduced basis formulation see Patera *et al.* [118] and Rovas [134].

5.10 Reduced basis approximation for adjoint problem

We next define our primal and dual reduced-basis approximation spaces. To wit, for the primal and dual problem we choose N and M points: $\mu^i,\ i = 1,\dots,N$ and $\mu^i,\ i = 1,\dots,M$, respectively, not necessarily the same as for the primal problem in our parameter set $\mathcal{D}$. We denote the collection of the samples as:

$$\mathcal{S}_N^{pr} = \left\{\mu^1,\dots,\mu^N\right\},\ \mathcal{S}_M^{du} = \left\{\mu^1,\dots,\mu^M\right\}.$$

We then compute $[\mathbf{u}(\mu^i), p(\mu^i)] \in Y \times Q$ and $[\psi(\mu^i), \lambda(\mu^i)] \in Y \times Q$, the solutions of (5.3.1) for the primal problem (pr) and (5.9.2)) for the dual one (du), respectively, for all $\mu^i \in \mathcal{S}_N^{pr}$ and $\mu^i \in \mathcal{S}_M^{du}$. We have to calculate the quantities $\sigma_{kn}^{pr} \in Y$, and $\sigma_{kn}^{du} \in Y\ q = 1,\dots,Q^b$, and $n = N+1,\dots 2N$ or $n = M+1,\dots,2M$, respectively, which satisfy the supremizer problem:

$$\left(\sigma_{kn}^{pr}, v\right)_Y = \mathcal{B}^k(v, p(\mu^{n-N})),\ \forall v \in Y,\ k = 1,\dots,Q^b,\ n = N+1,\dots,2N \tag{5.10.1}$$

$$\left(\sigma_{kn}^{du}, v\right)_Y = \mathcal{B}^k(v, \lambda(\mu^{n-M})),\ \forall v \in Y,\ k = 1,\dots,Q^b,\ n = M+1,\dots,2M. \tag{5.10.2}$$

We then define the primal and dual "pressure" approximation spaces Q_N^{pr} and Q_M^{du}

$$Q_N^{pr} = \operatorname{span}\left\{p(\mu^i),\ i = 1,\dots,N\right\} \equiv \operatorname{span}\left\{\xi_i^{pr},\ i = 1,\dots,N\right\}, \tag{5.10.3}$$

$$Q_M^{du} = \operatorname{span}\left\{\lambda(\mu^i),\ i = 1,\dots,M\right\} \equiv \operatorname{span}\left\{\xi_i^{du},\ i = 1,\dots,M\right\}; \tag{5.10.4}$$

and the "velocity" approximation spaces $Y_N^{pr}(\mu)$ and $Y_M^{du}(\mu)$ (referring to the first supremizer option with N or M pressure functions and $2N$ or $2M$ velocity functions for primal and dual problem, respectively)

$$Y_N^{pr}(\mu) = \operatorname{span}\left\{\mathbf{u}(\mu^i), \sum_{q=1}^{Q^b} \Phi^q(\mu)\sigma_{q(N+i)}^{pr},\ i = 1,\dots,N\right\} \equiv \operatorname{span}\left\{\sigma_i^{pr},\ i = 1,\dots,2N\right\}, \tag{5.10.5}$$

$$Y_M^{du}(\mu) = \operatorname{span}\left\{\psi(\mu^i), \sum_{q=1}^{Q^b} \Phi^q(\mu)\sigma_{q(M+i)}^{du},\ i = 1,\dots,M\right\} \equiv \operatorname{span}\left\{\sigma_i^{du},\ i = 1,\dots,2M\right\}; \tag{5.10.6}$$

with dimensions $\dim Q_N^{pr} = N$, $\dim Y_N^{pr}(\mu) = 2N$, $\dim Q_M^{du} = M$, and $\dim Y_M^{du}(\mu) = 2M$.
In the construction of the reduced-basis spaces, we do not necessarily need to choose an equal number of pressure and velocity modes for primal and dual problem. We can also choose N_u^{pr} velocity basis functions for $Y_N^{pr}(\mu)$, and N_p^{pr} basis functions for the for Q_N^{pr} and the same for the dual problem. Another remark deals with the existence of two different kinds of approach for the primal and dual reduced basis approximation. Here we have introduced the so-called "non-integrated" (building different spaces for primal and dual problem) approach, as used in [134], another method is introduced in [118] where the "integrated" approach is used: in this case the approximation space for primal and dual problem is the same and made up of

both ζ_i^{pr} and ζ_i^{du}. The approach used here (the "non-integrated") has significant advantages concerning computational costs and conditioning aspects.
Using the definitions of reduced basis approximation spaces we can define the reduced-basis problems for primal and dual problem. We look for $[\mathbf{u}_N(\mu), p_N(\mu)] \in Y_N^{pr}(\mu) \times Q_N^{pr}$ and $[\psi_M(\mu), \lambda_M(\mu)] \in Y_M^{du}(\mu) \times Q_M^{du}$, such that:

$$\begin{cases} \mathcal{A}(\mathbf{u}_N(\mu); \mu) + \mathcal{B}(\mathbf{v}, p_N(\mu); \mu) = \ell(\mathbf{v}; \mu) \ \ \forall \mathbf{v} \in Y_N^{pr}(\mu), \\ \mathcal{B}(\mathbf{u}_N(\mu), q; \mu) = 0 \ \ \forall q \in Q_N^{pr}, \end{cases} \tag{5.10.7}$$

and,

$$\begin{cases} \mathcal{A}(\mathbf{v}, \psi_M(\mu); \mu) + \mathcal{B}(\mathbf{v}, \lambda_M(\mu); \mu) = -\ell_u^O(\mathbf{v}; \mu) \ \ \forall v \in Y_M^{du}(\mu), \\ \mathcal{B}(\psi_M(\mu), q; \mu) = -\ell_p^O(q; \mu), \ \forall q \in Q_M^{du}, \end{cases} \tag{5.10.8}$$

respectively. The solution of the dual problem is carried out as already seen for the state problem with the splitting of the procedure into an off-line (performed once) and online part (performed many times). If $[\mathbf{u}_N, p_N] \in Y_N^{pr}(\mu) \times Q_N^{pr}$ and, $[e_u^{pr}, e_p^{pr}](\mu) \equiv [\mathbf{u} - \mathbf{u}_N, p - p_M](\mu)$ is the error, the residual $R_u^{pr}(\cdot; [\mathbf{u}_N, p_N]; \mu) \in Y'$ is defined

$$\begin{aligned} R_u^{pr}(\mathbf{v}; [\mathbf{u}_N, p_N]; \mu) &= \ell(\mathbf{v}; \mu) - \mathcal{A}(\mathbf{u}_N(\mu), \mathbf{v}; \mu) - \mathcal{B}(\mathbf{v}, p_N(\mu); \mu) = \\ &= \mathcal{A}(e_u^{pr}(\mu), \mathbf{v}; \mu) + \mathcal{B}(\mathbf{v}, e_p^{pr}(\mu)) \ \ \forall \mathbf{v} \in Y, \end{aligned} \tag{5.10.9}$$

where the second line follows from equation (5.3.1). Similarly the residual related to the incompressibility constraint $R_p^{pr}(\cdot; [\mathbf{u}_N, p_N]; \mu) \in Q'$ is

$$\begin{aligned} R_p^{pr}(q; [\mathbf{u}_N, p_N]; \mu) &= -\mathcal{B}(\mathbf{u}_N(\mu), q; \mu) \\ &= \mathcal{B}(e_u^{pr}(\mu), q; \mu) \ \forall q \in Q. \end{aligned} \tag{5.10.10}$$

We can the define the primal residual $R^{pr}(\cdot; [\mathbf{u}_N, p_N]; \mu) \in (Y \times Q)'$, from

$$\begin{aligned} R^{pr}([\mathbf{w}, q]; [\mathbf{u}_N, p_N]; \mu) &= R_u^{pr}(\mathbf{w}; [\mathbf{u}_N, p_N]; \mu) + R_p^{pr}(q; [\mathbf{u}_N, p_N]; \mu) = \\ &= \mathcal{A}(e_u^{pr}(\mu), \mathbf{w}; \mu) + \mathcal{B}(\mathbf{w}, e_p^{pr}(\mu)) + \mathcal{B}(e_u^{pr}(\mu), q; \mu) \ \forall [\mathbf{w}, q] \in Y \times Q. \end{aligned} \tag{5.10.11}$$

For the dual problem, if $[\psi_M, \lambda_M] \in Y_M^{du}(\mu) \times Q_M^{du}$ and, $[e_u^{du}, e_p^{du}](\mu) \equiv [\psi - \psi_M, \lambda - \lambda_M](\mu)$ is the error, we define in a similar way the residuals $R_u^{du}(\cdot; [\psi_M, \lambda_M]; \mu) \in Y'$ and $R_p^{du}(\cdot; [\psi_M, \lambda_M]; \mu) \in Q'$:

$$\begin{aligned} R_u^{du}(\mathbf{v}; [\psi_M, \lambda_M]; \mu) &= -\ell_u^O(\mathbf{v}; \mu) - \mathcal{A}(\mathbf{v}, \psi_M(\mu); \mu) - \mathcal{B}(\mathbf{v}, \lambda_M(\mu); \mu) = \\ &= \mathcal{A}(e_u^{du}(\mu), \mathbf{v}; \mu) + \mathcal{B}(\mathbf{v}, e_p^{du}(\mu)) \ \forall \mathbf{v} \in Y, \end{aligned} \tag{5.10.12}$$

and

$$\begin{aligned} R_p^{du}(q; [\psi_M, \lambda_M]; \mu) &= -\ell_p^O(q; \mu) - \mathcal{B}(\psi_M(\mu), q; \mu) = \\ &= \mathcal{B}(e_u^{du}(\mu), q; \mu) \ \forall q \in Q. \end{aligned} \tag{5.10.13}$$

The dual residual is then $R^{du}(\cdot; [\mathbf{w}_M, q_M]; \mu) \in (Y \times Q)'$ is then

$$\begin{aligned} R^{du}([\mathbf{w}, q]; [\psi_M, \lambda_M]; \mu) &= R_u^{du}(\mathbf{w}; [\psi_M, \lambda_M]; \mu) + R_p^{du}(q; [\psi_M, \lambda_M]; \mu) \\ &= \mathcal{A}(\mathbf{w}, e_u^{du}(\mu); \mu) + \mathcal{B}(\mathbf{w}, e_p^{du}(\mu)) + b(e_u^{du}(\mu), q; \mu) \ \forall [\mathbf{w}, q] \in Y \times Q. \end{aligned} \tag{5.10.14}$$

The output approximation is then obtained from

$$s_N(\mu) = \ell^O([\mathbf{u}_N, p_N](\mu);\mu) - R^{pr}([\psi_M, \lambda_M](\mu); [\mathbf{u}_N, p_N](\mu);\mu); \tag{5.10.15}$$

where the adjoint correction helps improving the accuracy of the approximation. In Patera and Rønquist [110] a detailed analysis concerning the output correction is provided. For a more general framework we suggest to see also Giles and Pierce [114]. For the computation of the primal and dual basis functions, a total of $N + M$ Stokes problems need to be solved. In addition, $(N+M)Q_b$ Y-solves are required for the calculation of supremizers σ_{kn}. Finally, a number of matrix-vector and inner products are required for the formation of a number of auxiliary quantities. The important thing to note it that once the expensive and memory intensive off-line part is completed, a database with $\mathcal{O}((N^2+M^2)Q_aQ_b^2)$ quantities, is created. In the on-line part, for each new $\mu \in \mathcal{D}$, and using this database: first, $\mathcal{O}((N^2+M^2)Q_aQ_b^2)$ operations are required to form the reduced-basis problems; and second $\mathcal{O}(N^3+M^3)$ operations are required to invert the resulting linear systems and compute the output approximation. Note that during on-line calculation no explicit reference is made to the continuous or, in practice, finite-element problem and so computational costs are not depending on the costs of finite-element solution. As N and M will typically be small, significant computational savings are expected.

5.10.1 Some elements for output error estimation

Let $[\mathbf{u}, p](\mu) \in Y \times Q$ be the exact solution for the primal problem (5.3.1), and $[\mathbf{u}_N, p_N](\mu) \in Y_N \times Q_N$ the reduced-basis approximation obtained by solving (5.10.7). Subtracting (5.3.1) and (5.10.7), the error $[e_u^{pr}, e_p^{pr}](\mu) \equiv [\mathbf{u} - \mathbf{u}_N, p - p_N] \in Y \times Q$ to the primal problem satisfies the following equation:

$$\begin{cases} \mathcal{A}(e_u^{pr}(\mu), \mathbf{v};\mu) + \mathcal{B}(\mathbf{v}, e_p^{pr}(\mu)) = R_u^{pr}(\mathbf{v}; [\mathbf{u}_N, p_N](\mu);\mu), \ \forall v \in Y, \\ \mathcal{B}(e_u^{pr}(\mu), q;\mu) = R_p^{pr}(q; [\mathbf{u}_N, p_N](\mu);\mu), \ \forall q \in Q, \end{cases} \tag{5.10.16}$$

with similar equation valid for the dual error $[e_u^{du}, e_p^{du}](\mu) \equiv [\psi - \psi_M, \lambda - p_M](\mu) \in Y \times Q$. We can get a posteriori error estimator for the output. From (5.9.1) and (5.10.15) the error in the output is given by

$$\begin{aligned} s(\mu) - s_N(\mu) &= \ell_u^O(\mathbf{u}(\mu);\mu) + \ell_p^O(p(\mu);\mu) \\ &\quad -\ell_u^O(\mathbf{u}_N(\mu);\mu) - \ell_p^O(p_N(\mu);\mu) + R^{pr}([\psi_M, \lambda_M](\mu); [\mathbf{u}_N, p_N](\mu);\mu) = \\ &= \ell_u^O(e_u^{pr}(\mu);\mu) + \ell_p^O(e_p^{pr}(\mu);\mu) + R^{pr}([\psi_M, \lambda_M](\mu); [\mathbf{u}_N, p_N](\mu);\mu) \end{aligned}$$

which from the definition of the adjoint problem (5.9.2) and the primal residual (5.10.11) can be written as

$$\begin{aligned} s(\mu) - s_N(\mu) &= -\mathcal{A}(e_u^{pr}(\mu), \psi(\mu);\mu) - \mathcal{B}(e_u^{pr}(\mu), \lambda(\mu);\mu) - \mathcal{B}(\psi(\mu), e_p^{pr}(\mu);\mu) \\ &\quad + \mathcal{A}(e_u^{pr}(\mu), \psi_M(\mu);\mu) + \mathcal{B}(e_u^{pr}(\mu), \lambda_M(\mu);\mu) + \mathcal{B}(\psi_M(\mu), e_u^{pr}(\mu);\mu) = \\ &= -\mathcal{A}(e_u^{pr}(\mu), e_u^{du}(\mu);\mu) - \mathcal{B}(e_u^{pr}(\mu), e_p^{du}(\mu);\mu) - \mathcal{B}(e_u^{du}(\mu), e_u^{pr}(\mu);\mu) = \\ &= -R_u^{du}(e_u^{pr}; [\psi_M, \lambda_M](\mu);\mu) - R_p^{du}(e_p^{pr}(\mu); [\psi_M, \lambda_M](\mu);\mu); \end{aligned}$$

here the definitions for the primal and dual residuals (5.10.11) and (5.10.14), respectively, have been used. We then have:

$$\begin{aligned} |s(\mu) - s_N(\mu)| &\leq \sup_{\mathbf{v}\in Y} \frac{R_u^{du}(\mathbf{v};[\psi_M,\lambda_M](\mu);\mu)}{\|\mathbf{v}\|_Y} \|e_u^{pr}(\mu)\|_Y + \sup_{q\in Q} \frac{R_p^{du}(q;[\psi_M,\lambda_M];\mu)}{\|q\|_Q} \|e_p^{pr}(\mu)\|_Q \\ &= \|R_u^{du}(\cdot;[\psi_M,\lambda_M](\mu);\mu)\|_{Y'} \|e_u^{pr}(\mu)\|_Y + \|R_p^{du}(\cdot;[\psi_M,\lambda_M];\mu)\|_{Q'} \|e_p^{pr}(\mu)\|_Q, \end{aligned} \tag{5.10.17}$$

obtaining a bound depending on the dual norms for the dual residuals multiplied for the primal error. We can conclude that if we consider corrected outputs with dual-residual we have a faster convergence and a greater accuracy with respect to the non-dual corrected version because in the dual corrected case the output error is bounded by a product of dual residuals and primal errors. There is a trade-off between accuracy and computational cost: for example, for exponentially convergent primal and dual approximation (the worst case concerning the advantage of the dual approach), the primal-dual combined approach gives comparable accuracy at 1/4 the computational cost even if the problem complexity has increased in solving an adjoint problem and assembling dual basis.

5.10.2 Results using non-compliant outputs

In Figure 5.23 we present a comparison considering the mean error on output using the dual residual correction with respect to the non-corrected one (considering only Stokes primal problem). The improvement in accuracy achieved is shown in the worst case, where the primal space has already some approximation properties for the dual problem. The test is concerned with a 4-parameters bypass configuration (using several parameters combinations) and the "non-compliant" output considered was the distributed vorticity:

$$s = \int_\Omega (\frac{\partial u_1}{\partial x_2} - \frac{\partial u_2}{\partial x_1}) d\Omega.$$

In Figure 5.24 we show the convergence for primal and dual error (H^1 velocity relative errors) and a mean relative error over the non-compliant vorticity output considering a great number of different 3-parameters bypass configuration. In this case we can see the "square effect" (the output error is bounded by the product between the primal error with the dual residual as shown in 5.10.17) and we have an accuracy in the dual corrected case for $N = 10$ which is the same we get for $N = 20$ in the non-corrected case and with computational costs which are 1/8 (based on LU scaling) with respect to the non-corrected approach. In Figure 5.25 we show some results dealing with the dual corrected output error, the relative H^1 velocity error for primal problem, the error for the non-corrected output ($\tilde{s}_N(\mu)$) and a theoretical upper bound for the non-corrected output. The latter is given by

$$\begin{aligned} s(\mu) - \tilde{s}_N(\mu) &= \ell_u^O(\mathbf{u}(\mu);\mu) + \ell_p^O(p(\mu);\mu) \\ &\quad -\ell_u^O(\mathbf{u}_N(\mu);\mu) - \ell_p^O(p_N(\mu);\mu) = \\ &= \ell_u^O(e_u^{pr}(\mu);\mu) + \ell_p^O(e_p^{pr}(\mu);\mu) = \\ &= \frac{\ell_u^O(e_u^{pr}(\mu);\mu)}{\|e_u^{pr}(\mu)\|_Y} \|e_u^{pr}(\mu)\|_Y + \frac{\ell_p^O(e_p^{pr}(\mu);\mu)}{\|e_p^{pr}(\mu)\|_Q} \|e_p^{pr}(\mu)\|_Q \\ &\leq \sup_{\mathbf{v}\in Y} \frac{\ell_u^O(\mathbf{v};\mu)}{\|\mathbf{v}\|_Y} \|e_u^{pr}(\mu)\|_Y + \sup_{q\in Q} \frac{\ell_p^O(q;\mu)}{\|q\|_Q} \|e_p^{pr}(\mu)\|_Q, \end{aligned}$$

where the upper bound is the dual norm of the linear functional times the primal error. Also in this case we can see how the dual correction improves the output accuracy.

Now we can turn our attention on our main application and study bypass parametrized

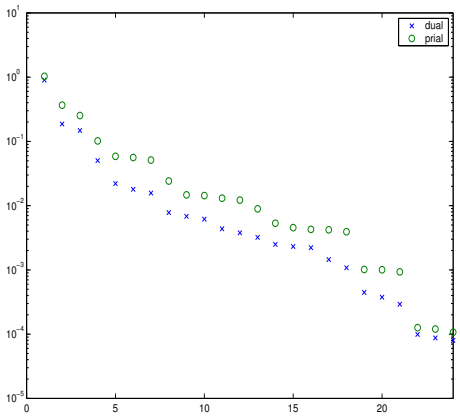

Figure 5.23: Max output error (comparison with and without correction).

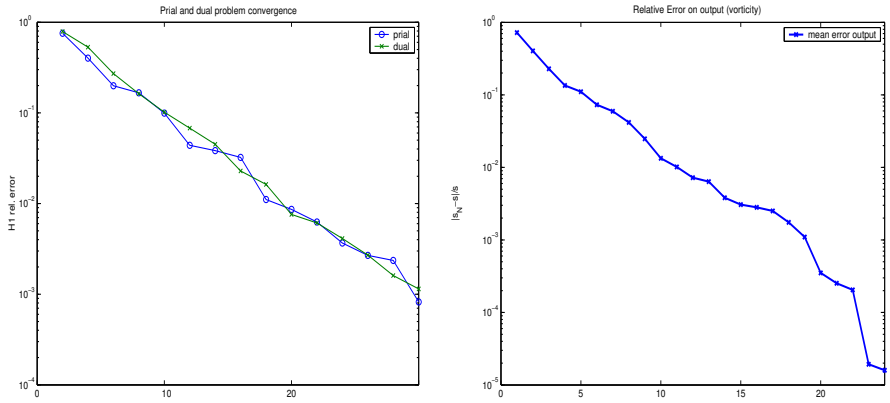

Figure 5.24: H^1 velocity relative error for dual and primal problems and output relative errors.

configuration with more complex outputs. We report some summary results dealing with 4 varying parameters (i.e t, D, S, θ). Results are an extension of the ones obtained considering the flow perturbation due to the increase of mean velocity. In Figures 5.26 and 5.27 we have summarized our results by reporting only few spots (each representing a different configuration) to keep the plot quite clear, which show the distributed vorticity $m^2 s^{-1}$ cost functional with respect to $\frac{S}{D}$ (reported in x_1 axis) and $\frac{t}{D}$ (represented by the colored scale) and θ graft angle (reported in x_2 axis and represented by the dimension of the colored spots). We can conclude that quantities $\frac{S}{D}$ and $\frac{t}{D}$ are more important and only freezing them the graft angle has a crucial role (to have a look on some numerical results dealing with blood recirculation at different graft angle see [141], where other geometrical parameters are frozen). Vorticity is reduced when the ratio $\frac{S}{D}$ is bigger than unity and when $\frac{t}{D}$ is smaller than unity. These

results are a further explanation of fluid mechanics phenomena related with geometry for incompressible flows. We want also to underline how the output seems to be sensible with the changes in bypass configuration.

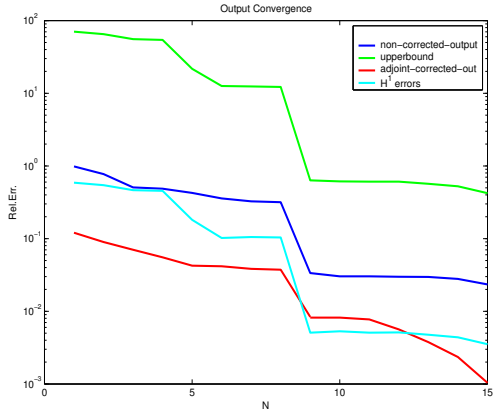

Figure 5.25: H^1 error, upper bound for output error (non-corrected), adjoint-corrected and non-corrected output error.

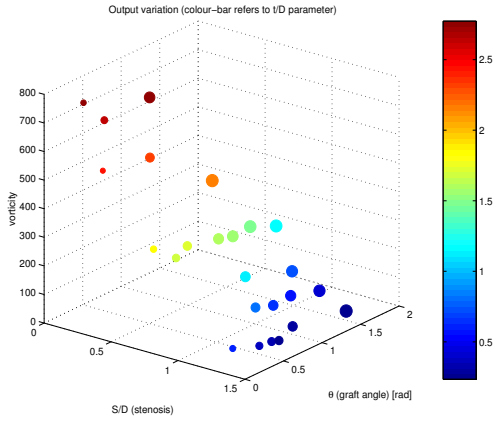

Figure 5.26: Output s_N $[m^2 s^{-1} \cdot 10^{-2}]$ versus θ parameter (spots dimension) and the ratios $\frac{t}{D}$ (colorbar) and $\frac{S}{D}$. Real-time "clinical" indications by a great number (i.e. hundreds) of bypass configurations (Re= 10^3).

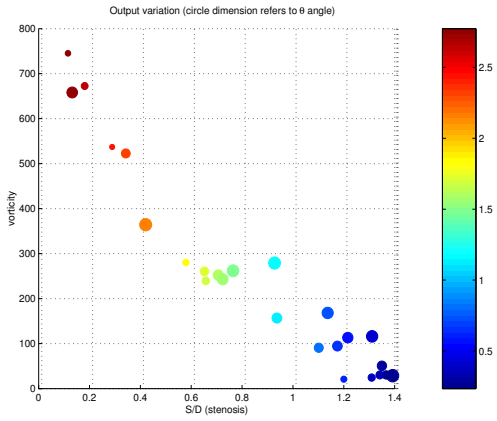

Figure 5.27: Bidimensional version of Figure 5.26.

5.11 Conclusions

We have provided some elements to solve rapidly and efficiently Stokes equations in parametrized domains and to extract information on some fluid mechanics outputs and a sensitivity analysis on some geometrical parameters, describing a complete configuration for a bypass. Reduced basis techniques allow us huge computational savings and real-time results and they guarantee at the same time the stability of the approximation. To complete this study we have to extend the application of reduced basis to Navier-Stokes equations in parametrized domains and in problems involving non-affine mapping dependence (i.e. shape design problem with curved walls). Some recent works are [159] for Navier-Stokes reduced basis formulation and references [145] and [12] dealing with non-affine parameter dependence. The latter especially introduces an efficient reduced basis discretization procedure replacing non-affine coefficient functions with a collateral reduced basis expansion which permits an offline-online computational decomposition by a stable and inexpensive empirical interpolation procedure. These issues will make the subject of the following chapter.

Chapter 6

Reduced Basis Methods for Stokes Equations in Domains with Non-Affine Parametric Dependence

In this chapter we extend reduced basis techniques applied to Stokes equations in domains parametrized by affine and non-affine maps with respect to a reference domain. The proposed method is ideally suited also for shape optimization problem with more realistic configuration. An "empirical", stable and inexpensive interpolation method has permitted to replace non-affine coefficient functions with an expansion which leads to a computational decomposition between the offline–parameters independent–stage for reduced basis generation and the online–parameters dependent–approximation stage based on Galerkin projection, used to find a new solution for a new set of parameters by a combination of previously computed stored solutions. As in the affine case this computational decomposition leads us to preserve reduced basis properties: rapid and accurate convergence and computational economies. The applications and results are based on parametrized geometries describing domains with curved walls, a preliminary test based on a stenosed channel and then some tests on the bypass configuration. This method is well suited to treat also problems in fixed domains with non-affine parameters dependence expressing varying physical coefficients.

6.1 An extension on the use of reduced basis

This chapter is an extension of applications and results collected in [138] dealing with the application of reduced basis techniques for Stokes equations in curved parametrized domains. After this introduction, in Section 6.2 the empirical interpolation procedure proposed by Maday *et al.* [12] and applied to non-affine transformation terms, mapping the real domain into a reference one, is briefly described. In this chapter we focus on the use of this interpolation procedure for geometrical non-affine transformation terms, the coupling with the affine ones and the introduction of parametrized complex geometries in the reduced basis problems. In Section 6.3 we recall the parametrized Stokes equations framework coupling affine and

non-affine parametric dependence. In Section 6.4 we introduce Stokes reduced basis formulation extended to the non-affine case. Then in Section 6.5 we introduce some numerical results based on two different geometries. Finally, in Section 6.6 we give a preview on the development guidelines for viscous flow and shape optimization problems.

6.2 Empirical interpolation for (coefficient) functions approximation

To start with we recall the empirical interpolation procedure, proposed in [12]. This procedure has been applied also in Grepl [44] for parabolic equations. We consider a (coefficient) function $g(x,\mu)$, depending on spatial coordinates and on a set of parameters $\mu \in \mathcal{D} \subset \mathbb{R}^P$ (for some $P \geq 1$). The function $g(x,\mu)$ represents, for example, a coefficient for a linear or bilinear form, that shows up when a non-affine mapping transformation of a physical domain into a reference one indicated with Ω is applied. We assume that $g(x,\mu) \in L^\infty(\Omega)$ for all choice of μ. Our goal is to rewrite this function as an expansion given by products between parameters dependent coefficients and "shape functions" depending only on spacial coordinates. We introduce Ξ^g as a suitably fine parameter sample over $\mathcal{D}$ and the related quantities

$$\mu_M^g = argmax_{\mu\in\Xi^g} inf_{z\in W_{M-1}^g} \|g(.,\mu) - z\|_{L^\infty(\Omega)}$$

to build the sets $S_M^g = \{\mu_m^g, 1 \leq m \leq M\}, 1 \leq M \leq M_{max}$, $S_M^g = S_{M-1}^g \cup \mu_M^g$ and the following approximation spaces

$$W_M^g = span\{\gamma_m = g(.,\mu_m^g), 1 \leq m \leq M\}, 1 \leq M \leq M_{max}.$$

The quantity μ_1^g is chosen "a priori" so that $\gamma_1(x) \neq 0$. We need to construct nested sets of interpolation points:

$$T_M = \{t_1, \ldots t_M\}, 1 \leq M \leq M_{max},$$

by the following algorithm. Starting from $M = 1$ we store

$$\gamma_1(x) = g(x,\mu_1^g), t_1 = argsup_{x\in\Omega}|\gamma_1(x)|,\ q_1(x) = \gamma_1(x)/\gamma_1(t_1),$$

for $M \geq 2$ we have to solve a linear system to get σ_{M-1} and then $r_M(x)$ in assembling T_M:

$$M = 2, \ldots, M_{max} : \Sigma_{j=1}^{M-1}\sigma_j^{M-1} q_j(t_i) = \gamma_M(t_i), 1 \leq i \leq M-1;$$

$$r_M(x) = \gamma_M(x) - \Sigma_{j=1}^{M-1}\sigma_j^{M-1} q_j(x), t_M = argsup_{x\in\Omega}|r_M(x)|,$$

$$q_M(x) = r_M(x)/r_M(t_M).$$

At the end of the algorithm our function is approximated by $g_M(x,\mu)$ and split into two parts (decoupled) each of them depending only on the μ parameter ($\lambda_m(\mu)$) or on x coordinates ($q_m(x)$), i.e:

$$g_M(x,\mu) = \Sigma_{m=1}^M \lambda_m(\mu) q_m(x),$$

where λ_j are given by the solution of the following linear system

$$\Sigma_{j=1}^{M} q_j(t_i)\lambda_j(\mu) = g(t_i,\mu), 1 \le i \le M.$$

We choose M_{max} as being the minimum M s.t. the maximum interpolation error:

$$\varepsilon_M(\mu) = \|g(.,\mu) - g_M(.,\mu)\|_{L^\infty(\Omega)} \tag{6.2.1}$$

satisfies $\varepsilon_M \le \varepsilon_{max}$ (for a prescribed tolerance ε_{max}).
This interpolation process can be justified. A priori we can introduce a Lebesgue constant $\Lambda_M = \sup_{x\in\Omega} \Sigma_{m=1}^{M} |V_m^M(x)|$, where V_m^M is the only element of W_M^g such that $V_m^M(t_i) = \delta_{im}$. It is possible to demonstrate ([12]) that Λ_M is bound by the quantity $2^M - 1$. For the interpolation error (6.2.1) we have:

$$\varepsilon_M \le (1 + \Lambda_M)\varepsilon_M^*(\mu),$$

where $\varepsilon_M^*(\mu) \equiv \inf_{z\in W_M^g} \|g(.,\mu) - z\|_{L^\infty(\Omega)}, \forall \mu \in \mathcal{D}$. The bound on the Lebesgue constant is pessimistic and compensated (as in polynomial approximation) by the rapid convergence of the term $\varepsilon_M^*(\mu)$.
The problem of locally non-affine dependence of $g(x,\mu)$ on parameter μ is also studied in Solodukhov [145].

6.3 The Stokes problem with non-affine parametric dependence

The parametrized Stokes equations have been formulated in Section 5.2 in a domain $\hat{\Omega} \in \mathbb{R}^2$ whose shape is depending affinely on a set of geometrical parameters in each subdomain $\hat{\Omega}^r$ such that $\hat{\Omega} = \bigcup_{r=1}^{R} \hat{\Omega}^r$.
In this section we build a system of P^2DEs (Parametrized Partial Differential Equations) depending on a set of geometrical parameters (μ) as coefficients whose dependence from parameters is both affine and non-affine (in different subdomains). As already seen, problem (5.2.7) can be traced back to a *reference domain*, in this case by an *affine mapping* on some subdomains $\hat{\Omega}_G^r$ into Ω_G^r and by a *non-affine mapping* on the remaining subdomains $\hat{\Omega}_T^r$ into Ω_T^r . In this case $R = R_G + R_T$ and $\Omega = \bigcup_{r=1}^{R_G} \Omega_G^r \cup \bigcup_{r=1}^{R_T} \Omega_T^r$. For any $\hat{x} \in \hat{\Omega}_G^r$, $r = 1, \ldots, R_G$, its image $x \in \Omega_G^r$ is given by

$$x = \mathcal{G}^r(\mu;\hat{x}) = G^r(\mu)\hat{x} + g^r, \quad 1 \le r \le R_G; \tag{6.3.1}$$

we thus write on Ω_r^G

$$\frac{\partial}{\partial \hat{x}_i} = \frac{\partial x_j}{\partial \hat{x}_i}\frac{\partial}{\partial x_j} = G_{ji}^r(\mu)\frac{\partial}{\partial x_j}. \tag{6.3.2}$$

For any $\hat{x} \in \hat{\Omega}_T^r$, $r = 1, \ldots, R_T$, its image $x \in \Omega_T^r$ is given by

$$x = \mathcal{T}^r(\mu;\hat{x}), \quad 1 \le r \le R_T; \tag{6.3.3}$$

we thus write on Ω_T^r

$$\frac{\partial}{\partial \hat{x}_i} = \frac{\partial x_j}{\partial \hat{x}_i}\frac{\partial}{\partial x_j} = T_{ji}^r(\mu, x)\frac{\partial}{\partial x_j}. \tag{6.3.4}$$

Referring to problem (5.2.7) and to formulation from (5.2.10) to (5.2.13), we can write with the current parametrization in the reference domain Ω:

$$\langle \mathcal{A}\mathbf{u}, \mathbf{w}\rangle = \sum_{r=1}^{R_G}\int_{\Omega_G^r}\frac{\partial \mathbf{u}}{\partial x_i}\Big(G_{ii'}^r(\mu)\hat{\nu}_{i'j'}G_{jj'}^r(\mu)det(G^r(\mu))^{-1}\Big)\frac{\partial \mathbf{w}}{\partial x_j}d\Omega + \tag{6.3.5}$$

$$\sum_{r=1}^{R_T}\int_{\Omega_T^r}\frac{\partial \mathbf{u}}{\partial x_i}\Big(T_{ii'}^r(\mu, x)\hat{\nu}_{i'j'}T_{jj'}^r(\mu, x)det(T^r(\mu, x))^{-1}\Big)\frac{\partial \mathbf{w}}{\partial x_j}d\Omega \ \forall \mathbf{w} \in Y,$$

$$\langle \mathcal{B}p, \mathbf{w}\rangle = -\sum_{r=1}^{R_G}\int_{\Omega_G^r} p\Big(G_{ij}^r(\mu)det(G^r(\mu))^{-1}\Big)\frac{\partial w_j}{\partial x_i}d\Omega + \tag{6.3.6}$$

$$-\sum_{r=1}^{R_T}\int_{\Omega_T^r} p\Big(T_{ij}^r(\mu, x)det(T^r(\mu, x))^{-1}\Big)\frac{\partial w_j}{\partial x_i}d\Omega \ \forall \mathbf{w} \in Y,$$

$$\langle F, \mathbf{w}\rangle = \langle F_s, \mathbf{w}\rangle + \langle F^0, \mathbf{w}\rangle, \tag{6.3.7}$$

where

$$\langle F_s, \mathbf{w}\rangle = \sum_{r=1}^{R_G}\int_{\Omega_G^r}\Big(\hat{\mathbf{f}}^r det(G^r(\mu))^{-1}\Big)\mathbf{w}d\Omega + \sum_{r=1}^{R_T}\int_{\Omega_T^r}\Big(\hat{\mathbf{f}}^r det(T^r(\mu, x))^{-1}\Big)\mathbf{w}d\Omega; \tag{6.3.8}$$

$$\langle F^0, \mathbf{w}\rangle = -\langle \mathcal{A}\mathbf{g}_{in}, \mathbf{w}\rangle; \ \langle G^0, q\rangle = \langle \mathcal{B}q, \mathbf{g}_{in}\rangle.$$

In Section 6.5 we introduce two different parametrizations based on different test cases and we show their explicit forms. The *transformation tensors* for bilinear forms with affine and non-affine mappings are defined, respectively, as follows:

$$\nu_{G_{ij}}^r(\mu) = G_{ii'}^r(\mu)\hat{\nu}_{i'j'}G_{jj'}^r(\mu)det(G^r(\mu))^{-1}, 1 \le i, j \le 2, r = 1, ..., R_G, \tag{6.3.9}$$

$$\nu_{T_{ij}}^r(\mu, x) = T_{ii'}^r(\mu, x)\hat{\nu}_{i'j'}T_{jj'}^r(\mu, x)det(T^r(\mu, x))^{-1}, 1 \le i, j \le 2, r = 1, ..., R_T, \tag{6.3.10}$$

The tensors for *pressure and divergence forms* are defined, respectively, for affine and non-affine mappings as:

$$\chi_{G_{ij}}^r(\mu) = G_{ij}^r det(G^r(\mu))^{-1}, \tag{6.3.11}$$

$$\chi_{T_{ij}}^r(\mu, x) = T_{ij}^r(\mu, x)det(T^r(\mu, x))^{-1}, \tag{6.3.12}$$

For the non-affine parts we apply the empirical interpolation procedure of Section 6.2 to expand non-affine mapping terms and decouple the parameters dependent contribution from the one depending only on spacial coordinates. We write:

$$\nu_{T_{ij}}^r(\mu, x) = \Sigma_{m=1}^{M_{ijr}^a}\beta_{ijm}^r(\mu)\gamma_{ijm}^r(x), \tag{6.3.13}$$

$$\chi_{T_{ij}}^r(\mu, x) = \Sigma_{m=1}^{M_{ijr}^b}\alpha_{ijm}^r(\mu)\omega_{ijm}^r(x), \tag{6.3.14}$$

where m refers to the number of interpolation functions we use for each form (related with max interpolation error), i and j are indexes related to linear/bilinear form, r refers to subdomains; β and α are weight quantities depending on the parameters μ, γ and ω are interpolation functions used as basis.
Furthermore, we may define

$$\Theta^{q(i,j,r)}(\mu) = \nu^r_{G_{ij}}(\mu),\ \mathcal{A}_G^{q(i,j,r)}(\mathbf{u},\mathbf{w}) = \int_{\Omega^r_G} \frac{\partial \mathbf{u}}{\partial x_i}\frac{\partial \mathbf{w}}{\partial x_j} d\Omega, \tag{6.3.15}$$

$$\Phi^{s(i,j,r)}(\mu) = \chi^r_{G_{ij}}(\mu),\ \mathcal{B}_G^{s(i,j,r)}(p,\mathbf{w}) = -\int_{\Omega^r_G} p\frac{\partial w_i}{\partial x_j} d\Omega, \tag{6.3.16}$$

for $1 \le r \le R_G$, $1 \le i,j \le d = 2$ (q and s are condensed indexes of i,j,r quantities) and

$$\Psi^{t(i,j,r,m)}(\mu) = \beta^r_{ijm}(\mu),\ \mathcal{A}_T^{t(i,j,r,m)}(\gamma(x),\mathbf{u},\mathbf{w}) = \int_{\Omega^r_T} \gamma^r_{ijm}(x)\frac{\partial \mathbf{u}}{\partial x_i}\frac{\partial \mathbf{w}}{\partial x_j} d\Omega, \tag{6.3.17}$$

$$\Upsilon^{p(i,j,r,m)}(\mu) = \alpha^r_{ijm}(\mu),\ \mathcal{B}_T^{p(i,j,r,m)}(\omega(x),p,\mathbf{w}) = -\int_{\Omega^r_T} \omega^r_{ijm}(x) p\frac{\partial w_i}{\partial x_j} d\Omega, \tag{6.3.18}$$

for $1 \le r \le R_T$, $1 \le i,j \le d = 2$, $1 \le m \le max(M^a_{ijr}, M^b_{ijr})$ (t and p are condensed indexes of i,j,r,m quantities). We apply an effectively affine decomposition:

$$\mathcal{A}(\mu,\mathbf{u},\mathbf{w}) = \sum_{q=1}^{Q^a_G} \Theta^q(\mu)\mathcal{A}^q_G(\mathbf{u},\mathbf{w}) + \sum_{t=1}^{Q^a_T} \Psi^t(\mu)\mathcal{A}^t_T(\gamma(x),\mathbf{u},\mathbf{w});$$

$$\mathcal{B}(\mu,p,\mathbf{w}) = \sum_{s=1}^{Q^b_G} \Phi^s(\mu)\mathcal{B}^s_G(p,\mathbf{w}) + \sum_{p=1}^{Q^b_T} \Upsilon^p(\mu)\mathcal{B}^p_T(\omega(x),p,\mathbf{w})\ ;$$

in general $\max(Q^a_G) = d \times d \times d \times R_G$, $\max(Q^b_G) = d \times d \times R_G$, $Q^a_T = \Sigma^d_{j=1}\Sigma^d_{i=1}\Sigma^{R_T}_{r=1} M^a_{ijr}$ and $Q^b_T = \Sigma^d_{j=1}\Sigma^d_{i=1}\Sigma^{R_T}_{r=1} M^b_{ijr}$. The Stokes problem rewritten on the reference domain Ω reads: find $(\mathbf{u}(\mu), p(\mu)) \in Y \times Q$ such that

$$\begin{cases} \mathcal{A}(\mu;\mathbf{u}(\mu),\mathbf{w}) + \mathcal{B}(\mu;p(\mu),\mathbf{w}) = \langle F,\mathbf{w}\rangle\ \forall\ \mathbf{w} \in\ Y, \\ \mathcal{B}(\mu;q,\mathbf{u}(\mu)) = \langle G^0, q\rangle\ \forall\ q \in\ Q. \end{cases} \tag{6.3.19}$$

We recall that this problem has an inf-sup condition (LBB) [127] to be guaranteed:

$$\beta(\mu) = \inf_{q\in Q}\sup_{\mathbf{w}\in Y} \frac{\mathcal{B}(\mu,q,\mathbf{w})}{\|\mathbf{w}\|_Y \|q\|_Q} \ge \beta_0 > 0, \forall\ \mu\ \in\ \mathcal{D};$$

here $Y = H^1_0 \times H^1_0$.
We re-introduce the supremizer operator T^μ: $Q \to Y$ so that

$$(T^\mu q, \mathbf{w})_Y = \mathcal{B}(\mu;q,\mathbf{w}),\ \forall\ \mathbf{w}\ \in\ Y$$

and

$$T^\mu q = \arg\sup_{\mathbf{w}\in Y} \frac{\mathcal{B}(\mu;q,\mathbf{w})}{\|\mathbf{w}\|_Y}.$$

Then

$$\beta^2(\mu) = \inf_{q \in Q} \frac{(T^\mu q, T^\mu q)_Y}{\|q\|_Q^2}.$$

For the proofs see the previous chapter. At this step we can solve the Stokes problem by Galerkin-Finite Element Method using Taylor-Hood $\mathbb{P}^2-\mathbb{P}^1$ elements for velocity and pressure, respectively. See Girault and Raviart [43], Gresho and Sani [46], and Gunzburger [48].

6.4 The Stokes reduced basis formulation with non-affine parameters

As seen, in the reduced basis approximation we construct a set of "$\boldsymbol{\mu}$" parameters samples $S_N^{\boldsymbol{\mu}} = \{\boldsymbol{\mu}^1, \dots, \boldsymbol{\mu}^N\}$, where $\boldsymbol{\mu}^n \in \mathcal{D}^\mu$, $n = 1, \dots, N$.
Correspondingly, we define a set of couples $(\mathbf{u}(\mu^n), p(\mu^n))$ which are approximate solutions of the Stokes problem. Then the *reduced basis pressure space* is $Q_N = \text{span}\,\{\xi_n,\ n = 1, \dots, N\}$, where $\xi_n = p(\mu^n)$, while the *reduced basis velocity space* is $Y_N = \text{span}\,\{\zeta_n,\ n = 1, \dots, N; T^{\mu^n}\xi_n,\ n = 1, \dots, N\}$, where $\zeta_n = \mathbf{u}(\mu^n)$.
The problem in reduced basis approximation reads: find $(\mathbf{u}_N(\mu), p_N(\mu)) \in Y_N \times Q_N$ s.t:

$$\begin{cases} \mathcal{A}(\mu; \mathbf{u}_N(\mu), \mathbf{w}) + \mathcal{B}(\mu; p_N(\mu), \mathbf{w}) = \langle F, \mathbf{w}\rangle \ \forall\ \mathbf{w} \in\ Y_N, \\ \mathcal{B}(\mu; q, \mathbf{u}_N(\mu) = \langle G^0, q\rangle \ \forall\ q \in\ Q_N. \end{cases} \tag{6.4.1}$$

This problem is well posed if it does admit an inf-sup property. We introduce

$$\beta_N(\mu) = \inf_{q \in Q_N} \sup_{\mathbf{w} \in Y_N} \frac{\mathcal{B}(\mu, q, \mathbf{w})}{\|\mathbf{w}\|_Y \|q\|_Q},$$

where $\beta(\mu)$ is the inf-sup constant related to Galerkin-Finite Element Method. We rewrite for computational convenience Y_N using the *effectively affine dependence* of $\mathcal{B}(\mu; q, \mathbf{w})$ on the parameter and the *linearity* of T^μ:

$$T^\mu \xi = \sum_{q=1}^{Q_G^b} \Phi^q(\mu) T_G^q \xi + \sum_{p=1}^{Q_T^b} \Upsilon^p(\mu) T_T^p \xi \tag{6.4.2}$$

for any ξ and μ, where:

$$(T_G^q \xi, \mathbf{w})_Y = \mathcal{B}_G^q(q, \mathbf{w}),\ \forall\ \mathbf{w}\ \in\ Y,$$
$$(T_T^p \xi, \mathbf{w})_Y = \mathcal{B}_T^p(\omega, q, \mathbf{w}),\ \forall\ \mathbf{w}\ \in\ Y,$$

which allows us to write:

$$Y_N = \text{span}\,\{\sum_{k=1}^{\overline{Q}_G^b} \Phi^k(\mu^n)\sigma_{kn} + \sum_{k'=1}^{Q_T^b} \Upsilon^{k'}(\mu^n)\widetilde{\sigma}_{k'n},\ n = 1, \dots, 2N\},$$

where $\overline{Q}_G^b = Q_G^b + 1, \Phi^{\overline{Q}_G^b} = 1$, $\mu^{N+j} = \mu^j, 1 \le j \le N$.
For $n = 1, \dots, N$:

$$\sigma_{kn} = 0, for\ k = 1, \dots, Q_G^b;$$

$$\widetilde{\sigma}_{k'n} = 0, for\ k' = 1, \ldots, Q_T^b;$$

$$\sigma_{\overline{Q}^b n} = \zeta_n = \mathbf{u}(\mu^n).$$

For $n = N+1, \ldots, 2N$:

$$(\sigma_{kn}, \mathbf{w})_Y = \mathcal{B}_G^k(\xi_{n-N}, \mathbf{w}), \forall \mathbf{w} \in Y, for\ k = 1, \ldots, Q_G^b; \tag{6.4.3}$$

$$\sigma_{\overline{Q}^b n} = 0;$$

$$(\widetilde{\sigma}_{kn}, \mathbf{w})_Y = \mathcal{B}_T^k(\omega, \xi_{n-N}, \mathbf{w}), \forall \mathbf{w} \in Y, for\ k = 1, \ldots, Q_T^b. \tag{6.4.4}$$

For a new "$\boldsymbol{\mu}$" we want a solution given by a combination of previously computed stored solutions as basis functions:

$$\mathbf{u}_N(\mu) = \sum_{j=1}^{2N} \mathbf{u}_{Nj}(\mu)\Big(\sum_{k=1}^{\overline{Q}_G^b} \Phi^k(\mu^j)\sigma_{kj} + \sum_{k'=1}^{Q_T^b} \Upsilon^{k'}(\mu^j)\widetilde{\sigma}_{k'j}\Big),$$

$$p_N(\mu) = \sum_{l=1}^{N} p_{Nl}(\mu)\xi_l,$$

whose weights $\mathbf{u}_{Nj}$ and p_{Nl} are given by the following reduced basis linear system:

$$\begin{cases} \sum_{j=1}^{2N} A_{ij}^{\mu}\mathbf{u}_{Nj}(\mu) + \sum_{l=1}^{N} B_{il}^{\mu} p_{Nl}(\mu) = F_i \quad 1 \le i \le 2N, \\ \sum_{j=1}^{2N} B_{jl}^{\mu}\mathbf{u}_{Nj}(\mu) = G_l \quad 1 \le l \le N; \end{cases} \tag{6.4.5}$$

where the sub-matrices A and B are built by online-offline computational decoupled procedure:

$$A_{ij}^{\mu} = \sum_{k=1}^{Q_G^a} \Theta^k(\mu)\mathcal{A}_G^k(\sum_{k'=1}^{\overline{Q}_G^b} \Phi^{k'}(\mu^i)\sigma_{k'i},\ \sum_{k''=1}^{\overline{Q}_G^b} \Phi^{k''}(\mu^j)\sigma_{k''j}) +$$

$$+ \sum_{k=1}^{Q_T^a} \Psi^k(\mu)\mathcal{A}_T^k(\gamma,\ \sum_{k'=1}^{\overline{Q}_T^b} \Upsilon^{k'}(\mu^j)\widetilde{\sigma}_{k'j},\ \sum_{k''=1}^{\overline{Q}_T^b} \Upsilon^{k''}(\mu^i)\widetilde{\sigma}_{k''i}),\ 1 \le i, j \le 2N;$$

$$B_{il}^{\mu} = \sum_{k=1}^{\overline{Q}_G^b} \Phi^k(\mu)\mathcal{B}_G^k(\sum_{k'=1}^{\overline{Q}_G^b} \Phi^{k'}(\mu^i)\sigma_{k'i}, \xi_l) +$$

$$+ \sum_{k=1}^{\overline{Q}_T^b} \Upsilon^k(\mu)\mathcal{B}_T^k(\omega,\ \sum_{k'=1}^{\overline{Q}_T^b} \Upsilon^{k'}(\mu^i)\widetilde{\sigma}_{k'i}, \xi_l),\ 1 \le i \le 2N,\ 1 \le l \le N;$$

where $\mathcal{A}_T^k, \mathcal{A}_G^k, \mathcal{B}_T^k$ and $\mathcal{B}_G^k$ are assembled offline, and:

$$F_i = \langle F, \sum_{k'=1}^{\overline{Q}_G^b} \Phi^{k'}(\mu^i)\sigma_{k'i}\rangle + \langle F, \sum_{k'=1}^{Q_T^b} \Upsilon^{k'}(\mu^i)\widetilde{\sigma}_{k'i}\rangle,\ 1 \le i \le 2N;$$

$$G_l = \langle G^0, \xi_l\rangle,\ 1 \le l \le N.$$

System (6.4.5) can therefore be written as:

$$\begin{pmatrix} \underline{A} & \underline{B} \\ \underline{B}^T & 0 \end{pmatrix} \begin{pmatrix} \underline{\mathbf{u}}_N \\ \underline{p}_N \end{pmatrix} = \begin{pmatrix} \underline{F} \\ \underline{G} \end{pmatrix}. \tag{6.4.6}$$

Remark 6.4.1 *We recall that more options dealing with the supremizer calculation and basis assembling procedures are available. At this step we have adopted, for simplicity, the second alternative option introduced in the previous chapter (and in [111]), where all the velocity reduced basis functions are μ (on-line) independent (they depend only on samples μ^j used to store basis). By using this option we cannot demonstrate the validity of the stability condition $\beta_N(\mu) \geq \beta(\mu) \geq \beta_0 > 0, \forall \mu \in \mathcal{D}^\mu$, even if results guarantee the stability of approximation. This option is competitive concerning computational costs dealing with $3N \times 3N$ reduced basis matrices (6.4.6) instead of $(\overline{Q}^b+1)N \times (\overline{Q}^b+1)N$ matrix (usually $(\overline{Q}^b+1) \gg 3$, $\overline{Q}^b = \overline{Q}^b_G + Q^b_T$), introduced as the first option to build reduced basis velocity space without the use of (6.4.2) and to apply orthonormalization, if needed. Also in this case first option is better, even if more expensive.* □

Remark 6.4.2 *We have the following computational costs to build reduced basis matrices, given also the supremizer components in the velocity space: $O(Q^a 4N^2)$ for sub-matrix $\underline{A}$, $O(\overline{Q}^b 2N^2)$ for $\underline{B}$, $O(N)$ for $\underline{F}$ and $O(9N^3)$ for the inversion of the full reduced basis matrix (6.4.6), where $Q^a = Q^a_T + Q^a_G$, $\overline{Q}^b = \overline{Q}^b_G + Q^b_T$. Note that the quantities Q^a_G and Q^b_G are depending only on the number of subdomains with affine mappings (R_G), while quantities Q^a_T and Q^b_T are depending also on the number of "shape functions" ($\gamma(x)$ and $\omega(x)$) related with interpolation error (ε_{max}) and the number of subdomains with non-affine mappings (R_T).* □

6.5 Numerical results

Numerical tests were carried out to develop Stokes reduced basis techniques with affine/non-affine mappings. Taylor-Hood finite elements have been used to store approximation basis functions: $\mathbb{P}^2-\mathbb{P}^1$ elements for velocity (with supremizer) and pressure, respectively [127]. The reduced basis solutions have been compared directly with approximate finite element solutions by computing the H^1 relative error for velocity and the L^2 relative error for pressure.

6.5.1 First test: curved upper wall

In this first test we apply empirical interpolation to describe a channel with a curved and parametrized upper wall. This simple geometry (see Figure 6.1) can be considered for example in the study of blood flow through an artery interested by a stenosis, i.e. featuring a reduced section (see Quarteroni and Formaggia [126]). A similar geometry can be used also in periodical series to set up and study an oxigenator for haemodinamic applications. In our application we have made the following assumptions:

- To solve the parametrized Stokes problem in the domain outlined in Figure 6.1 we have imposed zero Dirichlet conditions on the boundary Γ_D, Neumann non-homogeneous conditions on the inflow Γ_{Ni} ($\tau_{\hat{\mathbf{n}}} = 1, \tau_{\hat{\mathbf{t}}} = 0$, where $\tau = (\nu \frac{\partial \mathbf{u}}{\partial \hat{\mathbf{n}}} - p\hat{\mathbf{n}})$, with $\hat{\mathbf{n}}$ and $\hat{\mathbf{t}}$ normal and tangential directions, respectively) and Neumann homogeneous conditions on outflow Γ_{No} ($\tau_{\hat{\mathbf{n}}} = 0, \tau_{\hat{\mathbf{t}}} = 0$).

- We consider one parameter μ ranging in the interval $[-0.8, 0.8]$ to describe the upper arterial wall in the physical domain, through $\hat{x}_2 = f(\hat{x}_1, \mu) = 1 + \mu sin(2\pi\hat{x}_1)$ (we have a single domain subject to an unique non-affine mapping). Referring to Section 6.3 we have $\Omega_G = \emptyset$ and $\Omega_T = \Omega$, so $R_T = 1$.
  The coordinate transformation is $\mathcal{T} : \hat{\Omega} \to \Omega$ such as $\mathbf{x} = \mathcal{T}(\hat{\mathbf{x}})$ and:

$$(x_1, x_2) = \mathcal{T}(\hat{x}_1, \hat{x}_2) = (\hat{x}_1, \frac{1}{f(\hat{x}_1, \mu)}\hat{x}_2) \tag{6.5.1}$$

  in Ω. Then,

$$d\hat{x}_1 d\hat{x}_2 = f(x_1, \mu) dx_1 dx_2$$

  and the following relations hold:

$$\begin{cases} \frac{\partial \hat{\mathbf{u}}}{\partial \hat{x}_2} = \frac{1}{f(x_1,\mu)} \frac{\partial \mathbf{u}}{\partial x_2}, \\ \frac{\partial \hat{\mathbf{u}}}{\partial \hat{x}_1} = \frac{\partial \phi}{\partial x_1} - x_2 \frac{f_{x_1}(x_1,\mu)}{f(x_1,\mu)} \frac{\partial \mathbf{u}}{\partial x_2} \quad (with\ f_{x_1} := \frac{df}{dx_1}), \end{cases} \tag{6.5.2}$$

$$\nabla \cdot \hat{\mathbf{u}} = \frac{\partial u_1}{\partial x_1} - x_2 \frac{f_{x_1}(x_1, \mu)}{f(x_1, \mu)} \frac{\partial u_1}{\partial x_2} + \frac{1}{f(x_1, \mu)} \frac{\partial u_2}{\partial x_2}, \tag{6.5.3}$$

  Using the compact notation of Section 6.3 (6.3.10 and 6.3.12) and transformation (6.5.1) we get the following tensor for diffusion and divergence forms, respectively:

$$\nu_T = \nu \begin{bmatrix} f(x_1, \mu) & -f'_{x_1}(x_1, \mu) x_2 \\ -f'_{x_1}(x_1, \mu) x_2 & \frac{1}{f(x_1,\mu)} + \frac{f'^2_{x_1}(x_1,\mu)}{f(x_1,\mu)} {x_2}^2 \end{bmatrix}; \tag{6.5.4}$$

$$\chi_T = \begin{bmatrix} f(x_1, \mu) & -f'_{x_1}(x_1, \mu) x_2 \\ 0 & 1 \end{bmatrix}; \tag{6.5.5}$$

  where $\nu = 0.04 N s m^{-2}$ is the viscosity. Referring to notation of Section 6.2 we get 5 different coefficients functions $g_M^j(x, \mu)$ to expand.

- We apply empirical interpolation (6.3.13 and 6.3.14) to the tensors (6.5.4 and 6.5.5) and we impose a maximum interpolation error ε_{max}, thus considering different M_{max} "shape functions" for each $g_M^j(x, \mu)$. Each $g_M^j(x, \mu)$ refers to a different coefficient of a bilinear form of our Stokes problem ($j = 5$ in this test case). Owing to empirical interpolation we expand each tensor component to apply the effectively affine decomposition:

$$\nu_T = \nu \begin{bmatrix} \Sigma_{m=1}^{M_{11}^a} \beta_{11m}(\mu) \gamma_{11m}(x) & \Sigma_{m=1}^{M_{12}^a} \beta_{12m}(\mu) \gamma_{12m}(x) \\ \Sigma_{m=1}^{M_{21}^a} \beta_{21m}(\mu) \gamma_{21m}(x) & \Sigma_{m=1}^{M_{22}^a} \beta_{22m}(\mu) \gamma_{22m}(x) \end{bmatrix}.$$

Note that this tensor is symmetric. Moreover,

$$\chi_T = \begin{bmatrix} \Sigma_{m=1}^{M_{11}^b} \alpha_{11m}(\mu)\omega_{11m}(x) & \Sigma_{m=1}^{M_{12}^b} \alpha_{12m}(\mu)\omega_{12m}(x) \\ 0 & 1 \end{bmatrix}.$$

The index r referring to every different subdomain is omitted.

- At this step, having defined all the abstract formulation of the previous sections, we have applied the reduced basis method and assembled the approximation spaces as described in Section 6.4.

- Tables 6.1 and 6.2 (and Figures 6.3 and 6.4) show numerical results (mean H^1 relative errors on velocity, testing a large number of configurations) at different N and different max interpolation error ε_{max}. At the end of the test we have carried out a comparison between magic points interpolation (using $g_M^j(x,\mu)$) and true functions ($g^j(x,\mu)$). We can see that for $\varepsilon_{max} \leq 10^{-4}$ we have a good convergence and results are not dominated or influenced by interpolation error. When the interpolation error is dominating the reduced basis error is characterized by a constant "plateau" and is not diminished by increasing N (see for example the case in which $\varepsilon_{max} \geq 10^{-2}$).

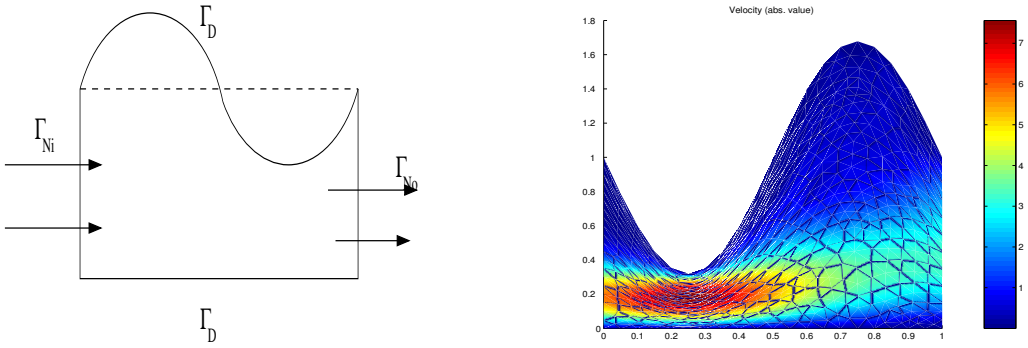

Figure 6.1: Geometrical scheme for the stenosis test problem (left) and velocity absolute value $[ms^{-1}]$ for $\mu = 0.5$ (right).

In Figure 6.5 we represent a possible configuration of interest for biomedical applications, for example an oxygenator. It is possible to understand how the geometry can be described using a periodic criterium by assembling a more complex configuration starting from a simple subdomain. The framework should be completed addressing our attention to periodic boundary conditions. This configuration has been studied also by Wei *et al.* in [163] considering a wavy-walled channel with a poroelastic layer to investigate physiological flows in capillaries and venules.

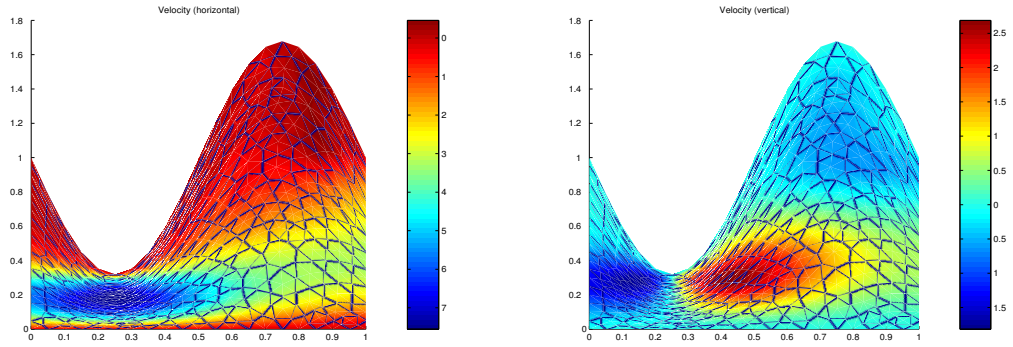

Figure 6.2: Horizontal and vertical velocity $[ms^{-1}]$ for $\mu = 0.5$.

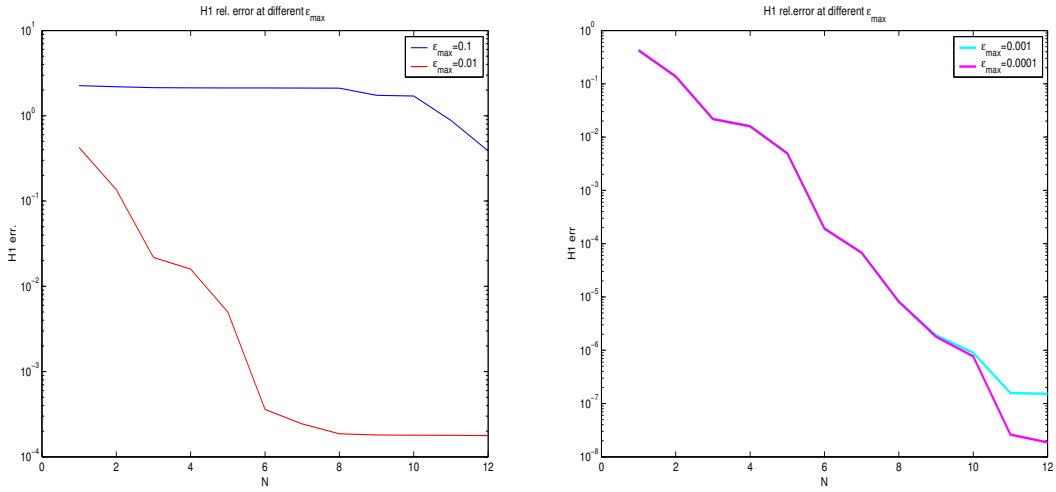

Figure 6.3: H^1 relative mean error on velocity for different ε_{max}, imposed on all $g_M^j(x,\mu)$, considering different μ test values.

N	$\varepsilon_{max} = 0.1$	$\varepsilon_{max} = 0.01$	$\varepsilon_{max} = 10^{-3}$	$\varepsilon_{max} = 10^{-4}$
1	$2.2549e+000$	$4.2557e-001$	$4.2656e-001$	$4.2653e-001$
2	$2.1926e+000$	$1.3614e-001$	$1.3708e-001$	$1.3709e-001$
3	$2.1361e+000$	$2.1768e-002$	$2.1880e-002$	$2.1886e-002$
4	$2.1267e+000$	$1.5939e-002$	$1.5963e-002$	$1.5964e-002$
5	$2.1226e+000$	$4.9955e-003$	$4.9358e-003$	$4.9388e-003$
6	$2.1172e+000$	$3.5905e-004$	$1.9177e-004$	$1.9183e-004$
7	$2.1131e+000$	$2.4352e-004$	$6.7685e-005$	$6.7584e-005$
8	$2.1080e+000$	$1.8644e-004$	$8.2645e-006$	$8.1374e-006$
9	$1.7357e+000$	$1.8016e-004$	$1.9044e-006$	$1.7880e-006$
10	$1.7043e+000$	$1.7929e-004$	$9.0032e-007$	$7.7022e-007$
11	$8.8174e-001$	$1.7868e-004$	$1.5746e-007$	$2.6138e-008$
12	$3.8732e-001$	$1.7743e-004$	$1.5181e-007$	$1.8676e-008$

Table 6.1: Mean H^1 velocity relative errors for different ε_{max}.

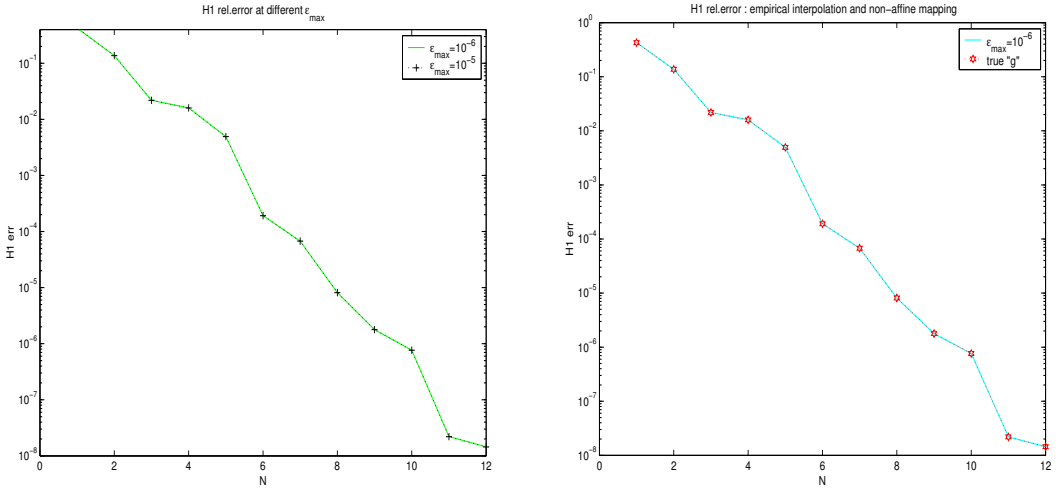

Figure 6.4: H^1 mean relative error on velocity for different ε_{max}, imposed on all $g_M^j(x,\mu)$ (left) and comparison with the use of "true" $g^j(x,\mu)$ functions, without empirical interpolation (right).

N	$\varepsilon_{max} = 10^{-5}$	$\varepsilon_{max} = 10^{-6}$	$exact\ g^j$
1	$4.2654e-001$	$4.2654e-001$	$4.2654e-001$
2	$1.3709e-001$	$1.3709e-001$	$1.3709e-001$
3	$2.1885e-002$	$2.1884e-002$	$2.1884e-002$
4	$1.5963e-002$	$1.5963e-002$	$1.5963e-002$
5	$4.9380e-003$	$4.9380e-003$	$4.9380e-003$
6	$1.9180e-004$	$1.9181e-004$	$1.9181e-004$
7	$6.7581e-005$	$6.7582e-005$	$6.7582e-005$
8	$8.1348e-006$	$8.1356e-006$	$8.1356e-006$
9	$1.7812e-006$	$1.7813e-006$	$1.7813e-006$
10	$7.6544e-007$	$7.6542e-007$	$7.6542e-007$
11	$2.2070e-008$	$2.1981e-008$	$2.1980e-008$
12	$1.4503e-008$	$1.4421e-008$	$1.4421e-008$

Table 6.2: Mean H^1 velocity relative errors for different ε_{max} and comparison with "true" g^j.

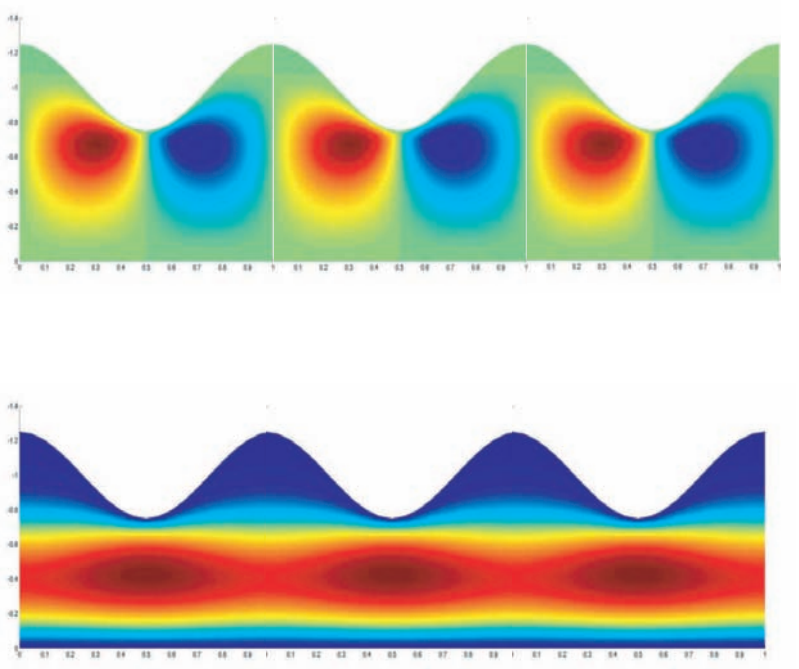

Figure 6.5: Periodic channel: vertical velocity (top) and horizontal velocity (bottom) $[ms^{-1}]$, same colorbars of Figure 6.1.

6.5.2 Second test: bypass with curved incoming branch

We introduce a vector of parameters $\boldsymbol{\mu} = \{t, D, L, S, H, \theta, \upsilon\} \in \mathcal{D}^{\mu} \subset \mathbb{R}^P$, $\mathcal{D}^{\mu}$ is given by: $[t_{min}, t_{max}] \times [D_{min}, D_{max}] \times [L_{min}, L_{max}] \times [S_{min}, S_{max}] \times [H_{min}, H_{max}] \times [\theta_{min}, \theta_{max}] \times [\upsilon_{min}, \upsilon_{max}]$. For a schematic view of the problem see Figure 6.6. The new element introduced in the study of the complete configuration is the curvature of the artery and of the bypass wall to deal with a more realistic configuration. In this problem we have affine and non-affine parameters dependence in different subdomains. The aim of the test is to combine the study of affine and the non-affine terms in the same problem by varying different geometrical parameters and then to test reduced basis convergence. Referring to notation in Section 6.3 we have $R_G = 3$ (number of subdomains with affine dependence, i.e. $\Omega^2, \Omega^3, \Omega^4$), $R_T = 1$ (number of subdomains with non-affine dependence, i.e Ω^1). For more info on this applications dealing only with affine parameters dependence we suggest to see [137]. The coordinate transformation in Ω^1 with non-affine parameter dependence is given by:

$$\begin{cases} x_1 = \frac{1}{H}\hat{x}_1 \\ x_2 = \frac{1}{t}(\hat{x}_2 - (\upsilon H^2 x_1(x_1 - 1) + H x_1 \tan(\theta))) \end{cases} \tag{6.5.6}$$

The role of parameters t and H is to stretch subdomain Ω^1 (as L, S, D stretch the remaining subdomains), the parameter υ introduces a curvature in the walls of the incoming branch of the bypass and θ is responsible for a rigid rotation varying the graft angle. The tensors for *viscous terms* are given by:

$$\nu_T^1 = \nu \begin{bmatrix} \frac{t}{H} & -(\tan\theta + 2\upsilon H x_1 - \upsilon H) \\ -(\tan\theta + 2\upsilon H x_1 - \upsilon H) & \frac{(1+(\tan\theta+2\upsilon H x_1-\upsilon H)^2)}{t} H \end{bmatrix}; \tag{6.5.7}$$

$$\nu_G^2 = \nu \begin{bmatrix} \frac{S}{D} & 0 \\ 0 & \frac{D}{S} \end{bmatrix}; \nu_G^3 = \nu \begin{bmatrix} \frac{t}{D} & 0 \\ 0 & \frac{D}{t} \end{bmatrix}; \ \nu_G^4 = \nu \begin{bmatrix} \frac{L}{D} & 0 \\ 0 & \frac{D}{L} \end{bmatrix}. \tag{6.5.8}$$

The tensors for *pressure and divergence forms* are given by:

$$\chi_T^1 = \begin{bmatrix} t & -H(\tan\theta + 2\upsilon H x_1 - \upsilon H) \\ 0 & H \end{bmatrix}; \ \chi_G^2 = \begin{bmatrix} S & 0 \\ 0 & D \end{bmatrix}; \tag{6.5.9}$$

$$\chi_G^3 = \begin{bmatrix} t & 0 \\ 0 & D \end{bmatrix}; \ \chi_G^4 = \begin{bmatrix} L & 0 \\ 0 & D \end{bmatrix}. \tag{6.5.10}$$

We have applied empirical interpolation expansion to the components of tensor ν_T^1 and χ_T^1 and built reduced basis approximation.

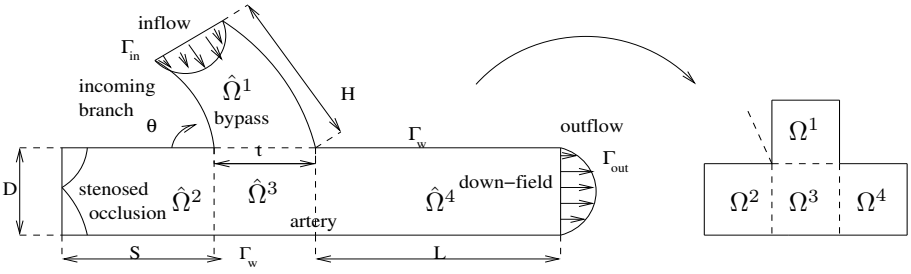

Figure 6.6: Geometrical scheme for the bypass test problem (physical domain and reference one).

We have carried out four different tests, based on the same geometry but with different parameters:

(a) we consider only υ parameter to create a curvature in the wall, we deal only with non-affine mapping in one subdomain where we apply empirical interpolation;

(b) then, we consider υ and also parameters L and S, each of them is operating into different subdomains and we combine affine and non-affine transformations;

(c) in the third test we consider parameters υ, L, S and t so that we have more parameters in the same subdomain subject to non-affine parametric dependence;

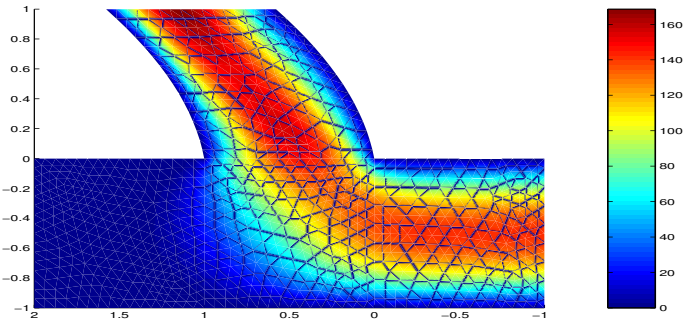

Figure 6.7: Haemodinamic flow: absolute value of velocity $[ms^{-1} \cdot 10^{-2}]$ in bypass subject to curved wall and graft angle ($\upsilon = 0.41$ and $\theta = \pi/3$).

(d) in the last term we introduce also graft angle θ so that we have rigid rotation, stretching (due to t or/and H) and curvature (due to υ) in the same subdomain. Figure 6.7 shows an example of haemodinamic flow in our curved geometry.

In Tables 6.3-6.6 we report numerical results (H^1 errors on velocity and L^2 errors for pressure) considering about 50 configurations at different N for different test cases (a)-(d). The maximum interpolation error considered has been $\varepsilon_{max} = 10^{-5}$ not to have interpolation error dominating our approximation and to avoid a constant "plateau" in error plots. In Figure 6.8 we report errors in log-log scale dealing with (d) test case. Figure 6.9 shows the offline set of parameters used to store the basis functions by the adaptive optimized assembling procedure we used, introduced in Veroy *et al.* [161] and Prud'homme [121].

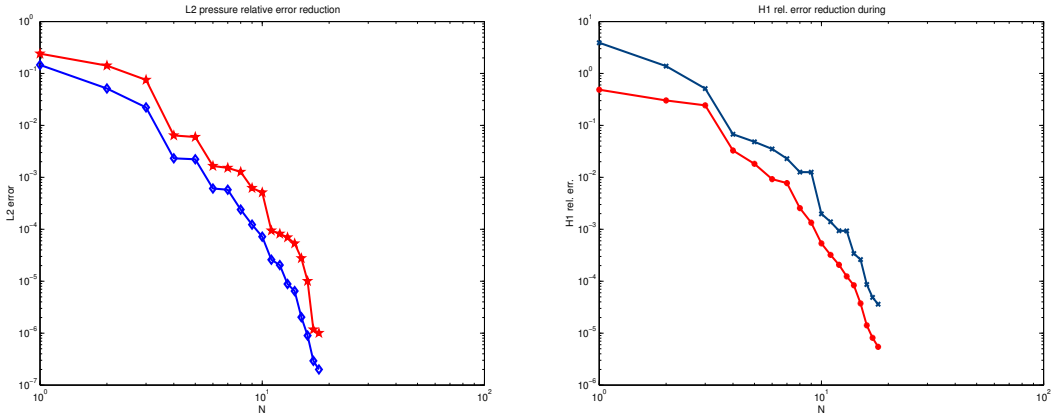

Figure 6.8: L^2 and H^1 relative errors for pressure and velocity, respectively (max and mean).

N	H^1 mean (a)	H^1 max (a)	H^1 mean (b)	H^1 max (b)
1	0.048058118	0.136051645	0.066384779	0.10111214
2	0.001552862	0.002320168	0.039400421	0.098294259
3	$7.1431E-06$	$1.03781E-05$	0.003468971	0.004683999
4	$1.62586E-07$	$8.24285E-07$	0.003163783	0.003657563
5	$6.101E-10$	$1.41057E-09$	0.000858429	0.00231849
6	$7.01E-12$	$3.212E-11$	0.000129567	0.000272338
7	–	–	$5.5189E-05$	$4.23899E-05$
8	–	–	$3.18091E-05$	$3.83384E-05$
9	–	–	$1.23528E-05$	$2.2659E-05$
10	–	–	$7.29802E-06$	$9.86723E-06$
11	–	–	$1.51548E-06$	$2.30932E-06$
12	–	–	$2.34584E-07$	$5.31751E-07$
13	–	–	$1.2129E-07$	$2.40584E-07$
14	–	–	$7.51433E-08$	$1.18963E-07$
15	–	–	$3.23837E-08$	$9.11491E-08$

Table 6.3: H^1 velocity relative errors for different number of varying parameters and $\varepsilon_{max} = 10^{-5}$: (a) only υ (non-affine) parameter varying, (b) υ, L, S (affine and non-affine) parameters (in different subdomains) varying.

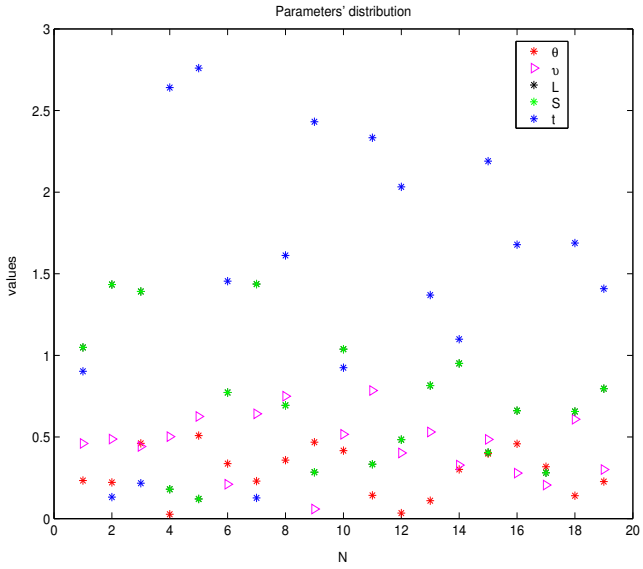

Figure 6.9: Parameters distribution during off-line optimized basis assembling procedures.

N	H^1 mean (c)	H^1 max (c)	H^1 mean (d)	H^1 max (d)
1	0.563465887	1.106596438	0.487915824	3.904000929
2	0.155181008	0.426078474	0.302592595	1.385050105
3	0.023388203	0.06289385	0.243772546	0.511847739
4	0.006968648	0.013543197	0.032855726	0.067523767
5	0.00241075	0.00754956	0.018203568	0.048221219
6	0.00074055	0.001924017	0.009246898	0.035139624
7	0.000442849	0.001727769	0.007747967	0.022901482
8	0.000224509	0.000784976	0.002552479	0.012609594
9	$6.57733E-05$	0.000360971	0.001338957	0.012582395
10	$1.22527E-05$	$8.0297E-05$	0.000534446	0.001979371
11	$3.46346E-06$	$2.09716E-05$	0.000321415	0.001391688
12	$1.011E-06$	$7.81558E-06$	0.000207283	0.000936665
13	$1.91343E-07$	$1.04166E-06$	0.000123885	0.000930468
14	$2.38061E-08$	$2.38061E-07$	$8.34764E-05$	0.000340849
15	–	–	$3.74193E-05$	0.000260742
16	–	–	$1.41356E-05$	$8.64251E-05$
17	–	–	$8.12437E-06$	$4.87599E-05$
18	–	–	$5.44325E-06$	$3.614E-05$

Table 6.4: H^1 velocity relative errors for different number of varying parameters and $\varepsilon_{max} = 10^{-5}$: (c) υ, L, S, t parameters varying, (d) $\upsilon, t, L, S, \theta$ parameters varying.

N	L^2 mean (a)	L^2 max (a)	L^2 mean (b)	L^2 max (b)
1	0.00131102	0.00330782	0.049765761	0.076442818
2	$4.84371E-05$	$7.21384E-05$	0.001443908	0.002404592
3	$2.00619E-07$	$3.03232E-07$	0.000218353	0.000223485
4	$2.06747E-09$	$1.09034E-08$	0.000117247	0.000154309
5	$8.91E-12$	$2.108E-11$	$2.26938E-05$	$5.85041E-05$
6	$1.1E-13$	$5.3E-13$	$2.98422E-06$	$7.29587E-06$
7	–	–	$9.68781E-07$	$2.04184E-06$
8	–	–	$4.43647E-07$	$5.17774E-07$
9	–	–	$1.55099E-07$	$2.51658E-07$
10	–	–	$7.90834E-08$	$1.29403E-07$
11	–	–	$1.86052E-08$	$2.98586E-08$
13	–	–	$2.30951E-09$	$6.43834E-09$
14	–	–	$1.5816E-09$	$2.43859E-09$
15	–	–	$6.0645E-10$	$1.32561E-09$

Table 6.5: L^2 pressure relative errors for different number of varying parameters and $\varepsilon_{max} = 10^{-5}$: (a) only υ (non-affine) parameter varying, (b) υ, L, S (affine and non-affine) parameters (in different subdomains) varying.

N	L^2 mean (c)	L^2 max (c)	L^2 mean (d)	L^2 max (d)
1	0.395384579	0.710666218	0.145944345	0.240938029
2	0.006901236	0.013288413	0.051283742	0.141755515
3	0.004135993	0.00882405	0.022163703	0.075274908
4	0.000917813	0.00212774	0.00232357	0.006473042
5	0.000217614	0.000709398	0.002227062	0.004974737
6	0.000102036	0.000478661	0.000609347	0.001651962
7	$4.40703E-05$	0.000189533	0.000577145	0.001413289
8	$2.55188E-05$	0.000105753	0.000239322	0.001273091
9	$4.03863E-06$	$2.22016E-05$	0.000122951	0.000623509
10	$5.14632E-07$	$3.87984E-06$	$7.2085E-05$	0.000511114
11	$3.35225E-07$	$2.72714E-06$	$2.59278E-05$	$9.45921E-05$
12	$3.06439E-07$	$2.68244E-06$	$2.04926E-05$	$8.20901E-05$
13	$2.11621E-08$	$1.12451E-07$	$8.85109E-06$	$6.95492E-05$
14	$3.04801E-09$	$3.04801E-08$	$6.46217E-06$	$5.3356E-05$
15	–	–	$2.0293E-06$	$2.76806E-05$
16	–	–	$8.98324E-07$	$1.00727E-05$
17	–	–	$2.92535E-07$	$1.1717E-06$
18	–	–	$1.99739E-07$	$1.0067E-06$

Table 6.6: L^2 pressure relative errors for different number of varying parameters and $\varepsilon_{max} = 10^{-5}$: (c) υ, L, S, t parameters varying, (d) $\upsilon, t, L, S, \theta$ parameters varying.

6.6 Conclusions

In this chapter we have shown how to expand and apply efficient, accurate and real-time reduced basis techniques to bio-mechanics problems using more realistic geometries such as in biomedical devices optimization problem and extended previous studies on bypass configuration (with curved walls). Interesting applications of the method presented in this chapter are shape optimization problems in which we may treat both affine and non-affine parametric dependence (see for example Cholaseuk [23], and Lim and Choi [81]): usually the affine parametric dependence could describe complete (macro and coarse) geometrical configuration, while the non-affine parametric dependence could describe local configuration. At this stage we may combine reduced basis techniques with shape design and optimal control related problem such as the ones considered in Chapter 3 and in [4], where shape optimization in reference domain and non-affine mapping have already been considered.
Results have shown that it is possible to consider more complex geometries in optimization problems using reduced basis techniques and introducing empirical, stable and inexpensive interpolation for non-affine mapping terms preserving reduced basis methods properties, first of all rapid and accurate convergence and computational online-offline decomposition. In the next chapter our attention will be devoted to the use of reduced basis for Navier-Stokes equations in parametrized domain. The following chapter is going to conclude the framework on the use of reduced basis for a (pre-process) macro-geometrical optimization on bypass and at the same time it allows us to extend methodology.

Chapter 7

Reduced Basis for Navier-Stokes Equations

In this chapter we introduce an extension of reduced basis methods for non-linear equations in parametrized domains. We deal with Navier-Stokes equations. The main difference with respect to the work described in the previous chapters, dealing with Stokes problem, is the introduction of a non-linear transport term and the extension of reduced basis machinery to this term, including the possibility to consider also non-affine parametric dependence by an empirical interpolation method. The extension to Navier Stokes equations allows us to have a feedback on the results from pre-process optimization based on complete configuration and on the results of local shape optimization carried out by optimal control techniques using low order (and low fidelity) methods on the proposed application.

7.1 Introduction

Until now, the use of reduced basis in this thesis and its related application was aimed at providing real time information on solutions and fluid mechanics related outputs, computed in parametrized domains by using low fidelity (simplified) model, such as the Stokes equations, used to approximate low Reynolds blood flows and provide an optimized configuration. In this chapter, with the extension of the reduced basis framework to the non-linear steady Navier-Stokes problem, we are going to complete our pre-process optimization toolbox, providing also some comparison to validate our results achieved using low order (and low cost) methods. But we are also going to provide a different perspective: reduced basis methods provide real time solutions for the design and the optimization of systems and can be used not only as a pre-process but as a complete optimization tool in itself. This extension has been possible thanks to the introduction of treatment for non-linearities and non-affine mappings. Another aspect will be considered in the next chapter which provides some perspectives on the use of reduced basis to solve optimal control (and parametrized) problems.
The present chapter is organized as follows: after this introduction, in Section 7.2 we report an excursus of references and aspects dealing with reduced basis for Navier-Stokes, then

Section 7.3 deals with the formulation of the steady Navier-Stokes problem and its related aspects. From Section 7.4 to Section 7.6 we build the reduced basis formulation for Navier-Stokes equations in parametrized domains with (i) affine, (ii) non-affine and (iii) affine/non-affine combined parametric dependence. In these sections aspects dealing with algebraic and approximation stability are recalled and extended. In Sections 7.7, 7.8 and 7.9 numerical results and computational costs and savings are reported. Some conclusions follow.

7.2 The state of the art

The application of reduced basis methods to non-linear problems in fluid mechanics is becoming a problem with growing interest. Previous works were carried out in the 1990*s* by Peterson [113] and by Ito and Ravindran in [64]. The former work was focused on stream function and vorticity formulation for various Reynolds number and using Taylor and Lagrangian type basis. In the latter the authors built a reduced basis approximation for a Navier-Stokes problem (both steady and unsteady) in a cavity using different techniques to build reduced basis approximation spaces (Hermite and/or Taylor spaces, incorporating the derivatives of velocity with respect to the parameter, the Reynolds number). The reduced basis formulation does not consider the pressure in the reduced-order model. Then Patera and Veroy since 2003 carried out intensive research on reduced basis in non-linear fluid mechanics using Lagrangian basis (i.e. global approximation functions) studying natural convection problem, parametrized by physical quantities (e.g. Grashof number [104], viscosity [160]) considering free-divergence spaces. In 2004 they developed rigorous a posteriori error estimation and bounds for real time computation based on the *Brezzi-Rappaz-Raviart* theory, see [159]. A review is provided also in the recent work [45]. In our work we have followed the guidelines provided by Patera *et al.* in their recent works and focused our attention on the following aspects: i) the efficient treatment of non-linear term; ii) the domain parametrization; iii) the incorporation of a stable approximation for pressure (useful in haemodynamic applications); iv) the use of non-affine transformation maps by an empirical interpolation method to consider more complex geometries, such as curved walls. Related aspects deals with the use of different options to build the reduced basis velocity spaces and the efficient offline selection of basis function.
More recently, researchers dealing with flow optimization and using sensitivity analysis have addressed their attention to the reduced basis method, see for example the recent works of Burkardt [21] and Gunzburger [50].

7.3 Steady Navier-Stokes equations

We consider the steady Navier-Stokes equations in a domain Ω with proper boundary conditions on $\Gamma = \Gamma_{in} \cup \Gamma_{out} \cup \Gamma_w$:

$$\begin{cases} -\nu\Delta\mathbf{u} + (\mathbf{u}\cdot\nabla)\mathbf{u} + \nabla p = \mathbf{f} \ in\ \Omega, \\ \nabla\cdot\mathbf{u} = 0 \ in\ \Omega, \\ \mathbf{u} = \mathbf{0} \ on\ \Gamma_w;\ \mathbf{u} = \mathbf{g}_{in} \ on\ \Gamma_{in}, \left(\nu\frac{\partial\mathbf{u}}{\partial\hat{\mathbf{n}}} - p\hat{\mathbf{n}}\right) = \mathbf{0} \ on\ \Gamma_{out}. \end{cases} \tag{7.3.1}$$

For the mathematical theory of the Navier-Stokes equations see e.g. Galdi [41] and for aspects dealing with their numerical solution see Temam [150], Girault and Raviart [43], Brezzi and Fortin [19].
Before proceeding we introduce the weak formulation of problem (7.3.1) which reads: find $\mathbf{u} \in Y = H^1_{\Gamma_D}(\Omega) \times H^1_{\Gamma_D}(\Omega),\ p \in Q = L^2(\Omega),\ \Omega \subset \mathbb{R}^2$:

$$\begin{cases} \nu\displaystyle\int_\Omega \nabla\mathbf{u}\cdot\nabla\mathbf{w}d\Omega - \int_\Omega p\,\nabla\cdot\mathbf{w}d\Omega + \int_\Omega (\mathbf{u}\cdot\nabla)\mathbf{u}\cdot\mathbf{w}d\Omega = \int_\Omega \mathbf{f}\cdot\mathbf{w}d\Omega + \langle F^0, \mathbf{w}\rangle \ \forall\mathbf{w}\in Y, \\ \displaystyle\int_\Omega q\,\nabla\cdot\mathbf{u}d\Omega = \langle G^0, q\rangle \ \ \forall q \in Q, \end{cases} \tag{7.3.2}$$

F^0, G^0 are terms due to non-homogeneous Dirichlet boundary condition ($\mathbf{u} = \mathbf{g}_{in}$) on Γ_{in}, $\Gamma_D = \Gamma_{in} \cup \Gamma_w$, on Γ_{out} we impose a free stress Neumann condition. Then we discretize problem (7.3.2) by a stable approximation using finite element method (Taylor-Hood $\mathbb{P}^2 - \mathbb{P}^1$ elements for velocity and pressure, respectively) on a fine mesh triangulation; see, for example, Quarteroni and Valli [127]. The numerical methods used to solve the system of non-linear equations (7.3.2) is the iterative Newton method and it involves the linerization of the advection term $(\mathbf{u}_h\cdot\nabla)\mathbf{u}_h$ considering its derivative in the *Frechet* sense. The linearized version of the discretized problem (7.3.2) at each iteration reads: given $\mathbf{u}_h^{(k)}$, find $\mathbf{u}_h^{(k+1)} \in Y_h,\ p_h^{(k+1)} \in Q_h,\ \Omega \subset \mathbb{R}^2$, such that

$$\begin{cases} \nu\displaystyle\int_\Omega \nabla\mathbf{u}_h^{(k+1)}\cdot\nabla\mathbf{w}_h d\Omega - \int_\Omega p_h^{(k+1)}\,\nabla\cdot\mathbf{w}_h d\Omega + \int_\Omega (\mathbf{u}_h^{(k)}\cdot\nabla)\mathbf{u}_h^{(k+1)}\cdot\mathbf{w}_h\ d\Omega + \\ + \displaystyle\int_\Omega (\mathbf{u}_h^{(k+1)}\cdot\nabla)\mathbf{u}_h^{(k)}\cdot\mathbf{w}_h\ d\Omega - \int_\Omega (\mathbf{u}_h^{(k)}\cdot\nabla)\mathbf{u}_h^{(k)}\cdot\mathbf{w}_h\ d\Omega = \int_\Omega \mathbf{f}\cdot\mathbf{w}_h d\Omega + \langle F^0, \mathbf{w}_h\rangle \ \forall\mathbf{w}_h\in Y_h, \\ \displaystyle\int_\Omega q_h\,\nabla\cdot\mathbf{u}_h^{(k+1)} d\Omega = \langle G^0, q_h\rangle \ \ \forall q_h \in Q_h, \end{cases} \tag{7.3.3}$$

till the convergence is reached. We can adopt a condition based on the difference between two estimates

$$\|\mathbf{u}_h^{(k+1)} - \mathbf{u}_h^{(k)}\| \le \epsilon$$

where ϵ is a small tolerance. We recall that the convergence for Newton method is quadratic [129]. To solve the linearized Navier-Stokes system (7.3.3) at each Newton step we can use the so-called *Pressure Matrix Method* to decouple the calculation of pressure from the velocity field. In this case we solve our problem in three steps: in the first one we get an auxiliary

velocity $\tilde{\mathbf{u}}_h$, in the second step we can calculate the pressure p_h and then the corrected velocity $\mathbf{u}_h$. See for example Quarteroni and Valli [127].

7.4 Parametrized formulation: affine parametric dependence

We suppose that the domain we are considering is composed of R subdomains: $\hat{\Omega} = \bigcup_{r=1}^{R} \hat{\Omega}^r$, so that we rewrite (7.3.3) as follows, introducing the "hat" notation to indicate equations in real domain without parametrization and dropping the subscript h for simplicity of notation:

$$\begin{cases} \hat{\mathcal{A}}(\hat{\mathbf{u}}^{(k+1)}, \hat{\mathbf{w}}) + \hat{\mathcal{B}}(\hat{p}^{(k+1)}, \hat{\mathbf{w}}) + \hat{\mathcal{C}}(\hat{\mathbf{u}}^{(k+1)}, \hat{\mathbf{u}}^{(k)}, \hat{\mathbf{w}}) + \hat{\mathcal{C}}(\hat{\mathbf{u}}^{(k)}, \hat{\mathbf{u}}^{(k+1)}, \hat{\mathbf{w}}) = \\ = \langle \hat{F}, \hat{\mathbf{w}} \rangle + \hat{\mathcal{C}}(\hat{\mathbf{u}}^{(k)}, \hat{\mathbf{u}}^{(k)}, \hat{\mathbf{w}}) \quad \forall \hat{\mathbf{w}} \in Y, \\ -\hat{\mathcal{B}}(\hat{q}, \hat{\mathbf{u}}^{(k+1)}) = \langle \hat{G}^0, \hat{q} \rangle \quad \forall \hat{q} \in Q, \end{cases} \tag{7.4.1}$$

where for $1 \leq i, j \leq d = 2$ and $\hat{\nu}_{i,j} = \nu \delta_{i,j}$:

$$\hat{\mathcal{A}}(\hat{\mathbf{u}}, \hat{\mathbf{w}}) = \sum_{r=1}^{R} \int_{\hat{\Omega}^r} \frac{\partial \hat{\mathbf{u}}}{\partial \hat{x}_i} \hat{\nu}_{ij} \frac{\partial \hat{\mathbf{w}}}{\partial \hat{x}_j} d\hat{\Omega}, \tag{7.4.2}$$

$$\hat{\mathcal{B}}(\hat{p}, \hat{\mathbf{w}}) = -\sum_{r=1}^{R} \int_{\hat{\Omega}^r} \hat{p} \nabla \cdot \hat{\mathbf{w}} d\hat{\Omega}, \tag{7.4.3}$$

$$\hat{\mathcal{C}}(\hat{\mathbf{u}}, \hat{\mathbf{v}}, \hat{\mathbf{w}}) = \sum_{r=1}^{R} \int_{\hat{\Omega}^r} (\hat{\mathbf{u}} \cdot \nabla) \hat{\mathbf{v}} \cdot \hat{\mathbf{w}} d\hat{\Omega}, \tag{7.4.4}$$

$$\langle \hat{F}, \hat{\mathbf{w}} \rangle = \langle \hat{F}_s, \hat{\mathbf{w}} \rangle + \langle \hat{F}^0, \hat{\mathbf{w}} \rangle, \tag{7.4.5}$$

and

$$\langle \hat{F}_s, \hat{\mathbf{w}} \rangle = \sum_{r=1}^{R} \int_{\hat{\Omega}^r} \hat{\mathbf{f}} \hat{\mathbf{w}} d\hat{\Omega}, \langle \hat{F}^0, \hat{\mathbf{w}} \rangle = -\langle \hat{\mathcal{A}} \hat{g}_{in}, \hat{\mathbf{w}} \rangle, \ \langle \hat{G}^0, \hat{q} \rangle = \langle \hat{\mathcal{B}} \hat{q}, \hat{g}_{in} \rangle. \tag{7.4.6}$$

Now we want to build a system of P^2DEs (Parametrized Partial Differential Equations) affinely depending on a set of geometrical parameters (μ). As already seen, problem (7.4.1) is traced back to a *reference domain* by an *affine mapping* on some subdomains $\hat{\Omega}_G^r$ into Ω^r. For any $\hat{x} \in \hat{\Omega}^r$, $r = 1, \ldots, R$, its image $x \in \Omega^r$ is given by

$$x = \mathcal{G}^r(\mu; \hat{x}) = G^r(\mu)\hat{x} + g^r, \quad 1 \leq r \leq R; \tag{7.4.7}$$

we thus write on Ω_r

$$\frac{\partial}{\partial \hat{x}_i} = \frac{\partial x_j}{\partial \hat{x}_i} \frac{\partial}{\partial x_j} = G^r_{ji}(\mu) \frac{\partial}{\partial x_j}. \tag{7.4.8}$$

We write the P^2DEs system depending on μ on a reference domain $\Omega \subset \mathbb{R}^2$. The problem reads: given $\mathbf{u}^{(k)}$, find $\mathbf{u}^{(k+1)} \in Y = H^1_{\Gamma_D}(\Omega) \times H^1_{\Gamma_D}(\Omega)$, $p^{(k+1)} \in Q = L^2(\Omega)$:

$$\begin{cases} \mathcal{A}(\mu; \mathbf{u}^{(k+1)}, \mathbf{w}) + \mathcal{B}(\mu; p^{(k+1)}, \mathbf{w}) + \mathcal{C}(\mu; \mathbf{u}^{(k+1)}, \mathbf{u}^{(k)}, \mathbf{w}) + \mathcal{C}(\mu; \mathbf{u}^{(k)}, \mathbf{u}^{(k+1)}, \mathbf{w}) = \\ \langle F_s + F^0, \mathbf{w} \rangle + \mathcal{C}(\mu; \mathbf{u}^{(k)}, \mathbf{u}^{(k)}, \mathbf{w}) \ \forall \ \mathbf{w} \in \ Y, \\ \mathcal{B}(\mu; q, \mathbf{u}^{(k+1)}) = \langle G^0, q \rangle \ \forall \ q \in \ Q, \end{cases} \tag{7.4.9}$$

where:

$$\mathcal{A}(\mu,\mathbf{u},\mathbf{w})=\sum_{r=1}^{R}\int_{\Omega^r}\frac{\partial\mathbf{u}}{\partial x_i}\Big(G^r_{ii'}(\mu)\hat{\nu}_{i'j'}G^r_{jj'}(\mu)|(G^r(\mu))^{-1}|\Big)\frac{\partial\mathbf{w}}{\partial x_j}d\Omega\ \forall\mathbf{w}\in Y,$$

$$\mathcal{B}(\mu,p,\mathbf{w})=-\sum_{r=1}^{R}\int_{\Omega^r}p\Big(G^r_{ij}(\mu)|(G^r(\mu))^{-1}|\Big)\frac{\partial w_j}{\partial x_i}d\Omega\ \forall\mathbf{w}\in Y,$$

$$\mathcal{C}(\mu,\mathbf{u},\mathbf{v},\mathbf{w})=-\sum_{r=1}^{R}\int_{\Omega^r}u_i\Big(G^r_{ij}(\mu)|(G^r(\mu))^{-1}|\Big)\frac{\partial v_j}{\partial x_i}\mathbf{w}d\Omega\ \forall\mathbf{w}\in Y,$$

$$\langle F_s,\mathbf{w}\rangle=\sum_{r=1}^{R}\int_{\Omega^r}\Big(\hat{f}^r|(G^r(\mu))^{-1}|\Big)\mathbf{w}d\Omega;\ \langle F^0,\mathbf{w}\rangle=-\langle\mathcal{A}g_{in},\mathbf{w}\rangle;$$

$\langle G^0,q\rangle=\langle\mathcal{B}q,\mathbf{g}_{in}\rangle$; the general formulation of the tensors for *viscous terms* is

$$\nu^r_{ij}(\mu)=G^r_{ii'}(\mu)\hat{\nu}_{i'j'}G^r_{jj'}(\mu)det(G^r(\mu))^{-1},1\le i,j\le 2,r=1,...,R,\tag{7.4.10}$$

the one of the tensors for *pressure, divergence and convective terms* is:

$$\chi^r_{ij}(\mu)=\pi^r_{ij}(\mu)=G^r_{ij}det(G^r(\mu))^{-1},1\le i,j\le 2,r=1,...,R.\tag{7.4.11}$$

Using the affine decomposition property to exploit and decouple the online computational stage (many queries) and the offline one (computed once) we introduce the following elements:

$$\Theta^{q(i,j,r)}(\mu)=\nu^r_{ij}(\mu),\ \mathcal{A}^{q(i,j,r)}(\mathbf{u},\mathbf{w})=\int_{\Omega^r}\frac{\partial\mathbf{u}}{\partial x_i}\frac{\partial\mathbf{w}}{\partial x_j}d\Omega,$$

$$\Phi^{s(i,j,r)}(\mu)=\chi^r_{ij}(\mu),\ \mathcal{B}^{s(i,j,r)}(p,\mathbf{w})=-\int_{\Omega^r}p\frac{\partial w_i}{\partial x_j}d\Omega,$$

$$\Upsilon^{s(i,j,r)}(\mu)=\pi^r_{ij}(\mu),\ \mathcal{C}^{s(i,j,r)}(\mathbf{u},\mathbf{u},\mathbf{w})=\int_{\Omega^r}u_j\frac{\partial u_i}{\partial x_j}\mathbf{w}d\Omega,$$

$$\mathcal{A}(\Theta(\mu),\mathbf{u},\mathbf{w})=\sum_{q=1}^{Q^a}\Theta^q(\mu)\mathcal{A}(\mathbf{u},\mathbf{w})^q;$$

$$\mathcal{B}(\Phi(\mu),p,\mathbf{w})=\sum_{s=1}^{Q^b}\Phi^s(\mu)\mathcal{B}(p,\mathbf{w})^s;$$

$$\mathcal{C}(\Upsilon(\mu),\mathbf{u},\mathbf{u},\mathbf{w})=\sum_{s=1}^{Q^c}\Upsilon^s(\mu)\mathcal{C}(\mathbf{u},\mathbf{u},\mathbf{w})^s;$$

where s and q are condensed indexes for i,j,r, $\max(Q^a)=d\times d\times d\times R$, $\max(Q^b)=d\times d\times R$ and $\max(Q^c)=d\times d\times d\times R$. The reduced basis approximation for the Navier-Stokes system

(7.4.9) reads: find $(\mathbf{u}_N^{(k+1)}(\mu), p_N^{(k+1)}(\mu)) \in Y_N \times Q_N$, given $\mathbf{u}_N^{(k)}$ as guess solution for the non-linear solver (taken from the previous iteration or given as $\mathbf{u}_N^{(0)}$), such that

$$\begin{cases} \mathcal{A}(\mu; \mathbf{u}_N^{(k+1)}(\mu), \mathbf{w}) + \mathcal{B}(\mu; p_N^{(k+1)}(\mu), \mathbf{w}) + \mathcal{C}(\mu; \mathbf{u}_N^{(k+1)}(\mu), \mathbf{u}_N^{(k)}(\mu), \mathbf{w}) + \\ \mathcal{C}(\mu; \mathbf{u}_N^{(k)}(\mu), \mathbf{u}_N^{(k+1)}(\mu), \mathbf{w}) = \langle F, \mathbf{w} \rangle + \mathcal{C}(\mu; \mathbf{u}_N^{(k)}(\mu), \mathbf{u}_N^{(k)}(\mu), \mathbf{w}) \ \forall \ \mathbf{w} \in \ Y_N, \\ \mathcal{B}(\mu; q, \mathbf{u}_N^{(k+1)}(\mu)) = \langle G, q \rangle \ \forall \ q \in \ Q_N. \end{cases} \tag{7.4.12}$$

As already seen we properly take some "μ" samples $S_N^\mu = \{\mu^1, \ldots, \mu^N\}$ (snapshots), where $\mu^n \in \mathcal{D}^\mu$, $n = 1, \ldots, N$.
The *reduced basis pressure space* is:

$$Q_N = \text{span}\ \{\xi_n,\ n = 1, \ldots, N\}, \tag{7.4.13}$$

where $\xi_n = p(\mu^n)$. We use the supremizer solutions to enrich Y_N, the *reduced basis velocity space* is given by:

$$\begin{aligned} Y_N &= \text{span}\ \{\sigma_n,\ n = 1, \ldots, 2N\} = \\ &= \text{span}\ \{\zeta_n, T^{\mu^n}\xi_n,\ n = 1, \ldots, N\}, \end{aligned} \tag{7.4.14}$$

where $\zeta_n = \mathbf{u}(\mu^n)$ and $T^{\mu^n}\colon\ Q \to Y$ is the supremizer operator

$$(T^\mu q, \mathbf{w})_Y = \mathcal{B}(\mu; q, \mathbf{w};),\ \forall\ \mathbf{w}\ \in\ Y. \tag{7.4.15}$$

We recall that we can write $T^{\mu^n}\xi = \sum_{q=1}^{Q^b} \Phi^q(\mu^n) T^q \xi$ for any ξ and μ.

Remark 7.4.1 *Note that in this case the reduced basis velocity space is not depending on the "online" value of the μ parameter because in the supremizer affine assembling procedure we use the values of μ^n corresponding at each solution $\xi_n = p(\mu^n)$, considered as basis function. This option allows us to simplify notation and to reduce complexity of the problem in this first case.* □

Other options are available to get a different space Y_N for velocity, for example: i) a space which is μ independent, using only $T^q\xi$ components to enrich velocity space. This option is useful if we want to apply an orthonormalization procedure to restore algebraic stability; or ii) a space μ dependent, using the online value of the parameter in Φ^q. For more elements on the choice of supremum space we recall what introduced in Section 5.7.2 dealing with Stokes flows and in [111]. We remind briefly also the reduced basis equivalent LBB inf-sup constant $\beta_N(\mu)$ with respect to $\beta(\mu)$ associated with the Galerkin method, and the LBB inf-sup condition which, if satisfied as in (ii), guarantees the stability of the approximation (Lemma 5.3.1): $\beta_N(\mu) \geq \beta(\mu) \geq \beta_0 > 0, \forall \mu \in \mathcal{D}^\mu$ where

$$\beta_N(\mu) = \inf_{q \in Q_N} \sup_{\mathbf{w} \in Y_N} \frac{\mathcal{B}(\mu, q, \mathbf{w})}{\|\mathbf{w}\|_Y \|q\|_Q},$$

and

$$\beta(\mu) = \inf_{q\in Q} \sup_{\mathbf{w}\in Y} \frac{\mathcal{B}(\mu, q, \mathbf{w})}{\|\mathbf{w}\|_Y \|q\|_Q}.$$

The reduced basis solution for a new sample μ is built as:

$$\mathbf{u}_N(\mu) = \sum_{j=1}^{2N} u_{Nj}(\mu)\sigma_j, \quad p_N(\mu) = \sum_{l=1}^{N} p_{Nl}(\mu)\xi_l;$$

and the reduced basis non-linear system for $1 \le i, j, h \le 2N,\ 1 \le l \le N$ is:

$$\begin{cases} \sum_{j=1}^{2N} A_{ij}^{\mu}\mathbf{u}_{Nj}^{(k+1)}(\mu) + \sum_{l=1}^{N} B_{il}^{\mu}p_{Nl}^{(k+1)}(\mu) + \sum_{h=1}^{2N}\sum_{j=1}^{2N} \mathbf{u}_{Nh}^{(k)}(\mu)C_{ijh}^{\mu}\mathbf{u}_{Nj}^{(k+1)}(\mu) + \\ + \sum_{h=1}^{2N}\sum_{j=1}^{2N} \mathbf{u}_{Nh}^{(k+1)}(\mu)C_{ijh}^{\mu}\mathbf{u}_{Nj}^{(k)}(\mu) = F_i^{\mu} + \sum_{h=1}^{2N}\sum_{j=1}^{2N} \mathbf{u}_{Nj}^{(k)}(\mu)C_{ijh}^{\mu}\mathbf{u}_{Nh}^{(k)}(\mu) \\ \sum_{j=1}^{2N} B_{jl}^{\mu}\mathbf{u}_{Nj}^{(k+1)}(\mu) = G_l^{\mu}, \quad 1 \le l \le N; \end{cases} \tag{7.4.16}$$

$$A_{ij}^{\mu} = \sum_{m=1}^{Q^a} \Theta^m(\mu)\mathcal{A}(\sigma_i, \sigma_j)^m,\ B_{il}^{\mu} = \sum_{m=1}^{Q^b} \Phi^m(\mu)\mathcal{B}(\sigma_i, \xi_l)^m;$$

$$C_{ijh}^{\mu} = \sum_{m=1}^{Q^c} \Upsilon^m(\mu)\mathcal{C}(\sigma_h, \sigma_j, \sigma_i)^m;$$

$$F_i^{\mu} = \langle F, \sigma_i\rangle,\ G_l^{\mu} = \langle G, \xi_l\rangle.$$

We recall that the k index refers to the Newton iteration. The form $\mathcal{C}^{\mu}$ is depending on 3 different indexes and is assembled online given the value of μ. Then for every k we have to incorporate in $\mathcal{C}^{\mu}$ the solution at the previous iteration to update the system matrix and the right-hand-side. We can adopt the following stopping criterium

$$\|\mathbf{u}_N^{(k+1)}(\mu) - \mathbf{u}_N^{(k)}(\mu)\| \le \epsilon_N$$

where ϵ_N is a prescribed tolerance. When the Stokes solution is available, as in our case, it may be used as initial guess $\mathbf{u}_N^{(0)}$. If we compare the assembling and computational costs of Navier-Stokes reduced basis problem with respect to Stokes problem we have to increase $O(9KN^3)$ operations for the solution of the non-linear system (K is the number of Newton iteration). In reality we are going to use more efficient and faster solver with splitting procedures. The other computational cost comes from the assembling procedure of $\underline{C}$ matrices (advection terms), whose theoretical assembling costs are $O(Q^c 8N^3)$. We recall that the assembling costs for $\underline{A}$, $\underline{B}$ and $\underline{F}$ are, respectively, $O(Q^a 4N^2)$, $O(Q^b 2N^2)$ and $O(N)$. The structure of the system (7.4.16) is

$$\begin{pmatrix} \underline{A} + \underline{C}^{(k+1)} & \underline{B} \\ \underline{B}^T & 0 \end{pmatrix} \begin{pmatrix} \underline{\mathbf{u}}_N^{(k+1)} \\ \underline{p}_N^{(k+1)} \end{pmatrix} = \begin{pmatrix} \underline{F}^{(k)} \\ \underline{G} \end{pmatrix}; \tag{7.4.17}$$

Numerical results dealing only with geometrical affine parametric dependence will be reported in Section 7.7.

7.5 Parametrized formulation: non-affine parametric dependence

In this section we extend the formulation given in the previous one dealing only with non-affine geometrical parametric dependence in the reduced basis framework for Navier-Stokes equations. We consider a *non-affine mapping* from the true subdomains $\hat{\Omega}^r$ into the reference ones denoted with Ω^r. For any $\hat{x} \in \hat{\Omega}^r$, $r = 1, \ldots, R$, its image $x \in \Omega^r$ is given by

$$x = \mathcal{T}^r(\mu; \hat{x}), \quad 1 \leq r \leq R; \tag{7.5.1}$$

we thus write on Ω^r

$$\frac{\partial}{\partial \hat{x}_i} = \frac{\partial x_j}{\partial \hat{x}_i}\frac{\partial}{\partial x_j} = T^r_{ji}(\mu, x)\frac{\partial}{\partial x_j}. \tag{7.5.2}$$

Referring to the problem (7.4.9) each elements in the system has the following form for $1 \leq i, j \leq 2$:

$$\mathcal{A}(\mu; \mathbf{u}, \mathbf{w}) = \sum_{r=1}^{R} \int_{\Omega^r} \frac{\partial \mathbf{u}}{\partial x_i}\Big(T^r_{ii'}(\mu, x)\hat{\nu}_{i'j'}T^r_{jj'}(\mu, x)det(T^r(\mu, x))^{-1}\Big)\frac{\partial \mathbf{w}}{\partial x_j}d\Omega \ \forall \mathbf{w} \in Y,$$

$$\mathcal{B}(\mu; p, \mathbf{w}) = -\sum_{r=1}^{R} \int_{\Omega^r} p\Big(T^r_{ij}(\mu, x)det(T^r(\mu, x))^{-1}\Big)\frac{\partial w_j}{\partial x_i}d\Omega \ \forall \mathbf{w} \in Y,$$

$$\mathcal{C}(\mu; \mathbf{u}, \mathbf{v}, \mathbf{w}) = -\sum_{r=1}^{R} \int_{\Omega^r} u_i\Big(T^r_{ij}(\mu, x)det(T^r(\mu, x))^{-1}\Big)\frac{\partial v_j}{\partial x_i}\mathbf{w}d\Omega \ \forall \mathbf{w} \in Y,$$

$$\langle F_s, \mathbf{w}\rangle = \sum_{r=1}^{R} \int_{\Omega^r} \Big(\hat{\mathbf{f}}^r det(T^r(\mu, x))^{-1}\Big)\mathbf{w}d\Omega.$$

In Section 7.8 we report a test case and we show the explicit forms of the previous terms. The *transformation tensors* for *diffusion bilinear forms* with non-affine mappings are defined as follows:

$$\nu^r_{T_{ij}}(\mu, x) = T^r_{ii'}(\mu, x)\hat{\nu}_{i'j'}T^r_{jj'}(\mu, x)det(T^r(\mu, x))^{-1}, 1 \leq i, j \leq 2, r = 1, ..., R. \tag{7.5.3}$$

The tensors for *pressure, divergence and advection forms* are defined for non-affine mappings as:

$$\chi^r_{T_{ij}}(\mu, x) = \pi^r_{T_{ij}}(\mu, x) = T^r_{ij}(\mu, x)det(T^r(\mu, x))^{-1}. \tag{7.5.4}$$

To decouple the non-affine contributions we apply the empirical interpolation procedure of Section 6.2 to expand mapping terms and split the parameters dependent contribution from the one depending only on spacial coordinates. We can write:

$$\nu^r_{T_{ij}}(\mu, x) = \Sigma_{m=1}^{M^a_{ijr}}\beta^r_{ijm}(\mu)\gamma^r_{ijm}(x), \tag{7.5.5}$$

$$\chi^r_{T_{ij}}(\mu, x) = \pi^r_{T_{ij}}(\mu, x) = \Sigma_{m=1}^{M^b_{ijr}}\alpha^r_{ijm}(\mu)\omega^r_{ijm}(x), \tag{7.5.6}$$

where m refers to the number of interpolation functions we use for each form (related with max interpolation error), i and j are indexes related to linear/bilinear form, r refers to subdomains. β and α are weight quantities depending on the parameters μ, while γ and ω are interpolation functions ("shape functions") used as basis.

Reminder 7.5.1 *We recall very briefly the algorithm based on the empirical interpolation method proposed by Maday et al. in [12]:*

$$g(x,\mu),\ is\ the\ non-affine\ mapping\ term\ (i.e.\ a\ shape).$$

The goal is to develop:

$$g_M(x,\mu) = \Sigma_{m=1}^{M}\beta_m(\mu)q_m(x),$$

as a sum of products decomposed in two parts: $\beta_m(\mu)$ parameters dependent weights; $q_m(x)$ shape functions without a parametric dependence.
The main elements are: test shape functions and service interpolation points, respectively:

$$W_M^g = \{\gamma_m = g(.,\mu_m^g), 1 \le m \le M\}, \mu_m^g\ properly\ chosen,$$

$$T_M = \{t_1, \dots t_M\}, 1 \le M \le M_{max},\ sets\ of\ interpolation\ points.$$

The interpolation algorithm is:

$$for\ M = 1, t_1 = argsup_{x\in\Omega}|\gamma_1(x)|,\ q_1 = \gamma_1(x)/\gamma_1(t_1), (off-line)$$

$$then,\ for\ M = 2, \dots, M_{max} : \Sigma_{j=1}^{M-1}\sigma_j^{M-1}q_j(t_i) = \gamma_M(t_i), 1 \le i \le M-1, (off-line)$$

$$r_M(x) = \gamma_M(x) - \Sigma_{j=1}^{M-1}\sigma_j^{M-1}q_j(x), t_M = argsup_{x\in\Omega}|r_M(x)|, (off-line)$$

$$q_M(x) = r_M(x)/r_M(t_M); g_M(x,\mu) = \Sigma_{m=1}^{M}\beta_m(\mu)q_m(x), (off-line)$$

$$\Sigma_{j=1}^{M}q_j(t_i)\beta_j(\mu) = g(t_i,\mu), 1 \le i \le M,\ (on-line).$$

To stop the procedure we impose $\|g(.,\mu) - g_M(.,\mu)\|_{L^\infty(\Omega)} \le \epsilon_{max}$ where ϵ_{max} is an interpolation error. □

We go back to our problem and, in order to build an *effectively affine* decomposition, we define:

$$\Psi^{t(i,j,r,m)}(\mu) = \beta_{ijm}^r(\mu),\ \mathcal{A}^{t(i,j,r,m)}(\gamma(x),\mathbf{u},\mathbf{w}) = \int_{\Omega^r}\gamma_{ijm}^r(x)\frac{\partial\mathbf{u}}{\partial x_i}\frac{\partial\mathbf{w}}{\partial x_j}d\Omega, \tag{7.5.7}$$

$$\Upsilon^{p(i,j,r,m)}(\mu) = \alpha_{ijm}^r(\mu),\ \mathcal{B}^{p(i,j,r,m)}(\omega(x),p,\mathbf{w}) = -\int_{\Omega^r}\omega_{ijm}^r(x)p\frac{\partial w_i}{\partial x_j}d\Omega, \tag{7.5.8}$$

$$\Upsilon^{p(i,j,r,m)}(\mu) = \alpha_{ijm}^r(\mu),\ \mathcal{C}^{p(i,j,r,m)}(\omega(x),\mathbf{u},\mathbf{v},\mathbf{w}) = -\int_{\Omega^r}\omega_{ijm}^r(x)u_j\frac{\partial v_i}{\partial x_j}\mathbf{w}d\Omega, \tag{7.5.9}$$

for $1 \le r \le R$, $1 \le i,j \le d = 2$, $1 \le m \le max(M_{ijr}^a, M_{ijr}^b)$ (t and p are condensed indexes of i,j,r,m quantities). We rewrite our terms as:

$$\mathcal{A}(\mu,\mathbf{u},\mathbf{w}) = \sum_{t=1}^{Q^a}\Psi^t(\mu)\mathcal{A}^t(\gamma(x),\mathbf{u},\mathbf{w});$$

$$\mathcal{B}(\mu, p, \mathbf{w}) = \sum_{p=1}^{Q^b} \Upsilon^p(\mu)\mathcal{B}^p(\omega(x), p, \mathbf{w}) \ ;$$

$$\mathcal{C}(\mu, \mathbf{u}, \mathbf{v}, \mathbf{w}) = \sum_{p=1}^{Q^c} \Upsilon^p(\mu)\mathcal{C}^p(\omega(x), \mathbf{u}, \mathbf{v}, \mathbf{w}) \ ;$$

in this case $Q^a = \Sigma_{j=1}^{d}\Sigma_{i=1}^{d}\Sigma_{r=1}^{R_T} M_{ijr}^a$; $Q^b = Q^c = \Sigma_{j=1}^{d}\Sigma_{i=1}^{d}\Sigma_{r=1}^{R_T} M_{ijr}^b$. We can now solve the Navier-Stokes problem written in (7.4.9) on the reference domain Ω for some values of parameter μ with the scope of building the reduced basis spaces. The formulation in this case is the same as the one in the previous section. We use the same supremizer option (the one with the μ^n offline value) so that we have a reduced basis velocity space Y_N (7.4.14) which is μ independent. The only difference is the use of the *effectively affine dependence* of $\mathcal{B}(\mu; q, \mathbf{w})$ on the parameter which reads:

$$T^{\mu^n}\xi = \sum_{p=1}^{Q^b} \Upsilon^p(\mu^n)T^p\xi \tag{7.5.10}$$

for any ξ and μ, where:

$$(T^p\xi, \mathbf{w})_Y = \mathcal{B}^p(\omega, q, \mathbf{w}), \ \forall \ \mathbf{w} \ \in \ Y.$$

Referring to the reduced basis non-linear system (7.4.16) we have the following sub-matrices A, B and C, respectively:

$$A_{ij}^{\mu} = \sum_{z=1}^{Q^a} \Psi^z(\mu)\mathcal{A}^z(\gamma, \sigma_i, \sigma_j), \ 1 \leq i, j \leq 2N;$$

$$B_{il}^{\mu} = \sum_{z=1}^{Q^b} \Upsilon^z(\mu)\mathcal{B}^z(\omega, \sigma_i, \xi_l), \ 1 \leq i \leq 2N, \ 1 \leq l \leq N;$$

and:

$$C_{ijh}^{\mu} = \sum_{z=1}^{Q^c} \Upsilon^z(\mu)\mathcal{C}^z(\omega, \sigma_i, \sigma_j, \sigma_h), \ 1 \leq i, j, h \leq 2N.$$

Numerical results dealing with a test case (a furrowed channel) will be reported in Section 7.8.

7.6 Parametrized formulation: affine and non-affine parametric dependence

In this section we are going to combine the formulation introduced in the two previous sections allowing us to prepare the framework for the application of reduced basis for Navier-Stokes equations to our problem of interest: the study of a bypass configuration. We deal with parametrized domains with both affine and non-affine parametric dependence (in different subdomains). In this case we are going to use a different supremizer option, building reduced

basis approximation space which is depending on the value of the "online" parameter μ. We consider again a P^2DEs (Parametrized Partial Differential Equations) system, whose formulation on the reference domain Ω is the following: find $(\mathbf{u}(\mu), p(\mu)) \in Y \times Q$:

$$\begin{cases} \mathcal{A}(\mu; \mathbf{u}(\mu), \mathbf{w}) + \mathcal{B}(\mu; p(\mu), \mathbf{w}) + \mathcal{C}(\mu; \mathbf{u}(\mu), \mathbf{u}(\mu), \mathbf{w}) = \langle F, \mathbf{w} \rangle \ \forall \ \mathbf{w} \in \ Y, \\ \mathcal{B}(\mu; q, \mathbf{u}(\mu)) = \langle G^0, q \rangle \ \forall \ q \in \ Q. \end{cases} \tag{7.6.1}$$

The problem has been traced back to a *reference domain* by an *affine mapping* on some subdomains $\hat{\Omega}_G^r$ into Ω_G^r and by a *non-affine mapping* on the remaining subdomains $\hat{\Omega}_T^r$ into Ω_T^r. More precisely, the physical domain $\hat{\Omega}$ is the union of two (finite) families of subdomains $\{\hat{\Omega}_G^r, r = 1, \ldots, R_G\}$ and $\{\hat{\Omega}_T^r, r = 1, \ldots, R_T\}$. Then $\hat{\Omega} = \bigcup_{r=1}^{R_G} \hat{\Omega}_G^r \cup \bigcup_{r=1}^{R_T} \hat{\Omega}_T^r$. For any $\hat{x} \in \hat{\Omega}_G^r$, $r = 1, \ldots, R_G$, its image $x \in \Omega_G^r$ is given by

$$x = \mathcal{G}^r(\mu; \hat{x}) = G^r(\mu)\hat{x} + g^r, \quad 1 \le r \le R_G, \tag{7.6.2}$$

therefore for $1 \le i, j \le 2$:

$$\frac{\partial}{\partial \hat{x}_i} = \frac{\partial x_j}{\partial \hat{x}_i} \frac{\partial}{\partial x_j} = G_{ji}^r(\mu) \frac{\partial}{\partial x_j}. \tag{7.6.3}$$

On the other hand, for any $\hat{x} \in \hat{\Omega}_T^r$, $r = 1, \ldots, R_T$, its image $x \in \Omega_T^r$ is given by

$$x = \mathcal{T}^r(\mu; \hat{x}), \quad 1 \le r \le R_T, \tag{7.6.4}$$

thus

$$\frac{\partial}{\partial \hat{x}_i} = \frac{\partial x_j}{\partial \hat{x}_i} \frac{\partial}{\partial x_j} = T_{ji}^r(\mu, x) \frac{\partial}{\partial x_j}. \tag{7.6.5}$$

In the reference domain Ω we have:

$$\mathcal{A}(\mu; \mathbf{u}, \mathbf{w}) = \sum_{r=1}^{R_G} \int_{\Omega_G^r} \frac{\partial \mathbf{u}}{\partial x_i} \Big(G_{ii'}^r(\mu) \hat{\nu}_{i'j'} G_{jj'}^r(\mu) det(G^r(\mu))^{-1} \Big) \frac{\partial \mathbf{w}}{\partial x_j} d\Omega + \tag{7.6.6}$$

$$\sum_{r=1}^{R_T} \int_{\Omega_T^r} \frac{\partial \mathbf{u}}{\partial x_i} \Big(T_{ii'}^r(\mu, x) \hat{\nu}_{i'j'} T_{jj'}^r(\mu, x) det(T^r(\mu, x))^{-1} \Big) \frac{\partial \mathbf{w}}{\partial x_j} d\Omega \ \forall \mathbf{w} \in Y,$$

$$\mathcal{B}(\mu; p, \mathbf{w}) = -\sum_{r=1}^{R_G} \int_{\Omega_G^r} p \Big(G_{ij}^r(\mu) det(G^r(\mu))^{-1} \Big) \frac{\partial w_j}{\partial x_i} d\Omega + \tag{7.6.7}$$

$$-\sum_{r=1}^{R_T} \int_{\Omega_T^r} p \Big(T_{ij}^r(\mu, x) det(T^r(\mu, x))^{-1} \Big) \frac{\partial w_j}{\partial x_i} d\Omega \ \forall \mathbf{w} \in Y,$$

$$\mathcal{C}(\mu; \mathbf{u}, \mathbf{v}, \mathbf{w}) = \sum_{r=1}^{R_G} \int_{\Omega_G^r} u_i \Big(G_{ij}^r(\mu) det(G^r(\mu))^{-1} \Big) \frac{\partial v_j}{\partial x_i} \mathbf{w} d\Omega + \tag{7.6.8}$$

$$-\sum_{r=1}^{R_T} \int_{\Omega_T^r} u_i \Big(T_{ij}^r(\mu, x) det(T^r(\mu, x))^{-1} \Big) \frac{\partial v_j}{\partial x_i} \mathbf{w} d\Omega \ \forall \mathbf{w} \in Y,$$

$$\langle F, \mathbf{w} \rangle = \langle F_s, \mathbf{w} \rangle + \langle F^0, \mathbf{w} \rangle, \tag{7.6.9}$$

where

$$\langle F_s, \mathbf{w}\rangle = \sum_{r=1}^{R_G}\int_{\Omega_G^r}\Big(\hat{\mathbf{f}}^r det(G^r(\mu))^{-1}\Big)\mathbf{w}d\Omega + \sum_{r=1}^{R_T}\int_{\Omega_T^r}\Big(\hat{\mathbf{f}}^r det(T^r(\mu,x))^{-1}\Big)\mathbf{w}d\Omega; \tag{7.6.10}$$

$$\langle F^0, \mathbf{w}\rangle = -\langle \mathcal{A}\mathbf{g}_{in}, \mathbf{w}\rangle;\ \langle G^0, q\rangle = \langle \mathcal{B}q, \mathbf{g}_{in}\rangle.$$

The *transformation tensors* for diffusion bilinear forms with affine and non-affine mappings are defined, respectively, as follows:

$$\nu_{G_{ij}}^r(\mu) = G_{ii'}^r(\mu)\hat{\nu}_{i'j'}G_{jj'}^r(\mu)det(G^r(\mu))^{-1}, 1\le i,j\le 2, r=1,...,R_G, \tag{7.6.11}$$

$$\nu_{T_{ij}}^r(\mu,x) = T_{ii'}^r(\mu,x)\hat{\nu}_{i'j'}T_{jj'}^r(\mu,x)det(T^r(\mu,x))^{-1}, 1\le i,j\le 2, r=1,...,R_T. \tag{7.6.12}$$

The tensors for *pressure, divergence and advection forms* are defined, respectively, for affine and non-affine mappings as:

$$\chi_{G_{ij}}^r(\mu) = \pi_{G_{ij}}^r(\mu) = G_{ij}^r det(G^r(\mu))^{-1}, \tag{7.6.13}$$

$$\chi_{T_{ij}}^r(\mu,x) = \pi_{T_{ij}}^r(\mu,x) = T_{ij}^r(\mu,x)det(T^r(\mu,x))^{-1}. \tag{7.6.14}$$

For the non-affine parts we apply, as already proposed, the empirical interpolation procedure of Section 6.2 (and recalled in the previous section) to expand non-affine mapping terms and decouple the parameters dependent contribution from the one depending only on spacial coordinates. We write:

$$\nu_{T_{ij}}^r(\mu,x) = \Sigma_{m=1}^{M_{ijr}^a}\beta_{ijm}^r(\mu)\gamma_{ijm}^r(x), \tag{7.6.15}$$

$$\chi_{T_{ij}}^r(\mu,x) = \Sigma_{m=1}^{M_{ijr}^b}\alpha_{ijm}^r(\mu)\omega_{ijm}^r(x), \tag{7.6.16}$$

where m refers to the number of interpolation functions we use for each form (related with max interpolation error), i and j are indexes related to linear/bilinear form, r is the subdomain index, β and α are weighing quantities depending on the parameters μ, γ and ω are interpolation functions used as basis.
Furthermore, we define

$$\Theta^{q(i,j,r)}(\mu) = \nu_{G_{ij}}^r(\mu),\ \mathcal{A}_G^{q(i,j,r)}(\mathbf{u},\mathbf{w}) = \int_{\Omega_G^r}\frac{\partial\mathbf{u}}{\partial x_i}\frac{\partial\mathbf{w}}{\partial x_j}d\Omega, \tag{7.6.17}$$

$$\Phi^{s(i,j,r)}(\mu) = \chi_{G_{ij}}^r(\mu) = \pi_{G_{ij}}^r(\mu),\ \mathcal{B}_G^{s(i,j,r)}(p,\mathbf{w}) = -\int_{\Omega_G^r}p\frac{\partial w_i}{\partial x_j}d\Omega, \tag{7.6.18}$$

$$\mathcal{C}_G^{s(i,j,r)}(\mathbf{u},\mathbf{v},\mathbf{w}) = \int_{\Omega_G^r}u_i\frac{\partial v_i}{\partial x_j}\mathbf{w}d\Omega, \tag{7.6.19}$$

for $1\le r\le R_G$, $1\le i,j\le d=2$ (q and s are condensed indexes of i,j,r quantities), and

$$\Psi^{t(i,j,r,m)}(\mu) = \beta_{ijm}^r(\mu),\ \mathcal{A}_T^{t(i,j,r,m)}(\gamma(x),\mathbf{u},\mathbf{w}) = \int_{\Omega_T^r}\gamma_{ijm}^r(x)\frac{\partial\mathbf{u}}{\partial x_i}\frac{\partial\mathbf{w}}{\partial x_j}d\Omega, \tag{7.6.20}$$

$$\Upsilon^{p(i,j,r,m)}(\mu) = \alpha^r_{ijm}(\mu),\ \mathcal{B}_T^{p(i,j,r,m)}(\omega(x), p, \mathbf{w}) = -\int_{\Omega_T^r} \omega^r_{ijm}(x) p \frac{\partial w_i}{\partial x_j} d\Omega, \tag{7.6.21}$$

$$\mathcal{C}_T^{p(i,j,r,m)}(\omega(x), \mathbf{u}, \mathbf{v}, \mathbf{w}) = \int_{\Omega_T^r} \omega^r_{ijm}(x) u_i \frac{\partial v_i}{\partial x_j} \mathbf{w} d\Omega, \tag{7.6.22}$$

for $1 \le r \le R_T$, $1 \le i, j \le d = 2$, $1 \le m \le max(M^a_{ijr}, M^b_{ijr})$ (t and p are condensed indexes of i, j, r, m quantities used to simplify notation: each value of t or p represents a different combination of the previous four indexes i, j, r, m). We apply an *effectively affine* decomposition:

$$\mathcal{A}(\mu, \mathbf{u}, \mathbf{w}) = \sum_{q=1}^{Q_G^a} \Theta^q(\mu) \mathcal{A}_G^q(\mathbf{u}, \mathbf{w}) + \sum_{t=1}^{Q_T^a} \Psi^t(\mu) \mathcal{A}_T^t(\gamma(x), \mathbf{u}, \mathbf{w});$$

$$\mathcal{B}(\mu, p, \mathbf{w}) = \sum_{s=1}^{Q_G^b} \Phi^s(\mu) \mathcal{B}_G^s(p, \mathbf{w}) + \sum_{p=1}^{Q_T^b} \Upsilon^p(\mu) \mathcal{B}_T^p(\omega(x), p, \mathbf{w}) \ ;$$

$$\mathcal{C}(\mu, \mathbf{u}, \mathbf{v}, \mathbf{w}) = \sum_{s=1}^{Q_G^c} \Phi^s(\mu) \mathcal{C}_G^s(\mathbf{u}, \mathbf{v}, \mathbf{w}) + \sum_{p=1}^{Q_T^c} \Upsilon^p(\mu) \mathcal{C}_T^p(\omega(x), \mathbf{u}, \mathbf{v}, \mathbf{w}) \ ;$$

in general, $\max(Q_G^a) = d \times d \times d \times R_G$, $\max(Q_G^b) = d \times d \times R_G$ $\max(Q_G^c) = d \times d \times d \times R_G$; $Q_T^a = \Sigma_{j=1}^d \Sigma_{i=1}^d \Sigma_{r=1}^{R_T} M^a_{ijr}$; $Q_T^b = \Sigma_{j=1}^d \Sigma_{i=1}^d \Sigma_{r=1}^{R_T} M^b_{ijr}$ and $Q_T^c = \Sigma_{j=1}^d \Sigma_{i=1}^d \Sigma_{r=1}^{R_T} M^b_{ijr}$;
The non-linear problem (7.6) has to be discretized and then linearized to be solved, by an iterative method as seen in Section 7.4.
In the reduced basis approximation we choose properly (i.e. by optimized algorithm as seen in Section 5.4) a set of sample parameters $S_N^{\boldsymbol{\mu}} = \{\boldsymbol{\mu}^1, \dots, \boldsymbol{\mu}^N\}$, where $\boldsymbol{\mu}^n \in \mathcal{D}^\mu$, $n = 1, \dots, N$. Correspondingly, we take a set of couples $(\mathbf{u}(\mu^n), p(\mu^n))$ which are approximate solutions of the Navier-Stokes problem (7.6.1). Then the *reduced basis pressure space* is always
$Q_N = \text{span}\ \{\xi_n,\ n = 1, \dots, N\}$, where $\xi_n = p(\mu^n)$, while for the *reduced basis velocity space* we take into consideration the option in which the space is μ dependent:
$Y_N^\mu = \text{span}\ \{\zeta_n,\ n = 1, \dots, N; T^\mu \xi_n,\ n = 1, \dots, N\}$, where $\zeta_n = \mathbf{u}(\mu^n)$.
The reduced basis approximation problem reads: find $(\mathbf{u}_N(\mu), p_N(\mu)) \in Y_N \times Q_N$ s.t.:

$$\begin{cases} \mathcal{A}(\mu; \mathbf{u}_N(\mu), \mathbf{w}) + \mathcal{B}(\mu; p_N(\mu), \mathbf{w}) + \mathcal{C}(\mu; \mathbf{u}_N(\mu), \mathbf{u}_N(\mu), \mathbf{w}) = \langle F, \mathbf{w} \rangle \ \forall\ \mathbf{w} \in\ Y_N, \\ \mathcal{B}(\mu; q, \mathbf{u}_N(\mu) = \langle G^0, q \rangle \ \forall\ q \in\ Q_N. \end{cases} \tag{7.6.23}$$

We rewrite for computational convenience Y_N^μ using the *effectively affine dependence* of $\mathcal{B}(\mu; q, \mathbf{w})$ on the parameter and the *linearity* of T^μ:

$$T^\mu \xi = \sum_{q=1}^{Q_G^b} \Phi^q(\mu) T_G^q \xi + \sum_{p=1}^{Q_T^b} \Upsilon^p(\mu) T_T^p \xi \tag{7.6.24}$$

for any ξ and μ, where:

$$(T_G^q \xi, \mathbf{w})_Y = \mathcal{B}_G^q(q, \mathbf{w}) \ \forall\ \mathbf{w}\ \in\ Y,$$

$$(T_T^p\xi,\mathbf{w})_Y=\mathcal{B}_T^p(\omega,q,\mathbf{w})\ \forall\ \mathbf{w}\ \in\ Y,$$

which allows us to write:

$$Y_N^\mu=\text{span}\,\{\sum_{k=1}^{\overline{Q}_G^b}\Phi^k(\mu)\sigma_{kn}+\sum_{k'=1}^{Q_T^b}\Upsilon^{k'}(\mu)\widetilde{\sigma}_{k'n},n=1,\dots,2N\},$$

where $\overline{Q}_G^b=Q_G^b+1,\Phi^{\overline{Q}_G^b}=1$.
For $n=1,\dots,N$:

$$\sigma_{kn}=0,for\ k=1,\dots,Q_G^b;$$
$$\widetilde{\sigma}_{k'n}=0,for\ k'=1,\dots,Q_T^b;$$
$$\sigma_{\overline{Q}^b n}=\zeta_n=\mathbf{u}(\mu^n).$$

For $n=N+1,\dots,2N$:

$$(\sigma_{kn},\mathbf{w})_Y=\mathcal{B}_G^k(\xi_{n-N},\mathbf{w}),\forall\mathbf{w}\ \in\ Y,for\ k=1,\dots,Q_G^b;\tag{7.6.25}$$

$$\sigma_{\overline{Q}^b n}=0;$$
$$(\widetilde{\sigma}_{kn},\mathbf{w})_Y=\mathcal{B}_T^k(\omega,\xi_{n-N},\mathbf{w}),\forall\mathbf{w}\ \in\ Y,for\ k=1,\dots,Q_T^b.\tag{7.6.26}$$

For a new "μ" we want a solution given by a combination of previously computed stored solutions as basis functions, i.e.:

$$\mathbf{u}_N(\mu)=\sum_{j=1}^{2N}\mathbf{u}_{Nj}(\mu)\Big(\sum_{k=1}^{\overline{Q}_G^b}\Phi^k(\mu)\sigma_{kj}+\sum_{k'=1}^{Q_T^b}\Upsilon^{k'}(\mu)\widetilde{\sigma}_{k'j}\Big),$$

$$p_N(\mu)=\sum_{l=1}^{N}p_{Nl}(\mu)\xi_l,$$

whose unknowns $\mathbf{u}_{Nj}$ and p_{Nl} satisfy the following non-linear system:

$$\begin{cases}\sum_{j=1}^{2N}A_{ij}^\mu\mathbf{u}_{Nj}(\mu)+\sum_{l=1}^{N}B_{il}^\mu p_{Nl}(\mu)+\sum_{h=1}^{2N}\sum_{j=1}^{2N}\mathbf{u}_{Nh}(\mu)C_{ijh}^\mu\mathbf{u}_{Nj}(\mu)=F_i,\quad 1\le i\le 2N,\\ \sum_{j=1}^{2N}B_{jl}^\mu\mathbf{u}_{Nj}(\mu)=G_l,\quad 1\le l\le N.\end{cases}\tag{7.6.27}$$

To solve it we apply the Newton method reads, yielding the following iteration: for $k\ge 0$ given $\mathbf{u}_{Nj}^{(k)}$, find $\mathbf{u}_{Nj}^{(k+1)}$ and $p_{Nl}^{(k+1)}$ such that

$$\begin{cases}\sum_{j=1}^{2N}A_{ij}^\mu\mathbf{u}_{Nj}^{(k+1)}(\mu)+\sum_{l=1}^{N}B_{il}^\mu p_{Nl}^{(k+1)}(\mu)+\sum_{h=1}^{2N}\sum_{j=1}^{2N}\mathbf{u}_{Nh}^{(k)}(\mu)C_{ijh}^\mu\mathbf{u}_{Nj}^{(k+1)}(\mu)+\\ +\sum_{h=1}^{2N}\sum_{j=1}^{2N}\mathbf{u}_{Nh}^{(k+1)}(\mu)C_{ijh}^\mu\mathbf{u}_{Nj}^{(k)}(\mu)=F_i^\mu+\sum_{h=1}^{2N}\sum_{j=1}^{2N}\mathbf{u}_{Nj}^{(k)}(\mu)C_{ijh}^\mu\mathbf{u}_{Nh}^{(k)}(\mu)\\ \sum_{j=1}^{2N}B_{jl}^\mu\mathbf{u}_{Nj}^{(k+1)}(\mu)=G_l^\mu,\quad 1\le l\le N,\ 1\le i\le 2N.\end{cases}\tag{7.6.28}$$

The sub-matrices A, B and C are given by:

$$A_{ij}^\mu=\sum_{z=1}^{Q_G^a}\sum_{k'=1}^{\overline{Q}_G^b}\sum_{k''=1}^{\overline{Q}_G^b}\Theta^z(\mu)\Phi^{k'}(\mu)\Phi^{k''}(\mu)\mathcal{A}_G^z(\sigma_{k'i},\sigma_{k''j})+$$

$$+\sum_{z=1}^{Q_T^a}\sum_{k'=1}^{\overline{Q}_T^b}\sum_{k''=1}^{\overline{Q}_T^b}\Psi^z(\mu)\Upsilon^{k'}(\mu)\Upsilon^{k''}(\mu)\mathcal{A}_T^z(\gamma,\widetilde{\sigma}_{k'i},\widetilde{\sigma}_{k''j}),\ 1\le i,j\le 2N;$$

$$B_{il}^{\mu}=\sum_{z=1}^{\overline{Q}_G^b}\sum_{k'=1}^{\overline{Q}_G^b}\Phi^z(\mu)\Phi^{k'}(\mu)\mathcal{B}_G^z(\sigma_{k'i},\xi_l)+$$

$$+\sum_{z=1}^{\overline{Q}_T^b}\sum_{k'=1}^{\overline{Q}_T^b}\Upsilon^z(\mu)\Upsilon^{k'}(\mu)\mathcal{B}_T^z(\omega,\widetilde{\sigma}_{k'i},\xi_l),\ 1\le i\le 2N,\ 1\le l\le N;$$

$$C_{ijh}^{\mu}=\sum_{z=1}^{\overline{Q}_G^c}\sum_{k'=1}^{\overline{Q}_G^b}\sum_{k''=1}^{\overline{Q}_G^b}\sum_{k'''=1}^{\overline{Q}_G^b}\Phi^z(\mu)\Phi^{k'}(\mu)\Phi^{k''}(\mu)\Phi^{k'''}(\mu)\mathcal{C}_G^z(\sigma_{k'i},\sigma_{k''j},\sigma_{k'''h})+$$

$$+\sum_{z=1}^{\overline{Q}_T^c}\sum_{k'=1}^{\overline{Q}_T^b}\sum_{k''=1}^{\overline{Q}_T^b}\sum_{k'''=1}^{\overline{Q}_T^b}\Upsilon^k(\mu)\Upsilon^{k'}(\mu)\Upsilon^{k''}(\mu)\Upsilon^{k'''}(\mu)\mathcal{C}_T^z(\omega,\widetilde{\sigma}_{k'i},\widetilde{\sigma}_{k'j},\widetilde{\sigma}_{k'h}),\ 1\le i,j,h\le 2N;$$

$$F_i=\sum_{k'=1}^{\overline{Q}_G^b}\Phi^{k'}(\mu)\langle F,\sigma_{k'i}\rangle+\sum_{k'=1}^{Q_T^b}\Upsilon^{k'}(\mu)\langle F,\widetilde{\sigma}_{k'i}\rangle,\ 1\le i\le 2N;$$

$$G_l=\langle G^0,\xi_l\rangle,\ 1\le l\le N.$$

In compact form the linearized problem (7.6.28) can therefore be written as:

$$\begin{pmatrix}\underline{A}+\underline{C}^{(k+1)} & \underline{B}\\ \underline{B}^T & 0\end{pmatrix}\begin{pmatrix}\underline{\mathbf{u}}_N^{(k+1)}\\ \underline{p}_N^{(k+1)}\end{pmatrix}=\begin{pmatrix}\underline{F}^{(k)}\\ \underline{G}\end{pmatrix}. \tag{7.6.29}$$

Remark 7.6.1 *This reduced basis formulation seems to be more involved than the one introduced in Section 7.5 due to the coupling between affine and non-affine maps in different subdomains from one hand, the use of a different supremizer which is μ dependent, yielding a different reduced basis velocity approximation space from the other hand.* □

Remark 7.6.2 *We have the following computational costs to build reduced basis matrices, accounting also for the computation of supremizer components in the velocity space: $O(Q^a(\overline{Q}^b)^2 4N^2)$ for sub-matrix $\underline{A}$, $O((\overline{Q}^b)^2 2N^2)$ for $\underline{B}$, $O(Q^c(\overline{Q}^b)^3 8N^3)$ for $\underline{C}$, $O(\overline{Q}^b N)$ for $\underline{F}$ and $O(9N^3)$ for the "inversion" of the full reduced basis matrix (7.6.29) at each Newton iteration, where $Q^a=Q_T^a+Q_G^a$, $\overline{Q}^b=\overline{Q}_G^b+Q_T^b$, $\overline{Q}^c=\overline{Q}_G^c+Q_T^c$. Note that the quantities Q_G^a, Q_G^b and Q_G^c are depending only on the number of subdomains with affine mappings (R_G), while quantities Q_T^a, Q_T^b and Q_T^c are depending also on the number of "shape functions" ($\gamma(x)$ and $\omega(x)$) related with interpolation error (ε_{max}) and the number of subdomains with non-affine mappings (R_T).* □

Some numerical results based on the reduced basis approximation introduced in this section will be reported in Section 7.9.

7.7 Some preliminary results

For our first test on the use of reduced basis for Navier-Stokes equations we deal only with affine mapping on a rectangular domain ($R = 1$), parametrized by two quantities D and t, see Figure 7.1 (right). We have used the formulation introduced in Section 7.4 and have considered a forced flow. The parameters range is: $0.1 \leq D \leq 1.5$ and $0.1 \leq t \leq 1.5$.

- To solve the parametrized Navier-Stokes problem in the domain outlined in Figure 7.1 we have imposed zero Dirichlet conditions on the boundary Γ_D, Neumann homogeneous conditions on the inflow Γ_{Ni} and outflow Γ_{No} ($\tau_{\hat{\mathbf{n}}} = 0, \tau_{\hat{\mathbf{t}}} = 0$, where $\tau = (\nu \frac{\partial \mathbf{u}}{\partial \hat{\mathbf{n}}} - p\hat{\mathbf{n}})$, with $\hat{\mathbf{n}}$ and $\hat{\mathbf{t}}$ normal and tangential directions, respectively).

- We have considered a forcing term $\mathbf{f} = 10 \cdot (x, y)^T$ in order to create a flow acceleration, to have a non-zero velocity in y-direction and not only a parabolic velocity profile. Using the compact notation of Section 7.4 (7.4.10 and 7.4.11) and transformation (7.4.8) we get the following tensor for diffusion, divergence and transport forms, respectively:

$$\nu = \tilde{\nu} \begin{bmatrix} \frac{t}{D} & 0 \\ 0 & \frac{D}{t} \end{bmatrix}, \chi = \pi = \begin{bmatrix} t & 0 \\ 0 & D \end{bmatrix},$$

  where $\tilde{\nu} = 0.04 N s m^{-2}$ is the viscosity.

- Taylor-Hood finite elements have been used to build offline approximation basis functions: $\mathbb{P}^2 - \mathbb{P}^1$ elements for velocity (with supremizer) and pressure, respectively [127]. The problem has been solved using the *Pressure-Matrix Method*. The mean *Reynolds* number considered was of order 10^2 (a low Reynolds number). Note, in fact, that the change of the value of the parameter D (channel diameter) implies also a Reynolds number variation (by definition).

- At this step we have applied the reduced basis method and assembled the approximation spaces as described in Section 7.4. The basis assembling is based on the optimized procedure introduced in Section 5.4, see Figure 7.1 for the basis construction when increasing N.

- Figure 7.2 shows numerical results (mean and max H^1 and L^2 relative errors on velocity and pressure, respectively, on a large number of configurations) at different N. The reduced basis solutions have been compared directly with the approximate finite element solutions: the associate H^1 relative error for velocity and L^2 relative error for pressure are computed.

7.8 Furrowed channel test

Our second test on the use of reduced basis for Navier-Stokes equations deals with non-affine mapping on a rectangular domain ($R = 1$), considering a channel with an upper wall

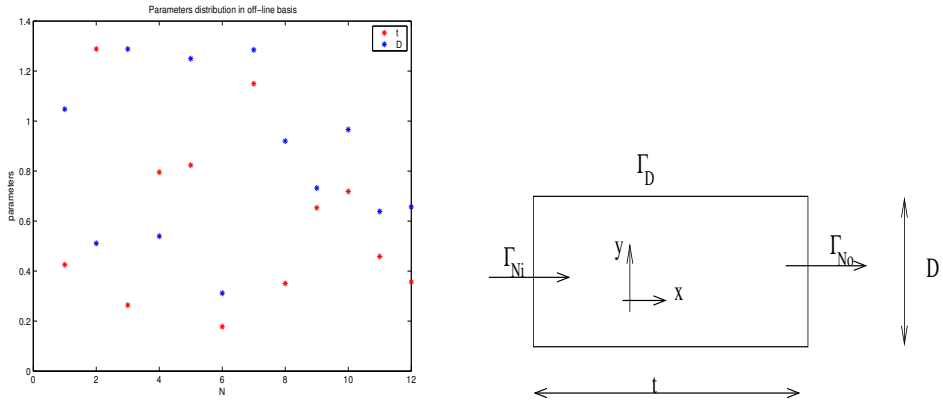

Figure 7.1: Parameters (D, t) distribution during basis assembling (left) and scheme of configuration (right).

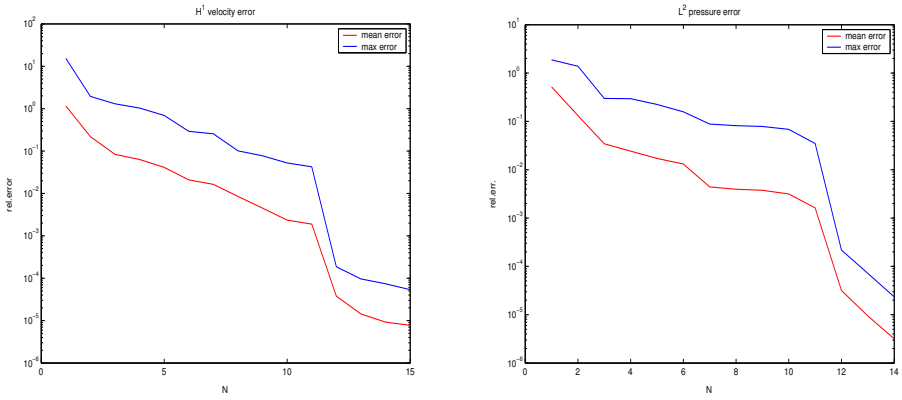

Figure 7.2: H^1 and L^2 relative errors on velocity and pressure, first test with 2 varying parameters (D, t).

parametrized by a sinusoidal law, see Figure 7.3 (left). This may be regarded as a simplified stenotic arterial flow, that was already investigated e.g. by Sobey and Stephanoff [143] and [148]. We have used the formulation introduced in Section 7.5. The test case is the same considered in Section 6.5.1 however here we consider Navier-Stokes equations whereas there we used Stokes equations. We briefly recall the assumptions that we have made during this study:

- To solve the parametrized Navier-Stokes problem in the domain outlined in Figure 7.3 we have imposed zero Dirichlet conditions on the boundary Γ_D, Neumann non-homogeneous conditions on the inflow Γ_{Ni} ($\tau_{\hat{\mathbf{n}}} = 1, \tau_{\hat{\mathbf{t}}} = 0$, where $\tau = (\nu \frac{\partial \mathbf{u}}{\partial \hat{\mathbf{n}}} - p\hat{\mathbf{n}})$, with $\hat{\mathbf{n}}$ and $\hat{\mathbf{t}}$ normal and tangential directions, respectively) and Neumann homogeneous conditions on outflow Γ_{No} ($\tau_{\hat{\mathbf{n}}} = 0, \tau_{\hat{\mathbf{t}}} = 0$).

- We consider one parameter μ ranging in $[-0.8, 0.8]$ to describe the upper arterial wall in the physical domain, through $\hat{x}_2 = f(\hat{x}_1, \mu) = 1 + \mu sin(2\pi\hat{x}_1)$ (we have a single

domain subject to a unique non-affine mapping). Figures 7.3-7.5 show some simulations to better describe the fluid dynamics phenomena involved in this case of study. The upper curved wall is responsible of the changing of the channel section and so of the velocity gradient. Interesting phenomena to be "captured" by reduced basis method are the vertical velocity behavior (see Figure 7.5 on the right) and the development of a secondary flow (to be added to the mainstream channel) when $|\mu|$ increases (see Figure 7.4 on the right). In Sobey [143] an accurate study of steady (and unsteady) flows has been carried out dealing with furrowed channels at different Reynolds number, in particular focusing the attention over the secondary flows in the hollow zone of the channel. In our case the Reynolds ranges between 10^2 and $4 \cdot 10^3$.

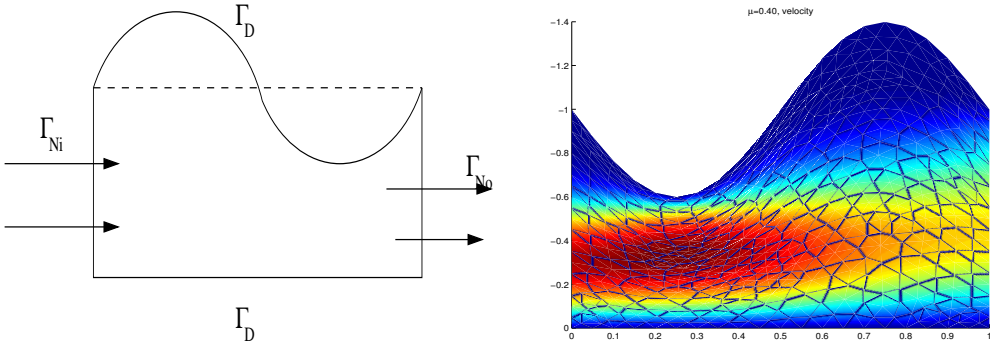

Figure 7.3: Geometrical scheme for curved wall test model problem (left) and velocity (absolute value) for $\mu = 0.4$, $Re = 100$ (right). The colorbar is the same as in Figure 6.1.

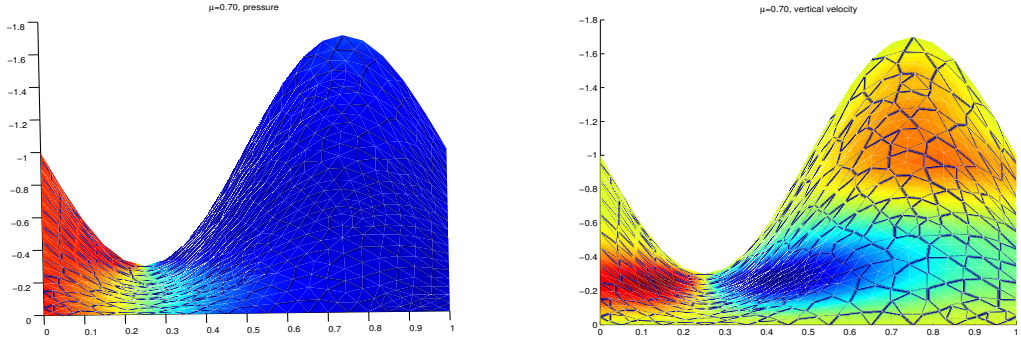

Figure 7.4: Pressure (left) and vertical velocity (right), for $\mu = 0.7$ and $Re = 100$.

Referring to Section 7.5 we have $\Omega_G = \emptyset$ and $\Omega_T = \Omega$, so $R_T = 1$.
The coordinate transformation is $\mathcal{T} : \hat{\Omega} \to \Omega$, $\mathbf{x} = \mathcal{T}(\hat{\mathbf{x}})$, with

$$(x_1, x_2) = \mathcal{T}(\hat{x}_1, \hat{x}_2) = (\hat{x}_1, \frac{1}{f(\hat{x}_1, \mu)}\hat{x}_2) \tag{7.8.1}$$

in Ω. Then,

$$d\hat{x}_1 d\hat{x}_2 = f(x_1, \mu) dx_1 dx_2,$$

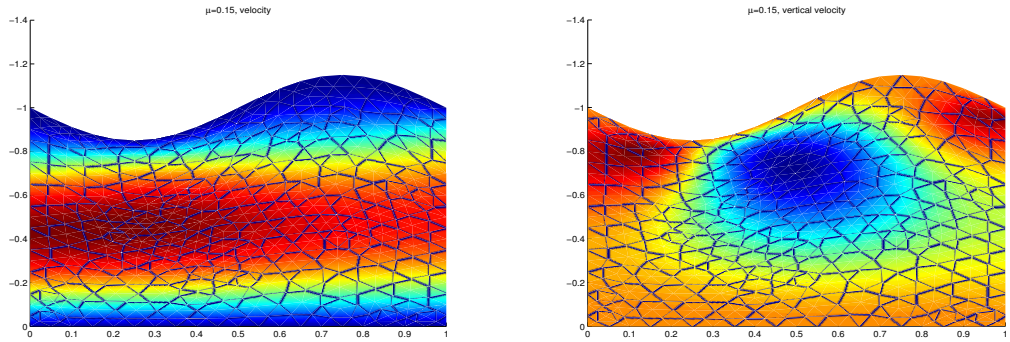

Figure 7.5: Absolute value of velocity (left) and vertical velocity (right), for $\mu = 0.15$ and $Re = 100$.

and the following relations hold:

$$\begin{cases} \frac{\partial \hat{\mathbf{u}}}{\partial \hat{x}_2} = \frac{1}{f(x_1,\mu)} \frac{\partial \mathbf{u}}{\partial x_2}, \\ \frac{\partial \hat{\mathbf{u}}}{\partial \hat{x}_1} = \frac{\partial \phi}{\partial x_1} - x_2 \frac{f_{x_1}(x_1,\mu)}{f(x_1,\mu)} \frac{\partial \mathbf{u}}{\partial x_2} \quad (with\ f_{x_1} := \frac{df}{dx_1}). \end{cases} \tag{7.8.2}$$

$$\nabla \cdot \hat{\mathbf{u}} = \frac{\partial u_1}{\partial x_1} - x_2 \frac{f_{x_1}(x_1,\mu)}{f(x_1,\mu)} \frac{\partial u_1}{\partial x_2} + \frac{1}{f(x_1,\mu)} \frac{\partial u_2}{\partial x_2}. \tag{7.8.3}$$

Using the compact notation of Section 7.5 (7.5.3 and 7.5.4) and transformation (7.8.1) we get the following tensor for diffusion and divergence (and advection) forms, respectively:

$$\nu_T = \nu \begin{bmatrix} f(x_1,\mu) & -f'_{x_1}(x_1,\mu)x_2 \\ -f'_{x_1}(x_1,\mu)x_2 & \frac{1}{f(x_1,\mu)} + \frac{f'^2_{x_1}(x_1,\mu)}{f(x_1,\mu)} {x_2}^2 \end{bmatrix}; \tag{7.8.4}$$

$$\chi_T = \pi_T = \begin{bmatrix} f(x_1,\mu) & -f'_{x_1}(x_1,\mu)x_2 \\ 0 & 1 \end{bmatrix}; \tag{7.8.5}$$

where ν is the viscosity $[Nsm^{-2}]$ whose value was varied in simulating flows at different Reynolds number. Referring to notation of Reminder 7.5.1 we get 5 different coefficient functions $g_M^j(x,\mu)$ to expand.

Reminder 7.8.1 *We recall here that the coordinate transformation (7.8.2) used in this example is the same one used in Chapters* 3 *and* 4. □

- We apply empirical interpolation (7.5.5 and 7.5.6) to the tensors (7.8.4 and 7.8.5) and we impose a maximum interpolation error ε_{max}, thus considering different M_{max} "shape functions" for each $g_M^j(x,\mu)$. Each $g_M^j(x,\mu)$ represents a different coefficient for a different term of our problem ($j = 5$ in this test case). Owing to empirical interpolation we expand each tensor component to apply the effectively affine decomposition:

$$\nu_T = \nu \begin{bmatrix} \Sigma_{m=1}^{M_{11}^a} \beta_{11m}(\mu)\gamma_{11m}(x) & \Sigma_{m=1}^{M_{12}^a} \beta_{12m}(\mu)\gamma_{12m}(x) \\ \Sigma_{m=1}^{M_{21}^a} \beta_{21m}(\mu)\gamma_{21m}(x) & \Sigma_{m=1}^{M_{22}^a} \beta_{22m}(\mu)\gamma_{22m}(x) \end{bmatrix}.$$

Note that this tensor is symmetric. Moreover,

$$\chi_T = \pi_T = \begin{bmatrix} \Sigma_{m=1}^{M_{11}^b} \alpha_{11m}(\mu)\omega_{11m}(x) & \Sigma_{m=1}^{M_{12}^b} \alpha_{12m}(\mu)\omega_{12m}(x) \\ 0 & 1 \end{bmatrix}.$$

The index r referring to every different subdomain is omitted (in this case $R = 1$).

- At this step we may apply the reduced basis formulation to this case and assemble the approximation spaces Y_N (7.4.14) and Q_N (7.4.13).

7.8.1 Results for low Reynolds number

We report some numerical results dealing with the solution of the furrowed channel rebuilt by reduced basis method. First we considered low Reynolds number (~ 100). Figures 7.6 and 7.7 show convergence results (mean and max H^1 and L^2 relative errors on velocity and pressure, respectively, testing a large number of configurations) at different N and at different imposition of max interpolation error ε_{max}. At the end of the test we have carried out also a comparison between empirical interpolation (using $g_M^j(x,\mu)$) and true functions ($g^j(x,\mu)$). We can see that for $\varepsilon_{max} \leq 10^{-8}$ we have accurate results that are not dominated or affected by interpolation error. When the interpolation error is dominating, the reduced basis error is characterized by a constant "plateau" and is not diminished by increasing N (see for example the case in which $\varepsilon_{max} \geq 10^{-6}$).

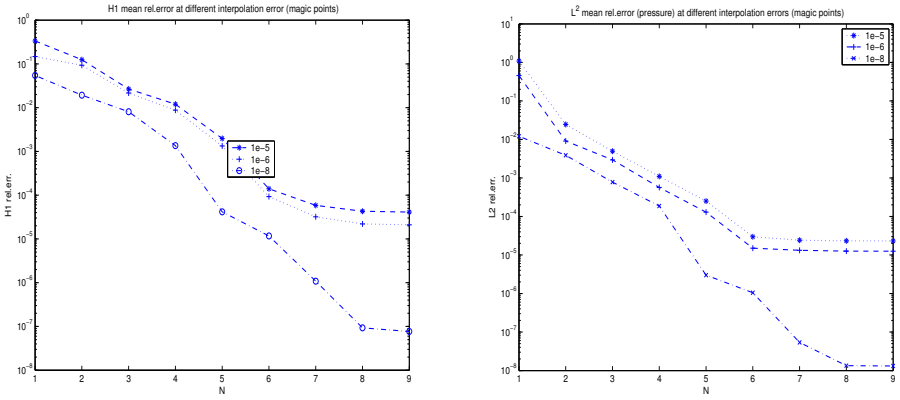

Figure 7.6: H^1 and L^2 relative mean error on velocity and pressure ($\nu = 0.1$) at different ϵ_{max} imposed on all $g_M^j(x,\mu)$ (great number of testing configurations).

7.8.2 Results for higher Reynolds number

A further test stage has been devoted to the increase of Reynolds number ($\sim 4 \cdot 10^3$). We have reported in Figure 7.8 convergence results using a max interpolation error $\varepsilon_{max} \geq 10^{-6}$. The comparison is always made between the "true" approximated solution by finite element method and the "interpolated" one by reduced basis.

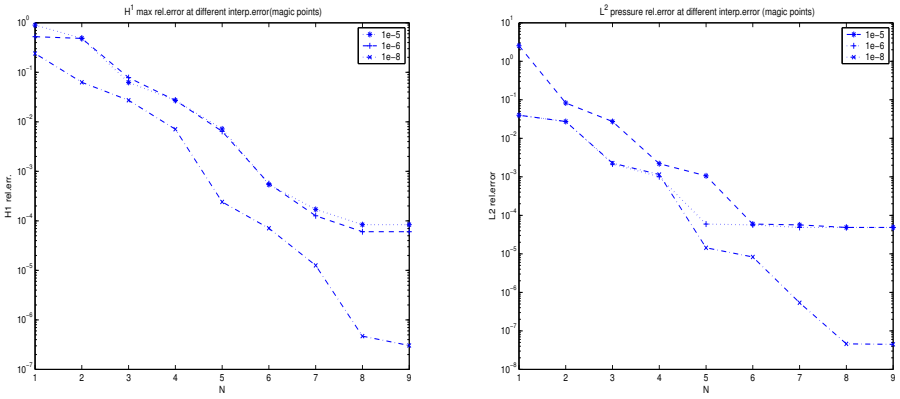

Figure 7.7: H^1 and L^2 relative max error on velocity and pressure ($\nu = 0.1$) at different ϵ_{max} imposed on all $g_M^j(x,\mu)$ (great number of testing configuration).

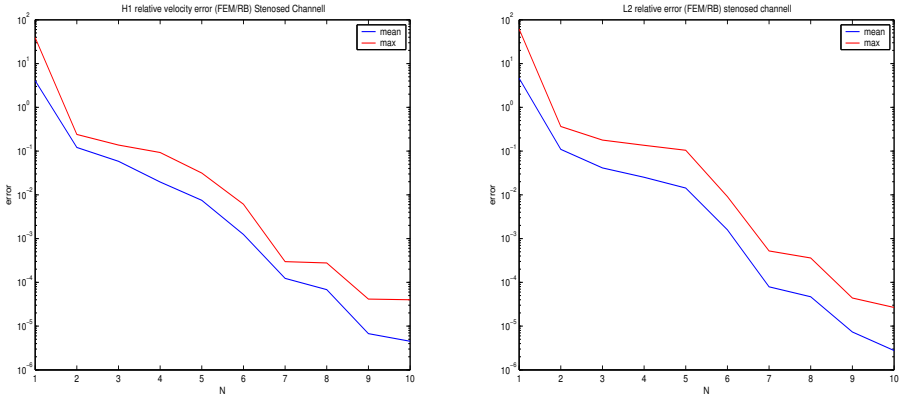

Figure 7.8: H^1 and L^2 relative error (max and mean) on velocity and pressure ($\nu = 0.04$) (testing a great number of configurations).

7.8.3 Reduced basis computational costs

At the end of this section we make some remarks on the computational costs in using the reduced basis in the online stage at different Reynolds number. This completes Remark 7.6.2 that was concerned with the assembling and computational costs. For simplicity we consider the case of the problem of the furrowed channel with one varying parameter and at different Reynolds number (at different viscosity values). Figure 7.9 shows online reduced basis computational cost (cputime, Pentium M 1.80 GHz, 1.0 Gb of Ram, IBM®T42 ThinkPad) for increasing N, compared with the computational cost of a finite element numerical simulation; the Reynolds number is $Re \leq 400$. We can see that reduced basis computational costs are $\sim 20\%$ of the finite element offline solutions if we choose $N = 12$ corresponding to an H^1 error on velocity of $O(10^{-6})$, as shown in the picture on the right. The reduces basis approximation spaces have been optimized during the assembling procedures. Increasing the Reynolds number ($400 \leq Re \leq 4000$) we can see how the computational saving of reduced basis techniques

are at least of two orders of magnitude (i.e 1%) as shown in Figure 7.10, where on the right we have also a zoom representing online computational cost when increasing N. Results in reality depend on the choice of the initial guess for Newton iterations: in our case we have used Stokes solution (already calculated and stored). Other elements influencing computational costs are the setting of the tolerance for the Newton algorithm (difference between the solutions of two successive iterations), in our case set to 10^{-8}. The numerical approximation of steady Navier-Stokes equations has been carried out by using a parametrized version of *MLife*, a FEM library [139] in Matlab-PDE toolbox environment where we have considered $\mathbb{P}^2 - \mathbb{P}^1$ elements for velocity and pressure, respectively, over a triangulation of $O(10^4)$ elements (see also Gresho and Sani [46]). The sparse linear system has been solved using *Pressure-Matrix Method* [127] (which is a block LU type decomposition of the system matrix) to compute velocity in two steps and to decouple the calculation of pressure from velocity (see [127]). The iterative methods used to solve the linearized system at each iteration have been *GMRES* and *Bi-CGSTAB* [129]. To improve computational efficiency we have used *Cahouet-Chabard Preconditioner*, see [22].

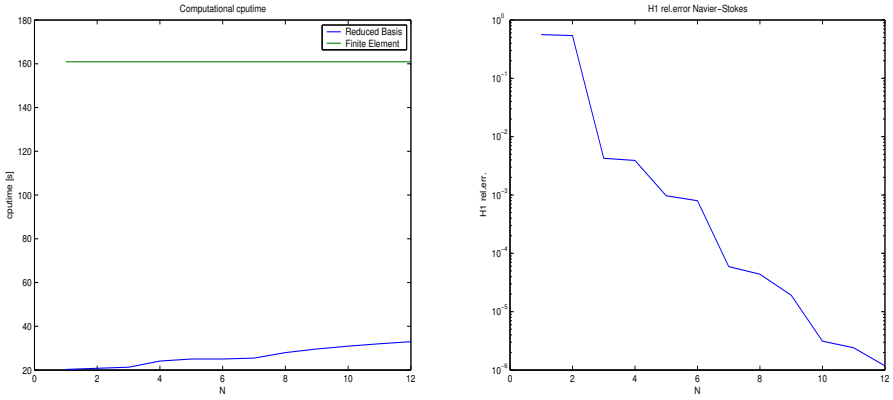

Figure 7.9: Reduced basis online mean computational costs in comparison with finite element simulation (left) and H^1 reduced basis velocity error increasing N (right) for channel flow at low Reynolds numbers.

We observe that the use of reduced basis is providing real time solutions (or related outputs) of a non-linear parametrized problems, whose solution would be quite expensive even if considering efficient FEM solvers. The importance of real time accurate solutions increases when considering optimization problems involving also non-affine geometrical parametric dependence, as seen in the example of the furrowed channel.

7.9 The bypass problem

We retake into consideration the parametrized bypass of Figure 7.11 configuration with the vector of parameters $\boldsymbol{\mu} = \{t, D, L, S, H, \theta, \upsilon\} \in \mathcal{D}^{\mu} \subset \mathbb{R}^P$ with $\mathcal{D}^{\mu}$ given by:
$[t_{min}, t_{max}] \times [D_{min}, D_{max}] \times [L_{min}, L_{max}] \times [S_{min}, S_{max}] \times [H_{min}, H_{max}] \times [\theta_{min}, \theta_{max}] \times$

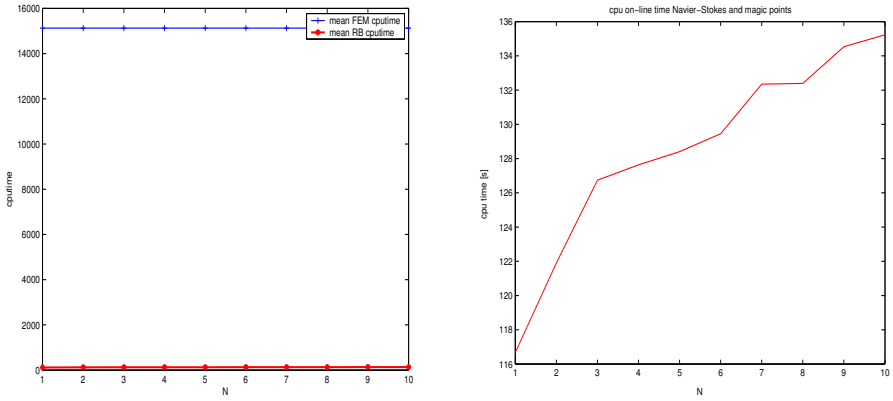

Figure 7.10: Reduced basis online mean computational costs for channel flow at higher Reynolds numbers.

$[\upsilon_{min}, \upsilon_{max}]$, already considered in Section 6.5.2. This test problem deals both with affine and non-affine parameters dependence in different subdomains and it is the application of the formulation introduced in Section 7.6. The aim of the test is to combine the study of affine and non-affine terms in the same non-linear problem by varying different geometrical parameters and then to test reduced basis convergence, extract output information and a sensitivity analysis on parameters. Referring to notation in Section 7.6 we have $R_G = 3$ (number of subdomains with affine dependence, i.e. $\Omega^2, \Omega^3, \Omega^4$), $R_T = 1$ (number of subdomains with non-affine dependence, i.e Ω^1). The coordinate transformation in Ω^1 with non-affine parameter dependence is given by:

$$\begin{cases} x_1 = \frac{1}{H}\hat{x}_1 \\ x_2 = \frac{1}{t}(\hat{x}_2 - (\upsilon H^2 x_1(x_1 - 1) + H x_1 \tan(\theta))). \end{cases} \tag{7.9.1}$$

We recall that the role of parameters t and H is to stretch subdomain Ω^1 (as L, S, D stretch the remaining subdomains), the parameter υ introduces a curvature in the walls of the incoming branch of the bypass and θ is responsible for a rigid rotation by letting the graft angle vary. The tensors for *viscous bilinear terms* are given by:

$$\nu_T^1 = \nu \begin{bmatrix} \frac{t}{H} & -(\tan\theta + 2\upsilon H x_1 - \upsilon H) \\ -(\tan\theta + 2\upsilon H x_1 - \upsilon H) & \frac{(1+(\tan\theta+2\upsilon H x_1 - \upsilon H)^2)}{t} H \end{bmatrix}; \tag{7.9.2}$$

$$\nu_G^2 = \nu \begin{bmatrix} \frac{S}{D} & 0 \\ 0 & \frac{D}{S} \end{bmatrix}; \nu_G^3 = \nu \begin{bmatrix} \frac{t}{D} & 0 \\ 0 & \frac{D}{t} \end{bmatrix}; \ \nu_G^4 = \nu \begin{bmatrix} \frac{L}{D} & 0 \\ 0 & \frac{D}{L} \end{bmatrix}. \tag{7.9.3}$$

The tensors for *pressure, divergence and transport terms* are given by:

$$\chi_T^1 = \pi_T^1 = \begin{bmatrix} t & -H(\tan\theta + 2\upsilon H x_1 - \upsilon H) \\ 0 & H \end{bmatrix}; \ \chi_G^2 = \pi_G^2 = \begin{bmatrix} S & 0 \\ 0 & D \end{bmatrix}; \tag{7.9.4}$$

$$\chi_G^3 = \pi_G^3 = \begin{bmatrix} t & 0 \\ 0 & D \end{bmatrix}; \ \chi_G^4 = \pi_G^4 \begin{bmatrix} L & 0 \\ 0 & D \end{bmatrix}. \tag{7.9.5}$$

We apply empirical interpolation expansion to the components of tensors ν_T^1, χ_T^1 and π_T^1 and we build the reduced basis approximation spaces for velocity and pressure.

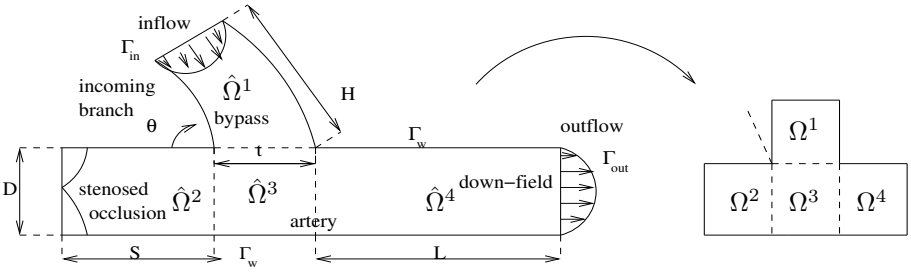

Figure 7.11: Geometrical scheme for the bypass test problem (physical domain and reference one).

We have carried out some tests based on the same geometry considering five different varying parameters (we have frozen L and H). In particular we are interested in varying graft angle θ and curvature υ (defining the upstream geometry) and the ratio $\frac{t}{D}$. In Figures 7.12 and 7.13 we report numerical results (max and mean H^1 errors on velocity and L^2 errors for pressure) considering several configurations at different N for two different maximum interpolation error $\varepsilon_{max} = 10^{-5}$ and then $\varepsilon_{max} = 10^{-8}$ to avoid to have interpolation error dominating our approximation with the constant "plateau" in error plots.

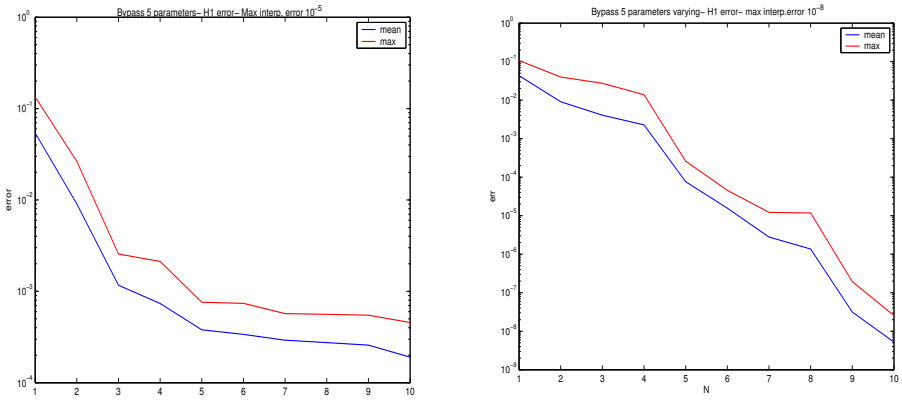

Figure 7.12: H^1 relative errors on velocity with different ϵ_{max} interpolation error imposed on all $g_M^j(x,\mu)$ (testing hundreds of different configurations with 5 different parameters varying).

7.9.1 Outputs sensitivities

We conclude this section with two different studies on the bypass problem providing a comparison between Stokes and Navier-Stokes solutions (and outputs) and some considerations about the influence of curvature of the upper stream geometry. The ratio $\frac{t}{D}$ is the most important parameter and it is responsible of recirculation in the host artery, but also curvature

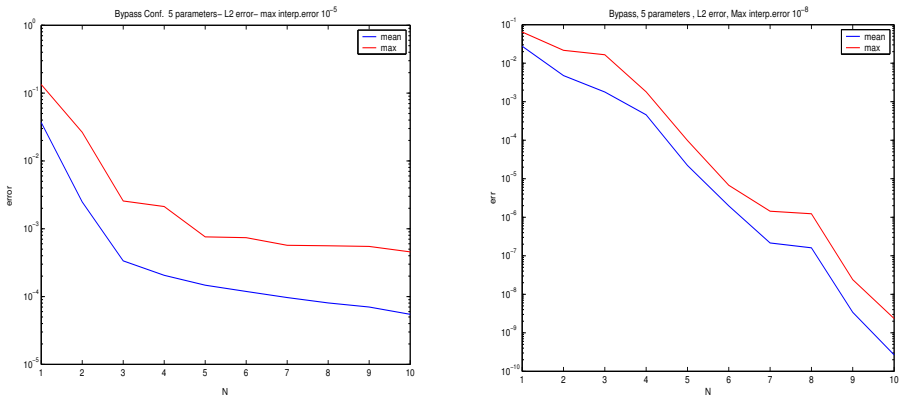

Figure 7.13: L^2 relative errors on pressure with different ϵ_{max} interpolation error imposed on all $g_M^j(x,\mu)$ (testing hundreds of configurations with 5 different parameters varying).

has a role. The ratio $\frac{S}{D}$ becomes important if we freeze $\frac{t}{D}$ and so the graft angle θ.
Figure 7.14 (left) shows a comparison between the vorticity output functional calculated with Stokes and Navier-Stokes equations. We can see that the "low fidelity" method is a good approximation only if the ratio $\frac{t}{D}$ is less than unity and this is our case, otherwise if the bypass diameter t is too small with respect to the arterial diameter D a strong recirculation arises in the host vessel and also vorticity increases considerably. These phenomena are not well captured by the linearized model. An optimized value of quantity $\frac{t}{D}$ is in the range $[0.85 - 0.96]$. This test gives us important information about the fidelity of our model and it allows a generalization of results available in the literature, especially provided by experimental research activity and surgical experience.
Figure 7.14 (right) shows the behavior of vorticity varying the curvature of the upstream (inflow) geometry. Increasing the curvature υ the vorticity diminishes: this behavior can be explained by the fact that curvature is guiding the flow more smoothly. An interesting analysis can be obtained introducing the *Dean* number, representing the ratio of the square root of the product of the inertial and centrifugal forces to the viscous forces, defined as follows

$$De = 4\Big[\frac{D}{R}\Big]^{\frac{1}{2}} Re, \tag{7.9.6}$$

where R is the radius of curvature and Re the Reynolds number. See also Doorly and Sherwin in [141]. If we do not have curvature the Dean number is equal to zero. In the case we have considered, the range of the Dean number was $[0, 2.31 \cdot Re]$. By increasing the Dean number (and so *curvature*, the inverse of the curvature radius) makes the peak velocity to increase, but at the same time the velocity peak is displaced away from the centre of curvature. Note that $De = 0$ corresponds to a case in which we have a centered velocity profile of *Hagen-Poiseuille* type. In our case the displacement of the peak velocity profile allows the blood to be driven into the host vessel more smoothly and to better adapt the upstream inflow condition at the junction geometry. In our case the critical zone of the bypass near the upper wall has lower mean velocity. The introduction of the upstream curvature has been discussed also in

Papaharilaou, Doorly and Sherwin [108]. Results in Figure 7.14 (right) refers to a graft angle of 45 degree and a ratio $\frac{t}{D} = 1$.

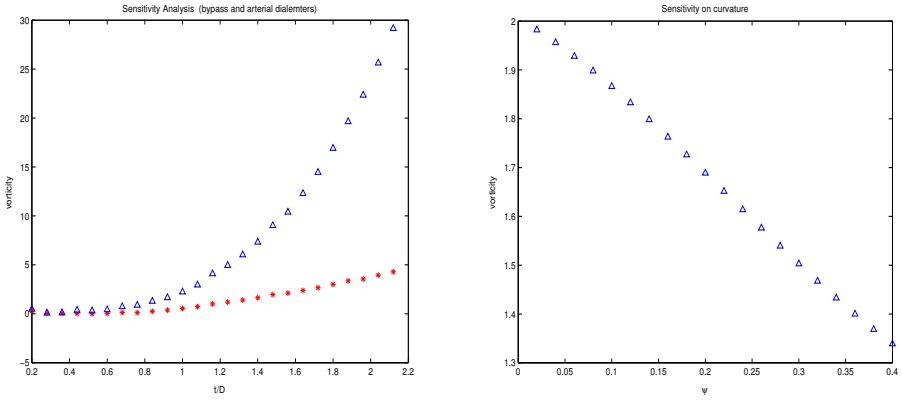

Figure 7.14: Distributed vorticity $[m^2 s^{-1}]$ varying $\frac{t}{D}$ and comparison between Stokes $(*)$ and Navier-Stokes (Δ) flows (left); distributed vorticity $[m^2 s^{-1}]$ and curvature (right).

7.10 Conclusions

In this chapter we have extended the use of reduced basis methodology to non-linear problems in domains with non-affine parametric dependence. This extension has allowed us (i) to get useful and more realistic information about parametrized bypass configuration; (ii) to compare previous results from low fidelity method (Stokes based) with the new higher fidelity ones; (iii) to use the reduced basis as an optimization method itself in our haemodynamic application and not only as a pre-process optimization tool to investigate a coarse bridge configuration.
When we are considering problems with an increasing complexity, such as the ones with non-linearities and non-affine parametrization, the use of reduced basis method becomes even more competitive and computational savings are more relevant.
In the next chapter we provide some perspectives in developing reduced basis for optimal control problems but with results not specifically oriented to our bypass application, but more oriented on haemodynamics related problems.

Chapter 8

Perspectives in Flow Control by Reduced Basis Methods

In this conclusive chapter we provide some perspectives on the use of reduced basis in parametrized flow control problems. We consider a different kind of problem: an advection-diffusion scalar problem in order to investigate possible extensions of the use of reduced basis for optimal control problems in parametrized domains by combining the solutions of state and adjoint problems. With this chapter we conclude the guidelines which led us from numerical simulation to optimal control by reduced basis methods.

8.1 Introduction

Control problems solved with the reduced basis methods were already presented by Ito and Ravindran since 1998 in [62], [63], and [64] without considering multi-parametric problems and geometrical parameters, and so adopting different solution procedures. Parameters can be divided into three classes: control (i.e depending, in some way, on control function), physical (like velocity field or diffusivity) and geometrical (i.e. related to different domain configuration). We are going consider all these parameter classes to be able to solve many different "kind" of control problems.
As a case study, we consider an advection-diffusion problem which can be seen in the framework of life sciences, considering, for example, an application related with the release of drugs or chemical elements (solutes) in blood or, more generally, physiological flows. See the work by Quarteroni, Veneziani and Zunino in [130] and [131]. The modelling of advection-diffusion phenomena can be useful in biomedical field for the setting, for example, of appropriate peritoneal dialysis procedures or the design of drug eluting stents. See, for example, Zunino [170]. The goal can be the regulation of the substance emission by some sources in order to keep concentration at a desired and/or acceptable level over an observation area. A similar problem arises in environmental fluid dynamics. See, for example, [122].
In Section 8.2 we formulate a generic control problem for a linear time-independent advection-diffusion equation using Lagrangian formulation. In Section 8.3 we describe the reduced basis

approximation for the solution of the parametrized equations governing the control problem. In Section 8.4 we describe very briefly an example of optimal flow control problem by applying the formulation presented in Section 8.2 to derive our model. In Section 8.5, 8.6 and 8.7 we present the parametrized state and adjoint equations, some results and an example in the case of control, physical and geometrical input, respectively. In Section 8.8 we report some concluding remarks and further perspectives. Section 8.9 is a quick note on time dependent problems. Other very recent applications of reduced basis methods are provided in the field of optimal control by Grepl [44] (unsteady advection-diffusion problems) and by Nguyen [103] in the field of inverse problems with non-affine parametric dependence.

8.2 Optimal control problem for advection-diffusion equations

8.2.1 A formulation for optimal control problem based on Lagrangian

We recall that the goal of an optimal control problem is to find the function $u \in \mathcal{U}$ in order to minimize the *cost functional* $J = J(u)$, where w is the solution of the *state equation*, i.e.:

$$find\ u \in \mathcal{U}\ so\ that\ J(u)\ is\ minimized\ and\ Aw = f + Bu, \forall v \in \mathcal{V}, \tag{8.2.1}$$

with $\mathcal{U}$ and $\mathcal{V}$ being two Hilbert spaces. The differential operator A is an elliptic operator defined on $\mathcal{V}$ with values in $\mathcal{V}'$, B is an operator defined on $\mathcal{U}$ and valued in $\mathcal{V}'$ which introduces control variable u in the state equation, f is a source field. To analyze optimal control problems, we adopt the *Lagrangian* approach [15], equivalent to optimal control classical analysis, developed for example by Lions in [82]. By introducing the Lagrangian multiplier p and the Lagrangian functional:

$$\mathcal{L}(w, p, u) = J(u) + \langle p, Aw - f - Bu \rangle,$$

the unique solution of problem (8.2.1) is determined by solving the PDE system:

$$\nabla \mathcal{L}(w, p, u) = 0.$$

The weak form of the state equation is:

$$a(w, \varphi) = (f, \varphi) + b(u, \varphi),\ \forall \varphi \in \mathcal{V},$$

where $a(\cdot, \cdot)$ is the bilinear form associated to the elliptic operator and $b(\cdot, \cdot)$ is the bilinear form associated to the control term Bu. The cost functional can be expressed as:

$$J(u) = \frac{1}{2}\|Cw - z_d\|^2 + \frac{1}{2}n(u, u), \tag{8.2.2}$$

where operator C brings state variable w into the observation space (an Hilbert space), z_d is the desired observation function, that is the optimal control problem goal, and $n(\cdot, \cdot)$ is an Hermitian form. Let's denote the product $(\cdot, \cdot)$ as the L^2 scalar product. The Lagrangian functional con be expressed as:

$$\mathcal{L}(w, p, u) = J(u) + b(u, p) + (f, p) - a(w, p),$$

so that the optimal control solution can be calculated solving the following problem:

$$find\ (w,p,u) \in \mathcal{V}\times\mathcal{V}\times\mathcal{U}:\ \nabla\mathcal{L}(w,p,u)[(\varphi,\phi,\psi)] = 0,\ \forall(\varphi,\phi,\psi)\in\mathcal{V}\times\mathcal{V}\times\mathcal{U}.$$

We have then:

$$\begin{cases} \mathcal{L}_w[\varphi] = (Cw - z_d, C\varphi) - a(p,\varphi) = 0,\ \forall\varphi\in\mathcal{V}, \\ \mathcal{L}_p[\phi] = (f,\phi) + b(u,\phi) - a(w,\phi) = 0,\ \forall\phi\in\mathcal{V}, \\ \mathcal{L}_u[\psi] = b(p,\psi) + n(u,\psi) = 0,\ \forall\psi\in\mathcal{U}. \end{cases}$$

The differential $\mathcal{L}_p$ corresponds to the weak form of the state equation, $\mathcal{L}_w$ to the *adjoint equation* and $\mathcal{L}_u$ is an optimal control constraint. The variable p is the adjoint variable and it expresses the cost functional sensitivity to the variations of the control variable u.
The optimal control constraint $\mathcal{L}_u[\psi]$ can be related to the strong derivative $J'(u)$ by means of the cost functional definition (8.2.2) and the Riesz theorem. In particular we can write $\mathcal{L}_u[\psi] = \langle J'(u),\psi\rangle = (J'(u),\psi)$, since the functional $\mathcal{L}_u[\psi]$ is linear and bounded and ψ belongs to an Hilbert space [127].

To solve the control problem, we adopt an iterative method. Starting from an initial value for control variable u_0, we solve the state equation; then we compute cost functional value and we resolve the adjoint equation. Once p is known, we determine cost functional derivative J' and apply a suitable stopping criterium. If this criterium is not fulfilled, we start an iterative process on control function u; we adopt, for instance, the *steepest descent* method:

$$u^{k+1} = u^k - \tau^k J'(u^k), \tag{8.2.3}$$

where τ^k is a relaxation parameter, whose value can be determined by control problem properties, see for example Agoshkov [6]. The iterative process ends with the optimal control criterium fulfillment.

8.2.2 Optimal control problem governed by advection-diffusion equations

Let us consider the following state equation of our problem:

$$\begin{cases} -\nabla\cdot(\nu\nabla w) + \mathbf{V}\cdot\nabla w = u\ in\ \ \Omega\subset\mathbb{R}^2, \\ w = 0 \quad on\ \Gamma_D, \\ \frac{\partial w}{\partial\hat{\mathbf{n}}} = 0 \quad on\ \Gamma_N, \end{cases} \tag{8.2.4}$$

where w is the state variable, u the control function defined on the domain, $\mathbf{V}$ is the velocity field and ν is the diffusivity, depending on the domain coordinates $\mathbf{x} = (x,y)^T$. A homogeneous Dirichlet condition is imposed on inflow boundary $\Gamma_D := \{\mathbf{x}\in\partial\Omega\ :\ \mathbf{V}(\mathbf{x})\cdot\hat{\mathbf{n}}(\mathbf{x}) < 0\}$, where $\hat{\mathbf{n}}(\mathbf{x})$ is the unit vector directed outward, and a homogeneous Neumann condition on the rest of the boundary ($\Gamma_N := \partial\Omega\backslash\Gamma_D$). Defining $H^1_{\Gamma_D}:= \{v\in H^1(\Omega)\ :\ v|_{\Gamma_D} = 0\}$, the weak form of the state equation is:

$$find\ w\in H^1_{\Gamma_D}\ :\ a(w,\varphi) = F(\varphi;u),\ \forall\varphi\in H^1_{\Gamma_D},$$

where

$$a(w,\varphi) := \int_\Omega \nu \nabla w \cdot \nabla \varphi \; d\Omega + \int_\Omega \mathbf{V} \cdot \nabla w \; \varphi \; d\Omega, \tag{8.2.5}$$

$$F(\varphi; u) := \int_\Omega u\varphi \; d\Omega. \tag{8.2.6}$$

We then define the observation of the system on a part D of the domain ($D \subset \Omega$) with the following cost functional:

$$J(u) = \frac{1}{2} \int_D \Big(w(u) - z_d)^2 dD,$$

where z_d is the desired observation.
It is now possible to write the Lagrangian functional:

$$\mathcal{L}(w,p,u) = J(u) + F(p;u) - a(w,p),$$

where $w, p \in H^1_{\Gamma_D}(\Omega)$ and $u \in L^2(\Omega)$. By differentiating it with respect to the state variable, we obtain the weak form for the adjoint equation:

$$find \; p \in H^1_{\Gamma_D} \; : \; a^{ad}(p,\phi) = F^{ad}(\phi; w), \; \forall \varphi \in H^1_{\Gamma_D},$$

where

$$a^{ad}(p,\phi) := \int_\Omega \nu \nabla p \cdot \nabla \phi \; d\Omega + \int_\Omega \mathbf{V} \cdot \nabla \phi \; p \; d\Omega, \tag{8.2.7}$$

$$F^{ad}(\phi, w) := \int_\Omega (w - z_d) \; g(x,y) \; \phi \; dD, \tag{8.2.8}$$

whose strong form is:

$$\begin{cases} -\nabla \cdot (\nu \nabla p + \mathbf{V} \cdot p) = m_D (w - z_d) \; in \;\; \Omega, \\ p = 0 \quad on \; \Gamma_D, \\ \nu \frac{\partial p}{\partial \hat{\mathbf{n}}} + \mathbf{V} \cdot \hat{\mathbf{n}} \; p = 0 \quad on \; \Gamma_N, \end{cases}$$

where m_D is the characteristic function of the subdomain D.
By differentiating the Lagrangian functional with respect to the control function u, we obtain the weak form of the optimal condition constraint:

$$\mathcal{L}_u[\psi] = \langle J'(u), \psi \rangle = (J'(u), \psi) = \int_\Omega p\psi \; d\Omega = 0, \;\; \forall \psi \in \text{Ł}^2(\Omega).$$

We solve our problem using an iterative method where the variation of control function is led by a gradient method. From the optimal control constraint, we can derive a stopping criterium for the iterative method. At $k-th$ step of the iterative method:

- we solve state equation

$$find \; w^k \in H^1_{\Gamma_D} \; : \; a(w^k, \varphi) = F(\varphi; u^k), \; \forall \varphi \in H^1_{\Gamma_D};$$

- we solve adjoint equation

$$find \; p^k \in H^1_{\Gamma_D} \; : \; a^{ad}(p^k, \phi) = F^{ad}(\phi; w^k), \; \forall \varphi \in H^1_{\Gamma_D};$$

- if the stopping criterium is not satisfied, we update control function

$$u^{k+1} = u^k + \delta u^k \qquad \delta u^k = -\tau^k p^k.$$

The stopping criterium adopted [32] is:

$$\|p^k\|_{L^2} < tol, \tag{8.2.9}$$

that is we check if adjoint variable p L^2-norm is too small (according to our fixed tolerance tol) to produce a significative variation δu^k on the new control function u^{k+1}.

8.2.3 Numerical discretization and stabilization

Since the state and adjoint equations are both advection-diffusion equations and transport term can dominate the diffusion one, a suitable stabilization is needed. We adopt the *Stabilized Lagrangian* [32], instead of stabilizing separately state and adjoint equations in a conventional manner [127]. In this way, stabilization is not only based on a strongly consistent method, but also there is coherence between state and adjoint stabilized equations.
In this thesis we have adopted the approach "optimize-then-discretize" to solve optimal control problems, as seen in Chapter 2, 3 and 4; we have firstly formulated an optimality condition, from this condition we have built an adjoint problem and then we have discretized both state and adjoint equations. In this chapter we use the same approach to be coherent; an alternative approach would be the so-called "discretize then optimize" which has been considered for the same kind of problem in [124].
Indicating with the subscript h the discretized quantities, the stabilized state equation reads:

$$find\ w_h \in \mathrm{X}_h \ :\ a_h(w_h, \varphi_h) = F_h(\varphi_h; u_h),\ \forall \varphi_h \in \mathrm{X}_h, \tag{8.2.10}$$

where:

$$a_h(w_h, \varphi_h) := a(w_h, \varphi_h) -$$

$$\sum_{K \in \mathcal{T}_h} \delta_K \int_K \Big(-\nabla \cdot (\nu \nabla w_h) + \mathbf{V} \cdot \nabla w_h \Big) \Big(-\nabla \cdot (\nu \nabla \varphi_h + \mathbf{V} \varphi_h) \Big)\, dK,$$

$$F_h(\varphi_h; u_h) := F(\varphi_h; u_h) - \sum_{K \in \mathcal{T}_h} \delta_K \int_K u_h \Big(-\nabla \cdot (\nu \nabla \varphi_h + \mathbf{V} \varphi_h) \Big)\, dK.$$

The terms $a(w_h, \varphi_h)$, $F(\varphi_h; u_h)$ are defined in (8.2.5), (8.2.6) and w_h, u_h are discrete approximation of the functions w, u. The space $\mathrm{X_h} \subset H^1_{\Gamma_D}$ is the finite element one. The finite element solution is computed over the grid $\mathcal{T}_h$, so that the computational domain is $\overline{\Omega} = \bigcup_{K \in \mathcal{T}_h} K$.
The adjoint equation is:

$$find\ p_h \in \mathrm{X}_h \quad :\quad a_h^{ad}(p_h, \phi_h) = F_h^{ad}(\phi_h; w_h; u_h),\ \forall \phi_h \in \mathrm{X}_h, \tag{8.2.11}$$

where:

$$a_h^{ad}(p_h, \phi_h) := a^{ad}(p_h, \phi_h) -$$

$$\sum_{K\in\mathcal{T}_h}\delta_K\int_K\Big(-\nabla\cdot(\nu\nabla p_h+\mathbf{V}p_h)\Big)\Big(-\nabla\cdot(\nu\nabla\phi_h)+\mathbf{V}\cdot\nabla\phi_h\Big)\,dK,$$

$$F_h^{ad}(\phi_h;w_h;u_h):=F^{ad}(\phi_h;w_h)-\sum_{K\in\mathcal{T}_h}\delta_K\int_K\Big(m_D\Big(w_h-z_d\Big)\cdot$$

$$\cdot\Big(-\nabla\cdot(\nu\nabla\phi_h)+\mathbf{V}\cdot\nabla\phi_h\Big)+\Big(-\nabla\cdot(\nu\nabla w_h)+\mathbf{V}\cdot\nabla w_h-u_h\Big)m_D\phi_h\Big)\,dK.$$

Note that the terms $F^{ad}(\phi_h;w_h)$ are defined in (8.2.7) and (8.2.8), while p_h is the discrete approximation of functions p.

8.3 Reduced basis method for optimal control

As anticipated in Section 8.1, we can consider an input parameter of three different types:

- control input μ_u, which define control function $u=u(\mu_u)$;
- physical input μ_p, for example, velocity field $\mathbf{V}$ and/or viscosity ν;
- geometrical input μ_g, that is geometrical parameters which can vary the configuration of the domain.

We make this distinction into parameter classes in order to be able to consider several aspects (advection fields, diffusivity terms, localization of sources for releases, ect.) of the same problem: even if, in reality, we are solving different "types" of problem. Of course, input can be combined together to form, for example, a control-physical input. In this section, for convenience, we refer to a generic input $\boldsymbol{\mu}=\{\mu_u,\mu_p,\mu_g\}$, without specifying its nature.
We introduce a set of parameter samples $S_N=\{\boldsymbol{\mu}^1,...,\boldsymbol{\mu}^N\}$, where $\boldsymbol{\mu}^n\in\mathcal{D}$, $n=1,...,N$. For each input vector in S_N, we calculate using the finite element method a solution of the state equation $w_h(\boldsymbol{\mu}^n)$ in the space X_h; we choose a discretization enough refined to ensure that the solution in the high-dimensional space X_h is "in good agreement" with the exact solution in $H^1_{\Gamma_D}$. We do the same for the adjoint problem (note the similarity of this approach with the one used to set the dual residual method to correct the cost functional in Section 5.10): find a set of N samples $S_N^{ad}=\{\boldsymbol{\mu}_{ad}^1,...,\boldsymbol{\mu}_{ad}^N\}$, where $\boldsymbol{\mu}_{ad}^n\in\mathcal{D}$, $n=1,...,N$, and compute the finite element approximation of the adjoint variable $p_h(\boldsymbol{\mu}_{ad}^n)\in X_h$. The two sets S_N and S_N^{ad} are chosen independently. Also the reduced basis formulation and the basis construction procedure have been influenced by our choice of using the approach "optimize-then-discretize" for optimal control problem. We introduce the following reduced basis spaces:

$$W_N=span\{\zeta^n\equiv w_h(\mu^n),\ n=1,...,N\} \tag{8.3.1}$$

for the state problem and

$$Z_N=span\{\xi^n\equiv p_h(\mu_{ad}^n),\ n=1,...,N\} \tag{8.3.2}$$

for the adjoint problem. Starting from the state variable, we look for an approximation $w_N(\mu)$ to $w_h(\mu)$ in W_N; in particular we express $w_N(\mu)$ as:

$$w_N(\mu) = \sum_{j=1}^{N} w_{N_j}(\mu)\zeta^j = (\underline{w}_N(\mu))^T \underline{\zeta}, \tag{8.3.3}$$

where $\underline{w}_N(\mu) \in \mathbb{R}^N$ is the column vector of the linear combination coefficient w_{N_j}, $j = 1, ..., N$. Let p_N be the reduced basis approximation of the adjoint variable:

$$p_N(\mu) = \sum_{j=1}^{N} p_{N_j}(\mu)\xi^j = (\underline{p}_N(\mu))^T \underline{\xi}. \tag{8.3.4}$$

The goal is to represent accurately the solution of state and adjoint problem at some new point in parameter space, $\boldsymbol{\mu}^{new}$, as an appropriate combination of solutions previously computed at a small number of sample points in parameter space ($\boldsymbol{\mu}^n$ and $\boldsymbol{\mu}^n_{ad}$, $n = 1, ..., N$). In this case we are interested in solving the optimal control problem and finding the control function evaluating the cost functional in a rapid, reliable and repeated way.
At each iterative step of the method adopted to solve the control problem, for the given $\mu \in \mathcal{D}$ and the given control function u (8.2.3):

- we compute the reduced basis approximation of the state variable $w_N(\mu) \in W_N$, where

$$a(w_N(\mu), v; \mu) \;=\; F(v; u), \quad \forall v \in W_N;$$

- once w_N is available, we determine the solution $p_N \in Z_N$ of the adjoint equation:

$$a^{ad}(p_N(\mu), \phi; \mu) \;=\; F^{ad}(\phi, w_N(\mu)), \quad \forall \phi \in Z_N;$$

- we evaluate the reduced basis approximation of our output, i.e. the cost function $J(u, w_N)$ and the adjoint variable p_N, which allows us to check whether the stopping criterium is satisfied.

To apply the reduced basis method, we suppose, as usual, that for some finite (preferably small) integers Q and Q^{ad}, the bilinear forms $a(\cdot, \cdot; \mu)$ and $a^{ad}(\cdot, \cdot; \mu)$ may be expressed as:

$$a(w, v; \mu) \;=\; \sum_{q=1}^{Q} \sigma^q(\mu) a^q(w, v), \quad \forall w, v \in H^1_{\Gamma_D}, \; \forall \mu \in \mathcal{D},$$

$$a^{ad}(p, \phi; \mu) \;=\; \sum_{q=1}^{Q^{ad}} \sigma^q_{ad}(\mu) a^q_{ad}(p, \phi), \quad \forall p, \phi \in H^1_{\Gamma_D}, \; \forall \mu \in \mathcal{D},$$

for some $\sigma^q(\mu) : \mathcal{D} \to \mathbb{R}$, $a^q : H^1_{\Gamma_D} \times H^1_{\Gamma_D} \to \mathbb{R}$, $q = 1, ..., Q$ and for some $\sigma^q_{ad}(\mu) : \mathcal{D} \to \mathbb{R}$, $a^q_{ad} : H^1_{\Gamma_D} \times H^1_{\Gamma_D} \to \mathbb{R}$, $q = 1, ..., Q^{ad}$. We assume also affine parameter dependence for the functionals F and F^{ad}.
Coming to the matrix form, we define the matrices $\underline{A}_N(\mu) = a(\zeta^i, \zeta^j; \mu)$ and $\underline{A}^{ad}_N(\mu) =$

$a^{ad}(\xi^i, \xi^j; \mu)$, $1 \le i, j \le N$ and the vectors $\underline{F}_N = F(\zeta^j, u)$ and $\underline{F}_N^{ad} = F^{ad}(\xi^j, w_N)$, $1 \le j \le N$. We observe that:

$$\underline{A}_N(\mu) = \sum_{q=1}^{Q} \sigma^q(\mu)\underline{A}^q, \tag{8.3.5}$$

$$\underline{A}_N^{ad}(\mu) = \sum_{q=1}^{Q^{ad}} \sigma_{ad}^q(\mu)\underline{A}_{ad}^q,$$

where $A_{i,j}^q = a^q(\zeta^i, \zeta^j)$, $1 \le i, j \le N$, $1 \le q \le Q$ and $A_{ad_{i,j}}^q = a_{ad}^q(\xi^i, \xi^j)$, $1 \le i, j \le N$, $1 \le q \le Q^{ad}$. Note that $\underline{A}^q$, $1 \le q \le Q$ and $\underline{A}_{ad}^q$, $1 \le q \le Q^{ad}$ are *independent* of input parameter μ.

We can then reformulate the state equation as: given $\mu \in \mathcal{D}$, find the unique solution $\underline{w}_N(\mu)$ to

$$\underline{A}_N(\mu)\underline{w}_N(\mu) = \underline{F}_N; \tag{8.3.6}$$

and the adjoint equation as: given $\mu \in \mathcal{D}$ and $\underline{w}_N(\mu)$, find the unique solution $\underline{p}_N(\mu)$ to

$$\underline{A}_N^{ad}(\mu)\underline{p}_N(\mu) = \underline{F}_N^{ad}. \tag{8.3.7}$$

8.3.1 Computational procedure: off-line/on-line decomposition

The matrices and vectors introduced in the previous section are assembled in two different steps: the parameter-dependent (online, many queries) and the parameter-independent ones (off-line, computed once).

In the *off-line* stage, we find the ζ^i, the ξ^i, $i = 1, ..., N$ and form the $\underline{A}^q$, for $1 \le q \le Q$, the $\underline{A}_{ad}^q$, for $1 \le q \le Q^{ad}$ and $\underline{F}_N$, $\underline{F}_N^{ad}$. The *online* stage, for any given new μ, we only need to form $\underline{A}_N(\mu)$ from the $\underline{A}^q$, $\underline{A}_N^{ad}(\mu)$ from the $\underline{A}_{ad}^q$, then solve (8.3.6) for $\underline{w}_N(\mu)$ and (8.3.7) for $\underline{p}_N(\mu)$ and finally evaluate $J(u, w_N; \mu)$.

Note that the two processes are completely decoupled. Also in this case the expensive off-line computation be processed at an early stage and needs to be done only once. The efficient online computation can then be used for very fast evaluations of outputs at different point in the parameter space. The incremental cost to evaluate, for example, $J_N(\mu)$ for any given new μ is very small: (i) N is very small, typically $\mathcal{O}(10)$ thanks to the good convergence properties of W_N and Z_N [134]; (ii) (8.3.6) and (8.3.7) can be assembled and inverted very rapidly.

8.3.2 Error on control and error on cost functional

As seen, while solving a simple equation, for example the state equation, the reduced basis approach looks for an approximation $w^N(\mu)$ to $w_h(\mu)$ in W_N, presuming that $w_h(\mu)$ is sufficiently close to $w(\mu)$. This means that we make no distinction between the actual solution and the finite element solution computed on a grid refined enough for our purposes. When dealing with an optimal control problem, it is important to check that the problem solved with the finite element method and the one solved with the reduced basis method converge to

the same solution, although they evolve separately. To this aim, we define ε_u as the L^2 error on control function u at convergence and ε_J as the L^2 error on cost functional at convergence:

$$\varepsilon_u = \int_Q (u_h^f - u_N^f)^2 d\Omega,$$

$$\varepsilon_J = |J^f(u_N, w_N) - J^f(u_h, w_h)|.$$

The index f refers to the values at convergence, i.e. at last iteration, and u_h^f and u_N^f are given by:

$$u_h^f = u_h^{f-1} - \tau J'(u_h^{f-1}) = u_0 - \tau \sum_{i=1}^{f-1} J'(u_h^i),$$

$$u_N^f = u_N^{f-1} - \tau J'(u_N^{f-1}) = u_0 - \tau \sum_{i=1}^{f-1} J'(u_N^i),$$

where u_0 is the initial control function.
We note that:

$$\varepsilon_u = \int_Q (u_h^f - u_N^f)^2 d\Omega = \int_Q \Big(\tau \sum_{i=1}^{f-1} \Big(J'(u_N^i) - J'(u_h^i)\Big)\Big)^2 d\Omega,$$

and, since $J' = p$ by means of Riesz theorem [32]:

$$\varepsilon_u = \int_Q \Big(\tau \sum_{i=1}^{f-1} \Big(p_N^i - p_h^i\Big)\Big)^2 d\Omega.$$

This means that the L^2 error on control function u at convergence depends on the sum, extended to all previous iterations, of the errors on adjoint variable, multiplied by relaxation parameter $\tau > 0$. So the larger number of iteration to converge, the larger ε_u is. We want that even in the worst case (many iteration before converging), ε_u is reasonably acceptable. We use an adaptive procedure for the construction of the basis as seen in Section 5.4 and A.5 (see also [135]), so that the dimension of the reduced basis N is large enough to ensure that the errors ε_u and ε_J are "small" in any case.
To have an idea of how $J(u_N, w_N)$, $J(u_h, w_h)$ and ε_u vary at each iteration, see Section 8.5.4 and Section 8.6.4.

8.4 An application to flow control

We consider now a type of control problem with the aim of regulating a generic substance emission by some sources into a fluid (for example a physiological flow) in order to achieve a desired concentration level or to maintain the concentration level below a fixed threshold over an observation area in the domain. This kind of problem is a parametrized extension of the one in [32]. Preliminary results are reported in [124] dealing with a different application.

We refer to the domain in Figure 8.1 where we have positioned three different sources Q_1,

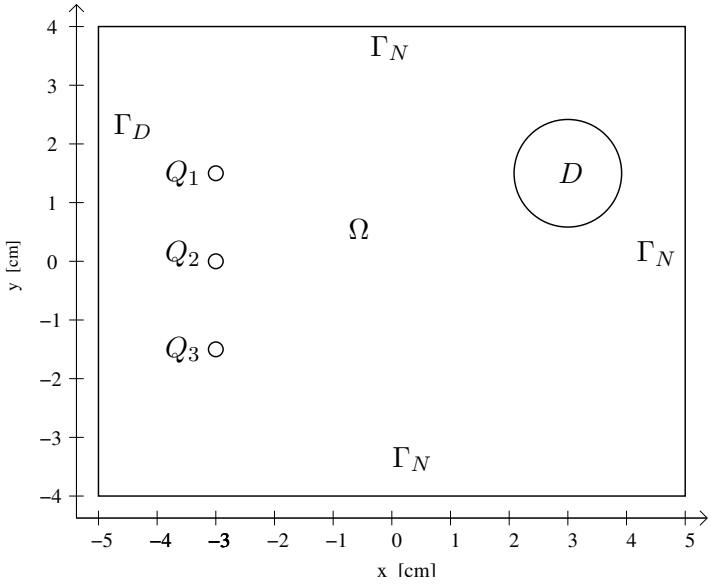

Figure 8.1: Reference domain for advection-diffusion problem.

Q_2, Q_3 emitting certain substances, while D is an observation area. Our goal is to provide an example of a systematical method to control emission by some release sources so that the concentration of the eluted substance over a certain area D is acceptable (i.e., at a desired level), taking into account advection field and diffusivity conditions in a stationary frame (an unsteady frame is provided in Section 8.9). In Figure 8.2 we report three different functions describing the diffusivity ν considered in our test cases. We consider the state equation

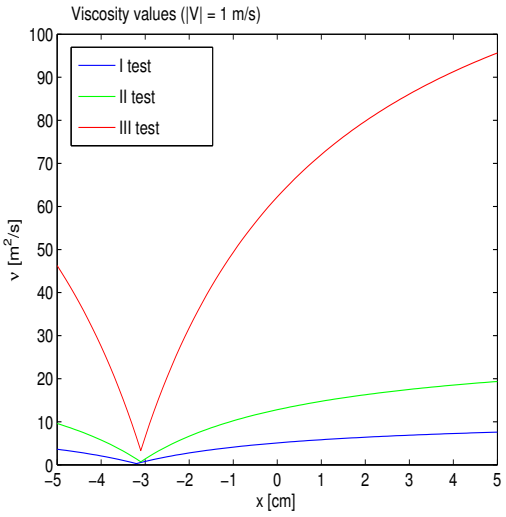

Figure 8.2: Three different diffusivity coefficients: ν_1, ν_2, ν_3.

(8.2.4), where ν can also be dependent on $\mathbf{V}$, describing the mean motion of the fluid, instead

of exactly representing pointwise velocity. Diffusivity ν may depend also on the problem type and domain geometry (x coordinate). We assume $u = \sum_{i=1}^{3} u_i m_{Q_i}$, being m_{Q_i} the characteristic function of the i-th source and u_i the rate of emission from the i-th source. Then quantity (8.2.6) can be written as:

$$F(\varphi; u) = \sum_{i=1}^{3} \int_{Q_i} u_i \varphi \, dQ_i.$$

Solving the control problem with the iterative method, at each step we update control function in the following way:

$$\delta u^k = \sum_{i=1}^{3} \delta u_i^k = -\tau \sum_{i=1}^{3} p m_{Q_i}.$$

8.5 Control input: variable emission rates

As first test we consider a two component control input parameter $\boldsymbol{\mu}_u = \{u_1, u_2\}$. We fix a total emission value $u_{tot} = 27\ mgs^{-1}$ corresponding to a certain release of substances in the physiological fluid, for example. Therefore we write $u_3 = 27 - u_1 - u_2$ and $\mu_u \in \mathcal{D}$, where $\mathcal{D} = [0, 27] \times [0, 27]$ with $u_1 - u_2 \leq 27$.

8.5.1 Parametrized state equation

To compute the reduced basis approximation of the state variable (8.3.3), we need to find the N unknown components $w_{N_j}(\mu_u)$ by solving the problem:

$$a_h(w_N(\mu_u), \zeta_i) = F_h(\zeta_i) \quad i = 1, ..., N, \tag{8.5.1}$$

where

$$a_h(w_N(\mu_u), \zeta_i) = \sum_{j=1}^{N} \sum_{i=1}^{N} w_{N_j}(\mu_u) \Big[\sum_{K \in \mathcal{T}_h} \int_K \nu \nabla \zeta_j \cdot \nabla \zeta_i + \sum_{K \in \mathcal{T}_h} \int_K (\mathbf{V} \cdot \nabla \zeta_j) \zeta_i + \tag{8.5.2}$$

$$\sum_{K \in \mathcal{T}_h} \delta_K \frac{h_K}{\|\mathbf{V}\|} \int_K \Big(-\nabla \nu \cdot \nabla \zeta_j + \mathbf{V} \cdot \nabla \zeta_j \Big) \Big(\mathbf{V} \cdot \nabla \zeta_i \Big) \Big],$$

and

$$F_h(\zeta_i) = \sum_{i=1}^{N} \Big[\sum_{K \in \mathcal{T}_h} \int_K u(\mu_u) \zeta_i + \sum_{K \in \mathcal{T}_h} \delta_K \frac{h_K}{\|\mathbf{V}\|} \int_K u(\mu_u) \Big(\mathbf{V} \cdot \nabla \zeta_i \Big) \Big]. \tag{8.5.3}$$

We define now the following matrices, related to the diffusive term, convective term and stabilization term:

$$C_{i,j} = \sum_{K \in \mathcal{T}_h} \int_K \nu \nabla \zeta_j \cdot \nabla \zeta_i, \tag{8.5.4}$$

$$B_{i,j} = \sum_{K \in \mathcal{T}_h} \int_K (\mathbf{V} \cdot \nabla \zeta_j) \zeta_i, \tag{8.5.5}$$

$$S_{i,j} = \sum_{K\in\mathcal{T}_h} \delta_K \int_K \Big(\nabla\nu\cdot\nabla\zeta_i + \nabla\cdot\mathbf{V}\zeta_i + \mathbf{V}\cdot\nabla\zeta_i\Big)\Big(-\nabla\nu\cdot\nabla\zeta_j + \mathbf{V}\cdot\nabla\zeta_j\Big)\Big]. \tag{8.5.6}$$

The term $\nabla\nu$ has only the component ν_x, being $\nu = \nu(x)$. The matrix $\underline{A}_N$ (8.3.5) can thus be written as:

$$A_{N_{i,j}} = C_{i,j} + B_{i,j} + S_{i,j}.$$

In this simple and particular case, $\underline{A}_N$ is independent of input parameter μ_u.
Let us define also the following column vectors:

$$G_i(\mu_u) = \sum_{K\in\mathcal{T}_h} \int_K u(\mu_u)\zeta_i, \tag{8.5.7}$$

$$H_i(\mu_u) = \sum_{K\in\mathcal{T}_h} \delta_K \frac{h_K}{\|\mathbf{V}\|} \int_K u(\mu_u)\Big(\mathbf{V}\cdot\nabla\zeta_i\Big), \tag{8.5.8}$$

so that $\underline{F}_N$ is:

$$F_{N_i}(\mu_u) = G_i(\mu_u) + H_i(\mu_u).$$

Both $\underline{G}$ and $\underline{H}$ depend on μ_u because $u_i = \mu_u^i$ on the $i-th$ source and set to zero over the remaining part of the domain. This assembling procedure of the right-hand-side is very fast. The unknown vector $\underline{w}_N(\mu_u)$ is the solution of the system:

$$\underline{A}_N\underline{w}_N(\mu_u) = \underline{F}_N(\mu_u). \tag{8.5.9}$$

8.5.2 Parametrized adjoint equation

The N unknown components $p_{N_j}(\mu_u)$ for the reduced basis approximation of adjoint variable (8.3.4) are the solution of the problem:

$$a_h^{ad}(p_N(\mu_u),\xi_i) = F_h^{ad}(\xi_i; w_N, u_h) \quad i = 1,...,N, \tag{8.5.10}$$

where

$$a_h^{ad}(p_N(\mu_u),\xi_i) = \sum_{j=1}^{N}\sum_{i=1}^{N} p_{N_j}(\mu_u)\Big[\sum_{K\in\mathcal{T}_i}\int_K \nu\nabla\xi_j\cdot\nabla\xi_i + \tag{8.5.11}$$

$$\sum_{K\in\mathcal{T}_h}\int_K \Big(\mathbf{V}\cdot\nabla\xi_i\Big)\xi_j + \sum_{K\in\mathcal{T}_h}\delta_K\int_K\Big(\nabla\nu\cdot\nabla\xi_j + \nabla\cdot\mathbf{V}\xi_j + \mathbf{V}\cdot\nabla\xi_i\Big)\Big(-\nabla\nu\cdot\nabla\xi_i + \mathbf{V}\cdot\nabla\xi_i\Big)\Big], \tag{8.5.12}$$

and

$$F_h^{ad}(\xi_i; w_N(\mu_u); u_h) = \sum_{i=1}^{N}\Big[\sum_{K\in\mathcal{T}_h}\int_K m_D(w_N(\mu_u) - z_d)\xi_i -$$

$$\sum_{K\in\mathcal{T}_h}\delta_K\int_K m_D(w_N(\mu_u) - z_d)\Big(-\nabla\nu\cdot\nabla\xi_i + \mathbf{V}\cdot\nabla\xi_i\Big) -$$

$$\sum_{K\in\mathcal{T}_h}\delta_K\int_K m_D\Big(-\nabla\nu\cdot\nabla w_N(\mu_u) + \mathbf{V}\cdot\nabla w_N(\mu_u) + u_h\Big)\xi_i\Big].$$

Let $\underline{C}$ be the matrix (8.5.4), we now introduce $\underline{B}^{ad}$ and $\underline{S}^{ad}$:

$$B^{ad}_{i,j} = \sum_{K\in\mathcal{T}_h} \int_K \Big(\mathbf{V}\cdot\nabla\xi_i\Big)\xi_j = B_{j,i}, \tag{8.5.13}$$

$$S^{ad}_{i,j} = \sum_{K\in\mathcal{T}_h} \delta_K \int_K \Big(\nabla\nu\cdot\nabla\xi_j + \nabla\cdot\mathbf{V}\xi_j + \mathbf{V}\cdot\nabla\xi_j\Big)\Big(-\nabla\nu\cdot\nabla\xi_i + \mathbf{V}\cdot\nabla\xi_i\Big)\Big] = S_{j,i}. \tag{8.5.14}$$

where $B_{j,i}$, $S_{j,i}$ are defined by (8.5.5), (8.5.6).
The matrix $\underline{A}^{ad}_N$ can be rewritten as:

$$A^{ad}_{N_{i,j}} = C_{i,j} + B^{ad}_{i,j} + S^{ad}_{i,j}.$$

Let $\underline{G}^{ad}$, $\underline{H}^{ad}$, $\underline{I}^{ad} \in \mathbb{R}^N$ be the column vectors defined as:

$$G^{ad}_i = \sum_{K\in\mathcal{T}_h} \int_K m_D\xi_i, \tag{8.5.15}$$

$$H^{ad}_i = -\sum_{K\in\mathcal{T}_h} \delta_K \int_K m_D\Big(-\nabla\nu\cdot\nabla\xi_i + \mathbf{V}\cdot\nabla\xi_i\Big), \tag{8.5.16}$$

$$I^{ad}_i = -\sum_{K\in\mathcal{T}_h} \delta_K \int_K m_D\Big(-\nabla\nu\cdot\nabla\xi_i + \mathbf{V}\cdot\nabla\xi_i\Big)\xi_i. \tag{8.5.17}$$

All the matrices $\underline{C}$, $\underline{B}^{ad}$, $\underline{S}^{ad}$ and the vectors $\underline{G}^{ad}$, $\underline{H}^{ad}$, $\underline{I}^{ad}$ are computed off-line (i.e only once and stored), while for every new μ_u we assemble online the right-hand-side $\underline{F}^{ad}_N$.
The unknown vector $\underline{p}_N(\mu_p)$ is the solution of system:

$$\underline{A}^{ad}_N\underline{p}_N(\mu_u) = \underline{F}^{ad}_N(\mu_u). \tag{8.5.18}$$

8.5.3 Some results

We report in Table 8.1 the number of basis functions (for both state and adjoint equation), the mean error on cost functional and on control function at convergence (computed on a high number of random inputs) and the computational saving in the case of $\nu = \nu_2$ and $\nu = \nu_3$. We have imposed $tol = 10^{-7}$. The computational saving compares the time needed to perform the on-line steps with the one necessary to complete a finite element simulation, using a mesh with $O(10^4)$ elements.
The number of basis functions and the saving percentage are the same for the two cases. The orders of magnitude of the errors are nearly the same.
In Table 8.2 we report some details regarding only state equation: the mean H^1 error with respect to the finite element solution (computed on a high number of random inputs) and the computational saving for the three different diffusivity conditions. The number of basis functions for the reduced basis approximation of state problem is $N = 7$ for the three cases. Dealing with a test case we calculated several errors on control function, on cost functional and its gradient.

ν	N	Mean error on J	Mean H^1 error on u	Saving
ν_1	7	$1.4E-11$	$2.5E-5$	90%
ν_2	7	$1.9E-12$	$6.1E-6$	90%

Table 8.1: Control input: number of basis functions, mean errors on cost functional and control function at convergence and time saving.

ν	mean H^1 error	Saving
ν_1	$1E-8$	96%
ν_2	$2.1E-8$	94%
ν_3	$3.7E-8$	90%

Table 8.2: Control input for state equation: mean H^1 error and time saving for control input.

8.5.4 Example

We start from the following test case, where $\nu = \nu_2$: the upper source is emitting at 45% of u_{tot} and the central one is not active, that is $\mu_u = \{1215, 0\}$ $[mgs^{-1}]$. The control problem solved by the two methods (finite element and reduced basis) leads to the optimal solution: the upper source emission rate is reduced to 3.49%, central source remains inoperating and the lower one is at 55.02% of u_{tot}. Figure 8.3 shows the reduced basis approximation of initial and optimal solution.
For this particular choice of μ_u, control problems solved with the two methods converge both after 21 iteration. Since the number of iteration is the same (in this case), we can compare cost functional values ($J(w_N, u_N)$ and $J(w_h, u_h)$) at each iteration and check the L^2 error on control function trend (Figure 8.4).

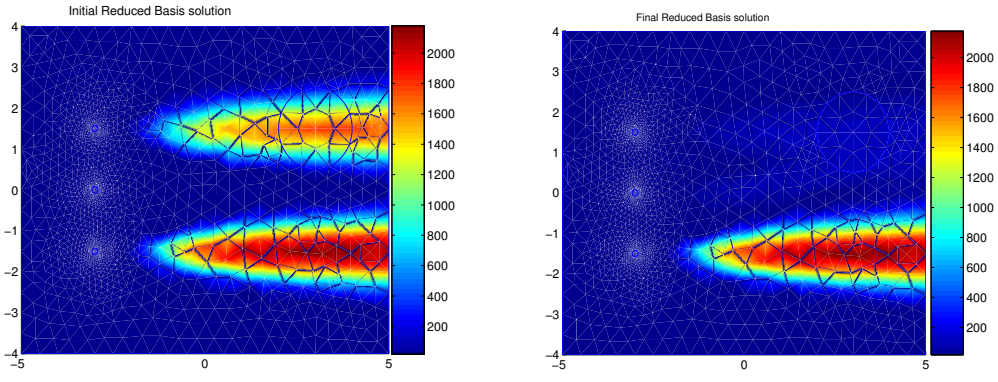

Figure 8.3: Control input: initial reduced basis solution (right) and final reduced basis solution (left) of state equation. Substance concentration is in $[\mu g]$.

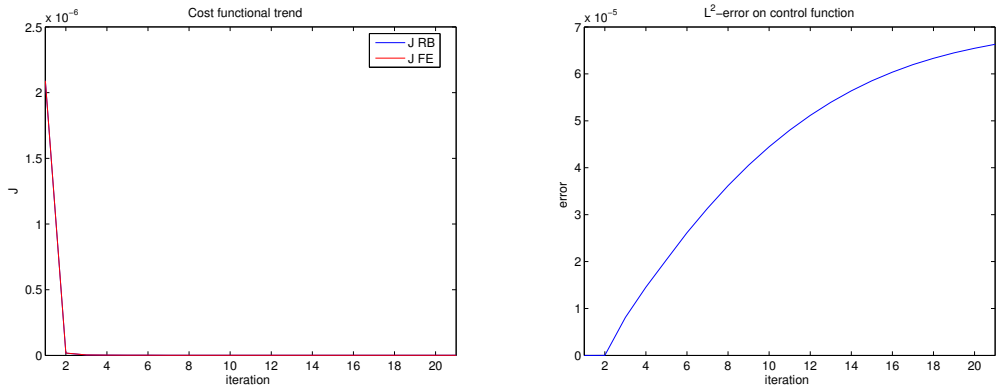

Figure 8.4: Control input: comparison between $J(w_N, u_N)$ and $J(w_h, u_h)$ at every iteration (right) and L^2-error on control function trend (left).

8.6 Physical input: variable emission rates and velocity field

This case is more complex: we consider an input made of four component $\mu_p = \{u_1, u_2, V_x, V_y\}$. Once again $u_3 = 27 - u_1 - u_2\ mgs^{-1}$, having imposed $u_1 + u_2 \leq u_{tot}$, and we fix the velocity absolute value $|\mathbf{V}| = 1$. We assume that the velocity field of the advection term can vary in direction of an angle ranging in $[-40^o, 90^o]$. As physical input one could also choose the "diffusivity coefficient" ν.

8.6.1 Parametrized state equation

The N unknowns $w_{N_j}(\mu_p)$ (8.3.3) are the solution of the problem (8.5.1), where a_h and F_h are respectively defined in (8.5.2) and (8.5.3).
The matrix $\underline{A}_N$ can be written as follows:

$$A_{N_{i,j}}(\mu_p) = C_{i,j} + V_x \cdot B_{x_{i,j}} + V_y \cdot B_{y_{i,j}} + S_{i,j}(\mu_p), \tag{8.6.1}$$

where $\underline{C}$ is the matrix (8.5.4), $\underline{S}$ is defined by (8.5.6) and $\underline{B}_x$ and $\underline{B}_y$ are given by:

$$B_{x_{i,j}} = \sum_{K \in \mathcal{T}_h} \int_K (\mathbf{U}_x \cdot \nabla \zeta_j)\zeta_i, \tag{8.6.2}$$

$$B_{y_{i,j}} = \sum_{K \in \mathcal{T}_h} \int_K (\mathbf{U}_y \cdot \nabla \zeta_j)\zeta_i, \tag{8.6.3}$$

with $\mathbf{U}_x = (1, 0)$ and $\mathbf{U}_y = (0, 1)$; $\underline{B} = V_x \cdot \underline{B}_x + V_y \cdot \underline{B}_y$, where $\underline{B}$ (8.5.5) is the matrix related to the convective term.
The source term $\underline{F}_N$ is given by:

$$F_{N_i}(\mu_p) = G_i(\mu_p) + H_i(\mu_p).$$

All the parameter-independent matrices ($\underline{C}$, $\underline{B}_x$, $\underline{B}_y$) are assembled in the off-line stage, while matrices $\underline{S}$, $\underline{G}$, $\underline{H}$, depending on the parameter in a non-affine way, must be built on-line for each new μ_p. Always in the on-line stage, matrices $\underline{A}_N(\mu_p)$ e $\underline{F}_N(\mu_p)$ are assembled.
The unknown vector $\underline{w}_N(\mu_p)$ is the solution of the system:

$$\underline{A}_N(\mu_p)\underline{w}_N(\mu_p) = \underline{F}_N(\mu_p). \tag{8.6.4}$$

The difference between (8.5.9) and (8.6.4) is that in the latter also $\underline{A}_N$ depends on input parameter μ_p. To improve efficiency of the assembling procedure described above we may apply the decomposition of non-affine terms by the empirical interpolation method described in Chapter 6 while assembling $\underline{S}$, $\underline{G}$ and $\underline{H}$, specified in (8.5.6)-(8.5.8).

8.6.2 Parametrized adjoint equation

We want to find the weights of the combination (8.3.4), in order to have the reduced basis approximation of the adjoint variable, solution of (8.5.10). Bilinear form a_h^{ad} and functional F_h^{ad} are the same as in (8.5.11) and (8.5.12).
Let $\underline{A}_N^{ad} \in \mathbb{R}^{N\times N}$ be the matrix:

$$A_{N_{i,j}}^{ad}(\mu_p) = C_{i,j} + V_x \cdot B_{x_{i,j}}^{ad} + V_y \cdot B_{y_{i,j}}^{ad} + S_{i,j}^{ad}(\mu_p),$$

where $\underline{C}$ is defined by (8.5.4), $\underline{S}^{ad}$ is the stabilization matrix (8.5.14), now parameter-dependent. The elements of matrices $\underline{B}_x^{ad}$ and $\underline{B}_y^{ad}$ are given by:

$$B_{x_{i,j}}^{ad} = \sum_{K\in\mathcal{T}_h} \int_K \Big(\mathbf{U}_x \cdot \nabla\xi_i\Big)\xi_j = B_{x_{j,i}},$$

$$B_{y_{i,j}}^{ad} = \sum_{K\in\mathcal{T}_h} \int_K \Big(\mathbf{U}_y \cdot \nabla\xi_i\Big)\xi_j = B_{y_{j,i}},$$

with $\mathbf{U}_x = (1,0)$ and $\mathbf{U}_y = (0,1)$, while $B_{x_{j,i}}$ and $B_{y_{j,i}}$ are (8.6.2) and (8.6.3). Moreover $\underline{B}^{ad} = V_x \cdot \underline{B}_x^{ad} + V_y \cdot \underline{B}_y^{ad}$, where $\underline{B}^{ad}$ is the matrix related to the convective term (8.5.13).
Source term $\underline{F}_N$ is given by:

$$F_{N_i}^{ad}(\mu_p) = G_i^{ad} + H_i^{ad}(\mu_p) + I_i^{ad}(\mu_p).$$

In this case, $\underline{H}^{ad}$ (8.5.16) and $\underline{I}^{ad}$ (8.5.17) are parameter-dependent, since they depend on velocity vector, while $\underline{G}^{ad}$ (8.5.15) is parameter-independent. Also in this case an efficient computational procedure should be used.
Unknown vector $\underline{p}_N(\mu_p)$ is the solution of system:

$$\underline{A}_N^{ad}(\mu_p)\underline{p}_N(\mu_p) = \underline{F}_N^{ad}(\mu_p). \tag{8.6.5}$$

Even in this case, the difference between (8.5.18) and (8.6.5) is that in the latter also $\underline{A}_N^{ad}$ depends on input parameter μ_p.

8.6.3 Some results

The use of the reduced basis method to solve both state and adjoint equations, at each step of our iterative method to solve control problem, implies several advantages from a computational point of view. In the case of control and physical input we have time savings up to $65 - 70\%$, which means that in the same time the finite element method solves just one iteration (state + adjoint equation using a mesh with $O(10^4)$ elements), the reduced basis method solves 3 iterations. This is a good result dealing with optimal control problems, which are not real-time problems, but time savings could be even improved if we can adopt a stabilization method based on terms which can be built off-line. At the present, stabilization is needed also for the reduced basis formulation; indeed, when using the non-stabilized Galerkin method, we have a "plateau" as $N \to \infty$, corresponding to the Galerkin residual evaluated for the stabilized "truth" solutions.
In our case, we can fix velocity field (the desired online value) before applying optimal control (at first iteration) and so we can build S and S^{ad} offline or at a step we can call "pre-online" for our optimal control problem. Note that the basis has been assembled offline considering different values for velocity field.
We report in Table 8.3 the number of basis function, the mean error on cost functional and on control function at convergence (computed on a high number of random inputs) and the computational saving (having fixed the "online" velocity field at first iteration) for $\nu = \nu_2$ and $\nu = \nu_3$, having imposed $tol = 10^{-7}$. To understand the slight difference in the number of basis functions, we need to compare the weight of the diffusive term and the one of the convective term in $\underline{A}_N$ (8.6.1). As diffusivity increases, diffusive term becomes dominant and so just "few" basis functions are needed to have a good approximation of the solution depending on convective velocity. Since for $\nu = \nu_3$ diffusivity absolute value is greater, the convective term is less influent and fewer basis functions are needed.
In Table 8.4 we report some details about only state equation: the mean H^1 error with respect to the finite element solution (computed on a high number of random inputs) and the computational saving for the three different diffusivity conditions. The number of basis functions for the reduced basis approximation of state variable is $N = 81$ for $\nu = \nu_3$ and $N = 132$ for $\nu = \nu_2$.

ν	N	Mean error on J	Mean H^1 error on u	Saving
ν_2	132	$0.9E-9$	$2.5E-7$	80%
ν_3	81	$0.5E-9$	$1.1E-7$	80%

Table 8.3: Physical input: number of basis functions, mean errors on cost functional and control function, at convergence, and time saving (including also error calculation).

ν	mean H^1-error	Saving
ν_1	$1.1E-6$	95%
ν_2	$3.8E-7$	95%
ν_3	$5.4E-5$	$90-95\%$

Table 8.4: Physical input for state equation during optimal control (velocity field is fixed at first iteration): mean H^1 error and time saving. Without fixing the online velocity field at first iteration computational saving are $\sim 65-70\%$.

8.6.4 Example

We choose the following input: $u_1 = 30\%$, and $u_2 = 40\%$, respectively, of u_{tot} and advection field direction at 45^o with respect to x-axis. Figure 8.5 shows the initial solution and the solution at convergence, with the upper source emitting at 30.02%, the central one at 38.81% and the lower one at 7.27%.
Also in this second case we choose a particular input parameter so that the control problems solved with the reduced basis method and with the finite element method converge in the same number of iteration. Once again we can compare cost functional values ($J(w_N, u_N)$ and $J(w_h, u_h)$) at each iteration and check the L^2 error on control function trend (Figure 8.6). We notice that till the 5^{th} iteration $J(w_N, u_N) < J(w_h, u_h)$, while from the 5^{th} till convergence $J(w_N, u_N) > J(w_h, u_h)$. The absolute value $|J(w_N, u_N) - J(w_h, u_h)|$ increases at each iteration till it sets on a constant value. At the beginning, $J(w_N, u_N) < J(w_h, u_h)$ because, as seen, reduced basis solution is always an under-estimation of the finite element solution (see Appendix A). After some iteration, instead, $J(w_N, u_N) > J(w_h, u_h)$ because, since reduced basis solution is an under-estimation, the source term of the adjoint problem is inferior and so $p_N(\mu) < p_h(\mu)$ on the whole domain; since $J' = p$, if $J'(u_N) < J'(u_h)$, it means that $J(w_N, u_N)$ decreases less rapidly and so $J(w_N, u_N)$ is greater.

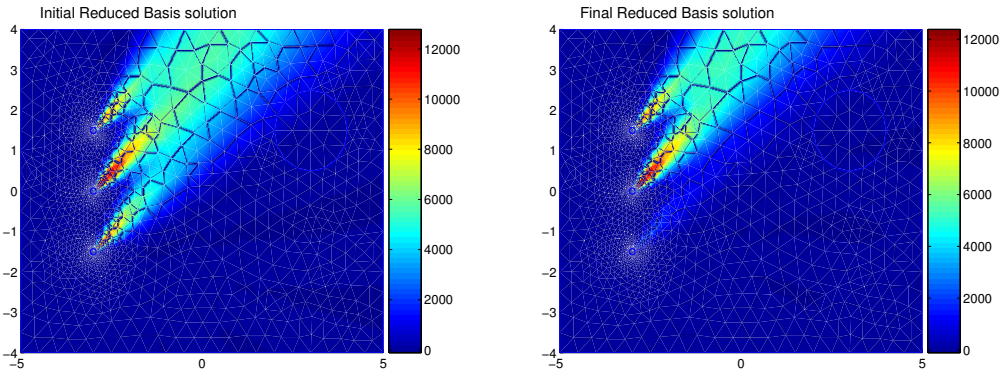

Figure 8.5: Physical input: initial reduced basis solution (right) and final reduced basis solution (left) of state equation. Concentration is in $[\mu g]$.

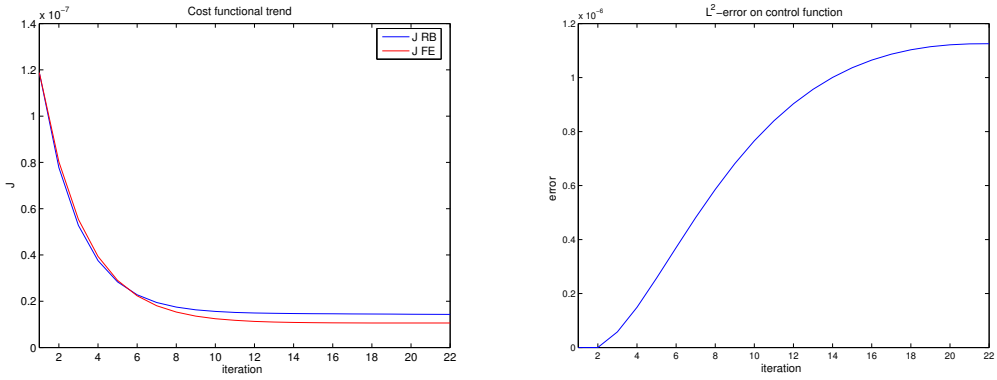

Figure 8.6: Physical input: comparison between $J(w_N, u_N)$ and $J(w_h, u_h)$ at every iteration (right) and L^2 error on control function trend (left).

8.7 Geometrical input: parametrized domains

The goal of this section is to show how to combine optimal control problems with the calculation of geometrical sensitivity analysis and to solve a problem with a double aim: to achieve the desired concentration into a zone and to optimize the distribution of sources by positioning them in the domain. The ultimate goal is, for example, the optimization of substances release in the domain or in a subset of it.
We refer to Figure 8.7, the physical domain $\hat{\Omega} \subset \mathbb{R}^2$ is divided in seven subdomains $\hat{\Omega}^r$, $r = 1, ..., 7$. We have chosen the parameters $\boldsymbol{\mu}_g$ as C_1, C_2, C_3 and C_4 $[cm]$, with $C_1 + C_2 = 3$ and $C_3 + C_4 = 3$. The position of the central source is fixed, while the position C_3 of the upper one and the position C_2 of the lower one can vary.
Moreover, we considered this kind of parametrized domain in order to be able to handle some practical situations: for example where to place a new emission source. The method is based on the affine mapping procedures from reference subdomains (the ones with $C_1 = 2$, $C_2 = 1$, $C_3 = 1$ e $C_4 = 2$) to the true ones ($\Omega^r \to \hat{\Omega}^r$). Also in this case we can extend this methodology to non-affine mappings dealing with non-Cartesian geometry.

8.7.1 Parametrized state equation

Let R be the number of subdomains in which the real domain is divided: $\hat{\Omega} = \bigcup_{r=1}^{R} \hat{\Omega}^r$. From the weak form of the state equation (8.2.10), we define the following bilinear and linear forms:

$$\hat{\mathcal{A}}(\hat{w}, \hat{v}) = \sum_{r=1}^{R} \int_{\hat{\Omega}^r} \frac{\partial \hat{w}}{\partial \hat{x}_i} \hat{\nu}_{ij}^r \frac{\partial \hat{v}}{\partial \hat{x}_j} d\hat{\Omega}, \tag{8.7.1}$$

$$\hat{\mathcal{B}}(\hat{w}, \hat{v}) = \sum_{r=1}^{R} \int_{\hat{\Omega}^r} V_i \frac{\partial \hat{w}}{\partial \hat{x}_i} \hat{v} d\hat{\Omega},$$

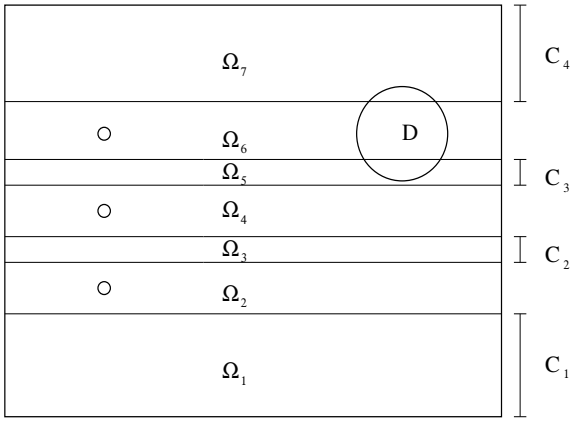

Figure 8.7: Scheme for the computational domain: subdomains and parameters.

$$\hat{\mathcal{F}}(\hat{v}) = \sum_{r=1}^{R} \int_{\hat{\Omega}^r} \hat{u}\hat{v} d\hat{\Omega},$$

$$\hat{\mathcal{S}}(\hat{w}, \hat{v}) = \sum_{r=1}^{R} \sum_{\hat{K} \in \mathcal{T}_h^r} \delta_{\hat{K}} \frac{h_{\hat{K}}}{\|\mathbf{V}\|} \int_{\hat{K}} \Big(V_i \frac{\partial \hat{w}}{\partial \hat{x}_i}\Big)\Big(V_j \frac{\partial \hat{v}}{\partial \hat{x}_j}\Big) d\hat{K},$$

$$\hat{\mathcal{G}}(\hat{v}) = \sum_{r=1}^{R} \sum_{\hat{K} \in \mathcal{T}_h^r} \delta_{\hat{K}} \frac{h_{\hat{K}}}{\|\mathbf{V}\|} \int_{\hat{K}} \hat{u}\Big(V_i \frac{\partial \hat{v}}{\partial \hat{x}_i}\Big) d\hat{K},$$

where $1 \leq i, j \leq d = 2$ e $\hat{\nu}_{i,j}^r = \hat{\nu}\delta_{i,j}$. For the sake of simplicity, we assume that diffusivity ν and $|\mathbf{V}|$ are constant over the whole domain. The weak form of the stabilized state equation in the real domain can be written as:

$$find\ \hat{w}_N(\mu) \in \hat{W}_N \quad : \quad \hat{\mathcal{A}}(\hat{w}_N, \hat{v}) + \hat{\mathcal{B}}(\hat{w}_N, \hat{v}) + \hat{\mathcal{S}}(\hat{w}_N, \hat{v}) = \hat{\mathcal{F}}(\hat{v}) + \hat{\mathcal{G}}(\hat{v}) \ \ \forall \hat{v} \in \hat{W}_N.$$

We are interested in writing a partial differential equation depending on the set of geometrical parameters given as input. We introduce an affine mapping from the "true" subdomains $\hat{\Omega}^r$ into the corresponding Ω^r. For any $\hat{x} \in \hat{\Omega}^r$, $r = 1, \ldots, R$, its image $x \in \Omega^r$ is given by:

$$x = \mathcal{G}^r(\mu_g; \hat{x}) = G^r(\mu)\hat{x} + g^r, \quad 1 \leq r \leq R.$$

For convenience, we rename μ_g with μ. We thus write:

$$\frac{\partial}{\partial \hat{x}_i} = \frac{\partial x_j}{\partial \hat{x}_i} \frac{\partial}{\partial x_j} = G_{ji}^r(\mu) \frac{\partial}{\partial x_j}, 1 \leq i, j \leq d = 2$$

and in the reference domain Ω we have:

$$\mathcal{A}(w, v; \mu) = \sum_{r=1}^{R} \int_{\Omega^r} \frac{\partial w}{\partial x_i} \Big(G_{ii'}^r(\mu) \hat{\nu}_{i'j'}^r G_{jj'}^r(\mu) |(G^r(\mu))^{-1}|\Big) \frac{\partial v}{\partial x_j} d\Omega,$$

$$\mathcal{B}(w,v;\mu)=\sum_{r=1}^{R}\int_{\Omega^r}V_i\frac{\partial w}{\partial x_i}\Big(G^r_{ii'}(\mu)|(G^r(\mu))^{-1}|\Big)vd\Omega,$$

$$\mathcal{F}(v;\mu)=\sum_{r=1}^{R}\int_{\Omega^r}\Big(\hat{u}|(G^r(\mu))^{-1}|\Big)vd\Omega,$$

$$\mathcal{S}(w,v;\mu)=\sum_{r=1}^{R}\sum_{K\in\mathcal{T}_h^r}\delta_K\frac{h_K}{\|\mathbf{V}\|}\int_K V_i\frac{\partial w}{\partial x_i}\Big(G^r_{ii'}(\mu)G^r_{jj'}(\mu)|(G^r(\mu))^{-1}|\Big)\frac{\partial v}{\partial x_j}V_j\ dK,$$

$$\mathcal{G}(v;\mu)=\sum_{r=1}^{R}\sum_{K\in\mathcal{T}_h^r}\delta_K\frac{h_K}{\|\mathbf{V}\|}\int_K \hat{u}V_i\frac{\partial v}{\partial x_i}\Big(G^r_{ii'}(\mu)|(G^r(\mu))^{-1}|\Big)dK,$$

for $1\le i,j\le 2,\ r=1,...,R$.

The *transformation tensors* for bilinear forms are defined as follows:

$$\nu^r_{ij}(\mu)=G^r_{ii'}(\mu)\hat{\nu}^r_{i'j'}G^r_{jj'}(\mu)|(G^r(\mu))^{-1}|,\ 1\le i,j\le 2,\ r=1,...,R,$$

$$\lambda^r_{ij}(\mu)=G^r_{ii'}(\mu)G^r_{jj'}(\mu)|(G^r(\mu))^{-1}|=\frac{\nu^r_{ij}}{\hat{\nu}^r_{i'j'}},\ 1\le i,j\le 2,\ r=1,...,R,$$

where ν^r is the diffusivity in the reference subdomains. For the linear forms we define:

$$\chi^r_i(\mu)=G^r_{ii'}(\mu)|(G^r(\mu))^{-1}|,\ 1\le i\le 2,\ r=1,...,R.$$

Furthermore, we may define:

$$\sigma^{q(i,j,r)}(\mu)=\nu^r_{ij}(\mu),\ \mathcal{A}^{q(i,j,r)}(w,v)=\int_{\Omega^r}\frac{\partial w}{\partial x_i}\frac{\partial v}{\partial x_j}d\Omega,$$

$$\Phi^{s(i,r)}(\mu)=\chi^r_i(\mu),\ \mathcal{B}^{s(i,r)}(w,v)=\int_{\Omega^r}V_i\frac{\partial w}{\partial x_i}v,\ d\Omega, \tag{8.7.2}$$

$$\Upsilon^{q(i,j,r)}(\mu)=\lambda^r_{ij}(\mu),\ \mathcal{S}^{q(i,j,r)}(w,v)=\sum_{K\in\mathcal{T}_h^r}\delta_K\frac{h_K}{\|\mathbf{V}\|}\int_K V_i\frac{\partial w}{\partial x_i}\frac{\partial v}{\partial x_j}V_j\ dK, \tag{8.7.3}$$

$$\mathcal{G}^{s(i,r)}(v)=\sum_{K\in\mathcal{T}_h^r}\delta_K\frac{h_K}{\|\mathbf{V}\|}\int_K \hat{u}V_i\frac{\partial v}{\partial x_i}dK,$$

for $1\le i,j\le 2,\ r=1,...,R$, with q and s "condensed" indexes for combinations of i,j,r and i,r.

We can now apply affine decomposition:

$$\mathcal{A}(\sigma(\mu),w,v)=\sum_{q=1}^{Q^a}\sigma^q(\mu)\mathcal{A}^q(w,v),\quad \mathcal{B}(\Phi(\mu),w,v)=\sum_{s=1}^{Q^b}\Phi^s(\mu)\mathcal{B}^s(w,v),$$

$$\mathcal{S}(\Upsilon(\mu),w_N,v)=\sum_{q=1}^{Q^a}\Upsilon^q(\mu)\mathcal{S}^q(w_N,v),\quad \mathcal{G}(\Phi(\mu),v)=\sum_{s=1}^{Q^b}\Phi^s(\mu)\mathcal{G}^s(v),$$

where $\max(Q^a)=d\times d\times R$ and $\max(Q^b)=d\times R$.

The reduced basis approximation of the stabilized state equation in the reference domain Ω reads: *find* $w_N(\mu)\in W_N$ *such that*

$$\mathcal{A}(w_N,v;\mu)+\mathcal{B}(w_N,v;\mu)+\mathcal{S}(w_N,v;\mu)=\mathcal{F}(v;\mu)+\mathcal{G}(v;\mu),\ \forall v\in W_N.$$

8.7.2 Parametrized adjoint equation

Let $\hat{\mathcal{A}}$ be the form (8.7.1); from the weak formulation of the adjoint problem (8.2.11), we define:

$$\hat{\mathcal{B}}^{ad}(\hat{p},\hat{v}) = \sum_{r=1}^{R}\int_{\hat{\Omega}^r} \hat{p}V_i\frac{\partial\hat{v}}{\partial\hat{x}_i}d\hat{\Omega} = \hat{\mathcal{B}}(\hat{v},\hat{p}),$$

$$\hat{\mathcal{F}}^{ad}(\hat{v}) = \sum_{r=1}^{R}\int_{\hat{\Omega}^r} \hat{m}_D\Big(\hat{w}-\hat{z}_d\Big)\hat{v}\ d\hat{\Omega},$$

$$\hat{\mathcal{S}}^{ad}(\hat{p},\hat{v}) = \sum_{r=1}^{R}\sum_{\hat{K}\in\mathcal{T}_h^r}\delta_{\hat{K}}\int_{\hat{K}}\Big(V_i\frac{\partial\hat{p}}{\partial\hat{x}_i}\Big)\Big(V_j\frac{\partial\hat{v}}{\partial\hat{x}_j}\Big)d\hat{K},$$

$$\hat{\mathcal{G}}^{ad}(\hat{v}) = -\sum_{r=1}^{R}\sum_{\hat{K}\in\mathcal{T}_h^r}\delta_{\hat{K}}\int_{\hat{K}}\hat{m}_D\ \Big(\hat{w}_N-\hat{z}_d\Big)\Big(V_i\frac{\partial\hat{v}}{\partial\hat{x}_i}\Big)d\hat{K},$$

$$\hat{\mathcal{H}}^{ad}(\hat{v}) = -\sum_{r=1}^{R}\sum_{\hat{K}\in\mathcal{T}_h^r}\delta_{\hat{K}}\int_{\hat{K}}\hat{m}_D\Big(V_i\frac{\partial\hat{w}_N}{\partial\hat{x}_i}\Big)\hat{v}\ d\hat{K},$$

for $1\le r\le R$, $1\le i,j\le 2$, where $\hat{\mathcal{B}}$ is defined by (8.7.1).
The reduced basis approximation of the stabilized adjoint problem in the real domain is: $find\ \hat{p}_N(\mu)\in\hat{Z}_N suchthat$:

$$\hat{\mathcal{A}}(\hat{p}_N,\hat{v})+\hat{\mathcal{B}}^{ad}(\hat{p}_N,\hat{v})+\hat{\mathcal{S}}^{ad}(\hat{p}_N,\hat{v}) = \hat{\mathcal{F}}^{ad}(\hat{v})+\hat{\mathcal{G}}^{ad}(\hat{v})+\hat{\mathcal{H}}^{ad}(\hat{v})\ \ \forall\hat{v}\in\hat{Z}_N.$$

In the reference domain, we have:

$$\mathcal{B}^{ad}(p,v;\mu) = \sum_{r=1}^{R}\int_{\Omega^r} V_i\frac{\partial v}{\partial x_i}\Big(G^r_{ii'}(\mu)|(G^r(\mu))^{-1}|\Big)p\ d\Omega,$$

$$\mathcal{F}^{ad}(v;\mu) = \sum_{r=1}^{R}\int_{\Omega^r}\Big(\hat{m}_D\Big(\hat{w}-\hat{z}_d\Big)|(G^r(\mu))^{-1}|\Big)v\ d\Omega,$$

$$\mathcal{S}^{ad}(p,v;\mu) = \sum_{r=1}^{R}\sum_{K\in\mathcal{T}_h^r}\delta_K\int_K V_i\frac{\partial p}{\partial x_i}\Big(G^r_{ii'}(\mu)G^r_{jj'}(\mu)|(G^r(\mu))^{-1}|\Big)\frac{\partial v}{\partial x_j}V_j\ dK,$$

$$\mathcal{G}^{ad}(v;\mu) = -\sum_{r=1}^{R}\sum_{K\in\mathcal{T}_h^r}\delta_K\int_K\hat{m}_D\Big(\hat{w}_N-\hat{z}_d\Big)\Big(V_i\frac{\partial v}{\partial x_i}\Big)\Big(G^r_{ii'}(\mu)|(G^r(\mu))^{-1}|\Big)dK,$$

$$\mathcal{H}^{ad}(v;\mu) = -\sum_{r=1}^{R}\sum_{K\in\mathcal{T}_h^r}\delta_K\int_K\hat{m}_D\Big(V_i\frac{\partial\hat{w}_N}{\partial x_i}\Big)\Big(G^r_{ii'}(\mu)|(G^r(\mu))^{-1}|\Big)v\ dK.$$

We introduce:

$$\Phi^{s(i,r)}(\mu)=\chi^r_i(\mu),\ \mathcal{B}^{s(i,r)}_{ad}(p,v) = \int_{\Omega^r}V_i\frac{\partial v}{\partial x_i}p\ d\Omega,$$

$$\mathcal{S}_{ad}^{q(i,j,r)}(p_N, v) = \sum_{K \in \mathcal{T}_h^r} \delta_K \int_K V_i \frac{\partial p_N}{\partial x_i} \frac{\partial v}{\partial x_j} V_j \; dK, \quad \forall v \in Z_N,$$

$$\mathcal{G}_{ad}^{s(i,r)}(v) = - \sum_{K \in \mathcal{T}_h^r} \delta_K \int_K \hat{m}_D \Big(\hat{w}_N - \hat{z}_d \Big) \Big(V_i \frac{\partial v}{\partial x_i} \Big) dK,$$

$$\mathcal{H}_{ad}^{s(i,r)}(v) = - \sum_{K \in \mathcal{T}_h^r} \delta_K \int_K \hat{m}_D \Big(V_i \frac{\partial w_N}{\partial x_i} \Big) v \; dK,$$

for $1 \leq i, j \leq 2$, $1 \leq r \leq R$, where $\chi_i^r(\mu)$ is defined by (8.7.1).
By the definitions above , we write:

$$\mathcal{B}^{ad}(\Phi(\mu), p, v) = \sum_{s=1}^{Q^b} \Phi^s(\mu) \mathcal{B}_{ad}^s(p, v), \quad \mathcal{S}^{ad}(\Upsilon(\mu), p, v) = \sum_{q=1}^{Q^a} \Upsilon^q(\mu) \mathcal{S}_{ad}^q(p, v),$$

$$\mathcal{G}^{ad}(\Phi(\mu), v) = \sum_{s=1}^{Q^b} \Phi^s(\mu) \mathcal{G}_{ad}^s(v), \quad \mathcal{H}^{ad}(\Phi(\mu), v) = \sum_{s=1}^{Q^b} \Phi^s(\mu) \mathcal{H}_{ad}^s(v),$$

where $\Upsilon^q(\mu)$ e $\Phi^s(\mu)$ are respectively defined in (8.7.3) and (8.7.2).
The reduced basis approximation of the stabilized adjoint equation in the reference domain Ω is: *find* $p_N(\mu) \in Z_N$ *such that*

$$\mathcal{A}(p_N, v) + \mathcal{B}^{ad}(p_N, v) + \mathcal{S}^{ad}(p_N, v) = \mathcal{F}^{ad}(v) + \mathcal{G}^{ad}(v) + \mathcal{H}^{ad}(v) \quad \forall v \in Z_N.$$

At this point we solve a *parametrized optimal control problem.*

8.7.3 Geometrical sensitivity analysis

We fix the source release rates ($u_1 = 20\%$ of $u_{tot} = 27 \; mgs^{-1}$, $u_2 = 5\%$ and so $u_3 = 75\%$), so that the only variable parameters will be the geometrical quantities in order to get important information on geometrical parameters sensitivity. With the adaptive assembling procedure of Section 5.4, we find 35 basis functions.
We report in Figure 8.8 the result of the analysis for the parameterized domain of Figure 8.7. We note that, fixing C_3 (i.e. for a determined upper source position), substance concentration over the observation zone decreases when C_2 goes from 0.1 to 1.3, while for $1.3 \leq C_2 \leq 2.9$ there are no important variations. This is due to the fact that for $C_2 \geq 1.3$ the observation area is out of the lower emission zone. If we keep constant the position C_2 of the lower source, we note that the concentration over the observation zone increases rapidly till it reaches its maximum around $C_3 = 1$ and then it decreases till $C_3 = 2.9$. The explanation of this behavior is that for $C_3 = 0.1$ the observation zone is partially inside the emission wake, while for $C_3 = 1$ it's totaly inside of it. For $C_3 \geq 1$ the zone comes gradually out of the emission wake.

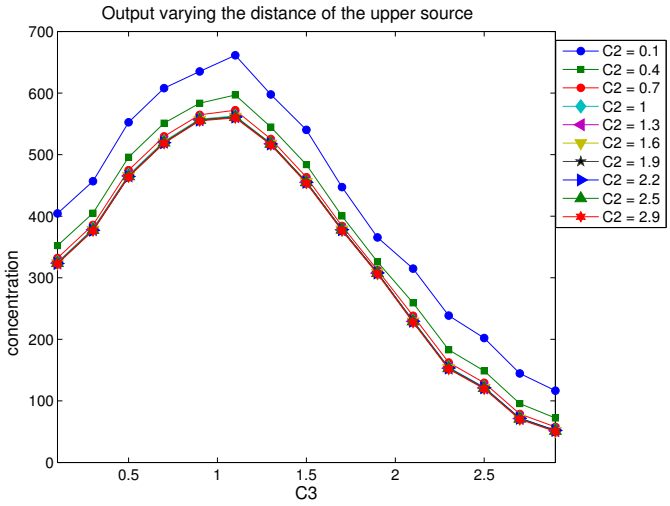

Figure 8.8: Variations of substance concentration (in μg) over the observation zone when the upper (C_3) and lower (C_2) source positions change.

8.7.4 Sensitivity analysis applied to control problem

The choice of geometrical inputs allows us to study the state variable sensitivity to domain variations, to know how the concentration over the observation area varies according to the geometrical changes. We want now to exploit this sensitivity analysis in solving the control problem, in order to optimize the source emission level while keeping the concentration level at an optimal level.

At this purpose we modify the iterative method adopted to solve the control problem. Starting always from an initial value for control variable u_0, we solve state and adjoint equations. Once p is known, we check if the stopping criterium (8.2.9) is satisfied. At every iterative step in which the adjoint variable does not satisfy the stopping criterium, instead of starting directly an iterative process on control variable u, we try first to fulfill the criterium only by varying the positions of upper and lower sources, for example. If we cannot satisfy it just by modifying the geometry, then we update control variable value adopting the steepest descent method (8.2.3). In this way we minimize the number of iteration on u. Figure 8.9 clarifies this new combined technique for solving the control problem.

The number of input parameters for this test problem is six: the emission rates of the two sources and the geometrical parameters of our model, i.e. $\boldsymbol{\mu} = \{u_1, u_2, C_1, C_2, C_3, C_4\}$. The set of parameters $\boldsymbol{\mu}$ belongs to $\mathcal{D} = [0, 27] \times [0, 27] \times [0.1, 2.9] \times [0.1, 2.9] \times [0.1, 2.9] \times [0.1, 2.9]$. We notice that for a number of basis functions $N = 80$, the reduced basis solution of the control problem is a "good" approximation of the finite element solution, i.e. the mean H^1 error for random input is about 10^{-5}. To verify that the control problem solved with the finite element method and the one solved with the reduced basis method converged to the same solution, we compute the two errors ε_u and ε_J for a certain number of random input.

Imposing $tol = 10^{-7}$, we find that the order of magnitude for ε_u mean value is 10^{-5}, while for ε_J mean value is 10^{-10}.
For each of the random input we solve also the simple control problem without geometrical sensitivity, that is the one which iterates only on control function: on an average the sensitivity analysis increases the diffusivity of the substances emitted of around 15% on the total.

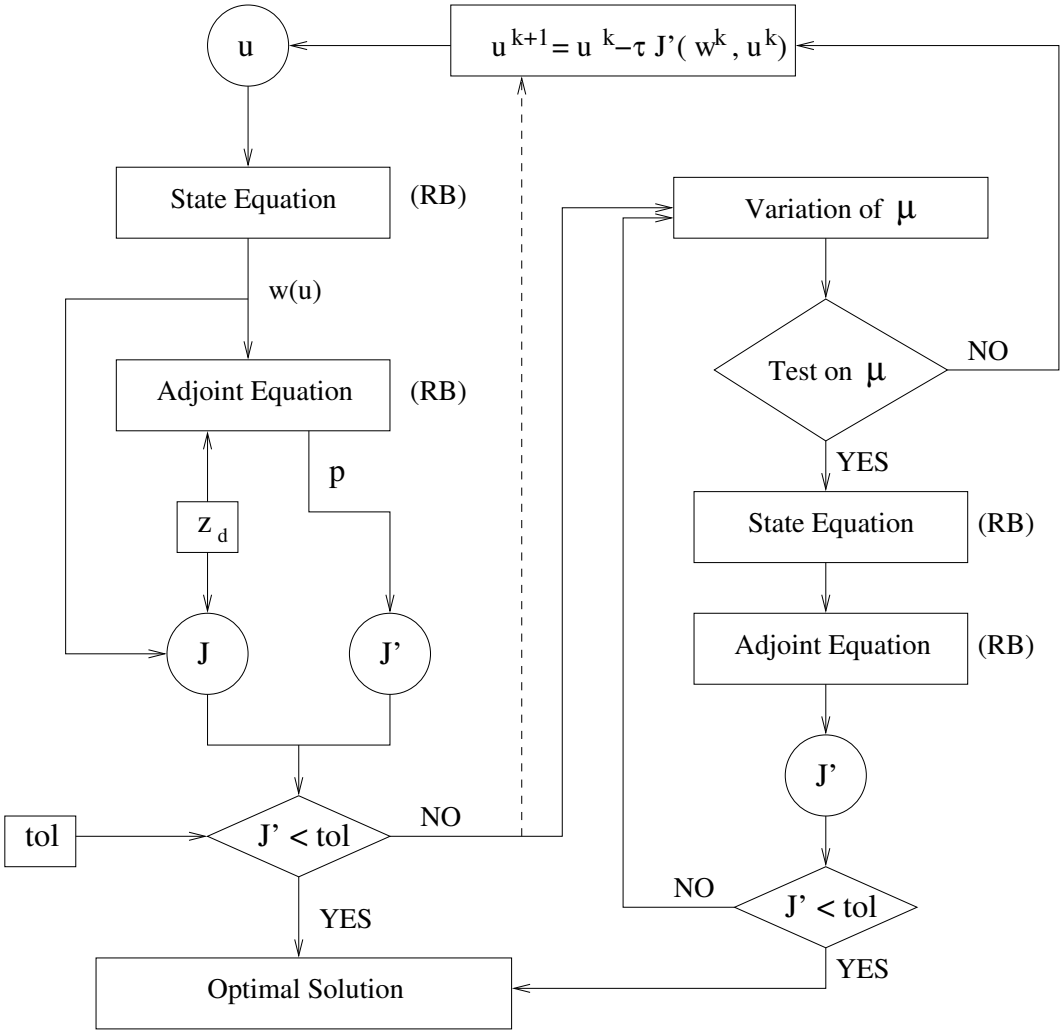

Figure 8.9: Scheme of the iterative process to solve control problem combined with sensitivity analysis.

8.8 Some concluding remarks

We found out that adopting the reduced basis method for the solution of both state and adjoint equations, at every steps of the iterative method used to solve the optimal control problem, implies important advantages from a computational point of view. In the analyzed

cases we found time savings up to 70%.
The reduced basis method shows also in this case great versatility. In fact we analyzed different input parameter classes:

- *control input* - in our application this kind of input is related to the emissions from sources, for example;
- *physical input* - this kind of input allows us to take into account advection and diffusivity conditions;
- *geometrical input* - in order to consider the position of the emitting sources with respect to the observation zone.

With all these different parametrization we are able to solve the control problem from a global and decisional point of view, being able to consider, at the same time, several aspects of the same problem. All the extensions to reduced basis methods introduced in the previous chapters (Stokes and Navier-Stokes problems in domains with also non-affine parametric dependence) are possible.
An other interesting aspect to consider in the efficient resolution of optimal control problems is the mesh adaptivity and the influence of the mesh on the accuracy of cost functional estimation. This aspect is developed in the work by Dedè and Quarteroni [32].
A further extension is the development of a posteriori error estimation in the reduced basis context dealing with problem with non-affine geometrical parametric dependence.

8.9 Appendix: reduced basis for time-dependent problem

In this appendix we show very briefly how to solve an unsteady problem with reduced basis considering also time as a parameter. An unsteady problem has been recently studied using reduced basis method by Grepl in [44] and before by Ito and Ravindran in [64].
Indicating with w the concentration of a substance, with $\mathbf{V}$ a velocity field (for example given by a Navier-Stokes simulation in the same domain) and with ν the diffusivity coefficient, we consider the following state equation in Ω completed with properly initial and boundary condition:

$$\begin{cases} \frac{\partial w}{\partial t} - \nu \triangle w + \mathbf{V} \cdot \nabla w = \beta(\mathbf{x}) u(t), \\ w = 0 \ on \ \Gamma_D, \\ \nabla w \cdot \hat{\mathbf{n}} = 0 \ on \ \Gamma_N, \\ y(t=0) = 0. \end{cases} \tag{8.9.1}$$

The right-hand-side is built as a product of two functions: β, depending on spacial coordinates, indicating for example the zone of emission of a source and u, time dependent, indicating an emission rate in time. Introducing $H^1_{\Gamma_D} = \{v \in H^1 \ : \ v|_{\Gamma_D} = 0\}$, we can write the weak formulation for the problem (8.9.1):

$$\forall \ 0 < t \leq 1 \ find \ w(t) \in H^1_{\Gamma_D} \quad : \quad a(w(t), \varphi) = F(\varphi, u(t)), \ \forall \varphi \in H^1_{\Gamma_D},$$

where

$$a(w(t),\varphi) := \int_\Omega \frac{\partial w}{\partial t}\ \varphi\ d\Omega + \int_\Omega \nu\nabla w\cdot\nabla\varphi\ d\Omega + \int_\Omega \mathbf{V}\cdot\nabla w\ \varphi\ d\Omega,$$

$$F(\varphi,u) := \int_\Omega \beta(\mathbf{x})u(t)\varphi\ d\Omega.$$

We introduce a triangulation $\mathcal{T}_h$ of the domain and a time discretization in the interval $[0,1]$ s. We approximate the temporal derivative with:

$$\frac{\partial w}{\partial t} = \frac{w^k - w^{k-1}}{\Delta t},$$

where $w^k = w(t^k = k\cdot\Delta t)$, for $k = 1,...,N_k$ with $N_k = 1/\Delta t$. Using a strategy based on *backward Euler* ([127]) we find the following discretized problem:

$$for\ 1\le k\le N_k\ find\ w^k\in H^1_{\Gamma_D}\quad :\quad a^k(w^k,\varphi) = F^k(\varphi,u^k),\ \forall\varphi\in H^1_{\Gamma_D},$$

where

$$a^k(w^k,\varphi) := \Delta t^{-1}\int_\Omega w^k\ \varphi\ d\Omega + \int_\Omega \nu\nabla w^k\cdot\nabla\varphi\ d\Omega + \int_\Omega \mathbf{V}^k\cdot\nabla w^k\ \varphi\ d\Omega,$$

$$F^k(\varphi,u^k) := \int_\Omega \beta(\mathbf{x})u^k\varphi\ d\Omega + \Delta t^{-1}\int_\Omega w^{k-1}\ \varphi\ d\Omega,$$

and $\mathbf{V}^k$ is the velocity field at the instance t^k, while $u^k = u(t^k)$.
For values of $\nu\in[0.1,10]$ we note that the local *Péclet* number is always greater than unity and so we need stabilization procedure (see [127]). Indicating with $w^k_h\in X_h$ the Galerkin-Finite Element approximation at instance t^k, the problem becomes the following:

$$find\ w^k_h\in X_h\quad :\quad a^k(w^k_h,\varphi_h) + \mathcal{L}^{(\rho)}_h(w^k_h,f,\varphi_h) = F^k(\varphi,u^k),\ \forall\varphi_h\in X_h.$$

so that $\mathcal{L}^{(\rho)}_h(w^k,f,\varphi_h) = 0$, $\forall\varphi_h\in X_h$. The formulation for $\mathcal{L}^{(\rho)}_h$ is:

$$\mathcal{L}^{(\rho)}_h(w_h,f,\varphi_h) = \sum_{K\in\mathcal{T}_h}\delta_K(Aw_h - f,\mathcal{S}^{(\rho)}_K(\varphi_h))_{L^2(K)}, \tag{8.9.2}$$

where $Aw = \frac{\partial w}{\partial t} - \nu\triangle w + \mathbf{V}\cdot\nabla w$ and $f = \beta(\mathbf{x})u(t)$, while

$$\mathcal{S}^\rho_K = \frac{h_K}{\|\mathbf{V}\|}\ [A_{SS}\varphi_h + \rho\cdot A_S\varphi_h],$$

with $A_{SS}\varphi_h$ and $A_S\varphi_h$ we indicate, respectively, the antisymmetric part and the symmetric part of the operator $A\varphi_h$. We decide to use SUPG method so that $\rho = 0$ and we consider only the following antisymmetric part of the operator A which is:

$$A_{SS}\varphi_h = \frac{1}{2}\Big(\nabla\cdot(\mathbf{V}\varphi_h) + \mathbf{V}\cdot\nabla\varphi_h\Big) = \frac{1}{2}\Big(\nabla\cdot\mathbf{V} + \mathbf{V}\cdot\nabla\varphi_h + \mathbf{V}\cdot\nabla\varphi_h\Big) = \mathbf{V}\cdot\nabla\varphi_h,$$

and the stabilized problem becomes:

$$for\ 1\le k\le N_k\ find\ w^k_h\in \mathrm{X}_h\quad :\quad a^k(w^k_h,\varphi_h) + s_h(w^k_h,\varphi_h;u^k) = F^k(\varphi_h;u^k),\ \forall\varphi_h\in \mathrm{X}_h,$$

$$s_h(w_h^k, \varphi_h; u^k) := \sum_{K \in \mathcal{T}_h} \delta_K \frac{h_K}{\|\mathbf{V}^k\|} \int_K (A w_h^k - f)(A_{SS}\varphi_h)\ dK$$

or its equivalent formulation:

$$for\ 1 \le k \le N_k\ find\ w_h^k \in \mathrm{X_h} \quad : \quad a_h^k(w_h^k, \varphi_h) = F_h^k(\varphi_h; u^k),\ \forall \varphi_h \in \mathrm{X_h}, \tag{8.9.3}$$

where

$$a_h^k(w_h^k, \varphi_h) := a^k(w_h^k, \varphi_h) + \sum_{K \in \mathcal{T}_h} \delta_K \frac{h_K}{\|\mathbf{V}^k\|} \int_K (\Delta t^{-1} w_h^k + \mathbf{V}^k \cdot \nabla w_h^k)(\mathbf{V}^k \cdot \nabla \varphi_h)\ dK,$$

$$F_h^k(\varphi_h; u^k) := F(\varphi_h; u^k) + \sum_{K \in \mathcal{T}_h} \delta_K \frac{h_K}{\|\mathbf{V}^k\|} \Big[\int_K (\Delta t^{-1} w_h^{k-1})(\mathbf{V}^k \cdot \nabla \varphi_h)\ dK +$$

$$+ \int_K \beta_h u^k (\mathbf{V}^k \cdot \nabla \varphi_h)\ dK \Big],$$

where h_K is the diameter of K, δ_K is a parameter depending on the local Péclet number, β_h is the discrete approximation of $\beta(\mathbf{x})$ function and $\mathrm{X_h} \subset \mathrm{H}^1_{\Gamma_\mathrm{D}}$ is the finite element space (for example $\mathbb{P}^1$). The contribution to stabilization is zero on the elements where $\mathbf{V}^k$ is zero. The output of interest (concentration) into a subdomain $\Omega_s \subset \Omega$ is:

$$s(\nu, t) = |\Omega_s|^{-1} \int_{\Omega_s} w(\nu, t)\ d\Omega. \tag{8.9.4}$$

8.9.1 Reduced basis formulation

We consider the input made up of the following vector of parameters: $\mu = (\nu, t^f)$, where $t^f \in [0, 1]$ s is the time instance of which we want to know the solution, $\mu \in \mathcal{D} \subset \mathbb{R}^2$, $\mathcal{D} = [0.1, 1] \times [0, 1]$.
The reduced basis solution of problem (8.9.3) is indicated with $y_N(\mu)$ and given by:

$$w_N(\nu, t^k) = \sum_{j=1}^{N} w_{N_j}^k(\mu)\zeta^j = \sum_{j=1}^{N} w_{N_j}^k(\mu) \sum_{i=1}^{\mathcal{N}} \zeta_i^j \varphi_i. \tag{8.9.5}$$

The N unknowns $w_{N_j}^k(\mu)$ are calculated by solving the following problem:

$$a_h^k(w_N(\mu), \zeta_h; \mu) = F_h^k(\zeta_h) \quad 1 \le h \le N \text{e } 1 \le k \le N_k,$$

where

$$a_h^k(w_N, \zeta_h; \mu) = \sum_{j=1}^{N}\sum_{h=1}^{N} w_{N_j}^k(\mu) \sum_{i=1}^{\mathcal{N}}\sum_{l=1}^{\mathcal{N}} \zeta_i^j \zeta_l^h \Big[\Delta t^{-1} \sum_{K \in \mathcal{T}_h} \int_K \varphi_i\ \varphi_l + \nu \sum_{K \in \mathcal{T}_h} \int_K \nabla \varphi_i \cdot \nabla \varphi_l +$$

$$\sum_{K \in \mathcal{T}_h} \int_K (\mathbf{V}^k \cdot \nabla \varphi_i)\varphi_l + \sum_{K \in \mathcal{T}_h} \delta_K \frac{h_K}{\|\mathbf{V}^k\|} \int_K (\Delta t^{-1} \varphi_i + \mathbf{V}^k \cdot \nabla \varphi_i)(\mathbf{V}^k \cdot \nabla \varphi_l) \Big]$$

and

$$F_h^k(\zeta_h) = \sum_{j=1}^{N}\sum_{h=1}^{N} w_{N_j}^{k-1} \sum_{i=1}^{\mathcal{N}}\sum_{l=1}^{\mathcal{N}} \zeta_i^j \zeta_l^h \Big[\Delta t^{-1} \sum_{K\in\mathcal{T}_h} \int_K \varphi_i\, \varphi_l + \Delta t^{-1} \sum_{K\in\mathcal{T}_h} \delta_K \frac{h_K}{\|\mathbf{V}^k\|} \int_K \varphi_i(\mathbf{V}^k\cdot\nabla\varphi_l)\Big] +$$

$$\sum_{h=1}^{N}\sum_{l=1}^{\mathcal{N}} \zeta_l^h \Big[\sum_{K\in\mathcal{T}_h} \int_K \beta_h u^k \varphi_l + \sum_{K\in\mathcal{T}_h} \delta_K \frac{h_K}{\|\mathbf{V}^k\|} \int_K \beta_h u^k (\mathbf{V}^k\cdot\nabla\varphi_l)\Big].$$

We define $\underline{M}$, $\underline{C}$, $\underline{B}$, $\underline{S}$, as mass matrix, stiffness matrix, transport related matrix and stabilization one, respectively:

$$M_{l,i} = \sum_{K\in\mathcal{T}_h} \int_K \varphi_i\, \varphi_l,$$

$$C_{l,i} = \sum_{K\in\mathcal{T}_h} \int_K \nabla\varphi_i \cdot \nabla\varphi_l,$$

$$B_{l,i} = \sum_{K\in\mathcal{T}_h} \int_K (\mathbf{V}^k\cdot\nabla\varphi_i)\varphi_l,$$

$$S_{l,i}(\mu) = \sum_{K\in\mathcal{T}_h} \delta_K \frac{h_K}{\|\mathbf{V}^k\|} \int_K (\Delta t^{-1}\varphi_i + \mathbf{V}^k\cdot\nabla\varphi_i)(\mathbf{V}^k\cdot\nabla\varphi_l).$$

We introduce matrix $\underline{A}_h$ given by:

$$A_{h_{l,i}}(\mu) = \Delta t^{-1}\cdot M_{l,i} + \nu\cdot C_{l,i} + B_{l,i} + S_{l,i}(\mu).$$

To write also the right-hand-side we define $\underline{D}$ e $\underline{G}$, $\underline{H}$:

$$D_{l,i}(\mu) = \sum_{K\in\mathcal{T}_h} \delta_K \frac{h_K}{\|\mathbf{V}^k\|} \int_K \varphi_i(\mathbf{V}^k\cdot\nabla\varphi_l),$$

$$G_l = \sum_{K\in\mathcal{T}_h} \int_K \beta_h u^k \varphi_l,$$

$$H_l(\mu) = \sum_{K\in\mathcal{T}_h} \delta_K \frac{h_K}{\|\mathbf{V}^k\|} \int_K \beta_h u^k (\mathbf{V}^k\cdot\nabla\varphi_l),$$

$\underline{S}$, $\underline{D}$ and $\underline{H}$ are depending on μ, because δ_K is depending on the Péclet number (an on ν) and they should be calculated online. All the other quantities are calculated offline.
The reduced basis solution $\underline{w}_N^k(\mu)$ is obtained by solving the following problem:

$$(\underline{W}^T \underline{A}_h(\mu)\underline{W})\ \underline{w}_N^k(\mu) = \Delta t^{-1}\cdot[\underline{W}^T(\underline{M} + \underline{D}(\mu))\underline{W}]\ \underline{w}_N^{k-1} + \underline{W}^T(\underline{G} + \underline{H}(\mu)), \tag{8.9.6}$$

where $\underline{w}_N^{k-1}$ is known by the solution at the previous time step $t = t^{k-1}$.
From solution (8.9.5) we can calculate the output approximation:

$$s_N^k(\nu, t^k) = |\Omega_s|^{-1} \int_{\Omega_s} w_N^k(\mu)\ d\Omega. = |\Omega_s|^{-1} \sum_{j=1}^{N} w_{N_j}^k(\mu) \sum_{i=1}^{\mathcal{N}} \zeta_i^j \int_{\Omega_s} \varphi_i\ d\Omega. \tag{8.9.7}$$

Basis assembling

As basis function we take solutions calculated at different time steps ($\delta t = 0.1$ s) and at different values of $\nu = 0.1, 0.3, 0.5, 0.7, 1$ as shown in Figure 8.10. With this kind of basis the relative H^1 max error for a great number of random configurations during the optimized assembling process is shown in Figure 8.11.

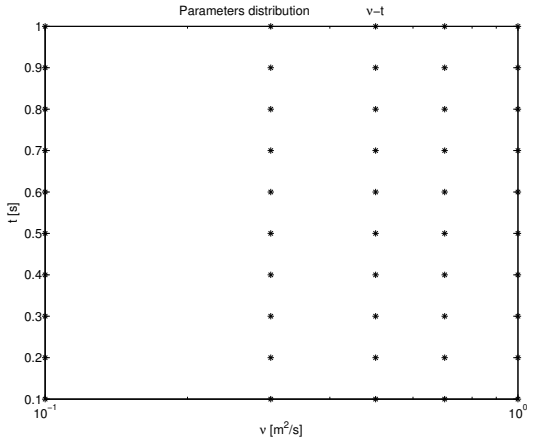

Figure 8.10: Basis construction.

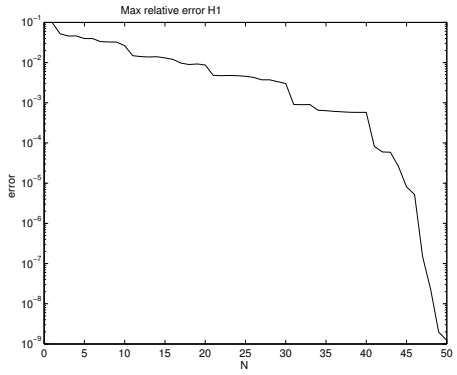

Figure 8.11: Max H^1 relative error during basis assembling and optimization.

Error on solutions

We can calculate the relative H^1 error considering a great number of different random configuration and using the basis assembled previously. Figure 8.12 shows max and mean error varying N. The same calculation is carried out considering the error on outputs and it is shown in Figure 8.13.

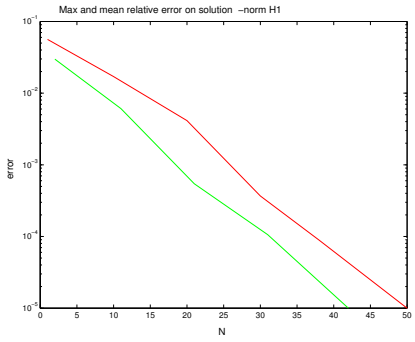

Figure 8.12: Max and mean H^1 relative error on solutions.

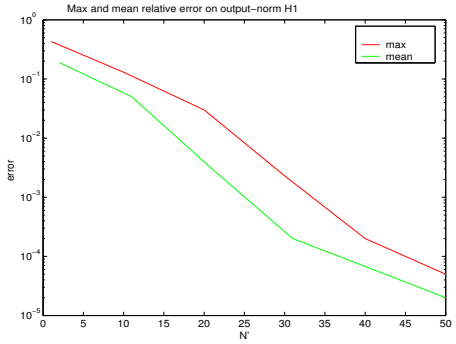

Figure 8.13: Max and mean H^1 relative error on output.

Appendix A

An Introduction to Reduced Basis Methods: Elliptic Equations in Parametrized Domains

In this appendix we review several aspects of reduced basis methods and we deal for simplicity with multi-parametrized subdomains in the elliptic case (introduced also in [135]). The essential components of the method are (i) (provably) rapidly convergent global reduced-basis approximations — Galerkin projection onto a space W_N spanned by solutions of the governing partial differential equation at N selected points in parameter space; (ii) a posteriori *error estimation — relaxations of the error-residual equation that provide inexpensive bounds for the error in the outputs of interest; and (iii) off-line/on-line computational procedures — methods which decouple the generation and projection stages of the approximation process. The operation count for the on-line stage — in which, given a new parameter value, we calculate the output of interest and associated error bound — depends only on N (typically very small) and the parametric complexity of the problem; the method is thus ideally suited for the repeated and rapid evaluations required in the context of parameter estimation, design, optimization, and real-time control. In [118] a rigorous* a posteriori *error bound framework for reduced-basis approximations of elliptic coercive equations is developed. The resulting error estimates are, in some cases, quite sharp: the ratio of the estimated error in the output to the true error in the output, or* effectivity*, is close to (but always greater than) unity. We use* a posteriori *bound error estimator applied also to an adaptive procedure in choosing the approximation space and its dimension, minimizing the estimated error or the* effectivity *[161].*

A.1 Overview on reduced basis

The optimization, control, design and characterization of an engineering component or system requires, as seen also in the first part of the thesis, the prediction of certain "quantities of interest," or performance metrics, which we shall denote *outputs* — for example velocity field, maximum stresses, maximum temperatures, heat transfer rates, flow rates, vorticity, or lifts

and drags. These outputs are typically expressed as functionals of field variables associated with a parametrized partial differential equation which describes the physical behavior of the component or system. The parameters, which we shall denote *inputs*, serve to identify a particular "configuration" of the components: these inputs may represent design or decision variables, such as geometry, or characterization variables, such as physical properties — for example in inverse design problems. We thus get an implicit *input–output* relationship, evaluation of which demands solution of the underlying partial differential equations. See [158] for a detailed presentation of the state of the art of the design problem and some examples.

The development of computational methods is permitting *rapid* and *reliable* evaluation of this partial-differential-equation-induced input-output relationship in the design, optimization and control contexts. See recent developments in [134]. The approach used is based on the reduced-basis method, first introduced in the late 1970s for non-linear structural analysis, and later developed more extensively in the 1980s and 1990s [11, 13, 37, 113, 117, 133]. The reduced basis method recognizes that the field variable is not, in fact, some arbitrary member of the infinite-dimensional solution space associated with the partial differential equation; rather, the field variable resides, or evolves, on a much lower-dimensional manifold induced by the parametric dependence.

In the application we use *global* approximation spaces; second, we make rigorous *a posteriori error estimations*; and third, we exploit *off-line/on-line* computational decompositions (see Balmes [11] for application of this strategy within the reduced–basis context). These three steps allow us — for the restricted but important class of "parameter-affine" problems, that it has been extended in Chapters 6 and 7 — to reliably decouple the generation and projection stages of reduced-basis approximation, thereby effecting computational economies of several orders of magnitude.

In Section A.2 we present the problem statement. In Section A.3 we describe the *a posteriori* error estimation framework. In Section A.4 we present the *a priori* convergence theory applied also to our output bounds and not only to approximate solution. In Section A.5 we study our procedure to control N more tightly and to apply our error bound adaptively in the choice of μ parameters family. Finally, in Section A.6, we present the application and in the Section A.7 the numerical results for our "model-problem" example, in Section A.8, we provide our guidelines for the development of reduced basis method in fluid mechanics and precisely in haemodynamics. These aspects are the subject of Chapters 5, 6, 7 and 8. Finally, in Section A.9 we provide an historical review on model-order reduction and some remarks on its development.

A.2 Problem formulation

We first introduce a Hilbert space Y, and an associated inner product and a norm, $(\cdot,\cdot)$ and $\|\cdot\| \equiv (\cdot,\cdot)^{1/2}$, respectively. We next introduce the dual space of Y, Y', and the associated duality pairing between Y and Y', ${}_{Y'}\langle\cdot,\cdot\rangle_Y \equiv \langle\cdot,\cdot\rangle$.

We then define, for any $\mu \in \mathcal{D}^\mu \subset \mathbb{R}^P$, the parametrized (distributional) operator $\mathcal{A}(\mu)\colon Y \rightarrow$

Y'. We assume that $\mathcal{A}(\mu) = A(\Theta(\mu))$, where, for any $\Theta \in \mathbb{R}^Q_+$, $A(\Theta)\colon Y \to Y'$ is given by

$$A(\Theta) = A_0 + \sum_{q=1}^{Q} \Theta_q \, A_q \ ,$$

and the $\Theta_q\colon \mathcal{D}^\mu \to \mathbb{R}_+$, $q = 1, \ldots, Q$, are non-negative functions. Here $\mathbb{R}_+$ refers to the non-negative real numbers. The range of Θ is denoted $\mathcal{D}^\theta$; and we define $\theta^{\min}$ (≥ 0), $\theta^{\max}$ (assumed finite), and $\mathcal{D}^\theta_{\rm box} \subset \mathbb{R}^Q_+$ as

$$\begin{aligned} \theta_q^{\min} &\equiv \sup t_{\{t\in\mathbb{R}_+ \,|\, \Theta_q(\mu)\geq t,\ \forall \mu\in\mathcal{D}^\mu\}}, \qquad q = 1, \ldots, Q \ , \\ \theta_q^{\max} &\equiv \inf t_{\{t\in\mathbb{R}_+ \,|\, \Theta_q(\mu)\leq t,\ \forall \mu\in\mathcal{D}^\mu\}}, \qquad q = 1, \ldots, Q \ , \end{aligned}$$

and $\mathcal{D}^\theta_{\rm box} \equiv \Pi_{q=1}^Q [\theta_q^{\min}, \theta_q^{\max}]$, respectively.
Finally, we require that A_0 is continuous, symmetric, and coercive, and that the A_q, $q = 1, \ldots, Q$, are continuous, symmetric, and positive-semidefinite ($\langle A_q v, v\rangle \geq 0$, $\forall\, v \in Y$); it follows that $A(\Theta)$ (respectively, $\mathcal{A}(\mu)$) is continuous, symmetric, and coercive for all θ in $\mathcal{D}^\theta_{\rm box}$ (respectively, for all μ in $\mathcal{D}^\mu$).
The general formulation for the problem can then be stated as: given $\mu \in \mathcal{D}^\mu$, and linear functional $F \in Y'$, evaluate the output

$$s(\mu) = \langle F, u(\mu)\rangle,$$

where $u(\mu) \in Y$ is the unique solution of $A(\Theta(\mu))\, u(\mu) = F$; we shall interpret the latter as

$$\langle A(\Theta(\mu))\, u(\mu), v\rangle = \langle F, v\rangle, \quad \forall\, v \in Y. \tag{A.2.1}$$

Output $s(\mu)$ may also be interpreted as the energy of the solution — $s(\mu) = \langle F, u(\mu)\rangle = \langle A(\Theta(\mu))\, u(\mu), u(\mu)\rangle$ — and is hence strictly positive. The output $s(\mu)$ is "compliant," and the operator $A(\Theta)$ is symmetric; however, the formulation will be readily extended [118] to treat both non-compliant outputs, $s(\mu) = \langle L, u(\mu)\rangle$ for given $L \in Y'$, and non-symmetric, but still coercive, operators. We may also express our output as

$$s(\mu) = \langle F, A^{-1}(\Theta(\mu))F\rangle. \tag{A.2.2}$$

Here, for any $\theta \in \mathcal{D}^\theta_{\rm box}$, $A^{-1}(\Theta)\colon Y' \to Y$ is the (continuous, symmetric, coercive) inverse of $A(\Theta)$; further, $\forall\, G \in Y'$, $\langle A(\Theta)\, A^{-1}(\Theta)\, G, v\rangle = \langle G, v\rangle$, $\forall\, v \in Y$.

A.2.1 Galerkin approximation

The $u(\mu)$ of (A.2.1) are, in general, not known exactly. In order to construct our reduced-basis space we will therefore require a *finite*-dimensional "truth" approximation to Y, which we shall denote $\tilde{Y}_h$; $\tilde{Y}_h$ is an $\mathcal{N}$-dimensional subspace of Y. For example, for $\Omega \subset \mathbb{R}^{d=1,\,2,\,\text{or}\,3}$, and $\tilde{Y}_h \subset H^1(\Omega)$, $\tilde{Y}_h$ will typically be a finite element approximation space associated with a very fine triangulation $\mathcal{T}_h$ of the computational domain. We assume that the triangles, denoted with T_h^j, also referred to as elements, cover the computational domain Ω , $\bar{\Omega} = \cup_{T_h\in\mathcal{T}_h} \bar{T}_h$ ($\bar{T}_h$

is the closure T_h) and that each of the elements do not overlap, $T_h^i \cap T_h^j = 0,\ \forall T_h^i,\ T_h^j \in \mathcal{T}_h$. The subscript h denotes the diameter of the triangulation defined as:

$$h = \sup_{T_h \in \mathcal{T}_h} \sup_{x,y \in T_h} |x - y|; \tag{A.2.3}$$

here $|\cdot|$ is the Euclidean norm.

Discrete Problem

Using then the triangulation $\mathcal{T}_h$, we define the space $\tilde{Y}_h$ as the space of continuous functions which are piecewise linear over each of the elements $T_h \in \mathcal{T}_h$:

$$\tilde{Y}_h = \{v \in C^0(\bar{\Omega})\ |v|_{T_h} \in \mathbb{P}^1(T_h),\ \forall T_h \in \mathcal{T}_h\}. \tag{A.2.4}$$

If $\mathcal{N}$ is the number of nodes in the triangulation, we introduce the Lagrangian basis functions $\phi_i \in \tilde{Y}_h$, such that $\phi_i(x_j) = \delta_{i\,j},\ i, j = 1, \ldots, \mathcal{N}$, where x_j are the coordinates of node j, and $\delta_{i\,i} = 1$ if $i = j$, or $\delta_{i\,j} = 0$ if $i \neq j$. Each function ϕ_i has compact support over the region defined by the elements surrounding node i . In general, we expect that $\mathcal{N}$ will be very large. See also [127] for more detailed studies on FEM approximation.
Our Galerkin-FEM approximation can be stated as: given a $\mu \in \mathcal{D}^\mu$, evaluate the output

$$\tilde{s}(\mu) = \langle F, \tilde{u}(\mu) \rangle, \tag{A.2.5}$$

where $\tilde{u}(\mu) \in \tilde{Y}_h$ is the unique solution of

$$\langle A(\Theta(\mu))\ \tilde{u}(\mu), v \rangle = \langle F, v \rangle, \quad \forall\, v \in \tilde{Y}_h. \tag{A.2.6}$$

As before, the output can be expressed as a (strictly positive) energy: $\tilde{s}(\mu) = \langle F, \tilde{u}(\mu) \rangle = \langle A(\Theta(\mu))\ \tilde{u}(\mu), \tilde{u}(\mu) \rangle$.
It is convenient to express (A.2.5)–(A.2.6) in terms of the basis for $\tilde{Y}_h = \{\phi_i,\ i = 1, \ldots, \mathcal{N}\}$. We first introduce the matrices $\underline{\tilde{A}}_q \in \mathbb{R}^{\mathcal{N} \times \mathcal{N}}$, $q = 0, \ldots, Q$, as $\tilde{A}_{q\,i\,j} = \langle A\phi_j, \phi_i \rangle$, $1 \leq i, j \leq \mathcal{N}$; it is readily shown that $\underline{\tilde{A}}_0$ (respectively, $\underline{\tilde{A}}_q$, $q = 1, \ldots, Q$) is symmetric positive-definite (respectively, symmetric positive-semidefinite). For any $\Theta \in \mathcal{D}^\theta_{\text{box}}$, we then define $\underline{\tilde{A}}(\Theta) \in \mathbb{R}^{\mathcal{N} \times \mathcal{N}}$ as

$$\underline{\tilde{A}}(\Theta) = \underline{\tilde{A}}_0 + \sum_{q=1}^{Q} \Theta_q\, \underline{\tilde{A}}_q;$$

$\underline{\tilde{A}}(\Theta)$ is symmetric positive-definite for all $\Theta \in \mathcal{D}^\theta_{\text{box}}$. In the same way we introduce $\underline{\tilde{F}} \in \mathbb{R}^{\mathcal{N}}$ as $\tilde{F}_i = \langle F, \phi_i \rangle$, $1 \leq i \leq \mathcal{N}$.
Our approximation can then be restated as: given $\mu \in \mathcal{D}^\mu$, evaluate the output

$$\tilde{s}(\mu) = \underline{\tilde{F}}^T\, \underline{\tilde{u}}(\mu),$$

where ^{T} refers to the algebraic transpose and $\underline{\tilde{u}}(\mu) \in \mathbb{R}^{\mathcal{N}}$ is the unique solution of

$$\underline{\tilde{A}}(\Theta(\mu))\ \underline{\tilde{u}}(\mu) = \underline{\tilde{F}}; \tag{A.2.7}$$

Note that $\tilde{u}(\mu)$ and $\underline{\tilde{u}}(\mu) = (\tilde{u}_1, \ldots, \tilde{u}_{\mathcal{N}})^T$ are related via

$$\tilde{u}(\mu) = \sum_{j=1}^{\mathcal{N}} \tilde{u}_j(\mu)\, \phi_j \ .$$

As always, our compliance output can be expressed as an energy:

$$\tilde{s}(\mu) = \underline{\tilde{u}}^T(\mu)\, \underline{\tilde{A}}(\Theta(\mu))\, \underline{\tilde{u}}(\mu),$$

or, equivalently,

$$\tilde{s}(\mu) = \underline{\tilde{F}}^T\, \underline{\tilde{A}}^{-1}(\Theta(\mu))\, \underline{\tilde{F}}, \tag{A.2.8}$$

where $\underline{\tilde{A}}^{-1}(\Theta)$ is the (symmetric, positive-definite) inverse of $\underline{\tilde{A}}(\Theta)$. Note that since $\mathcal{N}$ can be large, solution of (A.2.7), and hence evaluation of $\tilde{s}(\mu)$, will be computationally expensive.

Computational Complexity

We see that the original problem has been replaced by a finite-dimensional one. Assuming sufficient regularity of the solution $u(\mu)$ the *a priori* convergence theory for this type of finite-elements suggests that the error in the output $|s(\mu) - \tilde{s}(\mu)|$ will converge as h^2 (see Theorem 4.1 in Patera and Rønquist [110]), where h is defined in (A.2.3). Moreover as $h \to 0$, we get $\tilde{u}(\mu) \to u(\mu)$ and $\tilde{s}(\mu) \to s(\mu)$. The above *a priori* result suggests also that to decrease the error in the output by a factor $C > 0$, we need to increase the number of elements and therefore $\mathcal{N}$ roughly by the same factor. We see that as the requirements for accuracy increase or the geometric complexity increases, we need higher $\mathcal{N}$ to obtain accurate and reliable results (to ascertain the accuracy we need *a posteriori* error estimators). Moreover, in the presence of singularities or boundary layers, local refinement is essential, further increasing the required degrees of freedom.

The discussion above suggests that even for relatively simple problems in simple domains $\mathcal{N}$ is large, at least $\mathcal{O}(10^3)$, but it is not uncommon for $\mathcal{N}$ to be $\mathcal{O}(10^6)$ or higher. We also see the difficulty, as $\mathcal{N}$ increases, so does the size of the linear system (A.2.7), which has to be inverted. By virtue of the compact support of ϕ_i, the matrix $\underline{\tilde{A}}$ is sparse and therefore iterative solvers can be used to obtain a solution. The computational complexity scales as $\mathcal{O}(\mathcal{N}^a)$, where a depends on the condition number of the problem (which increases quadratically with $1/h$). Especially in contexts where repeated solution of (A.2.7) is required, the computational requirements soon become unacceptably large.

A.2.2 Reduced basis method

Identifying the problem in the high dimensionality of the finite-element spaces, we look for ways to further reduce the computational complexity. The large number of degrees of freedom required in the case of finite-element methods, is attributed to the particular choice of basis functions, which have general approximation properties for functions in Y. To further reduce the computational complexity we look for spaces with approximation properties specific to the problem of interest.

The critical observation is that the solution and the output evolve in a low-dimensional manifold induced by the parametric dependence of the problem. Central to reduced-basis methods, first introduced in Nagy [102], is constructing an approximation to this manifold. In our approach, slightly different from earlier approaches, we construct linear reduced-basis spaces comprising of solutions to (A.2.7) at different parameter points. We then use these spaces to find an approximation $u_N(\mu)$ to the exact solution.
Earlier approaches viewed the reduced-basis method as a combined projection and continuation method. A different view, suitable for our purposes, is that of multi-dimensional parameter-space interpolation. The required interpolation weights are obtained by solving suitably defined low-dimensional problems chosen to minimize the approximation error measured in problem-specific energy norms.

Reduced-basis space

We introduce some "μ" samples $S_N^\mu = \{\mu^1, \ldots, \mu^N\}$, where $\mu^n \in \mathcal{D}^\mu$, $n = 1, \ldots, N$. We then define our reduced basis space $W_N = \text{span}\{\tilde{\zeta}_n, n = 1, \ldots, N\}$, where $\tilde{\zeta}_n = \tilde{u}(\mu^n)$, $n = 1, \ldots, N$. Recall that $\tilde{u}(\mu^n)$ is the solution of (A.2.6) for $\mu = \mu^n$. We denote $\underline{\tilde{\zeta}}_n = \underline{\tilde{u}}(\mu^n)$, $n = 1, \ldots, N$. In the first step, given a $\mu \in \mathcal{D}^\mu$, we find $s_N(\mu) = \langle F, u_N(\mu)\rangle$, where $u_N(\mu) \in W_N$ satisfies

$$\langle A(\Theta(\mu))\, u_N(\mu), v\rangle = \langle F, v\rangle, \quad \forall\, v \in W_N.$$

Also in this case we can express the output as an energy, $s_N(\mu) = \langle A(\Theta(\mu))\, u_N(\mu), u_N(\mu)\rangle$. In terms of our basis functions, we define the symmetric positive-definite matrix $\underline{A}_N(\mu) \in \mathbb{R}^{N\times N}$ as $A_{N\,i\,j}(\mu) = \langle A(\Theta(\mu))\tilde{\zeta}_j, \tilde{\zeta}_i\rangle$, $1 \le i, j \le N$, and the vector $\underline{F}_N \in \mathbb{R}^N$ as $F_{N\,i} = \langle F, \tilde{\zeta}_i\rangle$, $1 \le i \le N$. It is a simple matter to observe that

$$\underline{A}_N(\Theta) = \underline{A}_{N\,0} + \sum_{q=1}^{Q} \Theta_q\, \underline{A}_{N\,q}, \tag{A.2.9}$$

where $(\underline{A}_{Nq})_{i\,j} = \langle A_q\, \tilde{\zeta}_j, \tilde{\zeta}_i\rangle$, $1 \le i, j \le N$, $0 \le q \le Q$; note that the $\underline{A}_{Nq} \in \mathbb{R}^{N\times N}$, $0 \le q \le Q$, are *independent* of θ.
We can then restate the formulation as: given $\mu \in \mathcal{D}^\mu$, find $s_N(\mu) = \underline{F}_N^T \underline{u}_N(\mu)$, where $\underline{u}_N(\mu) \in \mathbb{R}^N$ is the unique solution to

$$\underline{A}_N(\Theta(\mu))\, \underline{u}_N(\mu) = \underline{F}_N.$$

Note that $u_N(\mu) = \sum_{j=1}^N u_{N\,j}(\mu)\, \tilde{\zeta}_j$. The output may also be expressed as

$$s_N(\mu) = \underline{u}_N^T(\mu)\, \underline{A}_N(\Theta(\mu))\, \underline{u}_N(\mu) = \underline{F}_N^T\, \underline{A}_N^{-1}(\Theta(\mu))\, \underline{F}_N. \tag{A.2.10}$$

Remark A.2.1 *The* a priori *convergence theory, and extensive numerical tests, suggest that the convergence of the reduced-basis approximation to the exact will be very fast. In fact, exponential convergence is observed in all the numerical tests. This suggests that even with a very modest N, we can expect to achieve good accuracy. The linear system above can be formed and solved very efficiently in the case where the operator depends affinely on the parameters. In this case we can separate the computational steps into two stages:*

- *The* off-line *stage, in which the reduced-basis space is constructed and some pre-processing is performed. This is an expensive step, that needs to be performed only once, requiring solutions of finite-element problems.*

- *The* on-line *stage, in which for each new parameter value, the reduced-basis approximation for the output of interest is calculated.*

The on-line stage is "blackbox" in the sense that there is no longer any reference to the original problem formulation: the computational complexity of this stage scales only with the dimension of the reduced-basis space and the parametric complexity of the partial differential operator. The "blackbox" nature of the on-line component of the procedure has other advantages. In particular, the on-line code is simple, non-proprietary, and completely decoupled from the (often complicated) off-line "truth" code. This is particularly important in multidisciplinary design optimization, in which various models and approximations must be integrated.

A.3 Reduced basis output bounds

The computational relaxation introduced in the previous section, allows us to compute very efficiently accurate approximations to the solution and the output of interest. Thanks to the expected rapid convergence N could, in theory, be chosen quite small. However, in practice we do not know how small N should be: this will depend on the desired accuracy, the choice of μ^i in the construction of the reduced-basis spaces, the output of interest and the particular problem in question. Either too many or too few basis functions will be retained: the former results in computational inefficiency; the later in unacceptable uncertainty. For the successful application of reduced-basis methods it is therefore critical that we can ascertain the accuracy of our predictions; for this reason rigorous error-estimation approaches are needed, directly for outputs of interest, to validate *a posteriori* the accuracy of our predictions.
We prove that these estimators $s_N^+(\mu)$ and $s_N^-(\mu)$ are upper and lower bounds, respectively, to the "true" output $\tilde{s}(\mu)$ that would be obtained by solution of the expensive finite-element problem:

$$s_N^-(\mu) \leq \tilde{s}(\mu) \leq s_N^+(\mu). \tag{A.3.1}$$

Unlike the exact value, these error estimators can be computed inexpensively — with a complexity that scales only with the dimension of the reduced-basis space.
In reality the error in the output has two components:

$$|s(\mu) - s_N(\mu)| \leq |s(\mu) - \tilde{s}(\mu)| + |\tilde{s}(\mu) - s_N(\mu)|;$$

the first related to the discretization error (see in Section A.9.2); and the second to the reduced-basis error. In practice, both of these errors have to be estimated for reliability in our predictions. Estimation of the discretization error has been treated extensively in the literature; see Patera and Peraire [109] for a review. For our purposes, we assume that h is chosen very conservatively such that $\tilde{s}(\mu) \approx s(\mu)$ and the dominant error is due to the reduced-basis approximation.

A.3.1 Bound conditioner

In the previous section we have seen how to compute our *predictor*, $s_N(\mu)$ from equation (A.2.10); in the next steps we are going to compute our *bounds*, $s_N^-(\mu) \leq \tilde{s}(\mu) \leq s_N^+(\mu)$. The latter may be interpreted also as *a posteriori* estimators. We first define the error $\tilde{e}(\mu) \in Y$ as $\tilde{e}(\mu) = \tilde{u}(\mu) - u_N(\mu)$ and residual $R \in Y'$ as $\langle R(\mu), v\rangle \equiv \langle F - A(\Theta(\mu))\, u_N(\mu), v\rangle$, $\forall\, v \in Y$; and then $\underline{\tilde{R}}(\mu) \in \mathbb{R}^{\mathcal{N}}$ as $\tilde{R}_i(\mu) = \langle R(\mu), \phi_i\rangle$ $i = 1, \ldots, \mathcal{N}$. We note that

$$\underline{\tilde{R}}(\mu) = \underline{\tilde{F}} - \underline{\tilde{A}}(\Theta(\mu))\, \underline{u}_N(\mu)\ , \tag{A.3.2}$$

and that $u_N(\mu)$ is given by

$$u_N(\mu) = \sum_{n=1}^{N} u_{Nn}(\mu)\, \tilde{\zeta}_n\ ; \tag{A.3.3}$$

by construction: $\tilde{\zeta}_n = \sum_{i=1}^{\mathcal{N}} \tilde{u}_i(\mu^n)\, \phi_i$. We then introduce a symmetric, continuous, and coercive *bound conditioner* as in Veroy [158] $\mathcal{C}(\mu) : Y \to Y'$ such that the minimum and maximum eigenvalues

$$\rho_{min}(\mu) \equiv \min_{v\in Y} \frac{\langle \tilde{A}(\mu)v, v\rangle}{\langle \mathcal{C}(\mu)v, v\rangle}, \tag{A.3.4}$$

$$\rho_{max}(\mu) \equiv \max_{v\in Y} \frac{\langle \tilde{A}(\mu)v, v\rangle}{\langle \mathcal{C}(\mu)v, v\rangle}, \tag{A.3.5}$$

satisfy the following spectral condition:

$$1 \leq \rho_{min}(\mu), \quad \rho_{max} \leq \rho, \tag{A.3.6}$$

for some (preferably small) constant $\rho \in \mathbb{R}$.
We note that:

$$\rho_{min}(\mu) \leq \frac{\langle \tilde{A}(\mu)v, v\rangle}{\langle \mathcal{C}(\mu)v, v\rangle} \leq \rho_{max}(\mu) \quad \forall v \in Y, \tag{A.3.7}$$

and for any $\hat{e} \in Y$ and $\tilde{e} \in Y$ such that:

$$\langle \tilde{A}(\mu)\tilde{e}, v\rangle = \langle \underline{\tilde{R}}(\mu), v\rangle,\ \forall v \in Y, \tag{A.3.8}$$

and

$$\langle \mathcal{C}(\mu)\hat{e}, v\rangle = \langle \underline{\tilde{R}}(\mu), v\rangle,\ \forall v \in Y, \tag{A.3.9}$$

we can show that:

$$\rho_{min}(\mu) \leq \frac{\langle \tilde{A}(\mu)\tilde{e}, v\rangle}{\langle \mathcal{C}(\mu)\hat{e}, v\rangle} \leq \rho_{max}(\mu). \tag{A.3.10}$$

In addition to the spectral condition (A.3.6), we also require a "computational invertibility" hypothesis, in particular that $\mathcal{C}^{-1}(\mu)$ be of the form:

$$\mathcal{C}^{-1}(\mu) = \sum_{i\in\mathcal{I}(\mu)} \alpha_i(\mu)\, \mathcal{C}_i^{-1}$$

where (i) $\mathcal{I}(\mu) \subset \{1, \ldots, I\}$ is a parameter-dependent set of indices, I is a finite (preferably small) integer, and each $\mu \in \mathcal{D}^\mu$. (ii) The $\mathcal{C}_i : Y \to Y'$ are parameter-*indipendent* symmetric, coercive operators.

A.3.2 Error and output bounds

We now find $\underline{\hat{e}}(\mu) \in \mathbb{R}^{\mathcal{N}}$ such that

$$\underline{\mathcal{C}}(\mu)\,\underline{\hat{e}}(\mu) = \underline{\tilde{R}}(\mu); \tag{A.3.11}$$

this equation will of course have a unique solution since $\mathcal{C}(\mu)$ is symmetric positive-definite. We can now define our lower and upper bounds as

$$s_N^-(\mu) = s_N(\mu),$$

and

$$s_N^+(\mu) = s_N(\mu) + \Delta_N(\mu)\ ,$$

where $\Delta_N(\mu)$, the bound gap, is given by

$$\begin{aligned}\Delta_N(\mu) &\equiv \underline{\hat{e}}^T(\mu)\,\underline{\mathcal{C}}(\mu)\,\underline{\hat{e}}(\mu)\\ &= \underline{\tilde{R}}^T(\mu)\,\underline{\mathcal{C}}^{-1}(\mu)\,\underline{\tilde{R}}(\mu)\\ &= \underline{\tilde{R}}^T(\mu)\,\underline{\hat{e}}(\mu).\end{aligned}$$

The previous expressions for the bound gap will be useful in the theoretical and computational context.

A.3.3 Minimum coefficient bound conditioner

We now consider a method for choosing the $\mathcal{C}_i$ and the associated α_i called *Minimum Coefficient Bound Conditioner*.
To begin we recall our separability assumption on $\underline{\tilde{A}}(\Theta)$:

$$\underline{\tilde{A}}(\Theta(\mu)) = \underline{\tilde{A}}_0 + \sum_{q=1}^{Q} \Theta_q(\mu)\,\underline{\tilde{A}}_q \ \forall\ \mu \in \mathcal{D}^{\mu}_{box},$$

where $\Theta(\mu) : \mathcal{D}^{\mu} \to \mathbb{R}$ and the $\underline{\tilde{A}}_q : Y \to Y'$. We now define

$$\underline{\tilde{\mathcal{A}}}(\theta) = \underline{\tilde{\mathcal{A}}}_0 + \sum_{q=1}^{Q} \theta_q\,\underline{\tilde{\mathcal{A}}}_q,$$

where $\theta \in \mathbb{R}^Q$ and $\underline{\tilde{\mathcal{A}}}(\theta) : Y \to Y'$ and $\underline{\tilde{A}}_q \equiv \underline{\tilde{\mathcal{A}}}_q$. If $\Theta_q(\mu) = \theta_q$, we may then write

$$\underline{\tilde{A}}(\Theta(\mu)) = \underline{\tilde{\mathcal{A}}}(\theta),$$

where $\Theta : \mathcal{D}^{\mu} \to \mathcal{D}^{\theta}$ and $\mathcal{D}^{\theta} \equiv \mathit{Range}(\Theta) \in \mathbb{R}^Q$. Then we introduce I points θ_i as samples $S_I^{\theta} = \{\theta_1, \ldots, \theta_I\}$, where $\theta_i \in \mathcal{D}^{\theta}_{\rm box}$, $i = 1, \ldots, I$. We choose

$$\alpha_i(\mu) = \Big(\min_{1 \le q \le Q} \Big(\frac{\Theta^q(\mu)}{\theta_i^q} \Big) \Big)^{-1}, \tag{A.3.12}$$

and

$$\mathcal{C}_i = \sum_{q=1}^{Q} \theta_i^q \, \underline{\tilde{A}}_q. \tag{A.3.13}$$

Our bound conditioner $\mathcal{C}(\mu) \in \mathbb{R}^{\mathcal{N}\times\mathcal{N}}$ is

$$\mathcal{C}(\mu) = \left(\sum_{i\in\mathcal{I}(\mu)} \alpha_i(\mu) {\mathcal{C}_i}^{-1}(\theta^i) \right)^{-1}. \tag{A.3.14}$$

Clearly, $\mathcal{C}^{-1}$ and hence $\mathcal{C}$ are symmetric positive-definite. In words, $\mathcal{C}^{-1}$ is an approximation to $\underline{\tilde{A}}^{-1}(\Theta(\mu))$ In our application we used a single-point conditioner. We set $I = 1$, $S_I^\theta = \{\overline{\theta}\}$, $|\mathcal{I}(\mu)| = 1$, $\mathcal{I}(\mu) = \{1\}$. For further information and a detailed understanding of bound conditioner families (and special cases) we suggest to see [90, 118, 120].

A.3.4 Bounding properties

It remains to demonstrate our claim that $s_N^-(\mu) \le \tilde{s}(\mu) \le s_N^+(\mu)$ for all $N \ge 1$. We prove at first that for all $\mu \in \mathcal{D}^\mu$, and all $N \ge 1$, $s_N^-(\mu) \le \tilde{s}(\mu)$. We have that

$$\begin{aligned}
\tilde{s}(\mu) - s_N(\mu) &= \langle F, \tilde{u}(\mu) - u_N(\mu)\rangle \\
&= \langle A(\Theta(\mu))\, \tilde{u}(\mu), \tilde{u}(\mu) - u_N(\mu)\rangle \\
&= \langle A(\Theta(\mu))\, (\tilde{u}(\mu) - u_N(\mu)), \tilde{u}(\mu)\rangle \\
&= \langle A(\Theta(\mu))\, (\tilde{u}(\mu) - u_N(\mu)), \tilde{u}(\mu) - u_N(\mu)\rangle \\
&\ge 0
\end{aligned} \tag{A.3.15}$$

having used the definition of $s(\mu)$, (A.2.6), the symmetry of A, Galerkin orthogonality, and coercivity, respectively.

This lower bound proof is a standard result in variational approximation theory. We now turn to the upper bound to demonstrate that for all $\mu \in \mathcal{D}^\mu$, and all $N \ge 1$, $s_N^+(\mu) \ge \tilde{s}(\mu)$. We first define $\underline{\tilde{e}} \in \mathbb{R}^{\mathcal{N}}$ as $\underline{\tilde{e}} = \underline{\tilde{u}} - \underline{u}_N$; it then follows from (A.2.7) and (A.3.2) that

$$\underline{\tilde{A}}(\Theta(\mu))\, \underline{\tilde{e}}(\mu) = \underline{\tilde{R}}(\mu)\ , \tag{A.3.16}$$

which is the usual error-residual relationship. It then follows from (A.3.15) that

$$\begin{aligned}
\tilde{s}(\mu) - s_N(\mu) &= \underline{\tilde{e}}^T(\mu)\, \underline{\tilde{A}}(\Theta(\mu))\, \underline{\tilde{e}}(\mu) \\
&= \underline{\tilde{R}}^T(\mu)\, \underline{\tilde{A}}^{-1}(\Theta(\mu))\, \underline{\tilde{R}}(\mu)\ .
\end{aligned} \tag{A.3.17}$$

It thus only remains to write the *effectivity*:

$$\eta_N(\mu) \equiv \frac{s_N^+(\mu) - s_N(\mu)}{\tilde{s}(\mu) - s_N(\mu)} = \frac{\Delta_N(\mu)}{\tilde{s}(\mu) - s_N(\mu)} = \frac{\underline{\tilde{R}}^T(\mu)\underline{\mathcal{C}}^{-1}(\mu)\underline{\tilde{R}}(\mu)}{\underline{\tilde{R}}^T(\mu)\underline{\tilde{A}}^{-1}(\Theta(\mu))\underline{\tilde{R}}(\mu)}, \tag{A.3.18}$$

using the boundaries properties (A.3.7) and (A.3.10) and equations (A.3.11)-(A.3.16) we have:

$$\eta_N(\mu) \equiv \frac{\underline{\hat{e}}^T(\mu)\,\underline{\mathcal{C}}(\Theta(\mu))\,\underline{\hat{e}}(\mu)}{\underline{\tilde{e}}^T(\mu)\,\underline{\tilde{A}}(\Theta(\mu))\,\underline{\tilde{e}}(\mu)} = \frac{\langle \tilde{C}(\mu)\hat{e},\hat{e}\rangle}{\langle \underline{\tilde{A}}(\Theta(\mu))\tilde{e},\tilde{e}\rangle}, \tag{A.3.19}$$

therefore:

$$\rho_{min}(\mu) \le \eta_N(\mu) \le \rho_{max}(\mu); \tag{A.3.20}$$

by construction, $\rho_{min}(\mu) \ge 1$ for all $\mu \in \mathcal{D}^\mu$ and therefore:

$$\eta_N(\mu) \ge 1, \tag{A.3.21}$$

and $s_N^+(\mu) \ge s(\mu)$ as required. Note that the result (A.3.20) also indicates the sharpness of our bounds: it follows from (A.3.6) that:

$$\eta_N(\mu) \le \rho. \tag{A.3.22}$$

This result provides insight as to the properties of a good bound conditioner. Clearly, we wish $\rho_{max}(\mu)$ to be as close to unity, and hence as close to ρ_{min}, as possible.

A.3.5 Computational procedure: off-line/on-line decomposition

We review here arguments given in detail in [118]; early applications of this approach may be found in [11]. The theoretical and empirical results let us to apply separate *off-line* and *on-line* computational procedures that exploit the dimension reduction.
In an *off-line* stage, we find the $\underline{\tilde{\zeta}}_n$, $n = 1,\ldots,N$ ($N \times \underline{\tilde{A}}$-solves), and form the $\underline{A}_{N\,q}$, $0 \le q \le Q$ ($(Q+1)N^2$ $\times\underline{\tilde{A}}$-inner products), and $\underline{F}_N$ ($N \times \mathcal{N}$ operations). In the *on-line* stage — given any new μ — we need only form $\underline{A}_N(\mu)$ from the $\underline{A}_{Nq}$ ($(Q+1)N^2$ operations), find $\underline{u}_N(\mu)$ ($O(N^3)$ operations), and evaluate $s_N(\mu)$ (N operations). The most important point is that the on-line complexity (and storage — $O(QN^2)$) is *independent* of the very large dimension of the truth space $\tilde{Y}_h, \mathcal{N}$; in particular, since N is typically very small (as suggested in the previous sections), "real-time" response is obtained.

Computational Procedures for the upper bound $s_N^+(\mu)$

A computational procedure for the *upper bound* is very important and very useful in view of adaptivity procedures applied to basis $\underline{\tilde{\zeta}}^n$ storage and to test results with a cheap and fast procedure. See [118] for detailed bound conditioners presentation. We first note from (A.3.14)–(A.3.11) that

$$\underline{\hat{e}}(\mu) = \sum_{i\in\mathcal{I}(\mu)} \alpha_i(\mu)\,\underline{\tilde{A}}^{-1}(\theta^j)\left[\underline{\tilde{F}} - \sum_{q=0}^{Q}\sum_{n=1}^{N} \Theta_q(\mu)\,u_{Nn}(\mu)\,\underline{\tilde{A}}_q\,\underline{\tilde{\zeta}}_n\right];$$

recall that $\Theta_0 = 1$. It follows that we may express $\underline{\hat{e}}(\mu)$ as

$$\underline{\hat{e}}(\mu) = \sum_{i\in\mathcal{I}(\mu)} \alpha_j(\mu)\left[\underline{\tilde{z}}^i_{00} + \sum_{q=0}^{Q}\sum_{n=1}^{N} \Theta_q(\mu)\,u_{Nn}(\mu)\,\underline{\tilde{z}}^i_{qn}\right],$$

where for all $i \in \{1,\ldots,M\}$, $\tilde{\underline{A}}(\theta^i)\tilde{\underline{z}}^i_{00} = \tilde{\underline{F}}$, and $\tilde{\underline{A}}(\theta^i)\tilde{\underline{z}}^i_{qn} = -\tilde{\underline{A}}_q\,\tilde{\underline{\zeta}}_n$, $0 \le q \le Q$, $1 \le n \le N$. We may thus express our bound gap $\Delta_N(\mu)$ as the following (A.3.23):

$$\begin{aligned}
\Delta_N(\mu) &= \underline{\tilde{R}}^T(\mu)\,\underline{\hat{e}}(\mu) \\
&= \sum_{i\in\mathcal{I}(\mu)} \alpha_i(\mu) \left[\tilde{\underline{F}} - \sum_{q=0}^{Q}\sum_{n=1}^{N} \Theta_q(\mu)\,u_{Nn}(\mu)\,\tilde{\underline{A}}_q\,\tilde{\underline{\zeta}}_n\right]^T \\
&\qquad \left[\tilde{\underline{z}}^i_{00} + \sum_{q'=0}^{Q}\sum_{n'=1}^{N} \Theta_{q'}(\mu)\,u_{Nn'}(\mu)\,\tilde{\underline{z}}^i_{q'n'}\right] \\
&= \sum_{i\in\mathcal{I}(\mu)} \alpha_i(\mu) \left[c^i + \sum_{q=0}^{Q}\sum_{n=1}^{N} \Theta_q(\mu)\,u_{Nn}(\mu)\,\Lambda^i_{qn}\right. \\
&\qquad \left. + \sum_{q=0}^{Q}\sum_{n=1}^{N}\sum_{q'=0}^{Q}\sum_{n'=1}^{N} \Theta_q(\mu)\,\Theta_{q'}(\mu)\,u_{Nn}(\mu)\,u_{Nn'}(\mu)\,\Gamma^i_{qq'nn'}\right], \qquad \text{(A.3.23)}
\end{aligned}$$

where for all $i \in \{1,\ldots,M\}$, $c^i = \tilde{\underline{F}}^T\,\tilde{\underline{z}}^i_{00}$, $\Lambda^i_{qn} = \tilde{\underline{F}}^T\,\tilde{\underline{z}}^i_{qn} - \tilde{\underline{\zeta}}^T_n\,\tilde{\underline{A}}_q\,\tilde{\underline{z}}^i_{00}$ for $0 \le q \le Q$, $1 \le n \le N$, and $\Gamma^i_{qq'nn'} = -\tilde{\underline{\zeta}}^T_n\,\tilde{\underline{A}}_q\,\tilde{\underline{z}}^i_{q'n'}$ for $0 \le q, q' \le Q$, $1 \le n, n' \le N$.

The off-line/on-line decomposition is now clear. In the *off-line* stage we compute the $\tilde{\underline{z}}^i_{00}$ and $\tilde{\underline{z}}^i_{qn}$ ($M((Q+1)N+1)$ $\tilde{\underline{A}}$-solves) and the c^i, Λ^i_{qn}, and $\Gamma^i_{qq'nn'}$ (predominated by M $((Q+1)^2N^2 + (Q+1)N)$ $\tilde{\underline{A}}$-inner products). In the on-line stage we need "only" perform the sum (A.3.23), which requires $|\mathcal{I}(\mu)|((Q+1)^2N^2 + (Q+1)N + 1)$ operations. The essential point is that the on-line complexity (and storage — $O(M(Q+1)^2N^2)$) is independent of $\mathcal{N}$.

We note that the off-line/on-line decomposition depends critically on the "separability" of $\tilde{\underline{C}}^{-1}$ as a sum of products of parameter-*dependent* functions (the $\alpha_i(\mu)$) and parameter-*independent* operators (the $\tilde{\underline{A}}^{-1}(\theta^i)$). In turn, it is the direct approximation of $\tilde{\underline{A}}^{-1}(\Theta(\mu))$ (i.e., by a convex combination of $\tilde{\underline{A}}^{-1}(\theta^i)$) rather than of $\tilde{\underline{A}}(\Theta(\mu))$ (e.g., by a convex combination of $\tilde{\underline{A}}(\theta^i)$) that permits us to achieve this separability while simultaneously pursuing a "high-order" bound conditioner achieving some fixed (known, certain) accuracy — as measured by $\Delta_N(\mu)$ — at a lower computational effort. See [119].

A.4 A priori convergence theory

We recall *a priori* framework for a general a priori convergence theory. Depending on the context and application, we will either invoke the lower bound ($s^-_N(\mu)$) or upper bound ($s^+_N(\mu)$) as our estimator for $\tilde{s}(\mu)$. For example, in an optimization problem in which $\tilde{s}(\mu)$ enters as a constraint $\tilde{s}(\mu) \le s^{\max}$ (respectively, $\tilde{s}(\mu) \ge s^{\min}$), we will replace this condition with $s^+_N(\mu) \le s^{\max}$ (respectively, $s^-_N(\mu) \ge s^{\min}$) so as to ensure satisfaction/feasibility even in the presence of approximation errors. The rigorous bounding properties proven in Section A.3.4 provide the requisite certainty.

But we of course also require accuracy: if, in the optimization context cited above, $s_N^+(\mu)$ or $s_N^-(\mu)$ is not close to $\tilde{s}(\mu)$, then our design may be *seriously suboptimal*. Since $|s_N^+(\mu)-\tilde{s}(\mu)| \leq |s_N^+(\mu)-s_N^-(\mu)| = \Delta_N(\mu)$ and $|\tilde{s}(\mu)-s_N^-(\mu)| \leq |s_N^+(\mu)-s_N^-(\mu)| = \Delta_N(\mu)$, it is the convergence of $\Delta_N(\mu)$ as a function of N that we must understand. In particular, from (A.3.19) and (A.3.15) we may write

$$\begin{aligned}\Delta_N(\mu) = s_N^+(\mu) - s_N^-(\mu) &= (\tilde{s}(\mu) - s_N(\mu)) \left(\frac{s_N^+(\mu) - s_N^-(\mu)}{\tilde{s}(\mu) - s_N(\mu)} \right) \\ &= \langle A(\Theta(\mu))\, \tilde{e}(\mu), \tilde{e}(\mu) \rangle\, \eta_N(\mu),\end{aligned}$$

where $\tilde{e}(\mu) = \tilde{u}(\mu) - u_N(\mu)$. In some sense, the first factor, $\langle A(\Theta(\mu))\tilde{e}(\mu), \tilde{e}(\mu)\rangle$, measures the error in the solution $\tilde{u}(\mu) - u_N(\mu)$, while the second factor, the effectivity $\eta_N(\mu)$, measures the ratio of the actual and estimated errors; the former should be small, while the latter should be close to unity. As we shall see, this two-step factorization is important not only as a theoretical construct: it is this factorization which permits us to achieve high accuracy while simultaneously honoring our bound requirements. We would thus like to understand the convergence of $\Delta_N(\mu)$ to zero as a function of N. In particular, we consider the case in which $A(\mu) = A_0 + \mu A_1$ (and hence $\Theta_1(\mu) = \mu$), and $\mu \in \mathcal{D}^\mu \equiv [0, \mu^{\max}]$. From our continuity and coercivity assumptions, there exists a positive real constant γ_1 such that

$$\langle A_1 v, v\rangle \leq \gamma_1 \langle A_0 v, v\rangle; \tag{A.4.1}$$

it thus follows that $\langle A(\mu)v, v\rangle \leq (1 + \mu^{\max}\gamma_1)\, \langle A_0 v, v\rangle$. Defining $\|\cdot\|^2 \equiv \langle A_0 \cdot, \cdot\rangle$, we may thus write

$$\Delta_N(\mu) \leq (1 + \mu^{\max}\gamma_1)\, \|\tilde{u}(\mu) - u_N(\mu)\|^2\, \eta_N(\mu). \tag{A.4.2}$$

A.4.1 Best approximation

It remains to bound $\|\tilde{u}(\mu) - u_N(\mu)\|$ and $\eta_N(\mu)$; and, in particular, to understand the convergence rate of $\|\tilde{u}(\mu) - u_N(\mu)\| \to 0$ and $\eta_N(\mu) \to 1$ (or at least a constant) as N increases. The proofs for both $\|\tilde{u}(\mu) - u_N(\mu)\|$ [91] and $\eta_N(\mu)$ implicate a particular "optimal" logarithmic point distribution which we thus impose *a priori*. In particular, we introduce an upper bound for γ_1, γ, and a "log increment" $\delta_N = (\ln(\gamma\mu^{\max} + 1))/(N-1)$; we then define

$$\mu^n = \exp\{-\ln\gamma + (n-1)\delta_N\} - \gamma^{-1}, \quad 1 \leq n \leq N\ ,$$

and take $S_N^\mu = \{\mu^1, \ldots, \mu^N\}$. Clearly, $\ln(\mu^n + \gamma^{-1})$ is uniformly distributed. Note that for $N \geq N_{\rm crit} \equiv 1 + e\, \ln(\gamma\mu^{\max} + 1)$, $\delta_N \leq e^{-1} < 1$. We remind to the main result in [91, 92]: for $N \geq N_{\rm crit} \equiv 1 + e\, \ln(\gamma\mu^{\max} + 1)$ and all $\mu \in \mathcal{D}^\mu$ we find:

$$\|\tilde{u}(\mu) - u_N(\mu)\| \leq (1 + \mu^{\max}\gamma_1)^{1/2}\, \|\tilde{u}(0)\|\, e^{-(\frac{N}{N_{\rm crit}})}.$$

See Theorem 3 of [91] (for $c^* = 1$). We see that we obtain *exponential* convergence, *uniformly* for all μ in $\mathcal{D}^\mu$. Furthermore, our convergence threshold parameter $N_{\rm crit} = 1 + e\, \ln(\gamma\mu^{\max} + 1)$, and exponential convergence rate $1/N_{\rm crit}$, depend only weakly — *logarithmically* — on γ_1 and

$\mu^{\max}$ (which together comprise the continuity-coercivity ratio). In short, we expect extremely rapid convergence even for large parameter ranges. To obtain a bound for $\eta_N(\mu)$ (limited and close to unity) see [157].

A.5 Adaptive procedure for basis construction

Given the higher powers of N that appear in our complexity estimates, it is crucial (both as regards online and offline effort) to control N more tightly. To this end, we may gainfully apply our *a posteriori* error bounds adaptively. We first construct, offline, an approximation that, over most of the domain, exhibits an error (in the H^1-norm) less than ϵ_d^{prior}: we begin with a first point $\mu^1(S_{N'=1} = \{\mu^1\})$; we next (inexpensively) evaluate $\Delta_{N'=1}(\mu)$ over a large test sample of parameter points in $\mathcal{D}^\mu, \Sigma^{prior}$; we then choose for μ^2 (and hence $S_{N'=2} = \{\mu^1, \mu^2\}$) the maximizer of $\Delta_{N'=1}(\mu)$ over Σ^{prior}. We repeat this process until the maximum of $\Delta_{N'=N^{prior}}(\mu)$ over Σ^{prior} is less than ϵ_d^{prior}. Then, online, given a new value of the parameter, μ, and an error tolerance $\epsilon_d^{post}(\mu)$, we essentially repeat this adaptive process - but now our sample points are drawn from $S_{N^{prior}}$, and the test sample is a singleton - μ. Typically we choose $\epsilon_d^{prior} \ll \epsilon_d^{post}(\mu)$ since our test is not exhaustive; and therefore, typically, $N^{post}(\mu) \ll N^{prior}$. With the adaptive process we get higher accuracy at lower N: modest reductions in N can translate into measurable performance improvements. This procedure is very important not only to get a computationally cheaper and faster method but also to avoid ill-conditioning in matrix assembling procedures.

A.6 A multi-parameter application

We consider a physical domain $\hat{\Omega} \subset \mathbb{R}^2$ is divided in four subdomains $\hat{\Omega}^r, r = 1, ..., 4$, a "T"-shaped region with boundary $\hat{\Gamma}$, divided in $\hat{\Gamma}_D$ and $\hat{\Gamma}_N$ and associated, respectively, Dirichlet or Neumann condition. See Figures A.1 and A.2.

A.6.1 Geometrical model

The geometrical model is based on a simple and standard configuration made up of four square subdomains parametrized in their dimensions (lengths and angles). This is a first example towards a more relevant one concerning bypass anastomosis used in Chapters 6 and 7. We have chosen five geometrical parameters.

- The angle θ for the incoming branch of the bypass.
- The diameters t and D, respectively, of the bypass and the artery.
- The lengths L and S, respectively, the outflow length and the distance between the incoming new branch and the occlusion caused by a stenosis. See Figure A.1.

We underline that this is a macro geometrical structure, useful to study with low computational cost and sharp error bounds a possible configuration to be optimized by optimal shape

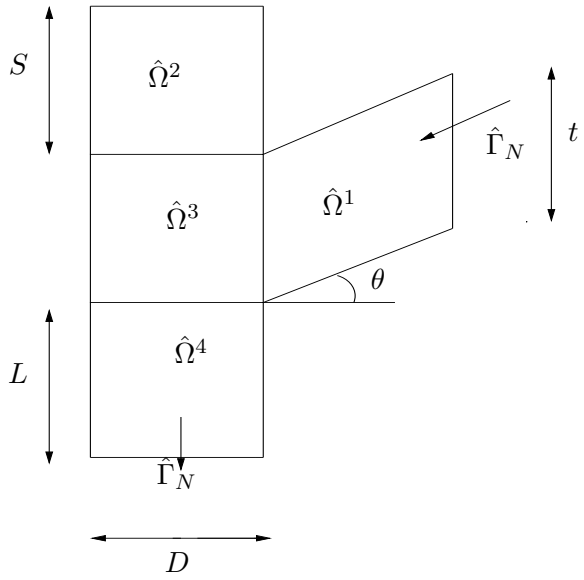

Figure A.1: Scheme for the reduced-basis multi-parameter problem.

design and control tools. This test case is studied to validate a methodological approach and to get a deep understanding of reduced-basis methodologies. The method is based on the affine mapping procedures from a sub-domain of reference (square) to the true one ($\Omega \rightarrow \hat{\Omega}$). Preliminary tests were made studying a simpler case based only on a square domain.

A.6.2 Formulation

We present the strong form of the equations governing our preliminary problem (in $\hat{\Omega}$), from which we derive the weak statement; we then reformulate the problem in terms of a reference (parameter-independent) domain (Ω), thus recovering the abstract formulation of Section A.2. We consider an elliptic equation, for example the equation of steady heat transfer with symmetric thermal diffusivity tensor $\hat{k}_{ij}$ (Poisson equation when $\hat{k}_{ij} = 1$) in $\hat{\Omega}^r \subset \mathbb{R}^d$, for $r = 1, \ldots, 4$ with boundary $\hat{\Gamma}$. The field $\hat{u}$ (i.e for example temperature) satisfies the partial differential equation

$$-\frac{\partial}{\partial \hat{x}_i}\Big(\hat{k}_{ij}\frac{\partial \hat{u}}{\partial \hat{x}_j}\Big) = \hat{f} \;\; in\ \hat{\Omega}, \tag{A.6.1}$$

where $1 \leq i, j \leq 2$ and with boundary conditions (see Figure A.1)

$$\hat{u} = 0 \ on\ \hat{\Gamma}_D, \quad \hat{k}_{ij}\frac{\partial \hat{u}}{\partial \hat{x}_j}\hat{n}_i = \hat{b} \ on\ \hat{\Gamma}_N, \tag{A.6.2}$$

where $\hat{f}$ can be seen as the rate of heat generated per unit volume, $\hat{b}$ is the prescribed heat flux input on the surface $\hat{\Gamma}_N$, and $\hat{n}_i$ is the $i-th$ component of the unit outward normal. We now derive the weak form of the governing equations. We introduce the function space:

$$\hat{Y} = \{\hat{v} \in H^1(\hat{\Omega}) | \hat{v} = 0 \ on\ \hat{\Gamma}_D\}, \tag{A.6.3}$$

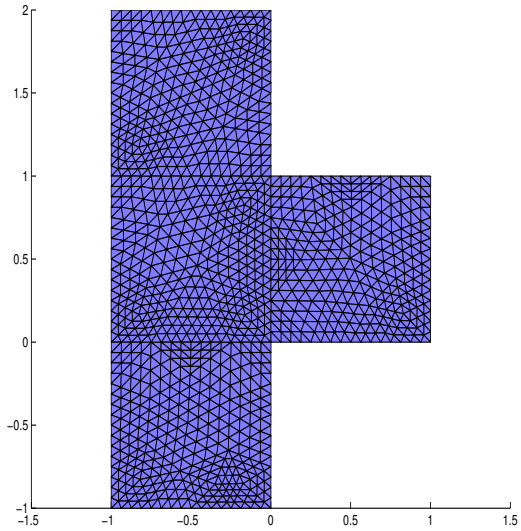

Figure A.2: Mesh for the reduced-basis problem (normalized domain).

and the associated norm

$$||\hat{v}||_{\hat{Y}} = \Big(\int_{\hat{\Omega}} \sum_{i=1}^{d} \Big(\frac{\partial \hat{v}}{\partial \hat{x}_i} \Big)^2 d\hat{\Omega} \Big)^{1/2}. \tag{A.6.4}$$

Multiplying (A.6.1) by a test function $\hat{v} \in \hat{Y}$, integrating over $\hat{\Omega}$ by parts and applying the divergence theorem we have for $1 \leq i, j \leq 2$:

$$-\int_{\hat{\Omega}} \hat{v} \frac{\partial}{\partial \hat{x}_i} \Big(\hat{k}_{ij} \frac{\partial \hat{u}}{\partial \hat{x}_j} \Big) d\hat{\Omega} = -\int_{\hat{\Gamma}} \hat{v} \hat{k}_{ij} \frac{\partial \hat{u}}{\partial \hat{x}_j} \hat{n}_i d\hat{\Gamma} + \int_{\hat{\Omega}} \frac{\partial \hat{v}}{\partial \hat{x}_i} \hat{k}_{ij} \frac{\partial \hat{u}}{\partial \hat{x}_j} d\hat{\Omega} = \int_{\hat{\Omega}} \hat{f} \hat{v} d\hat{\Omega} \quad \forall \hat{v} \in \hat{Y}. \tag{A.6.5}$$

Substituting boundary condition and by the fact that $\hat{v} = 0$ on $\hat{\Gamma}_D$, we obtain as our weak statement

$$\langle \hat{\mathcal{A}} \hat{u}, \hat{v} \rangle = \langle \hat{F}, \hat{v} \rangle, \ \forall \hat{v} \in \hat{Y}, \tag{A.6.6}$$

where

$$\langle \hat{\mathcal{A}} \hat{w}, \hat{v} \rangle = \int_{\hat{\Omega}} \frac{\partial \hat{v}}{\partial \hat{x}_i} \hat{k}_{ij} \frac{\partial \hat{w}}{\partial \hat{x}_j} d\hat{\Omega}, \tag{A.6.7}$$

$$\langle \hat{F}, \hat{v} \rangle = \langle \hat{F}_f, \hat{v} \rangle + \langle \hat{F}_b, \hat{v} \rangle, \tag{A.6.8}$$

here,

$$\langle \hat{F}_f, \hat{v} \rangle = \int_{\hat{\Omega}} \hat{f} \hat{v} d\hat{\Omega}, \quad \langle \hat{F}_b, \hat{v} \rangle = \int_{\hat{\Gamma}_N} \hat{b} \hat{v} d\hat{\Gamma}. \tag{A.6.9}$$

In our case $\hat{\Omega} = \bigcup_{r=1}^{R} \hat{\Omega}^r$, $R = 4$, so that the weak statement takes the form A.6.6 where

$$\langle \hat{\mathcal{A}} \hat{w}, \hat{v} \rangle = \sum_{r=1}^{R} \int_{\hat{\Omega}^r} \frac{\partial \hat{v}}{\partial \hat{x}_i} \hat{k}_{ij}^r \frac{\partial \hat{w}}{\partial \hat{x}_j} d\hat{\Omega}, \tag{A.6.10}$$

$$\langle \hat{F}, \hat{v} \rangle = \langle \hat{F}_f, \hat{v} \rangle + \langle \hat{F}_b, \hat{v} \rangle, \tag{A.6.11}$$

and

$$\langle \hat{F}_f, \hat{v} \rangle = \sum_{r=1}^{R} \int_{\hat{\Omega}^r} \hat{f}^r \hat{v} d\hat{\Omega}, \quad \langle \hat{F}_b, \hat{v} \rangle = \sum_{r=1}^{R} \int_{\hat{\Gamma}_N^r} \hat{b}^r \hat{v} d\hat{\Gamma}. \tag{A.6.12}$$

A.6.3 Affine mapping

The partition in subdomains $\hat{\Omega}^r$ is done such that there exists a reference domain Ω where, for any $\hat{x} \in \hat{\Omega}^r$, $r = 1, \ldots, R$, its image $x \in \Omega^r$ is given by

$$x = \mathcal{G}^r(\mu; \hat{x}) = G^r(\mu)\hat{x} + g^r, \quad 1 \le r \le R; \tag{A.6.13}$$

we thus write

$$\frac{\partial}{\partial \hat{x}_i} = \frac{\partial x_j}{\partial \hat{x}_i} \frac{\partial}{\partial x_j} = G_{ji}(\mu) \frac{\partial}{\partial x_j}, \tag{A.6.14}$$

where $x \in \Omega$, $\hat{x} \in \hat{\Omega}$, $G^r(\mu) \in \mathbb{R}^{d \times d}$ is a piecewise-constant matrix, $g^r(\mu) \in \mathbb{R}^d$ is a piecewise-constant vector, and $\mathcal{G}(\mu) : \hat{\Omega} \to \Omega$ is a piecewise-affine geometric mapping. We then denote the boundary of Ω as Γ, where $\Gamma(\mu, \overline{\Gamma})$. We now define the function space Y as $Y(\Omega) = \overline{Y}(\mathcal{G}^{-1}(\mu; \Omega)) = \overline{Y}(\overline{\Omega})$ such that

$$Y = \{v \in H^1(\Omega) | v = 0 \ on \ \Gamma_D\}, \tag{A.6.15}$$

and for any function $\overline{w} \in \overline{Y}$, we define $w \in Y$ such that $w(x) = \overline{w}(\mathcal{G}^{-1}(\mu; x))$. Furthermore, we have

$$d\hat{\Omega} = det G^{-1}(\mu) d\Omega, \ d\hat{\Gamma} = |G^{-1}(\mu)\hat{\mathbf{t}}| d\Gamma, \tag{A.6.16}$$

where $\hat{\mathbf{t}}$ is the unit vector tangent to the boundary Γ, and

$$|G^{-1}\hat{\mathbf{t}}| = \Big(\sum_{i=1}^{d} (G_{ij}\hat{t}_j)^2 \Big)^{1/2}. \tag{A.6.17}$$

It then follows that $\langle \mathcal{A}(\mu)w, v \rangle = \langle \hat{\mathcal{A}}\hat{w}, \hat{v} \rangle$ and $\mathcal{A}(\mu)$ given by

$$\langle \mathcal{A}w, v \rangle = \sum_{r=1}^{R} \int_{\Omega^r} \Big(G^r_{ii'}(\mu) \frac{\partial w}{\partial x_i} \Big) \hat{k}^r_{i'j'} \Big(G^r_{jj'}(\mu) \frac{\partial v}{\partial x_j} \Big) det(G^r(\mu))^{-1} d\Omega, \tag{A.6.18}$$

or

$$\langle \mathcal{A}w, v \rangle = \sum_{r=1}^{R} \int_{\Omega^r} \frac{\partial w}{\partial x_i} \Big(G^r_{ii'}(\mu) \hat{k}^r_{i'j'} G^r_{jj'}(\mu) det(G^r(\mu))^{-1} \Big) \frac{\partial v}{\partial x_j} d\Omega \ \forall w, v \in Y, \tag{A.6.19}$$

and $\langle F(\mu)w, v \rangle = \langle \hat{F}\hat{w}, \hat{v} \rangle$ and $F(\mu)$ given by

$$\langle F(\mu), v \rangle = \langle F_f, v \rangle + \langle F_b, v \rangle, \tag{A.6.20}$$

where

$$\langle F_f, v \rangle = \sum_{r=1}^{R} \int_{\Omega^r} \Big(\hat{f}^r det(G^r(\mu))^{-1} \Big) v d\Omega, \quad \langle F_b, v \rangle = \sum_{r=1}^{R} \int_{\Gamma_{N^r}} \Big(\hat{b}^r | (G^r(\mu))^{-1} \hat{\mathbf{t}}| \Big) v d\Gamma. \tag{A.6.21}$$

The abstract problem is then recovered for

$$\langle \mathcal{A}w, v\rangle = \sum_{r=1}^{R}\int_{\Omega^r}\frac{\partial w}{\partial x_i}k_{ij}^r\frac{\partial v}{\partial x_j}d\Omega\ \forall w, v \in Y, \tag{A.6.22}$$

$$\langle F(\mu), v\rangle = \langle F_f(\mu), v\rangle + \langle F_b(\mu), v\rangle, \tag{A.6.23}$$

$$\langle F_f, v\rangle = \sum_{r=1}^{R}\int_{\Omega^r} f^r v d\Omega,\quad \langle F_b, v\rangle = \sum_{r=1}^{R}\int_{{\Gamma_N}^r} b^r v d\Gamma. \tag{A.6.24}$$

Here $k_{ij}^r(\mu)$ is given by

$$k_{ij}^r = G_{ii'}^r(\mu)\hat{k}_{i'j'}^r G_{jj'}^r(\mu) det(G^r(\mu))^{-1}, \tag{A.6.25}$$

and $b^r(\mu)$, $f^r(\mu)$ are given by

$$f^r(\mu) = \hat{f}^r det(G^r(\mu))^{-1},\ b^r(\mu) = \hat{b}^r|(G^r(\mu))^{-1}\hat{\mathbf{t}}|. \tag{A.6.26}$$

Furthermore, we may define

$$\Theta^{q(i,j,r)}(\mu) = k_{ij}^r(\mu),\ \langle \mathcal{A}^{q(i,j,r)}w, v\rangle = \int_{\Omega^r}\frac{\partial v}{\partial x_i}\frac{\partial w}{\partial x_j}d\Omega, \tag{A.6.27}$$

for $1 \le r \le R$, $1 \le i, j \le d$.

A.6.4 Model problem

We now consider our model problem in detail. As already said the problem can be seen as a problem involving the flow of heat in a T-shaped region containing an internal heat source as shown in Figure A.2. Our output of interest is

$$s(\mu) = \sum_{r=1}^{R}\frac{1}{\xi_r}\int_{\hat{\Omega}^r}\hat{u}d\hat{\Omega}, \tag{A.6.28}$$

for $\boldsymbol{\mu} = \{t, D, L, S, \theta\} \in \mathcal{D}^\mu \subset \mathbb{R}^P$, where ξ_r is a normalizing factor (related to geometrical quantities in the subdomains $\hat{\Omega}^r$). Our problem can then be formulated as: given a $\mu \in \mathcal{D}^\mu \subset \mathbb{R}^P$, find $s(\mu) = \langle \hat{L}, \hat{u}\rangle$ where $\hat{u} \in \hat{Y}$ is the solution to:

$$\langle \hat{\mathcal{A}}\hat{w}, \hat{v}\rangle = \langle \hat{F}, \hat{v}\rangle, \forall \hat{v} \in \hat{Y}; \tag{A.6.29}$$

here, $\langle \hat{L}, \hat{v}\rangle = \langle \hat{F}, \hat{v}\rangle$, $\forall \hat{v} \in \hat{Y}$. In our case $\mathcal{D}^\mu$ is given by $[t_{min}, t_{max}] \times [D_{min}, D_{max}] \times [L_{min}, L_{max}] \times [S_{min}, S_{max}] \times [\theta_{min}, \theta_{max}]$, i.e: $[0.1, 1.5] \times [0.1, 1.5] \times [0.1, 5.0] \times [0.1, 5.0] \times [0^o, 60^o]$. We have $\hat{b} = 0$, $\hat{f} = \{\frac{1}{\xi_r}\}$ defined on $\hat{\Omega}^r$, so that:

$$\xi_1 = t,\ \xi_2 = SD,\ \xi_3 = tD,\ \xi_4 = LD. \tag{A.6.30}$$

The affine mapping $\mathcal{G}(\hat{x})(\mu) : \hat{\Omega} \to \Omega$ is given by (A.6.13) and we have

$$G^1(\mu) = \begin{pmatrix} 1 & -\tan(\theta) \\ 0 & 1 \end{pmatrix}\begin{pmatrix} 1 & 0 \\ 0 & \frac{1}{t} \end{pmatrix},\ G^2(\mu) = \begin{pmatrix} \frac{1}{D} & 0 \\ 0 & \frac{1}{S} \end{pmatrix}, \tag{A.6.31}$$

$$G^3(\mu) = \begin{pmatrix} \frac{1}{D} & 0 \\ 0 & \frac{1}{t} \end{pmatrix}, \; G^4(\mu) = \begin{pmatrix} \frac{1}{D} & 0 \\ 0 & \frac{1}{L} \end{pmatrix}. \tag{A.6.32}$$

Each mapping function is defined in $\hat{\Omega}^r$, furthermore $g^r = 0 \; \forall r$. We have

$$d\hat{\Omega}^1 = det(G^1)^{-1}(\mu) d\Omega^1 = t d\Omega, \; d\hat{\Gamma}^1 = |det(G^1)^{-1}(\mu)\hat{\mathbf{t}}| d\Gamma^1 = t d\Gamma, \tag{A.6.33}$$

$$d\hat{\Omega}^2 = det(G^2)^{-1}(\mu) d\Omega^2 = LD d\Omega, \quad d\hat{\Gamma}^2 = |det(G^2)^{-1}(\mu)\hat{\mathbf{t}}| d\Gamma^2 = LD d\Gamma, \tag{A.6.34}$$

$$d\hat{\Omega}^3 = det(G^3)^{-1}(\mu) d\Omega^3 = tD d\Omega, \quad d\hat{\Gamma}^3 = |det(G^3)^{-1}(\mu)\hat{\mathbf{t}}| d\Gamma^3 = tD d\Gamma, \tag{A.6.35}$$

$$d\hat{\Omega}^4 = det(G^4)^{-1}(\mu) d\Omega^4 = SD d\Omega, \; d\hat{\Gamma}^4 = |det(G^4)^{-1}(\mu)\hat{\mathbf{t}}| d\Gamma^4 = SD d\Gamma, \tag{A.6.36}$$

Figures A.3 and A.4 show the affine mapping procedures on two subdomains (Ω^1 and Ω^3 for example).

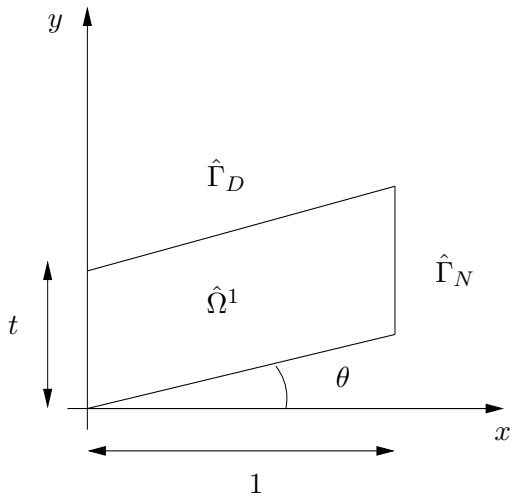

Figure A.3: Scheme of parameter-dependent domain Ω^1 undergoing vertical shear and rotation.

We may now re-formulate our problem in terms of our reference domain: find $s(\mu) = \langle L, u \rangle$ where $u \in Y$ is the solution to:

$$\langle \mathcal{A} w, v \rangle = \langle F, v \rangle, \forall v \in Y, \tag{A.6.37}$$

where $\langle L, v \rangle = \langle F, v \rangle \; \forall v \in Y$ and

$$\langle \mathcal{A} w, v \rangle = \sum_{r=1}^{R} \langle \mathcal{A}^r w, v \rangle = \langle F, v \rangle, \forall v \in Y, \tag{A.6.38}$$

$$\langle F, v \rangle = \sum_{r=1}^{R} \int_{\Omega_r} v d\Omega, \; \forall v \in Y, \tag{A.6.39}$$

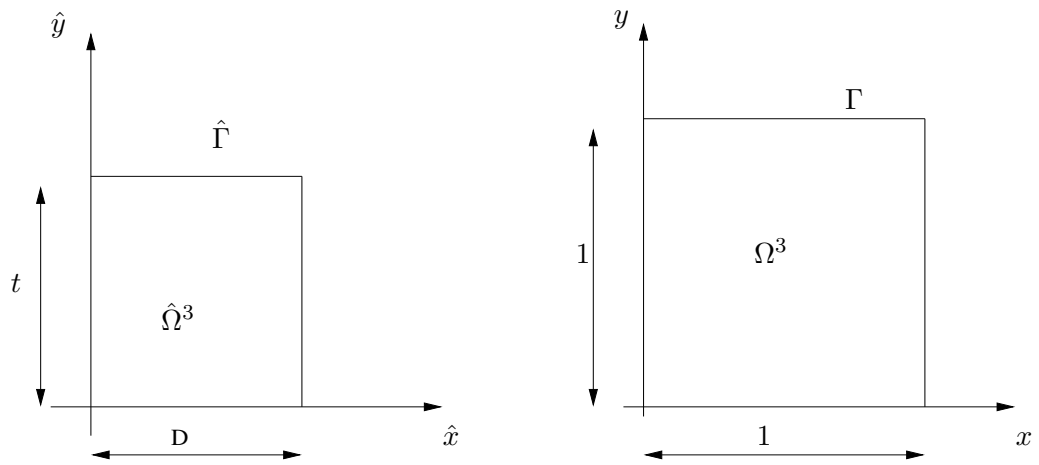

Figure A.4: Scheme for parameter-dependent domain Ω^3 and reference domain undergoing both stretch and shear.

$$\langle \mathcal{A}^r w, v\rangle = \int_{\Omega_r} \frac{\partial v}{\partial x_i} k^r_{ij} \frac{\partial w}{\partial x_j} d\Omega, \ \forall w, v \in Y, \tag{A.6.40}$$

and the effective diffusivity tensors $k^r_{ij}(\mu) = G_{ii'}(\mu)\hat{k}^r_{i'j'}G_{jj'}(\mu)detG^{-1}(\mu)$ are given by:

$$k^1 = \left[\begin{array}{cc} t & -\tan\theta \\ -\tan\theta & \frac{1+\tan^2\theta}{t} \end{array} \right]; \tag{A.6.41}$$

$$k^2 = \left[\begin{array}{cc} \frac{S}{D} & 0 \\ 0 & \frac{D}{S} \end{array} \right]; \tag{A.6.42}$$

$$k^3 = \left[\begin{array}{cc} \frac{t}{D} & 0 \\ 0 & \frac{D}{t} \end{array} \right]; \tag{A.6.43}$$

$$k^4 = \left[\begin{array}{cc} \frac{L}{D} & 0 \\ 0 & \frac{D}{L} \end{array} \right]. \tag{A.6.44}$$

The abstract problem formulation is then given for $P = 5$ (number of parameters), $R = 4$ (subdomains) and $Q = 9$ (different bilinear forms contributes to $\mathcal{A}$ over different portions of domain).

A.7 Some numerical results

In this section we present some numerical results obtained with the configuration previously described. We used a posteriori error bounds and adaptive procedures in basis-building process. Table A.1 shows a preliminary test based on two-parameters configuration and adaptivity procedures. We can see that the dimension of N is very small in reduced-basis

model. With adaptive procedures we get a 60% saving in computational cost related to off-line procedures using a triangulation with $O(10^3)$ elements. The information about the error bound is provided by Δ_N. Table A.2 gives us information about convergence (Δ_N), varying N,

N	Δ_N
7	0.1
9	0.01
13	0.001
20	0.0001

Table A.1: Δ_N and N using two-parameters configuration (L and D) and adaptive procedure (Section A.5). Without adaptive procedure we would need $N = 50$ to get a $\Delta_N < 10^{-3}$, we reach a consistent computational load reduction.

and about the effectivity η_N, studying a complete five-parameters configuration. With $N = 45$, for example, we get $\Delta_N \leq 10^{-4} = \varepsilon_d^{prior}$. Effectivity is near unity (always ≥ 1). The results are obtained testing at least 1000 different configurations Σ^{prior} and different parameters combinations (see Section A.5), the ones in the table are the worst gotten testing all the random configurations considered. It's important to underline that the adaptive procedure tested in the reduced-basis off-line building phase has permitted us to keep under control the condition number of the reduced-basis matrix, avoiding ill-conditioning problems caused by the random choice of parameters.
Figure A.5 shows the solution of the problem given by finite element method and by reduced basis for a certain combination of parameters (i.e $L = 1.0,\ D = 1.5, S = 1.0,\ t = 1.31,\ \theta = 16^o$). Figure A.6 shows the distribution of the error $\tilde{e}$ in Ω (difference between u_N and $\tilde{u}$) using $N = 60$ basis. This is not the error over the output $s(\mu)$ calculated by a posteriori error bounds, but it can be considered as a good indication how reduced-basis method is able to provide results close to the Finite-Elements solution. Figure A.7 shows the convergence of the method used in logarithmic scale increasing N, while Figure A.8 shows the upper and lower bound error estimator and their convergence to the true value of the output quantity of interest. Figures A.9 and A.10 represent effectivity η_N and the upper (η_{max}) and lower limit (η_{min}, i.e. unity). Figures A.11 and A.12 show parameters distribution in the parameters spaces during the off-line reduced-basis matrix construction. The former shows a two-parameters distribution region ($\mathcal{D}^\mu \subset \mathbb{R}^2$) around the first couple of parameters chosen in the centre of the region. Note that the parameters are distributed around the original starting point. The latter is a possible five-parameters distribution in the case studied applying the adaptive procedure.

N	η_N	Δ_{Nmax}	N	η_N	Δ_{Nmax}
1	3.1438	0.064589558	31	1.2802	0.000234237
2	4.4864	0.051445346	32	1.4427	0.000220116
3	4.6687	0.052944041	33	1.4321	0.000192997
4	4.5023	0.050876316	34	1.3848	0.000171898
5	4.0258	0.043368854	35	1.6566	0.000189594
6	2.9801	0.025041318	36	1.651	0.000176161
7	2.521	0.019830625	37	1.814	0.000185761
8	2.3531	0.018128973	38	1.8877	0.000192532
9	1.8848	0.012419358	39	1.9003	0.000187474
10	1.7454	0.010821934	40	1.8567	0.000179674
11	1.5322	0.008960269	41	1.6172	0.000140013
12	1.5339	0.008963254	42	1.6207	0.000139235
13	1.5327	0.008874298	43	1.6361	0.000140171
14	1.5052	0.008636955	44	1.7266	0.000146752
15	2.2945	0.008465466	45	1.6297	0.000101771
16	2.1233	0.008245741	46	1.6366	$9.74091E-05$
17	2.0121	0.007101543	47	1.6187	$9.63095E-05$
18	1.9571	0.005058438	48	1.6283	$9.64255E-05$
19	2.2285	0.003577518	49	1.481	$8.87554E-05$
20	2.3294	0.003595009	50	1.4757	$8.78055E-05$
21	1.9196	0.001392253	51	1.4802	$8.46522E-05$
22	1.882	0.00132827	52	2.8702	$8.46041E-05$
23	1.673	0.000950676	53	2.9196	$8.46041E-05$
24	1.6219	0.000783639	54	2.8235	$8.46041E-05$
25	1.655	0.000795108	55	2.6366	$8.47554E-05$
26	1.2313	0.000360924	56	2.7151	$7.8055E-05$
27	1.1243	0.000301648	57	2.6354	$7.65224E-05$
28	1.1096	0.000269211	58	2.6772	$7.46041E-05$
29	1.108	0.000268716	59	2.3726	$4.26101E-05$
30	1.1698	0.000275998	60	2.4882	$4.45111E-05$

Table A.2: Δ_{Nmax} and N using five-parameters configuration and adaptivity procedure to get a $\Delta_{Nmax} < 10^{-4} = \varepsilon_d^{prior}$ in the worst case. Note values of the effectivity η_N.

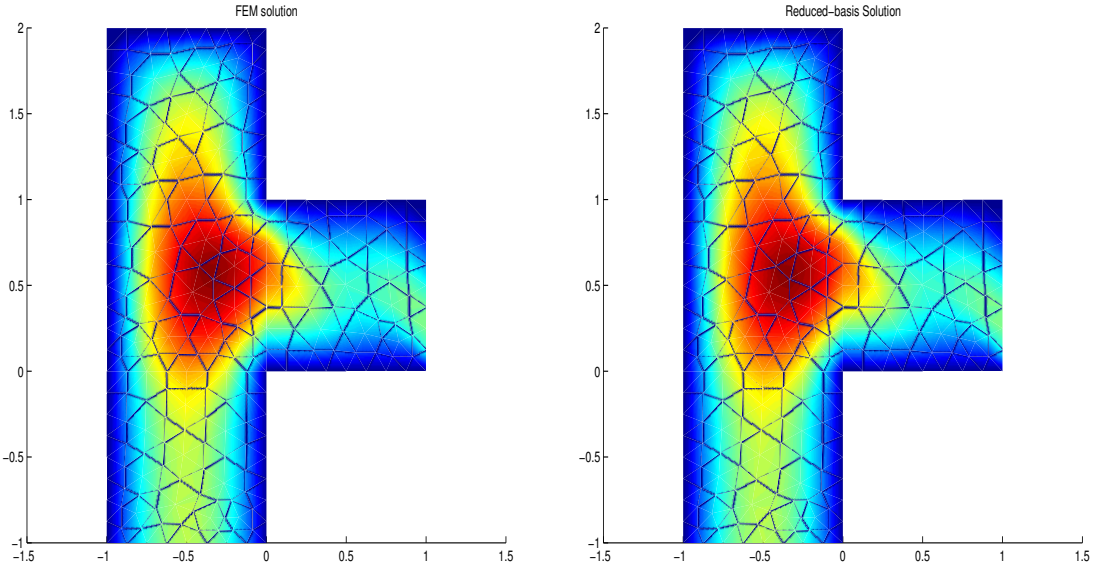

Figure A.5: Solution using FEM-Galerkin method for a 5-parameters configuration (left) and solution using reduced basis method with $N = 60$.

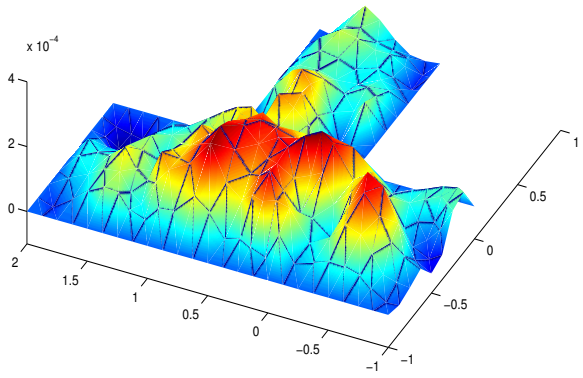

Figure A.6: Distributed error $\tilde{e}$ over the domain Ω between $\tilde{u}$ and u_N.

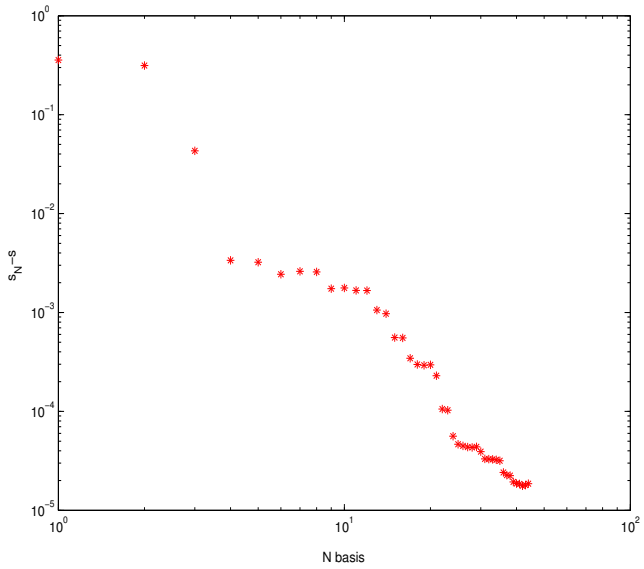

Figure A.7: Convergence of the difference $s_N - \tilde{s}$ increasing N.

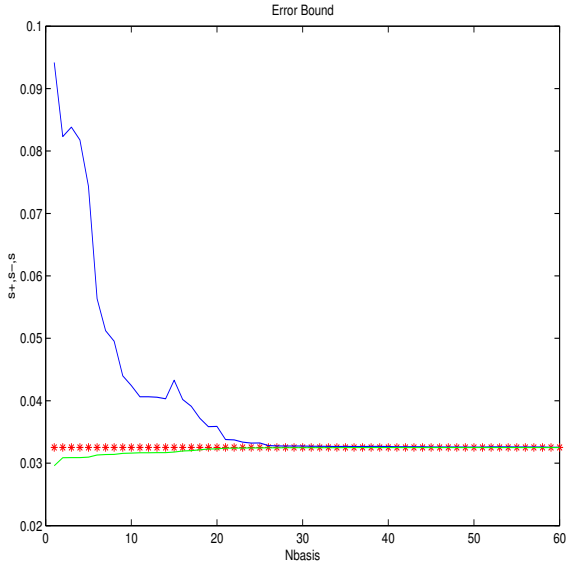

Figure A.8: Error Bounds s_N^+, s_N^- and their convergence to $s(*)$.

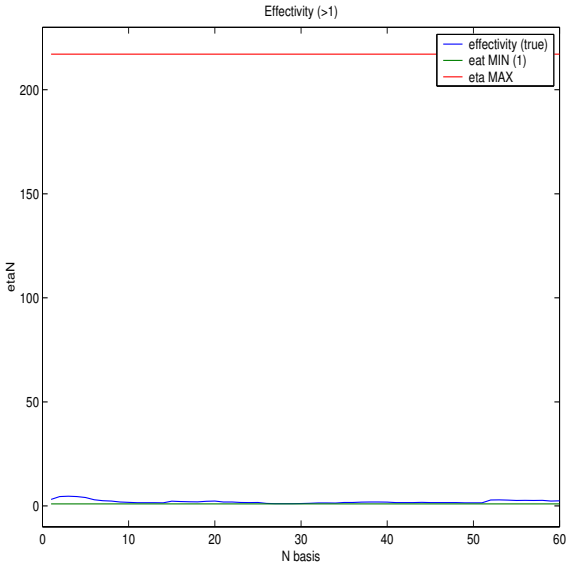

Figure A.9: Effectivity coefficient η_N and its bounds $\eta_{min}(=1)$ and η_{max}.

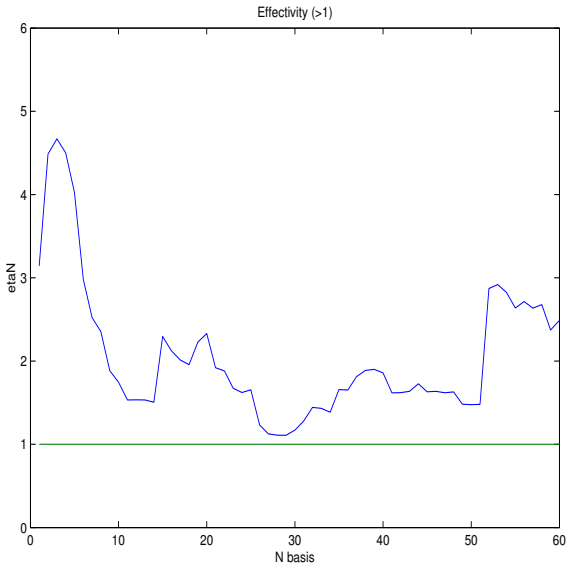

Figure A.10: Effectivity coefficient η_N with lower Bound (unity). Zoom.

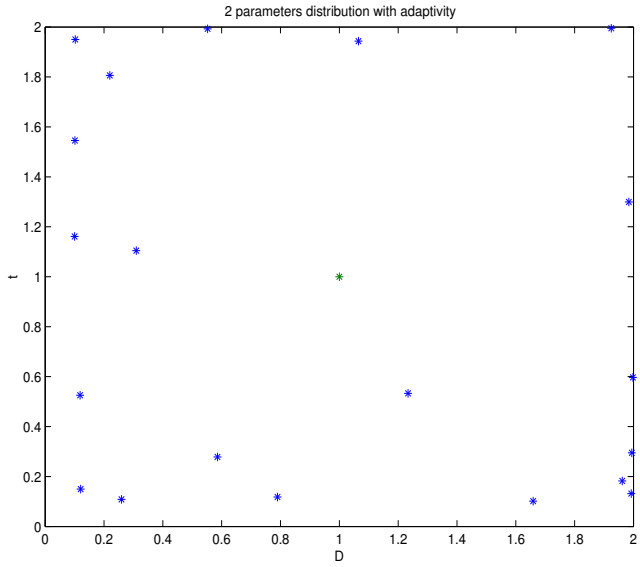

Figure A.11: 2-Parameters (t, D) distribution using adaptivity in basis building off-line process. The starting configuration is in the centre of the 2-parameters space.

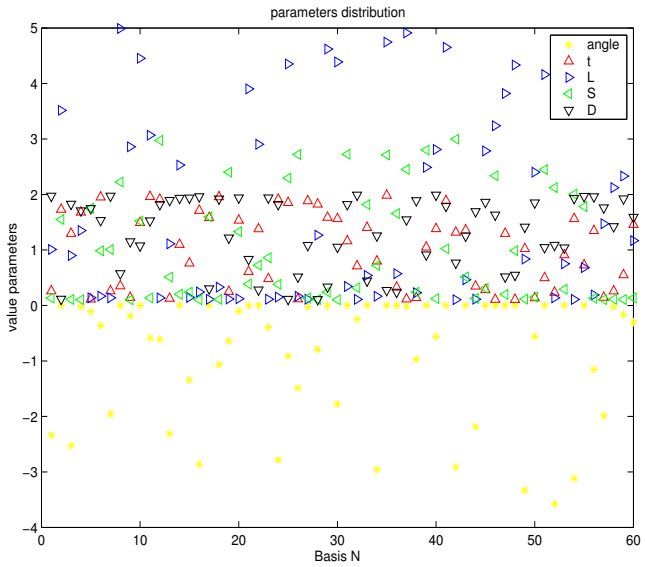

Figure A.12: 5-parameters distribution using adaptivity for reduced-basis matrix assembling.

A.8 Developments on reduced basis

In Chapters 5, 6 and 7 we extend the reduced basis technique to Stokes and Navier-Stokes equations and to problems involving also non-affine mapping (i.e. shape design). See also Grepl [44] and Solodukhov [145]. We are interested in studying a complete coarse configuration for the problem of aorto-coronaric bypass optimization but the procedures can be generalized for other design problems in engineering.

A.8.1 Reduced basis for the study of a complete geometrical configuration

The first step concerns the replacement of the elliptic state equation with Stokes equation (with Dirichlet in-flow condition and Neumann out-flow condition), see also Rovas [134]. The main steps are the following.

- Reformulation of the problem (new state equations, new bilinear forms) with the same geometry (4 subdomains) described in this appendix.
- Test of the bypass model with "macro" parameters in the haemodynamics background (5 macro-parameters) and a preliminary geometrical sensitivity analysis (diameter, stenosis lentgh, bypass angle,...).
- Test on a possible starting configuration to apply the tools of shape optimization and flow control (see Chapter 2-4 and [123]) with a more complex output of interest (e.g. vorticity).
- At the end of the study we get an optimized bridge configuration and useful indication for bypass construction. See Chapter 5.

A.8.2 Reduced basis for pre-process optimization

The problem can be studied at an intermediate level with an approach verified by feed-back procedures (a shell model).

- We use reduced-basis techniques to get a preliminary configuration for the bypass problem (coarse configuration) in a pre-process procedure for optimization.
- We apply tools for optimization based on flow control and optimal shape design technique, introduced in Chapter 2-4, using the starting configuration gotten from reduced basis model application. We use steady and unsteady Stokes equations.
- We take the new configuration (the local configuration optimized by shape design tools) for a further feedback using unsteady Navier-Stokes equations and other output of interest (such as unsteady quadratic functionals related to wall shear stress oscillations).

In conclusion at this step we have a "shell" model with three inner feedback procedure (see Figure A.13):

- Reduced-Basis method on a coarse "bridge" configuration.
- Optimal Shape design and Flow Control on fine configuration.
- Unsteady quantities and Navier Stokes equations as a feedback test for the final configuration.

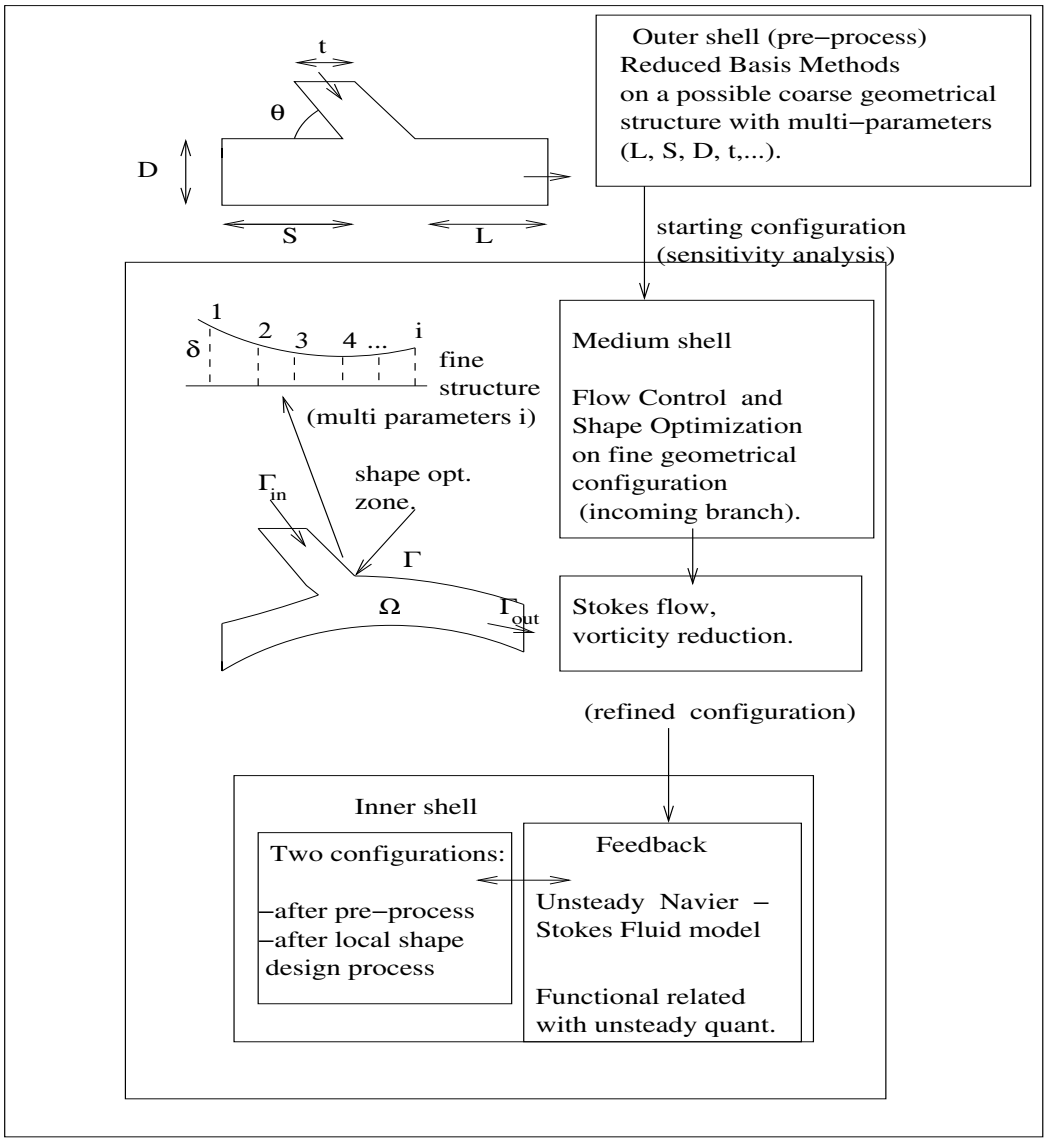

Figure A.13: "Shell" model scheme made up by consecutive steps.

A.8.3 Reduced basis for a shape optimization problem

The last step is the full extension of reduced basis model using more than five parameters and modelling the (curved) wall using non-affine mapping on reference domain. In this case

reduced basis can be used not only in the framework of a pre-process for optimization but as a shape optimization tool in itself. This aspect is considered in chapter 6. Then the introduction of non-linearities with the convective term allows us to study Navier-Stokes equation using reduced basis in parametrized domains. At this stage we can also carry out a comparison between the low fidelity fluid model based on the Stokes equation and the high fidelity one based on the Navier-Stokes equations. This aspect is developed in Chapter 7.

A.8.4 Reduced basis for optimal flow control

An other step to complete the present work is the creation of a link between optimal control (based on adjoint formulation) and reduced basis used to solve both state and adjoint problem with geometrical shape parameters. In this last case optimization would be driven by optimal control tools, while approximation by reduced-basis model. See Table A.3. This aspect is developed in Chapter 8.

Step	First Option	Second Option
Problem Approximation	Galerkin-Finite Element and Reduced-basis for state equation	Galerkin-Finite Element and Reduced-basis for state and adjoint equation
Optimization	Sensitivity Analysis	Optimal Control (adjoint formulation)

Table A.3: Third step future developments options.

It is evident that to expand and apply reduced-basis theory on biomechanics problems (i.e. biomedical devices such as bypass) the two most important phases are the use of a great number of geometrical parameters (non-affine mapping) and the use of Navier-Stokes equations to model fluid flow.

A.9 The model-order reduction

We give at the end of this appendix some relevant background (and historical) information on model-order reduction. The issue of reducing complexity while preserving all relevant information, has been a very active research area in many disciplines. A characteristic of systems whose behavior is governed by partial differential equations is that the resulting state models, obtained by a discretization procedure, are of very high-dimension. Therefore some of the existing methods developed, for example in control systems theory, are not directly applicable. In the last period the problem of model-order reduction is becoming more and more relevant due to the versatility that it allows in the parametrization of the problem. See for example the recent review work in *SIAM News* [51] by Gunzburger and Willcox. We

summarize in Section A.9.1 recent developments and relevant approaches. The references provided, although by no means exhaustive, should cover most of the recent work. As model-order reduction methods are by definition pre-asymptotic, validation of the obtained results has been recognized to be a critical ingredient. Even though residual-based error measures have been suggested, rigorous *a posteriori* error estimation procedures have been developed in the last years. In other contexts, like estimation of the discretization error in finite-element analysis, a plethora of *a posteriori* error estimation methods had already been existent for years. Some of these methods are relevant for our problems; we discuss in section A.9.2 the connection and differences between them.

A.9.1 Earlier Work

Proper Orthogonal Decomposition

We start our discussion with the proper orthogonal decomposition method, probably the most popular model-order reduction technique. Underlying this method is the solution of the following approximation problem: given a (possibly large) set of vectors, identify the best approximating N-dimensional plane (subspace) such that the root-mean square L_2-projection error is minimized. A solution to this problem can be obtained using the singular value (or Karhunen-Loève) decomposition [86].
The proper orthogonal decomposition has been applied and (re-)discovered in many different areas: system dynamics, stochastic processes, image processing, to name a few. For reduction of physical systems, it has been extensively applied to time-dependent problems. In this case, time is considered as the varying parameter, and "snapshots" of the field variable (e.g. temperature, displacement) at different times — parameter points — are obtained using numerical or experimental procedures. The optimal N-dimensional approximation space (for N small) is constructed by applying the singular-value decomposition to these vectors, and keeping only the N singular vectors corresponding to the largest singular values. As the singular values are related to the total "energy" of the approximation, these modes can be identified as the ones preserving most of the energy. The reduced model is then obtained by using a Galerkin projection to the space spanned by these vectors. More precisely, the POD algorithm is built as follows (see, for example, [50] and [132]):

- we start from a reduced basis $\{\phi_1, ..., \phi_{\widetilde{M}}\}$, a basis of finite element solutions associated to some "snapshots" (chosen parameters), where $\widetilde{M}$ is usually $\mathcal{O}(100)$, and we compute the mean value
$$\bar{\phi} = \frac{1}{\widetilde{M}} \sum_{j=1}^{\widetilde{M}} \phi_j.$$
We assume that ϕ_i, $i = 1, ..., \widetilde{M}$ has been computed by finite element method: $\phi_i \in \mathbb{R}^{\mathcal{N}}$, dove $\mathcal{N} \gg 1$ is the finite element space dimension.

- We build a correlation matrix $\underline{C} : \widetilde{M} \times \widetilde{M}$ (symmetric and positive semidefinite), whose elements are $C_{i,j} = \frac{1}{\widetilde{M}}(\phi_i - \bar{\phi})^T(\phi_j - \bar{\phi})$, $i, j = 1, ..., \widetilde{M}$.

- We compute eigenvalues $\{\lambda_1, ..., \lambda_{\widetilde{M}}\}$ and the corresponding eigenvectors $\{v_1, ..., v_{\widetilde{M}}\}$ of $\underline{C}$, ordering the eigenvalues by decreasing size.
- We choose M:
$$M = \min_{m \in [1, \widetilde{M}]} \text{such that } \frac{\sum_{j=1}^{m} \lambda_j}{\sum_{j=1}^{\widetilde{M}} \lambda_j} \geq \gamma,$$
where $0 \leq \gamma \leq 1$ is a fixed tolerance.
- We set $\Phi_i = \sum_{j=1}^{\widetilde{M}} (v_i)_j (\phi_j - \bar{\phi})$, for $i = 1, ..., M$. $(v_i)_j$ is the j-th component of the i-th eigenvector.
- We normalize $\hat{\Phi}_i = \frac{\Phi_i}{|\Phi_i|}$, where $|\Phi_i|^2 = \Phi_i^T \Phi_i$.

The set $B = span\{\hat{\Phi}_1, ..., \hat{\Phi}_M\}$ is the POD basis (orthonormal, i.e. $\Phi_i^T \Phi_j = \delta_{ij}$); the POD approximation is: find $u_M(\mu) \in B$ so that

$$a(u_M(\mu), v; \mu) = f(v), \ \forall v \in B. \tag{A.9.1}$$

The optimality property and generality of these ideas, has led to the successful application of the method in many areas: turbulent flows [89], fluid structure-interaction [34], non-linear structural mechanics [73], turbo-machinery flows [166]. Extension of these methods to general multi-parameter problems has been quite limited. The problem is that the singular values are not system invariants as they depend on the choice of "snapshots" and the particular configuration in consideration. It has been observed that reduced-order models obtained for one configuration were not optimal for other configurations; using such models often lead to inaccurate or, even worse, incorrect results. It has been suggested in [24] to give more weight or preselect some of the vectors in the starting basis, leading to "weighted-POD" or "predefined-POD" methods, but the selection of the required weights is not automatic limiting the generality of such approaches.
An analysis of the model-truncation error suggests that the error can be attributed to two sources: first in the inability of the low-order model to reproduce the exact loading; and second, for the approximated loading, in the inability of the low-order model to recover the exact solution [72] (see also [114] for similar ideas). Using terms from control-systems theory, the first error is related to the controllability (primal) and the second to the observability (dual) of the low-order model. In a similar manner, for our methods, we introduce at the end of Chapter 5 a combined primal-dual approach to estimate both of these errors. The notion that a truncation of the model should balance both of these errors, led to balanced-truncation methods [98].

Reduced Basis Methods

We turn now to reduced-basis approaches, upon which our method is also based. The reduced-basis method has been proposed in [8, 102] for the non-linear analysis of structures. In these approaches, only single-parameter problems were considered and the method was viewed

as a continuation procedure. The method has been further investigated and extended by Noor [105, 106], who realized that the method could be applied for general multi-parameter problems. Much of the earlier work focused: first, on the selection and efficient computation of basis functions; and second, on validation of the efficiency and accuracy of reduced-basis approaches in a number of test problems.

As seen in the introduction of this appendix the reduced-basis method recognizes that the field variable is not, in fact, some arbitrary member of the infinite-dimensional solution space associated with the partial differential equation; rather, it resides, or "evolves", on a much lower-dimensional manifold induced by the parametric dependence. In these earlier approaches, the approximation spaces for the low-dimensional manifold were typically defined "locally" — relative to a particular parameter point. Fink and Rheinboldt [37] placed the method in this geometric setting and carried out an error analysis for a general class of single-parameter problems. Porsching [117] considered Lagrangian, Taylor and discrete least squares approximation spaces, and extended some of the *a priori* analysis. In [38] a general local error estimation theory for single-parameter problems was developed containing the earlier estimates as special cases. The extension of the error analysis to multi-parameter problems was presented in [133]. Finally, evaluation of the constants that appear on the error bounds was considered in [13]. The *a priori* theory as developed in the works above concludes that, close to the parameter point selected for the construction of the reduced-basis spaces, the error converges to zero exponentially fast with the number of basis functions used.

Reduced basis approaches have been subsequently developed in many other areas. Peterson [113] applied it to fluid flow problems and the Navier-Stokes equations, and in [65, 64] it was used for control of fluid problems. The reduced-basis approach as earlier articulated was local in parameter space in both practice and theory. As a result, the computational improvements — relative to conventional (say) finite-element approximation — were often quite modest [117]. Balmes [11], was the first to consider general multi-parameter problems. In his approach he suggests choosing the basis functions by sampling globally in parameter space. The importance of error estimation has always been emphasized in the literature and rigorous *validation* methods have been developed by Patera, Maday *et al.* in [91], [92] and [134] and since then the range of reduced basis applications has increased a lot.

Other Methods

Krylov-subspace techniques like the Arnoldi or the Lanczos methods and their variants, have traditionally been used for the calculation of a small set of the extremal eigenvalues and eigenvectors for large-scale eigenproblems. But these are precisely the eigenvalues and eigenvectors of interest for model reduction. Many reduction approaches based on Krylov-subspace techniques have been developed; for an overview see [69] and the references contained therein. The iterative nature of the algorithms, makes it difficult to develop error bounds; moreover and the stability of the reduced-order problem is not always guaranteed.

A.9.2 Remarks on *a posteriori* error estimation

The issue of *a posteriori* error estimation and, more generally, validation of the numerical predictions has received considerable attention in the finite-element literature. The problem of interest is related to the choice of mesh to be used for the definition of the finite-element spaces. It is understood that there are certain trade-offs associated with the choice of the finite-element mesh: on one hand, a conservative choice, ensures high accuracy but also the computational costs become formidable; on the other hand, the choice of a relatively coarse mesh ensures efficiency but the accuracy is dubious. More to that, for a specific choice of mesh, the obtained accuracy is not easy to calculate as it depends on the topology of the mesh, the particular problem in consideration, the choice of finite-element spaces, or even the way we choose to measure the error. We can also relate a number of other problems like, for example, the choice of elements to be refined in adaptive refinement or, more generally the choice of "optimal" meshes (i.e. meshes which for a given accuracy minimize computational cost). For all these problems, the ability to estimate and therefore control, the discretization error is critical.

The extensive *a priori* theory can not be used as the provided error bounds depend on norms of the exact solution which, in general, is not known. Rather, the *a posteriori* error estimators give bounds which depend on computable quantities, like residuals. The study of these types of error estimators started in the 70s with the first paper by Babuska and Rheinboldt [10], and since then the literature has grown appreciably; a review can be found in [7]. Most error estimators developed give bounds for abstract norms of the error. Relevant to this thesis are *a posteriori* error estimators directly for outputs of interest; see for example [109, 110] for relevant work.

For the reduced-basis method instead of the finite-element mesh and the discretization error, we have the parameter space "discretization", and the reduced-basis approximation error; refinement of the mesh, corresponds to adding more basis-functions in the definition of the reduced basis global approximation space W_N. But there are also differences, the most important being the parameter-dependence of the operator, consideration of which is not required in the finite-element case. Even though the methodologies are distinctively different; some of the general ideas [110] for *a posteriori* error estimation are common.

Bibliography

[1] G. Abdoulaev, S. Cadeddu, G. Delussu, M. Donizelli, C. Manzi, L. Formaggia, A. Giachetti, E. Gobbetti, A. Leone, P. Pili, A. Schenine, M. Tuveri, A. Varone, A. Veneziani, G. Zanetti, A. Zorcolo. *VIVA: the virtual vascular project.* IEEE Transactions on Information Technology in Medicine, Vol. 22, No. 4 (1998), pp. 268–274.

[2] F. Abraham, M. Behr and M. Heinkenschloss. *Shape Optimization in Steady Blood Flow: A Numerical Study of Non-Newtonian Effects.* Computer Methods in Biomechanics and Biomedical Engineering, Vol. 8, No. 2 (2005), pp. 127–137.

[3] R. Adams. *Calculus of Several Variables: A Complete Course.* Addison-Wesley, fifth edition, 2002.

[4] V.I. Agoshkov, A. Quarteroni, G. Rozza. *Shape design approach using perturbation theory for bypass anastomoses.* To appear in Siam Journal of Numerical Analysis, 2005.

[5] V.I. Agoshkov, A. Quarteroni, G. Rozza. *A Mathematical approach in the design of arterial bypass using unsteady Stokes equations.* To appear in Journal of Scientific Computing, 2005.

[6] V.I. Agoshkov. *Optimal Control Approaches and Adjoint Equations in the Mathematical Physics Problems.* Institute of Numerical Mathematics, Russian Academy of Sciences, Moscow, 2003.

[7] M. Ainsworth, J. T. Oden. *A Posteriori Error Estimation in Finite Element Analysis.* Wiley-Interscience, 2000.

[8] B. O. Almroth, P. Stern, F. A. Brogan. *Automatic choice of global shape functions in structural analysis.* AIAA Journal, Vol. 16 (1978), pp. 525–528.

[9] A.K. Aziz, J.W. Wingate, M.J. Balas. *Control Theory of Systems Governed by Partial Differential Equations.* Academic Press, 1971.

[10] I. Babuska, W.C. Rheinboldt. *A posteriori error estimates for the finite-element method.* Int. J. Num. Meth. Engrg, Vol. 18 (1978), pp. 736–754.

[11] E. Balmes. *Parametric families of reduced finite element models. Theory and applications.* Mechanical Systems and Signal Processing Vol. 10, No. 4 (1996), pp. 381–394.

[12] M. Barrault, Y. Maday, N.C. Nguyen and A.T.Patera. *An "empirical interpolation" method: application to efficient reduced-basis discretization of partial differential equations.* C. R. Acad. Sci. Paris, Analyse Numerique, Serie I, 2004, Vol. 339, pp. 667–672.

[13] A. Barrett and G. Reddien. *On the reduced basis method.* Z. Angew. Math. Mech., Vol. 75, No. 7 (1995), pp. 543–549.

[14] R. Becker. *Mesh adaptation for stationary flow control.* Journal of Mathematical Fluid Mechanics, Vol. 3 (2001), pp. 317-341, Birkhäuser Verlag, Basel.

[15] R. Becker, H. Kapp, R. Rannacher. *Adaptive finite elements methods for optimal control of partial differential equations: basic concepts.* SIAM Journal on Control and Optimization. Vol. 39, No. 1 (2000).

[16] D. Bernardi, F. Hecht, T. Lachand-Robert, K.Ohtsuka, O. Pironneau. *Freefem+ for Macs, PCs, Linux: Documentation.* INRIA, Rocquencourt, 2001.

[17] M. Berggren. *Numerical solution of a flow-control problem: vorticity reduction by dynamic boundary action.* SIAM, Journal of Scientific Computing, Vol. 19, No. 3 (1998), pp. 829–860.

[18] C. Bertolotti, V. Deplano, J. Fuseri, P. Dupouy. *Numerical and experimental models of post-operative realistic flows in stenoses coronary bypasses.* Journal of Biomechanics, Vol. 34, No. 8 (2001), pp. 1049–1064.

[19] F. Brezzi, M. Fortin. *Mixed and Hybrid Finite Element Methods.* Springer and Verlag, New York, 1991.

[20] F. Brezzi, G. Gilardi. *Functional Analysis and Functional Spaces.* Mc-Graw Hill, NY, 1987.

[21] J. Burkardt. *Flow optimization using sensitivities.* Preprint, School of Computational Science, Florida State University, submitted, 2005.

[22] J. Cahouet, J.P. Chabard. *Some fast 3D finite element solvers for the generalized Stokes problem.* International Journal Numerical Methods for Fluids, Vol. 8, No. 8 (1988), pp. 869–895.

[23] D. Cholaseuk. *Shape Optimization for fluid flow problems using Bezier curves and designed numerical experiments.* Proceedings of the 1999 Asme Design Engineering Technical Conferences, September 12-15, 1999, Las Vegas, Nevada.

[24] E.A. Christensen, M. Brøns, J.N. Sørensen. *Evaluation of proper orthogonal decomposition-based decomposition techniques applied to parameter-dependent nonturbulent flows.* SIAM J. Scientific Computing, Vol. 21, No. 4 (2000), pp. 1419–1434.

[25] P.G. Ciarlet. *Introduction à l'Analyse Numérique Matricielle et à l'Optimisation.* Dunod, Paris, 1998.

[26] J.S. Cole, J.K. Watterson, M.J.G. O'Reilly. *Numerical investigation of the haemodynamics at a patched arterial bypass anastomosis.* Medical Engineering and Physics, Vol. 24 (2002), pp. 393–401.

[27] J.S. Cole, J.K. Watterson, M.J.G. O'Reilly. *Is there a haemodynamic advantage associated with cuffed arterial anastomoses.* Journal of Biomechanics, Vol. 35 (2002), pp. 1337–46.

[28] J.S. Cole, J.K. Watterson, S. Raghunathan and M.J.G. O'Reilly. *Numerical study of blood flow through the Taylor arterial bypass model.* 12^{th} Meeting of the European Society of Biomechanics, Dublin 2000.

[29] J.S. Cole, J.K. Watterson and M.J.G. O'Reilly. *Haemodynamics of modified distal bypass graft anastomoses.* 7^{th} Annual Conference of the Section of Bioengineering of the Royal Academy of Medicine in Ireland, Arklow 2001.

[30] J.S. Cole, L.D. Wijesinghe, J.K. Watterson and D.J.A. Scott. *Computational and experimental simulations of the haemodynamics at cuffed arterial bypass graft anastomoses.* Proceedings of the Institution of Mechanical Engineers, Part H: Journal of Engineering in Medicine, Vol. 216 (2002), pp. 135–143.

[31] R. Courant, D. Hilbert. *Methods of Mathematical Physics.* Wiley, New York, 1966.

[32] L. Dedè, A. Quarteroni. *Optimal control and numerical adaptivity for advection-diffusion equations.* M2AN, Vol. 39, No. 5 (2005), pp.1019–1040.

[33] N. Di Césaré. *Outils pour l'Optimisation de forme et le Contrôle Optimal, application à la Mécanique des Fluides.* Thèse de Doctorat de l'Université Paris VI, 2000.

[34] E.H. Dowell, K.C. Hall. *Modelling of fluid structure interaction.* Annual Rev. Fluid. Mech., Vol. 33 (2001), pp. 445–490.

[35] C. Fabre, G. Lebeau. *Prolongement unique des solutions de l'équation de Stokes.* Communications in Partial Differential Equations, Vol. 21, No. 3-4 (1996), pp. 573–596.

[36] C. Fabre, G. Lebeau. *Régularité et unicité pour le problème de Stokes.* Communications in Partial Differential Equations, Vol. 27, No. 3-4 (2002), pp. 437–475.

[37] J.P. Fink, W.C. Rheinboldt. *On the error behavior of the reduced basis technique for nonlinear finite element approximations.* Z. Angew. Math. Mech. Vol. 63, No. 1 (1983), pp. 21–28.

[38] J. P. Fink, W. C. Rheinboldt. *Local error estimates for parametrized non-linear equations.* SIAM J. Numerical Analysis, Vol.22 (1985), pp. 729–735.

[39] Y.C. Fung. *Biodynamics: Circulation.* Springer and Verlag, New York, 1984.

[40] G.P. Galdi. *An Introduction to the Mathematical Theory of the Navier-Stokes Equations, Volume I: Linearized Steady Problem.* Springer-Verlag, New York, 1994.

[41] G.P. Galdi. *An Introduction to the Mathematical Theory of the Navier-Stokes Equations, Volume II: Nonlinear Steady Problem.* Springer-Verlag, New York, 1994.

[42] J-F. Gerbeau, D. Chapelle. *Simulation numérique du système cardiovasculaire.* M/S Medecine Sciences, Vol. 21, No. 5 (2005), pp. 530–534.

[43] V. Girault, P.A. Raviart. *Finite Element Methods for Navier-Stokes Equations.* Springer-Verlag, Berlin, 1986.

[44] M. Grepl. *Reduced Basis Approximation and A posteriori Error Estimation for Parabolic Partial Differential Equations.* Phd thesis, MIT, Massachusetts Institute of Technology, 2005.

[45] M. Grepl, N.C. Nguyen, K. Veroy, A.T. Patera and G.R. Liu. *Certified rapid solution of parametrized partial differential equations for real-time applications.* 2^{nd} Sandia Workshop on PDE-Constrained Optimization: toward real-time and online PDE-Constrained Optimization. Submitted, 2005.

[46] P.M. Gresho, R.L. Sani. *Incompressible Flow and the Finite Elements Method.* J. Wiley, New York, 2000.

[47] Ph. Guillaume, M. Masmoudi. *Computational of high order derivatives in optimal shape design.* Numerische Mathematik, Vol. 67 (1994), pp. 231–250.

[48] M.D. Gunzburger. *Finite Element Method for Viscous Incompressible Flows: A Guide to Theory, Practice, and Algorithms.* Academic Press, Boston, 1989.

[49] M.D. Gunzburger, L. Hou, T. Svobodny. *Boundary velocity control of incompressible flow with an application to viscous drag reduction.* SIAM, Journal of Control and Optimization, Vol. 30, No. 1 (1992), pp. 167-181.

[50] M.D. Gunzburger. *Perspectives in Flow Control and Optimization.* SIAM, Advances in Design and Control, Philadelphia, 2003.

[51] M.D. Gunzburger, K. Willcox. *Reduced-order models of large-scale computational systems.* SIAM News, Vol. 38, No. 5, June 2005.

[52] J. Haslinger, R.A. Mäkinen. *Introduction to Shape Optimization: Theory, Approximation, and Computation.* SIAM, Advances in Design and Control, Philadelphia, 2003.

[53] F. Hecht, O. Pironneau. *Multiple unstructured meshes and the design of Freefem+.* INRIA, Rocquencourt, 1999.

[54] F. Hecht, O.Pironneau, K.Ohtsuka. *Freefem++ Manual 1.34.* http://www.freefem.org, 2003.

[55] F. Hecht. *BAMG: Bidimensional Anisotropic Mesh Generator.* User Guide. INRIA, Rocquencourt, 1998.

[56] E.J. Hinch. *Perturbation Methods.* Cambridge Texts in Applied Mathematics, Cambridge University Press, 1991.

[57] M. Hinze, K. Kunisch. *Second order methods for optimal control of time-dependent fluid-flow.* SIAM, Journal of Control Optimization, Vol. 40, No. 3 (2001), pp. 925–946.

[58] L. Hou, S. Ravindran. *Numerical approximation of optimal flow control problems by a penalty method: error estimates and numerical results.* SIAM, Journal of Scientific Computing, Vol. 20, No. 5 (1999), pp.1753–1777.

[59] L. Hou, S. Ravindran. *A penalized Neumann control approach for solving an optimal control problem for Navier-Stokes equation.* SIAM, Journal of Control and Optimization, Vol. 36, No. 5 (1998), pp. 1795–1814.

[60] P.E. Hughes, T.V. How. *Effects of geometry and flow division on flow structures in models of the distal end-to-dide anastomoses.* Journal of Biomechanics, Vol. 29, No. 7 (1996), pp. 855–872.

[61] V. Isakov. *Inverse Source Problem.* American Mathematical Society, Providence RI, USA, 1990.

[62] K. Ito, S.S. Ravindran. *A reduced basis method for control problems governed by PDEs.* In W. Desch, F. Kappel, and K. Kunish eds. *Control and Estimation of Distributed Parameter System*, pp. 153–168, *Birkäuser*, 1998.

[63] K. Ito, S.S. Ravindran. *Reduced basis method for optimal control of unsteady viscous flows.* International Journal of Computational Fluid Dynamics, Vol. 15 (2001), pp. 97–113.

[64] K. Ito, S.S. Ravindran. *A reduced-order method for simulation and control of fluid flow.* Journal of Computational Physics, Vol. 143, No. 2 (1998), pp. 403–425.

[65] K. Ito, J.D. Schroeter. *Reduced order feedback synthesis for viscous incompressible flows.* Mathematical And Computer Modelling, Vol. 33, No. 1-3 (2001), pp. 173–192.

[66] A. Jameson, J.C. Vassberg. *Computational fluid dynamics for aerodynamic design: its current and future impact.* AIAA Paper 2001-0538, 39^{th} AIAA Aerospace Sciences Meeting and Exibit, Jan 8-11 2001, Reno NV.

[67] A. Jameson. *Optimum aerodynamic design using CFD and control theory.* AIAA Paper 95-1729, 12^{th} AIAA Computational Fluid Dynamics Conference 1995.

[68] A. Jameson. *Aerodynamic design via control theory.* Journal of Scientific Computing, Vol. 3 (1988), pp. 233–260.

[69] M. Kamon, F. Wang, J. White. *Generating nearly optimally compact models from Krylov-subspace based reduced-order models.* IEEE Transactions on Circuits and Systems — II: Analog and Digital Processing. Vol. 47, No. 4 (2000), pp. 239–248.

[70] B. Kawohl, O. Pironneau, L. Tartar, J.-P. Zolésio. *Optimal Shape Design.* Springer, Berlin, 2000.

[71] J. Kevorkian, J.D. Cole. *Perturbation Methods in Applied Mathematics.* Springer-Verlag, New York-Heidelberg-Berlin, 1981.

[72] K. Kline. *Dynamic analysis using a reduced-basis of exact modes and Ritz vectors.* AIAA Journal, 1986, Vol. 24, No. 12, pp. 2022–2029.

[73] P. Krysl, S. Lall, J.E. Marsden. *Dimensional model reduction in non-linear finite element dynamics of solids and structures.* International Journal for Numerical Methods in Engineering, Vol. 51 (2001), pp. 479–504.

[74] S.M. Kute, D.A. Vorp. *The effect of proximal artery flow on the hemodynamics at the distal anastomosis of a vascular bypass graft: computational study.* ASME Journal of Biomechanical Engineering, Vol. 123 (2001), pp. 277–283.

[75] E. Laporte. *Optimisation de formes pour Écoulements Instationnaires.* Ph.D Thesis, École Polytechnique, Paris, 1998.

[76] E. Laporte, P. Le Tallec. *Shape optimization in unsteady flows.* INRIA, Rapport de Recherche, No. 3693, 1999.

[77] S.E. Lee, N. Piersol, F. Loth, P. Fischer, G. Leaf, B. Smith, R. Yedevalli, A. Yardimci, N. Alperin and L. Schwartz. *Automated mesh generation of an arterial bifurcation based upon in vivo MR images.* Proceedings of the 2000 World Congress on Medical Physics and Bioengineering, CD ROM.

[78] M. Lei, J.P. Archie, C. Kleinstreuer. *Computational design of a bypass graft that minimizes wall shear stress gradients in the region of the distal anastomosis.* Journal of Vascular Surgery, Vol. 25, No. 4 (1997).

[79] M. Lei, D.P. Giddens, S.A. Jones, F. Loth, H. Bassiouny. *Pulsatile flow in an end-to-side vascular graft model: comparison of computations with experimental Data.* ASME Journal of Biomechanical Engineering, Vol. 123 (2001), pp. 80–87.

[80] A. Leuprecht, K. Perktold, M. Prosi, T. Berk, W. Trubel, H. Schima. *Numerical study of hemodynamics and wall mechanics in distal end-to-side anastomoses of bypass graft.* Journal of Biomechanics, Vol. 35 (2002), pp. 225–236.

[81] S. Lim, H. Choi. *Optimal shape design of a two dimensional asymmetric diffuser in turbulent flow.* AIAA Journal, Vol. 42, No. 6 (2004).

[82] J.L. Lions. *Optimal Control of Systems Governed by Partial Differential Equations.* Springer-Verlag, 1971.

[83] J.L. Lions. *Some Aspects of the Optimal Control of distribuited parameter Systems.* SIAM, Philadelphia, 1972.

[84] J.L. Lions, E. Magenes. *Non-homogeneous Boundary Value Problems and Applications.* Springer-Verlag, 1972.

[85] P.L. Lions. *Mathematical Topics in Fluid Mechanics. Volume I: Incompressible Models.* Oxford Science Publications, Clarendon Press, Oxford, 1996.

[86] M. Loeve. *Probability Theory*, Van Nostrand, 1955.

[87] F. Loth, S.A Jones, D.P. Giddens, H.S Bassiouny, C.K Zarins, S. Glagov. *Measurement of velocity and wall shear stress inside a PTE vascular graft model under steady flow conditions.* Journal of Biomechanical Engineering, Vol. 119 (1997), pp. 187–194.

[88] A.E. Løvgren, Y. Maday, E.M. Rønquist. *A reduced basis element method for the steady Stokes problem.* Mathematical Modelling and Numerical Analysis M^2AN, submitted, 2004.

[89] J. Lumley, P. Blossey. *Control of Turbulence.* Annu. Rev. Fluid. Mech., Vol. 30 (1998), pp. 311–327.

[90] L. Machiels, Y. Maday, I.B. Oliveira, A.T. Patera and D.V. Rovas. *Output bounds for reduced-basis approximations of symmetric positive definite eigenvalue problems.* C. R. Acad. Sci. Paris, Série I, Vol. 331, No. 2 (2000), pp. 153–158.

[91] Y. Maday, A.T. Patera, and G. Turinici. *Global a priori convergence theory for reduced-basis approximations of single-parameter symmetric coercive elliptic partial differential equations.* C.R. Acad. Sci. Paris Série I, Vol. 335, No. 3 (2002), pp. 289-294.

[92] Y. Maday, A.T. Patera, and G. Turinici. *A priori convergence theory for reduced-basis approximations of single-parameter elliptic partial differential equations.* Journal of Scientific Computing, Vol. 17 No. 1-4 (2002), pp. 437–446.

[93] D.S. Malkus. *Eigenproblems associated with the discrete LBB condition for incompressible finite elements.* Int.J.Eng.Sci., Vol. 19 (1981), pp. 1299–1310.

[94] G.I. Marchuk. *Methods of Numerical Mathematics.* Nauka, Moscow, 1989.

[95] G.I. Marchuk. *Adjoint Equations and Analysis of Complex System.* Kluwer Academic Publisher, 1995.

[96] G.I. Marchuk, V.I. Agoshkov, V.P. Shutyaev. *Adjoint Equations and Perturbation Algorithms in Nonlinear Problems.* CRC Press, 1996.

[97] B. Mohammadi, O. Pironneau. *Applied Shape Optimization for Fluids.* Oxford University Press, Oxford, 2001.

[98] B.C. Moore. *Principal component analysis in linear systems: controllability, observability, and model reduction.* IEEE Transactions on Automatic Control, Vol. 26, No. 1 (1981), pp. 17–32.

[99] J.A. Moore, D.A. Steinman, S. Prakash, C.R. Ethier, K.W Johnston. *A numerical study of blood flow patterns in anatomically realistic and simplified end-to-side anastomoses.* ASME, J.Biomechanical Engineering, Vol. 121, No. 3 (1999), pp. 265–72.

[100] M. Moubachir, J.P. Zolésio. *Optimal control of fluid-structure interaction systems: the case of a rigid solid.* INRIA, Rapport de Recherche, No. 4611, 2002.

[101] W. Nichols, M. O'Rourke. *McDonald's Blood Flow in Arteries: Theoretical, Experimental and Clinical Principles.* Fourth edition, Arnold, London, 1998.

[102] D. A. Nagy. *Modal representation of geometrically nonlinear behaviour by the finite element method.* Computers and Structures, Vol. 10 (1979), pp. 683-688.

[103] N.C. Nguyen. *Reduced Basis Approximation and A Posteriori Error Bounds for Non-affine and Nonlinear Partial Differential Equations: Application to Inverse Analysis.* PhD Thesis, Singapore-MIT Alliance, National University of Singapore, 2005.

[104] N.C. Nguyen, K. Veroy, A.T. Patera. Certified Real-Time Solution of Parametrized Partial Differential Equations. *Handbook of Materials Modeling.* R. Catlow, H. Shercliff and S. Yip Eds. Kluwer Academic Publishing (Springer), 2005.

[105] A. K. Noor. *Recent advances in reduction methods for nonlinear problems*, Comput. Struct, Vol.13 (1981), pp. 31–44.

[106] A. K. Noor and J. M. Peters. *Reduced basis technique for nonlinear analysis of structures.* AIAA Journal, Vol. 18, No. 4 (1980), pp.455-462.

[107] T. P. O'Brien, T. McGloughlin. *Computational fluid dynamics analysis of blood flow in compliant arterial grafts.* 12^{th} Conference of the European Society of Biomechanics, Dublin, 2000.

[108] Y. Papaharilaou, D.J. Doorly, S.J. Sherwin. *The influence of out-of-plane geometry on pulsatile flow within a distal end-to-side anastomosis.* Journal of Biomechanics, Vol. 35 (2002), pp. 1225–1239.

[109] A.T. Patera, J. Peraire. *A general Langragian formulation for the computation of a posteriori finite element bounds.* In Error Estimation and Solution Adaptive Procedures in CFD. Springer-Verlag, 2002.

[110] A.T. Patera, E. M. Rønquist. *A general output bound result: application to discretization and iteration error estimation and control*. Mathematical Models and Methods in applied Sciences, Vol. 11, No.4 (2001), pp. 685–712.

[111] A.T. Patera, G. Rozza, K. Veroy. *Reduced basis methodologies for Stokes equations in parametrized domains*. EPFL-IACS Report 22.2004. Preprint.

[112] K. Perktold, M. Hofer, G. Karner, W. Trubel, H. Schima. *Computer simulation of vascular fluid dynamics and mass transport: optimal design of arterial bypass anastomoses.* Proceedings of ECCOMAS 98, pp. 484–489, K. Papailion and others Editors, John Wiley and Sons, Ltd, 1998.

[113] J.S. Peterson. *The reduced basis method for incompressible viscous flow calculations. SIAM J. Sci. Stat. Comput.*, Vol. 10, No. 4 (1989), pp. 777–786.

[114] N.A.Pierce and M.B. Giles. *Adjoint recovery of superconvergent functionals from PDE approximations.* SIAM review, Vol. 42, No.2 (2000), pp. 247–264.

[115] O. Pironneau. *Optimal Shape Design for Elliptic Systems.* Springer-Verlag, Springer Series in Computational Physics, New York, 1984.

[116] E. Polak. *Optimization: algorithms and consistent approximations*, Springer-Verlag, New York, 1997.

[117] T.A. Porsching. *Estimation of the error in the reduced basis method solution of nonlinear equations.* Math. of Comput., Vol. 45, No. 172 (1985), pp. 487–496.

[118] C. Prud'homme, D. Rovas, K. Veroy, Y. Maday, A.T. Patera and G. Turinici. *Reliable real-time solution of parametrized partial differential equations: reduced-basis output bound methods.* J. Fluids Engineering, Vol. 172 (2002), pp. 70–80.

[119] C. Prud'homme, D. Rovas, K. Veroy and A.T. Patera. *Mathematical and computational framework for reliable real-time solution of parametrized partial differential equations. M^2AN*, Mathematical Modelling and Numerical Analysis, Vol. 36, No. 5 (2002), pp. 747–771.

[120] C. Prud'homme, A.T. Patera. *Reduced-basis output bounds for approximately parametrized elliptic coercive partial differential equations.* Computing and Visualization in Science, Vol. 6, No. 2-3 (2004), pp. 147–162.

[121] C. Prud'homme. *Adaptive reduced basis space generation and approximation*, submitted, 2004.

[122] A. Quaini, A. Quarteroni, G. Rozza. *Reduced basis methods for advection-diffusion optimal control problems.* In progress, 2005.

[123] A. Quarteroni, G. Rozza. *Optimal control and shape optimization in aorto-coronaric bypass anastomoses. M^3AS*, Mathematical Models and Methods in Applied Sciences, Vol.13, No. 12 (2003), pp. 1801–23.

[124] A. Quarteroni, G. Rozza, L. Dedè, A. Quaini. *Numerical approximation of a control problem for advection-diffusion processes.* Proceedings of IFIP Conference 2005, Turin, Italy (Springer Ed.).

[125] A. Quarteroni, M. Tuveri, A. Veneziani. *Computational vascular fluid dynamics: problems, models and methods.* Computing and Visualization in Science, Vol. 2 (2000), pp. 163-197.

[126] A. Quarteroni, L. Formaggia. *Mathematical Modelling and Numerical Simulation of the Cardiovascular System* in Modelling of Living Systems, Handbook of Numerical Analysis Series (P.G. Ciarlet e J.L. Lions Eds), Elsevier, Amsterdam, 2004.

[127] A. Quarteroni, A. Valli. *Numerical Approximation of Partial Differential Equations.* Springer-Verlag, Berlin, 1994.

[128] A. Quarteroni, A. Valli. *Domain Decomposition Methods for Partial Differential Equations.* Oxford University Press, Berlin, 1999.

[129] A. Quarteroni, R. Sacco, F. Saleri. *Numerical Mathematics.* Springer, New York, 2000.

[130] A. Quarteroni, A. Veneziani, P. Zunino. *Mathematical modelling of solute dynamics in blood flow and arterial walls.* SIAM Journal on Numerical Analysis, Vol. 39 (2002), pp. 511–519.

[131] A. Quarteroni, A. Veneziani, P. Zunino. *A domain decomposition method for advection-diffusion processes with applications to blood solutes.* SIAM Journal on Scientific Computing, Vol. 23, No. 6 (2002), pp. 1659–1980.

[132] S.S. Ravindran. *A reduced-order approach for optimal control of fluids using proper orthogonal decomposition.* International Journal for Numerical Methods in Fluids, Vol. 34 (2000), pp. 425–448.

[133] W.C. Rheinboldt. *On the theory and error estimation of the reduced basis method for multi-parameter problems.* Nonlinear Analysis, Theory, Methods and Applications, Vol. 21, No.11 (1993), pp. 849–858.

[134] D. Rovas. *Reduced-Basis Output Bound Methods for Parametrized Partial Differencial Equations.* PhD Thesis, MIT, Massachusetts Institute of Technology (February 2003).

[135] G. Rozza. *Reduced basis methods for elliptic equations in sub-domains with a posteriori error bounds and adaptivity.* Applied Numerical Mathematics, Vol. 55, No. 4 (2005), pp. 403–424.

[136] G. Rozza. *On optimization, control and shape design of an arterial bypass.* International Journal for Numerical Methods in Fluids, Vol. 47, No. 10-11 (2005), pp. 1411–1419.

[137] G. Rozza. *Real time reduced basis techniques for arterial bypass geometries.* In K.J. Bathe (ed.), Computational Fluid and Solid Mechanics, Elsevier, 2005, pp. 1283–1287.

[138] G. Rozza. *Reduced basis methods for Stokes equations in domains with non-affine parameters dependence.* EPFL-IACS report 06.2005, submitted 2005.

[139] F. Saleri. *MLife, Finite Element Library Documentation.* In progress, 2005. Web: http://mox.polimi.it

[140] M. Sankaranarayanan, L.P. Chua, D.N. Ghista, Y.S. Tan. *Computational model of blood flow in the aorto-coronary bypass graft.* BioMedical Engineering OnLine, Vol. 4, No. 14 (2005).

[141] S.J. Sherwin, D.J. Doorly. *Flow dynamics within model distal arterial bypass graft.* Advances in Fluid Mechanics, Vol. 34 (2003), pp. 327–374.

[142] T. Slawig. *Domain Optimization for the stationary Stokes and Navier-Stokes Equations by an embedding domain Tecnique.* Ph.D. Thesis, Tu-Berlin, 1998.

[143] I.J. Sobey. *On flow furrowed channels. Part 1. Calculated flow pattern.* Journal of Fluid Mechanics, Vol. 96, Part I (1980), pp. 1–26.

[144] J. Sokoloski, J.-P. Zolésio. *Introduction to Shape Optimization: Shape Sensivity Analysis.* Springer-Verlag, 1992.

[145] Y. Solodukhov. *Reduced-Basis Methods Applied to Locally Non-Affine Problems.* PhD thesis, MIT, Massachusetts Institute of Technology, 2005.

[146] N. Staalsen, M.U. Ulrich, J. Winther, E.M. Pedersen, T. How, H. Nygaard. *The anastomosis angle does change the flow fields at vascular end-to-side anastomoses in vivo.* Journal of vascular surgery, Vol. 21 (3), 1995.

[147] D.A. Steinman, B. Vinh, C.R. Ethier, M. Ojha, R.S Cobbold, K.W Johnston. *A numerical simulation of flow in a two-dimensional end-to-side anastomosis model.* Journal of Biomechanical Engineering, Vol. 115, No. 1 (1993), pp. 112–118.

[148] K.D. Stephanoff, I.J. Sobey, B.J. Bellhouse. *On flow through furrowed chanels. Part 2. Observed flow patterns.* Journal of Fluid Mechanics, Vol. 96, Part I (1980), pp. 27–32.

[149] C.A. Taylor, C.P. Cheng, L.A. Espinosa, B.T. Tang, D. Parker, R.J. Herfkens. *In vivo quantification of blood flow and wall shear stress in the human abdominal Aorta during lower limb exercise.* Annals of Biomedical Engineering, Vol. 30 (2002), pp. 402–08.

[150] R. Temam. *Navier-Stokes Equations: Theory and Numerical Analysis.* North-Holland, Amsterdam, 1984.

[151] A.N. Tikhonov, V.Ya. Arsenin. *Methods for Solving Ill-Posed Problems.* Nauka, Moscow, 1974.

[152] J. Tuma. *CFD simulation of flow past end-to-side anastomosis.* Submitted, 2005.

[153] G.M. Vainikko, A.Yu. Veretennikov. *Iterative Procedures in ill-posed problems.* Nauka, Moscow, 1986.

[154] M. Van Dyke. *Perturbation Methods in Fluid Mechanics.* The Parabolic Press, Stanford, 1975.

[155] F.P. Vasiliev. *Methods for Solving the Extremum Problems.* Nauka, Moscow, 1981.

[156] A. Veneziani *Mathematical and Numerical Modelling of Blood Flow Problems.* Ph.D. Thesis, Politecnico di Milano, 1998.

[157] K. Veroy, D. Rovas and A.T. Patera. *A posteriori error estimation for reduced-basis approximation of parametrized elliptic coercive partial differential equations: "convex inverse" bound conditioners.* Control, Optimisation and Calculus of Variations, Vol. 8, pp. 1007–1028, June 2002. Special Volume: A tribute to J.L. Lions.

[158] K. Veroy, *Reduced-Basis Methods Applied to Problems in Elasticity.* PhD Thesis, MIT, Massachusetts Institute of Technology (June 2003).

[159] K. Veroy and A.T. Patera. *Certified real-time solution of the parametrized steady incompressible Navier-Stokes equations; Rigorous reduced-basis a posteriori error bounds.* International Journal Numerical Methods for Fluids, Vol. 47, No. 8-9 (2005), pp. 773–788.

[160] K. Veroy and A.T. Patera. *Reduced-basis approximation of the viscosity-parametrized incompressible Navier-Stokes equation: Rigorous a posteriori error bounds.* In Proceedings Singapore-MIT Alliance Symposium, January 2004.

[161] K. Veroy, C. Prud'homme, D. Rovas, A.T. Patera. *A Posteriori Error Bounds for Reduced-Basis Approximation of Parametrized Noncoercive and Nonlinear Elliptic Partial Differential Equations.* AIAA American Institute of Aeronautics and Astronatics. Paper 2003-3847 (2003).

[162] N. Weck. *Unique continuation for a generalized Stokes system.* Communications in Partial Differential Equations, Vol. 27, No. 3-4 (2002), pp. 425–436.

[163] H. H. Wei, S. L. Waters, S. Q. Liu and J.B. Grotberg. *Flow in a wavy-walled channel lined with a poroelastic layer.* Journal of Fluid Mechanics, Vol. 492 (2003), pp. 23–45.

[164] D. Wells, J.P. Archie, C. Kleinstreuer. *The effect of Carotid Artery geometry on the magnitude and distribution of Wall Shear Stress Gradients.* Journal of Vascular Surgery, Vol. 23 (1996), pp. 667–678.

[165] S.S. White, C.K. Zarins, D.P. Giddens, H.S. Bassiouny, F. Loth, A. Jones, S.Glagov. *Haemodynamic patterns in two flow models of end-to-side anastomoses: effect of pulsatility, flow division, Reynolds number and hood length.* Journal of Biomechanical Engineering, Vol. 115 (1993), pp. 104–111.

[166] K. Willcox, J. Peraire. *Balanced Model Reduction via the Proper Orthogonal Decomposition.* 15th AIAA Computational Fluid Dynamics Conference, 2001.

[167] K. Yosida. *Functional Analysis.* Springer-Verlag, Berlin, 1974.

[168] C. Zarins, D. Giddens, B. Bharadvaj, V. Sottiurai, R. Mabon, S. Glagov. *Carotid bifurcation atherosclerosis: quantitative correlation of plaque localization with flow velocity profiles and wall shear stress.* Circ. Res., Vol. 53 (1983), pp. 502–514.

[169] R.K. Zeytounian. *Theory and Applications of Viscous Fluid Flow.* Springer-Verlag Berlin-Heidelberg, 2004.

[170] P. Zunino. *Multidimensional pharmacokinetic models applied to the design of eluting stents.* Journal of Cardiovascular Engineering, Vol. 2, No. 4 (2004).

Index

Curriculum Vitæ

Gianluigi Rozza est né à Sant'Angelo Lodigiano (Lodi), Italie, le 20 Avril 1977. Il a fréquenté l'école secondaire au Lyceé "Giovanni Gandini" à Lodi où il a obtenu son Baccalauréat Scientifique en 1996. Ensuite, il poursuit ses études au Politecnico di Milano pour obtenir en 2002 un diplôme d'ingénieur aerospatiale, séction aerodinamique, avec mention apres un travail de diplome à l'École Polytechnique Fédérale de Lausanne – dans le cadre du projet Socrates de l'Union Europeenne – et au MOX – Modeling and Scientific Computing – centre du Politecnico. Depuis novembre 2002, il est engagé comme assistant dans la Chaire de Modelisation et Calcul Scientifique. A cette période, il commence son travail de thèse de doctorat en Analyse Numerique dans le reseau EU-RTN (Research Training Network of European Union) projet HaeMOdel sous la direction du Prof. A. Quarteroni et en collaboration avec Prof. V.I. Agoshkov de l'Academie Russie de la Science et Prof. A.T. Patera du MIT, Massachusetts Institute of Technology. En 2004 il partecipe à la Conference ICFD – Methodes Numeriques pour les Fluides – de l' Université de Oxford (UK) et il reçoit le Prix *Bill Morton* pour son travail sur l'optimization en mecanique des fluides. Il a participé à plusieurs conférences internationales (*Third MIT Conference on Computational Fluid and Solid Mechanics Young Researcher Fellowship Award en 2005*) et il est auteur et co-auteur des publications suivantes:

- A.Quarteroni, G.Rozza. *Optimal control and shape optimization of aorto-coronaric bypass anastomoses.* M^3AS Mathematical Models and Methods in Applied Sciences, Vol. 13, No. 12 (2003), pp. 1801–23.

- G.Rozza. *On optimization, control and shape design for an arterial bypass.* International Journal for Numerical Methods in Fluids, *Bill Morton Prize Paper*, Vol. 47, No. 10-11 (2005), pp. 1411–1419.

- G.Rozza. *Reduced basis methods for elliptic equations in sub-domains with a-posteriori error bounds and adaptivity.* Applied Numerical Mathematics, Vol. 55, No. 4 (2005), pp. 403–424.

- V.Agoshkov, A.Quarteroni, G.Rozza. *Shape design in aorto-coronaric bypass using perturbation theory.* To appear in SIAM Journal on Numerical Analysis, 2005.

- G.Rozza. *Real time reduced basis techniques in arterial bypass geometries.* Computational Fluid and Solid Mechanics, Elsevier, (K.J. Bathe Ed.), pp. 1283–1287, 2005.

- A.T.Patera, G.Rozza, K.Veroy. *Reduced basis methodologies for Stokes equations in parametrized domains.* IACS Report No. 22, 2004. Preprint.

- V.Agoshkov, A.Quarteroni, G.Rozza. *A mathematical approach in the design of arterial bypass using unsteady Stokes equations.* To appear in Journal of Scientific Computing, 2005.

- G.Rozza. *Reduced basis methods for Stokes equations in domains with non-affine parameters dependence.* IACS Report No. 06, 2005. Submitted.

- A.Quarteroni, G.Rozza. *Tecniche a basi ridotte per l'ottimizzazione di configurazioni di innesto per bypass coronarici.* Istituto Lombardo Accademia di Scienze e Lettere, 2005. MOX Report No. 67.

- A.Quarteroni, G.Rozza, L.Dedè, A.Quaini. *Numerical approximation of a control problem for adevection-diffusion processes,* in *System Modeling and Optimization*, Springer Ed., Proceedings of IFIP-TC7 Conference, Torino, Italy, 2005. IACS Report No. 14, 2005. Submitted.

- A.Quaini, A.Quarteroni, G.Rozza. *Reduced basis methods for advection-diffusion optimal control problems.* In preparation, 2005.

- G.Rozza. *Reduced basis techniques for Navier-Stokes equations in parametrized domains.* In progress, 2005.